Pure

Bangor University

DOCTOR OF PHILOSOPHY

Low latitude Pacific palaeoceanographic change across the Eocene/Oligocene boundary

Broadbent, Tom

Award date:
2010

Awarding institution:
Bangor University

Link to publication

General rights
Copyright and moral rights for the publications made accessible in the public portal are retained by the authors and/or other copyright owners and it is a condition of accessing publications that users recognise and abide by the legal requirements associated with these rights.

- Users may download and print one copy of any publication from the public portal for the purpose of private study or research.
- You may not further distribute the material or use it for any profit-making activity or commercial gain
- You may freely distribute the URL identifying the publication in the public portal ?

Take down policy
If you believe that this document breaches copyright please contact us providing details, and we will remove access to the work immediately and investigate your claim.

Download date: 13. Nov. 2024

Low latitude Pacific palaeoceanographic change across the Eocene/Oligocene boundary

Tom Broadbent

Bangor University

U.W.B LIBRARY
P.C.B LLYFRGELL

Abstract:

Evidence from both terrestrial and marine environments indicates a cooling of Earth's climate across the Eocene/Oligocene boundary (EOB), with the likely development of continental scale glaciation. The most geographically widespread and persuasive line of evidence for the shift in Earth's climate comes from variation in stable isotopes measured from benthonic foraminiferal carbonate, with a geologically rapid and globally observed >1 ‰ increase in $\delta^{18}O$. Increasing foraminiferal $\delta^{18}O$ reflects either a cooling in the deep ocean or an increase in the $\delta^{18}O$ of seawater, which is related to removal of light oxygen isotopes through continental glaciation. However, despite the global recognition of an increase of >1.0 ‰ in benthonic foraminiferal $\delta^{18}O$ and fundamental change in Earth's climate, the proportion of change, i.e. temperature decrease and/or ice volume development, is poorly constrained. Deconvolution of the foraminiferal $\delta^{18}O$ requires and independent proxy to isolate the temperature or ice-volume change, one such proxy is foraminiferal Mg/Ca ratios. Foraminiferal Mg/Ca ratios are a palaeotemperature proxy, however, their application has lead to the observation of bottom-water warming and thus suggesting bipolar glaciation; a scenario inconsistent with a warmer Earth and unsupported by sedimentary evidence. The warming observed in bottom-water Mg/Ca palaeotemperatures, however, was determined from a deep-ocean site that experienced significant deepening of the carbonate compensation depth (CCD) concomitant with Mg/Ca increase, leading to the hypothesis increasing carbonate ion saturation ($\Delta[CO_3^{2-}]$) caused enhanced foraminiferal uptake of Mg and thus the observed temperature increase. This study aimed to deconvolute the foraminiferal $\delta^{18}O$ record using paired benthonic foraminiferal records from a site with minimal change in $\Delta[CO_3^{2-}]$. Paired benthonic and planktonic foraminiferal stable-isotope and Mg/Ca records have been developed from Site 1211, Shatsky Rise; Site 1211 hypothesised to have a much reduced increase in $\Delta[CO_3^{2-}]$. Foraminiferal geochemical records were supplemented with CCD proxy records, i.e. %calcium carbonate, to allow relative constraint $\Delta[CO_3^{2-}]$ change. Foraminiferal stable-isotope records from Site 1211 exhibit a positive $\delta^{18}O$ shift and $\delta^{13}C$ excursion similar to published records, which lag a deepening of CCD by several hundred thousand years. Mg/Ca palaeotemperatures display a high degree of scatter hindering clear identification of EOB change, although an average increase is suggested. The similarity of palaeotemperature evolution from a range of water depths and postulated $\Delta[CO_3^{2-}]$ histories has been interpreted to show that changing $\Delta[CO_3^{2-}]$ has minimal control on benthonic foraminifera Mg/Ca. Estimation of ice-volume suggests a maximum ice-volume equivalent to the last glacial maximum was sustained for several hundred thousand years, with ice volumes reducing to modern day levels during the Early Oligocene.

Contents

List of Figures

List of plates

List of Tables

Acknowledgements

In the five years it has taken to complete this thesis there are too many people to acknowledge for their contribution in a single short page, however, there are those who deserve special mention. I would like to thank my main supervisor, Dr Leon Clarke, for his help, guidance and never (at least to my knowledge) despairing with me. Many were his helpful suggestions that pointed me in the correct direction during the writing of the thesis, not to mention the development of my analytical and lab skills during the practical element.

I am most grateful to my co-supervisor, Professor Melanie Leng, and the staff of the stable-isotope facility at the NERC Isotope Geosciences Laboratory (NIGL) who provided me with training and undertook many of the isotopic analyses upon which this thesis is based. Equally, I would like to thank Benoit Disch at the NERC ICP-MS facility (then) at the University of Kingston for his training and assistance in analysing my foraminifera for their element/Ca ratios. It is fair to say that the analytical support of these two groups of people were key to making this project successful.

I would also like to thank the other scientists who helped me along the way: Dr Ian Miller and Dr Tom Dunkley-Jones, for their valuable guidance in the development of the age-depth relationship, perhaps the single most troublesome aspect of the thesis as a whole. Professor Paul Pearson for his help with the difficult Oligocene planktonic foraminiferal taxonomy. Steve Wyatt for his assistance in the determination of the $\%CaCO_3$. The staff at the ODP core repository at the Marum Institute, Bremen for opportunity to both develop the XRF records and study ODP Leg 198 cores in detail.

Lastly, I would like to thank my parents for their support during the final, traumatic stages of writing up, without which finishing would have been a much more difficult prospect. My two brothers, Harry and Will, for their unfailing humour and courage in the face of adversity that spurred me on. Neither can I leave out mention of Izzy, Mark, Holly and the UMWC for the many good memories with which my time researching this thesis at Bangor University will always be linked.

1.0 Introduction

The Palaeogene (65.50 to 23.03 Ma before present) was a period of significant climate evolution, during which Earth's climate changed from a generally equable globally ice-free "greenhouse" in the Late Palaeocene to Early Eocene (~65 to ~50 Ma) to a much cooler glaciated "icehouse" by the early Oligocene (~33.9 Ma). Climate proxy data from terrestrial and marine environments are available for much of the Palaeogene, with the most stratigraphically continuous and globally distributed palaeoclimate archives being those of deep-sea sediment cores. The international science programs the Ocean Drilling Program (ODP) and its predecessor the Deep Sea Drilling Project Study (DSDP) recovered a globally comprehensive suite of sediment cores. These programs set out to conduct research into the evolution of Earth's climate and history of ocean basins and oceanic crust, through use of the drilling vessels *Glomar Challenger* and *JOIDES Resolution*. It is the study of these deep-sea sediment cores and, in particular, the generation of benthonic foraminiferal stable-isotope records (see Chapter 2 for details) that has allowed the compilation of a global dataset showing climate evolution through the Palaeogene (Figure 1.1; Zachos et al., 2001).

The gradual evolution of climate during Earth history is to be expected from the ever-changing boundary conditions of plate tectonics and orbital parameters. Plate tectonics acts to influence ocean and atmospheric circulation through changes in the location, elevation and distribution of the continents over geological time, while orbital parameters change the angle of the axis of Earth's rotation and the shape of the orbit on a series of cyclical timescales; these changes altering the solar insolation and Earth's energy budget. Superimposed on long-term climate evolution are more sudden and geologically rapid shifts in climate state, such as the Palaeocene–Eocene Thermal Maximum (PETM) and the Eocene–Oligocene boundary (EOB). These abrupt changes to Earth's climate have been the subject of much research in order to understand how global climate responds to changes in different forcing factors. Similarly, this study is concerned with the reconstruction of climate and ocean changes across the EOB, as described below.

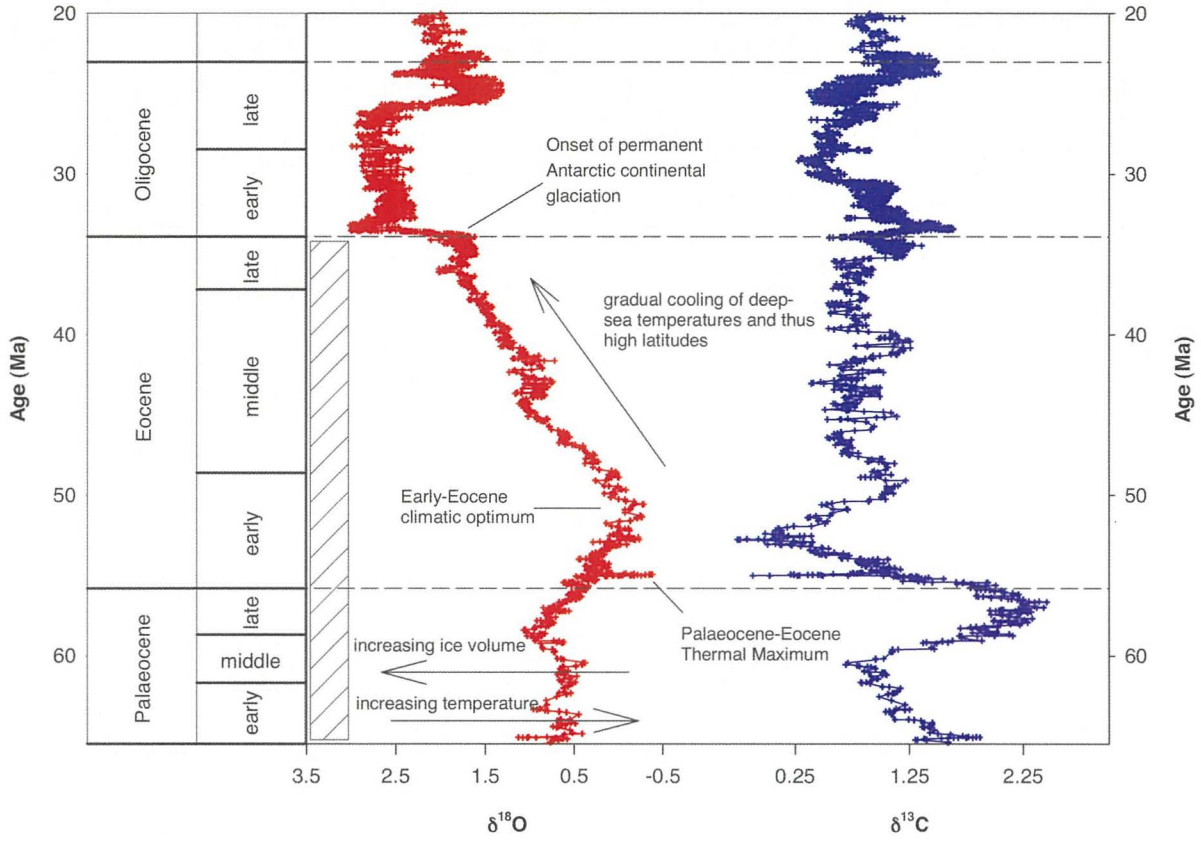

Figure 1.1: Compilation of global benthonic foraminiferal $\delta^{18}O$ and $\delta^{13}C$ stable-isotope records from Zachos et al. (2001). The hatched grey bar depicts the time period during which continental ice is believed to be absent or geographically restricted. A detailed discussion of the controls on benthonic foraminiferal stable-isotope ratios can be found in Chapter 2; in brief, foraminiferal $\delta^{18}O$ ratios depend on changes in seawater temperature ($\delta^{18}O$ values decreasing as temperatures increase) and the $\delta^{18}O$ composition of the seawater ($\delta^{18}O_{sw}$), the $\delta^{18}O_{sw}$ being controlled predominantly by the volume of continental ice (greater volumes of continental ice cause more positive seawater $\delta^{18}O$ values); foraminiferal $\delta^{13}C$ values depend on the CO_2 cycle as well as productivity and ocean circulation, e.g. isotope fractionation favours uptake of ^{12}C during the photosynthetic synthesis of organic matter, enriching the remaining dissolved inorganic carbon in seawaters in ^{13}C, leading to higher $\delta^{13}C$ values.

There is abundant sedimentary, geochemical and palaeontological evidence for a significant change in global climate at the EOB (33.9 Ma). The occurrence of dropstones and ice-rafted debris (IRD) and changes in sediment clay mineralogy on and around Antarctica suggests a change in climate and glaciation of that continent at the EOB (Coxall and Pearson, 2007). Perhaps the most significant geochemical proxy for documenting the EOB climate shift is that of benthonic foraminiferal stable-isotope ratios, in particular oxygen-isotope ratios (expressed as $\delta^{18}O$ values). A positive step change of ~1.0 ‰ in $\delta^{18}O$ ratios is seen at the EOB (Figure 1.1), these higher $\delta^{18}O$ values being sustained for ~400 kyrs, prior to a new steady state with Oligocene $\delta^{18}O$ values ~1 ‰ more positive than those of the Eocene. These changes in benthonic foraminiferal $\delta^{18}O$ values reflect cooling of deep waters and/or growth of (a) continental ice sheets. Synchronous with the well-documented $\delta^{18}O$ step is a positive excursion in $\delta^{13}C$ isotopes and a global deepening of

the carbonate compensation depth (CCD; Zachos et al., 1996; 2001; Coxall et al., 2005), indicative of changes in global carbon cycling, either as a cause or effect of the EOB.

Two main hypotheses have been suggested to explain the significant climate change at the EOB (e.g., Coxall and Pearson, 2007, and references therein). The first relates cooling of Antarctica to the onset of the Antarctic Circumpolar Current (ACC) following the opening of the Drake Passage and the Tasman Gateway, leading to the thermal isolation of the Antarctica and ice sheet growth. The second relates global cooling to a decrease in atmospheric CO_2, either through a reduction in volcanic outgassing throughout the Palaeogene or by drawdown of CO_2 by enhanced silicate weathering on the newly uplifted Tibetan Plateau (Raymo and Ruddiman, 1992). Modelling of the EOB has suggested that once a critical pCO_2 threshold has been reached, development of a continental ice sheet occurs rapidly, modelled oxygen isotope and ice volume scenarios closely following high-resolution deep-sea records (DeConto and Pollard, 2003; Coxall et al., 2005; DeConto et al., 2008). Many aspects of the EOB, such as the extent of Antarctic glaciation, the role of the ACC and the precise relationship with atmospheric pCO_2 levels are, however, still uncertain. As such further work is required to facilitate greater understanding of both the causes and effects within the Earth system during this significant change in global climate.

1.1 Study rationale

As indicated above, foraminiferal oxygen-isotope ratios are dependant on two main controls, the seawater temperature during calcification (increases in temperature cause a decrease in $\delta^{18}O$ values) and the ambient $\delta^{18}O$ composition of seawater ($\delta^{18}O_{sw}$). The latter is dependant on the volume of continental ice, since isotope fractionation in the hydrological cycle results in continental ice being relatively enriched in the "light" ^{16}O isotope (more negative $\delta^{18}O$ values), leaving seawater relatively enriched with the "heavy" ^{18}O isotope (more positive $\delta^{18}O$ values). Thus, the ~1.5 ‰ positive shift in benthonic foraminiferal oxygen isotopes at the EOB is as a result of either a decrease in temperature, an increase in ice volume or a combination of these two factors. Quantification of the relative magnitudes of these two principal influences on the ~1.5 ‰ positive step in benthonic foraminiferal $\delta^{18}O$ records is important to help reconstruction of the magnitude and improve understanding of the cause of glaciation at the EOB.

Deconvolution of these two influences on the benthonic foraminiferal $\delta^{18}O$ record is, however, a difficult undertaking, requiring an independent proxy for either temperature or ice volume that can be used to estimate the contribution of that specific variable to the oxygen-isotope record and thus derive the magnitude of the other controlling factor. The most promising approach suggested to date for such a deconvolution is that of the generation of paired foraminiferal geochemical proxy records. For the purposes of the deconvolution of bottom-water temperature and continental ice volume from foraminiferal oxygen-isotope records, paired proxies entail the use of foraminiferal Mg/Ca ratios as an independent proxy for palaeotemperature estimations. Foraminiferal Mg/Ca ratios have been demonstrated to vary depending on the temperature of calcification and thus can be used to calculate the relative proportions of the foraminiferal $\delta^{18}O$ record that is related to temperature and ice-volume (e.g., Lear et al., 2004; see also Chapter 2 for further discussion).

Application of this paired proxy deconvolution technique to EOB foraminiferal samples has, however, produced unexpected results. An early Oligocene increase in benthonic foraminiferal Mg/Ca ratios suggests that bottom-water temperatures increased by ~2°C across the EOB (Lear et al., 2004; Figure 1.2). Such a bottom-water temperature increase has two significant implications: 1) it counter-intuitively suggests that glaciation occurred synchronous with high-latitude warming (ocean bottom-waters form at the surface in the high latitudes in the modern ocean, so it is assumed that this occurred in the Palaeogene also; thus increasing bottom-water temperatures is as a result of warming at high-latitudes), and 2) it suggests that the entire positive step in $\delta^{18}O$ values is related to changes in continental ice volume, without any of the ~1.5 ‰ positive step in $\delta^{18}O$ values being due to a temperature decrease. The former implication questions the causal mechanism of the EOB and would suggest that ice growth did not result from decreasing temperatures, but as a result of an alternative causal factor such as increased moisture supply to the continent (Lear et al., 2000). The latter implication indicates the development of ice volumes too great to have been held on the Antarctic continent alone suggesting the requirement for additional Northern Hemisphere glaciation (Coxall et al., 2005).

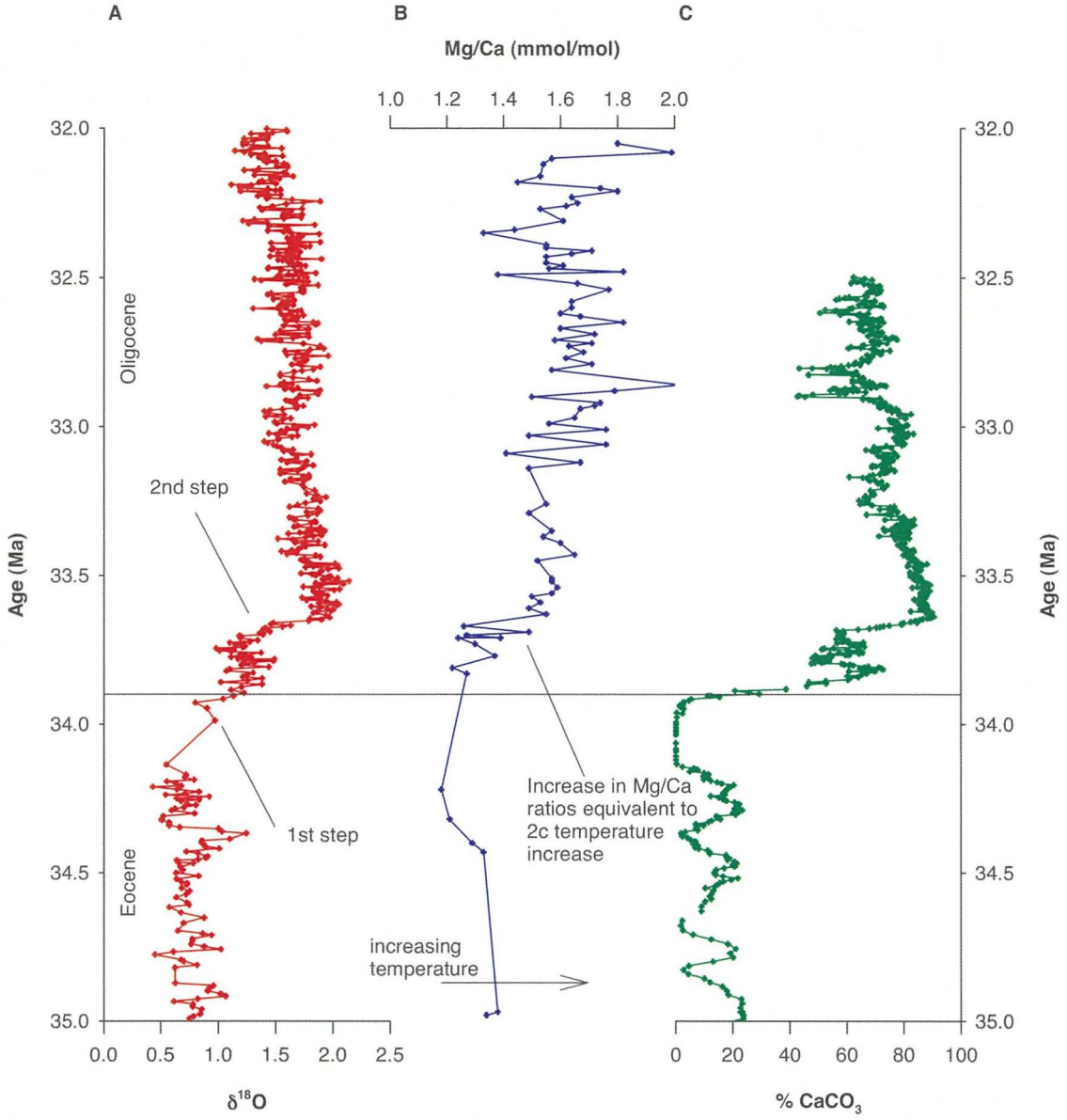

Figure 1.2: Existing Pacific Ocean geochemical proxy data from ODP Site 1218 (Coxall et al., 2005; Lear et al., 2004). A) Oxygen-isotope ratio data for benthonic foraminifera *Cibicidoides* spp. (Coxall et al., 2005). B) Mg/Ca ratio (mmol/mol) data for *Oridorsalis umbonatus*; ratios increase synchronously with the second step in the oxygen-isotope records (Lear et al., 2004). C) % calcium carbonate data from Coxall et al. (2005), showing the dramatic increase in the proportion of calcium carbonate within the sediment synchronous with the increase in benthonic foraminiferal $\delta^{18}O$ values at the EOB.

While there is some limited evidence for late Eocene to early Oligocene Northern Hemisphere glaciation from ice-rafted debris (Eldrett et al., 2007; Tripati et al., 2008), an alternative hypothesis that would explain current observations is that benthonic foraminiferal Mg/Ca ratios are not solely controlled by calcification temperature. The benthonic foraminiferal Mg/Ca ratio dataset of Lear et al. (2004), that described a warming trend across the EOB, was obtained from ODP Site 1218 which was located at a palaeodepth of ~3800m during the late Eocene to Oligocene (Coxall et al., 2005). The Eocene CCD was close to this depth (~3500m), and deepened dramatically at the EOB (synchronously with the positive step in oxygen-isotope ratios) by ~1 km as a result of increased deep-sea carbonate ion concentration (Figures 1.2 and 1.3; Coxall et al., 2005).

The increased deep-sea carbonate ($[CO_3^{2-}]$) would have caused the carbonate saturation ($\Delta[CO_3^{2-}]$) state at Site 1218 to change from undersaturation to likely oversaturation across the EOB, as indicated by the increase in calcium carbonate content of the sediment (Figure 1.2C).

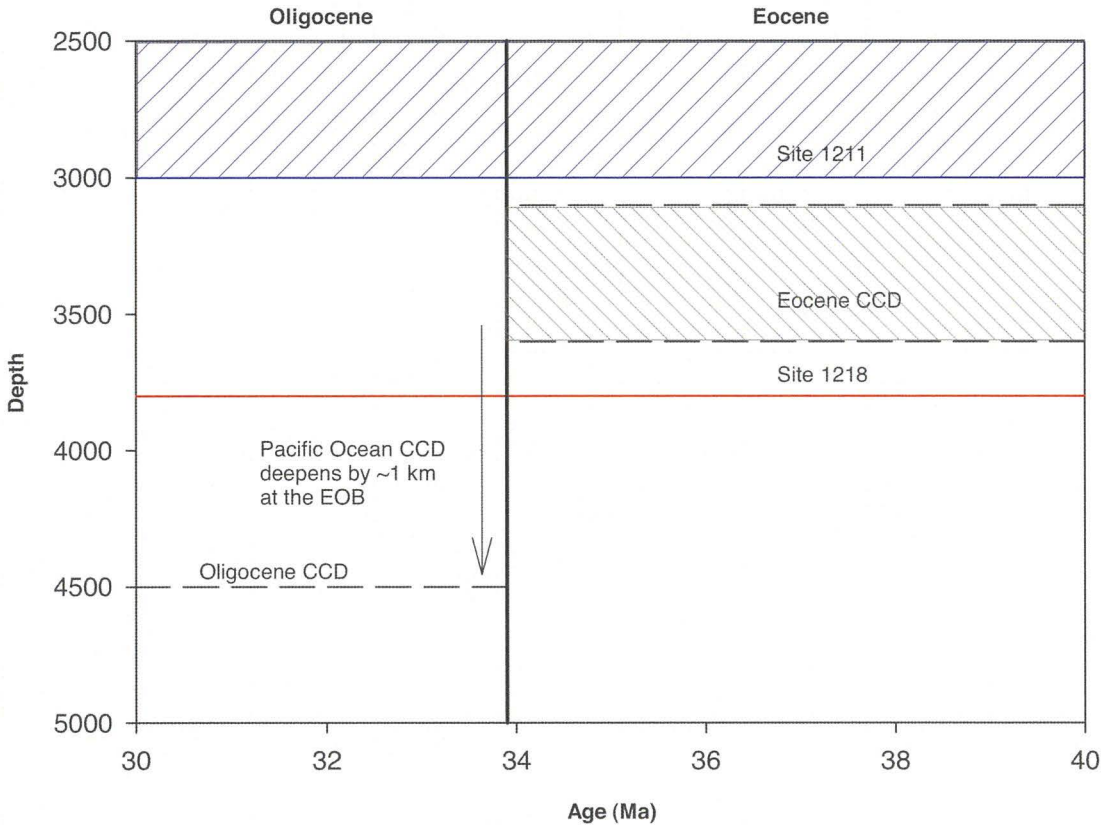

Figure 1.3: Eocene and Oligocene CCD (Tripati et al., 2005) with the palaeodepths of ODP Sites 1211 and 1218 (Shipboard Scientific Party, 2002a; Coxall et al., 2005) plotted across the EOB (shown as thick vertical line at 33.9 Ma). The Site 1211 palaeodepth is shown as a blue-hatched area corresponding to the palaeodepths allowed by benthonic foraminiferal assemblages (Shipboard Scientific Party, 2002a). The Eocene CCD is shown as a grey-hatched area across the range of CCD variation. Whilst Site 1211 was within a few hundred metres of the Eocene CCD, undersaturation with respect to the carbonate ion was not sufficient to cause a complete loss of sedimentary carbonate, as evidenced by the continuous nannofossil ooze sediment (Shipboard Scientific Party, 2002b). Thus the degree of increase in carbonate ion saturation across the EOB should be much less than at Site 1218 and therefore there should be a reduced influence of increasing carbonate ion saturation state on Mg/Ca ratios recorded within benthonic foraminiferal tests relative to Site 1218.

Billups and Schrag (2003) and Lear et al. (2004) have suggested that the EOB change in carbonate saturation state may have enhanced the uptake of Mg into benthonic foraminiferal tests and thus affected Mg/Ca ratios. This effect would have had a masking effect on the expected decrease in benthonic foraminiferal Mg/Ca ratios that would have been associated with a decrease in bottom-water palaeotemperatures. In contrast to the EOB benthonic foraminiferal Mg/Ca ratio increase observed by Lear et al. (2004), recent Mg/Ca records from planktonic foraminifera obtained from sediment cores representative of the low-latitude Indian Ocean suggest surface-ocean cooling across the EOB (Lear et al., 2008), and result in $\delta^{18}O_{sw}$ estimates that do not require the existence of Northern

Hemisphere ice sheets, thus lending further support to the hypothesis of a further influence of benthonic foraminiferal Mg/Ca ratios during EOB time.

The influence of carbonate saturation state described above has, however, very recently been challenged by findings that, for *Oridorsalis umbonatus*, the benthonic foraminiferal species used for Mg/Ca ratio investigations by Lear et al. (2004), with neither $[CO_3^{2-}]$ or $\Delta[CO_3^{2-}]$ having a clear influence on Mg/Ca ratios (Rathmann and Kuhnert, 2008). Therefore, it is important that new records of benthonic foraminiferal Mg/Ca ratios are developed from deep-sea locations that were less influenced by changing carbonate saturation state, i.e. at sites that were located at depths shallower than the CCD prior to the EOB, so that any change in deep-water carbonate saturation state is reduced relative to that evident at Site 1218. In this way better deconvolution of the relative contributions of seawater temperature and $\delta^{18}O_{sw}$ and further understanding of the potential effects of carbonate saturation state on benthonic foraminiferal Mg/Ca ratios will be possible.

The primary aim of this study thus was to produce new records of benthonic foraminiferal stable-isotope and Mg/Ca ratios across the EOB. A study site was chosen so as to be located at a palaeodepth above the Eocene and Oligocene CCD (~3500–4500 m), throughout the late Eocene to early Oligocene, thereby reducing the influence of any change in deep-water carbonate saturation state on geochemical proxy data. Based on the hypothesis that Site 1218 benthonic foraminiferal Mg/Ca ratios (Lear et al., 2004) predominantly reflect increasing carbonate ion saturation state and a related enhanced uptake of Mg into the foraminiferal test, Mg/Ca ratios for a site above the CCD (with reduced change in carbonate saturation state) should not show the increase in Mg/Ca ratios observed previously (Figure 1.2). Provided the carbonate ion saturation state, inferred from proxies for carbonate dissolution (e.g., % sand fraction and % calcium carbonate), remained sufficiently high that deep waters were not undersaturated and calcium carbonate was the dominant sedimentary component, Mg/Ca ratios at this above CCD locality should display a decrease across the EOB, as a result of deep water cooling, in line with those observed for the surface ocean by Lear et al. (2008).

Eocene–Oligocene geochemical proxy records across the EOB exist primarily from the Atlantic, Indian and Southern Oceans and, while there is close agreement between the magnitude and timing of the oxygen-isotope shift between these globally distributed datasets, their remains a paucity of data from the Pacific Ocean. The Pacific Ocean accounts for ~50% of the present-day global ocean, having been greater in size during the Palaeogene, and is globally important in influencing present-day climates through teleconnections, i.e. the Pacific Ocean effects the climate of a distant region by variation in its own climate (Lyle et al., 2008). Consequently, an improved understanding of how the EOB is manifested within and affected the Pacific Ocean is of great importance.

Recently, ODP Legs 198 and 199 (Leg 199 Site 1218 geochemical proxy data shown in Figure 1.2 and discussed above) sought to recover EOB sedimentary records from the Pacific Ocean in order to begin to fill such a gap in scientific knowledge. ODP Leg 198 recovered sediment from the Shatsky Rise, a medium-sized large igneous province situated in the northwest Pacific Ocean (Figure 1.4), with an overall goal to investigate the transient climate events that occurred during the Cretaceous and Cenozoic, e.g. the Palaeocene–Eocene Thermal Maximum and the Eocene–Oligocene boundary, amongst others. Particular aims were to "*address questions concerning the nature of chemical (i.e. calcite compensation depth, nutrients, and oxygenation) and physical oceanographic changes (temperature gradients) during these events*" (Shipboard Scientific Party, 2002a).

A series of eight sites were cored during the Leg 198 expedition, covering each of the highs on, and a range of water depths across, Shatsky Rise (Table 1.1; Figure 1.5); a transect of sites from the Southern High (Sites 1209 to 1212) recovered broadly similar sedimentary records (Shipboard Scientific Party, 2002a). Each of the sites recovered a Plio–Pleistocene interval of nannofossil oozes and clays and a near complete early Oligocene to Maastrichtian stratigraphic section dominated by nannofossil ooze. The dominance of nannofossil ooze in the recovered Palaeogene sediments indicates that sedimentation was above the CCD throughout that time period (Figure 1.3). Carbonate sedimentation throughout the late Eocene and into the Oligocene across Shatsky Rise contrasts with Site 1218 where carbonate sedimentation was sporadic (see $\%CaCO_3$ in Figure 1.2), thus the increase in bottom water carbonate ion saturation will have

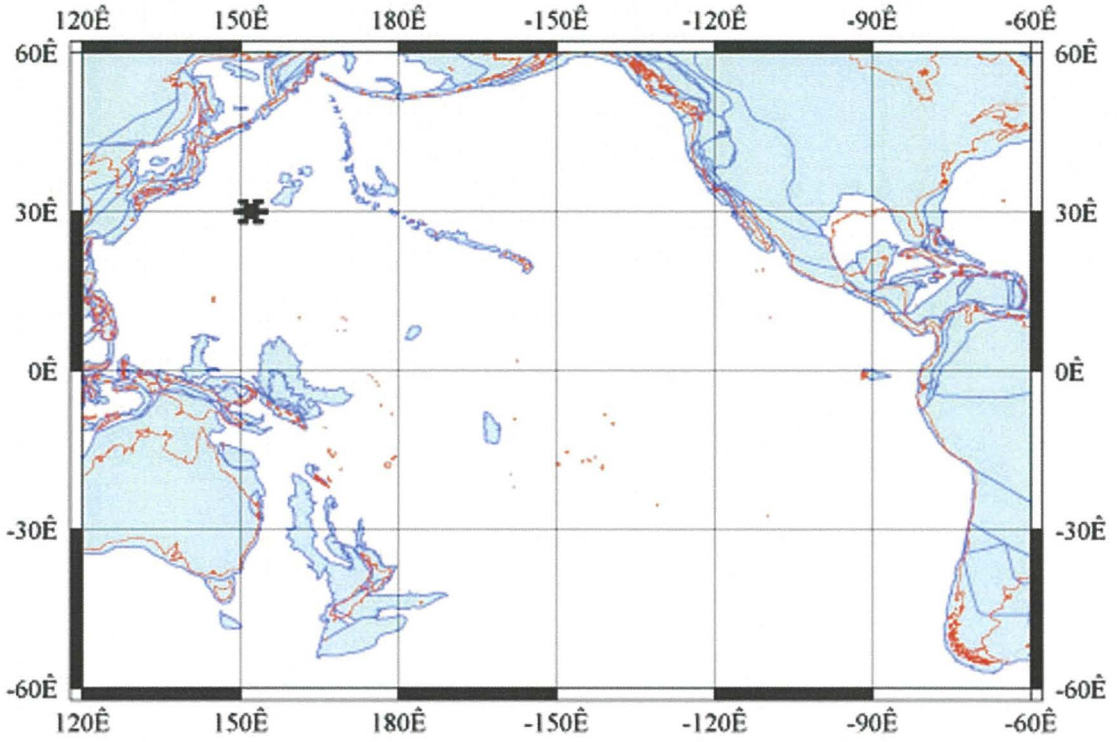

0 Ma Reconstruction

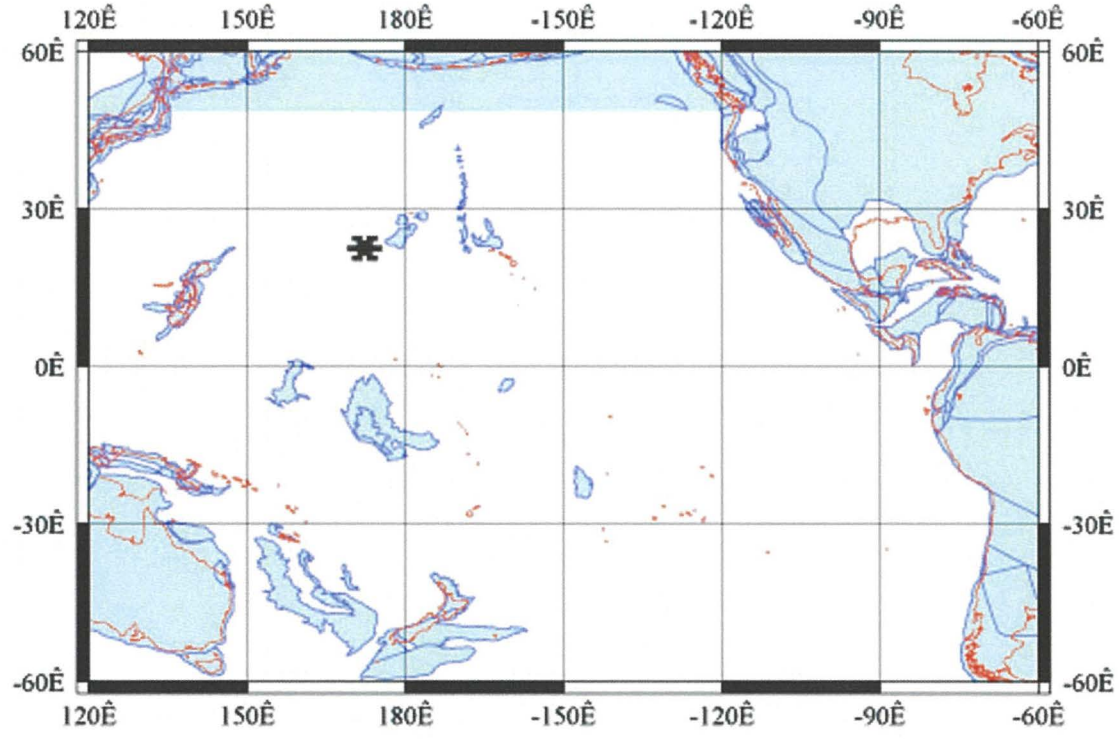

34 Ma Reconstruction

Figure 1.4: Present-day (0 Ma) and Eocene–Oligocene boundary (34 Ma) position of the Shatsky Rise (*). Modern shorelines are shown in red and plate boundaries in blue. Maps are plotted on an equidistant cylindrical projection using the ODSN plate tectonic reconstruction service (www.odsn.de)

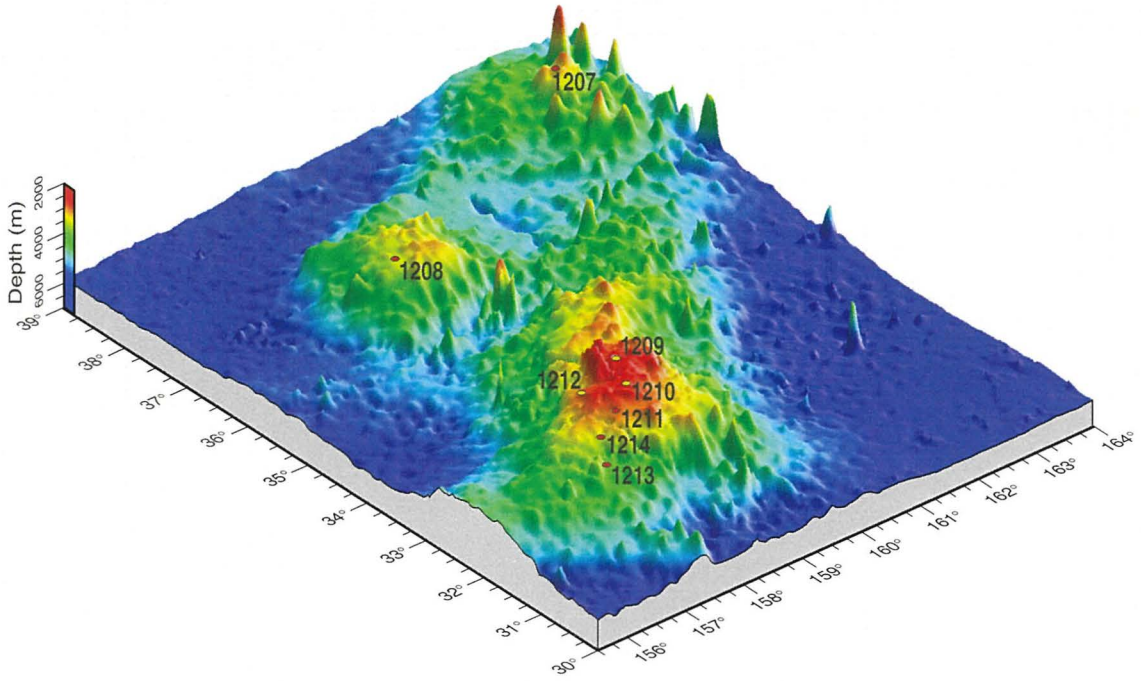

Figure 1.5: Relief map of Shatsky Rise. Sites 1207 and 1208 are situated on the Northern and Central Highs, respectively, with the other sites located on the Southern High (Shipboard Scientific Party, 2002a)

ODP site	Latitude	Longitude	Depth (metres below sea level, mbsl)	Metres Composite Depth of Sediment Recovered	Previous DSDP sites
1207	37°47.433'N	162°45.053'E	3100	622.8	
1208	36°07.630'N	158°12.095'E	3346	392.3	
1209	32°39.102'N	158°30.359'E	2387	307.5	
1210	32°13.416'N	158°15.562'E	2574	377.0	
1211	32°00.131'N	157°51.000'E	2907	169.9	DSDP Site 305
1212	32°26.903'N	157°42.701'E	2641	207.6	DSDP Site 47
1213	31°34.649'N	157°17.861'E	3883	494.4	
1214	31°52.025'N	157°28.717'E	3402	235.9	DSDP Site 306

Table 1.1: Leg 198 Shatsky Rise sites, sediment recovery and association with previous DSDP sites cored prior to Leg 198.

been reduced. The reduced increase in bottom water carbonate ion saturation across the EOB makes Shatsky Rise sediments suitable to test the hypothesis that the increase in carbonate ion saturation resulted in the increase in foraminiferal Mg/Ca ratios observed at Site 1218 (Figure 1.2), as described above. The most complete Shatsky Rise sedimentary record of Eocene–Oligocene climate change was recovered at Site 1211, with biostratigraphic data suggesting recovery of Late Eocene to Late Oligocene sediments (Shipboard Scientific Party, 2002a,b). Thus, this study has focused on Site 1211 to provide new Eocene to Oligocene geochemical datasets for the Pacific Ocean.

Using sediments recovered in ODP Leg 198 Site 1211, located at a palaeodepth of ~2000–3000 m (Figure 1.3; Shipboard Scientific Party, 2002 a,b), a range of geochemical analyses have been carried out to produce a new Pacific Ocean integrated geochemical proxy dataset for the EOB. Paired stable-isotope and Mg/Ca ratio analyses have been carried out on benthonic foraminifera to allow deconvolution of the ice-volume and temperature components of the foraminiferal oxygen-isotope record. These foraminiferal data were supplemented with proxies relating to the CCD and carbonate dissolution, i.e. % sand fraction and % calcium carbonate, in order to assess changes in carbonate saturation state across the Eocene–Oligocene boundary at Site 1211. The new foraminiferal Mg/Ca ratios and palaeotemperature estimates have been compared to the published data for Site 1218 (Lear et al., 2004; Coxall et al., 2005) to test the carbonate saturation state hypothesis. Planktonic foraminiferal and <38 μm fine-fraction stable-isotope and planktonic foraminiferal Mg/Ca ratio records have also been developed allowing assessment of palaeoceanographic change in surface-ocean waters and to enable reconstruction of surface-deep water geochemical gradients. Coupled deconvolution of benthonic and planktonic foraminiferal stable-isotope and Mg/Ca ratios allows a more robust assessment of the magnitude of change of $\delta^{18}O_w$ and thus of ice sheet growth. Interpretation of this new integrated geochemical dataset has been considered in comparison with published records.

1.2 Thesis structure

This chapter briefly covers the background to this study, its aims and rationale. Chapter Two then details the major evidence for climate change at the Eocene–Oligocene boundary, and discusses the likely causes and feedbacks that were in operation. It also

covers key concepts and gives a background to the key geochemical proxies used within the study, in particular those of foraminiferal stable-isotope and element/Ca ratio determinations. Materials and methods used in this study are discussed in Chapter Three, focusing in detail on the choice of samples, processing and geochemical methods used. Details as to the analytical accuracy and precision of the methods used are also covered in Chapter Three. The development of a robust depth–age model for Site 1211, using existing biostratigraphic data and a new Sr-isotope ratio dataset generated by this study is covered in Chapter Four. Chapter Five describes the new Site 1211 geochemical proxy data derived during this study, as well as an assessment of the affects of diagenesis and state of preservation of the calcareous nannofossil and foraminiferal samples investigated. Interpretation and discussion of this study's geochemical proxy dataset follows in Chapter Six, which also includes comparison to existing datasets. Finally, Chapter Seven details the main conclusions of the study and includes suggestions for further work.

Chapter 2: The Eocene–Oligocene Transition

2.0 Introduction

The following chapter describes the oceanographic evidence for significant climate change in the Late Eocene to Early Oligocene. Particular attention is paid to evidence from geochemical proxies that have been used within this study, i.e. foraminiferal stable-isotope and element/Ca ratios. Following the description of the evidence for climate change at the Eocene Oligocene Boundary (EOB), hypotheses as to the causal factors will be described and the results of recent modelling investigations will be considered in order to build a synthesis as to what happened at the EOB.

As briefly described in Chapter One, the Palaeogene was a period of significant climatic evolution (Zachos et al., 2001; 2008), this study focuses on one aspect of Palaeogene change: the Eocene-Oligocene boundary (EOB). There is a wealth of evidence from both terrestrial and oceanographic realms for a relative rapid and permanent shift in global climates at the EOB (33.9 Million years ago (Ma)). As this study is based on deep-sea sediment geochemical proxies, the following review deals mainly with evidence from such sources in the oceanographic realm. The oceanographic evidence for the EOB can be broadly split into two main groups; that is sedimentary and geochemical.

2.1 Sedimentary evidence

2.1.1 Glaciomarine sediments

The sediment record reveals much about the changes in climate leading up to and across the EOB, especially in sediments recovered from around Antarctica (e.g. Zachos et al., 1992; Ehrmann and Mackensen,1992; Diester-Haass 1996 among others). The most direct evidence of the development of ice on Antarctica is that of glaciomarine sediments (e.g. dropstones, ice rafted debris (IRD)) from locations around the modern-day East Antarctic ice sheet (e.g. Maud Rise, Kerguellen Plateau). While occasional layers of IRD have been identified prior to the EOB (Ehrmann and Mackensen 1992), the occurrence of IRD shows a marked increase at the EOB (Zachos et al., 1992; Ehrmann and Mackensen, 1992; Diester-Haass, 1996). The increase is synchronous with increases in the proportion of opal in the sediment and the shift in stable isotope records described below (Zachos et al. 1992,

Ehrmann and Mackensen 1992). These increases are thought to mark the onset of major glaciation over the area occupied by the modern-day East Antarctic ice sheet.

Records from west Antarctica have been more elusive but recently detailed glaciomarine sediments from the Antarctic Peninsula suggest that regional ice development across the EOB occurred here too (Ivany et al., 2006). Evidence of glaciation is also emerging from the Northern Hemisphere, Eldrett et al. (2007) and Tripati et al. 2008) reporting IRD in the Norwegian-Greenland Sea sediments deposited between ~44 to 30 Ma. IRD and dropstones have also been observed in middle Eocene sediments from the Lomonsov Ridge in the central Arctic Ocean (Moran et al., 2006; John 2008). The Northern Hemispheric evidence, however, does not allow for determination of the source or extent of glaciation so may be a result of calving of icebergs from mountain glaciers as opposed to ice sheets.

2.1.2 Clay mineralogies

Further sedimentary evidence is available from clay mineralogies, revealing information about the geology, level of weathering and environment of the source region. Four clay minerals (kaolinite, smectite, illite and chlorite) are typically the result of weathering, each forming in different environmental conditions and degrees of weathering (Diester-Haass et al., 1993). Kaolinite develops in warm environments where precipitation favours weathering of the bedrock, smectite develops in warm, wet seasonal environments where chemical weathering is able to proceed to completion. Illite and chlorite, however, are typical of areas where rock is being freshly eroded and environmental conditions are unfavourable for chemical weathering (i.e. steep relief, cold, dry). Other clay minerals may result from unchanged source rock (e.g. presence of micas) or from early diagenesis of biogenic silica (clinoptilolite).

Several sites surrounding Antarctica have had their clay assemblages studied (Diester-Haass et al., 1993; Zachos et al., 1999; Robert et al., 2002; Ehrmann and Mackensen 1992; Robert and Kennett 1997), these studies all record broadly the same trend of increasing proportions of illite/chlorite at the expense of smectite across the EOB. Diester-Haass et al. (1993) studied intervals of Eocene and Oligocene climate from Site 689 (Weddel Sea,

Southern Ocean) that reveal much about the environmental change during the Middle Eocene to Oligocene. The earliest sediment studied is from the Middle Eocene (~46 Ma), here clay is dominated by smectite; by the next interval in the late Middle Eocene (~41 Ma) smectite is still dominant but kaolinite and illite appear (up to 20 % total respectively). Across the EOB the proportion of illite increases up to 40 % of the clay assemblage, this trend continuing into the Oligocene with illite contributing up to 60 % of the clay assemblage. Similar trends are seen both in sediments recovered from the Weddell Sea and from the Kerguelen Plateau by Ehrmann & Mackenson (1992), Zachos et al. (1999) and Robert et al. (2002). The sequence of clay mineralogies, initially smectite rich but with increasing proportions of illite and chlorites, allows an interpretation of the source environments climate to be made (Ehrmann et al., 1992; Diester-Haass et al., 1993). Smectite, dominant during the Middle Eocene, forms during pedogenesis in warm, seasonally wet climates. Inland cooling and a shift to more year round rainfall are suggested by the appearance of illite and kaolinite by the late Middle Eocene. While the change in mineralogies is not dramatic at the EOB, increased illite as well as the appearance of fresh metamorphic and plutonic minerals (muscovite, talc, amphiboles) within the clay fraction, suggest decreased chemical weathering. The minor changes later in the Oligocene suggest that climate remains cold and physical weathering dominated beyond the boundary itself.

2.1.3 Radiogenic isotopes

Records of two radiogenic isotope ratios, $^{87}Sr/^{86}Sr$ and $^{187}Os/^{186}Os$, have been determined across the EOB, both of which appear to be demonstrating behaviour linked to the climatic change. Sr-isotopes are uniform throughout the ocean due to a residence time much greater than oceanic mixing time (Broecker and Peng, 1982) and are believed to be linked to changes in flux from two sources, weathering of continental rocks and removal at mid-ocean ridge basalts (Zachos et al., 1999). Ratios derived from continental rocks are dependent on the lithologies of rock available for weathering and the rate of weathering (Palmer and Edmond 1992; Zachos et al., 1999). Towards the end of the Eocene, the marine carbonate Sr-isotope ratio record is seen to inflect sharply with ratios increasing rapidly, becoming more radiogenic, throughout the remainder of the Palaeogene (Figure 2.1; Howarth and McArthur, 1997; McArthur et al., 2001; Zachos et al., 1999). The close relationship between the end of Eocene inflection in Sr-isotopes with oxygen isotopes, clay mineralogy changes and IRD suggests a relationship between each of these records

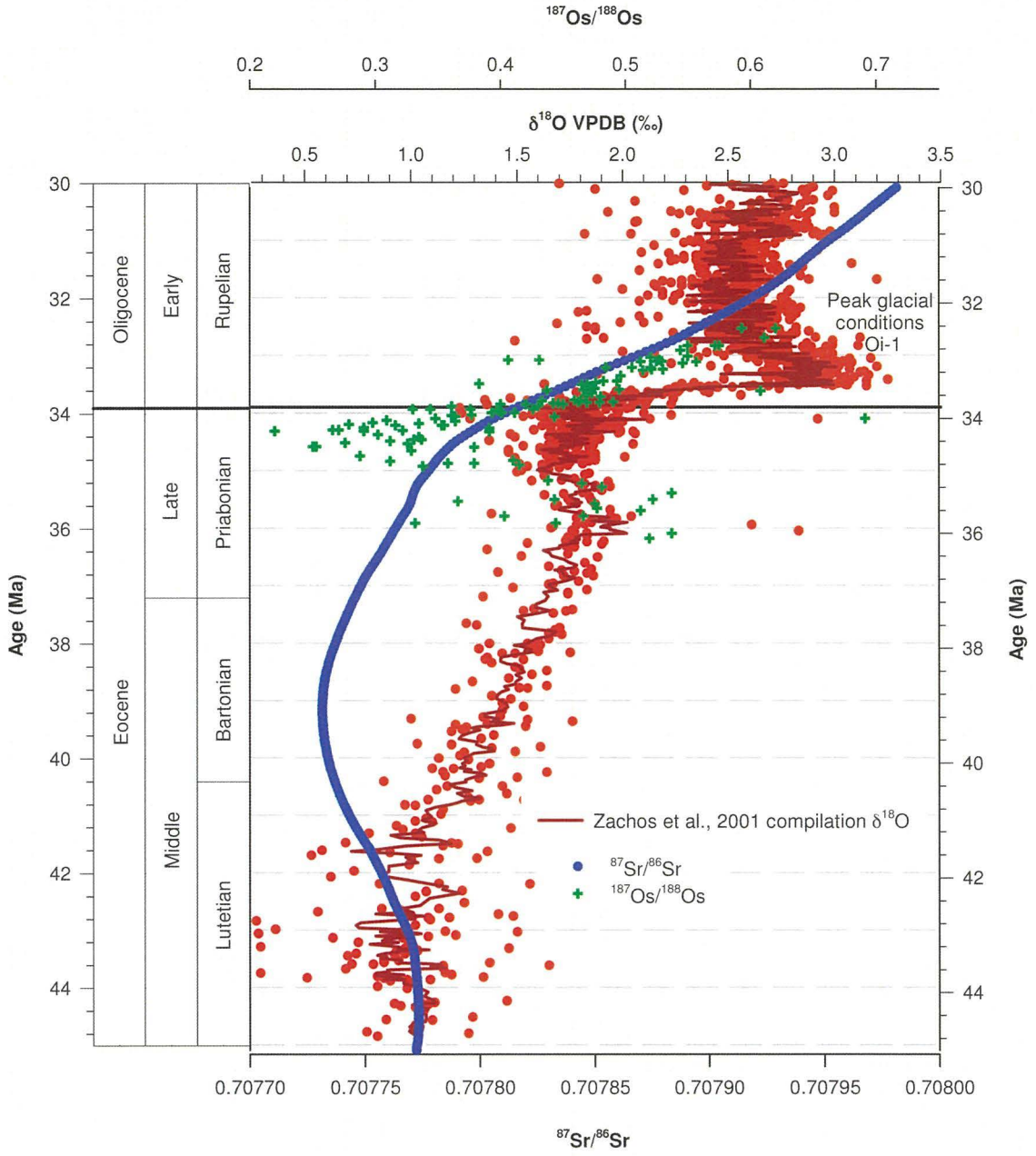

Figure 2.1: The relationship between radiogenic isotopes $^{87}Sr/^{86}Sr$ and $^{187}Os/^{188}Os$ to the benthonic foraminiferal $\delta^{18}O$ compilation curve (Howarth and McArthur, 1997; McArthur et al., 2001; Zachos et al., 2001; Ravizza and Peucker-Ehrenbrink, 2003). Both radiogenic isotope curves how significant inflections close to the EOB suggesting a link through weathering related to continental ice sheet growth (Lear et al., 2003; Ravizza and Peucker-Ehrenbrink, 2003).

(Zachos et al., 1999). The exact relationship between Sr-isotope ratios and the other evidence of EOB climate change is uncertain but much research has focused on the increase in Sr-isotopes over the last 40 million years being a result of increased weathering (Raymo et al., 1988; Zachos et al. 1999). Increased weathering has been suggested as a possible cause of global cooling and thus the EOB. The theory being that increased weathering of silicate rocks due to uplift caused the drawdown of atmospheric pCO_2 leading to global cooling that resulted in the glaciation of Antarctica (Raymo and Ruddiman, 1992). The uplift in question being that of the Himalayas, an idea supported by the highly radiogenic Sr-isotope ratios of modern-day Himalayan rivers and the fact these

rivers account for 25% of modern day Sr-isotope inputs (Edmond, 1992; Palmer and Edmond, 1992). However, while Himalayan uplift initiated in the middle Eocene, the influence of weathering of the Himalayas is uncertain prior to relief increasing significantly during the early Miocene (Zachos et al. 1999). Oslick et al. (1994) and Zachos et al. (1999) suggest the close relationship between Sr-isotope curve inflections and evidence of EOB glaciation may indicate climate enhanced chemical weathering related to Antarctic (de)glaciation as opposed to the relief related changes. Studies have shown that early stage glacial weathering of continental shields has enhanced $^{87}Sr/^{86}Sr$ ratios (Blum and Erel, 1995), Zachos et al. (1999) suggesting the temperate Oligocene Antarctic ice sheet fluctuated in a manner similar to the Pleistocene Northern Hemisphere ice sheets, leading to a regular supply and exposure of fresh material for weathering. Findings of Reilly et al. (2002) would appear to contradict this suggestion with an inflection seen during a period of minimum glaciation during the Oligocene, but this observation may be reconciled as a result of increased supply of material weathered during the previous glacial maxima. At the present time, it would seem that late Cenozoic Sr-isotope variation is a function of mainly relief related weathering with a component from rock freshly exposed by deglaciation.

The second Cenozoic radiogenic isotope record, that of $^{187}Os/^{188}Os$ is superficially similar to that of $^{87}Sr/^{86}Sr$ but unlike Sr-isotopes, Os-isotopes are not solely related to weathering and hydrothermal fluxes (Peucker-Ehrenbrink and Ravizza, 2000). Os-isotopes can also be affected by large bolide impacts and the weathering of organic-rich sediments. The residence time of Os within the oceans is also much less than that of Sr allowing discrimination between high frequency climatic and low frequency tectonic events given sufficient sampling density (Peucker-Ehrenbrink and Ravizza, 2000). While the Os-isotope record is much less well constrained than Sr-isotopes over the Cenozoic, studies indicate an asymmetric shift from Eocene values ($^{187}Os/^{188}Os$ ~0.4) to late Eocene minimum ($^{17}Os/^{188}Os$ ~0.25) followed by a marked increase over the EOB and into the Oligocene ($^{187}Os/^{188}Os$ ~0.6, Pegram and Turekian, 1999; Ravizza and Peucker-Ehrenbrink, 2003; Ravizza and Paquay, 2008; Figure 2.1). Two hypotheses have been suggested for the initial decrease in Os-isotope ratios: a decline in supply of radiogenic Os-isotopes or an increase in non-radiogenic Os-isotopes (Ravizza and Peucker-Ehrenbrink, 2003). Evidence for increased Os burial (Ravizza and Peucker-Ehrenbrink, 2003; Dalai et al., 2006) at the time of the Eocene minimum suggests that an increase in non-radiogenic Os is more likely than the significant decrease in radiogenic inputs required to recreate the isotope excursion.

Two sources are suggested for the non-radiogenic Os, weathering of ultramafic ophiolite complexes or the increased flux of cosmic dust (Ravizza and Peucker-Ehrenbrink, 2003; Dalai et al., 2006), the latter suggestion being favoured by Dalai et al. (2006) although investigation did not lead to unequivocal results.

Os-isotope ratio increase across the EOB broadly tracks the benthonic foraminiferal $\delta^{18}O$, but values plateau during the glacial maximum (See Section 2.2.3), increasing once again following the termination of peak glacial conditions (Figure 2.1; Ravizza and Peucker-Ehrenbrink, 2003). Ravizza and Peucker-Ehrenbrink (2003) interpret the increase in Os-isotopes on deglaciation from peak glacial conditions as evidence for increased supply of Os to the ocean from freshly exposed source rocks and enhanced weathering. Thus the increase in Os-isotopes agrees with the observations regarding increased weathering flux of radiogenic Sr upon deglaciation (Oslick et al., 1994; Zachos et al., 1999). The shorter oceanic residence time of Os allowing the Os-isotope record to reveal abrupt changes in the riverine flux that are hidden by the much longer residence time of Sr (Ravizza and Peucker-Ehrenbrink, 2003). These authors also suggest that if the Os-isotope record details weathering increases then it supports a possible feedback acting to stabilise Oligocene ice sheets; the feedback being the weathering of glacially exposed sediments causing the drawdown of atmospheric pCO_2 on deglaciation, preventing further ice-sheet wasting. Dalai et al. (2006) consider the possibility that an increase in cosmic dust supply, cosmic dust having a low $^{187}Os/^{188}Os$ ratio, caused the Os-isotope minimum and also may have influenced climate change at the EOB. The increased cosmic dust flux over the period of declining Os-isotopes (~1.5 Myr) lead to an enhanced supply of biologically important trace elements leading to a period of sustained enhanced productivity. Enhanced biological productivity could have lowered atmospheric CO_2 to a critical threshold allowing the development of a continental ice sheet on Antarctica (DeConto and Pollard, 2003).

2.2 Temperature and ice volume – foraminiferal $\delta^{18}O$ and Mg/Ca ratios

Stable isotope studies make use of the fact that oxygen and carbon have several stable isotopic species in nature. Oxygen has three: ^{16}O, ^{17}O, ^{18}O making up 99.76 %, 0.04 % and 0.2% respectively and carbon has two: ^{12}C and ^{13}C making up 98.89 % and 1.11 % of natural abundances. Of the oxygen isotopes, the isotopic ratios focus on $^{18}O/^{16}O$ ratios due to the higher abundances and greater mass difference. It is not possible to accurately

determine absolute abundances of minor isotopes such as $\delta^{18}O$ or $\delta^{13}C$ but through comparison of a sample to a defined standard, estimations can be made. These estimations are made through the use of the following formulae:

$$\delta^{18}O = \frac{^{18}O/^{16}O_{sample} - ^{18}O/^{16}O_{standard}}{^{18}O/^{16}O_{standard}} * 1000$$

$$\delta^{13}C = \frac{^{13}C/^{12}C_{sample} - ^{13}C/^{12}C_{standard}}{^{13}C/^{12}C_{standard}} * 1000$$

Variations such as this are given in delta (δ) notation, being reported in parts per thousand (‰). With this definition, positive values depict enrichment in the heavier isotope relative to the standard, and conversely negative values depletion. The most commonly referred to standard is the, now unavailable, Pee Dee Belemnite (PDB), a guard from Cretaceous belemnite *Belemnitella americana* found in the Pee Dee formation, South Carolina, having by definition $\delta^{18}O$ and $\delta^{13}C$ values of 0. Modern standards have been developed and defined against PDB to allow studies to make comparison to PDB. All biogenic carbonate $\delta^{18}O$ and $\delta^{13}C$ values referred to or plotted within this study are quoted relative to the Vienna PDB, a new reference sample to the original PDB.

2.2.1 Influences on foraminiferal $\delta^{18}O$

Foraminifera precipitate the carbonate for their tests from the ambient seawater following the reaction $Ca^{2+} + 2HCO_3^- \Rightarrow CaCO_3 + H_2O + CO_2$. Precipitation of both inorganic and biogenic carbonates, e.g. mollusc and foraminifera, $\delta^{18}O$ has been observed to occur in thermodynamic equilibrium with the precipitation solution (Urey, 1947; Epstein et al., 1953; Neil et al., 1969; Shackleton, 1974; Erez and Luz, 1983; Bemis et al., 1998; Ravelo and Hillaire-Marcel, 2007). Fractionation occurs during precipitation that leads to the preferential incorporation of ^{16}O rather than ^{18}O into the carbonate leading to biogenic carbonate $\delta^{18}O$ declining with increasing temperature, a 1 °C increase in temperature causing a ~0.21 to ~0.23 ‰ decrease in carbonate $\delta^{18}O$ (Ravelo and Hillaire-Marcel, 2007). The thermodynamic equilibrium of foraminiferal $\delta^{18}O$ allows the development of palaeotemperature equations, such as those of Shackleton, 1974; Erez and Luz, 1983; Bemis et al., 1998; Ravelo and Hillaire-Marcel, 2007). Whilst both quadratic and linear calibrations have been determined, Bemis et al. (1998) note that the relationship seen can

be calibrated to equivalent accuracies using either type of calibration. Palaeotemperature calibrations take the form of the following equation:

$$T = a - b * (\delta^{18}O_c - \delta^{18}O_{sw}) \qquad \text{Equ. 2.1}$$

Where T is the temperature (°C), *a* and *b* are constants, $\delta^{18}O_c$ is the $\delta^{18}O$ of the carbonate and $\delta^{18}O_{sw}$ is the $\delta^{18}O$ of the precipitating solution, i.e. seawater. Values of the two constants depend on the calibration used but *a* is typically ~16.5 and *b* ~ 4.5 (Bemis et al., 1998). Foraminiferal $\delta^{18}O$ values, however, are typically not the result of simple thermodynamic equilibrium values but are deviated from equilibrium by a variety of other factors, including ontogeny, presence of symbionts and gametogenic carbonate (Grossman, 1984a;b Spero & Lea, 1993; 1996; Cooke and Rohling, 1999). Variation in $\delta^{18}O_{sw}$ also prevents direct temperature estimation, as this value can vary with time and location (See Section 2.2.2).

Stable isotopic values from some species of foraminifera have been demonstrated to vary with size or stage of growth, i.e. with ontogeny. $\delta^{18}O$ from individual chambers of *Globogerina bulloides* grown in culturing experiments, a symbiont-free temperate to sub polar species commonly used in palaeoceanographic studies (Spero and Lea, 1996), has been observed to become more positive in later chambers. Spero and Lea (1996) attribute the ^{18}O enrichment to a decreasing proportion of ^{16}O from metabolic CO_2 in the chamber wall as test size increase, allowing chamber carbonate $\delta^{18}O$ to be closer to equilibrium. Ontogenetic enrichment has also been observed in fossil foraminifera samples, though the magnitude is less than would be expected from culturing (Spero & Lea, 1996; Cooke & Rohling, 1999). The reduced enrichment has been explained by changes in living depth across the formanifer life cycle. Spero & Lea (1996) suggest that calcification in a deeper, cooler environments during early life would lead to more enriched $\delta^{18}O$ values, a suggestion supported by comparison of cultured and fossil $\delta^{18}O$ growth plots. However, ontogeny is species specific with *Globigerinoides sacculifer* grown in culturing experiments showing no size–$\delta^{18}O$ relationship (Spero and Lea, 1993).

While ontogenetic calcite (that is calcite precipitated during the non reproductive stage) can differ for the reasons described above, a further complication is that of gametogenetic calcite. Some planktonic species (*G. sacculifera, Globigerinoides conglobatus, Orbulina*

universa) have been observed to deposit a further calcite crust over their last formed chambers immediately prior to gametogenesis (Be, 1980; Hamilton et al., 2008). Such gametogenetic layers can contribute a significant proportion of the shell's mass; Bé (1980) measured the addition of, on average, 28% by weight to the shells of *G. sacculifer*. Other species (*Neogloboquadrina dutertrei, Globorotalia* spp.) may deposit a crust as the organism descends through the water column towards the end of its life cycle (Hamilton et al., 2008). The isotopic signatures of the gametogenic carbonate may differ from that of ontogenetic carbonate, thick gametogenetic shells of *O. universa* having an enrichment with respect to $\delta^{18}O$ of 0.5‰ over thin, non-gametogenetic ones (Spero & Lea, 1993), as would be expected for carbonate precipitating in cooler, deeper waters. Quantification of the amount of gametogenetic calcite would be preferable, prior to interpretation of geochemical records from species displaying these behaviours. Gametogenetic calcite has been estimated to account for between 14 and 28 % of shell weight (Bé, 1980; Hamilton et al., 2008), although despite refined estimations of gametogenetic calcite within a shell, controls or reasons for calcification during gametogenesis remain elusive. Hamilton et al. (2008) hypothesise that gametogenetic calcification results from an internal discharge of Ca^{2+} or alkalinity that increases the carbonate saturation state prior to gametogenesis leading to carbonate precipitation.

Symbiont-bearing species, such as *G. sacculifer* and *O. universa*, $\delta^{18}O$ values have been observed to vary inversely correlated to the irradiance (Spero and Lea, 1993). Enhanced calcification rates also observed under high irradiance conditions have been hypothesised to lead to greater oxygen isotope fractionation and thus relative $\delta^{18}O$ depletion (Spero & Lea, 1993; Cooke & Rohling, 1999; Hamilton et al., 2008).

Recent work has demonstrated a carbonate ion ($[CO_3^{2-}]$) (or pH) effect on the $\delta^{18}O$ of planktonic foraminifera, although the effect has not been identified on the infaunal benthonic foraminifera *O. umbonatus* suggesting the effect may be species/habitat specific (Rathmann and Kuhnert, 2008). Spero et al. (1997) and Bijma et al. (1999) show that increasing $[CO_3^{2-}]$ results in a decrease in $\delta^{18}O$ in planktonic foraminifera *O. universa* and *Globigerina bulloides*. Observation has shown the $[CO_3^{2-}]$ effect behaviour to be independent of temperature and symbiont activity in *O. universa* and ontogenetic effects in *G. bulloides* (Bijima et al., 1999). The covariation of $\delta^{13}C$ and $\delta^{18}O$ decreasing with

increasing $[CO_3^{2-}]$ is a behaviour seen in many carbonate and aragonite secreting organisms (Bijma et al., 1999 and references therein) suggesting a common kinetic control, foraminiferal $\delta^{13}C$ reviewed in Section 2.3.1. Two alternate and probably complementary hypotheses have been suggested for why the $\delta^{18}O$ decreases with increasing $[CO_3^{2-}]$: either increasing $[CO_3^{2-}]$ causes increased calcification and thus greater fractionation (Bijma et al., 1999), or fractionation is a result of the changing balance of $[HCO_3^{-1}]$ and $[CO_3^{2-}]$ within the ocean as $[CO_3^{2-}]$ increases, $[CO_3^{2-}]$ having more negative $\delta^{18}O$ and thus foraminiferal $\delta^{18}O$ becomes more negative (Zeebe, 1999).

The influences that move foraminiferal carbonate away from thermodynamic equilibrium can, to an extent, be minimised through the use of single-species foraminiferal records and restricted size-fraction records, i.e. 150–250 μm. Single species records avoid the potential for the effects of differing species specific effects being present within a record (Vinot-Bertouille and Duplessy, 1972), i.e. species with or without symbionts, whilst a restricted size fraction excludes foraminifera from a significantly different ontogenetic stage. Benthonic foraminiferal $\delta^{18}O$ should have reduced potential for effects such as gametogenesis or ontogeny, as a consequence of the limited variation in $\delta^{18}O$ at or near the seabed (not the case for benthonic foraminiferal $\delta^{13}C$, see Section 2.3.1), however, the same strategies employed with planktonic foraminifera reduce the non-temperature related variation. Changes in carbonate ion saturation are more difficult to remove, especially in deep-time intervals where constraint on water chemistry is reduced, more work is required on carbonate ion effects to allow full understanding of foraminiferal stable-isotope records (Bijma et al., 1999; Lea et al., 1999a). Consideration of any of these effects on extinct foraminifera is difficult as the methods involved in identification, i.e. laboratory culturing, are not applicable, thus modern-day relationships have to be assumed to hold true during the geological past.

2.2.2 Influences on $\delta^{18}O_{sw}$

The predominant control on the variation in oxygen isotope ratios is fractionation during the hydrological cycle. Seawater naturally contains both ^{16}O and ^{18}O; upon evaporation the isotopically light water (i.e. H_2O where O is ^{16}O) is preferentially evaporated, with cooler temperatures leading to greater fractionation. Thus atmospheric moisture is isotopically lighter than its parent seawater. Upon precipitation of the atmospheric moisture, water

containing the $\delta^{18}O$ isotope condenses more readily, which leads to progressive enrichment in $\delta^{16}O$ of the remaining water vapour as the vapour moves from the source region following a Rayleigh distillation process. The fractionation of seawater during evaporation and condensation has local surface water effects, creating isotopically heavy areas where evaporation is occurring, isotopically lighter surface waters in high precipitation areas or around freshwater inlets (a coastal effect), that do not effect mean global ocean $\delta^{18}O_{sw}$. Evaporation/precipitation does effect global $\delta^{18}O_{sw}$ if the isotopically light water vapour is removed for timescales $>10^4$ years, i.e. by continental ice sheets. The Rayleigh fractionation of water vapour leads to highly ^{18}O depleted precipitation at high latitudes resulting in ice sheets having isotopic compositions of -30 to -50 ‰ (Huybrechts, 2002). Development of significant ice sheets, i.e. that cause global sea-level falls of >10 m, can effect global $\delta^{18}O_{sw}$. Fairbanks and Matthews (1978) quantify the effect of a drop in sea level by ~10 m as causing a 0.11 ‰ increase in $\delta^{18}O_{sw}$ for the Last Glacial Maximum (LGM).

While the lock up of "light" water in continental ice sheets affects global ocean $\delta^{18}O_{sw}$, precipitation and evaporation have local effects on surface water $\delta^{18}O_{sw}$ and thus surface water biogenic carbonate $\delta^{18}O$ records. Evaporation will locally increase the $\delta^{18}O_{sw}$ and also increase the salinity, while precipitation will have the opposite effect. Zachos et al. (1994) note that there is significant variation in surface water $\delta^{18}O$ as a result of evaporation and precipitation (low latitude being 1–1.5 ‰ higher than mean ocean/high latitude surface waters). Further variability is added if near shore waters are included. This variability can bias sea surface temperature estimations especially in areas where the effect is greatest (i.e. tropical surface waters), leading to calculation of cooler palaeotemperatures. Without independent palaeosalinity and $\delta^{18}O_{sw}$ proxies it is impossible to calculate the magnitude of this effect. Zachos et al. (1994) assume latitudinal gradients are akin to modern day, based on assumptions about heat transport and limits set by ocean density gradients. Using these assumptions they derive an expression describing present-day distribution of $\delta^{18}O_{sw}$, which adjusts Holocene values to a better fit with mean zonal temperatures. Given the uncertainty as to salinity gradients and distributions during the Palaeogene, the correction is unnecessary if surface-water records are being produced from a single location, as the shifts in surface-water $\delta^{18}O_{sw}$ as a result of evaporation/precipitation will not alter relative temperature variation or $\delta^{18}O_{sw}$ shifts within a record.

2.2.3 Eocene–Oligocene $\delta^{18}O$ record

Early work on benthonic foraminifera recognised a rapid (75-100 kyrs) positive shift of ~1 ‰ in $\delta^{18}O$ at the Eocene Oligocene boundary, the boundary then placed at 38 Ma (Shackleton and Kennett, 1975; Shackleton & Kennett, 1976; Kennett, 1977). Initial interpretation of the positive shift in $\delta^{18}O$ ratios was a decrease in bottom-water temperatures by ~5 °C close to the Eocene–Oligocene boundary caused by the onset of modern thermo-haline circulation, i.e. the formation of cold deep-waters at high latitude (Shackleton and Kennett, 1975; Kennett and Shackleton, 1976). The above authors cite the increased frequency of breaks in the stratigraphic record immediately prior to the $\delta^{18}O$ positive shift, turnover of benthonic faunal assemblages and an increase in biogenic carbonate sedimentation after the $\delta^{18}O$ shift as support for their hypothesis. Development of continental ice was believed to occur much later in the Middle Miocene (Shackleton and Kennett, 1975), based primarily on the assumption that $\delta^{18}O$ was insufficiently positive to require continental scale ice, although minor Antarctic glaciation was expected (Kennett, 1976). Planktonic foraminiferal $\delta^{18}O$ records across the EOB were more ambiguous than the benthonic foraminiferal $\delta^{18}O$ ratios, with low-latitude planktonic foraminifera exhibiting only a minor increase in $\delta^{18}O$ (Keigwin, 1980; Keigwin and Corliss, 1986). This was interpreted to support the positive shift in $\delta^{18}O$ resulting mainly from temperature increase.

Early stable-isotope records (Shackleton and Kennett, 1975; Shackleton & Kennett, 1976; Kennett, 1977, Keigwin, 1980; Keigwin and Keller, 1984; Miller and Thomas, 1985; Keigwin and Corliss, 1986) across the Eocene/Oligocene boundary were, however, hampered by poor biostratigraphic age constraints and incomplete Eocene/Oligocene sections leading to limited constraint on the magnitude and timing of the EOB event. Advances in drilling, improvements in the correlation of biostratigraphy and magnetostratigraphy and the targeting of shallowly buried, expanded Cenozoic sections have lead to the recovery of more complete EOB sections. These advances have resulted in a better understanding of many aspects of the EOB. Recent studies (Zachos et al., 1996; Diester-Haass & Zahn, 1996; Coxall et al., 2005; Riesselman et al., 2007; Katz et al., 2008,

Site	Location	Palaeodepth (mbsl)	EOT change $\delta^{18}O$	EOT change $\delta^{13}C$	EOT interval	Species	Publication
19	S. Atlantic	3730	0.7	0.4		*O. tener*	Keigwin & Corliss, 1986
19	S. Atlantic		0.42	-0.9		*G. subglobosa*	Keigwin & Corliss, 1986
77	Western Equatorial Pacific	2700	1.19	0.69		*Cibicidoides* spp.	Keigwin & Keller, 1984
253	Tropical Indian Ocean	606	1.04	0.3		*O. tener*	Keigwin & Corliss, 1986
253	Tropical Indian Ocean	606	0.4	0.4		*C. ungerianus*	Keigwin & Corliss, 1986
253	Tropical Indian Ocean		~	~		*T. ampliapertura*	Keigwin & Corliss, 1986
277	Southern Ocean	1232	1.01	0.25		mixed benthonic	Shackleton & Kennett, 1975
277	Southern Ocean	1232	1.2		~100 kyr	mixed benthonic	Shackleton & Kennett, 1975
277	Southern Ocean	1232	~1	~0.8	~800 kyr	*O. umbonatus*	Keigwin, 1980
277	Southern Ocean		~0.9	~0.9		*G. angiporoides*	Keigwin, 1980
292	Western Equatorial Pacific	1068	~1.5	~1		*O. umbonatus*	Keigwin, 1980
292	Western Equatorial Pacific		~0.3	~0.7		*T. ampliapertura*	Keigwin, 1980
362	S. Atlantic	1325	1.04	0.33		*C. ungerianus*	Keigwin & Corliss, 1986
363	S. Atlantic	2216	0.62	0.36		*O. tener*	Keigwin & Corliss, 1986
363	S. Atlantic		0.4	0.49		*T. ampliapertura*	Keigwin & Corliss, 1986
522	S. Atlantic	2963	1.2	0.52	<600 kyrs	*Cibicidoides* spp.	Miller et al., 1988
522	S. Atlantic	2963	1.55	1.76	~400kyr	*Cibicidoides* spp.	Zachos et al., 1996
563	western North Atlantic	2200	>0.76	>0.31		mixed benthonic	Miller & Fairbanks, 1980
574	Equatorial Pacific	3200	1.03	0.83	<700 kyrs	*Cibicidoides* spp.	Miller & Thomas, 1985
689	Southern Ocean, Atlantic	1500	1.44	0.88		*Cibicidoides* spp.	Stott et al., 1990 ;Diester-Haas & Zahn, 1996
744	Southern Ocean, Indian	1500	1.52	1.12	~400 kyr	*Cibicidoides* spp.	Zachos et al., 1996
748	Southern Ocean, Indian	1300	~1.5	~1.1	<200 kyrs	*Cibicidoides* spp.	Zachos et al., 1992
1218	Equatorial Pacific	3500	1.75	1.4	~300 kyrs	*Cibicidoides* spp.	Coxall et al., 2005
1263	subtropical South Atlantic	2100	~2.5	~1.5	~130 kyrs	*O. umbonatus*	Riesselman et al., 2007
SSQ	Gulf of Mexico	<150	1.87	2.75	~400 kyr	*Cibicidoides* spp.	Katz et al., 2008
TDP	Tropical Indian Ocean		~1	0.7	~400 kyrs	*T. ampliapertura*	Pearson et al., 2008

Table 2.1: Summary of published magnitudes and, where well constrained, timings of the Eocene–Oligocene transition. All $\delta^{18}O$ excursion magnitudes are determined from the minimum $\delta^{18}O$ value at the EOT to the maximum value at Oi-1a.

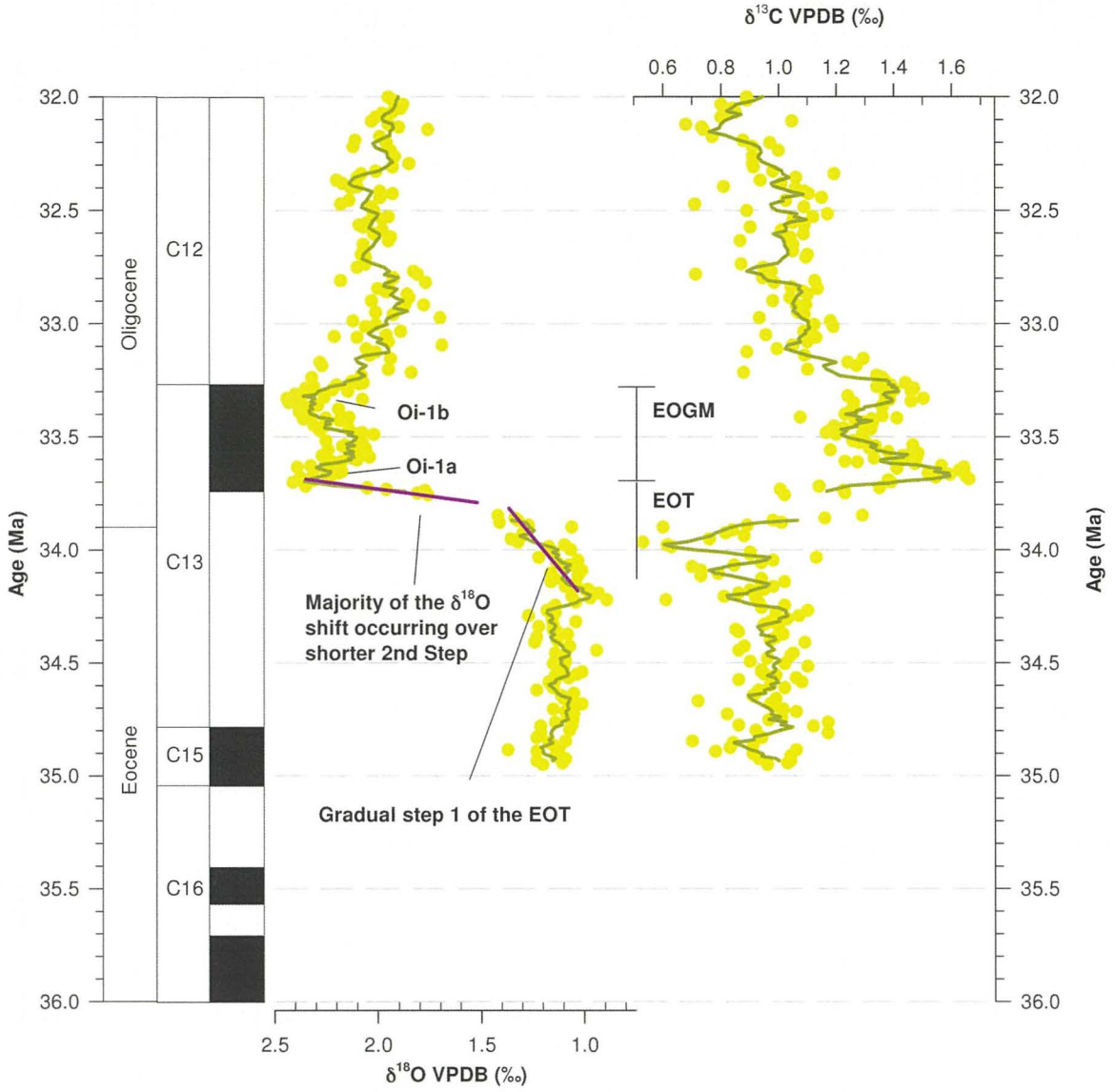

Figure 2.2: Benthonic foraminiferal stable-isotope plots for Site 744 in the Indian Ocean (Zachos et al., 1996; normalised to equilibrium using the offsets of Shackleton et al. (1984). $\delta^{18}O$ shows a gradual increase from the Late Eocene, accelerating at ~33.75 Ma reaching peak values (Oi-1) at ~33.65 Ma. Extreme $\delta^{18}O$ of the Eocene–Oligocene glacial maximum (EOGM) are maintained for ~400 kyr terminating prior to the end of C13r, post–EOGM Oligocene values are then ~1.0 ‰ greater than Eocene values. A transient two-step excursion is observed within the $\delta^{13}C$, with $\delta^{13}C$ values returning to approximate Eocene values on termination of the EOGM.

Lear et al., 2008) have identified a consistent magnitude and timing of the $\delta^{18}O$ shift over a global spread of locations (Table 2.1). These studies also record a similar evolution of the $\delta^{18}O$ record; from Eocene levels there is a ~1.5 ‰ positive shift in $\delta^{18}O$ known as the Eocene-Oligocene transition (EOT) followed by a ~400 kyr period of high $\delta^{18}O$ values, labelled the Eocene-Oligocene Glacial Maximum (EOGM; Coxall and Pearson, 2007).

During the EOGM two extreme periods of glaciation have been identified in records from Site 744 (Zachos et al., 1996), being labelled Oi-1a and Oi-1b following Miller et al.

(1991; Figure 2.2). Following the termination of the EOGM, $\delta^{18}O$ decreased and settled at a new equilibrium value ~1 ‰ higher than during the Eocene. Beyond the termination of the EOGM, the Oligocene was dominated by a pronounced orbital "heartbeat" (Diester-Haass and Zahn, 1996; Wade and Palike, 2004; Palike et al., 2006), with cycles within $\delta^{18}O$ and $\delta^{13}C$ records being present on both eccentricity and obliquity frequencies (in particular ~405, ~112 and ~96 kyr eccentricity cycles and ~1.2 Myr obliquity cycles).

Much of the EOT stable-isotope shift and the EOGM occurred within magnetic Chron C13n, constraining the duration of the EOGM to ~400 kyr (Zachos et al., 1996; Coxall et al., 2005). The EOT occurred over two steps, a gradual increase of less than half the total shift over ~300 kyr followed by a more rapid ~50 kyr increase to the EOGM, in records from the southern Atlantic and Southern (Indian) Oceans (Zachos et al. 1996; Figure 2.2). A similar pattern is also noted for Site 1263 in the subtropical south Atlantic by Riesselman et al. (2007). Records from Site 1218 also suggest two-step behaviour for the EOT, however, two roughly equal steps lasting 40 kyr are separated by 200 kyr plateau are observed (Coxall et al., 2005). The typical deep-sea positive $\delta^{18}O$ step has also been observed in hemipelagic records from both planktonic and benthonic foraminifera (Katz et al., 2008; Lear et al., 2008). However, differences do exist between both the hemipelagic records and the deep-sea records. Benthonic foraminiferal records from St Stephens Quarry, Alabama have been interpreted to have an extra stage of increase in the $\delta^{18}O$ record and a much less clear EOGM. Whilst the positive shift in Lear et al.'s (2008) planktonic foraminiferal $\delta^{18}O$ record is reduced compared to the deep-sea record, the significance of these differences is uncertain and requires further high-resolution hemipelagic and deep-sea records to resolve.

2.2.4 Cause of the $\delta^{18}O$ shift

As discussed in Section 2.2.1, foraminiferal $\delta^{18}O$ is controlled principally by temperature at which calcification occurs and the $\delta^{18}O_{sw}$. However, early studies attributed the entire positive shift in benthonic foraminiferal $\delta^{18}O$ as being a result of temperature change (Shackleton & Kennett, 1975; 1976; Kennett, 1977), suggesting only limited alpine glaciation on Antarctica. The assumption of a temperature, as opposed to $\delta^{18}O_{sw}$ increase, was a consequence of the absence of evidence for glaciation and that Eocene/Oligocene $\delta^{18}O_{sw}$ corresponded to that of an ice-free Earth, meaning benthonic foraminiferal $\delta^{18}O$

was insufficient to indicate the presence of continental ice. This assumption was challenged by both Matthews and Poore (1980) and Miller and Fairbanks (1983), whose earliest Oligocene $\delta^{18}O$ values would require bottom-water temperatures less than modern-day, a scenario incompatible with an ice-free world. The subsequent recognition of widespread glaciomarine sediments providing further evidence for continental ice development (Miller et al., 1991 and references therein). Miller et al. (1991) also dismiss suggestions that positive deep-ocean $\delta^{18}O$ values correspond to warm saline deep waters, as salt conservation constraints would result in surface water salinities below the tolerance of many marine organisms.

Subsequent work has attempted to isolate and quantify the ice volume component of the foraminiferal $\delta^{18}O$ change (Miller et al., 1987; 1991; 2008; Pekar et al., 2002; Lear et al., 2004; 2008; Coxall et al., 2005; Katz et al., 2008 among others). Miller et al. (1987; 1991) approached the problem of quantifying ice volume using strategies that had been applied to Pleistocene glacial records. Based on the assumption that $\delta^{18}O_{sw}$ change must be present in both low-latitude planktonic and benthonic foraminiferal $\delta^{18}O$ records, the magnitude of covariation in the two records can be attributed to the $\delta^{18}O_{sw}$ change. The covariation approach, however, requires surface-water records that display little annual variation in temperature, i.e. from western equatorial regions (Miller et al., 1991), which were not available. Using sub-tropical planktonic foraminiferal stable-isotope records, Miller et al. (1987) observed covariation showing $\delta^{18}O_{sw}$ increases of between 0.3 to 0.5 ‰, meaning the remainder resulted from bottom-water temperature decrease. The covariation values were then used to calibrate the increase in $\delta^{18}O_{sw}$ to sea level decline observed by using assumptions regarding the $\delta^{18}O$ content of Antarctic ice. The assumption was made that Early Oligocene ice sheets would have had $\delta^{18}O$ of ~-17 ‰, equivalent to the most positive snowfall on Antarctica today, rather than the average present day Antarctic ice (-50 ‰), leading Miller et al. (1987) to suggest a sea level–$\delta^{18}O$ calibration of 0.055 ‰ per 10 m change. Miller et al.s (1987) calibration being double that observed (0.11 ‰ per 10 m) for the LGM (Fairbanks and Matthews, 1978). However, the later Miller et al. (1991) study recognise a ~1.0 ‰ planktonic–benthonic covariation in $\delta^{18}O$ and suggest that the sea level–$\delta^{18}O$ calibration was closer to the LGM estimates. Pekar et al. (2002) considered the benthonic foraminiferal $\delta^{18}O$ through time from records obtained from high to low-latitude locations compared to apparent sea level variation, measuring a range of sea level–$\delta^{18}O$ relationships between 0.13 and 0.22 ‰ per 10 m. Greater changes in $\delta^{18}O_{sw}$ per 10 m sea

level fall were identified at low-latitudes than high latitudes, leading Pekar et al. (2002) to suggest greater cooling occurred across the EOB at low-latitudes. Using their high-latitude relationship, Pekar et al. (2002) suggest ~1.0 ‰ of benthonic foraminiferal $\delta^{18}O$ change resulted from ice-volume and the remaining $\delta^{18}O$ increase could be accounted for by a 1 °C cooling.

Whilst calibrating covariation of foraminiferal $\delta^{18}O$ or changes in benthonic foraminiferal $\delta^{18}O$ to apparent sea level allows estimation of the $\delta^{18}O_{sw}$, both methods lack a constraint on temperature changes. Use of Mg/Ca palaeothermometry (see Section 2.2.6) with $\delta^{18}O$ values should allow isolation of the $\delta^{18}O_{sw}$ component, and has been attempted for the EOB with contrasting results (Lear et al., 2000; 2004; 2008; Katz et al., 2008). Deep-sea records from the Southern Ocean and Equatorial Pacific (Sites 522 and 1218) have revealed $\delta^{18}O_{sw}$ increases of ~1.5 ‰ (Lear et al., 2000; 2004), whilst hemipelagic records indicate lesser changes of between 0.6 and 1.2 ‰ (Katz et al., 2008; Lear et al., 2008). Changes in $\delta^{18}O_{sw}$ can be converted to ice volumes, if the $\delta^{18}O$ of the ice sheet is known. Early studies (e.g. Miller et al., 1987) assumed that early ice sheets would be more positive than modern day, both as a result of size and warmer global temperatures. However, use of more positive, i.e. >-40 ‰, ice sheet $\delta^{18}O$ and estimated deep-sea $\delta^{18}O_{sw}$ change (~1.5 ‰) leads to estimations of ice-volumes greatly in excess of modern-day (by ~2.7 x assuming -25 ‰ ice $\delta^{18}O$) requiring significant northern hemisphere ice (Lear et al., 2004; Coxall et al., 2005). Evidence for such ice sheets has not been observed with sedimentological evidence being relatively restricted (e.g. Moran et al., 2006; Eldrett et al., 2007), thus ice volume constraints suggest Oligocene ice sheet $\delta^{18}O$ was similar to modern day (Pekar et al., 2002; Katz et al., 2008). Even with revised (modern) ice-sheet $\delta^{18}O$, deep-sea estimates of $\delta^{18}O_{sw}$ lead to EOB Antarctic ice volumes equivalent to that of the LGM (Lear et al., 2004; Katz et al., 2008), which has lead to questions as to the veracity of the deep-ocean benthonic Mg/Ca palaeotemperature records (see Section 2.2.7).

2.2.5 Late Eocene $\delta^{18}O$ variation

In considering the Eocene Oligocene transition, it seems remiss to not consider the build up to the transition during the Eocene. Considering the Late Eocene onwards (~41.3 Ma to 34 Ma), values start at ~1 ‰ gradually increasing to about ~1.6 ‰ over the next ~5 million

years before a very slight negative shift prior to the Eocene Oligocene transition (Figure 1.1; Kennett & Stott, 1990; Zachos et al., 2001). Historically much of this trend in Eocene $\delta^{18}O$ values has been attributed to temperature, specifically global cooling in the build up to the Eocene–Oligocene transition. Zachos et al. (2001) suggest a cooling of up to ~4 °C from the Middle Eocene to ~36 Ma. The period between ~36 Ma and the EOB has some fluctuation (~0.5 ‰) with postulated warming and cooling events (Vonhof et al., 2000; Zachos et al., 2003). The late Eocene has been referred to as a "doubthouse" climate, in that the presence or absence of continental ice has been uncertain during the period. Some sedimentary evidence has suggested that ice was at least transiently present (Zachos et al., 1999; Eldrett et al., 2007; Tripati et al., 2008) but isotopic evidence is less clear.

The long-term compilation of results shown in Figure 1.1 is useful in allowing an understanding of trends in global climate but suggests that change was rather gradual and monotonic. High-resolution studies of the Middle to Late Eocene demonstrate this not to be the case. Diester-Haass & Zahn (1996) record 100 – 400 kyr fluctuations in benthonic foraminiferal $\delta^{18}O$ superimposed on the larger scale changes in $\delta^{18}O$ from the Maud Rise, Southern Ocean (Site 689); the similarity of the timescales of stable-isotope fluctuations to the duration of orbital cycles suggesting an orbital control on climate. Another such feature is an abrupt ~1.0 per mille negative shift at ~41.5 Ma lasting less than 500 kyr. This event was shown to be Southern Ocean wide by Bohaty and Zachos (2003), whose benthonic and fine fraction $\delta^{18}O$ records reveal a 1.0 ‰ negative shift over about 600 kyr interrupting the general positive trend in $\delta^{18}O$ during the Middle Eocene. The ~1.0 ‰ decrease in $\delta^{18}O$ is interpreted as brief period of warming in both surface and bottom waters of ~4 °C.

The ice-free Eocene assumption has been questioned by Tripati et al. (2005) who identify a transient 1.5 ‰ shift in $\delta^{18}O$ synchronous with changes in the carbonate compensation depth of the equatorial Pacific at ~42.0 Ma, a $\delta^{18}O$ shift warranting both Northern and Southern Hemisphere ice. This interpretation has been questioned by Edgar et al. (2007), whose more complete Atlantic record suggests only half the isotopic variation, leading to a transient volume of ice easily sustainable by the Antarctic alone. The transient presence of continental scale ice sheets during the Middle Eocene also raises the question as to why the EOB glaciation was permanent, a question that will be discussed subsequently (See Section 2.4)

2.2.6 Mg/Ca–palaeotemperature calibrations

The use of foraminiferal Mg/Ca palaeothermometry has become widespread over the last decade (e.g. Nurnberg et al., 2000; Tripati et al., 2003; Dutton et al., 2005; Farmer et al., 2005; Bice et al., 2006), as a result of foraminiferal Mg/Ca ratios apparent independence from other oceanic parameters and thus allowing the development of paired foraminiferal $\delta^{18}O$ – Mg/Ca records to devolve the temperature and $\delta^{18}O_{sw}$ (e.g. Billups and Schrag, 2002; 2003). Carbonate Mg/Ca ratios were noted in early work as showing an apparent temperature control, subsequent studies have demonstrated similar exponential Mg/Ca–temperature relationship for planktonic foraminifera from a range of calibration methods such as planktonic foraminiferal culturing within known laboratory conditions (Nurnberg et al., 1996; Lea et al., 1999b), comparison of sediment trap samples with ambient ocean temperature (Anand et al., 2003), and comparison of core-top foraminifera to surface waters (Elderfield and Ganssen, 2000; Table 2.2). This exponential relationship has been quantified to give an equation of:

$$Mg/Ca_{foram}(mmol\ mol^{-1}) = B\ exp\ A * T \qquad \text{Equ. 6.2}$$

where Mg/Ca_{foram} is the Mg/Ca of the foraminifera, B is a pre-exponential constant, A an exponential constant and T is the water temperature, both A and B are species or calibration specific. A summary of the species pre-exponential and exponential constants calculated and related errors are shown in Table 2.2. Looking at the Mg/Ca–temperature equation, the A constant controls the temperature sensitivity typically leading to a foraminiferal Mg/Ca ratio sensitivity of ~10 % per °C. Whilst A is species specific (Table 2.2), the magnitude of the difference in relative temperatures resulting from values of A is similar to the errors within calibrations themselves (Elderfield and Ganssen, 2000), an error of ±0.7 °C due to variation in constant A compared to an error in single species calibrations of ±0.6 °C and ±1.1 °C in *Globigerina bulloides* culture data (Lea et al., 1999b). The similarity of extant foraminiferal Mg/Ca sensitivities supports the assumption of modern calibrations in deep-time studies using extinct foraminifera.

Culturing experiments allow investigations into the effects of other variables, such as seawater pH and salinity. Lea et al. (1999b) found that pH and salinity were both secondary in importance to temperature. Increasing salinity causes a 4 % increase

Location	Species	Calibration Method	Constants A	Constants B	Temperature Range	Cleaning	r^2	Study
Benthonic								
Little Bahamas Bank	*C. floridanus*	*Core-top*	0.085	1.36	4 to 18	Leaching		Rosenthal et al., 1997
	O. umbonatus		0.1	1.06				Lear et al., 2000
Global	*Cibicidoides* spp.	*Core-top*	0.109±0.007	0.867±0.049	0.8 to 18.4	Reductive	0.94	Lear et al., 2002
Global	*Uvigerina* spp.	*Core-top*	0.061	0.924	1.8 to 18.4	Reductive	0.69	Lear et al., 2002
Global	*O. umbonatus*	*Core-top*	0.114	1.008	0.9 to 9.9	Reductive	0.4	Lear et al., 2002
Global	*Melonis* spp.	*Core-top*	0.101	0.982	0.8 to 18.4	Reductive	0.84	Lear et al., 2002
Global	*Cibicidoides* spp.	*Core-top*	0.109±0.007	1.22±0.08	-1.1 to 18	Combination	0.95	Martin et al., 2002
Namibia	*O. umbonatus*	*Core-top*	0.09	1.528	2.9 to 10.4	None	0.93	Rathman et al.,2004
Namibia	*O. umbonatus*	*Core-top*	0.078	1.72	1.62 to 10.4	None	0.75	Rathmann & Kuhnert, 2008
Florida Straits	*C. pachyderma*	*Core-top*	0.042±0.005	1.55±0.12	5.8 to 17.6	Reductive	0.7	Marchitto et al., 2007
Florida Straits*	*C. pachyderma*	*Core-top*	0.116±0.014	1.2±0.18	5.8 to 17.6	Reductive	0.73	Marchitto et al., 2007
Planktonic								
Laboratory	*Orbulina universa*	Culture	0.085±0.011	1.36±0.24	17 to 27	Leaching	0.76	Lea et al., (1999)
Laboratory	*Globigerina bulloides*	Culture	0.102±0.008	0.53±0.17	16 to 25	Leaching	0.93	Lea et al., (1999)
North Atlantic	Multispecies	Core-top	0.1	0.52±0.0.0085	8 to 22	Oxidative		Elderfield and Ganssen, 2000
Tropical Pacific	*Globigerinoides ruber*	Core-top	0.089	0.3	~22 to ~30	Oxidative	0.95	Lea et al., (2000)
Sargasso Sea	Multispecies	Sediment trap	0.09±0.003	0.38±0.0.02	13 to 27	Oxidative	0.93	Anand et al., (2003)
North Atlantic	Multispecies (Deepwater)	Core-top	0.052±0.003	0.78±0.04	10.5 to 25.2	Oxidative	0.75	Cleroux et al., (2008)
Equatorial Atlantic	Multispecies (Warm >19 °C)	Core-top	0.101±0.003	0.29±0.08	19 to 28	Oxidative	0.9	Regenberg et al,. (2009)
Equatorial Atlantic	Multispecies (Cold <15 °C)	Core-top	0.083±0.005	0.84±0.06	8 to 15	Oxidative	0.85	Regenberg et al., (2009)

Table 2.2: Benthonic and planktonic foraminiferal Mg/Ca–water temperature calibrations. Constant A controls the temperature sensitivity and can be observed to be similar at about 0.1 or 10 % per °C for all foraminiferal calibrations. Elderfield and Ganssen (2000) suggest the error associated with choice of A is less than the error associated with a single species calibration. * is the linear calibration of Marchitto et al. (2007).

in Mg/Ca per salinity unit, while pH decreases Mg/Ca ratios by 6 % per 0.1 pH unit. Lea et al.s (1999b) study also looked at the effects of pH and salinity on Sr/Ca ratios, here the effect was close to the limits of measurement due to the analytical precision. With Lea et al.'s (1999b) additional controls on Mg/Ca by salinity and pH considered as potential error within the palaeothermometry equations, error increases to ±1.3 ˚C.

Benthonic foraminiferal Mg/Ca–temperature calibrations have been developed through depth transects and comparison to overlying bottom-water conditions (Rosenthal et al., 1997; Lear et al., 2002; Martin et al., 2002; Marchitto et al., 2007; Table 2.2). The calibrations of Lear et al. (2002) suggest that Mg/Ca has the potential to resolve bottom water temperatures to an accuracy of better than ±1 °C, although below 3 °C the natural variability of benthic foraminiferal Mg/Ca may act to obscure temperature changes (Lear et al., 2002; Rathmann and Kuhnert, 2008). The assumption of an exponential relationship between Mg/Ca and temperature for benthonic foraminifera has been questioned (Lear et al., 2002; Marchitto et al., 2007), with linear calibrations observed to fit the data in a statistically similar way. Marchitto et al. (2007) identify a linear calibration for the relationship of *Cibicidoides pachyderma* Mg/Ca–bottom water temperatures, however, this calibration appears to be species-specific and predicts unfeasibly high bottom-water temperatures (>40 °C) if applied to other species (Lear et al., 2008). The exact nature of individual benthonic foraminiferal species Mg/Ca–temperature relationships requires species-specific calibrations (Lear et al., 2002; Marchitto et al., 2007), but existing *Cibicidoides* spp. calibrations have been demonstrated to fit other benthonic species Mg/Ca–temperature relationships, e.g. *Melonis* spp, *Oridorsalis umbonatus* and *Planulina* spp. (Lear et al., 2002).

The exponential nature of the calibration means that at low temperatures (<3 °C) the magnitude of the temperature change that can be resolved becomes much less due to analytical accuracy constraints. The temperature change may also become obscured by other controls on Mg/Ca (Lear et al., 2002; Martin et al., 2002) such as dissolution or carbonate saturation. Study of benthonic foraminiferal Mg/Ca calibrations by Elderfield et

al. (2006) observed a departure from the expected exponential calibration for temperatures below ~3 °C. Similar departures from the expected exponential Mg/Ca–temperature calibration line were also seen by Martin et al. (2002) for deep Atlantic and Pacific Ocean ratios. Elderfield et al.'s (2006) plots of Mg/Ca against bottom water temperature show a well-defined inflection at ~3 °C for *Cibicidoides wuellerstorfi*, with the gradient of Mg/Ca change to temperature increasing by an order of magnitude below ~3 °C. The change in Mg/Ca–temperature relationship appears to be related to changing carbonate ion saturation ($\Delta[CO_3^{2-}]$), with the inflection point marking a change from a mainly temperature control (>3 °C) to a $\Delta[CO_3^{2-}]$ control. The precise temperature of inflection also shows a relationship with the $[CO_3^{2-}]$, with greater $[CO_3^{2-}]$ acting to depress the temperature of inflection. Interestingly the effect of $\Delta[CO_3^{2-}]$ variation appears to be less for infaunal benthonic foraminifera than for epifaunal species (Elderfield et al., 2006; Rathmann and Kuhnert, 2008), equilibration with respect to $[CO_3^{2-}]$ within the sediment pore waters hypothesised to reduce the influence of $\Delta[CO_3^{2-}]$ variation.

2.2.7 Eocene–Oligocene Mg/Ca palaeotemperature estimation

Calculation of palaeotemperatures from Cenozoic foraminiferal Mg/Ca ratios is more complex than simply inserting foraminiferal Mg/Ca into Equation 6.2 (Lear et al., 2000). Choice of palaeotemperature equation, preservation state of foraminiferal carbonate and sea water Mg/Ca ratios all have to be determined, whilst species-specific effects can influence multi-species records. Table 2.2 shows that for extant planktonic and benthonic foraminifera temperature sensitivities are similar, the absolute temperature estimated depending on the pre-exponential constant. The similarity of temperature sensitivity should mean that even if absolute temperature is questionable, relative variation is robust. Secondly, older sediments have a greater potential for chemical alteration or diagenesis, here "primary" signals may be overprinted or removed by dissolution or recrystallisation. Foraminiferal preservation can be assessed through careful examination of the foraminiferal test under a SEM microscope as well as consideration of the geochemistry of the whole dataset. Lear et al. (2004) eliminate foraminiferal data from Site 1218 older than 35 Ma due to an inverse correlation between Mg/Ca and Sr/Ca ratios as well as dolomite contamination leading to elevated foraminiferal Mg/Ca ratios in the deeper intervals of the core. Thirdly, to calculate absolute temperatures from foraminiferal Mg/Ca, seawater Mg/Ca ratios for the studied interval have to be determined. Over geological timescales both Mg and Ca are variable in the oceans with residence times of over 10 and 1 million

years respectively (Broecker & Peng, 1982). The oceanic budget of Mg and Ca is controlled by changes in supply by weathering and removal through carbonate production, hydrothermal circulation and dolomitisation (Wilkinson and Algeo, 1989). Modelling of geochemical processes has been used to estimate evolution of seawater Mg/Ca ratios throughout the Phanerozoic, however, very different evolutions of Cenozoic seawater Mg/Ca ratios have been predicted due to different initial assumptions (see Wilkinson and Algeo, 1989; Hardie, 1996; Stanley and Hardie, 1998; Berner et al., 2004; Figure 6.15**).** Across the Late Eocene to Early Oligocene, seawater Mg/Ca ratios between 2 and 5 mol/mol have been modelled (Figure 6.15), choice of seawater Mg/Ca having a profound influence on palaeotemperature estimation (Billups and Schrag, 2003; see also Figure 6.16), with lower seawater Mg/Ca ratios leading to increased temperature estimates. The poor constraint on Eocene–Oligocene seawater Mg/Ca means that absolute temperatures are uncertain, however, over time intervals less than the residence time of Ca, i.e. 1 Myrs, relative temperature changes should be robust (Lear et al., 2002), and are not dependant on the seawater Mg/Ca chosen.

Mg/Ca ratio palaeotemperature records developed for the EOB are limited, with only two deep-sea and one hemipelagic benthonic foraminiferal record and one hemipelagic planktonic foraminiferal record published (Lear et al., 2000; 2004; 2008; Katz et al., 2008). As discussed above, given the use of different Mg/Ca–temperature calibrations and sea-water Mg/Ca ratios, relative changes across the EOB are discussed. The two deep-sea records are from Sites 522 and 1218, in the southern Atlantic Ocean and Equatorial Pacific Ocean respectively. Benthonic foraminiferal Mg/Ca from Site 522 shows a 2 °C decrease across the first stage of the EOT and a 2 °C increase across the second (Lear et al., 2000), i.e. no overall temperature change over the EOT. The first stage of the EOT was absent at Site 1218 due to a dissolution event, but the second stage also shows a ~2 °C warming (Lear et al., 2004; Coxall et al., 2005). Site 522 records were interpreted as showing a deep-water cooling related to the initial cause of the glaciation of Antarctic, followed by a warming that resulted from a decline in the drawdown of atmospheric CO_2 as a result of glaciation (Lear et al., 2000).

The lack of temperature change or even an increase in EOB bottom-water temperatures was unexpected, as glaciation of Antarctica was expected to have resulted in deep-sea cooling (Zachos et al., 1996), and would suggest ice-growth was unrelated to high-latitude

temperature decrease (Lear et al., 2000). A further implication of the lack of deep-sea cooling is that the entire benthonic foraminiferal $\delta^{18}O$ shift resulted from ice-growth, leading to the requirement for EOGM ice equal in magnitude to the LGM (see Section 2.2.4; Lear et al., 2004; Coxall et al., 2005). However, the apparent absence of cooling and overall warming at Site 1218 lead to the hypothesis that a further control was acting on deep-water Mg/Ca ratios and masking the expected cooling (Lear et al., 2004; Katz et al., 2008). Site 1218 was located at a palaeodepth of ~3800 m across the EOB (Coxall et al., 2005), close to the Eocene CCD (~3500 m; Tripati et al., 2005). Coxall et al. (2008) record a >1 km deepening of carbonate compensation depth (CCD) at the EOB, which would have meant that there was a significant increase in $\Delta[CO_3^{2-}]$ at the palaeodepth of Site 1218. The increase in $\Delta[CO_3^{2-}]$ across the EOB hypothesised to lead to an increase in the uptake of Mg into the foraminiferal test, masking the decrease in deep-sea temperatures as per the observations of Martin et al. (2002) and more recently Elderfield et al. (2006). The carbonate ion saturation hypothesis, however, does not explain all features of the Sites 522 or 1218 records. A 1 km shift in CCD leads to an increase equivalent to ~2 °C (Martin et al., 2002; Lear et al., 2004), but the CCD deepening occurred equally across both stages of the EOT (Coxall et al., 2005), thus changing $\Delta[CO_3^{2-}]$ cannot entirely explain either the absence of cooling or overall warming. Equally, Site 522 did not experience the dramatic changes in $\Delta[CO_3^{2-}]$ observed at Site 1218, yet the ~2 °C increase was still observed. Further questions about the presence of the $\Delta[CO_3^{2-}]$ effect are raised by Rathmann and Kuhnert (2008), who do not observe a control on *O. umbonatus* Mg/Ca, the foraminifera species used by Lear et al. (2000; 2004) for Mg/Ca ratios, by either $\Delta[CO_3^{2-}]$ or $[CO_3^{2-}]$.

The hemipelagic records of Katz et al. (2008) and Lear et al. (2008) were developed to provide foraminiferal $\delta^{18}O$ and Mg/Ca records free of the hypothesised $\Delta[CO_3^{2-}]$ effect. Mg/Ca palaeotemperature records from benthonic foraminifera at St Stephens Quarry, Alabama (SSQ; Katz et al., 2008) and planktonic foraminifera from clay-rich sediments from Tanzania Drilling Project sites (TDP; Lear et al., 2008), both indicate cooling. The pattern of temperature decrease differs, however, with TDP sites showing a surface-water ~2 °C cooling across the entire transition, whereas SSQ shows two transient cooling intervals of ~2 °C related to the first stage of the EOT and the Oi-1 (identified from the foraminiferal $\delta^{18}O$); the two transient cooling intervals at SSQ being separated by an equivalent warming. As described in Section 2.2.4, $\delta^{18}O_{sw}$ increase estimates for these two sites were 0.6 ‰ for TDP sediments and 1.2 ‰ for SSQ, Katz et al. (2008) suggesting the

lower estimates from the TDP sites result from under sampling. Whilst both the TDP and SSQ sites were located in waters super-saturated with respect to [CO_3^{2-}] and thus free of $\Delta[CO_3^{2-}]$ effects, their hemipelagic rather than pelagic settings raises questions as to whether either site is truly representative of the global ocean changes. There are differences between SSQ and deep-sea $\delta^{18}O$ records (Figure 6.7), i.e. the much briefer Oi-1 event and absence of a clear EOGM, suggesting local factors may be influencing SSQ and that a robust record of global EOB $\delta^{18}O_{sw}$ change remains elusive. Thus, the evolution of bottom-water temperatures and ice-volume across the EOB are still ambiguously defined and require better constraints.

2.3 Eocene–Oligocene carbon-cycle variation

2.3.1 Foraminiferal $\delta^{13}C$

Foraminiferal $\delta^{13}C$ is obtained from the dissolved inorganic carbon (DIC) pool of sea water, uptake from this DIC pool is complicated by the nature of the oceanic carbon cycle. Within the oceans, DIC exists as a number of species in the ocean: $CO_{2\ (aqueous)}$, HCO_3^-, and CO_3^{2-} (Figure 2.3). At modern ocean pH values, the majority of the DIC exists as HCO_3^-, but can interchange with the other reservoirs through a series of equilibrium reactions.

$$H_2O + CO_2 \Leftrightarrow HCO_3^- + H^+ \text{ and } HCO_3^- \Leftrightarrow CO_3^{2-} + H^+$$

Foraminiferal calcium carbonate is formed through interaction with this inorganic carbon pool through the reaction $2HCO_3^- + Ca^{2+} \Leftrightarrow CaCO_3 + CO_2$. It is the nature of this reaction that controls whether foraminifera record DIC changes faithfully. The fractionation of ^{13}C between foraminiferal calcite and DIC is poorly understood, although, unlike foraminiferal $\delta^{18}O$, temperature is not a dominant control (Grossman, 1984; Romanek et al., 1992). Species-specific effects appear to control the relationship between foraminiferal and DIC $\delta^{13}C$ (Mulitza et al., 1999), in addition to the balance of carbonate species in the ocean (Romanek et al., 1992). Species-specific changes in the $\delta^{13}C$ record arise from a number of causal factors, such as presence of symbionts, "vital" effects, changes in environment during growth and changes in water chemistry. Studies have made use of culturing experiments to assess the scope of these factors to deviate $\delta^{13}C$ from the $\delta^{13}C_{DIC}$.

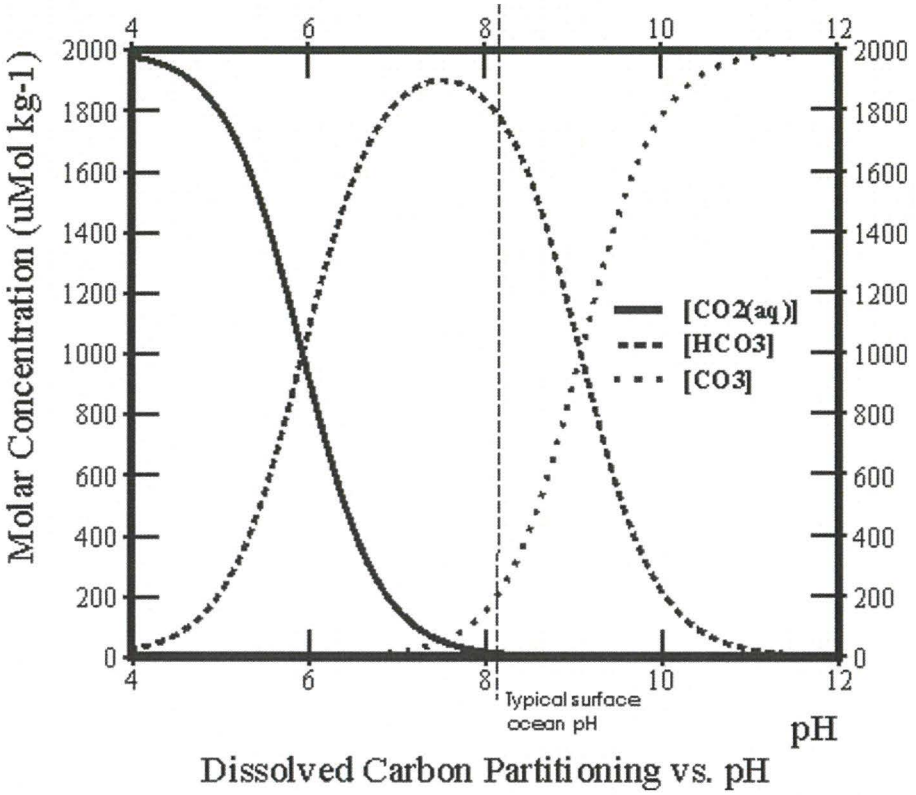

Figure 2.3: The predominant form of dissolved inorganic carbonate within the ocean depends on the pH of seawater. At typical seawater pH, the [HCO_3^-] ion is the dominant species and so is typically used in foraminiferal calcification. Shifts in seawater pH lead to a change in proportion of the carbonate ions and can lead to variation in foraminiferal stable-isotope chemistry. Figure courtesy of www.noc.soton.ac.uk/soes/staff/tt/eh/pics/bjerrum.jpg

Vital effects in foraminifera stem from the inclusion of metabolic CO_2 produced by respiration into the internal DIC pool from which the foraminifera calcifies (Vinot-Bertouille and Duplessy, 1972). Metabolic CO_2 is typically less ^{13}C enriched than $^{13}C_{DIC}$ values, thus as metabolic rates increase more light metabolic CO_2 enters the internal carbon pool. Metabolic CO_2 quickly hydrates (Spero & Lea, 1996) and thus becomes available for use in the calcification of the shell. A control on metabolic $\delta^{13}C$ by the $\delta^{13}C$ of food has also been suggested, however, Ortiz et al. (1996) and Spero and Lea (1996) both observed negligible changes in shell $\delta^{13}C$ for large changes in the $\delta^{13}C$ of the food. Ortiz et al. (1996) and Bemis et al. (2000) suggesting that temperature, through its influence on metabolic rates, controls the metabolic $\delta^{13}C$ and thus the degree of the vital effect.

Changes in the internal DIC reservoir are not solely controlled by foraminiferal respiration. Some species of planktonic foraminifera live with symbiotic algae. The presence of symbiotic algae has been demonstrated through culturing studies to move the $\delta^{13}C$ away from equilibrium fractionation values. Studies have shown that increasing irradiance leads

to progressive $\delta^{13}C$ enrichment (Spero & Williams, 1988; Spero, 1992; Spero & Lea, 1993 among others), this relationship disappearing if symbionts are removed (Berger & Wefer, 1991), suggesting that enrichment is linked to the increasing photosynthetic activity of the symbionts. For the two species studied during culturing experiments (*Orbulina universa* and *Globogerinoides sacculifer*), low light levels produced shell $\delta^{13}C$ values depleted relative to 1:1 fractionation while moderate and high irradiance both showed enrichments (Spero, 1992; Spero and Lea, 1993). This behaviour was attributed to the preferential use of "light" carbon in the waters surrounding the calcifying shell while symbionts were photosynthesising, leading to enrichment in the $\delta^{13}C$ values of the DIC pool being used for calcification. The low irradiance depletion suggests that foraminiferal metabolic carbon, i.e. $\delta^{13}C$ depleted carbon, is being used during calcification. In oceanic samples, the effect of irradiance will be complicated by changes in foraminiferal depth habitat or seasonality of calcification (Spero, 1992), e.g. flux of *O. universa* to the sediment depends on latitude with tropical to temperate zones having a year round flux while sub-polar sediments have a seasonal summer dominated flux.

Some species of planktonic foraminifera (e.g. *Globigerina bulloides* and *G.sacculifer*) have been observed to have increasing $\delta^{13}C$ with shell size (Oppo and Fairbanks, 1989; Spero and Lea, 1993). Culturing experiments by Spero & Lea (1993 & 1996) were designed to determine the reasons for the observed behaviours. While the two example species display the same behaviour, they are biologically different in that *G. bulloides* is not a symbiont bearing species while *G. sacculifer* is; this has implications on the possible causal mechanisms. Under constant irradiance, the symbiont baring *G. sacculifer* chambers does not show any relationship between $\delta^{13}C$ and size, indicating the observed increasing $\delta^{13}C$ results from greater symbiont activity increasing the internal carbon pool $\delta^{13}C$ (Spero and Lea, 1993). *G. bulloides*, however, shows clear ontogeny most likely related to incorporating reduced quantities of metabolic CO_2 with increasing shell size (Spero and Lea, 1996).

Some changes in $\delta^{13}C$ attributed to vital effects may actually be as a result of variation in the carbonate ion. As discussed in Section 2.2.1, Bijma et al. (1999) observe a covariance of $\delta^{13}C$ with $\delta^{18}O$ with increasing $[CO_3^{2-}]$, suggesting an underlying common factor controlling fractionation. The controlling factor is likely to be that of a pH dependant

balance between hydration and hydroxylation reactions. $\delta^{13}C$ though is likely to be further controlled by metabolic effects, greater quantities of respired CO_2 ($\delta^{13}C$ depleted) may be incorporated at higher pH while symbionts may act to scavenge "light" respired CO_2 causing further enrichment (Bijma et al., 1999). As such $[CO_3^{2-}]$ control is likely to be highly species specific, as the large differences in slope of $\delta^{13}C$ against $[CO_3^{2-}]$ observed by Bijma et al. (1999) for *O.universa* and *G.bulloides* suggest.

The $[CO_3^{2-}]$ control on $\delta^{13}C$ may have implications for palaeoclimatic interpretations concerning differences between glacial and interglacial carbon cycling. Foraminifera from glacial sediments have decreased $\delta^{13}C$ when compared to that of interglacial records; this decreasing $\delta^{13}C$ interpreted as the input of terrestrial carbon into the marine environment but this interpretation may need to be revised. Glacial atmospheric and thus, ocean CO_2 was approximately 200 p.p.m.v. as seen in ice core records (Barnola et al., 1987), this would cause $[CO_3^{2-}]$ to increase by at least 40 $\mu mol\ kg^{-1}$ (Spero et al., 1997). Spero et al.'s relationships between $[CO_3^{2-}]$ and $\delta^{13}C$ suggest an increase of this magnitude is sufficient to cause a drop similar in magnitude to the to 0.7 ‰ seen between glacial and interglacial foraminiferal $\delta^{13}C$. The importance of $[CO_3^{2-}]$ as a control of planktonic foraminiferal $\delta^{13}C$ is, however, questioned by low latitude records across the last glacial (Lea et al., 1999). Here $\delta^{13}C$ values do not show the expected $[CO_3^{2-}]$ control, the lowest vales of $\delta^{13}C$ occurring with glacial termination (i.e. when pCO_2 and $[CO_3^{2-}]$ values are returning to normal), while highest values are found in the early Holocene not in core tops. The lack of expected response would suggest that $[CO_3^{2-}]$ is not a principal control on shell $\delta^{13}C$. These uncertainties mean that further work on the effect of $[CO_3^{2-}]$ is required. As yet studies on benthonic foraminifera and whether they demonstrate $[CO_2^{2-}]$ akin to planktonic foraminifera have not been carried out, but these could have significant implications for interpretation of glacial/interglacial surface to deep-water records (Lea et al., 1999).

$\delta^{13}C$ variation between benthonic species is also common; Berger & Wefer (1991) plot data for several species of benthic foraminifera, and while the general pattern of variation is uniform throughout, the absolute $\delta^{13}C$ values differ by up to ~1 ‰. The $\delta^{13}C$ variation may be a result of changes in microhabitat as opposed to varying fractionation. Sedimentary $\delta^{13}C$ has been observed to be lowered by respiration of organic matter and may lead to pore-water $\delta^{13}C$ values 20 ‰ less than the bottom water immediately above

(Grossman, 1984b and references therein), explaining the observation of generally lower $\delta^{13}C$ values for infaunal species compared to epifaunal species from the same samples (McCorkle et al., 1995). Study of live benthic foraminifera (Grossman, 1989a) demonstrates that behaviour is not uniform for all species; some appear to be in equilibrium with the surrounding $\delta^{13}C$ while others vary in manners suggestive of strong vital effect control or microhabitat control. Vital effect control is believed to act as it does in planktonic foraminifera through the inclusion of metabolic CO_2 in the internal DIC reservoir.

Despite the many possible controls on $\delta^{13}C$ of foraminifera, foraminiferal $\delta^{13}C$ records from different locations and foraminifera have been observed to record similar variation over a given interval of time, e.g. records of the EOB from Sites 522, 744 and 1218 (Zachos et al., 1996; Coxall et al., 2005), thus the primary control on a single-species foraminiferal $\delta^{13}C$ appears to be the $\delta^{13}C$ of the ocean water. Controls on ocean water $\delta^{13}C$ are covered below.

2.3.2 Controls on ocean water $\delta^{13}C$

The controls on carbon isotopes in the ocean are intimately linked to the global carbon cycle and the behaviour of dissolved carbonate in the marine system. Changes in the partitioning between organic and inorganic carbon reservoirs and changes in sources and sinks can all affect the whole ocean $\delta^{13}C$. Within the ocean carbonate exists as four species, the proportions of which being determined by ocean pH (Figure 6.3). The species are CO_2, H_2CO_3, HCO_3^- and CO_3^{2-}, of these H_2CO_3 is found at low concentrations across the range of pH found in the oceans; the transition from CO_2 to HCO_3^- and CO_3^{2-} resulting in enrichment of $\delta^{13}C$ compared to the initial CO_2. These four species interact through the following reactions:

$$CO_2 + H_2O \leftrightarrow H_2CO_3,$$

$$H_2CO_3 \leftrightarrow H^+ + HCO_3^-$$

$$HCO_3^- \leftrightarrow H^+ + CO_3^{2-}$$

Photosynthesis discriminates against ^{13}C in favour of ^{12}C, meaning that an increase in the size of the terrestrial biosphere or burial of organic matter will enrich the dissolved

inorganic carbon (DIC) in the oceans with respect to $\delta^{13}C$. This ocean wide control on carbon isotopes is further controlled by local photosynthetic and respiratory changes. Photosynthetic action (i.e. plant growth) occurs within the surface waters, leading to enrichment in $\delta^{13}C$. The level of enrichment will depend on the level of export of organic matter into deeper waters and the amount of in-situ regeneration of organic matter. For example, if the same amount of organic matter is being regenerated within surface waters as is being used by photosynthesis, and then the surface water $\delta^{13}C$ will not change. However, if organic matter is exported then surface-water enrichment occurs. The level of export is related to volume and rate of photosynthesis in the surface waters, high productivity will lead to greater export and thus enhanced enrichment. The export of material from the surface waters has the opposite effect below the thermocline, where once in deeper waters respiration becomes the dominant process. The majority of organic material is regenerated as it travels through the water column through bacterial respiration, which leads to depletion of the deep ocean with respect to $\delta^{13}C$. This creates a typical cross sectional profile throughout the ocean of $\delta^{13}C$ enrichment at the surface and gradual depletion with depth.

The $\delta^{13}C$ of seawater is also affected by its "source" region, in the modern ocean deep waters form from surface waters at high latitudes, namely the North Atlantic and the Antarctic. These waters have different $\delta^{13}C_{DIC}$ signatures owing to their different origins. North Atlantic Deep Water (NADW) has $\delta^{13}C_{DIC}$ enrichment and low nutrients, reflecting its source region. This contrasts with Antarctic Bottom Water (AABW) that has high nutrients and low $\delta^{13}C_{DIC}$ as a result of ABW being a combination of surface waters and deep waters from all basins. NADW are thought of as young deep waters, ageing as both nutrients and $\delta^{13}C_{DIC}$ are exported into it from surface waters.

These processes all combine to create a complex series of inter-reactions controlling ocean $\delta^{13}C_{DIC}$, a system that can only be interpreted fully with a suite of proxies covering all aspects of the system. Such a suite of proxies is, in practice, virtually impossible to obtain especially from "deep time" periods, but careful use of the proxies that are available can still lead to palaeoceanographic insights.

2.3.3 Eocene–Oligocene carbon ($\delta^{13}C$) isotope records

The EOB $\delta^{13}C$ record consists of a ~0.5 ‰ negative excursion in the very late Eocene, followed by a ~1 ‰ transient positive excursion (trough to peak) occurring with the $\delta^{18}O$ increase, gradually recovering to pre-event levels ~1 Myrs following the initiation of the event (Figure 2.2; Diester-Haass & Zahn, 1996; Zachos et al., 1992; 1996; 2001; Coxall et al., 2005). High-resolution studies (Zachos et al., 1996; Coxall et al., 2005) show the $\delta^{13}C$ excursion has a similar two-stepped evolution as the $\delta^{18}O$ shift, occurring over a ~350 to ~400 kyr period. The $\delta^{13}C$ excursion lags the $\delta^{18}O$ event by between ~10 and 20 kyrs (Zachos et al, 1996; Coxall et al., 2005), suggesting $\delta^{13}C$ increase is a response to the development of ice rather than a cause. Throughout the Oligocene $\delta^{13}C$ has been found to oscillate on the 400 kyr eccentricity cycle, as well as show response to the longer 1.2 Myr obliquity cycle (Wade and Palike, 2004; Palike et al., 2006). Prior to the EOB, Eocene $\delta^{13}C$ shows no significant long-term change, values merely oscillate around an average value of ~0.75 ‰ from the Middle Eocene to the negative excursion prior to EOB (Figure 1.1; Zachos et al., 2001).

As described in Section 2.3.1, controls on oceanic and foraminiferal $\delta^{13}C$ are more complex to identify than those of foraminiferal $\delta^{18}O$, and as such several hypotheses and interpretations of the $\delta^{13}C$ record have been made. The $\delta^{13}C$ excursion has been seen to lag $\delta^{18}O$ by 10 – 20 kyrs (Zachos et al., 1996; Coxall et al., 2005), thus occurs as a result of the EOB rather than a cause, although the possibility of a carbon-cycle related feedback remains. Zachos et al. (1996) suggest that changes of a global nature such as the EOB must result from a change in global storage of carbon. Sustained increase in the proportion of organic carbon relative to inorganic carbon removed from the ocean has potential to cause a $\delta^{13}C$ excursion such as that observed across the EOB. Such a change in carbon burial could result from changes in the terrestrial biosphere or shifting primary production from carbonate to siliceous organisms (Zachos et al., 1996). The $\delta^{13}C$ excursion observed at the EOB, however, would require a sudden change in organic carbon production or burial. Such an increase in production and/or organic carbon burial could be increased vigour of atmospheric/oceanic circulation as a result of the cooling of high-latitudes and steepening of latitudinal temperature gradients (Diester-Haass, 1991; 1995; Zachos et al., 1996; Zachos and Kump, 2005). To test the export productivity hypotheses requires further

evidence concerning productivity and biogenic sedimentation across the EOB to be considered (Section 2.3.5).

2.3.5 Eocene–Oligocene productivity

Records of marine productivity have the potential to further the understanding as to the cause of the EOB $\delta^{13}C$ excursion, and as such significant amounts of work have gone into understanding changes across the boundary. Several methods have been used to quantify change depending on the sediments available, and the general findings of these approaches are described below.

Records documenting increases in benthonic foraminiferal accumulation rates (BFAR), opal accumulation as well as documenting other fossil increases across the EOB, have been produced across high to low-latitudes, e.g. Southern Ocean Sites 689 and 744 on the Maud Rise and Kerguelen Plateau respectively, mid-latitude Sites 592 and 763 on the Lord Howe Rise and Exmouth Plateau respectively and the equatorial Atlantic Site 925 on the Ceara Rise (Diester-Haass, 1995; Diester-Haass, 1996; Diester-Haass & Zahn, 1996; Salamy and Zachos, 1999; Diester-Haass and Zahn, 2001; Robert et al., 2002; Diester-Haass and Zachos, 2003). Although the magnitude of increase varies between sites, all show increase BFARs at the EOB reaching a maximum during the EOGM. Benthonic foraminiferal accumulation corresponding to export productivity, thus an increase in BFARs suggests an increase in export productivity. At Sites 689, 744 and 763, BFAR productivity highs are synchronous with bottom-water $\delta^{13}C$ decrease (Diester-Haass, 1996; Diester-Haass & Zahn, 1996; 2001), suggesting enhanced supply of $\delta^{13}C$ depleted organic material to deep waters from the surface (i.e. increased export productivity); at Site 744 the increase in BFARs is also observed to increase synchronously with the appearance of IRD across the EOB (Diester-Haass, 1996). Thus, there appears to be a close relationship between $\delta^{13}C$ increase, ice development and changes in productivity. Opal accumulation or % opal in the sediments is also observed to increase with foraminiferal $\delta^{18}O$ and the occurrence of IRD (Ehrman and Mackensen, 1992; Diester-Haass, 1996; Salamy and Zachos, 1999; Nilsen et al., 2003; Anderson and Delaney, 2005). However, several records of opal microfossil accumulation and BFARs from the Southern Ocean show increases equivalent to that observed at the EOB prior to the EOB (Diester-Haass, 1995; Diester-Haass and Zahn, 1996); these productivity increases are not observed away from the

Southern Ocean (Diester-Haass and Zahn, 2001; Diester-Haass and Zachos, 2003). Apparent increase in productivity prior to the EOB within the Southern Ocean has been suggested to correspond to the (partial) opening of the Drake Passage and development of proto-polar fronts (Diester-Haass and Zahn, 1996), although constraint on the timing of the opening of the Drake Passage is weak (see Barker et al., 2007 for review; also Section 2.4.1).

Alternative proxies, other than biogenic accumulation studies, have been applied to the EOB. Nilsen et al. (2003) developed export productivity records through biogenic Ba, nutrient burial through reactive phosphorus ($P_{reactiv}$) and biogenic silica records from the Ceara Rise (equatorial western Atlantic). Ratios of biogenic Ba/ $P_{reactive}$ (i.e. burial of total reactive phosphorus) are interpreted as a measure of the efficiency of the removal of organic matter from the ocean, important for the EOB where removal of organic carbon is a possible contributory factor for causing the $\delta^{13}C$ excursion. As with accumulation rate proxies, dissolution and diagenesis are possible complicating factors in the records developed, so no record can be interpreted without an assessment of its quality. Nilsen et al. (2003) using uranium and manganese enrichment factors as such an assessment criteria. In line with other studies (Diester-Haass, 1996; Salamy & Zachos, 1999; Diester-Haass & Zahn, 2001), biogenic silica productivity at the Ceara Rise is seen to increase across the EOB. However, the increase in biogenic silica does not appear to result in any increase in export productivity or nutrient burial at the site as indicated by barium and phosphorous records. An increase in siliceous microfossils without a concomitant increase in productivity, however, would contribute to the $\delta^{13}C$ excursion through the change in burial proportion of organic carbon to $CaCO_3$ (Salamy and Zachos, 1999).

Anderson and Delaney (2005) studied changes in export productivity and organic carbon burial at Site 1090 in the southern Atlantic Ocean. Multiple proxies, including $P_{reactive}$, biogenic Ba and opal mass accumulations, indicate increase in productivity at Site 1090 lead the EOB by as much as 1 Myrs. An earlier period of enhanced productivity occurred was also observed ~36.5 Ma. Whilst increase at the EOB is less pronounced at Site 1090, the pattern of enhanced productivity during the Late Eocene is similar to that observed at Southern Ocean sites (Diester-Haass, 1995; Diester-Haass and Zahn, 1996). Anderson and Delaney suggest that the increase in opal sedimentation observed prior to the EOB across a

wide latitudinal range may have lead to the decline in pCO_2 modelled to be the fundamental cause of EOB ice sheet development (DeConto and Pollard, 2003; See Section 2.4.2). The presence of organic rich sediments from the West African margin, dated by Os-isotopes as being Late Eocene age, adds further credence to Anderson and Delaney's hypothesis (Ravizza and Paquay, 2008).

Much of the productivity evidence indicates broad agreement with the hypothesis of Zachos et al. (1996) and Salamy and Zachos (1999), that glaciation lead to an increase in productivity through an increase in the intensity of atmospheric and oceanic circulation, particularly around the Antarctic. Increased opal microfossils suggest increased upwelling during the EOGM, especially within the Southern Ocean (Diester-Haass, 1995; 1996; Salamy and Zachos, 1999). Modern day seasonal upwelling zones are more effective at exporting organic carbon to the sediment than regions of constant production so an intensification of upwelling may have lead to a temporary increase in organic carbon burial increasing ocean $\delta^{13}C$. Evidence for increased seasonality at high latitudes has been described by Thomas & Gooday (1996) for the EOB from benthonic foraminiferal assemblage data, facilitating the burial of organic matter and thus removing $\delta^{12}C$. Equally, evidence for increased opal microfossil sedimentation prior to and at the EOB (Diester-Haass, 1995; Diester-Haass and Zahn, 1996; Anderson and Delaney, 2005), with or without increases in overall productivity (Nilsen et al., 2003), could shift the balance of organic carbon to $CaCO_3$ burial, away from $CaCO_3$ burial leading to both the $\delta^{13}C$ excursion and lowering of atmospheric pCO_2 (Zachos et al., 1996; Salamy and Zachos, 1999; Anderson and Delaney, 2005). The causes of the EOB are examined further in Section 2.4.

2.3.6 Carbonate sedimentation and the CCD

A feature of carbon-cycle change observed from oceanographic records across the EOB was variation in carbonate sedimentation and the CCD. Within the ocean, carbonate sedimentation is essentially controlled by the balance between the rain rate from surface waters and the increasing solubility of $CaCO_3$ with increasing depth (pressure) and decreasing temperature. The increasing solubility with depth leads to a carbonate compensation depth (CCD) where the rain rate is equal to the rate of dissolution and percent calcium carbonate in the sediment is zero. The zone of increasing undersaturation

above the CCD is called the lysocline, where carbonate preservation declines from ~90 % to a few percent over a few hundred metres (Broecker & Peng, 1982).

The CCD has been observed from DSDP and ODP records to deepen over the EOB in the Atlantic, Indian and Pacific Oceans (Figure 2.4; Van Andel, 1975; Hsü et al., 1984; Moore et al., 1984; Peterson and Backman, 1990; Rea et al., 1995; Coxall et al., 2005; Rea and Lyle, 2005; Tripati et al., 2005; Kroon et al., 2007). Rea & Lyle (2005) recognise a 1200 m deepening at the EOB, while noting other studies indicate a deepening of ~1 km in the Atlantic Ocean and ~700 m in the Indian Ocean from the Eocene to Oligocene (van Andel, 1975; Moore et al., 1984; Peterson and Backman, 1990; Tripati et al., 2005; Kroon et al., 2007), indicating that there was a significant change in global carbonate sedimentation across the EOB.

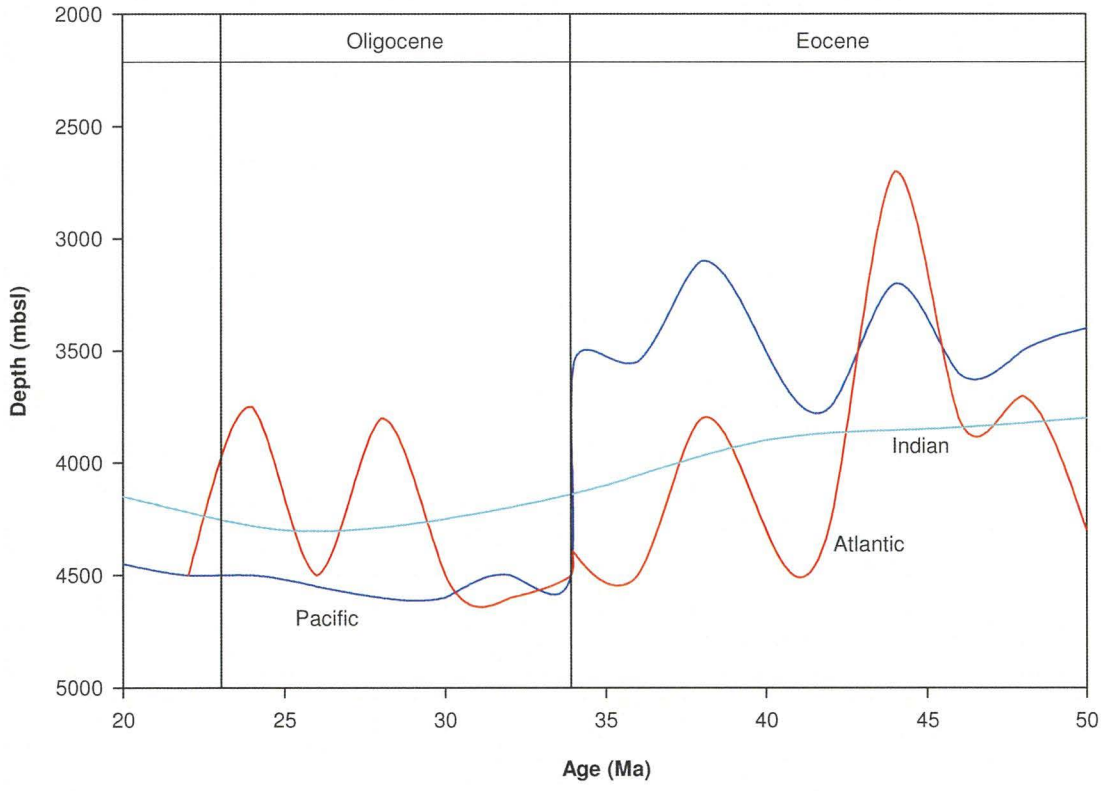

Figure 2.4: CCD variation during the Eocene and Oligocene for the Indian Ocean (Van Andel, 1975), tropical Atlantic Ocean and equatorial Pacific Ocean (Coxall et al., 2005; Tripati et al., 2005).

Coxall et al.s (2005) high resolution study of % $CaCO_3$ and $CaCO_3$ mass accumulation rates from Site 1218, identifies the deepening of CCD as occurring in two steps of ~40 kyr separated by a ~200 kyr plateau. The deepening of CCD occurs synchronously ("lockstep") with the $\delta^{18}O$ isotope change in the equatorial Pacific at Site 1218, whilst the

$\delta^{13}C$ lags by <10 kyr (Coxall et al., 2005). The synchronicity of CCD deepening and increase in $\delta^{18}O$, i.e. development of continental ice, indicates the two events are closely linked. The CCD deepening, however, is unlikely to have caused the growth of continental ice at the EOB, as assuming Pleistocene-like conditions the ~1 km deepening would only lower atmospheric pCO_2 by ~20 p.p.m.v. (Zeebe and Westbroek, 2003). Thus CCD deepening is likely to have occurred as a result of the continental glaciation (Coxall et al., 2005; Merico et al., 2008). Several hypotheses have been suggested to account for the CCD deepening; i) changes in seasonality and an increase in the proportion of siliceous to calcareous primary producers responsible for surface-ocean productivity (as described in Section 2.3.4); ii) changes in the inputs of Ca^{2+} and $[CO_3^{2-}]$ into the oceans as result of increased glacial weathering; and iii) shifts in the location of carbonate burial as a result of sea-level fall (Zachos et al., 1996; Salamy and Zachos, 1999; Ravizza and Peucker-Ehrenbrink, 2003; Coxall et al., 2005; Zachos and Kump, 2005). Merico et al. (2008) used a biogeochemical box model to test the above hypotheses; their results indicate that only a shift in the locus of carbonate burial from the continental shelf to the deep-ocean is able to replicate the form of both the $\delta^{13}C$ and CCD variation observed, although the study did not consider the magnitude of the effects. However, Rea and Lyle (2005) observe that a CCD deepening of ~1 km would lead to a further 25 % of Earths surface area covered by carbonate sedimentation, whilst the sea-level decrease would expose continental shelf equivalent to ~4 % Earths surface area. These authors suggest the exposure of continental shelf would be insufficient to account for the area of deep-ocean covered, indicating there must be a further control from the input of Ca^{2+} ions from weathering. The observations of Rea and Lyle (2005) are seemingly incompatible with the modelling of Merico et al. (2008). Tripati et al. (2005) note that the equatorial Pacific CCD change was more extreme than other regions as a result of large changes in productivity/accumulation across the EOB (Moore et al., 2004), an observation clear from Figure 2.4 for the Atlantic, Indian and Pacific Oceans. Thus, the deepening used by Rea and Lyle (2005) was likely in excess of the average global change and thus would overestimate the new extent of carbonate sedimentation. It is clear that understanding of the causes of the CCD deepening at the EOB is relatively poor, and that further records from a global spread of locations are required to enable the magnitude, timing and cause of the CCD deepening to be constrained better.

2.3.7 EOB carbon dioxide levels

Atmospheric pCO_2 levels having been gradually drawndown during the early Cenozoic, by mountain uplift or a gradual decrease in tectonic outgassing (Raymo and Ruddiman, 1992; Berner, 2003), have been suggested as a primary cause for the climate shift at the EOB (DeConto and Pollard, 2003; DeConto et al., 2008; See Section 2.4.2). Several approaches have been used to estimate palaeo-pCO_2: planktonic foraminiferal boron isotopes, leaf stomatal density, carbon stable isotope values of di-unsaturated alkenones (Pearson and Palmer, 2000; Royer et al., 2001; Pagani et al., 2005). The geochemical proxy records of Pearson and Palmer (2000) and Pagani et al. (2005) suggest an erratic decline during the Palaeogene, from pCO_2 of ~2000ppm in the late Palaeocene to earliest Eocene, ranging between ~1000 to ~1500 ppm throughout the Middle to Late Eocene before declining during the Oligocene to values <500 ppm (Figure 2.5); the high pCO_2 determined for the Eocene contrasting strongly with fossil leaf stomatal indices of Royer et al. (2001) that suggest levels of between 300 to 400 ppm. Constraint on pCO_2 across the EOB, however, is limited to Late Eocene and Early Oligocene data points from Pagani et al. (2005) and entirely absent from Pearson and Palmer (2000) and Royer et al. (2001).

Recently, Pearson et al. (2008) produced the first EOB record of pCO_2 levels using boron isotopes measured from foraminifera recovered from TDP sediments. The $\delta^{11}B$ of foraminifera is positively correlated with pH, which is negatively correlated with $[CO_3^{2-}]$ (see Figure 2 in Pearson et al., 2008), allowing relative changes in pCO_2 to be determined, if the $\delta^{11}B$ of seawater ($\delta^{11}B_{sw}$) is known. Pearson et al. (2008) use the results of geochemical modelling to predict $\delta^{11}B_{sw}$, allowing estimation of pCO_2. Figure 2.5 shows the evolution of pCO_2 calculated using a middle estimate of $\delta^{11}B_{sw}$ (~38 ‰) over the EOT, with a decline observed over the first stage of the EOT from ~1000 to ~800 p.p.m.v. and a recovery to Eocene levels across the second stage. Estimates of pCO_2 using the middle $\delta^{11}B$ estimate are similar in absolute magnitude to those of Pagani et al. (2005), who used carbon-isotope values from alkenones produced by haptophyte algae. Section 6.4.2 considers the implications of the changes in atmospheric pCO_2 on development of continental glaciation at the EOB.

2.4 Causal mechanisms

Several hypotheses as to the cause of the EOB climate change have been suggested and discussed; the thermal isolation of Antarctica due to the opening of the Drake Passage and

Tasman Gateway allowing the development of an (proto) Antarctic circum-polar current (ACC; e.g., Kennett, 1977) or global cooling resulting from either the drawdown of the atmospheric pCO_2 by enhanced silicate weathering of newly exposed terrains, i.e. the Himalayas and Tibetan Plateau (Raymo and Ruddiman, 1992), or as a result of decreasing volcanic outgassing throughout the Palaeogene (Berner, 1993). These hypotheses are discussed in the following sections.

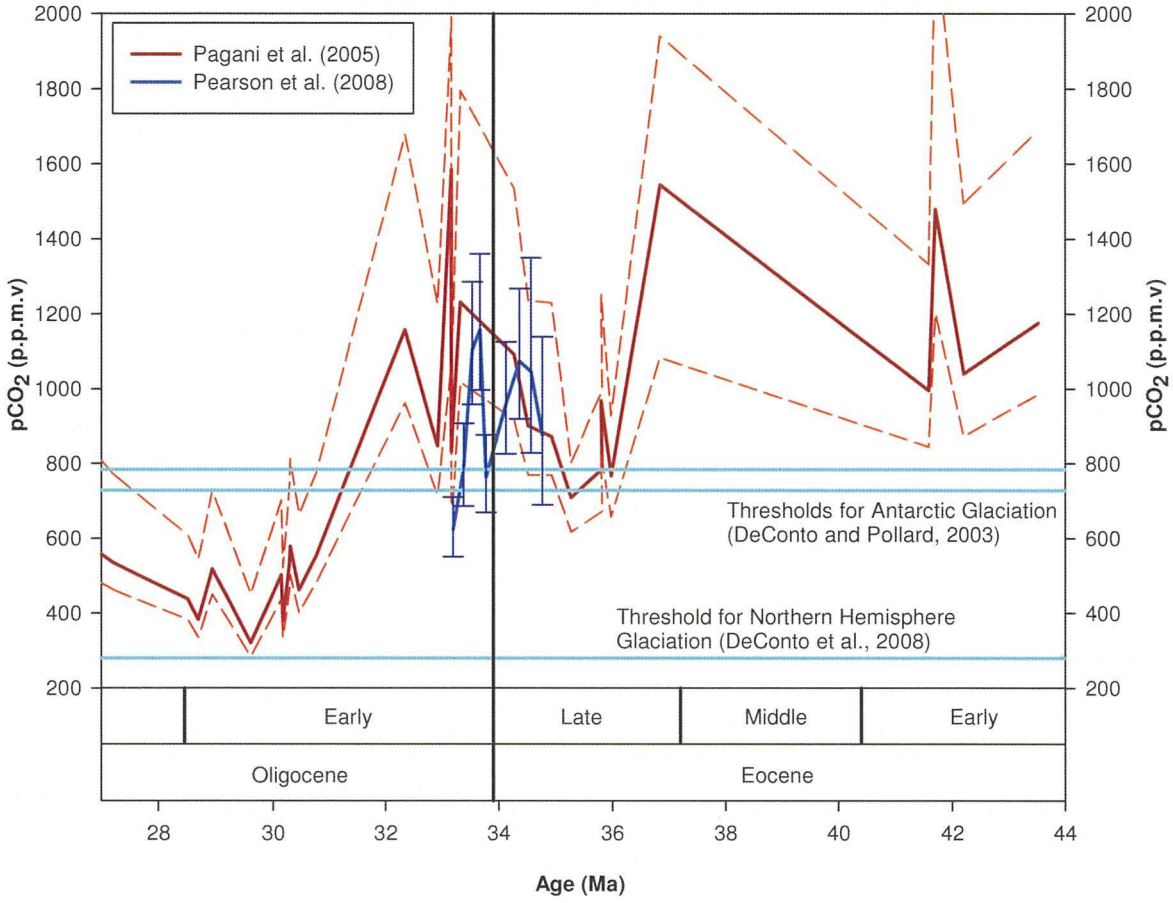

Figure 2.5: Evolution of atmospheric pCO_2 across the Eocene and Oligocene as determined by Pagani et al. (2005) and Pearson et al. (2009); the dashed lines indicating the maximum and minimum range of estimates depending on the assumptions made regarding either temperature (Pagani et al., 2005) or $\delta^{11}B_{sw}$ values (Pearson et al., 2009). The records suggest that pCO_2 declined erratically throughout the Eocene, approaching the threshold for Antarctic glaciation during the Late Eocene. Thresholds for Antarctic and Northern Hemisphere glaciation are those determined in ice-sheet modelling studies by DeConto and Pollard (2003) and DeConto et al. (2008). Atmospheric pCO_2 does not appear to have approached levels sufficiently low to allow Northern Hemispheric glaciation until ~30 Ma at the earliest, apparently ruling out the occurrence of bipolar EOB continental ice sheet development.

2.4.1 Development of the AAC

The thermal isolation of Antarctica by the ACC was first proposed by Kennett (1977) following early DSDP work in the Tasman Sea; development of the ACC reducing meridional heat transport causing cooling of Antarctica and thus ice sheet development.

Detailed description of the modern-day ACC and its associated fronts and zones is beyond the scope of this review, but suffice to say that for the development of the wind driven ACC, an open seaway around the circumference of Antarctica is required. Two likely final barriers to this open seaway have been identified in the Tasman Gateway and the Drake Passage (Barker et al., 2007, and references therein). Tectonic evidence indicates that subsidence at sites in the area of the Tasman Gateway initiated at ~35.5 Ma, lasting ~5 million years, with a deep-water (>2000 m) opening present at the Tasman Gateway by 32 Ma (Lawver and Gahagan, 2003).

Evidence for the opening of the Drake Passage, however, is less certain with estimates ranging from the Middle Eocene (~40 Ma) to the Miocene (~17 Ma; Barker et al., 2007). The lack of certainty stems from the complex nature of the opening of the Drake Passage; the result of the splitting of an active subduction zone, rather than the simple continental rifting, leading to the development of multiple passage ways (Lyle et al., 2008). A change in motion of the South American plate with respect to the Antarctic plate occurred at ~50 Ma, together with an acceleration of separation rate, is likely to have allowed a shallow <1000 m seaway between the Atlantic and Pacific during the Middle Eocene (Livermore et al., 2005). A shallow water connection during the Middle Eocene is supported by a decrease in Nd isotope ratios on the Atlantic side of the Drake Passage ~41 Ma, interpreted to be as a result of the input of radiogenic Pacific seawater in to the Atlantic (Scher and Martin, 2006). Further increases in Nd isotope ratios at ~37 and ~34 Ma were interpreted as resulting from the progressive opening of Drake Passage and strengthening of the ACC (Scher and Martin, 2004; 2006). Lawver and Gahagan (2003) reconstruct plate locations suggesting that an open deep-water Drake Passage is required by 30 Ma, most likely opening earlier at ~31±2 Ma.

Increase in Nd isotopes at ~37 Ma occurs at the same time as an increased amplitude in benthonic foraminiferal $\delta^{18}O$ and $\delta^{13}C$ variations at the same site, ODP Site 689 (palaeodepth ~1500 m) on the Maud Rise. Diester-Haass and Zahn (1996) interpreted the change in pattern of stable-isotope ratios as evidence for a change in ocean circulation, which they attribute to the development of the ACC and, thus the opening of the Drake Passage. Increases in palaeoproductivity, opal and benthonic foraminiferal accumulation rates also occur between 37 and 36 Ma (Diester-Haass, 1995; Diester-Haass and Zahn, 1996), which could result from an increase in vigour of ocean circulation resulting from

the development of a proto-ACC. Elsewhere, Latimer and Fillipelli (2001) observed a distinct change in proxies for terrigenous inputs and export productivity at ODP Site 1090 (water depth ~3700 m) on the Agulhas Ridge at 32.8 Ma, a change they attribute to the opening of the Drake Passage and onset of ACC. The difference between these to predictions may lie in the widely differing depths of the Maud Rise (~1500 m) and the Agulhas Ridge (~3700 m), a progressive opening and deepening suggested by onset of the ACC first at shallow sites and then at deeper levels. The identification of onset of ACC at 32.8 Ma by Latimer and Fillipelli (2001) is of similar age to the final deepening of the Tasman Gateway (Barker et al., 2007). The proximity of these ages may suggest that it was the opening of the Tasman Gateway as opposed to the Drake Passage that lead to a deeper ACC, although commencement of the ACC at ~32.8 Ma would suggest the ACC was not a causal factor for the EOB. Evidence from other sites, i.e. the Kerguelen Plateau and continental shelf sediments from New Zealand, suggests that current speeds, as determined by sediment size, sedimentation and unconformities, increase in the late Oligocene, close to the Oligocene–Miocene boundary (Lyle et al., 2008 and references therein). Barker et al. (2007) tabulate the estimates of ACC onset that range from the Middle Eocene to the latest Miocene, noting that the observations used to indicate the onset of ACC may be influenced by other factors, especially biogenic proxies such as opal or benthonic foraminiferal accumulation. The available data suggests that an ACC equivalent to that of modern-day is not likely to have developed until much later than the EOB, but that a shallow ("proto" ACC) may have developed as early as ~41 Ma.

Assuming that the Drake Passage was open in the Middle Eocene and a proto-ACC developed shortly afterwards, could this have lead to cooling that triggered the EOB; to assess this it is necessary to use general circulation models (GCMs) to provide simplified approximations. Toggweiler and Bjornsson (2000) model the effect of the opening of Drake Passage and the onset of a circum-polar current on climate using a coupled atmosphere-ocean GCM. Their results suggest that the presence of the ACC leads to a temperature drop of ~3 °C around Antarctica as a result of ocean-atmospheric circulation transporting heat from the southern hemisphere to the northern hemisphere. Toggweiler and Bjornssons (2000) results also suggest that the depth of the Drake Passage has only limited effect on the magnitude of the cooling seen. This latter finding would suggest that circumpolar circulation and thus cooling would occur relatively rapidly once the passage was open. Toggweiler and Bjornssons (2000) findings are at odds with those of other modelling studies (DeConto and Pollard, 2003; Huber and Nof, 2006), Huber and Nof

(2006) analyse the results of modelling studies to consider the effects of heat transfer on climate. Their findings suggest that ocean heat transfer would have to have been three time present levels to account for the changes at the EOB; a suggestion Huber and Nof (2006) dismiss as implausible due to the lack of supporting modelled scenarios for such an increase. The requirement and improbability of such a large change in heat transfer related to the onset of the ACC, suggests the opening of the oceanic gateways and thermal isolation of Antarctic is not a primary cause of the EOB. This suggestion reiterates the results of DeConto and Pollard (2003), whose coupled GCM-ice sheet model indicates that the effect of an open Drake Passage is only important within a restricted atmospheric pCO_2 range (~2.5–~3 x present atmospheric pCO_2). Within this range, the closure of the Drake Passage and hence absence of ACC delays glacial inception, as pCO_2 has to decrease further to account for the increased heat transport southwards.

The modelling of Eocene oceans has typically indicated that the basic structure of Eocene oceans is similar to that of modern-day (Lyle et al., 2008; and references therein), i.e. similar distribution and scale of oceanic gyres and upwelling zones, despite the very different climate and differences in continental organisation. Hay et al. (2005), however, challenge the occurrence of modern-day style ocean circulation present in the climate models such as those of Huber and Nof, (2006). Hay et al. (2005) suggest that in the absence of ice cover at the poles, seasonal alternation of low and high pressure could occur at the poles. The seasonal alteration of high and low pressure would prevent the development of the frontal systems, leading to a less well defined thermocline and a pycnocline dominated by salinity differences. The combination of these effects, Hay et al (2005) suggest would lead to ocean circulation dominated by eddies and small-scale gyres which, due to the less well defined thermocline, would promote ocean mixing and increase poleward heat transport in the absence of polar fronts. Hay et al. (2005) use their theory to suggest that the ubiquitous benthonic foraminiferal $\delta^{18}O$ positive step results, not from ice development, but from the cooling of the deep-ocean to form the pyschrosphere, much like early interpretations of the EOB (Kennet and Shackleton, 1976).

The hypothesis of Hay et al. (2005) regarding the EOB benthonic foraminiferal $\delta^{18}O$ shift is counter to current thinking, and based on uncertain assumptions with regards to sea level change at the EOB. A different mode of Eocene circulation and subsequent change at the

EOB would rehabilitate the opening of the Drake Passage and onset of the ACC as a primary cause of the EOB, but would require both evidence and assessment through modelling to test the ideas proposed. Equally, until there is an accurate constraint on the timing of the opening of the Drake Passage and the resulting onset of ACC, its role in the Late Eocene to Early Oligocene climate will remain controversial. Despite the indications of climate models, with their inherent assumptions concerning climate forcing, the occurrence of such a significant change in ocean circulation, coincidental with a major change in climate, remains a credible hypothesis.

2.4.2 Atmospheric pCO_2

Global cooling as a result of declining pCO_2 is the current favoured hypothesis to explain the dramatic climate shift seen in EOB records and across the Palaeogene in general (Coxall and Pearson, 2007). DeConto and Pollard (2003) and DeConto et al. (2008) model the development of both Antarctic and Northern Hemispheric ice sheets in response to declining pCO_2 and orbital forcing. Antarctic ice development commences with restricted high altitude ice caps once atmospheric pCO_2 declines below 6x pre-industrial levels (~1800 p.p.m.v.), and with declining pCO_2 and changing orbital parameters these small ice caps coalesce and separate. At a critical threshold of 2.6 to 2.8x pre industrial levels (~750 to ~800 p.p.m.v), a single ice sheet is formed within a few hundred thousand years, which is insensitive to further orbital forcing. The DeConto and Pollard (2003) model indicates that a sudden and extreme climatic transition occurs even with low rates of forcing, i.e. pCO_2 declining at a low rate. Coxall et al. (2005) note that the modelled increase in ice sheet size of DeConto and Pollard (2003) are similar to their own $\delta^{18}O$ records, although the modelled $\delta^{18}O$ shift is a third of the magnitude as the Site 1218 shift. DeConto et al. (2008) built upon the earlier DeConto and Pollard model using it to model ice sheet $\delta^{18}O$ development and thresholds for bipolar glaciation (as suggested by Coxall et al., 2005; Tripati et al., 2005). The model indicates that significant Northern Hemispheric ice does not develop until pCO_2 reaches pre-industrial levels, i.e. 280 p.p.m.v., thus if bipolar glaciation occurred pCO_2 had to decline rapidly during the EOT from ~800 to ~280 p.p.m.v.

Section 2.3.6 described the records of Eocene–Oligocene pCO_2 with both Pagani et al. (2005) and Pearson et al. (2009) indicating pCO_2 levels were close to the threshold for

Antarctic glaciation determined by DeConto and Pollard (2003; Figure 2.5). However, pCO_2 values were not observed to reach the levels required for Northern Hemisphere glaciation until the Miocene (Pagani et al., 2005), thus bipolar glaciation seems to have been unlikely. The ice-sheet $\delta^{18}O$ component of the DeConto et al. (2008) model suggests that Antarctic ice had a $\delta^{18}O$ of -35 to -30 ‰, lower than the -45 ‰ previously suggested (Lear et al., 2004; 2008; Katz et al., 2008). Together, the pCO_2 threshold for Northern Hemispheric glaciation and constraint on Antarctic ice $\delta^{18}O$ indicates that there must have been a deep-sea cooling component within the benthonic foraminiferal $\delta^{18}O$ and that the carbonate ion effect masked the cooling in the Mg/Ca records (Lear et al., 2004; 2008; Katz et al., 2008).

2.4.4 Orbital configuration

While it seems likely that a tectonic control (either through opening of ocean gateways or tectonic drawdown of pCO_2) was the driving force behind Cenozoic and EOB climate change, high-resolution benthonic foraminiferal stable-isotope records as well as modelling have suggested a close link between the EOB and variation in orbital parameters (DeConto and Pollard, 2003; Wade and Palike, 2004; Coxall et al., 2005). As previously described, the modelling of ice sheet development by DeConto and Pollard (2003) suggested a threshold for pCO_2 for ice sheet growth. DeConto and Pollards (2003) model then suggests that, prior to continental scale glaciation, ice sheet growth occurs during periods of minimum summer insolation increasing in size with subsequent eccentricity cycles until ice extends over the entire continent. Coxall et al. (2005) noted that initiation of the benthonic foraminiferal $\delta^{18}O$ step at the EOB corresponded to a node of minimal eccentricity, and low-amplitude obliquity that would favour cool summers, i.e. minimise snowmelt throughout the summer months allowing the build up of continental ice. Further evidence of an orbital component to Oligocene climate change comes from the exceptionally high-resolution (~6kys per sample) Oligocene benthonic foraminiferal stable isotope records of Wade and Palike (2004). Wade and Palike's records show cyclical variation on timescales of 40, ~110 and 405 kyr suggestive of an orbital control by obliquity (40 kyr) and eccentricity (~110 and 405 kyr) variations.

2.5 EOB synthesis

The weight of oceanographic evidence across the Eocene–Oligocene boundary indicates a rapid and permanent change in global climate. Glaciomarine sediments combined with the global increase in deep-sea $\delta^{18}O$ and decline in sea levels indicates the development of significant glaciation on a scale equivalent to, if not greater than, that of modern-day Antarctica. Increase in proxies for productivity and microfossil accumulation suggest an increase in vigour of oceanic circulation as a result of increased latitudinal temperature gradients. However, beyond these general observations, climate change across the EOB is still poorly understood. Key questions remain as to the extent of glaciation and the evolution of deep-waters, what mechanism lead to the CCD deepening as well as the underlying question of causal mechanism.

A clear, unambiguous record of deep-sea stable-isotope and element/Ca change would be beneficial for the understanding of the EOB. Ideally such a record would come from a site that can be observed to be free from any $\Delta[CO_3^{2-}]$ effect, i.e. above the lysocline throughout the Late Eocene to Early Oligocene. However, such a site may not be available so the development of a multiproxy record including benthonic foraminiferal element/Ca ratios such as Ba/Ca, Li/Ca, Zn/Ca and Cd/Ca that show relationships to bottom-water $[CO_3^{2-}]$ (McCorkle et al., 1995; Elderfield et al., 1996; Marchitto et al., 2002; Lear and Rosenthal, 2006), in addition to stable-isotope and Mg/Ca ratios would allow the greatest constraint on the influence and change in bottom-water chemistry. With such a record, constraint of bottom-water temperature and ice volume may be determined more robustly. Whilst hemipelagic records have been used to approach the ice-sheet magnitude problem (Katz et al., 2008; Lear et al., 2008), the discrepancy between the two records raises questions as to whether one or both sites has an unidentified local control.

Better constraint of the ice sheet magnitude and bottom water temperature change would also allow refinement of the climate/ice sheet models used to model the EOB change. DeConto and Pollard (2003) and DeConto et al. (2008) models currently under predict the $\delta^{18}O$ change observed in deep-water records, a fact they attribute to the $\Delta[CO_3^{2-}]$ effect; although the mismatch is also observed with $\delta^{18}O_{sw}$ records from the hemipelagic SSQ record (Katz et al., 2008). The causal mechanism of the EOB and the carbon cycle changes observed remains perhaps the biggest uncertainty; although a variety of modelling studies

have produced scenarios that approximate observed data (e.g. DeConto et al., 2003; Zachos and Kump, 2005; Merico et al., 2008). Declining pCO_2 levels do appear to provide the key threshold for the development of Antarctic ice at the EOB, but equally, until the timing of the opening of the Drake Passage and development of the ACC is identified unambiguously, the causal mechanism must remain uncertain.

Chapter 3 – Materials & Methods

3.0 Introduction

This chapter details the deep-sea core materials, collected by ODP Leg 198, that are investigated in this study. This chapter describes the location of the sediment cores, their collection, existing work completed prior to this study and the rationale behind sample selection. Beyond this, the methods used and, where applicable, the analytical precisions of those methods are described.

3.0.1 Terminology

Prior to discussion of the sediment core materials used, it is prudent to define ODP abbreviations and sample notation used within this study. Water depths are measured in metres below sea level (mbsl), while core depths are measured in metres below sea floor (mbsf), metres composite depth (mcd) or revised metres composite depth (rmcd). The latter two depth scales (mcd and rmcd) facilitate the compilation of a complete composite sedimentary record from sites, which have been cored several times in different holes. The multiple holes recovered from a single site typically have staggered starting depths, which means that the breaks between individual cores, that are inherent with any deep-sea coring technique, occur at different depths within each hole thereby allowing a complete stratigraphic section to be recovered. ODP sample notation describes samples as follows: Leg-Site-Hole-Core-Section and sample depth interval, e.g sample 198-1211C-9H-3, 55–57 cm would be from Leg 198, Site 1211, Hole C, Section 9, Core 3, sampling interval 55–57 cm. Site 1211 was recovered by use of advance piston coring, a technique used to recover soft sediments with minimal disturbance. Advanced piston coring has a maximum piston stroke of 9.5 m, these 9.5 m lengths are the cores described in the sample notation. Once recovered these are split into 7 sections, each up to 1.5 m in length. These sections are halved to produce an archive and a working half; the former is kept for reference purposes while the working half is used for subsequent research. Within individual cores the sediment record recovered is essentially the complete record of that drilled, but at the end of each core there is often some loss of sediment as a result of the coring operation. As previously described, Site 1211 was triple cored to enable derivation of a complete stratigraphic section that is recorded against a composite depth scale.

3.1 Materials

3.1.1 ODP Leg 198

ODP Leg 198 took place in the late summer of 2001, setting out to build on previous DSDP legs by recovering a more complete sedimentary record from the Shatsky Rise, northwest Pacific Ocean (Figure 1.4). ODP 198 and its aims were briefly touched upon in Chapter 1; most importantly, these objectives were to investigate transient climatic events that occurred during the Cretaceous and Cenozoic and to "*address questions concerning the nature of chemical (i.e. calcite compensation depth, nutrients, and oxygenation) and physical oceanographic changes (temperature gradients) during these events*" (Shipboard Scientific Party, 2002a). The addition of new palaeoclimatic and palaeoceanographic data from the Pacific Ocean, an ocean basin with few existing datasets for these critical time periods, will allow a more global dataset to be considered when modelling Earth's past climates.

3.1.2 Site 1211

Of the sites cored during ODP Leg 198, Site 1211 has been chosen for study. Site 1211 was selected, as it was from this site that the most complete late Eocene to Oligocene sedimentary record was recovered. Burial depths are also the shallowest of any of the carbonate-rich ODP 198 Leg sites, meaning that the possibility of burial diagenesis is minimized.

ODP Leg 198, Site 1211 was located at 32°0.13'N, 157°51.00'E and at a lower bathyal water depth of 2907m, on the southern flank of the Southern High of Shatsky Rise (Figure 1.5). Benthonic foraminiferal assemblages suggest an Eocene palaeodepth near to that of the present day (2000 to 3000m; Shipboard Scientific Party, 2002a,b). For the preservation of carbonate sediments a water depth above the CCD is necessary. Colour reflectance data position the Eocene CCD between the palaeowater depths of Sites 1208 and 1211, with the sporadic occurrence of calcareous microfossils at the former site suggesting the CCD was nearer Site 1208 (Shipboard Scientific Party, 2002a). Thus Site 1211 should have remained above the CCD throughout the Eocene–Oligocene stratigraphic range that is the focus of this study.

Site 1211 is located at the same position as DSDP Leg 32, Site 305. DSDP Site 305 was cored using a rotary core barrel and so the unlithified portion of the core was highly disturbed by coring, leading to low sediment recovery for much of the Cenozoic. As mentioned above, Site 1211 was triple cored using advanced piston coring so as to recover a complete, undisturbed record of the original DSDP sequence. The shipboard composite depth scale (Shipboard Scientific Party, 2002b) for Site 1211 was revised by Westerhold and Rohl (2006) and is based on the correlation of magnetic susceptibility records between the three holes drilled, i.e. 1211A, 1211B and 1211C. The resulting composite stratigraphic section reaches the lowermost Maastrichtian at a depth of over 160 rmcd (Westerhold and Rohl, 2006).

The sediments recovered at Site 1211 were sub-divided into three lithologic units based on sediment composition. Briefly, these units, as described by the Shipboard Scientific Party (2002b), are as follows:

Unit 1 – alternating nannofossil clays and oozes of Holocene to early Miocene age (0 to 58.26 rmcd in Hole C)

Unit 2 – homogenous nannofossil ooze of late Oligocene to early Paleocene age, averaging ~94% carbonate with varying amounts of clay (58.26 to 147.06 rmcd in Hole C). An unconformity separates Miocene clay from the upper Oligocene nannofossil ooze.

Unit 3 – nannofossil ooze of late to early Maastrichtian age, averaging ~95% carbonate with some centimetre-scale clayey intervals (147.06 to 152.68 rmcd in Hole C). Unit 3 is differentiated from unit 2 by a higher abundance of foraminifera (15%).

As this study is concerned with the Eocene to Oligocene transition, lithologic Unit 2 is of primary interest. Shipboard Scientific Party (2002b) suggested that sedimentation of Unit 2 was influenced by fluctuations in the lysocline, since smear slide estimates and coulometric analyses indicated that $CaCO_3$ content varied, dropping as low as 50 %. Prior to the EOB, records of colour reflectance and magnetic susceptibility display low amplitude cyclicity, suggesting a possible orbital control on the lysocline through variation in productivity and/or deepwater mass carbonate saturation (Shipboard Scientific Party, 2002b). Shipboard Scientific Party (2002a) identified the depth of the late Eocene CCD as being between Sites 1208 and 1211, thus Site 1211 was within a few hundred metres of the

CCD during that time period. Such a close proximity to the CCD would mean that relatively small CCD position fluctuations could have affected sedimentation at Site 1211 greatly.

The presence of the Eocene–Oligocene boundary (EOB) within cores from Site 1211 was indicated by biostratigraphic study of calcareous nannofossil and planktonic foraminifera (Shipboard Scientific Party, 2002b). In brief, the disappearance of EOB marker species, the planktonic foraminifera *Hantkenina* spp., was identified initially in core sections 1211A-9H-5 and 1211C-9H-4 and the last occurrence (LO) of calcareous nannofossil *Discoaster barbadiensis* was identified in samples 1211A-10H-1-140 cm and 1211B-9H-7-45 cm, thus demonstrating recovery of the EOB (Shipboard Scientific Party, 2002b). Further to these observations Shipboard Scientific Party (2002b) did not identify any major hiatus within the Site 1211 sedimentary record immediately prior to the EOB, suggesting a complete record of this key climatic transition was recovered.

The original depth–age control for Site 1211 used the biostratigraphic datums of Shipboard Scientific Party (2002b; Figure 3.1). Their predicted sedimentation rates indicated that sedimentation was uniform from the middle to late Eocene (~40 Ma to 33.9 Ma) at ~1.5 metres per million years (m/Mys), increasing at the EOB to a rate of ~3.5 m/Myrs throughout the Oligocene (Shipboard Scientific Party, 2002b). This depth–age model is, however, poorly constrained by the relative paucity of biostratigraphic depth–age control points, inconsistencies between planktonic foraminifera and calcareous nannofossil datums and the absence of a palaeomagnetic record for Site 1211 (Shipboard Scientific Party, 2002b; see Chapter 4 for further discussion). Thus, in the absence of a robust depth–age model, further work has been carried out to improve constraint of the depth–age relationships at Site 1211, using more recent higher stratigraphic resolution biostratigraphies (Bralower, 2005; Petrizzo et al., 2005) and Sr-isotope ratio derived numerical ages developed as part of this study, which are detailed in Chapter 4.

3.2 Sample selection

As described in Chapter 2, the EOB was a dramatic shift in global climate state. The transition from Eocene greenhouse climate state to extreme Oligocene glaciation and

subsequent shift to a new "steady-state" in the Oligocene occurred over ~1 Myrs (Zachos, et al., 1996). It is necessary to put this change in the context of the palaeoceanographic conditions prior to and subsequent to the EOB transition, so sampling was undertaken to allow the production of the most complete and accurate geochemical proxy records of palaeoceanographic change at Site 1211.

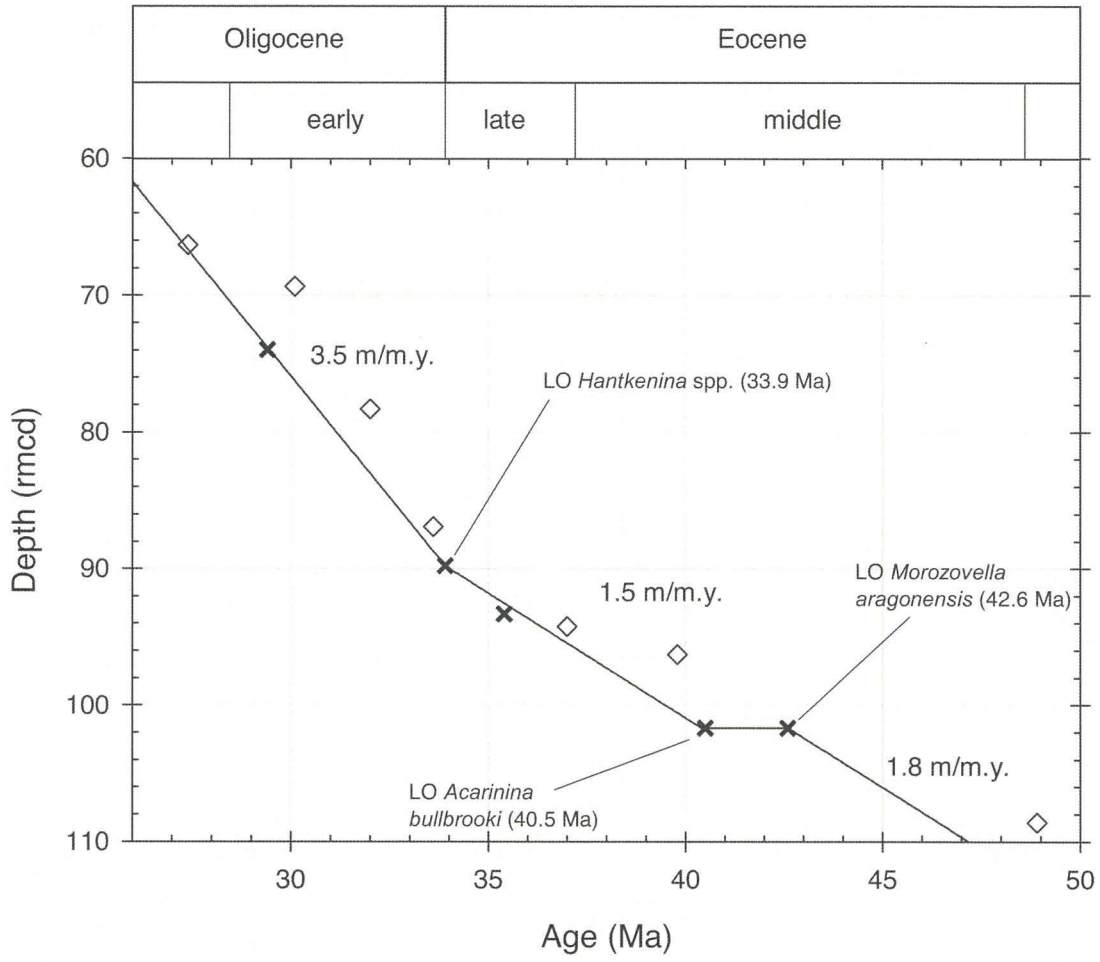

Figure 3.1: Modified depth-age model with sedimentation rates based on Figure 18 of Shipboard Scientific Party (2002b). Modifications from Figure 18 of Shipboard Scientific Party (2002b) are conversion of the depth scale to rmcd and the interpolation of biostratigraphic age datums onto the Palaeogene time scale of Luterbacher et al. (2004), rather than that of Berggren et al. (1995). The revised depths and biostratigraphic ages modify the predicted sedimentation rates for the Oligocene from 3.4 to 3.5 metres/million years (m/Myrs), whereas the Eocene sedimentation rate remains the same.

As described previously, the EOB can be identified within Site 1211 by calcareous nannofossil and planktonic biostratigraphic datums (Shipboard Scientific Party, 2002b). To further aid development of a sampling strategy, colour reflectance data and core photographs collected by the ODP during shipboard operations (Shipboard Scientific Party, 2002b) were considered. Colour reflectance is closely related to $\%CaCO_3$ (Shipboard Scientific Party, 2002b) and core photographs display this change also, with

increases in $\%CaCO_3$ leading to increased colour reflectance values or a lightening in colour of core material. Since the palaeodepth of Site 1211 was relatively close to the CCD during the Eocene (Shipboard Scientific Party, 2002b), deepening of the CCD at the EOB likely would have impacted on sedimentation rates at Site 1211. A CCD deepening would be expected to lead to enhanced carbonate sedimentation, as bottom waters would be less corrosive to the sinking carbonate particles. CCD deepening and thus enhanced carbonate sedimentation would be seen from the sediment becoming paler and an increase in colour reflectance values. Colour reflectance data measured by the Shipboard Scientific Party (2002b) (Figure 3.2), display a clear change around the stratigraphic interval identified by the biostratigraphic markers. Below ~90 rmcd colour reflectance values fluctuate between ~45 to ~75, but are generally around ~60, whereas above ~88 rmcd colour reflectance values are more uniform (with variance no more than ~± 2). The shift in colour reflectance values occurs monotonically over ~2 metres and is also visible to the naked eye as a distinct lightening in core colour in the core photos. This latter change is from the middle of Core 10 to the middle of Core 9, the exact position varying between Holes 1211A, 1211B and 1211C (Figure 3.2). From Figure 3.2, it can be seen that the colour change in Hole 1211A occurs at the top of core 10, close to the core gap, while in Hole 1211B the change occurs at the base of Core 9H, again close to the core gap. In contrast, the colour reflectance change in Hole 1211C occurs at the base of Section 1211C-9H-5. Positioning of each of the cores from the three Site 1211 holes on the revised composite depth scale is shown in Figure 3.2, indicating that Cores 1211C-10H and 1211C-9H recovered an apparently complete stratigraphic section. By comparison, Holes 1211A and 1211B both have several metre gaps between Cores 9 and 10, such that the stratigraphic record after and before the EOB event is lost in each hole, respectively. This evidence indicates that Hole 1211C recovered the most complete record of EOB change at Site 1211 and thus was selected for study.

The critical time period for this study is the immediate build up to the EOB, the event itself and the period following the early Oligocene glacial maximum (termed Oi-1; Miller et al., 1991). A sampling strategy was adopted to sample this stratigraphic interval at appropriate temporal resolutions. Samples were spaced at 10 cm intervals throughout Core 1211C-9H and the uppermost part of Core 1211C-10H. As it is important to place the EOB event in the broader scheme of Palaeogene change, a lower-resolution sampling scheme also was completed beyond the critical EOB interval, with samples taken at 20 cm intervals from Cores 1211C-7H, -8H and the remainder of -10H. In addition to these samples, further

materials were requested from Cores 1211A-7H, -8H, -9H and -10H, at 20 cm resolution, to fill core gaps existing in the Hole 1211C stratigraphic record (e.g. for core sediment lost during core recovery between Cores 1211C-8H and -9H). The samples taken are shown on Figure 3.2 and all data are plotted on the rmcd scale.

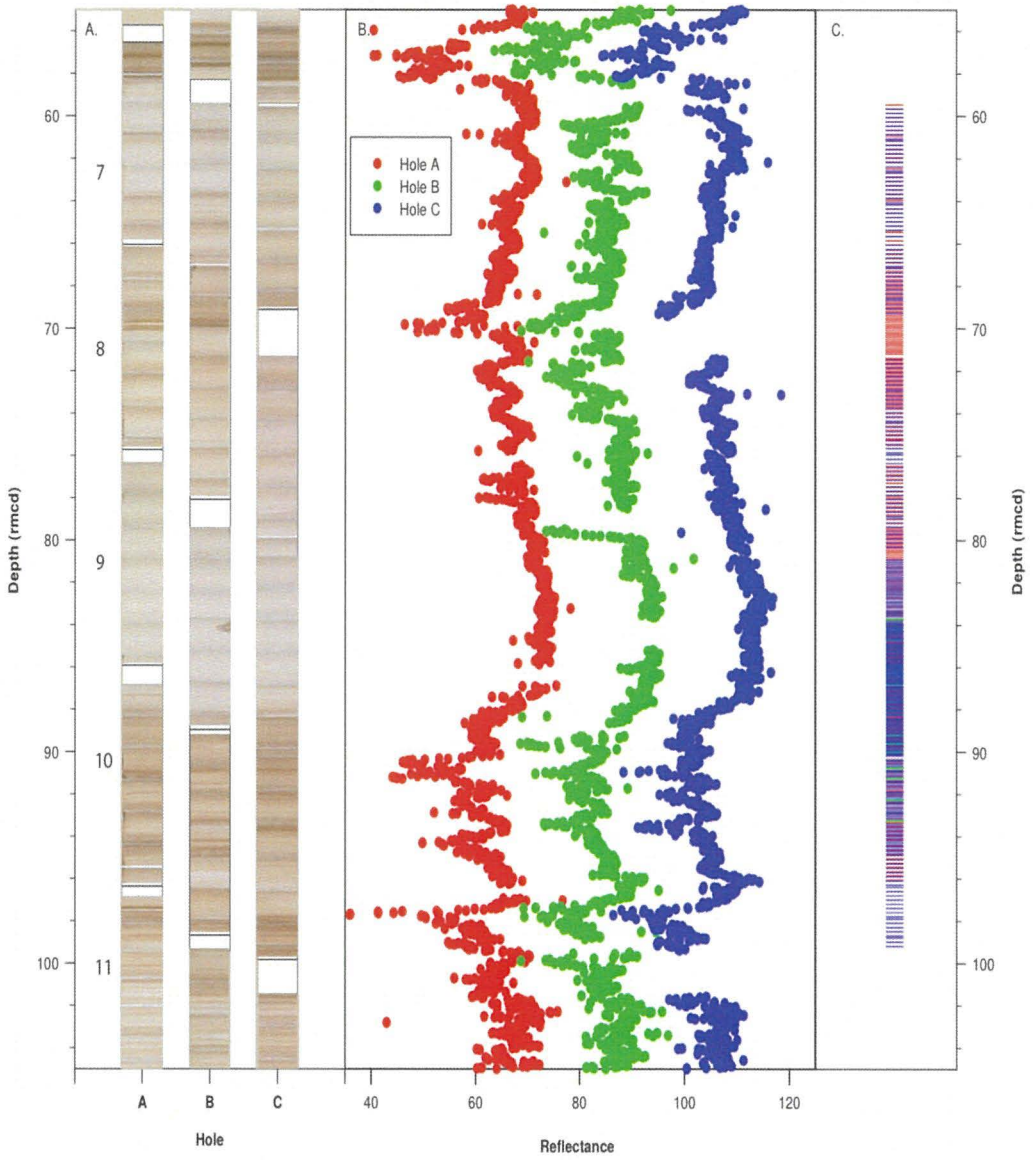

Figure 3.2: Summary of samples taken from Site 1211: a.) Core photographs; b.) L* Colour reflectance data (Holes B and C are offset from A by + 20 and +40 respectively); c.) Samples taken.

3.3 Methods

3.3.1 Sediment preparation

Upon receipt of samples from the ODP core repository, the raw sediment (bags ~20 cm^3) was batch dried until the sediment was seen to be dry. The resulting dry sediment was then split, with a proportion (up to 25 %) kept as bulk sediment to which no further processing occurred. The remaining sample was weighed and disaggregated in high-purity (18.2 MΩ) water on a rotating shaker table for a period of at least 24 hours. Upon complete disaggregation, the resulting slurry was wet-sieved at 63 μm, with the <63 μm proportion being retained and allowed to settle in 1 litre glass beakers. Once settling had occurred, the supernatant was siphoned off and the resulting <63 μm fraction dried at 60°C; the material was then bagged. The >63 μm fraction was dried at 60 °C, weighed and dry sieved at 450, 355, 250 and 150 μm. The resulting size fractions were transferred to glass vials ready for picking of foraminifera.

3.3.2 % Sand fraction

The percent sand fraction record, i.e. % >63 μm, was calculated from the dry weight of the sample, prior to disaggregation, and the dry weight of the >63 μm fraction. The % sand within deep-water marine sediments typically comprises of foraminifera, in particular planktonic foraminifera. There are several influences on the concentration of planktonic foraminifera in deep-sea sediments, including dissolution, productivity (or rain rate) and winnowing (Zachos et al., 1996). Planktonic foraminifera tend to be susceptible to syn-depositional dissolution in the water column and post-depositional dissolution on the seafloor, if deep-waters are under-saturated with respect to $CaCO_3$. Deep-water mass carbonate saturation (or under-saturation) depends on the water temperature and depth, saturation with respect to carbonate leading to preservation of planktonic foraminifera, dissolution increasing as the magnitude of the under-saturation increases. Thus, dissolution can be a significant influence on their concentration within the sediment. Rain rates depend on productivity within the surface waters; high productivity and hence high rain rate will depress the CCD, leading to planktonic foraminifera being deposited in the seafloor. Once at the seafloor, high rain rates also lead to rapid burial, thereby reducing the length of time for post-depositional dissolution of foraminifera on the seafloor. Periods of high productivity resulting in high organic accumulations at the seafloor, however, have been seen to lead to increased carbonate dissolution due to greater levels of bacterially respired

CO_2 (Diester-Haass, 1996). This phenomenon can be identified by observation of benthonic foraminiferal accumulation rates, which are thought to increase as export productivity increases (Diester-Haass, 1996). Winnowing results from the action of currents on % sand fraction sized and smaller particles, moving and focusing the location of deposition of the finer end of the particle scale downstream. The % sand fraction record thus is potentially very complex to interpret in terms of the derivation of a single reliable proxy. Wu et al. (1990) noted that % sand fraction is correlated with % carbonate for a modern-day near CCD deep-water Pacific Ocean site (4000m), suggesting that as % carbonate is controlled by dissolution at or near CCD water depths (~4100 m), correlation between the % sand and % carbonate records is a result of dissolution. Shallower than CCD/lysoclinal depths, this correlation breaks down, and Wu et al. (1990) have suggested that the >63μm fraction is more sensitive to dissolution than percentage carbonate when sediment is dominated by carbonate. Such an enhanced sensitivity to dissolution is due to the predominantly foraminiferal content of the sand fraction, with foraminifera breaking up into smaller fragments after relatively small amounts of dissolution, thereby decreasing the magnitude of the % sand fraction, transferring carbonate into the smaller fractions (Bassinot et al., 1994). The close correlation between % sand fraction and foraminiferal fragmentation observed by Bassinot et al. (1994) supports this suggestion.

The palaeodepth of Site 1211, within a few hundred metres of the Eocene CCD (Shipboard Scientific Party, 2002a,b), means that the site was likely to be below the lysocline and thus subject to varying degrees of dissolution through the Eocene and into the Oligocene. As such % sand content should primarily be a record of dissolution at Site 1211. % sand fraction records will be combined with % $CaCO_3$ records in this study to provide an assessment of such changes in dissolution across the EOB interval.

3.3.3 % $CaCO_3$

A percentage calcium carbonate (% $CaCO_3$) record has been produced for Site 1211. Percentage $CaCO_3$ was measured at the Department of Earth Sciences, University of Oxford, on a Coulomat 702 Analyser. Prior to analysis, an aliquot (~0.250 g) of each bulk unprocessed sediment sample was dried at 60 °C and then powdered using a pestle and mortar. Two splits of this powder were weighed (~20 mg and ~40 mg) in pre-combusted (to remove any existing organic carbon) ceramic boats. The ~40 mg boat was roasted over

night at ~600°C to oxidise organic material, thereby allowing measurement of both % Total C and % $CaCO_3$. These boats were then each individually combusted in pure O_2 at 1200 °C, the resulting gas being passed across urea peroxide tablets to remove SO_2 before absorption of the CO_2 into barium perchlorate solution at pH 10 and constant temperature of 35°C. The absorption of CO_2 lowers the pH of the solution, this change being monitored by a pH electrode; electrolysis occurs to restore the pH to 10, the current being measured and displayed as a number of counts, allowing conversion into % Total C and % $CaCO_3$. Conversion is through use of the formulae:

$$(\text{Counts} * 0.2)/\text{weight} = \% \text{ Total C}$$

$$\% \ CaCO_3 = \% \text{ Total C} * 100/12$$

The % Total C is calculated from the uncombusted sample, while % $CaCO_3$ is calculated from the combusted sample; the percentage organic carbon (% C_{org}) is then calculated from the difference between the % Total C and % $CaCO_3$.

% $CaCO_3$ in the deep-sea sedimentary record is thought to vary as a result of two primary variables in the oceans: productivity and deep-ocean carbonate ion concentration (Anderson et al., 2008, and references therein). Records from Pleistocene glacial–interglacials have provided much of the evidence that has been used to propose either productivity or carbonate ion concentration as the dominant control (Anderson et al., 2008). Apparent co-variation of % $CaCO_3$ with productivity related accumulation rates, such as siliceous microfossils or organic matter, supports a dominant productivity influence. Indicators of dissolution, such as foraminiferal preservation and ratios of dissolution resistant to dissolution prone species, however, vary with % $CaCO_3$ with preservation being poor when % $CaCO_3$ is low. Recent work (Zhang et al., 2007; Anderson et al., 2008,) has suggested that deep-water carbonate ion concentration is the dominant control, with changes in productivity not correlating with changes in % $CaCO_3$. Based on the findings of Zhang et al. (2007) and Anderson et al. (2008), % $CaCO_3$ can be used as proxy for relative changes in carbonate ion concentration, with higher concentrations of sedimentary $CaCO_3$ associated with an increased carbonate ion concentration (i.e. deeper CCD) for a given site. The latest Eocene CCD was positioned at

water depths between Sites 1211 and 1208 (Scientifc Shipboard Party, 2002b), being between ~3000–3500 m (Van Andel, 1975; Tripati et al., 2005). As previously described, the CCD deepened by ~1km at the EOB (Coxall et al., 2005), so it would be expected that Site 1211 would undergo an increase in carbonate ion saturation, which could be identified by $\%CaCO_3$ records.

3.3.4 Core-scanning X-ray fluorescence

High-resolution core-scanning X-ray fluorescence (XRF) studies, to determine elemental concentrations, were carried out using the XRF core scanner at the Centre for Marine Environmental Sciences (MARUM), University of Bremen, Germany (Röhl and Abrams, 2000; Röhl et al., 2000). Descriptions of the methods involved can be found in Jansen et al. (1998) and Röhl and Adams (2000). Basically, X-ray fluorescence uses primary X-rays to excite secondary X-rays from the sample (Fitton, 1999), with dispersion of secondary X-rays into a spectrum allowing identification of those specific elements present. Being a non-destructive and very rapid analysis system, the core-scanning XRF allows near continuous scanning of the pristine archive sections of cores to be made, with no detrimental effect to the sample material.

For this study, a total of ~90 m of core were analysed, i.e. Cores 8, 9 and 10 of each of the three Site 1211 holes. X-ray fluorescence measurements were taken at 2 cm spacing, over a 1 cm^2 area, using a 30-second count time, producing intensity counts for Fe, Ca and the minor elements K, Ti, Mn, Cu and Sr. Element intensity counts were then normalised by dividing the number of counts for each element by the sum of all counts plus the individual element counts again. Such a normalisation of intensity counts was undertaken due to the fact that variation in core wetness results in variation in the intensity counts measured (Westerhold, *pers. comm.*, 2006). Scanning XRF data thus are presented as normalised ratios of counts.

3.3.5 Fine-fraction stable-isotope records

The <63 μm fraction, obtained following the sieving of the original samples, was dry sieved at 38 μm to remove any larger pieces of broken foraminifera. Light microscopy of the sieved samples from across the stratigraphic range did not reveal any visible

foramininferal fragments within the resulting <38 μm fraction, indicating that the <38 μm fraction was predominantly comprised of calcareous nannofossils. <38 μm fraction samples were photographed by scanning electron microscope at a later date to reveal further information as to their composition (see Chapter 5).

The <38 μm fine fractions were then measured for $\delta^{13}C$ and $\delta^{18}O$ values using the following off-line procedure at the NERC Isotope Geosciences Laboratory (NIGL) situated at the British Geological Survey site in Keyworth, Nottingham. Sample material was reacted with anhydrous phosphoric acid in vacuum vessels overnight in a water bath held at a constant temperature of 25°C. The resulting CO_2 was separated from water vapour under vacuum and collected for analysis. Isotope-ratio analyses were undertaken on a VG Optima mass spectrometer. Overall analytical reproducibility for these samples was 0.08‰ for $\delta^{13}C$ and $\delta^{18}O$ values (N=60, 2σ). Isotope ratios ($\delta^{13}C$ and $\delta^{18}O$) are reported as per mil (‰) deviations of the isotope ratios ($^{13}C/^{12}C$, $^{18}O/^{16}O$) relative to the VPDB scale, using a within-run laboratory standard-calibrated against the NBS standards.

3.4 Selection and picking of foraminifera

3.4.1 Benthonic foraminifera

Identification and picking of benthonic foraminifera was carried out from the 150–250 and 250–355 μm size fractions. In the 355–450 μm and >450 μm size fractions there were relatively few benthonic foraminifera in the majority of samples, while picking the number of individual specimens required from the <150 μm size fraction would be likely have been too time consuming. The 250–355 μm size fractions contained variable numbers of benthonic foraminifera, but on the whole too few to pick any species consistently across the stratigraphic range of sampling. In contrast, the 150– 250 μm size fraction contained benthonic foraminifera across the range of sampling, except for the base of Cores 1211C-9H and the top of -10H (87.5 to ~90 rmcd).

Using the taxonomic descriptions of Bolli et al. (1994), *Oridorsalis umbonatus* was selected as the main species of study. This species is a transitional infaunal benthonic foraminiferan that lives in the uppermost sediment (0–4 cm; Rathburn et al., 1996) and was present throughout the time period investigated in this study. Rathburn et al. (1996)

reported $\delta^{18}O$ values for this species to be in near isotopic equilibrium, while $\delta^{13}C$ was recorded as being ~1 ‰ lower than the near-isotope values of epifaunal species, such as *Cibicidoides wuellerstorfi*. These offsets from equilibrium for $\delta^{13}C$ values and near equilibrium values for $\delta^{18}O$ values are similar to those measured by Woodruff et al. (1980) for *O. umbonatus*. As *O. umbonatus* is an extant species, a number of species-specific Mg/Ca ratio to temperature calibration equations (Lear et al., 2002; Rathmann et al., 2004; Healey et al., 2008) are in existence, thereby minimizing a potential error for palaeotemperature estimations based on this species.

Further benthonic foraminiferal species also were identified from the descriptions of Bolli et al. (1994): the extinct *Nuttaloides truempyi* and *Osungularia mexicana*, while extant species *Gyrinoides* sp., *Cibicidoides* sp., and *Melonis* sp. were also picked for geochemical analyses. *N.truempyi* was identified and commonly present in Core 1211C-10H (below 91.24 rmcd) and this species was picked extensively for stable-isotope ratio analyses. The other species were picked where possible to provide coverage and overlap for gaps in the *O. umbonatus* stable-isotope ratio records. Where possible, species were also picked from the same samples as *O. umbonatus* to allow quantification of any offsets in stable-isotope ratios. Early Cenozoic (Palaeocene and Eocene) stable-isotope offsets have been assessed previously by Katz et al. (2003) for some of these species (*Cibicidoides* spp., *N. truempyi* and *Oridorsalis* spp.), suggesting that carbon- and oxygen-isotopic ratio offsets are consistent between each of these species, except for $\delta^{18}O$ differences between *N. truempyi* and *Oridorsalis.* spp. While the inter-species offsets, observed by Katz et al. (2003), were not statistically valid for the Oligocene, comparison of the offsets measured by this study and those previously measured should reveal whether changes occur across the EOB.

In line with the available samples, benthonic foraminifera were picked, if present, at intervals of 10 cm throughout Core 1211C-9H. In Cores 1211C-8H and 10H picking was completed at intervals of 20 cm, while picking of Core 1211C-7H was undertaken at intervals of 40 cm. Sample coverage for the intervals between cores (core gaps), where there was a break in sediment recovery due to coring operations (i.e. between Cores 1211C-8H and 9H), or where foraminifera were sparse, was taken from stratigraphically equivalent sections of Hole 1211A. These samples, identified from the rmcd scale

(Westerhold and Rohl, 2006) were taken from Sections 1211A-8H-2 and -3, -9H-3, -6 and -7, and 10H-1 and -2 and were picked at 20 cm intervals where possible.

The key benthonic foraminiferal species (*O. umbonatus* and *N. truempyi*) were photographed under SEM to detail preservation. Only *O. umbonatus* was subject to element/Ca ratio analyses due to picking time constraints, as well as insufficient specimen numbers of other species being available for both stable-isotope and element/Ca ratio determinations. The pairing of these geochemical analyses allows independent temperature estimates from Mg/Ca ratios to be used to deconvolute the $\delta^{18}O$ of seawater, with both estimates being derived from the same source material, i.e. *O. umbonatus*.

3.4.2 Planktonic foraminifera

Unlike benthonic foraminifera, planktonic foraminifera were picked from both 150–250 and 250–355 μm size fractions, as a result of two distinct assemblages being present in the study material. Planktonic foraminiferal assemblages from samples deeper than ~94 rmcd contained more cosmopolitan Eocene assemblages, which were picked from the 250–350 μm size fraction. The cosmopolitan nature of these samples and relative low resolution of sampling completed, at ~40 cm spacing, has meant that the stratigraphic ranges of single species were short, i.e. limited to a few samples, which hindered picking of a continuous species-specific planktonic foraminiferal record.

Planktonic foraminiferal species were identified following Pearson et al. (2006) and consultation with Prof Paul Pearson (*pers. comm.*, 2008). Two of the more prominent species were chosen: *Acarinina bullbrooki* and *Subbotina senni.* These were two surface mixed-layer species, as identified by stable-isotope ratios (Pearson et al., 2006 and references therein), although the latter species has stable-isotope values associated with a deeper water column habitat than that of the former species. *A. bullbrooki* was only present in the lower two sections of Core 1211C-10H, while *S. senni* was present to ~94 rmcd. These species were both picked and used for stable-isotope and element/Ca ratio analyses. Between ~87.5 and ~94 rmcd few planktonic foraminifera were present within either size fraction, meaning that this stratigraphic interval could not be picked for planktonic foraminifera for either stable-isotope or element/Ca ratio determinations.

At depths shallower than ~87.5 rmcd, Oligocene planktonic foraminifera are dominant. The species *Catapsydrax unicavus* and *Turborotalia ampliapertura* were picked from the 150–250 μm fraction, up core at intervals of 20 cm throughout Core 1211C-9H and at 40 cm spacing in core 1211C-8H, until species numbers became insufficient to pick for both stable-isotope and element/Ca ratio determinations (*C. unicavus*: sample 1211C-8H-3, 65–67 cm at 75.05 rmcd; *T. ampliapertura*: 1211C-8H-6, 25–27 cm at 79.55 rmcd). Previous stable-isotope ratio studies have suggested that *C. unicavus* was a deep-dwelling species calcifying sub-thermocline (Van Eijden and Ganssen, 1995), while *T. ampliapertura* has stable-isotope values typical of a surface-water habitat (Pearson et al. 2006). Thus, these two planktonic foraminiferal species, in combination with benthonic foraminifera, allow for the reconstruction of a vertical oceanographic cross-section for the EOB and Oligocene.

3.5 Foraminiferal stable-isotope analyses

Between ~40 to ~100 mg of foraminifera (between 5 and 15 individuals depending on species and preservation) were weighed and subject to measurement of stable-isotope ratios. Benthonic foraminiferal analyses were undertaken on two mass spectrometers: initial analyses were completed using an automated VG Isocarb common acid bath system linked to an Optima mass spectrometer, with the bulk of the analyses completed on a GV IsoPrime mass spectrometer and Multiprep device, both systems again located at the NIGL analytical facility. Planktonic foraminiferal stable-isotope analyses were only undertaken on the GV IsoPrime mass spectrometer and Multiprep device.

Long-term analytical precision for analyses made on the VG Isocarb and Optima mass spectrometer was 0.22 ‰ for $\delta^{13}C$ and 0.14‰ for $\delta^{18}O$ (N=25, 2σ). For the GV IsoPrime mass spectrometer and Multiprep device, long-term analytical precision was 0.06 ‰ for $\delta^{13}C$ and 0.12 ‰ for $\delta^{18}O$ (N=86, 2σ). Foraminiferal stable-isotope ratios ($\delta^{13}C$ and $\delta^{18}O$) are reported as per mil (‰) deviations of the isotope ratios ($^{13}C/^{12}C$, $^{18}O/^{16}O$) relative to the VPDB scale, using a within-run laboratory standard-calibrated against the NBS standards.

3.6 Determination of foraminiferal element/Ca ratios

3.6.1 Selection of cleaning method

Variations on two methods are in widespread use for the physical and chemical cleaning and preparation of foraminifera for element/Ca analyses; choice of method depending on the desired elemental ratios to be measured. The two methods are the Cambridge 'oxidative' cleaning method (Barker et al., 2003) and the combined 'reductive' and 'oxidative' cleaning method (Boyle and Keigwin, 1985; modified by Boyle and Rosenthal, 1996). The combined 'reductive' and 'oxidative' cleaning method is typically used to measure trace element/Ca ratios, i.e. Cd/Ca, Li/Ca, Zn/Ca, in addition to the Mg/Ca and Sr/Ca ratios measurable after preparation using the 'oxidative' cleaning method. The reductive stage is thought to remove adsorbed or authigenic phases (Martin and Lea, 2002) that occur on and/or within the test, thus allowing measurement of trace elements that could easily be contaminated (Boyle and Keigwin, 1985), in comparison to the 'oxidative' methods that removes organic matter from the foraminiferal test (Martin and Lea, 2002). Studies comparing the efficacy of the two cleaning methods record Mg/Ca ratios 10–15% lower following 'reductive' cleaning compared with 'oxidative' cleaning only (Barker et al., 2003; Yu and Elderfield, 2008). Barker et al. (2003) note that the differences between the two cleaning methods for determination of Mg/Ca ratio palaeotemperature estimates are small relative to the uncertainties in palaeotemperature calibrations, and that removal of silicate phases is of primary importance, rather than the use or not of the 'reductive' cleaning step.

As discussed in Chapter 2, foraminiferal Cd/Ca, Li/Ca and Zn/Ca ratios are influenced by the carbonate saturation state of seawater. One of the aims of this study was to look at proxies of carbonate saturation state in relation to foraminiferal Mg/Ca ratios, and associated palaeotemperature estimates. This was to consider whether there was a dramatic change in seawater carbonate saturation across the EOB at Site 1211, which could hide any potential palaeotemperature signal in the foraminiferal Mg/Ca record. Consequently, it was decided to use the combined 'reductive' and 'oxidative' cleaning protocol in this study to allow determination of the trace element/Ca ratios. The method used is broadly outlined below:

- 5 – 10 benthonic or planktonic foraminifera (depending on species, size and availability) were broken open using a pin. The resulting fragments were transferred to acid-leached 1.5 ml micro-centrifuge tubes.

- In addition to the foraminiferal samples, at least two empty 1.5 ml micro-centrifuge tubes were also subject to the entire cleaning and dissolution procedure applied to the foraminifera. These were then measured to assess the inherent background contamination levels caused by the cleaning method.

- Four rinsing and ultrasonification steps were completed in ultra high quality (18.2 MΩ) H_2O, methanol (two times) and 18.2 MΩ H_2O again (two times).

- 'Reductive' cleaning in 100 µl of 0.25M ammonium citrate and 30 % ammonium hydroxide buffered hydrazine solution was completed for 30 minutes in a hot (sub-boiling) water bath, followed by rinsing a further five times in 18.2 MΩ H_2O.

- 'Oxidative' cleaning in 250 µl of 0.1M NaOH buffered H_2O_2 was completed for 10 minutes in a hot (90°C) water bath, followed by rinsing a further four times in 18.2 MΩ H_2O.

- Acid leaching in 0.001M HNO_3 was completed for a 30-second ultrasonification, followed by three further rinses in 18.2 MΩ H_2O and complete liquid removal via pipette.

- Dissolution was completed in 500 µl of 0.075M HNO_3, the samples being ultrasonified for 30 minutes, or until dissolved, followed by transfer of the solution to clean acid-leached 1.5 ml micro-centrifuge tubes for subsequent ICP-MS analyses.

A complete description of the combined 'reductive' and 'oxidative' cleaning method is found as an appendix to Martin and Lea (2002). All reagents are Merck Aristar with the exception of the Merck Ultrapur® HNO_3.

Following the first day of ICP-MS analyses, it was observed that concentrations of the trace elements Ba, Cd, Li and Zn within the dissolved foraminiferal samples were below the detection limits of the ICP-MS instrument used in this study. Despite this observation, the combined 'reductive' and 'oxidative' cleaning technique was used for all benthonic foraminiferal element/Ca ratio analyses, to maintain consistency between the element/Ca ratios measured. Subsequently, the Cambridge 'oxidative' cleaning method, without any 'reductive' cleaning steps, was used for the planktonic foraminiferal preparation. This decision was made in light of time constraints due to the imminent closure of the NERC ICP-MS Facility at Kingston University. The method used is broadly as described above but without the 'reductive' step; for a complete description see Barker et al. (2003).

3.6.2 ICP-MS setup

The Agilent 7500 series ICP-MS was initially set up to measure the following elements/isotopes: ^{7}Li, ^{11}B, ^{24}Mg, ^{42}Ca, ^{44}Ca, ^{66}Zn, ^{68}Zn, ^{88}Sr, ^{111}Cd and ^{137}Ba, with ^{29}Si, ^{47}Ti and ^{55}Mn included to monitor contamination. The trace elements (Li, B, Zn, Cd and Ba) concentrations were, however, below ICP-MS limits of detection and later analysis runs were setup to measure only Mg, Si, Ca, Ti, Mn and Sr.

For each day's analyses the same analysis sequence was completed: 1) procedural and certified reference materials (CRM) blanks followed by a "drift solution"; 2) the three series of standard solutions, each at different Ca concentrations, with each suite of standards being followed by a "drift solution"; 3) three unknown solutions, a CRM solution and a "consistency solution" were run, followed by a "drift solution"; 4) step 3 was repeated, changing the CRM each time until all unknown solutions had been analysed; 5) upon analysis of all unknowns a final "drift solution" was run. The purpose of the "drift solution" and "consistency solution" is described in the following section.

While the ICP-MS used in this study is capable of automatic sampling, the 500 µl volume of sample solutions available meant that manual sampling and initiation of measurement was necessary. The ICP-MS was set up to undertake five replicate analyses of each blank solution, and three replicate analyses of the known ("drift solution", standards, CRMs and

a "consistency solution") and unknown solutions (samples). Each solution analysis was followed by a two-minute wash in 10 % HNO_3.

3.6.3 Element/Ca ratio data processing

The raw data from the ICP-MS are in the form of counts per second (cps) for each isotope measured, output detailing the individual replicates for all solutions; the mean, standard deviation (σ) and %relative standard deviation (%RSD) of the individual replicates. Before element/Ca ratio concentration results could be determined from the cps data, these data had to be worked up in a standardised way, as follows:

- Raw cps results with %RSD >5% were highlighted (with the exception of blanks), since this variability suggested that the cps were unreliable and thus might have to have be discounted. Blanks were excluded from this criterion due to the near detection limits cps levels expected/measured.

- Means of all individual solutions were assigned a solution number, starting with the first "drift solution", i.e. excluding blanks. Run numbers were assigned to allow subsequent drift correction, hence starting at the first "drift solution" (run number = 0).

- Cps data were split into appropriate Excel worksheets, i.e. "drifts solutions", "consistency solutions", unknowns etc., and blank corrected using appropriate blanks. The blank corrected cps were then ratioed to the less abundant Ca isotope (^{42}Ca in this study) to give the greater signal ratio.

- In the "drift solution" worksheet, element/Ca ratios were plotted against run number. A linear regression was applied to the data forcing the y-axis intercept to be the value of "drift solution" number 1 (run number 0), followed by calculation of the regression and the r^2 of the relationship. The necessity to drift correct the raw cps data was assessed by considering a summary %RSD values of all the "drift" solutions, it was decided if this %RSD >2% for Mg and Sr (>5% for Mn and Ti) then drift correction was required, which was completed by the following equation:

Drift corrected = Sample cps – (((regression gradient/initial drift value)*solution number)*sample cps)

If resulting %RSD values of the "drift solutions" were <2% (or <5%) then the drift correction was applied to all worksheets.

- In the standards worksheet, element/Ca cps ratios were plotted against the known elemental ratios for each Ca solution (i.e. 10, 25 and 50 µg/ml), and regressions were then calculated forcing the y-axis intercept through 0. The calculated regressions allow direct calibration of the ratioed cps data to element/Ca ratios. Prior to calculation of unknown molar ratios for the unknown solutions, the average Ca (µg/ml) of the unknown solutions was calculated and the calibration curve with the closest Ca concentration applied (see Section 3.6.4)

- Elemental ratio data were then normalised, using the known element/Ca ratio of the synthetic "consistency solution" and calculating the offset between known and measured ratios. The following equation was then used to normalise the calibrated element/Ca ratios:

Normalised ratio = calculated ratio + ((offset/measured consistency ratio)*calculated ratio)

This normalisation procedure allows assessment of the analytical precision across all days of the study and removes inter-day bias in measured element/Ca ratios, thereby allowing compilation of the entire dataset.

3.6.4 Calibration, precision and accuracy of element/Ca ratios

Molar ratios have been used to calibrate the output signal of the Agilent 7500 series ICP-MS following Rosenthal et al. (1999). Use of output signal ratios, calibrated against a

series of synthetic standard solutions of known molar (element/Ca) ratios, facilitates more precise calculation of sample molar ratios (Rosenthal et al., 1999). The synthetic standard solutions containing known molar ratios of the elements investigated in this study (B, Li, Mg, Zn, Sr, Cd and Ba) were prepared initially at Ca concentrations of 1000 µg/ml. In addition to these elements, element/Ca ratios for elements used to monitor contamination (Si, Ti and Mn) were also included. These stock solutions contained a range of element/Ca ratios, increasing from 0 mmol/mol across a range of element/Ca ratios, chosen so as to be similar to those found in foraminiferal samples (Table 3.1). Standards were made up in Merck Ultrapur® 0.075M HNO_3. From each of the stock solutions, three solutions at 10, 25 and 50 µg/ml were prepared by dilution, with 0.075 M HNO_3, to provide Ca concentrations similar to those estimated to be present in the unknown sample solutions. As described above, these standard solutions were analysed sequentially in order of increasing Ca concentration, prior to any unknown solutions. Upon data processing, the resulting signal ratios for each Ca concentration were plotted against their known molar ratio and the relationships between them calculated (Figure 3.3). The resulting calibration equations allowed unknown isotope ratios to be converted into element/Ca molar ratios.

	mmol/mol				
	Mg/Ca	Sr/Ca	Si/Ca	Ti/Ca	Mn/Ca
0	0.00	0.00	0.00	0.00	0.00
1	1.00	0.25	0.50	0.50	0.50
2	2.00	0.75	1.00	1.00	1.00
3	4.00	1.10	1.50	1.50	1.50
Drift	6.00	1.50	2.00	2.00	2.00
Consistency	7.00	2.00	2.50	2.50	2.50
4	8.00	3.00	3.50	3.50	3.50
5	10.00	4.00	5.00	5.00	5.00

	µmol/mol				
	Li/Ca	B/Ca	Zn/Ca	Cd/Ca	Ba/Ca
0	0.00	0.00	0.00	0.00	0.00
1	4.00	170.00	1.00	0.01	0.50
2	6.00	180.00	2.00	0.04	0.90
3	8.00	190.00	3.50	0.07	1.20
Drift	10.00	200.00	5.00	0.10	1.50
Consistency	12.00	210.00	6.50	0.13	1.90
4	14.00	220.00	8.00	0.16	2.30
5	16.00	230.00	10.00	0.19	2.70

Table 3.1: Element/Ca ratios made up for synthetic standard solutions, made up at 1000ppm Ca in ultrapur 0.075 M HNO_3.

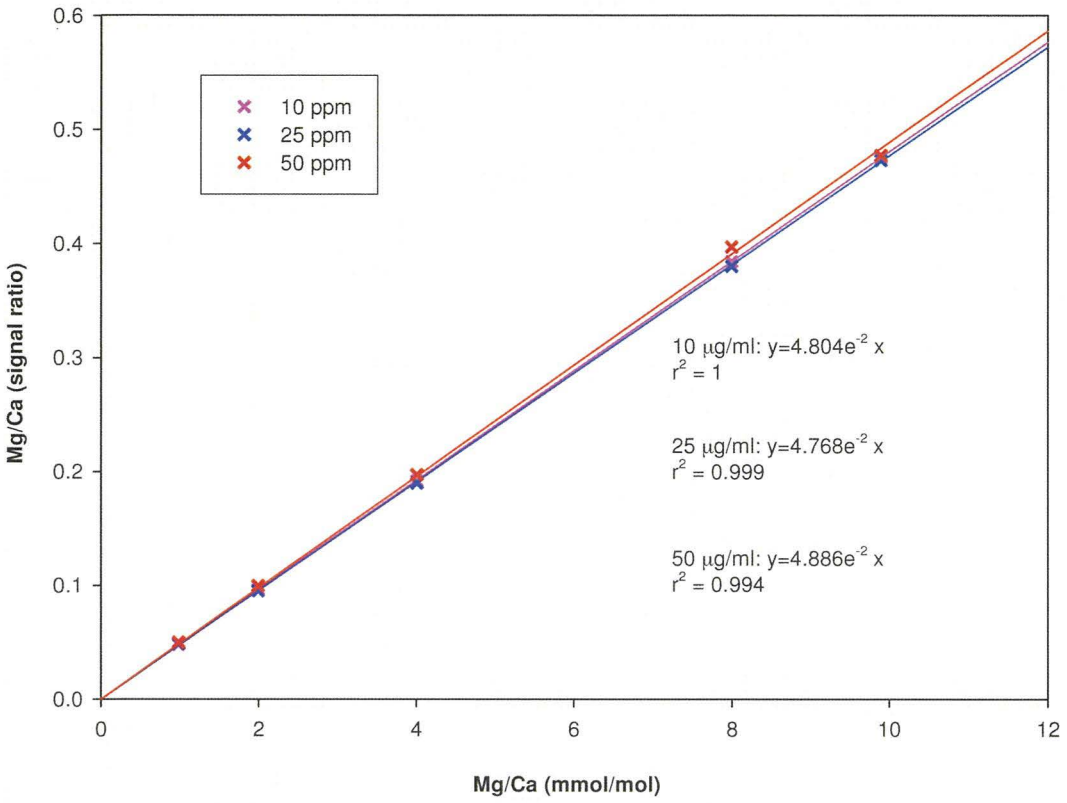

Figure 3.3: Plot of measured ICP-MS $^{24}Mg/^{42}Ca$ signal ratios versus expected molar Mg/Ca ratios, with regression lines for different Ca concentrations, for analyses measured on the 14th February 2008. It can be seen that over the range of Mg/Ca ratios typically found in benthonic foraminifera, i.e. 1–4 mmol/mol, there is minimal difference between the calibration lines.

Calculations of unknown sample Mg/Ca ratios were undertaken using the calibration line with the Ca concentration that was closest to the mean Ca concentration of the unknown samples, since this method was simple and quick to use. Assessments on which calibration line to use were completed independently for each individual analysis day. Rosenthal et al. (1999) and Lear et al. (2002) noted, however, so-called matrix (or mass bias) effects during ICP-MS analyses, whereby the variable Ca concentration of the unknown solutions can change the determined Mg/Ca ratios. A decrease in determined Mg/Ca ratios with increasing Ca concentrations has been observed with identical Mg/Ca ratio concentration consistency solutions declining from ~5.6 mmol/mol to ~5.0 mmol/mol over Ca concentrations typical of this study, i.e. ~1 to ~17 µg/ml (Lear et al., 2002).

Because the total sample volumes available in this study for ICP-MS analyses were small, ~500 µl, it was not possible to determine independently the Ca concentration of the unknown samples and subsequently dilute those solutions to a relatively consistent Ca concentration. Dilution to a single unknown sample Ca concentration could be matched to standards with the same Ca concentration, as carried out by Lear et al. (2004) to minimise

matrix effects. Thus, it has been necessary to determine in this study whether variable Ca concentrations in the unknown sample solutions and the use of a simple linear, rather than a mass bias corrected, calibration approach makes a significant difference to determined Mg/Ca ratios. Figure 3.3 shows the individual calibration lines for the 10, 25 and 50 μg/ml Ca standards for the 14th February 2008. It can be observed that over the range of expected benthonic foraminiferal ratios, i.e. 1–4 mmol/mol, there was little difference in the calibration lines for the different absolute Ca concentrations; planktonic foraminifera Mg/Ca ratios were also typically between 1–4 mmol/mol and the same relationship was observed (not shown).

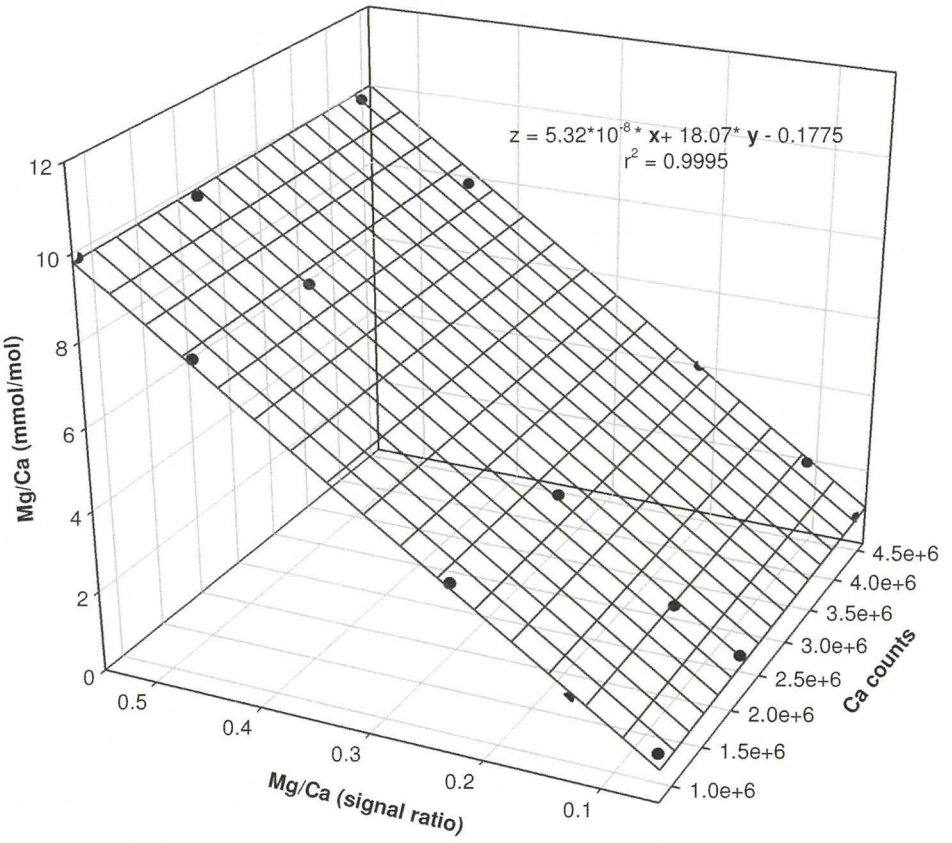

Figure 3.4: Example slope calibration for the synthetic standards measured on the 14th February, 2008. Calibrations using this approach calculate unknown sample Mg/Ca ratios using the slope of the plane through the Ca counts, the Mg/Ca signal ratio and the Mg/Ca molar ratio, using the equation shown on the figure.

To assess further whether the effect of different Ca concentrations on unknown sample Mg/Ca ratios was significant, separate mass bias (slope) calibrations where calculated for two of the analysis days, i.e. 10th December 2007 and 14th February 2008 (the latter shown on Figure 3.4; Table 3.2). These slope calibrations were used to determine the unknown Mg/Ca ratios for the two analysis days, which then were compared to the ratios determined using the simple linear calibration approach (Figure 3.5 and Table 3.3). This comparison shows no consistent relationship between the Mg/Ca ratios determined using the linear and

mass bias calibrations, with the differences between the Mg/Ca ratios calculated for each calibration being within ±2σ of the analytical precision. From the unknown sample population standard deviations it is evident that the mass bias calibration approach increases the scatter of the data, although the difference was relatively minor and still within ±2σ of the analytical precision. As the differences in Mg/Ca ratios resulting from the simple linear and mass bias (slope) calibration approaches were within ±2σ of the analytical precision and much less than the error associated with calculation of Mg/Ca palaeotemperatures (see Section 6.4) it was decided that there was no advantage in using the more complex mass bias calibration. The near identical range of Mg/Ca ratio data (Figure 3.5) shows that even if absolute determined molar ratios were slightly inaccurate, the relative changes between data points are unlikely to be the significantly different, such that estimations of relative Mg/Ca-derived palaeotemperature change would not be compromised. The similarity between mass bias and linear calibrations observed for the 10th December, 2007 and 14th February, 2008 is also observed throughout each of the other analysis days.

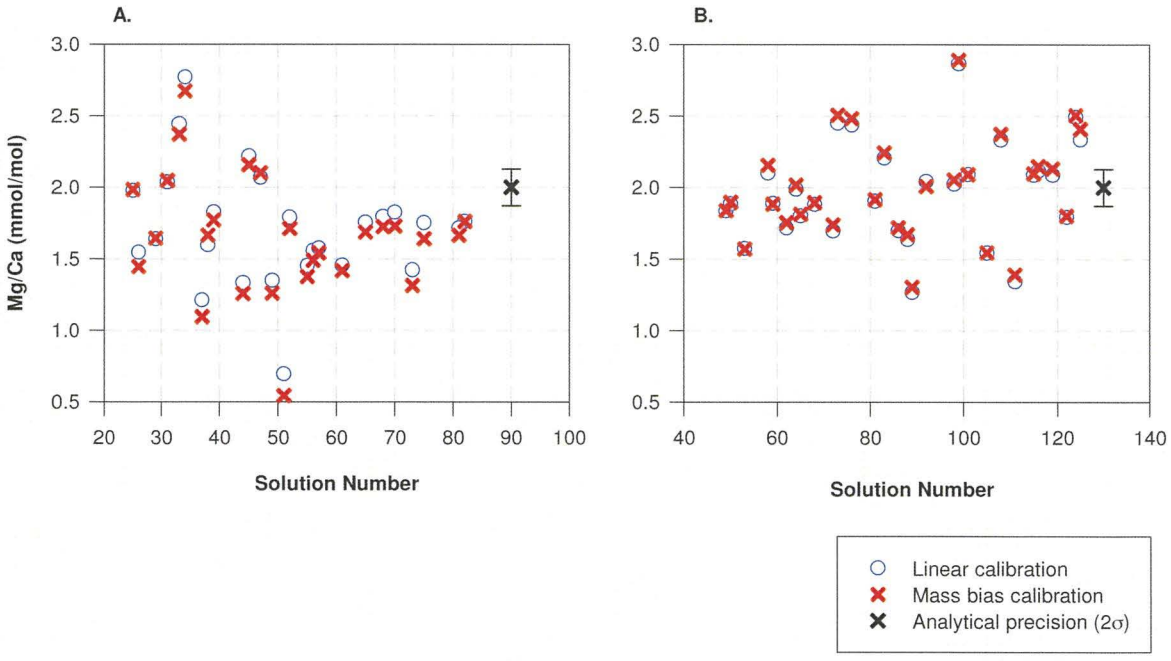

Figure 3.5: Plots of unknown sample Mg/Ca ratios for analysis days 10th December 2007 (panel A) and 14th February 2008 (panel B) using the simple linear calibration and more complex mass bias calibration approaches. It can be observed that the relationship between the two calibration approaches was different on each day of analysis and that the overall difference in determined Mg/Ca ratios was within ±2σ of the analytical precision.

A.	Equations					
	Linear (10 ppm)		Mass bias (slope) calibration			
	$z = mx$		$z = ax + by + c$			
	m		a	b	c	
10th December 2007	5.67E-02	$r^2 = 0.98$	18.07	5.32E-08	-1.78E-01	$r^2 = 1$
14th February 2008	4.89E-02	$r^2 = 0.99$	20.83	-3.55E-08	4.81E-02	$r^2 = 1$

B.	Linear calibration		Mass bias calibration	
	mean	σ	mean	σ
10th December 2007	1.71	0.41	1.66	0.42
14th February 2008	1.97	0.35	2.00	0.36

Table 3.2: A - Equations calculated for simple linear and more complex mass bias (slope) calibration approaches, with correlation coefficients, where x is the $^{24}Mg/^{42}Ca$ signal ratio and y is the Ca concentration in µg/ml. B. Mean and standard deviations of the unknown samples for each of the two days of analysis. No consistent relationship between linear and mass bias calibrations can be observed, with calculated overall population means being within the ±2σ of the analytical precision. Standard deviations of the determined unknown sample Mg/Ca ratios for each day were very similar with the mass bias calibration approach being within +0.01 of the linear calibration approach.

To assess intra- and inter-day analytical precision over the course of the ICP-MS analyses completed in this study, a "consistency solution" and a "drift solution" also were used. These solutions were prepared identically to the standards and diluted to 25 µg/ml Ca, so as to match the Ca concentration of the middle set of standards. Initially, the intention was to use a single 50 ml "consistency solution" for multiple days of ICP-MS analyses, which prior to exhaustion of the solution would be overlapped with a freshly diluted "consistency solution" to provide a continuous assessment of precision. When comparing day-to-day ICP-MS analyses, however, this policy had to be altered following evidence of leaching of contamination from the 50 ml centrifuge tubes containing the first batch of diluted "consistency solution". Fortunately, an uncontaminated "consistency solution" was measured with the contaminated batch, allowing precision to be assessed across all runs.

Accuracy across the days of ICP-MS analyses was assessed by use of three certified reference materials (CRMS; Table 3.3). Powders of these materials had been dissolved in Merck Ultrapur® 0.075M HNO_3 at a stock solution of 400 µg/ml Ca concentration prior to this study. For each set of ICP-MS analyses, fresh batches of each CRM and matching blank were made up to 25 µg/ml Ca in Merck Ultrapur® 0.075 M HNO_3 and, apart from the first three days of analyses, the CRM stock solutions were centrifuged for 10 minutes prior to dilution, to remove any insoluble contaminant silicate phases (Greaves et al., 2005;

2008). To monitor the significance of the centrifugation procedure both centrifuged and non-centrifuged CRMs were measured on three days of the analyses.

CRM	Mg/Ca (mmol/mol)		Sr/Ca (mmol/mol)		Mn/Ca (mmol/mol)	
	Quoted	Greaves	Quoted	Greaves	Quoted	Greaves
BAM RS3	0.800	0.791	0.200	0.184	n/a	n/a
ECRM 752-1	3.900	3.761	0.190	0.175		0.132
CMSI 1767	6.100	5.556		1.507	0.150	0.069

Table 3.3: Element/Ca ratios for CRMs used in this study, both quoted and Greaves values from Greaves et al. (2008).

	Mg/Ca Mean ± σ	Sr/Ca Mean ± σ	Mn/Ca Mean ± σ	Ti/Ca Mean ± σ
26.10.07	7.00 ± 0.052	2.00 ± 0.011	0.0132 ± 0.00035	2.5 ± 0.021
10.12.07	7.00 ± 0.026	2.00 ± 0.012	0.0132 ± 0.0002	2.5 ± 0.003
11.12.07	7.00 ± 0.021	2.00 ± 0.021	0.0132 ± 0.00062	2.5 ± 0.034
14.02.08	7.00 ± 0.105	2.00 ± 0.017	0.0132 ± 0.00030	2.5 ± 0.032
15.02.08	7.00 ± 0.045	2.00 ± 0.015	0.0132 ± 0.00013	2.5 ± 0.021
11.03.08	7.00 ± 0.081	2.00 ± 0.015	0.0132 ± 0.00032	2.5 ± 0.014
18.08.08	7.00 ± 0.046	2.00 ± 0.021	0.0132 ± 0.00034	2.5 ± 0.026
19.08.08	7.00 ± 0.064	2.00 ± 0.020	0.0132 ± 0.00053	2.5 ± 0.016
03.09.09	7.00 ± 0.062	2.00 ± 0.031	0.0132 ± 0.00038	2.5 ± 0.015
25.09.08	7.00 ± 0.065	2.00 ± 0.027	0.0132 ± 0.00012	2.5 ± 0.011
Overall	7.00 ± 0.064	2.00 ± 0.021	0.0132 ± 0.00031	2.5 ± 0.019

Table 3.4: Normalised consistency element/Ca concentrations (mmol/mol) and standard deviations measured during this study. Overall value used to assess precision across all analyses.

3.6.5 Assessment of analytical precision

Analytical precision was measured through the use of the "consistency solution", both for each day of ICP-MS analyses (intra-day) and across all analyses after normalisation (inter-day) (Figure 3.6 and Table 3.4). Figure 3.6 displays the drift corrected and normalised "consistency solution" data for each of the measured element/Ca ratios. Figure 3.7 shows the differences between inter-day element/Ca prior to normalisation, and illustrates the importance of normalisation in removing inter-day analytical variation, prior to compilation and interpretation of the unknown element/Ca ratios.

In summary, for the minor element/Ca ratios, intra-day precision was better than 1.5 %RSD and 1.55 %RSD for Mg and Sr, respectively, while the overall inter-day precision, for all ICP-MS runs, was 0.91 %RSD and 1.03 %RSD for Mg and Sr, respectively. For the trace element/Ca ratios, intra-day precision was better than 4.71 %RSD and 1.37 %RSD for Mn and Ti, respectively, and the overall inter-day precision was 2.35 %RSD and 0.75 %RSD for Mn and Ti, respectively. Si counts, and also Si/Ca ratios, of the "drift solution" when plotted versus solution number were variable and typically non-linear, with this variability hampering drift correction for the majority of the analysis days. As such, it was not possible to correct and compare "consistency solution" data reliably, such that an analytical precision for Si could not be assessed.

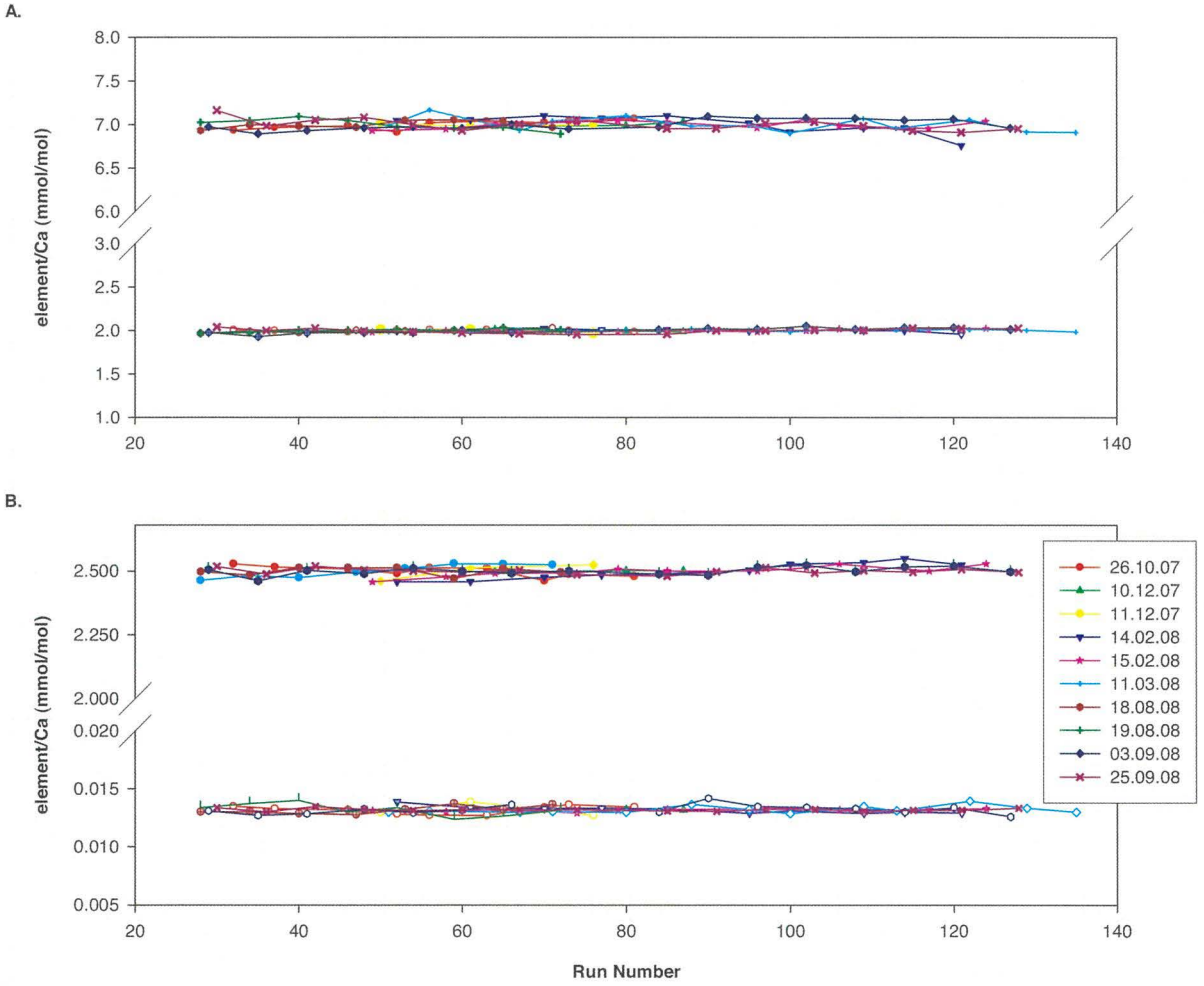

Figure 3.6: Plots of intra-day "consistency solution" element/Ca ratio data showing variance with run number: A.) Mg/Ca (closed symbols, upper) and Sr/Ca (open symbols, lower); B.) Ti/Ca (open symbols, upper) and Mn/Ca (closed symbols, lower).

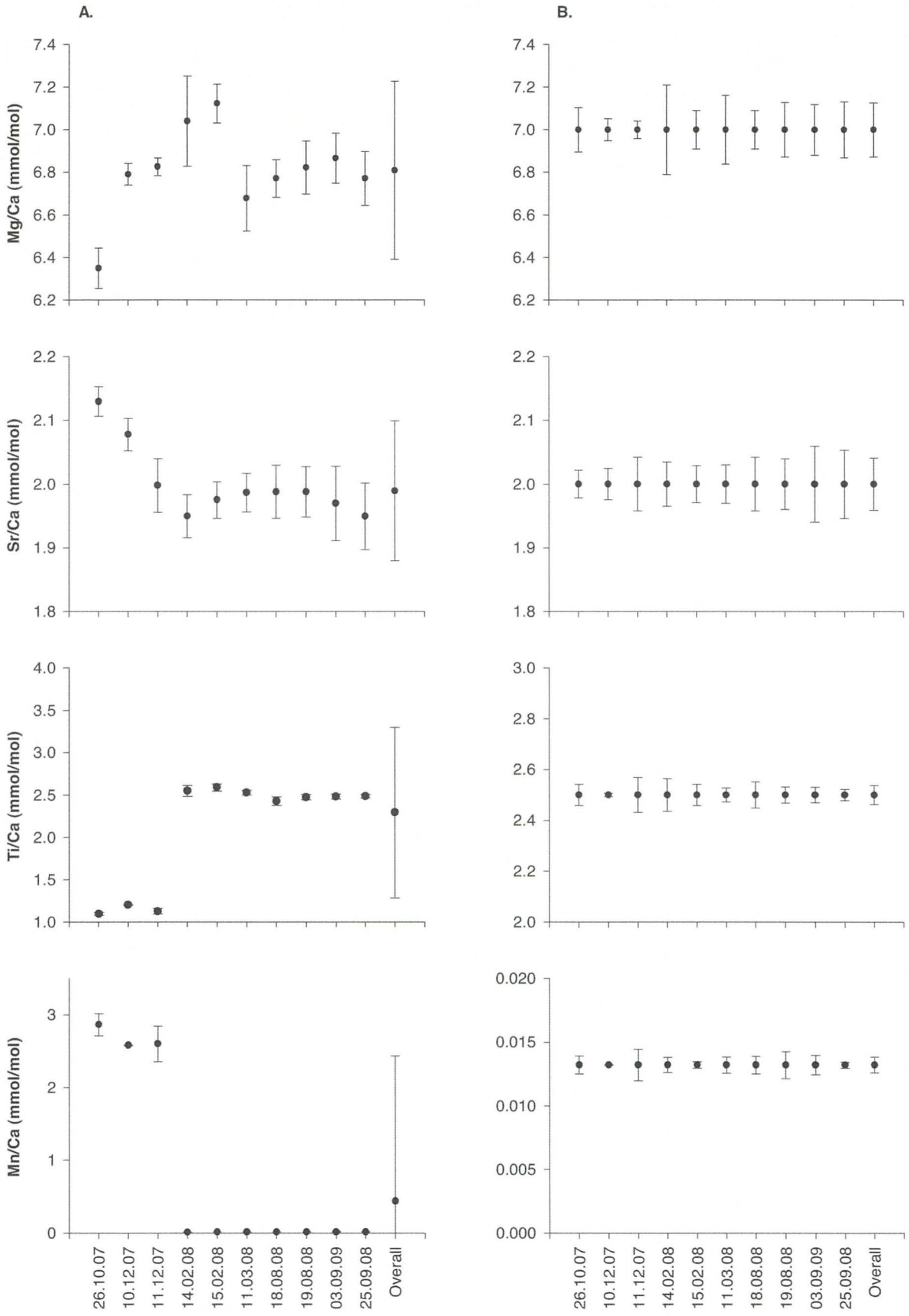

Figure 3.7: Plots of inter-day "consistency solution" element/Ca data (error bars ±2σ), A.) Pre-normalisation; B.) Post normalisation

3.6.6 Assessment of accuracy

Accuracy of element/Ca ratios was assessed through the use of three certified reference materials (BAM RS3, CMSI 1767 and ECRM 752-1; Table 3.3). BAM RS3 and ECRM 752-1 were included in all foraminiferal element/Ca analyses, whereas CMSI 1767 was used for all benthonic analyses, but not for planktonic analyses, due to time and number of analyses per day constraints following the imminent closure of the NERC ICP Facility. Greaves et al. (2005, 2008) noted that to ensure homogeneity of these CRMs it is necessary to centrifuge the stock solutions prior to dilution, since centrifuging removes any insoluble non-carbonate phases present. The presence of these insoluble non-carbonate phases offsets the CRM element/Ca ratios away from those of the carbonate phase and increases variability of the measured ratios across different sample sizes (see Figure 1a and b of Greaves et al., 2008). Within this study, however, CRMs used during the first three days of ICP-MS analyses were not centrifuged, so to assess the significance of this oversight on the accuracy of the measured values, later ICP-MS analyses measured element/Ca ratios for both centrifuged and non-centrifuged CRM solutions.

ICP-MS analysis days that yielded both non-centrifuged and centrifuged CRM element/Ca ratio data are plotted in Figure 3.8 to assess the presence of insoluble non-carbonate phases within the CRM stock solutions used in this study and whether there was a detrimental effect from the non-carbonate phases on the use of element/Ca ratios for determination of accuracy. Figures 3.8 A and B shows that a regression through all the available data has a gradient indicating that the non-centrifuged CRM solutions have elevated Mg/Ca and Sr/Ca ratios compared to the equivalent measured ratio from the centrifuged CRM solutions. For each single day of analyses, however, the mean measured element/Ca ratios for the non-centrifuged CRMs are within two σ of the measured ratios for the centrifuged CRMs (Figure 3.8C and D, except ECRM 752-1 Mg/Ca ratios for 11th March 07). The similarity of the measured centrifuged and non-centrifuged element/Ca ratios suggests that the presence of any insoluble non-carbonate phases is minimal within the non-centrifuged CRM solutions used. As such a combined mean of both centrifuged and non-centrifuged CRM solutions has been used for the purposes of assessing accuracy of measured element/Ca ratios. Figure 3.9 and Tables 3.5, 3.6 and 3.7 show the element/Ca ratios measured for each CRM in this study. Table 3.3 details the expected element/Ca ratios, as well as those measured by Greaves et al. (2008) in a recent inter-laboratory comparison study. Element/Ca ratios for the three CRMs were initially inferred from the concentrations

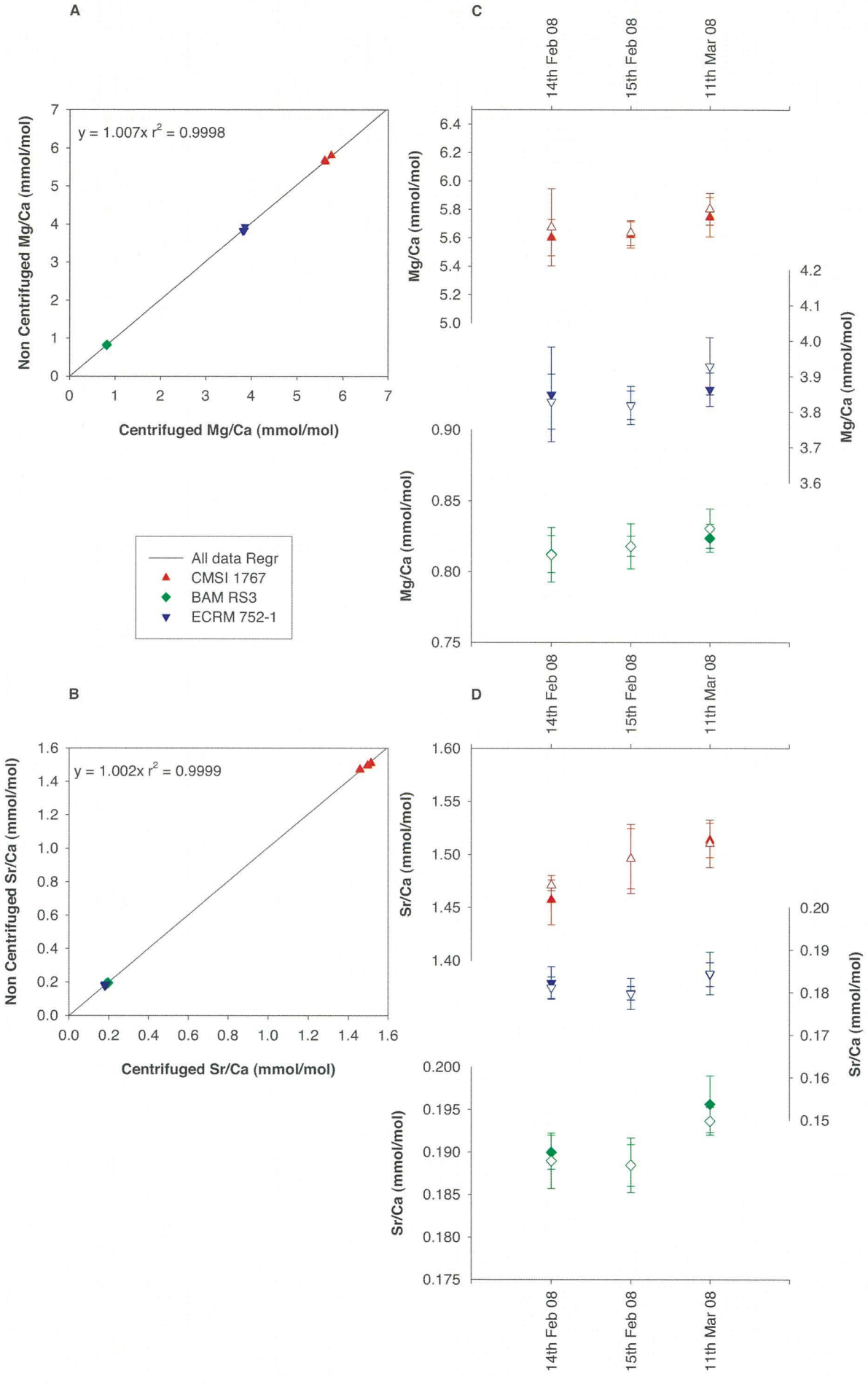
A
y = 1.007x r2 = 0.9998
Non Centrifuged Mg/Ca (mmol/mol)
Centrifuged Mg/Ca (mmol/mol)
All data Regr
CMSI 1767
BAM RS3
ECRM 752-1
C
14th Feb 08
15th Feb 08
11th Mar 08
Mg/Ca (mmol/mol)
B
y = 1.002x r2 = 0.9999
Non Centrifuged Sr/Ca (mmol/mol)
Centrifuged Sr/Ca (mmol/mol)
D
Sr/Ca (mmol/mol)

Figure 3.8: Cross plots of non-centrifuged versus centrifuged Mg/Ca (A) and Sr/Ca (B) ratios for three CRMs. Regression equations and lines indicate that the non-centrifuged CRMs have slightly higher element/Ca ratios. Measured Mg/Ca (C) and Sr/Ca (D) ratios (error bars ± 2σ) for centrifuged (closed, light coloured) and non-centrifuged (open, dark coloured) CRMs are plotted by day of analysis. It can be seen that only the non-centrifuged Mg/Ca ratio for the ECRM on the 11th March plots outside of ± 2σ of the measured centrifuged ratio mean.

Mg/Ca (mmol/mol) Date	Centrifuged Mean ± σ	Not Centrifuged Mean ± σ	Combined Mean ± σ
26.10.07		0.770 ± 0.0023	0.770 ± 0.0023
10.12.07		0.920 ± 0.0226	0.920 ± 0.0226
11.12.07		0.946 ± 0.0116	0.946 ± 0.0116
14.02.08	0.812 ± 0.0066	0.812 ± 0.0097	0.812 ± 0.0074
15.02.08	0.816 ± 0.0080	0.818 ± 0.0035	0.817 ± 0.0057
11.03.08	0.824 ± 0.0049	0.831 ± 0.0069	0.827 ± 0.0067
18.08.08	0.943 ± 0.0144		0.943 ± 0.0144
19.08.08	0.846 ± 0.0066		0.846 ± 0.0066
03.09.08	0.766 ± 0.0059		0.766 ± 0.0059
25.09.08	0.815 ± 0.0071		0.815 ± 0.0071
Measured Mean	0.823 ± 0.0051	0.866 ± 0.0064	0.840 ± 0.0598
Expected	0.791	0.791	0.791
% Difference	4.06	9.43	6.19

Sr/Ca (mmol/mol) Date	Centrifuged Mean ± σ	Not Centrifuged Mean ± σ	Combined Mean ± σ
26.10.07		0.135 ± 0.0003	0.135 ± 0.0003
10.12.07		0.208 ± 0.0028	0.208 ± 0.0028
11.12.07		0.207 ± 0.0045	0.207 ± 0.0045
14.02.08	0.190 ± 0.0010	0.189 ± 0.0016	0.189 ± 0.0013
15.02.08	0.189 ± 0.0011	0.188 ± 0.0016	0.189 ± 0.0013
11.03.08	0.196 ± 0.0017	0.194 ± 0.0008	0.195 ± 0.0016
18.08.08	0.193 ± 0.0028		0.193 ± 0.0028
19.08.08	0.188 ± 0.0025		0.188 ± 0.0025
03.09.08	0.190 ± 0.0029		0.190 ± 0.0029
25.09.08	0.192 ± 0.0030		0.192 ± 0.0030
Measured Mean	0.191 ± 0.0033	0.193 ± 0.0020	0.192 ± 0.0013
Expected	0.184	0.184	0.184
% Difference	3.91	5.02	4.35

Table 3.5: Measured element/Ca ratios (and standard deviations) for CRM BAM RS3, expected values from Greaves et al. (2008).

Mg/Ca (mmol/mol) Date	Centrifuged Mean ± σ	Not Centrifuged Mean ± σ	Combined Mean ± σ
26.10.07		3.586 ± 0.011	3.586 ± 0.011
10.12.07		3.886 ± 0.021	3.886 ± 0.021
11.12.07		3.855 ± 0.016	3.855 ± 0.016
14.02.08	3.849 ± 0.067	3.829 ± 0.039	3.841 ± 0.052
15.02.08	3.820 ± 0.002	3.818 ± 0.027	3.819 ± 0.020
11.03.08	3.863 ± 0.023	3.930 ± 0.040	3.897 ± 0.047
18.08.08	4.323 ± 0.070		4.323 ± 0.070
19.08.08	3.951 ± 0.018		3.951 ± 0.018
03.09.08	3.950 ± 0.055		3.950 ± 0.055
25.09.08	3.920 ± 0.028		3.920 ± 0.028
Measured Mean	3.939 ± 0.015	3.847 ± 0.10	3.903 ± 0.14
Expected	3.761	3.761	3.761
% Difference	4.73	2.27	3.78

Sr/Ca (mmol/mol) Date	Centrifuged Mean ± σ	Not Centrifuged Mean ± σ	Combined Mean ± σ
26.10.07		0.127 ± 0.0004	0.127 ± 0.0004
10.12.07		0.194 ± 0.0047	0.194 ± 0.0047
11.12.07		0.190 ± 0.0014	0.190 ± 0.0014
14.02.08	0.182 ± 0.0019	0.181 ± 0.0013	0.182 ± 0.0016
15.02.08	0.180 ± 0.0008	0.180 ± 0.0018	0.180 ± 0.0010
11.03.08	0.184 ± 0.0014	0.185 ± 0.0025	0.184 ± 0.0019
18.08.08	0.184 ± 0.0018		0.184 ± 0.0018
19.08.08	0.179 ± 0.0025		0.179 ± 0.0025
03.09.08	0.183 ± 0.0021		0.183 ± 0.0021
25.09.08	0.183 ± 0.0026		0.183 ± 0.0026
Measured Mean	0.182 ± 0.0032	0.181 ± 0.0192	0.181 ± 0.0115
Expected	0.175	0.175	0.175
% Difference	3.81	3.49	3.66

Mn/Ca (mmol/mol) Date	Centrifuged Mean ± σ	Not Centrifuged Mean ± σ	Combined Mean ± σ
14.02.08	0.135 ± 0.0052	0.133 ± 0.0032	0.134 ± 0.0042
15.02.08	0.144 ± 0.0012	0.143 ± 0.0001	0.143 ± 0.0011
11.03.08	0.156 ± 0.0011	0.156 ± 0.0015	0.156 ± 0.0012
18.08.08	0.143 ± 0.0004		0.143 ± 0.0004
19.08.08	0.133 ± 0.0007		0.133 ± 0.0007
03.09.08	0.143 ± 0.0030		0.143 ± 0.0030
25.09.08	0.153 ± 0.0011		0.153 ± 0.0011
Measured Mean	0.145 ± 0.0082	0.148 ± 0.0103	0.146 ± 0.0115
Expected	0.132	0.132	0.132
% Difference	10.20	12.11	10.55

Table 3.6: Measured element/Ca ratios (and standard deviations) for CRM ECRM 752-1, expected values from Greaves et al. (2008).

of the elements within the CRM (Greaves et al., 2005). Greaves et al. (2008) then measured element/Ca ratios of the same CRMs and these values differed from those inferred previously, a difference that likely results from imprecision in the original concentration measurements. Greaves et al. (2008) also made direct measurements of Sr/Ca ratios for the CMSI 1767, as well as of Mn/Ca ratios for each CRM. Thus, assessment of accuracy of the element/Ca ratios measured in this study has been completed against the Greaves et al. (2008) summary element/Ca ratios.

Mg/Ca ratios in foraminifera are typically on the order of 1–4 mmol/mol, thus assessment of the accuracy of this study's Mg/Ca ratios has been completed using the BAM RS3 and ECRM 752-1 CRMs, which have ratios at either end of this range. Tables 3.5 and 3.6 summarise the results for these standards, and show that accuracy of the mean of the CRMs (centrifuged and non-centrifuged) is better than 7 % for BAM RS3 and is within 4 % for ECRM 752-1.

Sr/Ca ratios in foraminifera typically exhibit much less variation than Mg/Ca ratios, varying between 1–2 mmol/mol. From the stated concentration ratios, neither of these CRMs has a Sr/Ca ratio in this range, but Greaves et al. (2008) measured a Sr/Ca ratio for CMSI 1767 within this range and showed it to be consistent throughout multiple aliquots of the CRM. Table 3.7 summarises measured Sr/Ca ratios for CMSI 1767, and that the accuracy of data generated by this study was within ~1 % of the Greaves et al. (2008) measured Sr/Ca ratio. For ICP-MS analyses where the CMSI 1767 CRM was not measured, Sr/Ca ratio accuracy has been assessed using the BAM RS3 and ECRM 752-1 CRMs; Tables 3.5 and 3.6 show that this accuracy is within 5 % for both CRMs.

Foraminiferal Mn/Ca ratios are typically much lower than the levels measured in the CRMs, so like-for-like values cannot be compared. Greaves et al. (2008) measured Mn/Ca ratios for both CMSI 1767 and ECRM 752-1 and the accuracy for these CRMs was better than 11% for CMSI 1767 and better than 20% for ECRM 752-1 in this study. The concentrations of Mn/Ca in the CRMs (Table 3.3) are approximately equivalent to the level (~0.1 mmol/mol, Yu et al., 2006) assigned to indicate contamination of foraminiferal tests by MnO indicating the presence of authigenic phases (Boyle, 1983). As Mn/Ca ratios were used as a threshold to identify contaminated or uncontaminated phases, the poor

accuracy observed for Mn/Ca ratios did not hinder the palaeoceanographic interpretation of the data. No assessment of the accuracy of Ti/Ca ratios could be made in this study since the Ti signal was below that of the blank in all CRM measurements.

Mg/Ca Date	Centrifuged Mean ± σ	Non Centrifuged Mean ± σ	Combined Mean ± σ
26.10.07		5.68 ± 0.142	5.68 ± 0.142
10.12.07		5.77 ± 0.035	5.77 ± 0.035
11.12.07		5.73 ± 0.015	5.73 ± 0.015
14.02.08	5.60 ± 0.064	5.67 ± 0.135	5.64 ± 0.105
15.02.08	5.62 ± 0.046	5.64 ± 0.043	5.63 ± 0.042
11.03.08	5.75 ± 0.069	5.80 ± 0.056	5.63 ± 0.066
Measured Mean	5.66 ± 0.089	5.72 ± 0.091	5.70 ± 0.094
Expected	5.556	5.556	5.556
% Difference	1.93	3.00	2.62

Sr/Ca Date	Centrifuged Mean ± σ	Non Centrifuged Mean ± σ	Combined Mean ± σ
26.10.07		1.51 ± 0.002	1.51 ± 0.002
10.12.07		1.50 ± 0.023	1.50 ± 0.023
11.12.07		1.56 ± 0.010	1.56 ± 0.010
14.02.08	1.46 ± 0.012	1.47 ± 0.003	1.46 ± 0.011
15.02.08	1.50 ± 0.014	1.50 ± 0.016	1.50 ± 0.014
11.03.08	1.51 ± 0.008	1.51 ± 0.011	1.51 ± 0.009
Measured Mean	1.49 ± 0.027	1.51 ± 0.030	1.50 ± 0.0066
Expected	1.507	1.506	1.507
% Difference	-1.07	0.09	-0.37

Mn/Ca (mmol/mol) Date	Centrifuged Mean ± σ	Non Centrifuged Mean ± σ	Combined Mean ± σ
14.02.08	0.064 ± 0.0026	0.065 ± 0.0021	0.065 ± 0.0023
15.02.08	0.069 ± 0.0009	0.069 ± 0.0006	0.069 ± 0.0007
11.03.08	0.076 ± 0.0003	0.077 ± 0.0008	0.076 ± 0.0006
Measured Mean	0.070 ± 0.0053	0.071 ± 0.0052	0.071 ± 0.0051
Expected	0.0687	0.0687	0.0687
% Difference	2.30	3.12	3.00

Table 3.7: Measured element/Ca ratios (and standard deviations) for CRM CMSI 1767, expected values from Greaves et al. (2008).

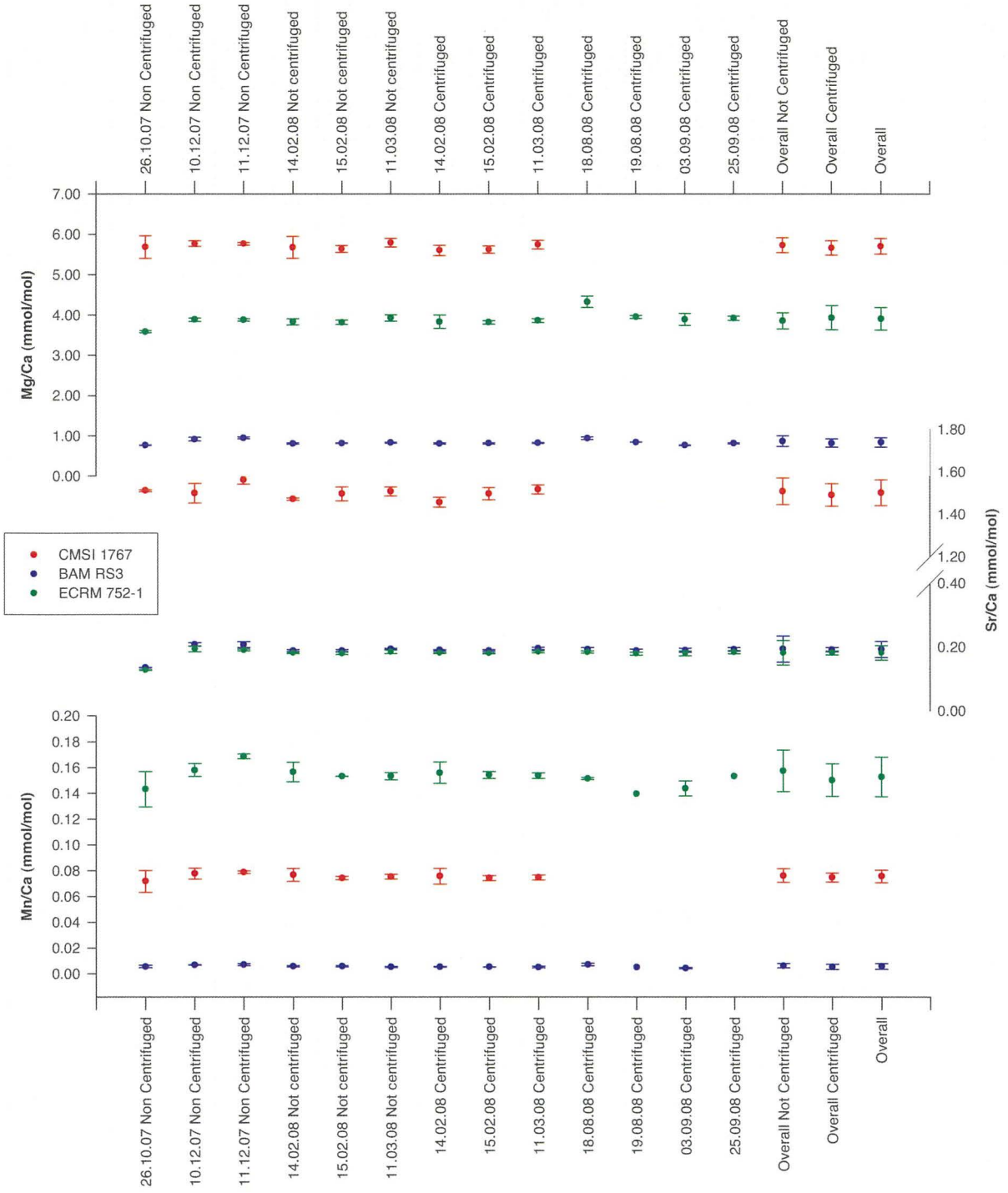

Figure 3.9: Plots of inter-day element/Ca variance of all CRMs (error bars ±2 σ).

Chapter 4: Depth–age model development

This chapter details the development of a depth–age model for ODP Site 1211, since a depth–age model is necessary to convert core sample depths to numerical ages, and thus allow this study's data to be interpreted in terms of timings and rates of change, as well as facilitate comparison with published datasets. Production of a depth–age model for Site 1211 requires the use of defined depth–age control points that are accurately calibrated within the geochronological record. Two key methods of depth–age control were applied during ODP Leg 198: biostratigraphy and magnetostratigraphy (Shipboard Scientific Party, 2002a,b).

Biostratigraphy is based on the positioning of defined first occurrence (FO) or last occurrence (LO) events (biostratigraphic datums) that have been identified as occurring at a particular geological time. At these datums species appear (FO) or disappear (LO) from the fossil record. Biostratigraphic correlation is complicated, however, as species are frequently not globally distributed (provincialism), while their appearances/disappearances in the fossil record may vary diachronously across latitudes and even between ocean basins. ODP Leg 198 biostratigraphies (Shipboard Scientific Party, 2002a) are based on the low-latitude calcareous nannofossil biozonations of Bukry (1973, 1975; modified by Okada and Bukry, 1980) and the planktonic foraminiferal biozonation of Berggren et al. (1995). Figure 4.1 details the biozones used for Site 1211, with the microfossil datum ages interpolated from the Palaeogene timescale of Luterbacher et al. (2004), rather than those datum ages used by Shipboard Scientific Party (2002a). Site 1211 biostratigraphies are described in more detail in Section 4.1.

Magnetostratigraphy is the measurement of the inclination of the natural remnant magnetism (NRM) of recovered cores by passing through a whole-core magnetometer. Following deposition, sediment retains an imprint of Earth's geomagnetic field, such that measurement of the inclination of this imprint can then be used to determine whether Earth's magnetic field was in a normal or reversed polarity state (Ogg and Smith, 2004). The sequence of geomagnetic polarity reversals is well defined and globally synchronous, thus providing an excellent method of age correlation at and between locations.

Palaeogene magnetostratigraphy is shown on Figure 4.1, following the numerical ages of chrons in Ogg and Smith (2004). Palaeomagnetic records were measured for cores recovered from Site 1211, but prior to the Plio-Pleistocene the core record showed erratic inclination values and there is little correlation of inclinations between holes, preventing reliable stratigraphic correlation and interpretation of individual chrons (Shipboard Scientific Party, 2002b). The erratic inclination values have been attributed to deformation of the sediment during core recovery (Shipboard Scientific Party, 2002b); thus, a potentially very useful tool in establishing a depth–age relationship is unavailable for Site 1211.

4.1 Biostratigraphy

Biostratigraphies have been established for Site 1211 based on calcareous nannofossils and planktonic foraminifera (Shipboard Scientific Party, 2002b; Bralower, 2005; Petrizzo et al., 2005). Shipboard Scientific Party (2002b) biostratigraphic age assignments were based on examination of core-catcher samples, with additional samples analysed around key stratigraphic intervals or possible unconformities, leading to ~4 to ~10 m separation between biostratigraphic samples. The biostratigraphic age assignments of Bralower (2005) and Petrizzo et al. (2005) were completed at higher stratigraphic resolution, with at least one sample per 1.5 m core section, thus allowing greater refinement of biozones and subzones. The age assignments of Shipboard Scientific Party (2002b), Bralower (2005) and Petrizzo et al. (2005) were all against the Cenozoic timescale of Berggren et al. (1995), but this timescale has been recently revised by Luterbacher et al. (2004). Consequently, the existing Site 1211 age assignments for biostratigraphic datums have been converted to the numerical timescale of Luterbacher et al. (2004) by interpolation of relevant biozonal ages. This interpolation procedure has an associated error of approximately ± 100 kyrs.

4.1.1 Planktonic foraminifera

Figure 4.2 shows Shipboard Scientific Party (2002b) and Petrizzo et al. (2005) planktonic foraminiferal biostratigraphies for Site 1211. Both Shipboard Scientific Party (2002b) and Petrizzo et al. (2005) Palaeogene planktonic foraminiferal biostratigraphies for Site 1211 are hindered by poor preservation/fragmentation of planktonic foraminifera and an absence of key marker species (e.g., *Orbulinoides beckmanni* for the base and the top of biozone

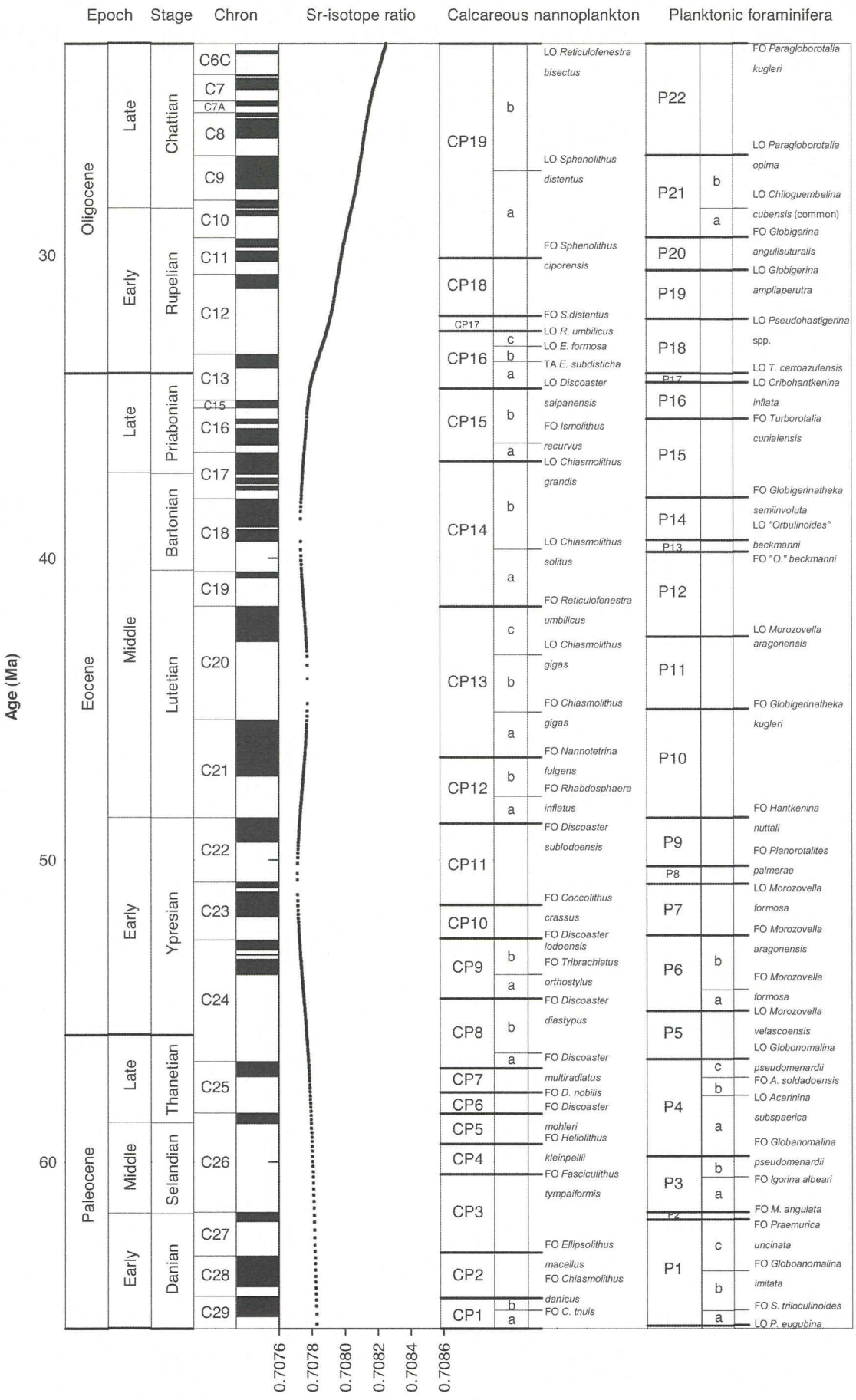
Epoch
Stage
Chron
Sr-isotope ratio
Calcareous nannoplankton
Planktonic foraminifera
Age (Ma)
Oligocene
Eocene
Paleocene
Late
Early
Middle
Chattian
Rupelian
Priabonian
Bartonian
Lutetian
Ypresian
Thanetian
Selandian
Danian
C6C
C7
C7A
C8
C9
C10
C11
C12
C13
C15
C16
C17
C18
C19
C20
C21
C22
C23
C24
C25
C26
C27
C28
C29
30
40
50
60
0.7076
0.7078
0.7080
0.7082
0.7084
0.7086
CP19
CP18
CP17
CP16
CP15
CP14
CP13
CP12
CP11
CP10
CP9
CP8
CP7
CP6
CP5
CP4
CP3
CP2
CP1
LO Reticulofenestra bisectus
LO Sphenolithus distentus
FO Sphenolithus ciporensis
FO S.distentus
LO R. umbilicus
LO E. formosa
TA E. subdisticha
LO Discoaster saipanensis
FO Ismolithus recurvus
LO Chiasmolithus grandis
LO Chiasmolithus solitus
FO Reticulofenestra umbilicus
LO Chiasmolithus gigas
FO Chiasmolithus gigas
FO Nannotetrina fulgens
FO Rhabdosphaera inflatus
FO Discoaster sublodoensis
FO Coccolithus crassus
FO Discoaster lodoensis
FO Tribrachiatus orthostylus
FO Discoaster diastypus
FO Discoaster multiradiatus
FO D. nobilis
FO Discoaster mohleri
FO Heliolithus kleinpellii
FO Fasciculithus tympaiformis
FO Ellipsolithus macellus
FO Chiasmolithus danicus
FO C. tnuis
P22
P21
P20
P19
P18
P17
P16
P15
P14
P13
P12
P11
P10
P9
P8
P7
P6
P5
P4
P3
P2
P1
FO Paragloborotalia kugleri
LO Paragloborotalia opima
LO Chiloguembelina cubensis (common)
FO Globigerina angulisuturalis
LO Globigerina ampliaperutra
LO Pseudohastigerina spp.
LO T. cerroazulensis
LO Cribohantkenina inflata
FO Turborotalia cunialensis
FO Globigerinatheka semiinvoluta
LO "Orbulinoides" beckmanni
FO "O." beckmanni
LO Morozovella aragonensis
FO Globigerinatheka kugleri
FO Hantkenina nuttali
FO Planorotalites palmerae
LO Morozovella formosa
FO Morozovella aragonensis
FO Morozovella formosa
LO Morozovella velascoensis
LO Globonomalina pseudomenardii
FO A. soldadoensis
LO Acarinina subspaerica
FO Globanomalina pseudomenardii
FO Igorina albeari
FO M. angulata
FO Praemurica uncinata
FO Globoanomalina imitata
FO S. triloculinoides
LO P. eugubina

Figure 4.1: Leg 198 Palaeogene timescale with primary calcareous microfossil datums. Datums are from Shipboard Scientific Party (2002a). Palaeogene epoch ages and biostratigraphic datum ages are interpolated from Luterbacher et al. (2004). Palaeomagnetic chronology is from Ogg and Smith (2004), and the Sr-isotope curve is from "Look-Up Table Version 4: 08/04" of Howarth and McArthur (1997) and McArthur et al. (2001), see Figure 4.4 for an expanded Eocene Sr-isotope record.

P14). Shipboard Scientific Party (2002b) identified the EOB based on the LO of the Hantkeninids (base of biozone P18), and the Oligocene by the recognition of base of biozone P19; further subdivision of the Eocene and Oligocene was not possible due to the paucity of marker species, low resolution sampling and poor preservation of the Eocene and Oligocene foraminifera despite the high $CaCO_3$ content. The base of biozone P21 is tentatively defined within this study as the LO of *Subbotina angiporoides,* a secondary marker species identified by Shipboard Scientific Party (2002b), in Figure 4.2. However, the base of biozone P19 identified by the LO of *Pseudohastigerina* spp. is placed at 93.62 rmcd, a mean depth derived from the LO horizon observed in samples core-catcher samples (1211A-11H-CC and 1211C-8H-CC). These two core-catcher samples are ~25 m apart on the composite rmcd scale and hence does not reflect a well-constrained biozone base. Identification of other datums (the base of biozone P18 at 89.80 rmcd, the base of biozone P12 at 101.67 rmcd; i.e. two older datums identified stratigraphically higher within the recovered sediment) also suggests that the identification of the base of biozone P19 at 93.62 rmcd is at too great a depth, thus in this study the base of P19 is not used when determining the depth–age model. Shipboard Scientific Party (2002b) biostratigraphy suggests a hiatus or highly condensed interval at ~101 rmcd, identified by the synchronous presence of the LO of *Acarinina bullbrooki* (~40.50 Ma) and LO of *Morozovella aragonensis* (base of biozone P12; 42.6 Ma).

Petrizzo et al. (2005) identified a greater number of Eocene biozones (P16/17, P15, P14, P12), as well as P18 (the LO of the Hantkeninids) for the EOB. However, few of their biozones were based on the defined zonal species, instead being reliant on secondary markers that have LO or FO close to the true marker species, e.g., the top of biozone P14 is identified by the FO of *Subbotina praeturritilina,* due to the absence of the marker species *Truncorotaloides rohri*, while the basal biozone P14 datum of LO *Orbulinoides beckmanni* is absent from Site 1211, introducing potential sources of error when comparing to geochemical proxy datasets with chronologies based on zonal species. Petrizzo et al. (2005) also failed to define biozones younger than P18 (EOB) which, with the Shipboard Scientific Party (2002b) uncertainty for Oligocene planktonic foraminiferal biozones, means no reliable planktonic foraminiferal biostratigraphy is available for the Oligocene.

A further point of note is the stratigraphic proximity of the base of biozone P12 (42.6 Ma) and the base of biozone P14 (39.4 Ma) within a few centimetres at ~97.60 rmcd, suggesting a hiatus or condensed interval at this depth of ~3 Ma duration (Petrizzo et al., 2005).

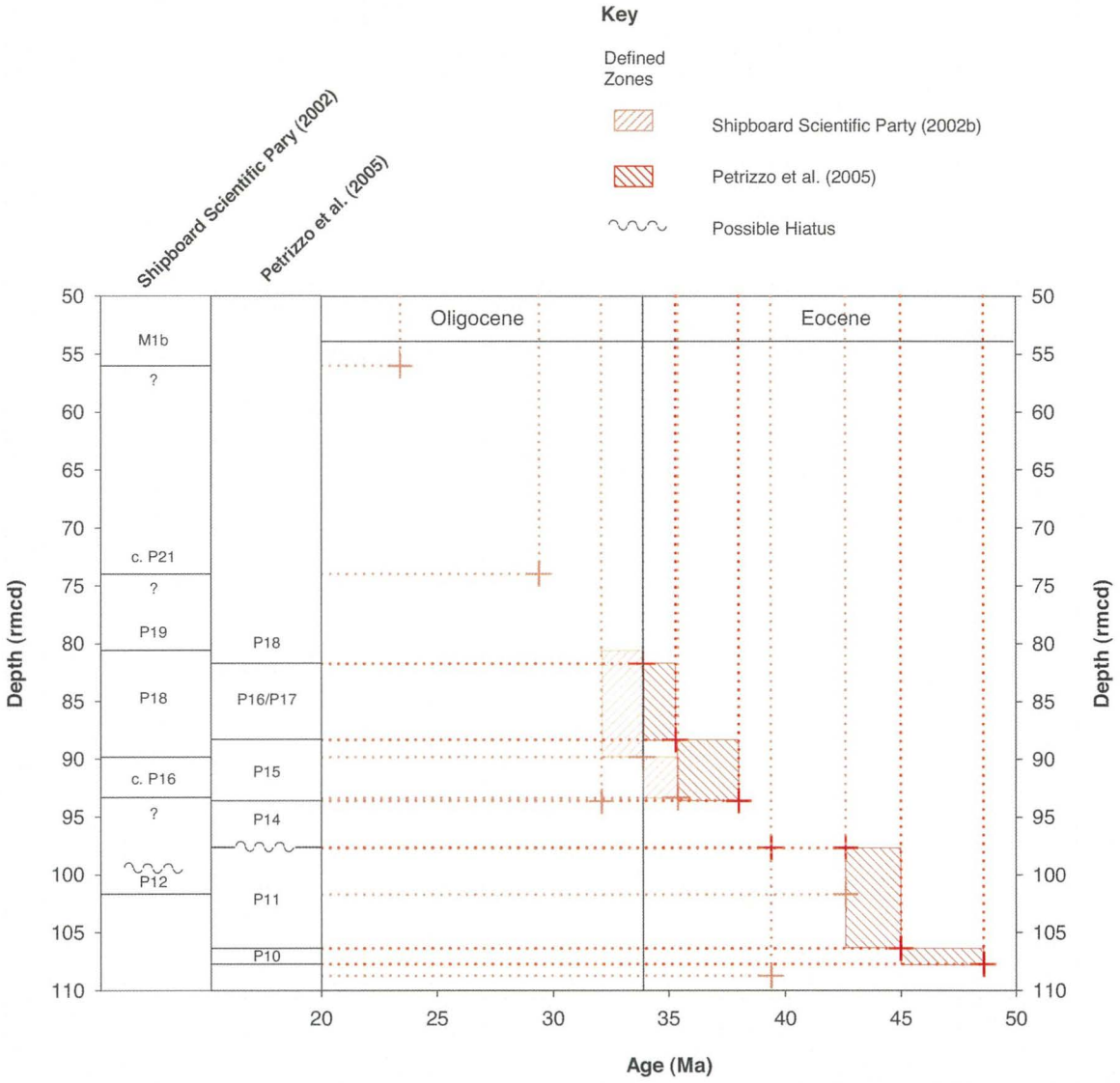

Figure 4.2: Planktonic foraminiferal biostratigraphy of Shipboard Scientific Party (2002b; pale red) and Petrizzo et al. (2005; dark red). Shaded areas delimit biozones with top and base identified. Crosshairs mark positions of planktonic foraminiferal datums. Ages interpolated onto the timescale of Luterbacher et al. (2004).

4.1.2 Calcareous nannofossils

Figure 4.3 shows Shipboard Scientific Party (2002b) and Bralower (2005) calcareous nannofossil biostratigraphies. Preservation of Palaeogene calcareous nannofossils was moderate (Shipboard Scientific Party 2002b; Bralower, 2005), thus generally better than the poor preservation of Palaeogene planktonic foraminifera (Shipboard Scientific Party 2002b; Petrizzo et al., 2005); however, samples did exhibit moderate overgrowths and some etching within the recovered Palaeogene section (Bralower, 2005). Overgrowths

masked some species (e.g. *Nannotetrina*) and made consistent interpretation of the discoaster ray form difficult, while etching removed central areas of species (e.g., *Toweius;* Bralower, 2005). Accurate biozonal positioning was also hindered by the rarity of marker species within samples (e.g. the FO of *Reticulafenestra umbilicus* for the base of biozone CP14a and the top acme of *Ericsonia subdisticha* for the base of CP16b) leading to difficulty in establishing true FO or LO depths (Bralower, 2005). Both Shipboard Scientific Party (2002b) and Bralower (2005) determined the occurrence of the majority of the low-latitude Palaeogene marker species of Bukry (1973, 1975), although the presence within a single sample (1211C-10H-6, 0–1 cm) of marker species for the bases of biozones CP13b, CP14a and CP14b suggests a hiatus or condensed interval at 97.6 rmcd (Bralower, 2005). As with Petrizzo et al. (2005), Bralower (2005) did not identify Oligocene biostratigraphic datums, thus limiting Oligocene biostratigraphy to the lower stratigraphic resolution study of Shipboard Scientific Party (2002b). Further biostratigraphic determinations were carried out by Dunkley Jones (*pers. comm.,* 2008), and these were in close agreement with those of Bralower (2005) but added a further datum, the FO of *Ismolithus recurvus* for the base of biozone CP15b (36.2 Ma) in sample 1211C-9H-6, 135–137 cm (89.72 rmcd). While not identified by Bralower (2005), positioning the base of biozone CP15b at 89.72 rmcd is very close to the depth identified for the base biozone CP15b by Shipboard Scientific Party (2002b).

For use in the determination of the depth–age relationship derived for this study, two modifications are made to the biostratigraphy of Bralower (2005). Bown (*pers. comm.* 2006) has suggested that the LO of *Discoaster barbadiensis* (the base of biozone CP16a) may have been identified by Bralower (2005) at too shallow a stratigraphic level (sample 1211C-9H-5, 102–103 cm; 87.89 rmcd). The LO of *D. barbadiensis* is based on rare specimens in samples 1211C-9H-5, 102–103 cm, -9H6, 22–23 cm and 1211A-10H-1, 105–106 cm, in the next studied sample (1211A-10H-2, 133–134 cm) the species is common. Bown (*pers. comm.* 2006) has suggested that these rare occurrences of *D. barbadiensis* are reworked specimens, with likely reworked specimens of other species (*D. multiradiatus, D. lodoensis* among others) also occurring at these sample depths. Thus for the purposes of this study, the base of biozone CP16a is identified by the last common occurrence of this species leading to a new depth of 88.80 rmcd for the base of this biozone.

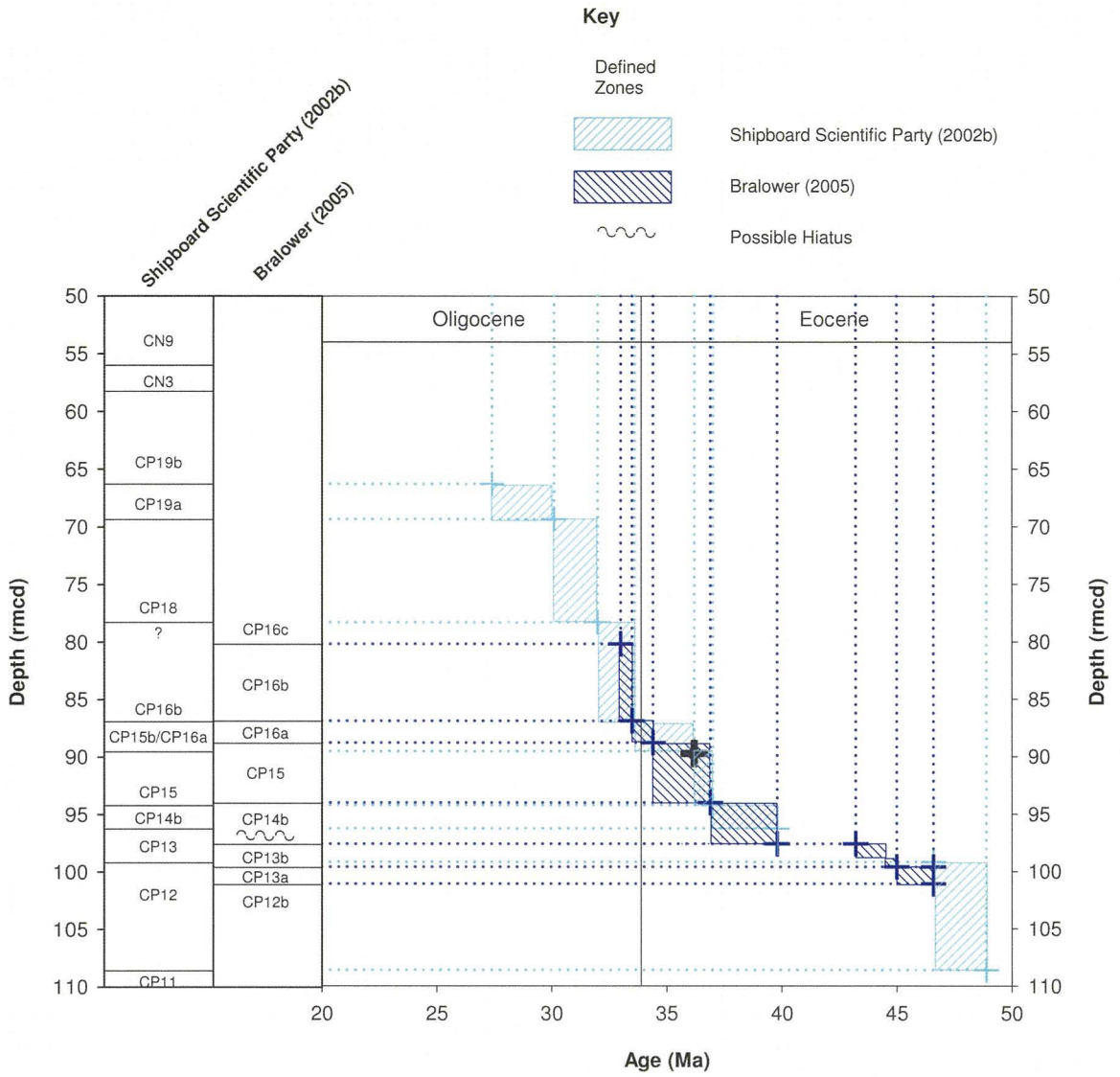

Figure 4.3: Calcareous nannofossil biostratigraphy of Shipboard Scientific Party (2002b; pale blue) and Bralower (2005; dark blue). Shaded areas delimit biozones with top and base identified. Cross hairs mark positions of identified datums, the colours as per defined zones; black crosshairs mark position of the Dunkley-Jones (*pers. comm.*, 2008) datum. Ages interpolated onto the timescale of Luterbacher et al. (2004).

The re-interpretation of the base of biozone CP16a leads to further consideration of the calcareous nannofossil stratigraphy of Bralower (2005), in particular for the base of biozone CP15, which was previously identified at 88.80 rmcd (i.e. the re-interpreted depth of the base of biozone CP16a). Identification of the base of biozone CP15 by the LO of *Chiasmolithus grandis* was based upon the presence of fragments of this species (Bralower, 2005). The age determination of the base of biozone CP15 (~36.8 Ma) at 88.60rmcd is in poor agreement with the calcareous nannofossil biostratigraphies of Shipboard Scientific party (2002b) and the planktonic foraminiferal biostratigraphy of Petrizzo et al. (2005), as well as Sr-isotope ratio derived ages developed within this study (Section 4.2). Bralower (2005) noted the likely reworking of *Discoaster multiradiatus* within the same sample as the first identification of fragments of *C. grandis* (sample 1211A-10H-5, 45–46 cm), which suggests the fragments may also be reworked. Thus, for

this study, the LO of whole specimens of *C. grandis* is used to determine the mean depth of the base of CP15, redefining the base of biozone CP15 as 94.03 rmcd. This revised depth places this biozone in much better agreement with Shipboard Scientific party (2002b) calcareous nannofossil and Petrizzo et al. (2005) planktonic foraminiferal biostratigraphies as well as this study's Sr-isotope ratio derived ages.

4.2 Sr-isotope chemostratigraphy

The absence of detailed Oligocene biozonation limits the potential of biostratigraphy to resolve a robust depth–age model for ages younger than the EOB, i.e. shallower than ~88 rmcd. This study's geochemical proxy dataset covers the stratigraphic range between 60 and 100 rmcd, thus a depth–age calibration is necessary for depths shallower than 88 rmcd, so further depth–age correlation was required prior to depth–age model development. One method identified to provide depth–age constraint was that of Sr-isotope chemostratigraphy, making use of the well-documented variation through geological time of the marine Sr-isotope ($^{87}Sr/^{86}Sr$) record to establish sediment age. Sr-isotope variation across the EOB has been discussed previously (Chapter 2); in brief, the Sr-isotope ratios curve, as recorded by marine carbonates, shows a distinct inflection in the latest Eocene, providing a well-constrained Oligocene marine Sr-isotope curve that offers unique numerical solutions (Figure 4.4). Prior to the latest Eocene, however, Sr-isotope ratios permit derivation of multiple age solutions (Figure 4.4; see example Sr-isotope ratio measured for 95.49 rmcd), with determination of the most likely numerical age solution requiring further independent age constraint.

4.2.1 Sr-isotope ratio methodology

A Sr-isotope chemostratigraphic record was developed for Site 1211 through analysis of mixed species of planktonic foraminifera and <38 μm fine-fraction carbonate samples. Analyses took place in two batches. A ten sample (planktonic foraminiferal) pilot study was initially undertaken to establish the suitability of Site 1211 foraminiferal Sr-isotope data for the purpose of providing a Sr-isotope chemostratigraphy. Subsequently, a further 27 samples (13 of planktonic foraminifera and 14 of <38 μm fine-fraction carbonate) were analysed to provide coverage over the total range of Site 1211 sampling (60–100 rmcd).

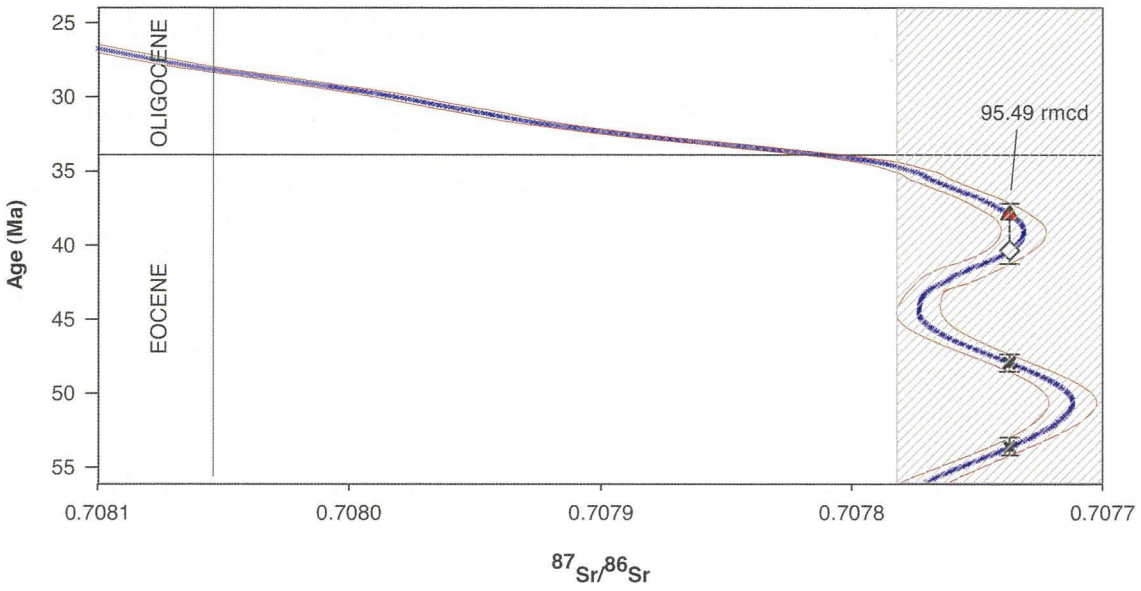

Figure 4.4: Eocene–Oligocene Sr-isotope curve (blue line) with 95% confidence interval (red lines) taken from the "Look-Up Table Version 4: 08/04" of Howarth and McArthur (1997) and McArthur et al. (2001). Shaded area indicates Sr-isotope ratios with more than one unique numerical age solution. The measured Sr-isotope ratios for 95.49 rmcd are plotted to demonstrate such a non-unique age. The youngest age (red infilled triangle) is the most likely solution as determined by the Site 1211 biostratigraphy (Shipboard Scientific Party, 2002b; Bralower, 2005; Petrizzo et al., 2005); the positioning of this Sr-isotope value on the curve leads to an asymmetric error biased towards older ages and a second possible numerical age determination within the 95% confidence limits (open diamond). Crosses mark the further unlikely age solutions for this example measured Sr-isotope ratio.

Selection of samples (Figure 4.5) was guided by the <38 μm fine-fraction $\delta^{18}O$ record and aimed to provide improved age constraint across the entire range of sampling, in combination with detailed records across the positive steps evident in the oxygen-isotope record (between 85 and 90 rmcd). For the Sr-isotope ratio analyses, samples consisted of ~200 mixed planktonic foraminifera picked from the 250–350 μm size fraction. For sample 1211C-10H-1, 120–122 cm (91.64 rmcd), there were insufficient planktonic foraminifera in the 250–350 μm size fraction so planktonic foraminifera from the 150–250 μm size fraction were also picked to obtain sufficient specimens. Prior to analyses foraminifera were broken open with a pin, then washed in a 1.5 ml micro-centrifuge tube in 0.5 ml of 18.2 MΩ H_2O, with ultrasonification for one minute before removal of the supernatant. This washing step was repeated until the supernatant was free of visual contaminants.

Across the interval ~88–93 rmcd, planktonic foraminifera were not present in sufficient quantities, as described above, and samples were taken from the <38 μm fine-fraction carbonate. Accurate age constraint of this stratigraphic interval was considered particularly important due to the unexpected negative step in <38 μm fine-fraction oxygen-isotope ratios observed at ~89 rmcd, a feature not seen in existing records, e.g. see the benthonic foraminiferal $\delta^{18}O$ compilation curve of Zachos et al. (2001; Figure 1.1). Further <38 μm

fine-fraction samples were taken from the same stratigraphic levels as planktonic foraminiferal analyses to enable assessment of any differences in Sr-isotope values between these two carbonate substrates. Sr was separated using Dowex AG50 ion exchange columns and then measured on a Thermo-Electron Triton mass spectrometer at the NIGL. Samples were run with the NBS987 standard and are quoted relative to a preferred $^{87}Sr/^{86}Sr$ value of 0.710250 (Miller, *pers. comm.*, 2009); measured standard values for the pilot study were 0.710282±0.000002 (1 sigma, N=9) and for the main sample batch 0.710255±0.000002 (1 sigma, N=17) prior to normalisation. The main sample batch data Sr-isotope ratio fall closer to the preferred standard value because an improved collection algorithm was used (Miller, *pers. comm.*, 2009). Internal sample precisions were ±0.000005, or better, for all samples.

4.2.2 Sr-isotope results

Foraminiferal $^{87}Sr/^{86}Sr$ isotope ratios were converted to numerical ages (Figure 4.6) using "Look-Up Table Version 4: 08/04" of Howarth and McArthur (1997) and McArthur et al. (2001). This table assigns a best-fit age, as well as 95% confidence limits, for the Sr-isotope curve throughout the Phanerozoic (Eocene and Oligocene are shown in Figure 4.4). For samples below ~90 rmcd (~36 Ma), multiple best-fit ages exist due to the non-unique age solutions that result from the variation in the Sr-isotope curve; ratios between 0.7077 and 0.7078 allowing several numerical ages to be assigned to a single measured Sr-isotope ratio (shaded area in Figure 4.6). In the first instance, where multiple numerical age solutions exist the simplest stratigraphically consistent age is assumed, i.e. sample age must increase with depth thus the next oldest sample age is chosen. For completeness all alternative ages are plotted in Figure 4.6.

The Sr-isotope value measured for the sample at 95.49 rmcd has a much greater 95% confidence limit range than the other Sr-isotope ratios, due to the shape of Sr-isotope curve as shown on Figure 4.4. Two data points (at 94.19 and 96.39 rmcd) have age solutions that would require a substantial (~10 Myr) hiatus at Site 1211, which based on the earlier discussion of biostratigraphic data is unlikely. On this basis these anomalous Sr-isotope data have been discounted from the depth–age model (filled blue diamonds on Figure 4.6).

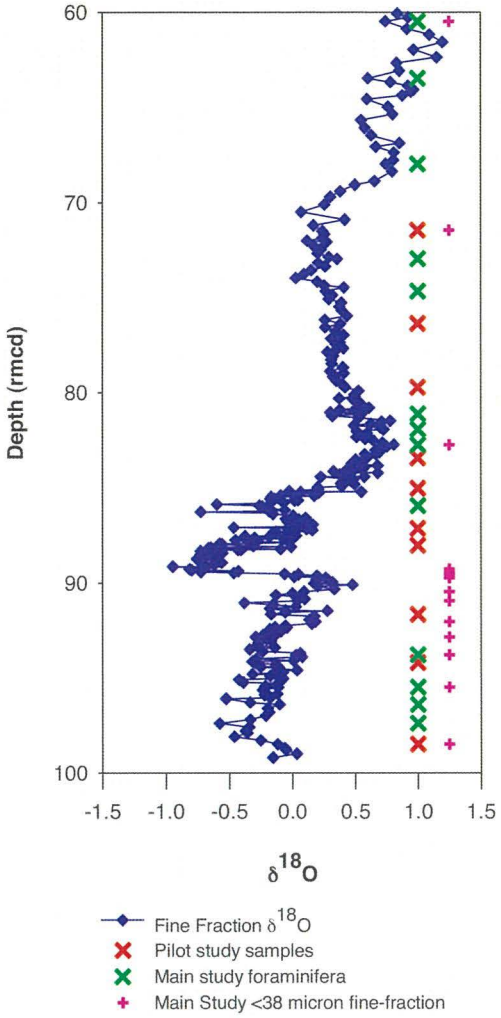

Figure 4.5: Sampling strategy for Sr-isotope ratio analyses, with <38 µm fine-fraction $\delta^{18}O$ used to aid selection.

Comparison of <38 µm fine-fraction carbonate to foraminiferal carbonate $^{87}Sr/^{86}Sr$ isotope ratios show that the offset is not consistent between the fractions, varying between -0.000008 (error ±0.000003) and 0.000040 (error ±0.000003). Plotting the <38 µm fine-fraction $^{87}Sr/^{86}Sr$ ratios against foraminiferal $^{87}Sr/^{86}Sr$ ratios results in a regression that does not lie parallel to a one-to-one relationship (Figure 4.7). As such, without a consistent offset between the two carbonate substrates, it has not been possible to use the <38 µm fine-fraction Sr-isotope data to establish either numerical ages for samples or the expected stratigraphic trends within the Sr-isotope values. Consequently, only foraminiferal $^{87}Sr/^{86}Sr$ isotope ratios have been considered for depth–age model purposes.

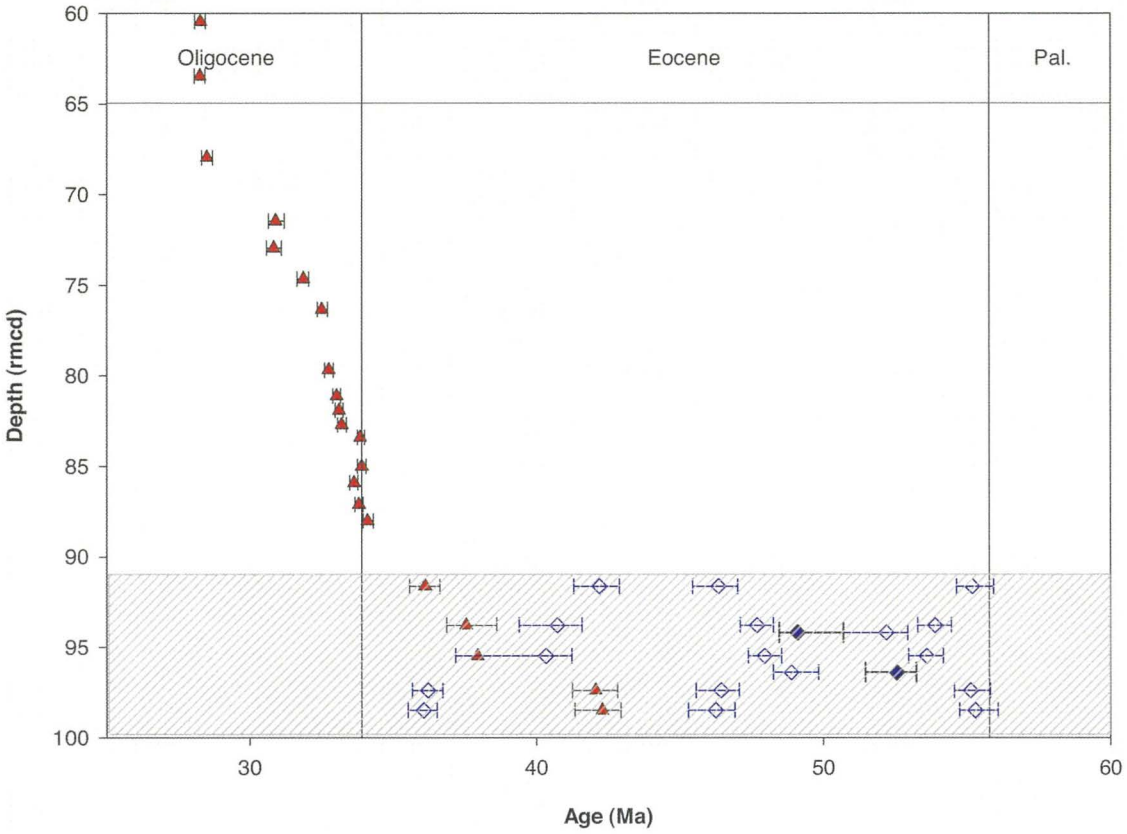

Figure 4.6: Sr-isotope ratio derived numerical ages for Site 1211 planktonic foraminiferal Sr-isotope data, using "Look-up Table Version 4: 08/04" of Howarth and McArthur (1997) and McArthur et al. (2001). Red triangles are the most likely numerical age solution. Open diamonds are alternative solutions, blue filled diamonds are anomalous age determinations for 94.19 and 96.39 rmcd. Error bars correspond to 95% confidence limits. The shaded zone marks the Site 1211 depth range where multiple numerical age solutions are possible, whereas it can be seen that the very latest Eocene and Oligocene have unique numerical age solutions. See text for more detailed discussion.

4.3 Depth–age model development

The first step of depth–age model development carried out was to establish which of the Sr-isotope values with multiple numerical age assignments were in agreement with the biostratigraphic data. To achieve this objective, Sr-isotope ratio numerical age assignments were plotted along with all biostratigraphic datums (Figure 4.8); Sr-isotope derived ages were deemed reliable if the derived ages, or range of 95% confidence intervals, overlapped with biostratigraphic datum assignments. If Sr-isotope ratio derived age or 95% confidence intervals did not satisfy this criterion then they were rejected.

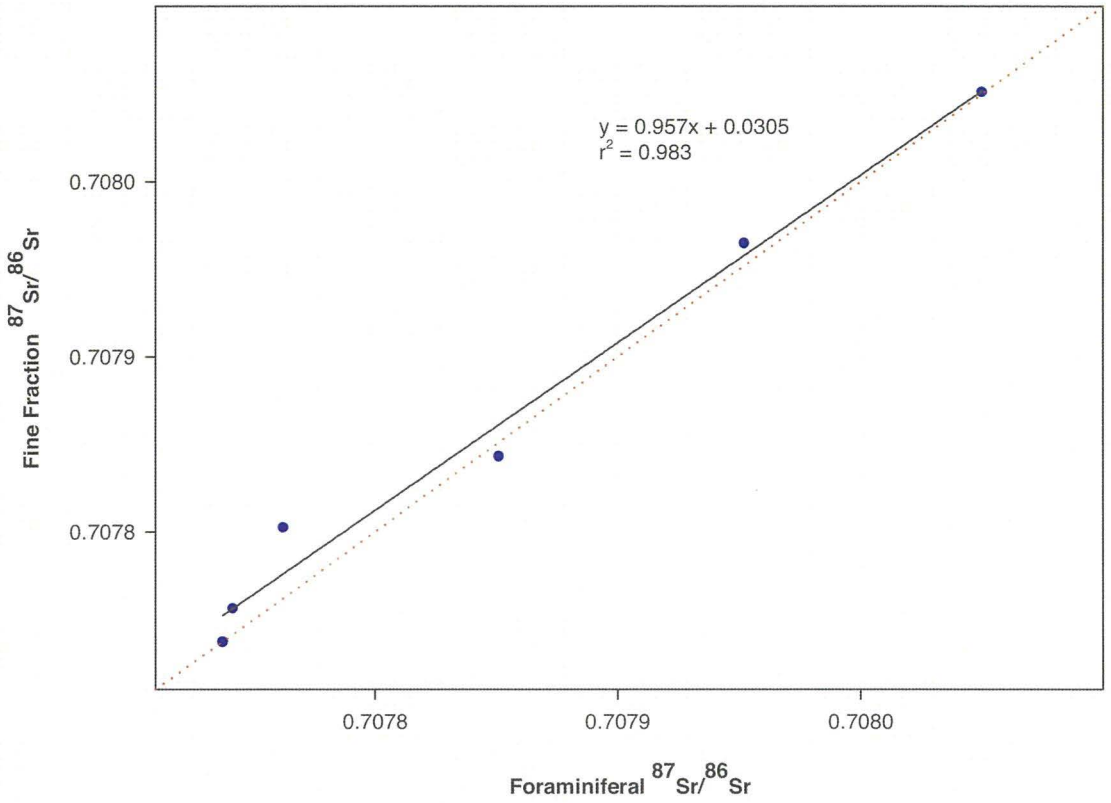

Figure 4.7: Cross plot of <38 µm fine-fraction carbonate Sr-isotope ratios versus planktonic foraminiferal Sr-isotope ratios for Site 1211 (blue circles). Solid blank line shows the regression through the Sr-isotope values. Dotted red line indicates a 1:1 relationship. It can be seen that the regression line does not lie parallel to the 1;1 line showing a variable offset between carbonate substrates.

With the identification of Sr-isotope derived ages for use within the depth–age model, the depth–age model was developed using these Sr-isotope numerical age assignments and the biostratigraphies of Bralower (2005) and Petrizzo et al. (2005). These biostratigraphic datasets have been preferred to those of Shipboard Scientific Party (2002b), due to their higher stratigraphic resolution. Construction of the depth–age model was undertaken by visually identifying trends or agreement within the different datasets, and then considering each stratigraphic interval individually. Figure 4.9 provides a guide to the intervals and sedimentation rates described in the text.

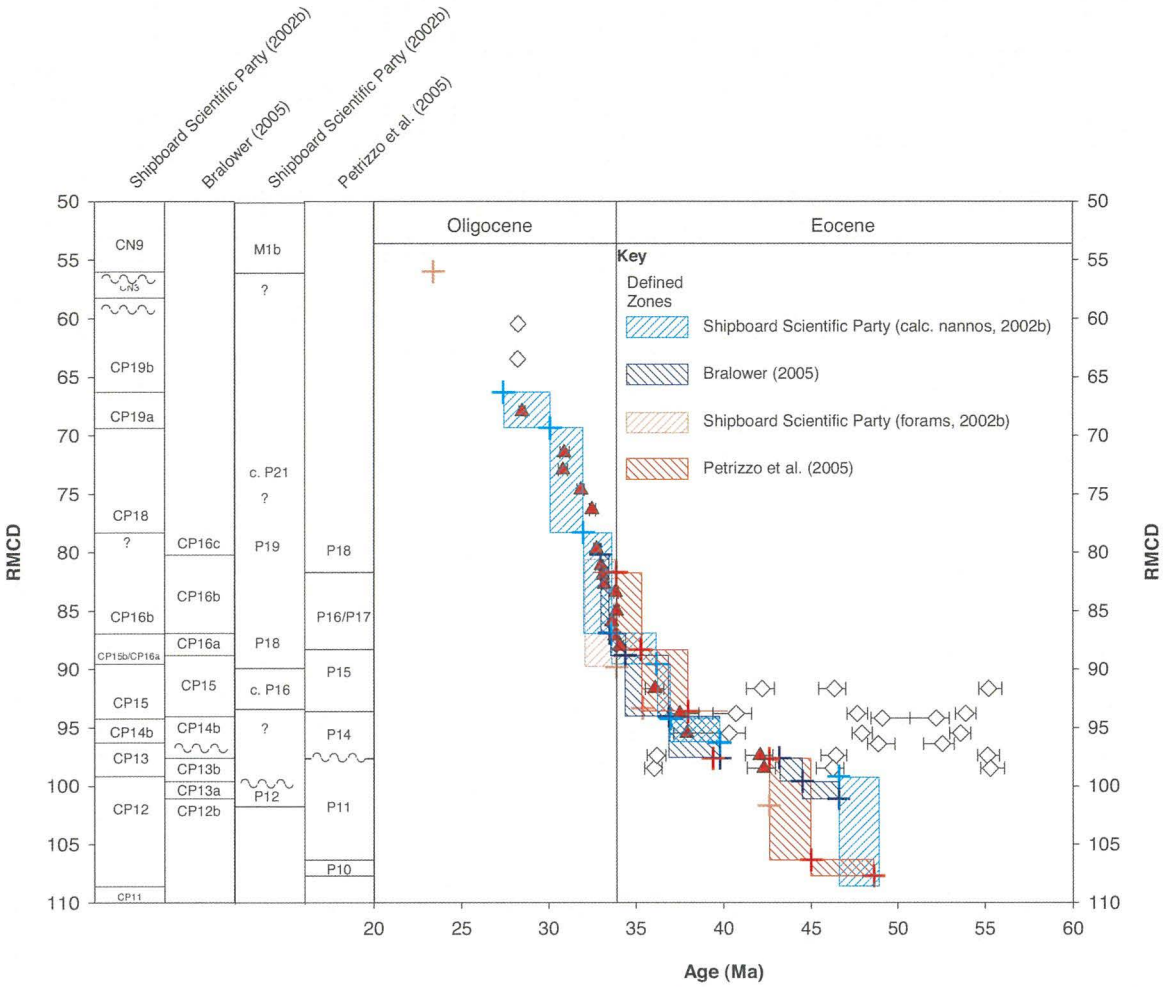

Figure 4.8: Plot of Shipboard Scientific Party (2002b), Bralower (2005) and Petrizzo et al. (2005) biostratigraphic data combined with Sr-isotope derived numerical ages. Biostratigraphy is as shown in Figures 4.2 and 4.3. Red infilled triangles are Sr-isotope values in agreement with the biostratigraphic data, whereas unfilled diamonds are incompatible with biostratigraphic data.

With the identification of Sr-isotope derived ages for use within the depth–age model, the depth–age model was developed using these Sr-isotope numerical age assignments and the biostratigraphies of Bralower (2005) and Petrizzo et al. (2005). These biostratigraphic datasets have been preferred to those of Shipboard Scientific Party (2002b), due to their higher stratigraphic resolution. Construction of the depth–age model was undertaken by visually identifying trends or agreement within the different datasets, and then considering each stratigraphic interval individually. Figure 4.9 provides a guide to the intervals and sedimentation rates described in the text.

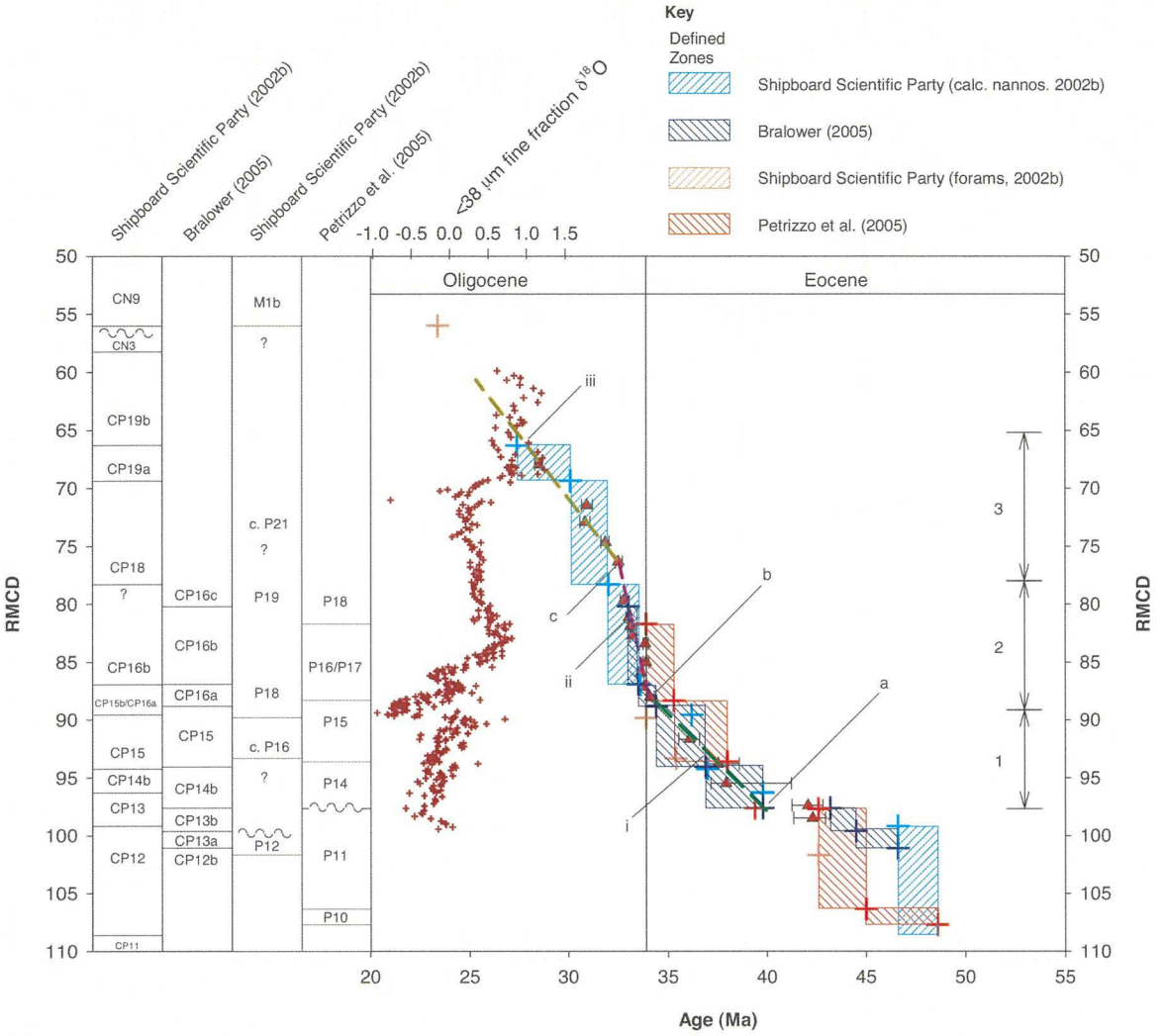

Figure 4.9: "Working" depth–age model, with biostratigraphic and Sr-isotope ratio data as in Figures 4.2, 4.3 and 4.7. Three stratigraphic intervals are labelled 1, 2 and 3, with contrasting sedimentation rates (dashed/dotted lines) labelled i, ii and iii. Labels a,b and c correspond to points of sedimentation rate inflection. Also plotted are < 38 µm fine-fraction $\delta^{18}O$ isotope data generated by this study; see Chapter 6.2 for further consideration of these latter data.

An obvious feature within Figure 4.9 is an apparent mismatch in planktonic foraminiferal and calcareous nannofossil age assignments between 98 and 110 rmcd. At ~97.60 rmcd (labelled a in Figure 4.8) there is agreement between the Bralower (2005) and Petrizzo et al. (2005) biostratigraphies for a condensed interval and/or hiatus in sedimentation; within a few centimetres of this depth biostratigraphic markers for the bases of planktonic foraminiferal biozones P12 (42.6 Ma; 97.66 rmcd) and P14 (39.4 Ma; 97.62 rmcd), and for the bases of calcareous nannofossil biozones CP13c (43.2 Ma; 97.60 rmcd), CP14a (41.6 Ma; 97.60 rmcd) and CP14b (39.8 Ma; 97.60 rmcd) were identified. The stratigraphic proximity of these datums suggests that between 43.2 to 39.4 Ma, sedimentation at Site 1211 was virtually non-existent or subject to post depositional erosion/dissolution and removal. During this study, geochemical proxy data collected at depths deeper than 97.6 rmcd were limited to only a few data points, especially for the key foraminiferal stable-

isotope and element/Ca ratio records, thus the inconsistent depth–age relationships below 97.6 rmcd have not been resolved.

With the base of this study's depth–age model established at 97.6 rmcd, three distinct stratigraphic intervals with different sedimentation rates are apparent (Figure 4.9): interval 1 (Late Eocene) between 97.6 and ~88 rmcd; interval 2 (latest Eocene to earliest Oligocene) between ~88 rmcd and ~77 rmcd, and interval 3 (Early Oligocene) between ~77 and ~65 rmcd. It can be seen that sedimentation rates increased at the EOB and into the earliest Oligocene. Sedimentation rates and thus depth–age relationships for each of the three intervals have been determined by regressions through all relevant depth–age datums. For stratigraphic interval 1, the relationship was based on datums between 88.02 and 97.6 rmcd; for stratigraphic interval 2, datums between 88.02 and 76.35 rmcd; for stratigraphic interval 3, datums above 76.35 rmcd. Sedimentation rate intervals are labelled i, ii and iii respectively, in Figure 4.9. At depths less than 65 rmcd, there are insufficient data to establish robust depth–age relationships such that the depth–age model was terminated at this stratigraphic level. The only modifications to the datums used were the inclusion of the base of biozone CP15b at 89.72 rmcd (Dunkley-Jones, *pers. comm.,* 2008) in the derivation of stratigraphic interval 1 and the omission, from the derivation of stratigraphic interval 2, of the LO of *Hantkenina* spp. (the base of biozone P18) of Petrizzo et al. (2005). Omission of the LO of *Hantkenina* spp. is based on two lines of evidence: first that the depth control on the datum is poor (± ~3 m) and second that, identification of the marker at this depth is not in agreement with observations made during this study, which positions the LO of *Hantkenina* spp. at 86.89 rmcd, between sample 1211C-9H-5, 45–47cm and -9H-5, 65–67 cm. Thus, this study's determination of the base of biozone P18 is used to calculate the sedimentation rate and depth–age relationship of stratigraphic interval 2.

Accurate identification of the inflection point between stratigraphic intervals 1 and 2 is paramount to the development of the Site 1211 depth–age model. To facilitate identification of this point, the fine-fraction $\delta^{18}O$ record from this study was plotted with the bio- and chemo-stratigraphic datums (dark red symbols in Figure 4.9), and the apparent inflection in sedimentation rate (labelled b in Figure 4.9) occurs close to the initiation of the increase in $\delta^{18}O$ values. The sedimentation rate and increase in $\delta^{18}O$ occur at depths that correspond to the LO of *D. barbadiensis* (88.80 rmcd; base of biozone CP16a; 34.4

Ma). However, as this LO marker is a relatively poorly constrained biostratigraphic datum (see discussion in Section 4.1.2), this study has used the intercept of the depth–age relationships for stratigraphic intervals 1 and 2 to establish the position of the sedimentation rate inflection point (labelled b in Figure 4.9). Similarly, positioning of the inflection in sedimentation rates between stratigraphic intervals 2 and 3 (labelled c in Figure 4.9) is also calculated by the intercept of the two depth–age relationships. The resulting depth–age relationships and sedimentation rates are summarised in Table 4.1, along with the corresponding age and depth ranges.

Section	Depth Range (rmcd)		Age Range (Ma)		Regression Equation		r^2
	min	max	min	max	gradient	intercept	
1	87.48	97.6	34.07	39.62	1.82	25.51	0.92
2	74.7	87.48	32.07	34.07	6.39	-130.07	0.88
3	65	74.7	27.07	32.07	1.94	12.52	0.94

Table 4.1: Depth and age ranges and regression equations for depth–age model shown in Figure 4.8.

4.4 Depth–age model refinement

Subsequent to the development of the depth–age model described above, Site 1211 benthonic foraminiferal stable-isotope records were compiled (as discussed in Section 5.5.4) and compared to the benthonic foraminiferal stable-isotope records of Site 1218 (Section 6.2.3, Lear et al., 2004; Coxall et al., 2005) to facilitate final "tuning" of the Site 1211 depth–age relationships. Tuning the depth–age model of Site 1211 to that of Site 1218 was undertaken to provide a further line of evidence for the interpretation of Site 1211 model rather than an absolute correction; thus the subsequent Site 1218 to 1211 tie-points have been considered with same merit as the biostratigraphy and Sr-isotope stratigraphy to produce a refined depth–age model. The benthonic foraminiferal stable-isotope records from Site 1218 are well suited for "tuning" of the Site 1211 depth–age relationships primarily as a result of the high-resolution nature of the study (~2.5 kyrs between data points) and the astronomical tuning of those stable-isotope records to calculated Oligocene orbital parameters (Supplementary material in Palike et al., 2006), which led to an exceptionally well-constrained depth–age model for Site 1218. Numerical ages for Site 1218 were converted from the astronomically tuned site model to the Gradstein et al. (2004) timescale by interpolating between geomagnetic polarity chron ages used by Gradstein et al. (2004) and those for the Site 1218 (Supplementary material in Palike et al., 2006). The benthonic foraminiferal stable-isotope record for Site 1218 was plotted against these new ages and tie-points were identified between the 5-point running means for Sites 1211 (plotted against rmcd) and 1218 (Figure 4.10; Table 4.2).

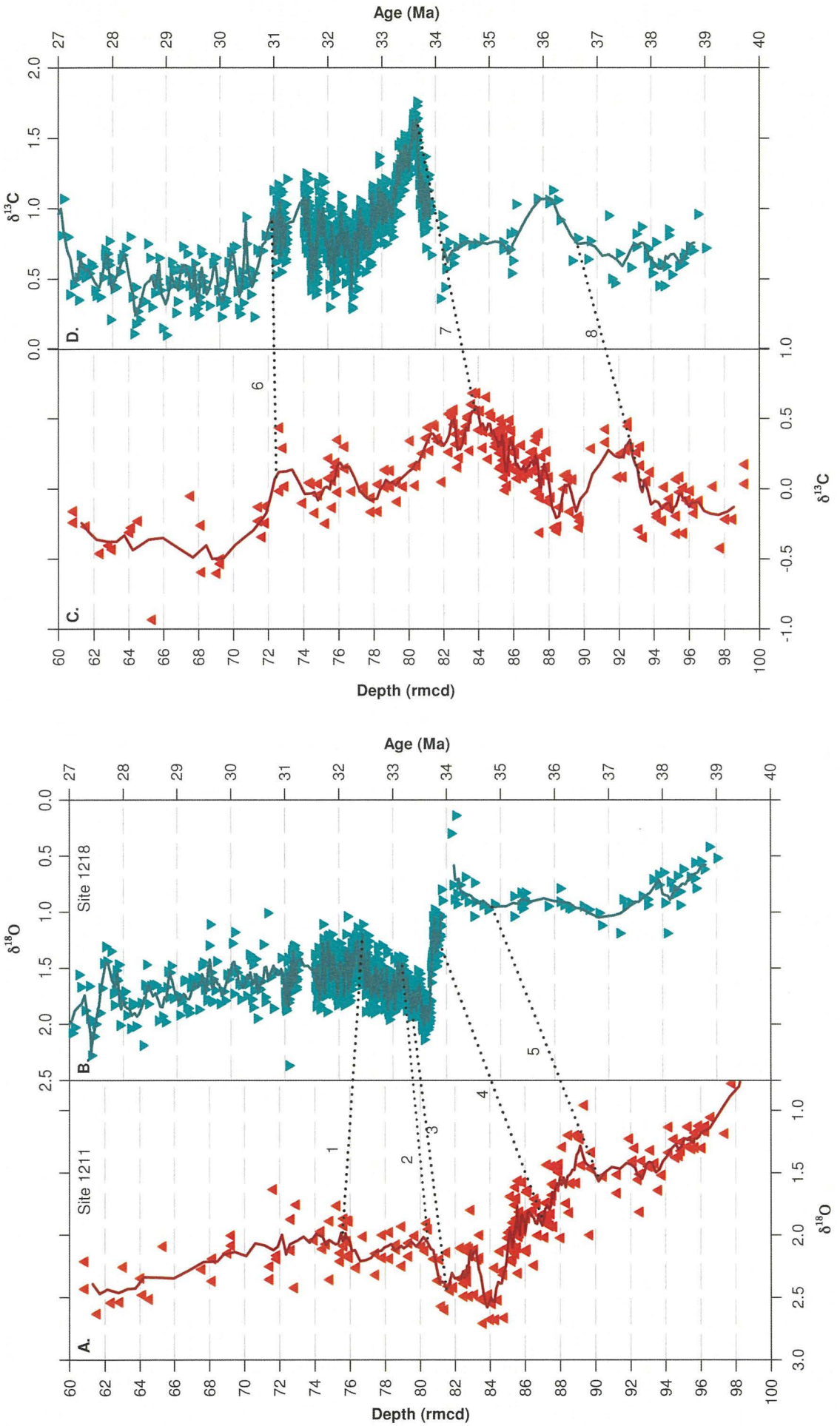
Age (Ma)
Depth (rmcd)
δ18O
δ13C
Site 1211
Site 1218
A.
B.
C.
D.
1
2
3
4
5
6
7
8

Figure 4.10: Plots of benthonic foraminiferal stable-isotope ratios, including 5-point running means for Sites 1211 (A and C) and 1218 (B and D; Lear et al., 2004; Coxall et al., 2005), plotted on the Gradstein et al. (2004) geologic timescale. Tie-points (numbered) were identified based on correlation of the 5-point running means as described in Table 4.2. Compilation of the benthonic foraminiferal stable-isotope records is detailed in Section 5.5.4, whilst Site 1218 data are discussed in Section 6.2.3.

Tie-points

	Site 1211	Site 1218	Description
1	75.49	32.4364	Minimum at ~75.5 rmcd in $\delta^{18}O$
2	80.188	33.1808	Minimum following clear decrease between 81 to 80 rmcd in $\delta^{18}O$
3	81.5	33.3365	"Oi-1b" maximum in $\delta^{18}O$
4	86.976	33.8503	Maximum prior to pause in $\delta^{18}O$ increase from 89 to 84 rmcd
5	90.172	34.8234	Minor peak prior to a ~0.2 negative shift in $\delta^{18}O$ at ~90 rmcd
6	72.59	31.0795	Initiation of major decrease in $\delta^{13}C$ at ~72.2 rmcd
7	83.838	33.7194	Peak $\delta^{13}C$
8	93.32	36.6345	Initiation of increase of ~0.5 in $\delta^{13}C$ at ~93 rmcd

Table 4.2: Identified tie-points (numbered on Figure 4.10) between the benthonic foraminiferal stable-isotope records of Sites 1211 (rmcd) and Site 1218 (numerical ages).

The new depth–age tie-points developed by correlation with the Site 1218 isotope dataset then were integrated into the previously described depth–age model (Figure 4.11). Final depth–age relationship segments were chosen based on the identification of the key trends in all of the depth-age control points, and the range of each "trend" was determined by assessing the most robust groupings of depth–age tie-points, based on r^2 values. Regressions were then calculated for each of these depth-age relationships (Table 4.3). All data shown in Figure 4.11 were assumed to be of equal significance and no omissions were made. As described in Section 4.3, inflections between the key depth–age trends were positioned through the calculation of the intercepts between the derived regression equations.

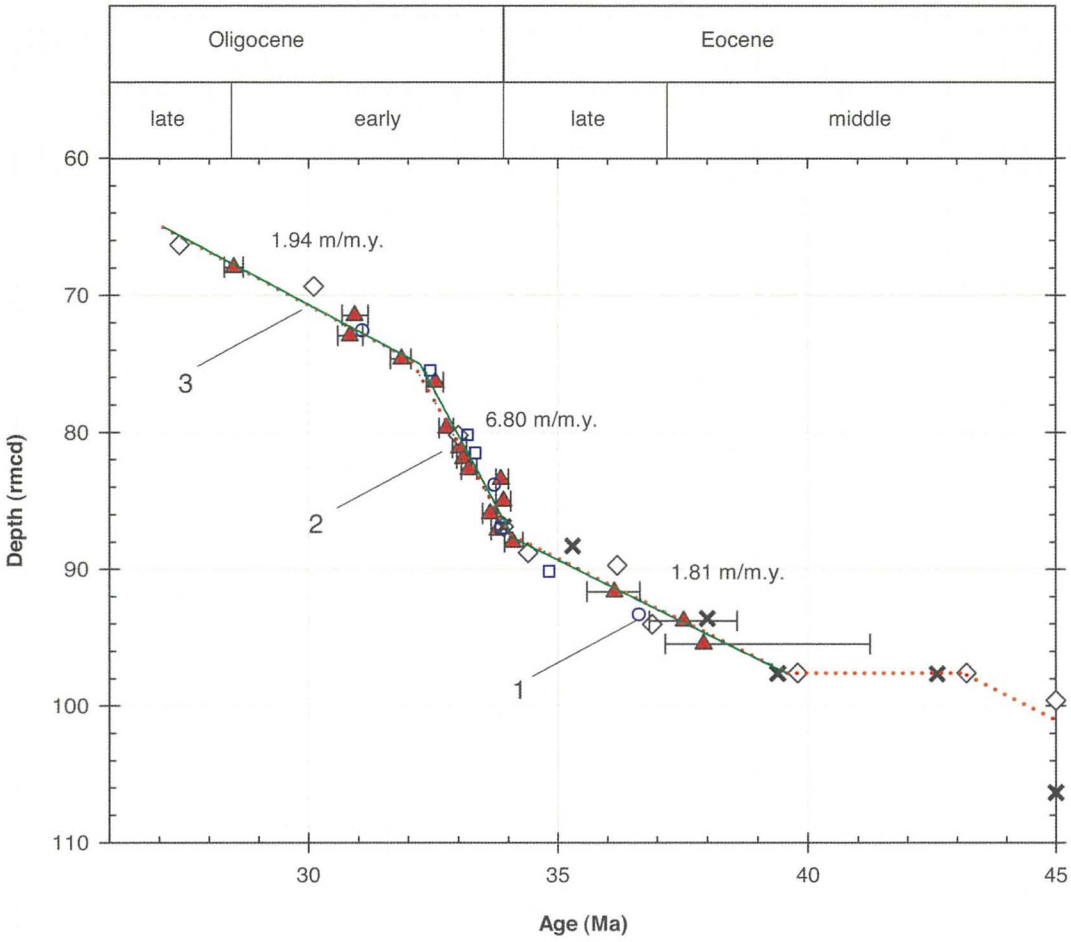

Figure 4.11: The depth–age relationships for Site 1211 following incorporation of the depth-age tie-points determined from correlation of the Site 1211 benthonic stable-isotope records with those of Site 1218 (Lear et al., 2004; Coxall et al., 2005). Dark green solid lines show the revised "tuned" depth–age relationships, whereas red dotted lines show the untuned depth–age relationships based solely on Site 1211 data. Diamonds are calcareous nannofossil datums. Crosses are planktonic foraminiferal datums. Triangles are Sr-isotope derived ages (with 95% confidence intervals). Squares and circles are Site 1218 $\delta^{18}O$ and $\delta^{13}C$ depth–age tie-points respectively (Table 4.2).

Both the "tuned" and "original" depth–age relationships are plotted in Figure 4.11 and reveal only minor differences between the two interpretations. The inclusion of stable-isotope ratio based tie-points leads to a small increase in the predicted sedimentation rates across the EOB (from 6.4 to 6.8 m/m.yrs), as well as increases in the r^2 value for each stratigraphic interval with a unique depth–age relationship. The "tuning" of the depth–age relationships also can be observed to improve the correlation of the Site 1211 and 1218 stable-isotope records (Figure 4.12), although some discrepancies still remain (see Section 6.2.3 for related discussion). The "tuned" age model was used to determine numerical ages for samples in subsequent chapters.

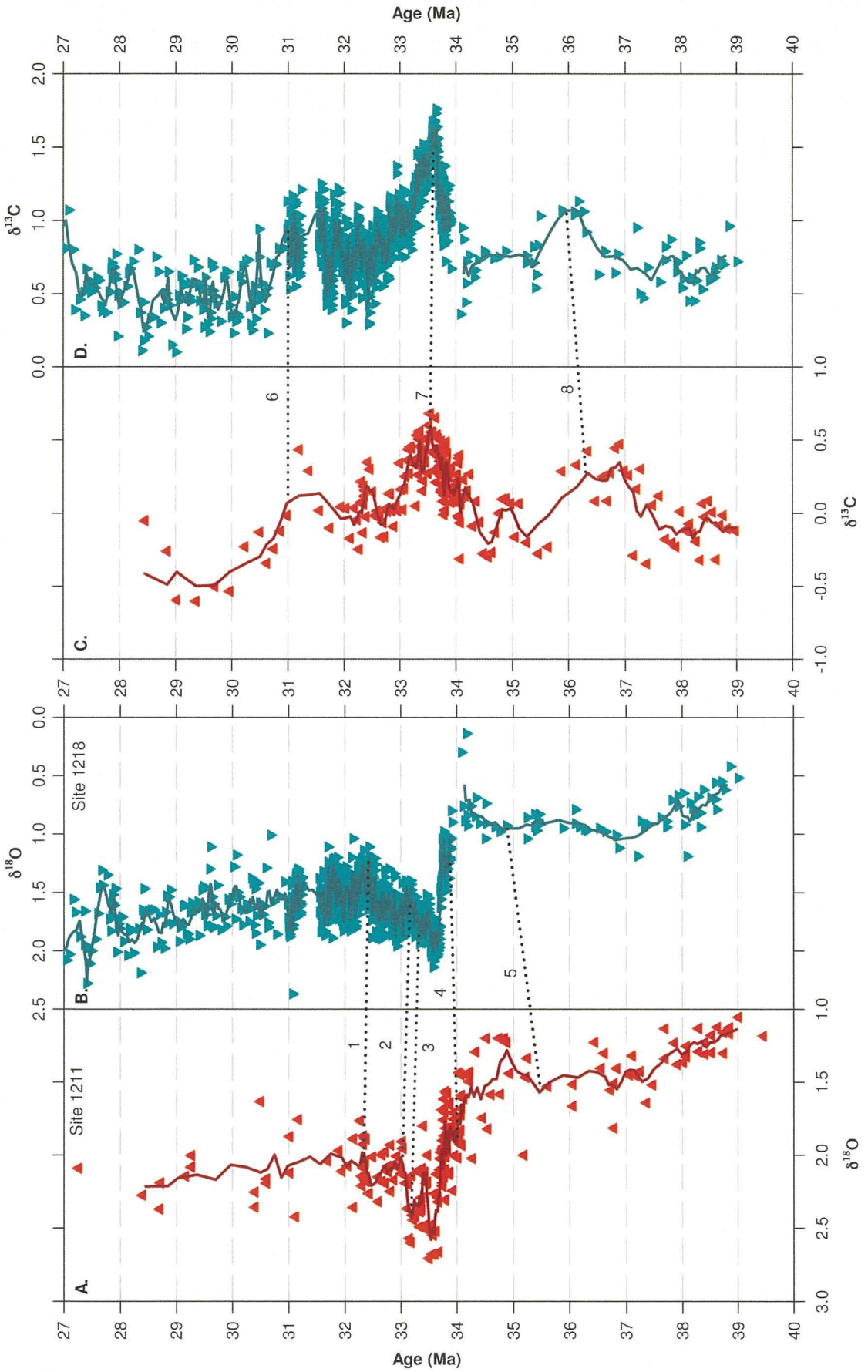
Age (Ma)
A.
Site 1211
B.
Site 1218
C.
D.
δ18O
δ13C
1
2
3
4
5
6
7
8

Figure 4.12: Benthonic foraminiferal stable-isotope records for Site 1211 (A and C) and 1218 (B and D) following "tuning" of the Site 1211 depth–age model to the Site 1218 stable-isotope ratio data. It can be observed that correlation between the records is not exact as the tie-points are integrated with the biostratigraphic and chemostratigraphic depth-age markers and not used as an absolute correction. Reasons for the discrepancies between Sites 1211 and 1218 are discussed in Section 6.2.3. Numbered tie-points correspond to those described in Table 4.2 and shown on Figure 4.10.

Section	Depth Range (rmcd)		Age Range (Ma)		Regression Equation		r^2
	min	max	min	max	gradient	intercept	
1	87.715	97.6	34.03	39.57	1.81	26.072	0.95
2	75.02	87.715	32.24	34.03	6.8	-144.12	0.89
3	65	75.02	27.07	32.24	1.94	12.45	0.94

Table 4.3: Depth and age ranges and associated regression equations and statistics for the depth–age model shown in Figure 4.11.

Chapter 5: Geochemical proxy data

This chapter describes the geochemical proxy data determined by this study. It is broken down into sections relating to each of the datasets collected, dealing with the sediment proxies first (% sand fraction, % calcium carbonate and scanning X-ray fluorescence data, colour reflectance, magnetic susceptibility), followed by the <38 μm fine-fraction stable-isotope data, along with SEM photomicrographs from across the stratigraphic range of the study, the latter to assess preservation. Benthonic and planktonic foraminiferal stable-isotope data follow, with further SEM photomicrographs of key species (*Catapsydrax unicavus, Nuttaloides truempyi, Oridorsalis umbonatus* and *Turborotalia ampliapertura*) also described in the context of preservation. Benthonic and planktonic foraminiferal element/Ca ratio data are then described. All data are presented against both the revised metres composite depth (rmcd) scale of Westerhold and Röhl (2006) and numerical ages determined using the depth–age model developed in Chapter 4. Data from Hole C are plotted and considered as a single dataset for the numerical age plots rather than the use of a "spliced" section, except for the continuously scanned XRF, L* reflectance and magnetic susceptibility datasets. Data was presented in this way to produce the most complete single body of data to aid subsequent interpretation and discussion. Data from Holes A and B is also plotted but not considered in Chapter 6. The calcareous nannofossil biostratigraphy of Bukry (1973, 1975), as modified by Okada and Bukry, 1980), is also shown as a reference between depth and numerical age plots. Stable-isotope and element/Ca ratio datasets are described using 5-point running averages and associated 95% confidence intervals to help identify the key trends.

5.1 % sand fraction (>63 μm)

Percent sand fraction is plotted against rmcd and numerical age in Figure 5.1 (A and B, respectively). The bulk of the data are from Hole C (60.0–100.0 rmcd), with gaps between cores filled with data from Hole A (~68.0–73.0 rmcd and ~80.0–84.0 rmcd). Limited data from Holes A and B also exist across the range ~85.0–96.0 rmcd. All of the data plot in a coherent manner, with no offsets evident between holes.

The % sand fraction varies between ~0.1 and ~3.5 %, with maximum values during calcareous nannofossil biozone CP13b (~99.0 rmcd, outside of the depth–age model but older than 43.0 Ma) and Early Oligocene biozones CP16c/CP17 (~80.0 rmcd; ~33.0 Ma).

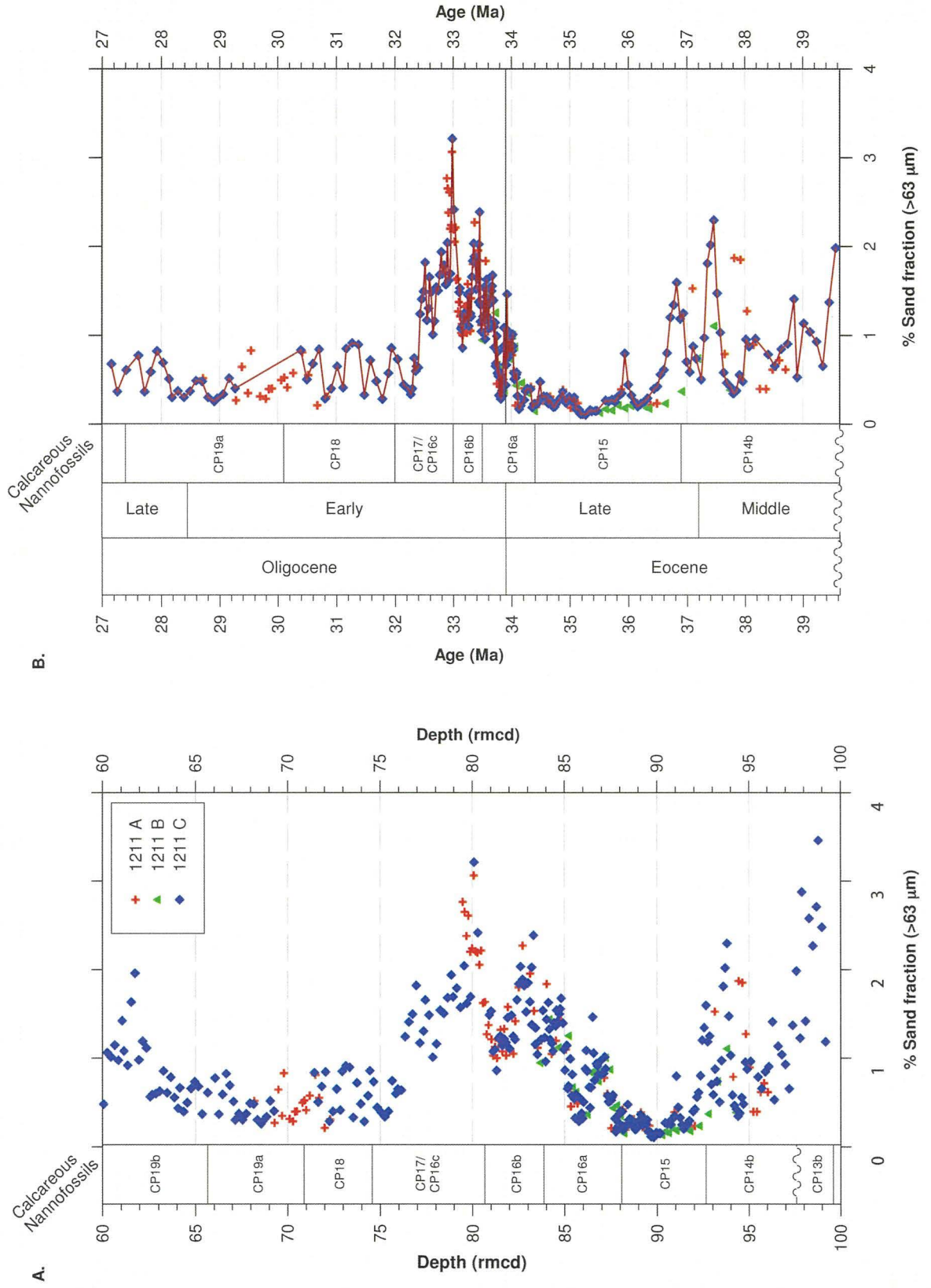

Figure 5.1: % sand fraction versus depth (A) and numerical age (B). Data from all three Site 1211 holes are plotted and show that the trends and variation in % sand fraction are common between them, thus data are interpreted as one group (dark red line in panel B).

Minimum values were during Late Eocene biozone CP15 (~92.0 to 88.0 rmcd; 36.5 to 34.2 Ma). % sand fraction ranged between ~0.5 and ~2.25 % and oscillated around ~1.0 % through Middle Eocene biozone CP14b (~39.8 to ~36.8 Ma; ~97.6–92.0 rmcd), before decreasing and becoming more stable following the base of the Late Eocene around the

base of biozone CP15 (~36.5 Ma; ~91.5 rmcd). Towards the end of the Late Eocene (~34.2 Ma; the base of biozone CP16a; ~88.0 rmcd) % sand fraction started to increase and became more variable, a trend that continued into the Early Oligocene. During the Early Oligocene, between 33.6 and 32.4 Ma (~85.0 to ~76.0 rmcd), % sand fraction varied between ~1.0 and ~3.0 %, with two peaks of ~2.4 % and ~3.2 % observed within the dataset at 33.5 and 33.0 Ma (~83.0 and ~80.0 rmcd), separated by a minima where values decreased to ~1.0 % at 33.2 Ma. At 32.4 Ma (~76.0 rmcd) % sand fraction decreased to ~0.7 % for the remainder of the Early–Late Oligocene and exhibited less variability, between ~0.3 and 1.0 %, compared to the earliest Oligocene.

5.2 % calcium carbonate

Figure 5.2 displays the % calcium carbonate data for each Site 1211 hole against both rmcd and numerical age (plots A and B, respectively). The bulk of the data are from Hole C with core gaps filled by data from Hole A (~69.0–71.0 and ~80.0–83.0 rmcd). Additional % calcium carbonate data from Holes A and B are plotted for the interval ~84.0–93.0 rmcd.

Percent calcium carbonate varies from ~83.0 to ~99.0 %, averaging ~97.0 % within the majority of the stratigraphic interval investigated, i.e. between ~60.0–68.0 and ~73.0–88.0 rmcd. During the Middle to latest Eocene (~39.6–34.4 Ma; 97.6–88.0 rmcd) % calcium carbonate values exhibited a much greater range, varying between ~84.0 and ~97.0 %, compared to the earliest Oligocene. From ~34.4–34.2 Ma (~88.5–87.0 rmcd) % calcium carbonate increased to an average of ~97.0 %, then varied between ~95.5 and ~98.5 % into the Early Oligocene at ~33.0 Ma (the base of biozone CP16c; ~80.6 rmcd), when values decreased gradually to about 95.0 % at ~30.0 Ma (the base of biozone CP19a; ~71.0 rmcd). The available data suggest little scatter about this trend. During the late Early Oligocene, at ~29.8 Ma (~70.0 rmcd), there was a minimum in the % calcium carbonate with values in Hole A of ~83.0 %, with values recovering within ~0.5 Ma (by ~69.0 rmcd) to ~94.0 %. % calcium carbonate then increased gradually into the Late Oligocene to ~98.0 % by 27.2 Ma (65.0 rmcd).

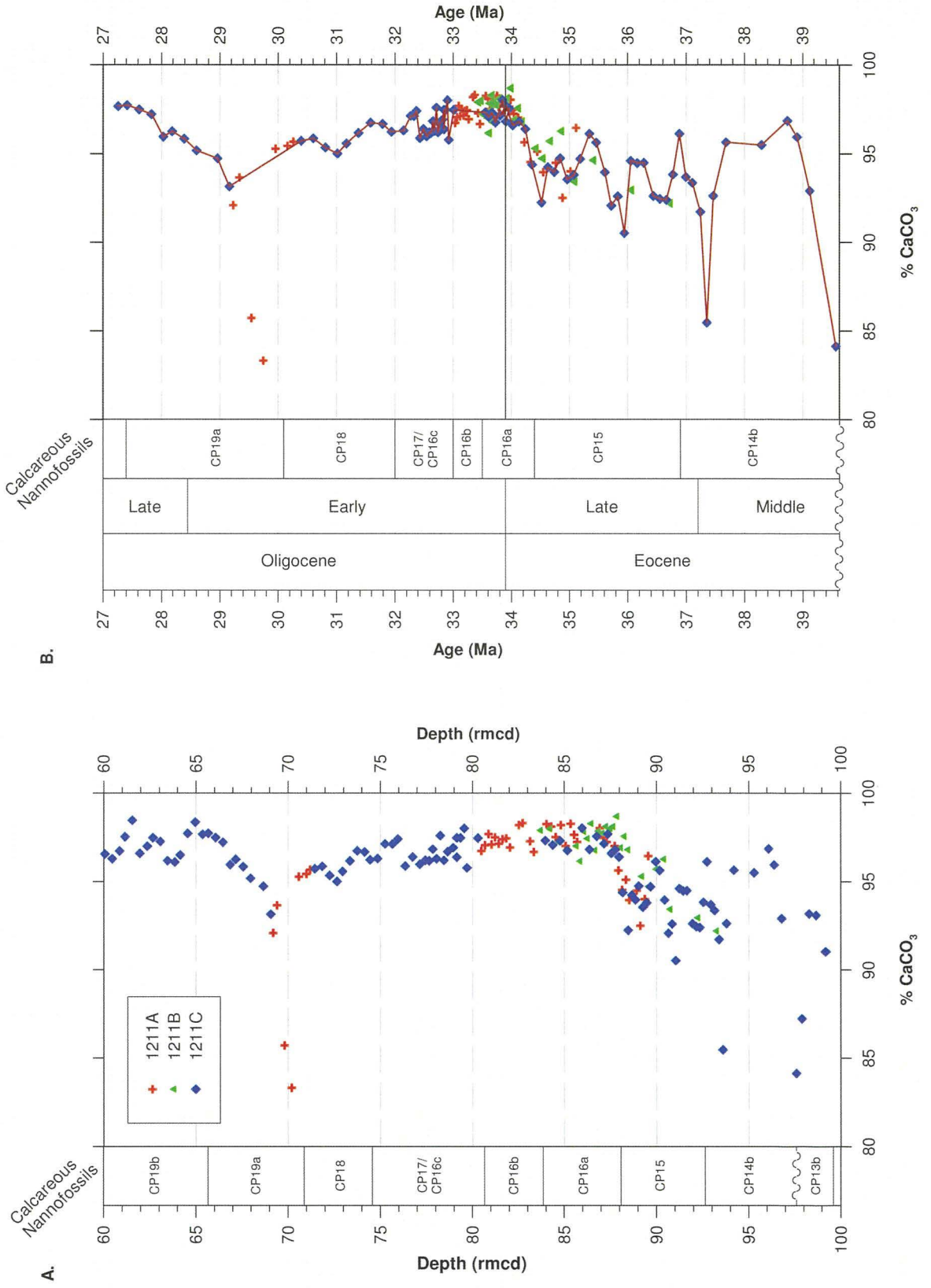

Figure 5.2: % calcium carbonate versus depth (A) and numerical age (B). Data from all three Site 1211 holes are plotted and show that the trends and variation in % calcium carbonate are common between them, thus data are interpreted as one group (dark red line in panel B).

5.3 Core-scanning X-ray fluorescence data

Core-scanning X-ray fluorescence (XRF) data are plotted as normalised element ratios (see Section 3.3 for further discussion). Seven elements were measured: K, Ca, Ti, Mn, Fe, Cu and Sr. These data are plotted for each Site 1211 hole against depth and, excepting Ti and Cu, also plotted as a splice section against numerical age (Figures 5.3 and 5.4, respectively). Ti and Cu were omitted due to the exceptionally low numbers of counts measured for Ti, and both the low counts measured for Cu and poor correlation of this element between the three holes at Site 1211. The dominant element in all samples was Ca. XRF counts for Ca were of the order 11,000, compared to hundreds of counts for K, Fe and Sr, tens of counts for Mn and Cu and single digit counts for Ti.

On a >5.0 m scale, each of the element datasets, with the exception Cu, exhibit general correlations between Holes A, B and C, although <5.0 m correlations are less closely matched (e.g. Ca between 74.0 and 70.0 rmcd and Ca, Mn and Fe between 95.0 and 90.0 rmcd; Figure 5.3). Such a lack of correlation is likely explained by one or more of the following reasons: first, any errors within the rmcd depth scale would offset excursions between holes, which would be observed as a simple offset between records; second, whilst post-depositional cracks and changes to the sediment, i.e. sediment that had dried out, were noted and those XRF results omitted, it is possible that not all such characteristics were noted; and third, counts for the majority of these elements were very low meaning that actual minor differences may exist between the cores, despite the close proximity of their locations. A similar mismatch between the three holes is evident within the magnetic susceptibility and colour reflectance records (Section 5.4), perhaps indicating that there is not a perfect match between holes using the rmcd scale of Westerhold and Röhl (2006). Such a mismatch has the potential to introduce artefacts into the geochemical records described later across the intervals they have been identified in.

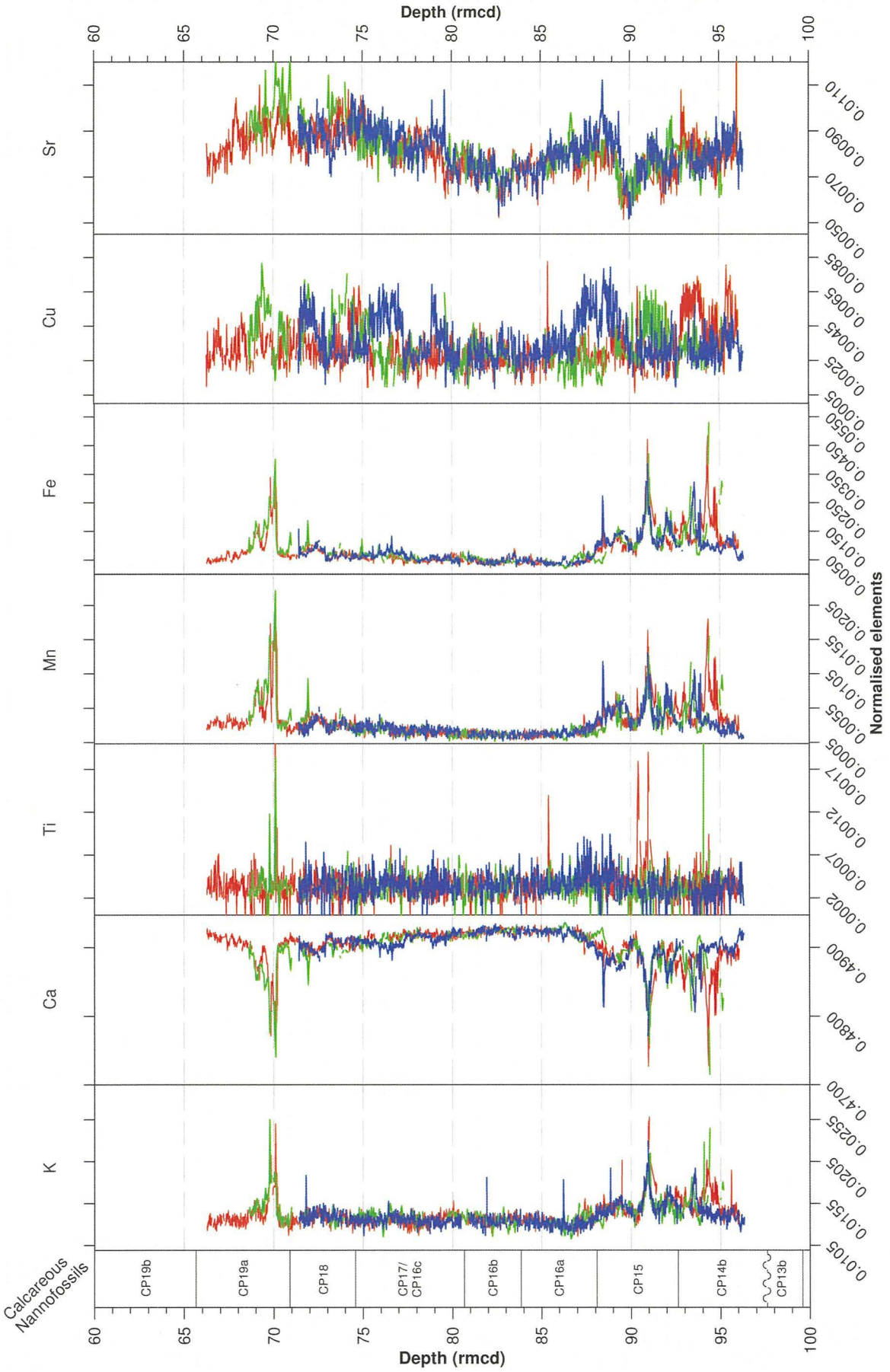

Figure 5.3: Normalised element count ratios (see Section 3.3.4 for explanation) for Site 1211 Holes A (red), B (green) and C (blue) plotted against depth. Macroscale correlation (>5.0 m depth range) between holes can be observed for all elements except Cu, but variability at scales <5.0 m is less well correlated.

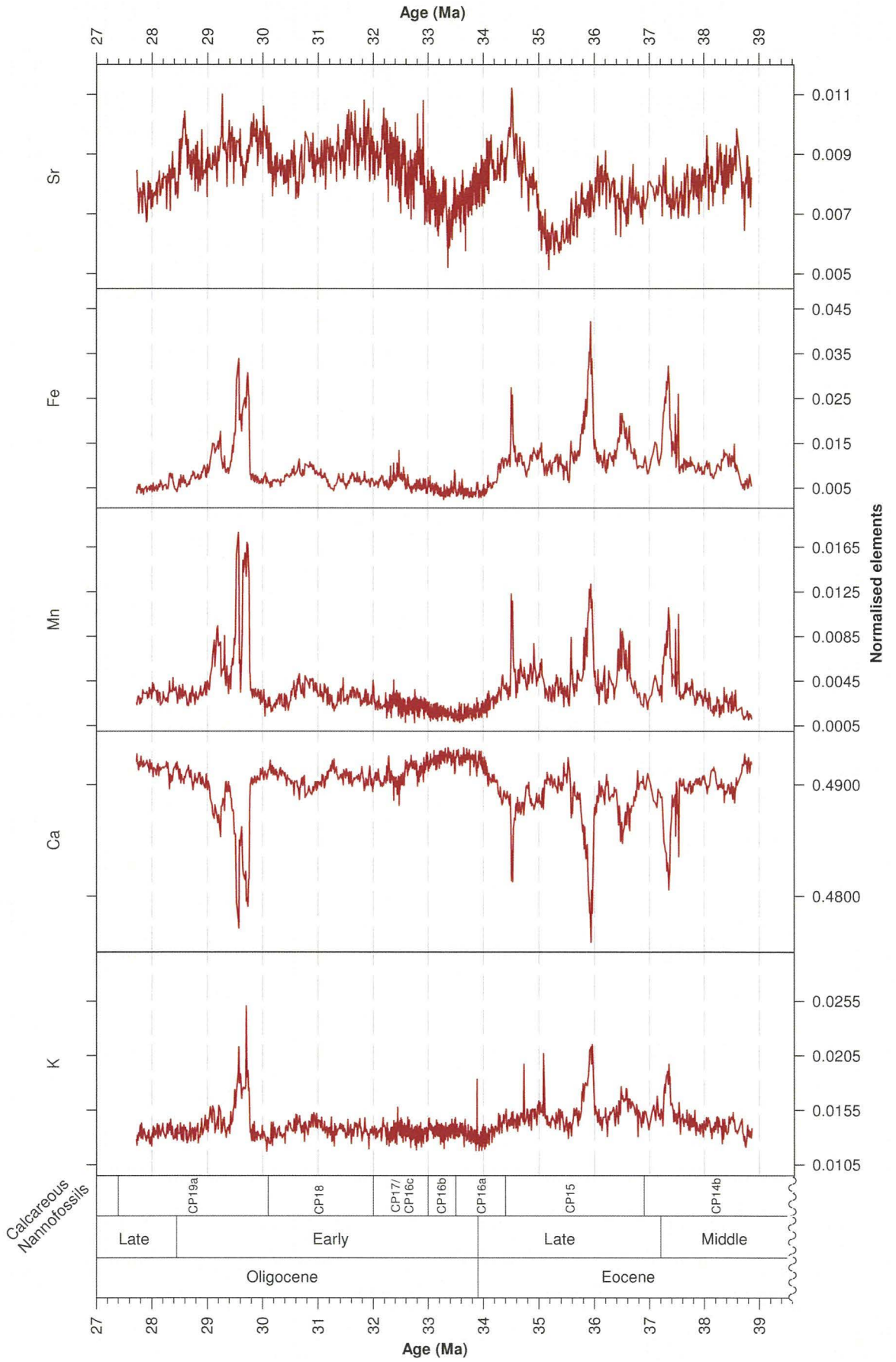

Figure 5.4: Normalised element count ratios for the Site 1211 rmcd splice of Westerhold and Rohl (2006), converted to numerical ages using the depth–age model developed in Chapter 4.

The elemental datasets are described using the spliced section of Westerhold and Röhl (2006) converted into numerical age (Figure 5.4). Compilation of the splice section

involves creating a single "spliced" record from the sections of each holes identified by Westerhold and Röhl (2006) as being typical for the depth. The predominant element, Ca, is described first, with K, Mn and Fe all mirroring Ca, such that the trends in those latter elements are generally opposite to those shown by Ca. Ca normalised element ratios typically averaged ~0.49, varying between ~0.4750 and ~0.4925, throughout the record. Middle to latest Eocene (biozones CP14b and CP15; ~39.0 to ~34.5 Ma, ~96.0 to ~88.0 rmcd) Ca normalised element ratios averaged ~0.49, oscillating slightly about this average, although occasional larger variances occurred, where Ca normalised element ratios drop as low as ~0.475 (e.g. ~34.5 Ma, ~88.0 rmcd; ~36.0 Ma, ~91.0 rmcd and ~37.4 Ma, ~94.2 rmcd). These drops in Ca signal are mirrored by peaks in the K, Mn and Fe records. During the latest Eocene, at ~34.4 Ma (slightly shallower than the base of biozone CP16a), Ca normalised element ratios values increased from ~0.4890 to ~0.4925 into the Oligocene, i.e. by 33.9 Ma (~87.0 rmcd). Values then remained at this level, with low amplitude variations of ~0.001, during the earliest Oligocene, until ~33.0 Ma (~80.6 rmcd), after which they decreased to 0.4900 by ~32.5 Ma (~77.0 rmcd). From ~32.5 until the late Early Oligocene at 29.8 Ma (~80.6 to ~70.2 rmcd) Ca normalised element ratios remained around ~0.490, albeit with low amplitude oscillations of ~0.001. During the interval 29.8–29.0 Ma (~70.2 to ~68.5 rmcd) in the late Early Oligocene there were two excursions to lower Ca normalised element ratios (lowest ~0.48), which are mirrored by peaks in K, Mn and Fe, after which values returned to pre-excursion levels and magnitude of variability into the Late Oligocene.

Throughout the Eocene K normalised element ratios ranged between of ~0.0120 and ~0.0210, the latter as discrete excursions. During the latest Eocene the range of variation declined to between ~0.0120 and ~0.0150 and remained at this magnitude throughout the Early Oligocene, except for the positive excursion between ~29.8 and ~29.0 Ma, where values peaked at ~0.0255. Mn normalised element ratios varied over a range of ~0.0005 to ~0.0125 throughout the Eocene, before the amplitude of oscillations decreased from the latest Eocene until late Early Oligocene at 29.8 Ma. Mn increased to peak values of ~0.0175 synchronously with the decrease in Ca between 29.8 and 29.0 Ma. Fe normalised element ratios displayed a similar trend to Mn and K, with an Eocene range between 0.005 and 0.0425; values then declined and oscillated about ~0.007 throughout the Oligocene, except for an excursion to ~0.035 between 29.8 and 29.0 Ma. Eocene Fe and Mn records have spikes that occur synchronously with minima in the Ca ratio values.

The Sr normalised element ratio record is the only element that displays variation independent of the Ca dataset (Figures 5.3 and 5.4). Sr values vary between ~0.005 and ~0.011, with few of the short-term peak events (<200 kyrs duration) seen in the other elemental records. From the Middle Eocene to the middle Late Eocene (39.0 to ~35.2 Ma, ~96.0 to ~90.0 rmcd) values decreased from ~0.009 to ~0.005, the rate of decrease increasing at ~36.2 Ma (~91.0 rmcd). Sr normalised element ratios then returned to middle Eocene values by ~34.8 Ma (~89.0 rmcd), before decreasing to another minimum of ~0.0055 during the earliest Oligocene at ~33.4 Ma (~83.0 rmcd). Values then again increased to an average of ~0.009 by ~31.8 Ma in the middle Early Oligocene (~74.0 rmcd). Sr normalised element ratios then decreased until ~30.2 Ma (~71.0 rmcd), before increasing until ~30.0 Ma (~70.0 rmcd). Between ~30.0 and ~28.5 Ma, values varied between ~0.0075 and ~0.0110 on a ~100–200 kyr time scale before decreasing from 28.6 Ma (~70.0 rmcd) to the end of the record. Low amplitude oscillations in normalised Sr element ratio of ± ~0.001 occurred during the Late Oligocene from 28.6–27.5 Ma (~70.0 to ~65.0 rmcd).

5.4 Shipboard measurements

Two Site 1211 physical property datasets that were measured during ODP Leg 198 (Shipboard Scientific Party, 2002b) are considered in the context of this study. These datasets are colour reflectance and magnetic susceptibility and are presented, for the splice section of Westerhold and Röhl (2006), against rmcd and numerical age in Figure 5.5.

5.4.1 Colour reflectance

Colour reflectance data from all three Site 1211 holes across the stratigraphic interval covered by this study are plotted against rmcd in Figure 5.5A and against numerical age in Figure 5.5C, the latter for the Site 1211 splice of Westerhold and Röhl (2006). As with the scanning-XRF records, colour reflectance data for the three individual holes show good correlation on a >5 m scale but this correlation breaks down over shorter stratigraphic intervals; in particular correlation was reduced between 95.0 and 88.0 rmcd and between 75.0 and 60.0 rmcd. This lack of correlation appears to result both from inter-hole differences and rmcd errors. Between 75.0 and 70.0 rmcd colour reflectance records for Hole 1211B appear to exhibit a greater magnitude of variation than those from Holes

1211A and 1211C, whereas a minimum at 94.5 rmcd in the Hole 1211A dataset would appear to correspond to minima at ~93.5 rmcd in Holes 1211B and 1211C (grey shaded interval, Figure 5.5A).

Between 39.6 and 38.6 Ma (97.6 to 96.0 rmcd) colour reflectance values increased from 50 to 75 by 38.8 Ma before decreasing again to ~65. During Middle to Late Eocene biozones CP14b and CP15 (38.5 to 34.5 Ma; 96.0 to 88.0 rmcd) colour reflectance typically ranged between 60 and 65, with occasional excursions to lower values between 45 and 50 at ~37.4, ~36.5 and 35.6 Ma. At the base of Eocene–Oligocene boundary biozone CP16a (34.4 Ma, ~88 rmcd), colour reflectance values increased to between 70 and 75 by 34.0 Ma (~87 rmcd), and remained at such values into Early Oligocene biozone CP16b. Colour reflectance values then decreased from 33.2 to 32.4 Ma (82.0 to 76.0 rmcd) to ~65 during Early Oligocene biozones CP16c/17. From 32.4 to 30.0 Ma (Early Oligocene biozone CP18, ~75.0 to ~71.0 rmcd), colour reflectance values varied between ~70 and ~55 on a wavelength of ~1 Myrs. At 30 Ma (~70 rmcd, late Early Oligocene biozone CP19a), colour reflectance values decreased to <50, before increasing by ~28.5 Ma (68 rmcd) to values of ~60. Colour reflectance values remained at that level until the youngest sample at ~27 Ma. Colour reflectance values follow the $\%CaCO_3$ records closely indicating that colour reflectance can be used as an indicator for sedimentary carbonate.

5.4.2 Magnetic susceptibility

Magnetic susceptibility across the stratigraphic interval covered by this study is plotted against rmcd in Figure 6.5B for all three Site 1211 holes and against numerical age in Figure 6.5C on the Site 1211 splice of Westerhold and Röhl (2006). As with the scanning-XRF and colour reflectance records, magnetic susceptibility data for the three individual holes show good macroscale (>2 m) correlation, but with differences in the fine-detail of the records. Correlation between the three Site 1211 holes was particularly poor between 96.0 and 91.0 rmcd and, to a lesser extent, between 90.0 and 88.0 rmcd; an observation also made for XRF and colour reflectance records. Misaligned peaks in magnetic susceptibility at ~94 rmcd for Site 1211A and ~93 rmcd for Sites 1211B and 1211C again suggest that Hole 1211A is expanded relative to the other two holes; however, much of the fine-scale differences in magnetic susceptibility would appear to be inter-hole differences (grey shaded interval in Figure 5.5B).

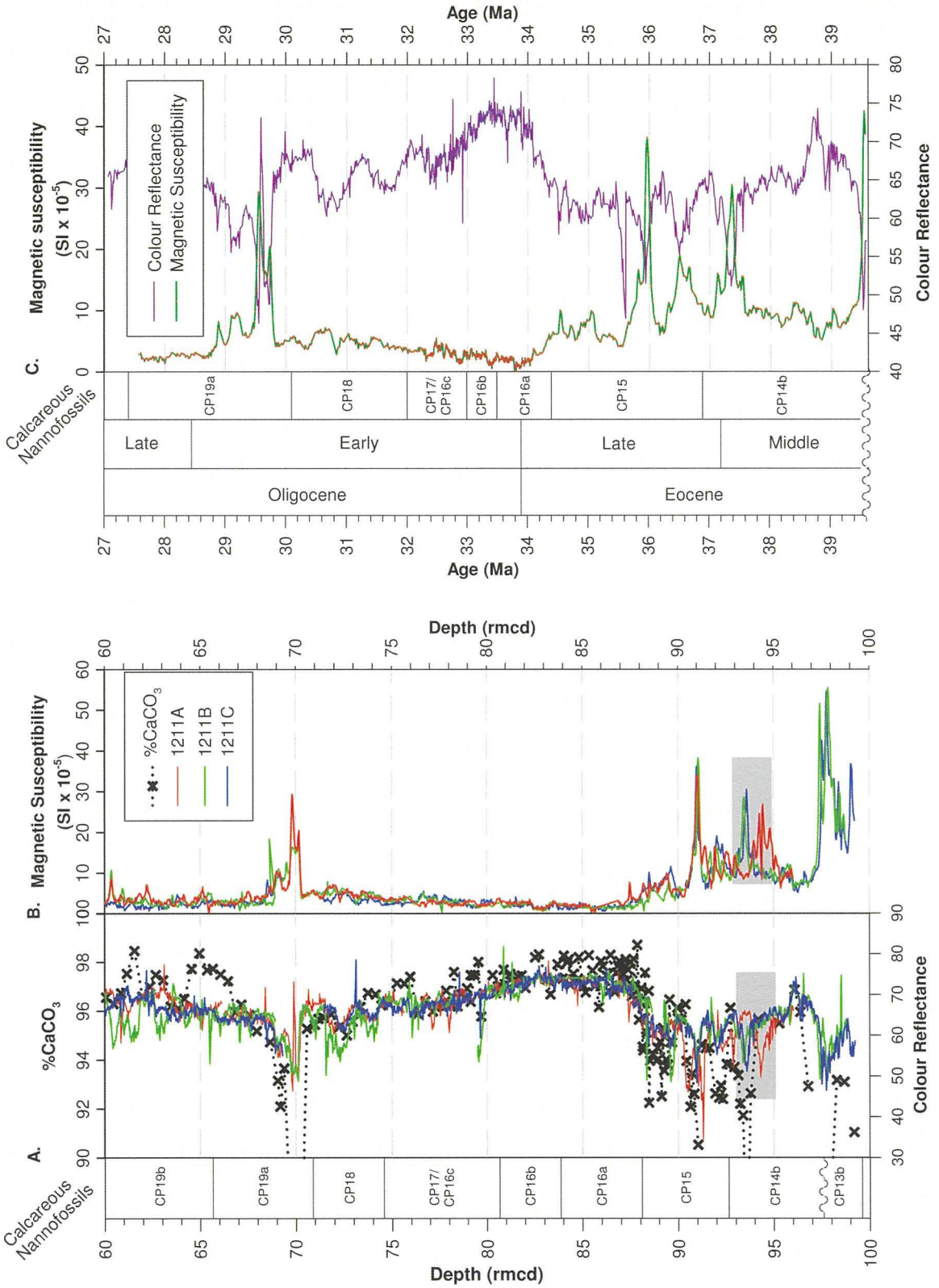

Figure 5.5: Site 1211 colour reflectance overlain with $\%CaCO_3$ and magnetic susceptibility data presented against rmcd (plots A and B, respectively) and numerical age (plot C). When records for each individual hole are plotted against rmcd, there is a general correlation between large-scale features (>2 m), but there are differences between the holes below this stratigraphic scale. The grey shaded interval in plots A and B shows a clear mismatch for both records, suggesting that core recovery at Hole 1211A was expanded relative to Holes 1211B and 1211C. L* colour reflectance can be observed to closely follow Hole C $\%CaCO_3$ value, thus is related to the sedimentary carbonate content. Data are presented using the rmcd splice of Westerhold and Rohl (2006), and converted to numerical age in panel C using the depth–age model developed in Chapter 4. It can be observed that colour reflectance and magnetic susceptibility records mirror each other, indicating an inter-relationship between the two measurements.

Magnetic susceptibility was relatively high during Middle Eocene biozone CP13b (>97.6 rmcd), with SI values between 20 and 55 x 10^{-6}. From the base of biozone CP14b to the top of biozone CP15, during the Middle to Late Eocene (39.6 to ~34.4 Ma, 97.6 to ~88.0 rmcd), magnetic susceptibility SI values were typically between 5 and 10 x 10^{-6}, with SI values up to ~40 x 10^{-6} coinciding with the decreases in colour reflectance and XRF at 37.4, 36.5 and 36.0 Ma (~94.5, ~93.5 and ~91.0 rmcd). Magnetic susceptibility SI values declined to <3 x 10^{-6} at the base of Eocene–Oligocene boundary biozone CP16a, at 34.4 Ma (~88 rmcd), remaining below this level until the top of Early Oligocene biozone CP16b (~33.0 Ma; ~81 rmcd). From the middle of biozone CP16a, magnetic susceptibility values increased gradually, reaching SI values of ~5 x 10^{-6} by the middle of Early Oligocene biozone CP18 (~31.0 Ma; ~75.0 rmcd). Above the base of late Early Oligocene biozone CP19a (~29.2 Ma; ~70.5 rmcd), magnetic susceptibility SI values increased to >40 x 10^{-6} at 29.6 Ma (~70.0 rmcd), before rapidly reducing to varying between 5 and 10 from ~29.5 to ~28.8 Ma (~70.0 to ~68.0 rmcd). Magnetic susceptibility SI values then remained <3 x 10^{-6} for the remaining age assigned interval, i.e. to 27.0 Ma (~65.0 rmcd).

5.5 <38 μm fine-fraction stable-isotope data

Stable-isotope ratios for the <38 μm fine-fraction are described below, following assessment of heterogeneity within aliquots of the <38 μm fine fraction. Preservation and composition of the <38 μm fine-fraction carbonate is then considered through the use of scanning electron microscopy.

5.5.1 <38 μm fine-fraction sample heterogeneity

In order to obtain the <38 μm fine-fraction material, the <65 μm fine-fraction was sieved at 38 μm and an aliquot of the resulting size fraction used for stable-isotope ratio determinations. Prior to description of the temporal variation in <38 μm fine-fraction stable-isotope values, it is necessary to consider whether within sample heterogeneity introduced artefacts into these stable-isotope records. To assess heterogeneity, 5–6 aliquots taken from each of five of the sieved <38 μm fraction samples spread over the stratigraphic range of the study were analysed for stable-isotope ratios (Figures 5.6 and 5.7A and Table 5.1). The standard deviations for these repeat analyses varied between 0.01 ‰ and 0.17 ‰ for $\delta^{18}O$ and 0.02 ‰ and 0.12 ‰ for $\delta^{13}C$. The highest standard deviations of 0.17 ‰ and 0.12 ‰, for $\delta^{18}O$ and $\delta^{13}C$ values, respectively, came from one sample (1211C-9H-6, 35–

37 cm), and are the result of a single analysis (Sample TB18, circled in Figure 5.6) that measured $\delta^{18}O$ and $\delta^{13}C$ values significantly different from the other five replicates). Excluding these anomalous data, the standard deviation of replicate analyses improves to 0.05 ‰ and 0.06 ‰ for $\delta^{18}O$ and $\delta^{13}C$, respectively. Based on the individual standard deviations of each set of replicate <38 μm fraction sample analyses (Table 5.1), all standard deviations are the same order of magnitude as the long-term analytical precision measured during fine-fraction stable-isotope determinations (0.08 ‰; N=60, 2σ; Section 3.4) and replicate run precision (N=6) measured for repeat analyses of the laboratory MCS-18 standard during the heterogeneity assessment (Table 5.1). The similarity between reference material and sample replicate standard deviations indicates that stable-isotope ratio heterogeneity is not a significant issue within the <38μm fine-fraction stable-isotope records generated by this study.

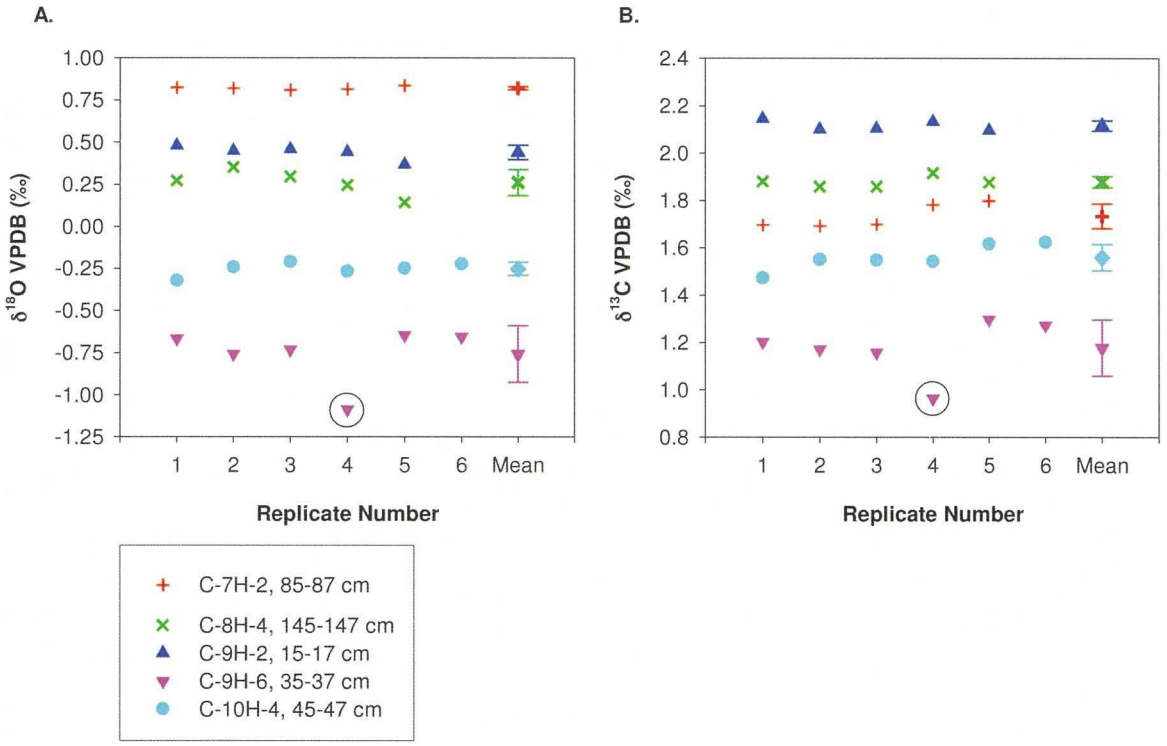

Figure 5.6: Plots of replicate $\delta^{18}O$ (A) and $\delta^{13}C$ (B) analyses to assess sample-isotope ratio heterogeneity for five selected samples (from across the stratigraphic range of this study) identified in the key. These replicate data values correspond to the data listed in Table 5.1. The circled value is considered to be an erroneous value, as discussed in the text.

Sample	$\delta^{18}O$ Replicates							
	1st	2nd	3rd	4th	5th	6th	Mean	SD
1211C-7H-2, 85-87 cm	0.83	0.82	0.81	0.82	0.84		0.82	0.01
1211C-8H-4, 145-147 cm	0.27	0.35	0.30	0.25	0.14		0.26	0.08
1211C-9H-2, 15-17 cm	0.48	0.45	0.46	0.44	0.37		0.44	0.04
1211C-9H-6, 35-37 cm	-0.67	-0.76	-0.73	***-1.09***	-0.64	-0.65	-0.76 (-0.69)	0.17 (0.05)
1211C-10H-4, 45-47 cm	-0.32	-0.24	-0.21	-0.27	-0.25	-0.22	-0.25	0.04
MCS-18	-9.21	-9.15	-9.17	-9.13	-9.19	-9.21	-9.18	0.03

Sample	$\delta^{13}C$ Replicates							
	1st	2nd	3rd	4th	5th	6th	Mean	SD
1211C-7H-2, 85-87 cm	1.70	1.69	1.70	1.78	1.80		1.73	0.05
1211C-8H-4, 145-147 cm	1.88	1.86	1.86	1.92	1.88		1.88	0.02
1211C-9H-2, 15-17 cm	2.15	2.10	2.11	2.13	2.10		2.12	0.02
1211C-9H-6, 35-37 cm	1.20	1.17	1.16	***0.96***	1.30	1.27	1.18 (1.22)	0.12 (0.06)
1211C-10H-4, 45-47 cm	1.47	1.55	1.55	1.54	1.62	1.62	1.56	0.06
MCS-18	-0.74	-0.71	-0.66	-0.64	-0.74	-0.74	-0.70	0.04

Table 5.1: <38 μm fine-fraction stable-isotope ratio replicates for the five samples plotted in Figure 5.6, as well as the stable-isotope ratio determinations for the MCS-18 standard that were run with these samples. All samples are ‰ and are reported relative to VPDB. The "flier" identified in the text and circled in Figure 5.5 is shown in bold and italics. Numbers in parentheses are the mean and standard deviation (SD) with the "flier" removed.

5.5.2 <38 μm fine-fraction $\delta^{18}O$ data

<38 μm fine-fraction stable-isotope ratios for Site 1211 are plotted against both depth and numerical age (Figure 5.7A and B, respectively). As with the other datasets, the data for Holes A and B plot on the same trend as those from Hole C that make up the bulk of the dataset, but data from Hole C alone is used in subsequent sections. Data from Hole C was then filtered by splitting the dataset into one million year segments and by calculating means and standard deviations for each segment. Any samples with stable isotope values that fell outside of the calculated mean $\pm 2\sigma$ of either or both $\delta^{18}O$ or $\delta^{13}C$ are discarded from subsequent consideration (Figure 5.7 B). The filtering lead to the omission of 10 of 238 samples (~4 %). To assist description a five-point running average and 95% confidence intervals have been drawn through the Hole C <38 μm fine-fraction stable-isotope ratio dataset (Figure 5.7B).

<38 μm fine-fraction $\delta^{18}O$ ($\delta^{18}O_{ff}$) values range between ~-1.0 and ~1.3 ‰ throughout the stratigraphic interval assigned numerical ages by the depth–age model. Values were typically more positive during the Oligocene, with an average $\delta^{18}O$ >0.0 ‰, than during the Eocene when $\delta^{18}O$ values averaged <0.0 ‰. $\delta^{18}O_{ff}$ values increased by ~0.2 ‰, from ~-0.4 to ~-0.2 ‰, through the Middle Eocene until the base of Late Eocene biozone CP15,

5-point running mean $\delta^{18}O_{ff}$ values then increased through a series of irregular steps to ~0.3 ‰ by the middle Late Eocene (~35.5 Ma). Throughout the Middle Eocene and much of the Late Eocene (~39.6 to ~35.2 Ma), sample-to-sample $\delta^{18}O_{ff}$ values exhibited greater variability than can be accounted for by analytical precision. $\delta^{18}O_{ff}$ values decreased by ~1.0 ‰ over <500 kyrs during the late Eocene (~35.2 Ma, ~90.0 to ~88.0 rmcd) within biozone CP15. Approximately half of this negative $\delta^{18}O_{ff}$ shift occurred within a restricted range of samples (35.2 to 35.0 Ma; ~89.5 to ~89.4 rmcd; ~0.1 to ~-0.4 ‰, respectively). A positive $\delta^{18}O_{ff}$ trend of ~1.5 ‰ initiated at ~34.4 Ma (~88.0 rmcd), before the base of latest Eocene to earliest Oligocene biozone CP16a, and consisted of a series of steps. ~1.0 ‰ of the $\delta^{18}O_{ff}$ shift occurred in a series of three steps of approximately equal magnitude (~0.4 ‰) each lasting ~100 to ~150 kyrs and separated by minor ~200 kyr reversals of between ~0.2 and ~0.3 ‰ (Figure 5.8 for expanded section). The final $\delta^{18}O_{ff}$ change of ~0.3 ‰ occurred over ~300 kyrs within the early Oligocene from ~33.7 Ma. Following attainment of maximum values (~0.8 ‰) $\delta^{18}O_{ff}$ decreased relatively monotonically from ~33.7 to 32.8 Ma to ~0.3 ‰, when the rate of decrease slowed but continued to 29.6 Ma. A further positive change in $\delta^{18}O$ values occurred during the late Early Oligocene at ~29.6 Ma, within biozone CP19a (~70.0 rmcd) in samples from Hole A, when $\delta^{18}O_{ff}$ values increased from ~0.2 to ~1.0 ‰ over ~600 kyrs. From ~33.0 to ~31.5 Ma variability in $\delta^{18}O_{ff}$ decreases to a magnitude approximately equal to the $\pm 2\sigma$ analytical precision.

5.5.3 <38 μm fine-fraction $\delta^{13}C$ data

<38 μm fine-fraction $\delta^{13}C$ ($\delta^{13}C_{ff}$) values ranged between 0.9 and ~2.5 ‰ throughout the stratigraphic interval sampled by this study. During Middle Eocene biozone CP14b (~39.6 to ~37.2 Ma; 97.6 to ~92.5 rmcd) $\delta^{13}C_{ff}$ values varied between ~1.5 and 2.0 ‰ with a periodicity of ~500 kyrs, followed by an increase at the early Late Eocene base of biozone CP15 (37.0 Ma, ~93.0 rmcd) with $\delta^{13}C_{ff}$ values then varying between ~2.0 and ~2.5 ‰ until ~35.2 Ma (~89.5 rmcd). A negative shift in $\delta^{13}C_{ff}$ values then occurred over two ~0.7 ‰ steps each of ~300 kyrs duration, interrupted by an ~100 kyr pause, between ~35.2 and ~34.5 Ma (~89.5 to ~88.0 rmcd). At the base of latest Eocene to Early Oligocene biozone CP16a (34.4 Ma, ~88.0 rmcd), $\delta^{13}C_{ff}$ increased in three ~0.5 ‰ steps each of ~200 kyrs duration, synchronously with the overall $\delta^{18}O_{ff}$ increase across the Eocene–Oligocene boundary, from <1.0 ‰ to ~2.3 ‰ by ~33.6 Ma (close to the base of Early Oligocene biozone CP16b, ~84.0 rmcd; see Figure 5.8). The brief (<100 kyrs) reversals seen in the

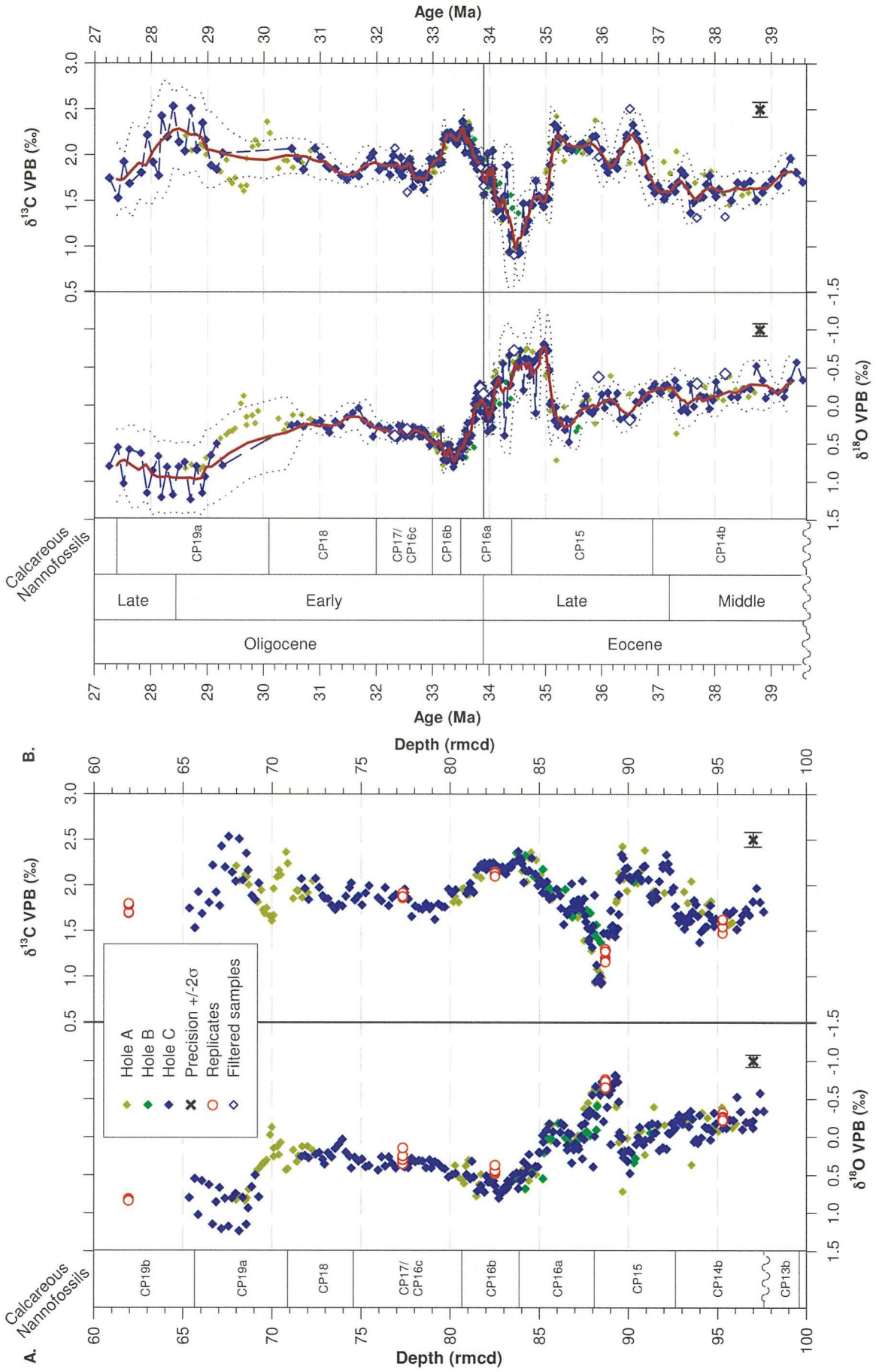
B.
Age (Ma)
δ13C VPB (‰)
δ18O VPB (‰)
Calcareous Nannofossils
CP19a
CP18
CP17/ CP16c
CP16b
CP16a
CP15
CP14b
Late
Early
Late
Middle
Oligocene
Eocene
A.
Depth (rmcd)
Hole A
Hole B
Hole C
Precision +/-2σ
Replicates
Filtered samples
CP19b
CP19a
CP18
CP17/ CP16c
CP16b
CP16a
CP15
CP14b
CP13b

Figure 5.7: Plots of stable-isotope ratio ($\delta^{18}O$ and $\delta^{13}C$) determinations for the Site 1211 <38 μm fine-fraction, plotted against depth (A) and numerical age (B). Open red circles are the replicate analyses described in Section 5.4.1 (without the flier, as discussed in the text). Open blue diamonds represent the filtered samples from the Hole C dataset (see text). The purple line in panel B is a 5-point running average of the entire dataset with 95% (2σ) confidence intervals (dotted lines). Data from Hole A are shown in dark yellow, Hole B are in green and Hole C are in blue.

$\delta^{18}O_{ff}$ record are of lower magnitude (~0.1 ‰) in the $\delta^{13}C_{ff}$ record. Following a brief (~400 kyrs) plateau from ~33.6 to ~33.2 Ma (~84.0 to ~81.5 rmcd), when $\delta^{13}C_{ff}$ values were ~2.2 ‰ and varied less than ±2σ of the analytical precision, $\delta^{13}C_{ff}$ values decreased until 32.9 Ma (~80.0 rmcd) to ~1.7 ‰. Early Oligocene $\delta^{13}C_{ff}$ values then oscillated on an ~1.0 Myr wavelength between ~1.8 and ~2.3 ‰ into the Late Oligocene, with the amplitude of $\delta^{13}C_{ff}$ variability increasing at the base of late Early Oligocene biozone CP19a. Sample-to-sample $\delta^{13}C_{ff}$ variability (scatter) shows little difference between the post-biozone CP17 Oligocene and Eocene, being typically of the order twice ±2σ of the analytical precision.

5.5.4 <38 μm fine-fraction SEM microscopy

The composition, i.e. presence of non-calcareous nannofossil material, and preservation of the <38 μm fine-fraction samples have been described by scanning electron microscopy (SEM). Samples were selected across the stratigraphic range of stable-isotope ratio analyses, with particular attention being paid to samples at the extremes of the isotope ratio changes described above, and observed under a SEM (Plates 5.1, 5.2, 5.3 and 5.4).

Calcareous nannofossils are the dominant component in all observed samples, with occasional foraminiferal fragments and no clear evidence for the occurrence of small juvenile foraminiferal specimens being present (see the low magnification micrographs on each plate). Preservation of the calcareous nannoplankton is variable, from moderate to good, throughout the stratigraphic interval studied (cf. Bralower, 2005), with varying degrees of coccolith fragmentation and dissolution. Preservation is generally poorer, and coccolith fragmentation appears to be greater, in samples from section 1211C-9H-6 and from the lowest sample observed 1211C-10H-6, 85–87 cm (Plates 5.2G and H, 5.3 and 5.4C and D; Table 5.2). This latter sample is, however, from ~98.7 rmcd and hence older than 43 Ma and, as such, lies outside of the stratigraphic range assigned numerical ages and thus is not a focus of this study. The poorer preservation evident within section 1211C-9H-6 is equivalent in depth to the negative step observed in $\delta^{18}O_{ff}$ and $\delta^{13}C_{ff}$ values (~89.5 to 88.5 rmcd; ~35.2 to ~34.9 Ma; Figure 5.7), but does not coincide with any clear change

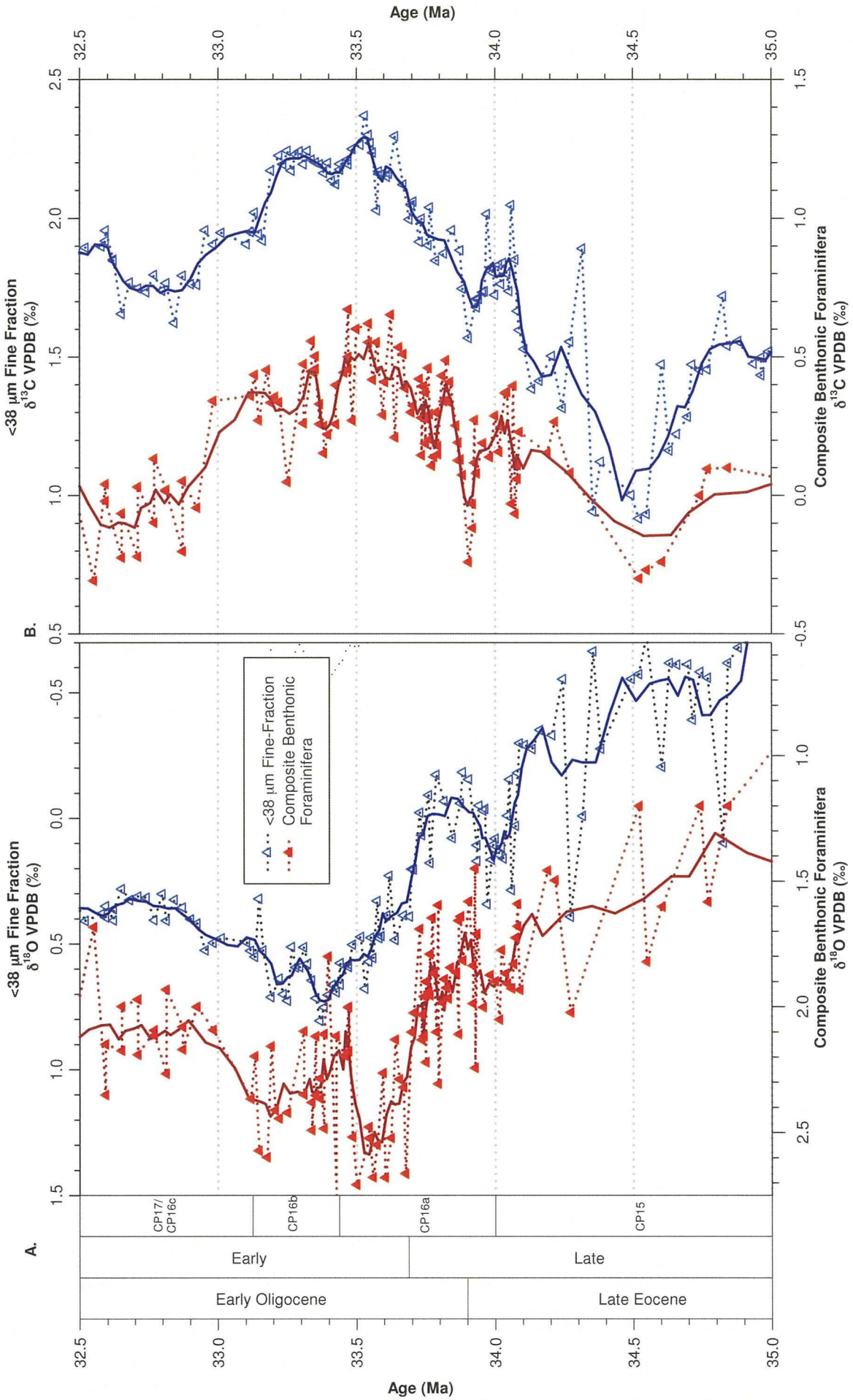

Figure 5.8: Expanded Eocene–Oligocene boundary section for <38 µm fine-fraction and composite benthonic foraminiferal stable-isotope records (see Section 5.6.3).

Sample	Depth (rmcd)	Age (Ma)	Estimate of coccolith fragmentation (%)
7-1, 85-87 cm	60.46		30
7-3, 105-107 cm	63.66		30
8-2, 5-7 cm	72.95	31.17	20
8-4. 45-47 cm	76.35	32.43	20
9-1, 105-107 cm	81.92	33.25	20
9-5, 115-117 cm	88.02	34.27	20
9-6, 15-17 cm	88.52	34.55	50
9-6, 65-67 cm	89.02	34.83	50
9-6, 90-92 cm	89.27	34.96	60
9-6, 115-117 cm	89.52	35.10	60
9-6, 135-137 cm	89.72	35.21	40
10-1, 115-117 cm	91.49	36.18	50
10-3, 85-87 cm	94.19	37.68	20
10-6, 65-67 cm	98.49		40

Table 5.2: Estimate of the volume of coccolith fragmentation and foraminiferal debris within the samples shown in the SEM images that follow. Estimates were based on a subjective observation of the volume of whole calcareous nannofossils to other material within a sample. The increase in coccolith fragmentation occurs at the interval were $\delta^{18}O$ and $\delta^{13}C$ values show negative excursions, although there is no systematic change in fragmentation that would account for these excursions.

in species composition. Even in these samples coccoliths are observed with clear proximal and distal shields (Plates 5.2 and 5.3), while rare Discoasters with relatively little overgrowth are present. Van der Lingen and Packham (1975) identified the presence of secondary calcite growth on the margins of coccoliths with euhedral crystal faces as a clear sign of burial diagenesis. Such secondary carbonate is not a common feature in the SEMs of the Site 1211 <38 μm fine-fraction samples, although there may be a slight increase in the proportion of such secondary euhedral minerals with depth in the Eocene samples, albeit limited to the edges of coccoliths or the highly susceptible to diagenetic overgrowth Discoasters (Plates 5.3H and 5.4B). Within many of the samples observed by SEM there are what appear to be sub-micron sized euhedral crystals (e.g. highlighted in Plates 5.1B,F; 5.2B,F and 5.3F), but these are interpreted in this study as fragments of coccoliths, due to their close resemblance to the segments that made up the coccolith shields.

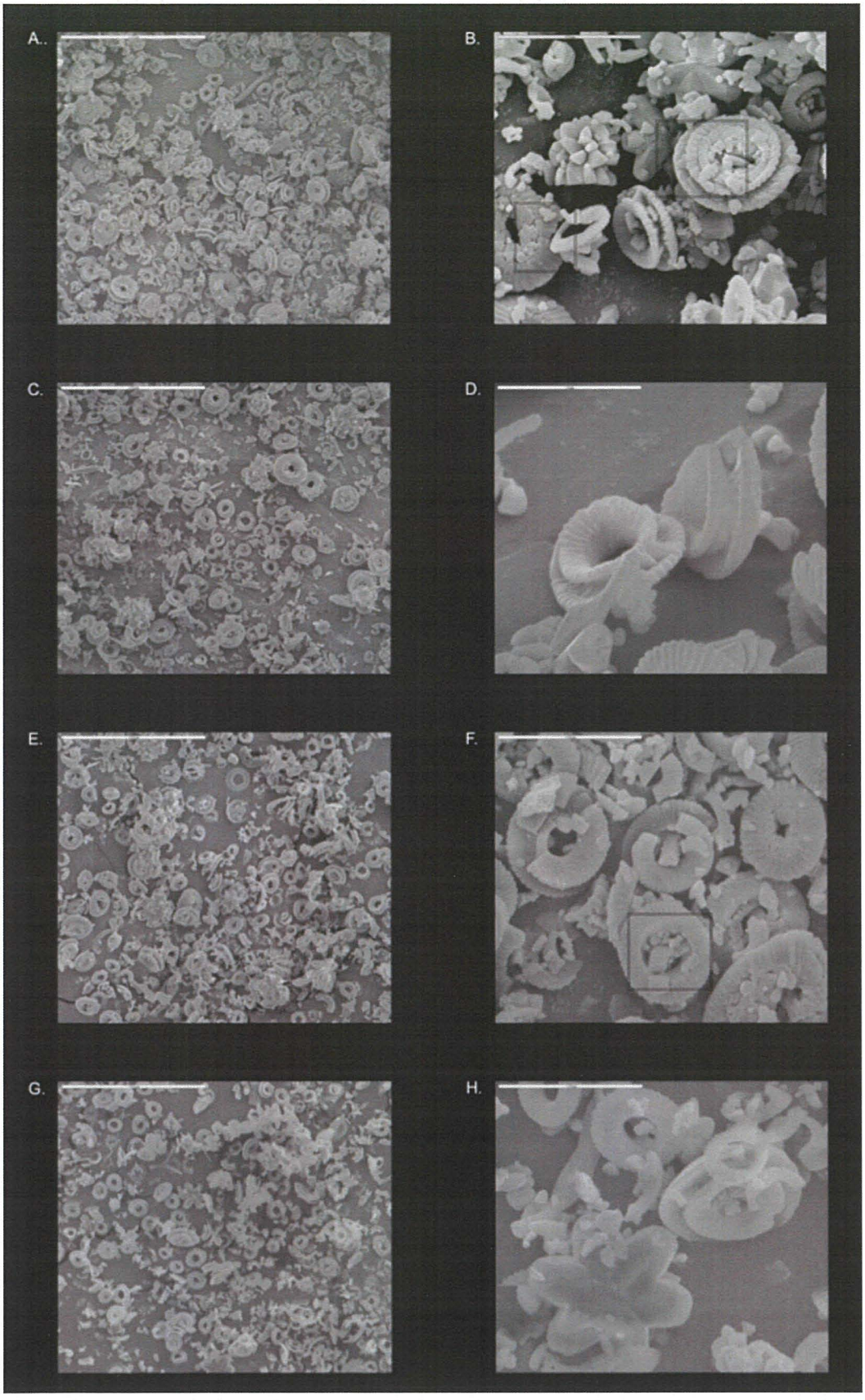

Plate 5.1: SEM photomicrographs from samples 1211C-7H-1, 85–87 cm (A and B); 1211C-7H-3, 105–107 cm (C and D); 1211C-8H-2, 5–7 cm (E and F), highlights in B and F are euhedral coccolith fragments and 1211C-8H-4, 45–47 cm (G and H). Images A, C, E and G are at 1000x magnification and scale bars = 50 μm. Images B, F and H are at 5000x magnification and scale bars = 10 μm. Image D is at 10000x magnification and scale bar = 5 μm.

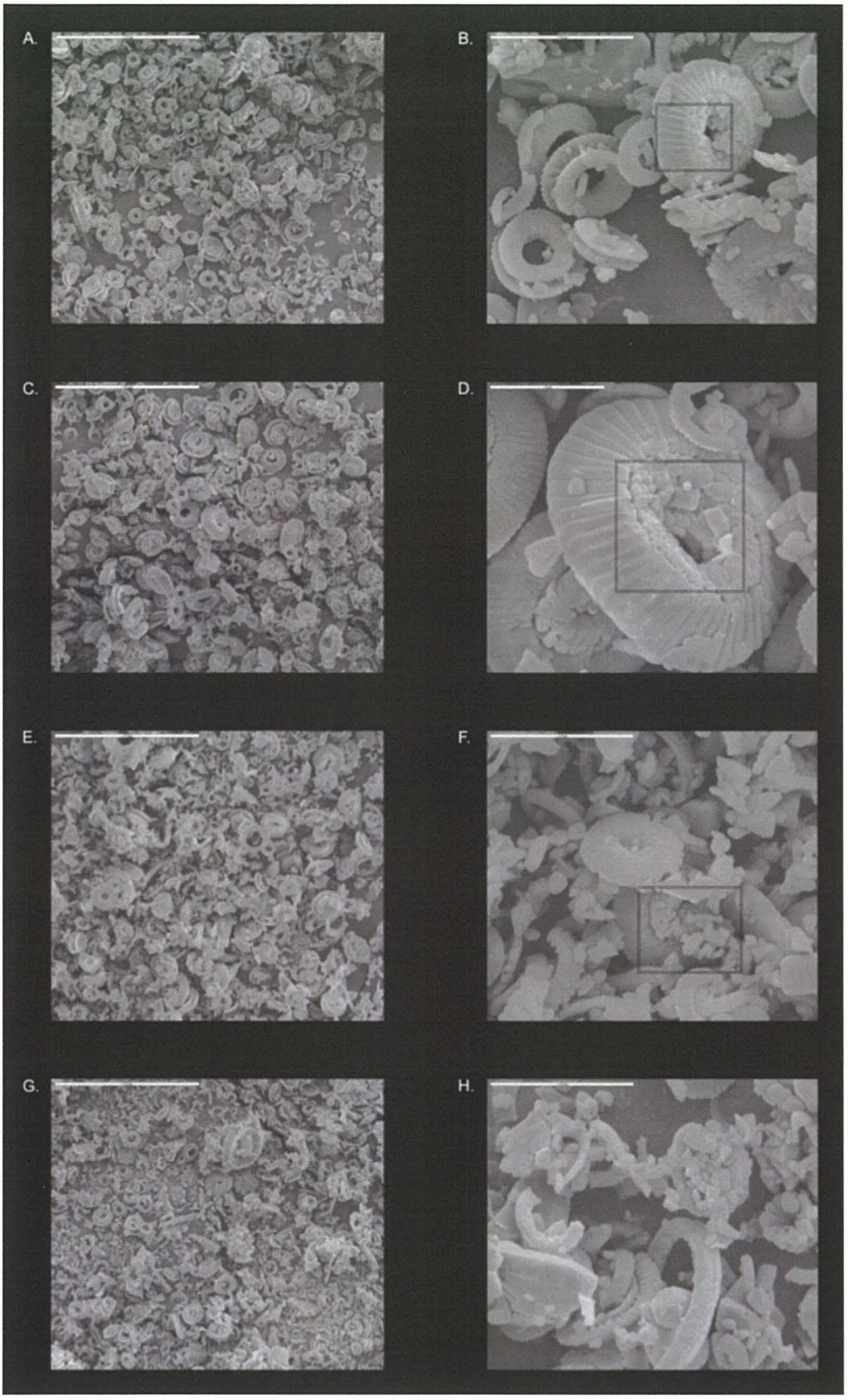

Plate 5.2: SEM photomicrographs from samples 1211C-9H-1, 105–107 cm (A and B); 1211C-9H-5, 115–117 cm (C and D), highlights in B and D euhedral crystals in place in coccolith plate; 1211C-9H-6, 15–17 cm (E and F), highlights are coccolith fragments and 1211C-9H-6, 65–67 cm (G and H). Images A, C, E and G are at 1000x magnification and scale bars = 50 μm. Images B, F and H are at 5000x magnification and scale bars = 10 μm; Image D is at 8000x magnification and scale bar = 5 μm.

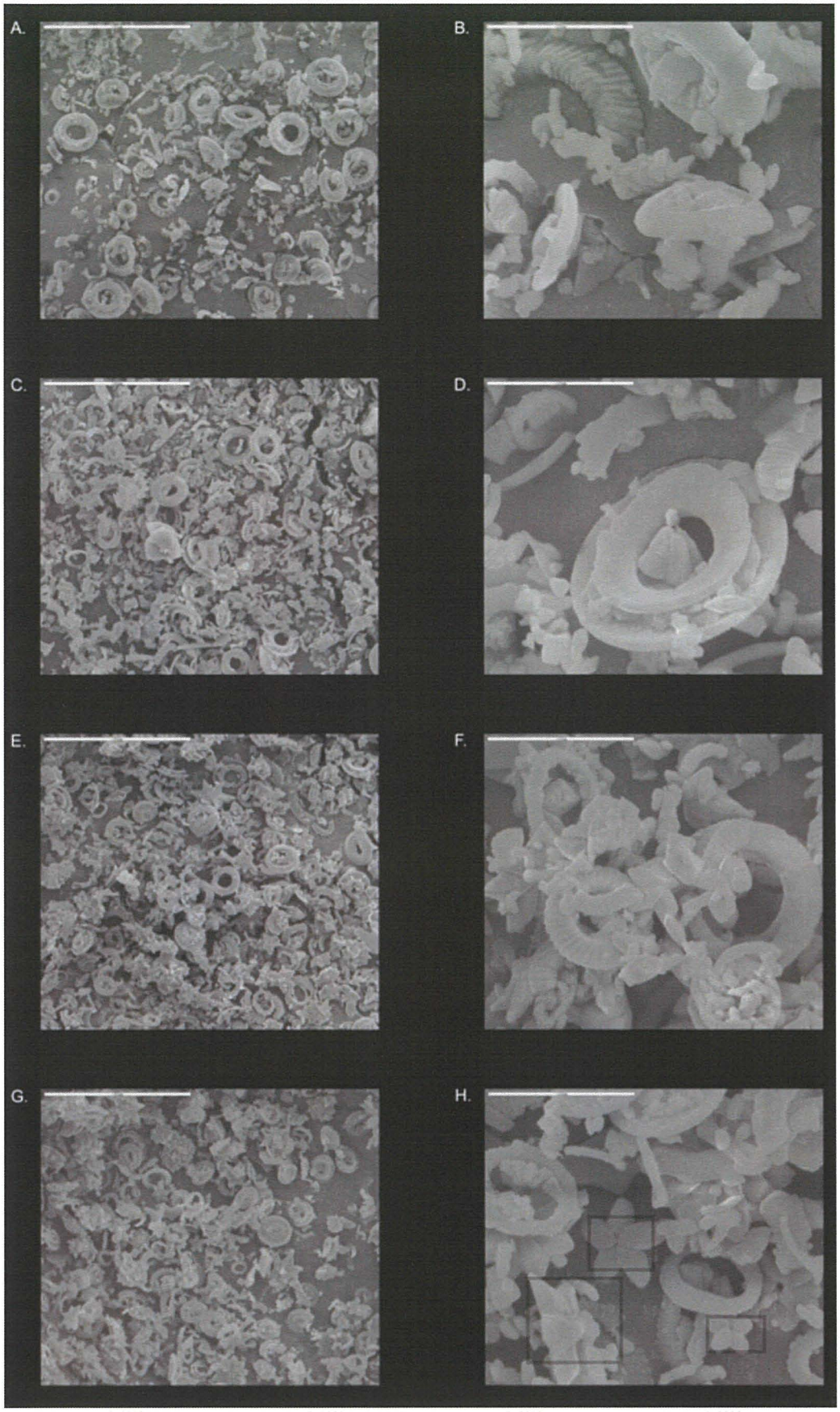

Plate 5.3: SEM photomicrographs from samples 1211C-9H-6, 90–92 cm (A and B); 1211C-9H-6, 115–117 cm (C and D); 1211C-9H-6, 135–137 cm (E and F) and 1211C-10H-1, 115–117 cm (G and H), highlighted images are overgrown Discoasters. Images A, C, E and G are at 1000x magnification and scale bars = 50 μm. Images B, D, F and H are at 5000x magnification and scale bars = 10 μm.

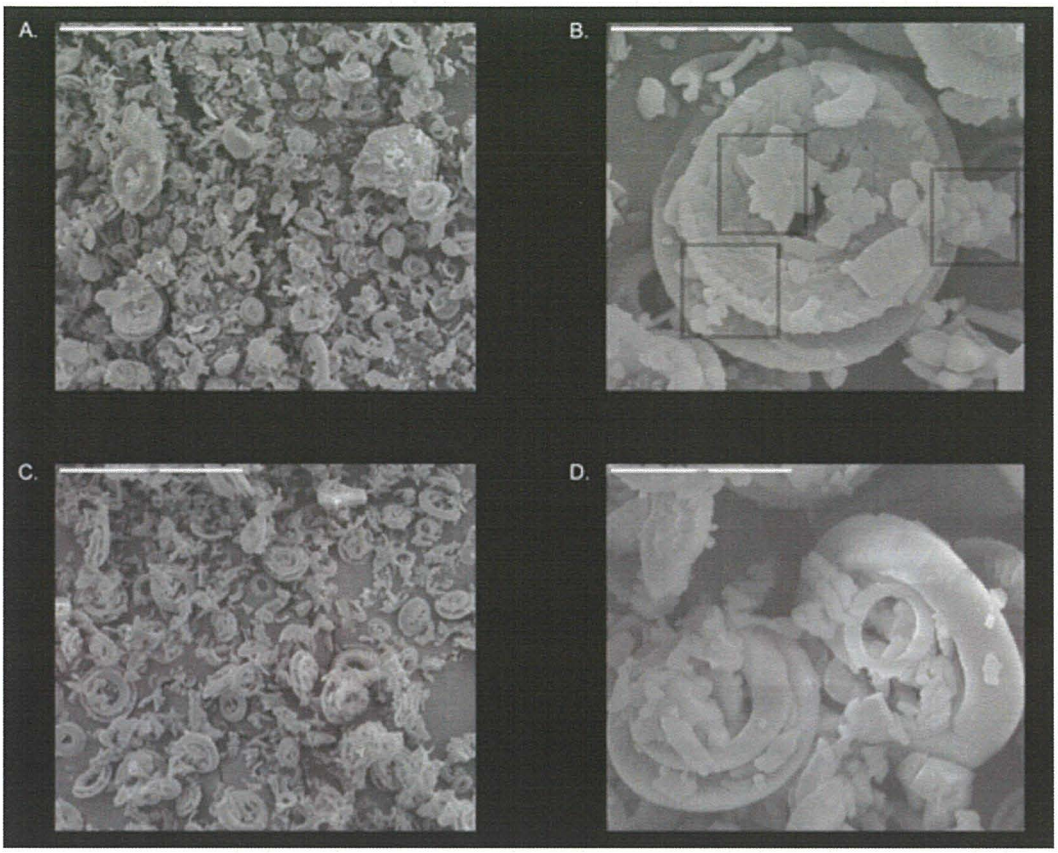

Plate 5.4: SEM photomicrographs from samples 1211C-10H-3, 85–87 cm (A and B), highlighted are overgrowths on both Discoasters and a whole coccolith; 1211C-10H-6, 65–67 cm (C and D). Figures A and C are at 1000x magnification and scale bars = 50 μm. Images B and D are at 5000x magnification and scale bars = 10 μm.

5.6 Benthonic foraminiferal stable-isotope data

The stable-isotope records from Hole C of the individual benthonic foraminiferal species analysed (Figure 5.9) are described below. Records for Holes A and B are plotted but not desribed. Short-term (over ~1.0 m) scatter within the $\delta^{18}O$ and $\delta^{13}C$ values was typically about two times the analytical precision ($\pm 2\sigma$). *Oridorsalis umbonatus* was used to generate the bulk of the isotope records, being supplemented by four additional species (*Cibicidoides* spp., *Gyrinoides* spp., *Nuttaloides truempyi* and *Osungularia mexicana*) that were analysed in a sufficient number of samples to permit comparisons between these species and *O. umbonatus*. Of these four species, *Osungularia mexicana* was only present within two stratigraphically restricted sections of the *O. umbonatus* stable-isotope records, limiting its usefulness in describing trends in the Eocene–Oligocene stable-isotope records. The remaining three species are described below.

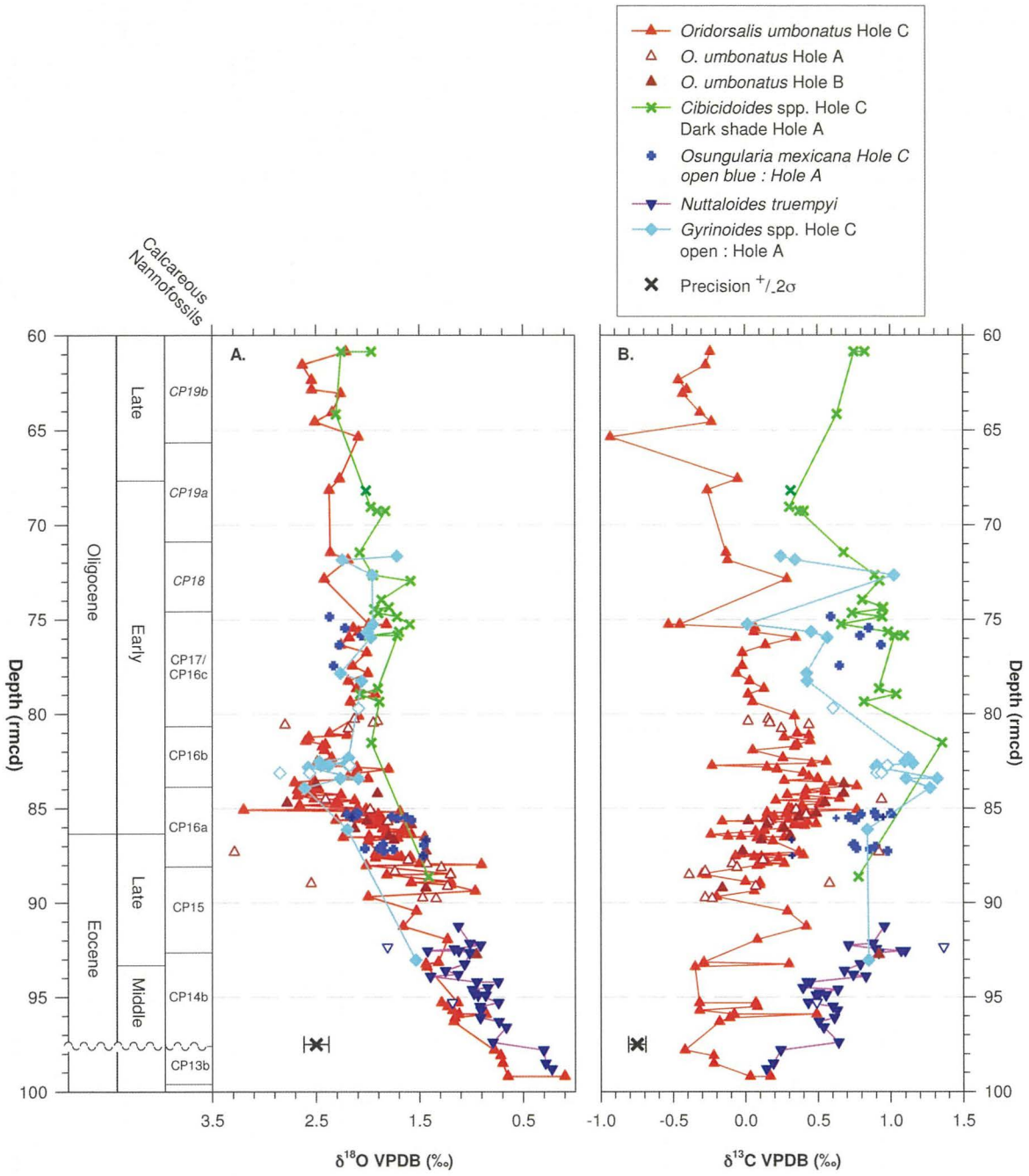

Figure 5.9: Plot of benthonic foraminiferal stable-isotope data for the each of the species analysed from Site 1211. Note that no inter-species correction factors have been applied to the stable-isotope data plotted in this figure.

5.6.1 Benthonic foraminiferal $\delta^{18}O$ data

Oridorsalis umbonatus

$\delta^{18}O$ values for *O. umbonatus* ranged between ~0.1 and ~2.8 ‰ (Figures 5.9). $\delta^{18}O$ values were lowest within the Middle Eocene biozone CP13b (~99.0 rmcd), prior to the hiatus in sedimentation at 97.6 rmcd. *O. umbonatus* $\delta^{18}O$ values then increased from the base of Middle Eocene biozone CP14b to the middle of Late Eocene biozone CP15 (97.6 to ~90.0 rmcd), although the sparser nature of the data within biozone CP15 mean that it is not possible to assess the degree of variability within the observed increase of *O. umbonatus*

$\delta^{18}O$ values. From the end of biozone CP15 (~88.0 rmcd) into latest Eocene to Early Oligocene biozone CP16a (~88.0 to ~86.0 rmcd) *O. umbonatus* $\delta^{18}O$ values increased from ~1.5 to ~1.8 ‰. At ~86.0 rmcd *O. umbonatus* $\delta^{18}O$ values then increased more rapidly to the most positive value of ~2.8 ‰ at ~84.7 rmcd. *O. umbonatus* $\delta^{18}O$ values then remained high (~2.5 ‰) throughout Early Oligocene biozone CP16b, before declining by ~0.5 ‰ towards the base of Early Oligocene biozones CP16c/CP17 (~80.7 rmcd). Between ~80.0 and 75.0 rmcd, within Early Oligocene biozones CP16c/CP17, *O. umbonatus* $\delta^{18}O$ values remained >2.0 ‰, while at depths shallower than ~75.0 rmcd, between Early Oligocene biozone CP18 and Late Oligocene biozone CP19b, data becomes sparser but seem to show a trend to more positive $\delta^{18}O$ values.

Nuttaloides truempyi

Stable-isotope ratio analyses for *N. truempyi* were limited to samples deeper than ~91.2 rmcd, but provide a greater density of data throughout Middle Eocene biozone CP14b and the early part of Late Eocene biozone CP15 (~97.6 to ~91.0 rmcd) than the *O. umbonatus* data. *N. truempyi* $\delta^{18}O$ values varied between 0.3 and ~1.4 ‰ (Figure 5.9). Like the *O. umbonatus* $\delta^{18}O$ record, the lowest *N. truempyi* $\delta^{18}O$ value was observed within biozone CP13b, before the identified hiatus (~97.8 rmcd). Above the hiatus *N. truempyi* $\delta^{18}O$ values increased from ~0.7 to ~1.0 ‰ throughout biozones CP14b and the lower part of biozone CP15, a trend similar to that seen in the *O. umbonatus* record, albeit with the *N. truempyi* offset to lower $\delta^{18}O$ values compared to *O. umbonatus*.

Cibicidoides spp.

The *Cibicidoides* spp. $\delta^{18}O$ record is predominantly from the Oligocene (biozones CP16b to CP19b), with one Late Eocene data point (at ~88.6 rmcd; biozone CP15). $\delta^{18}O$ ratios varied from ~1.4 to ~2.3 ‰ across the range of sampling (Figure 5.9), the former value being the single Late Eocene data point, while the latter value occurs near the top of the sampling range during the Late Oligocene (~64.2 rmcd). Oligocene *Cibicidoides* spp. $\delta^{18}O$ values varied between ~1.6 and ~2.3 ‰, around an average of ~1.9 ‰ throughout this time period. The major positive shift in $\delta^{18}O$ values evident in the *O. umbonatus* record was not sampled in detail for *Cibicidoides* spp., although between the Late Eocene and Early Oligocene samples, which sample before and after the Eocene–Oligocene boundary, there

was a ~0.5 ‰ increase in $\delta^{18}O$ values. *Cibicidoides* spp. $\delta^{18}O$ values were slightly lower than those measured for *O. umbonatus*.

Gyrinoides spp.

The *Gyrinoides* spp. $\delta^{18}O$ record is predominantly from the Early Oligocene (biozone CP16a to the end of biozone CP18), with an isolated data point within Middle Eocene biozone CP14b. $\delta^{18}O$ values varied from ~1.5 to ~2.9 ‰ (Figure 5.9). Sampling across the major positive shift in $\delta^{18}O$ values observed in the *O. umbonatus* record was limited, but the changes in *Gyrinoides* spp. $\delta^{18}O$ values from Middle Eocene biozone CP14b to the earliest Oligocene CP16a show an increase of 0.7 ‰. *Gyrinoides* spp. $\delta^{18}O$ values were highest, at ~2.6 ‰, during the earliest Oligocene, plotting close to the most positive values measured for *O. umbonatus* around ~84.0 rmcd. *Gyrinoides* spp. $\delta^{18}O$ values then twice decreased by 0.5 ‰, interrupted by an ~0.5 ‰ increase, across ~1.5 m during Early Oligocene biozone CP16b, after which values remained at about 2.0 ‰ through Early Oligocene biozones CP16c/CP17 to CP18. The *Gyrinoiodes* spp. $\delta^{18}O$ values plot close to the *O. umbonatus* record, indicating little offset in $\delta^{18}O$ values between these two species.

5.6.2 Benthonic foraminiferal $\delta^{13}C$ data

Oridorsalis umbonatus

$\delta^{13}C$ values for *O. umbonatus* range between -0.9 and ~0.9 ‰ over the stratigraphic range investigated (Figure 5.9). The sparse nature of the dataset hinders unequivocal identification of $\delta^{13}C$ trends during Middle Eocene biozones CP13b and CP14b and much of Late Eocene biozone CP15 (99.0 to 90.0 rmcd), with *O. umbonatus* $\delta^{13}C$ values being relatively scattered (between ~-0.4 and ~0.9 ‰). The density of data increases at depths shallower than 90.0 rmcd and *O. umbonatus* $\delta^{13}C$ values increased from ~0.1 ‰, at the base of latest Eocene to Early Oligocene biozone CP16a (~88.0 rmcd) to 0.7 ‰ at the base of Early Oligocene biozone CP16b (~84.0 rmcd). From the base of biozone CP16b to the middle of Early Oligocene biozones CP16c/CP17 (~77.5 rmcd) *O. umbonatus* $\delta^{13}C$ values decreased to 0.0 ‰. At depths shallower than ~77.5 rmcd, the data are relatively sparse, but *O. umbonatus* $\delta^{13}C$ values decrease by ~0.5 ‰ towards the end of the Early Oligocene and into the Late Oligocene, i.e. from biozones CP16c/CP17 to biozone CP19b.

Nuttaloides truempyi

$\delta^{13}C$ values for *N. truempyi* vary between ~0.1 and ~1.4 ‰ (Figure 5.9) and have a distinct offset to higher values, by upto ~1.0 ‰, from the $\delta^{13}C$ values recorded by *O. umbonatus*. The lowest *N. truempyi* $\delta^{13}C$ values were recorded during Middle Eocene biozone CP13b and increased by ~0.5 ‰ across the hiatus into Middle Eocene biozone CP14b. *N. truempyi* $\delta^{13}C$ values remained relatively constant throughout most of biozone CP14b, averaging ~0.5 ‰ (~97.6 to ~94.2 rmcd), before increasing in magnitude to ~1.0 ‰ by the base of Late Eocene biozone CP15 (92.6 rmcd), these values being maintained to the top of the dataset (~91.0 rmcd). The $\delta^{13}C$ values measured for *N. truempyi* exhibit reduced amplitude fluctuations compared to the *O. umbonatus* $\delta^{13}C$ dataset for the equivalent stratigraphic interval.

Cibicidoides spp.

Cibicidoides spp. $\delta^{13}C$ values range between ~0.3 and ~1.4 ‰. *Cibicidoides* spp. $\delta^{13}C$ values increased across the Eocene–Oligocene boundary, from ~0.8 ‰ to ~1.4 ‰, albeit a difference recorded in only two samples. From the most positive *Cibicidoides* spp. $\delta^{13}C$ value of ~1.4 ‰ within Early Oligocene biozone CP16b (~81.5 rmcd), $\delta^{13}C$ values decreased in magnitude to ~0.9 ‰ by ~79.0 rmcd within biozone CP17/CP16c, after which values varied between ~0.7 to ~1.1 ‰ to the end of Early Oligocene biozone CP18 (71.0 rmcd). The limited data within late Early Oligocene biozone CP19a and Late Oligocene biozone CP19b indicate a trend to higher *Cibicidoides* spp. $\delta^{13}C$ values. $\delta^{13}C$ values. *Cibicidoides* spp. are consistently offset to higher $\delta^{13}C$ values than those recorded by *O. umbonatus*.

Gyrinoides spp.

Gyrinoides spp. $\delta^{13}C$ values ranged between ~0.0 and ~1.3 ‰ (Figure 5.9). *Gyrinoides* spp. $\delta^{13}C$ values do not exhibit any change through the Late Eocene, but increase by Early Oligocene biozone CP16b. Maximum *Gyrinoides* spp. $\delta^{13}C$ values were evident during biozone CP16b (~84.0 rmcd), paralleling the *O. umbonatus* record, after which $\delta^{13}C$ values first decreased by <0.5 ‰ and then increased by ~0.2 ‰ within ~2 m. *Gyrinoides* spp.

$\delta^{13}C$ values decreased by up to ~1.0 ‰ into Early Oligocene biozone CP16c/CP17 by 75.0 rmcd. *Gyrinoides* spp. $\delta^{13}C$ values then increased to ~1.0 ‰ in Early Oligocene biozone CP18 (~72.5 rmcd) before decreasing to <0.5 ‰ within the same biozone. $\delta^{13}C$ values for *Gyrinoides* spp. were offset to higher values compared to *O. umbonatus*, and generally are lower than those measured for *Cibicidoides* spp.

5.6.3 Benthonic foraminiferal inter-species offsets in $\delta^{13}C$ and $\delta^{18}O$ data

Multiple species of benthonic foraminifera, as described above, were measured to fill gaps present within the *O. umbonatus* stable-isotope records, in order to produce the most detailed record of stable-isotope ratio variation at Site 1211 (see Section 5.5.4). To compile composite bottom water stable-isotope records, using several species of benthonic foraminifera, it is necessary to correct for species-specific offsets that result from differences in benthonic foraminiferal microhabitats, e.g. epifaunal *versus* infaunal, and associated vital effects (see Section 2.2.1) through use of inter-species correction factors. Correction factors have been determined and applied within the published literature for many species (see Shackleton et al., 1984 and Katz et al., 2003, among others) to correct either to isotope equilibrium or to an individual species, the latter typically *Cibicidoides* spp., to produce normalised isotope records. Within this study, correction factors that describe species-specific $\delta^{18}O$ and $\delta^{13}C$ offsets, relative to *O. umbonatus*, have been determined by calculating the mean of the offset observed for each species pair, where *O. umbonatus* and other species occurred in the same sample, (Figure 5.10 and Table 5.3).

Inter-species correction factors determined in this study are compared to published inter-species offsets in Table 5.4. The different correction factors for the benthonic foraminiferal species shown in Table 5.4 do not agree in terms of absolute magnitude, although in most cases they are of similar orders of magnitude, with the exception of the offset between *N. truempyi* and *O. umbonatus* reported by Shackleton et al. (1984). Use of generalised isotope ratio correction factors makes the assumption that inter-species offsets remained constant over time. Katz et al. (2003) noted that there is disagreement in the magnitude of offsets between many published records, such as Shackleton et al. (1984), Katz and Miller (1990), Pak and Miller (1995), as highlighted in Table 5.4, although Katz and Miller (1990) and Pak and Miller (1995) did not measure offsets relative to *O. umbonatus*. The disagreement between offsets may result either from evolutionary change or

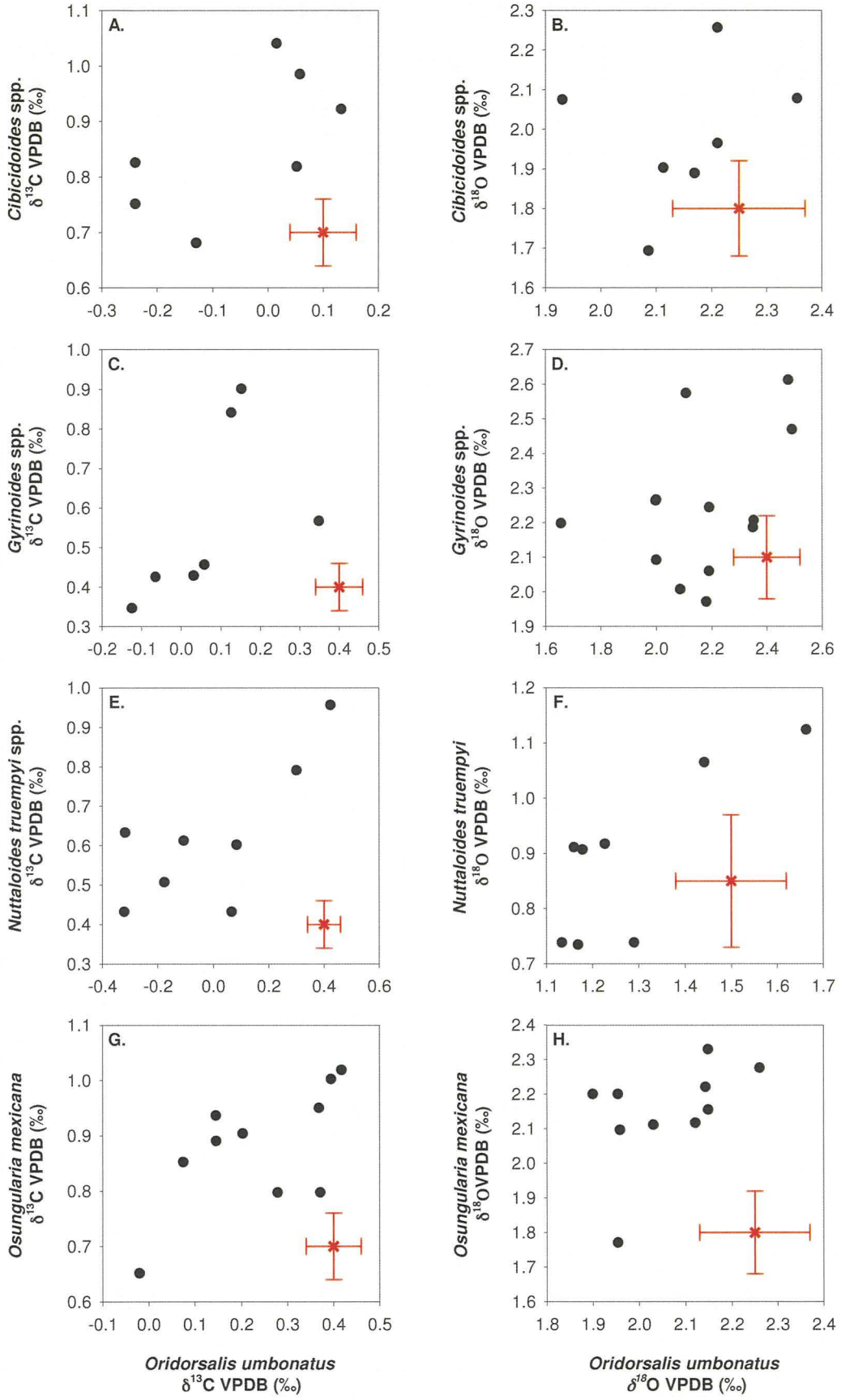

Figure 5.10: Cross-plots of *O. umbonatus* stable-isotope ratios against other benthonic foraminiferal species from the same samples. Isotope ratio pairs generally fall in a linear pattern, indicating constant $\delta^{13}C$ and $\delta^{18}O$ offsets between species, although there is scatter about these average offsets. Analytical precision ±2σ is shown on all plots.

Species to *O. umbonatus*	Depth	Age (Ma)	$\delta^{13}C$ VPDB (‰)	$\delta^{18}O$ VPDB (‰)
***Cibicidoides* spp.**				
C-7H-1, 125-127 cm	60.86		-1.07	0.25
C-7H-1, 125-127 cm	60.86		-0.99	-0.05
C-8H-1, 5-7 cm	71.45	30.4	-0.81	0.28
C-8H-3, 125-127 cm	75.65	32.33	-0.93	0.39
C-8H-5, 125-127 cm	78.65	32.77	-0.79	0.21
C-8H-6, 5-7 cm	78.95	32.81	-1.02	-0.14
C-8H-6, 45-47 cm	79.35	32.87	-0.77	0.28
	Mean		-0.91	0.17
	SD		0.12	0.19
***Gyrinoides* spp.**				
C-8H-1, 45-47 cm	71.85		-0.47	-0.05
C-8H-3, 125-127 cm	75.65	32.33	-0.40	0.08
C-8H-4, 5-7 cm	75.95	32.37	-0.22	0.21
C-8H-5, 45-47 cm	76.35	32.43	-0.49	-0.27
C-8H-5, 85-87 cm	78.25	32.71	-0.40	0.13
C-9H-1, 145-147 cm	82.32	33.31	-0.86	0.16
C-9H-2, 15-17 cm	82.52	33.34	-0.54	0.02
C-9H-2, 25-27 cm	82.62	33.35	-0.70	0.14
C-9H-2, 45-47 cm	82.82	33.38	-0.75	-0.47
C-9H-2, 105-107 cm	83.42	33.47	-0.82	-0.09
C-9H-2, 105-107 cm	83.42	33.47	-0.61	-0.27
C-9H-3, 5-7 cm	83.92	33.54	-0.72	-0.13
C-9H-4, 75-77 cm	86.12	33.87	-0.71	-0.54
	Mean		-0.59	-0.08
	SD		0.19	0.24
Osungularia mexicana				
C-8H-3, 105-107 cm	75.45	32.3	-0.78	-0.08
C-8H-4, 45-47 cm	76.35	32.43	-0.79	-0.02
C-8H-5, 5-7 cm	77.45	32.59	-0.67	-0.18
C-9H-2, 105-107 cm	83.42	33.47	-0.70	0.18
B-9H-5, 30-32 cm	84.46	33.62	-0.58	-0.01
C-9H-3, 135-137 cm	85.22	33.74	-0.75	-0.08
C-9H-3, 140-142 cm	85.27	33.74	-0.61	-0.14
C-9H-3, 145-147 cm	85.32	33.75	-0.52	-0.30
C-9H-3, 145-147 cm	85.32	33.75	-0.43	-0.25
A-9H-6, 141-143 cm	85.34	33.75	-0.60	0.00
C-9H-4, 25-27 cm	85.62	33.79	-0.58	0.73
	Mean		-0.64	-0.01
	SD		0.11	0.28

Nuttaloides truempyi				
C-10H-1, 90-92 cm	91.24	36.05	-0.53	0.54
C-10H-2, 140-147 cm	93.24	37.16	-0.49	0.38
C-10H-4, 45-47 cm	95.29	38.29	-0.75	0.40
C-10H-4, 45-47 cm	95.29	38.29	-0.37	0.55
C-10H-4, 65-67 cm	95.49	38.41	-0.52	0.31
C-10H-4, 85-87 cm	95.69	38.52	-0.95	0.27
C-10H-4, 125-127 cm	96.09	38.74	-0.72	0.25
C-10H-4, 145-147 cm	96.29	38.85	-0.68	0.43
Mean			-0.63	0.39
SD			0.18	0.11

Table 5.3: Benthonic foraminiferal inter-species offsets for individual samples with species pairs and the mean and standard deviation of offsets for all pairs. The mean offset has been used as the correction factor and applied to the benthonic foraminiferal isotope ratio datasets to produce the composite benthonic foraminiferal stable-isotope records shown in Figure 5.11.

methodological bias between studies, i.e. through assumptions of a regression slope of 1 between two species and that there was normal distribution of standard errors when calculating correction factors, leading to a potential uncertainty of at least 1–2 °C in bottom-water palaeotemperature estimations through the Cenozoic. While the least median squares regression method used by Katz et al. (2003), on a much larger paired foraminiferal isotope ratio dataset than that developed within this study, is more robust than the simple linear regression used in this study, the correction factors that they developed were not demonstrated to be statistically valid for post-Eocene applications and, as such, are not directly applicable to this study without further investigation. Unfortunately, the benthonic foraminiferal pairs identified within this study were insufficiently numerous to allow for a rigorous assessment and comparison of correction factors, thus it is not possible to say whether the Katz et al. (2003) corrections factors can be used for the Oligocene. As a consequence of this limitation, those correction factors developed within this study have been used to compile benthonic foraminiferal composite stable-isotope records.

	Calculated offset to *O. umbonatus* (VPDB; ‰)					
	Shackleton et al. (1984)		Katz et al. (2003)		This Study	
Species	$\delta^{13}C$	$\delta^{18}O$	$\delta^{13}C$	$\delta^{18}O$	$\delta^{13}C$	$\delta^{18}O$
Cibicidoides spp.	-1.00	0.50	-0.72	0.28	-1.02	0.19
Nuttaloides truempyi	-1.00	-0.35	-0.46	x*0.79+0.36	-0.61	0.34
Osungularia mexicana	-1.00	0.00			-0.61	0.02
Gyrinoides spp.					-0.65	-0.09

Table 5.4: Benthonic foraminiferal inter-species correction factors determined in this study compared to those calculated by Katz et al. (2003) for the Eocene. (It should be noted that the correction factors of Katz et al. (2003) have not been shown to be valid for the Oligocene.)

5.6.4 Benthonic foraminiferal composite isotope records

In order to produce the highest-resolution and most complete benthonic foraminiferal stable-isotope records for Site 1211, the individual species isotope data described above have been combined to form a composite dataset. This compilation was achieved using the benthonic foraminiferal inter-species correction factors described in Section 5.6.3, i.e. by correcting data for all other species to *O. umbonatus*. The composite isotope records were corrected to *O. umbonatus* for two reasons: first, the majority of the stable-isotope analyses completed in this study were for this species and, second, *O. umbonatus* has been shown to calcify in near oxygen-isotope equilibrium (Woodruff et al., 1980; Rathburn et al., 1996). Near equilibrium $\delta^{18}O$ values for *O. umbonatus* mean that there is no need to apply a further offset to the $\delta^{18}O$ record in order to produce accurate palaeotemperature estimates, removing a possible source of error from palaeotemperature calculations.

The composite benthonic foraminiferal stable-isotope records were filtered by splitting the data into one-million-year segments and rejecting any values that fell outside of $\pm 2\sigma$ of the mean for that interval. This filtering removed 10 of 187 data points (~5 %). The resulting filtered composite isotope ratio datasets are plotted, along with five-point running averages and 95% confidence intervals for descriptive purposes, in Figure 5.8 and 5.11. The stable-isotope values for each individual benthonic foraminiferal species are plotted as different symbols (same as in Figure 5.9) as a first-order check as to whether the inter-species offsets applied have introduced any secondary variability within the isotope records. For neither $\delta^{18}O$ nor $\delta^{13}C$, no species used in the benthonic compilation appears to depart from

the main body of *O. umbonatus* data suggesting description and interpretation of the compilation dataset does not introduce any artefacts into the Site 1211 record.

5.6.5 Benthonic foraminiferal composite $\delta^{18}O$ record

Composite $\delta^{18}O$ ratios range between ~0.9 and 2.8 ‰. Scatter within the dataset is approximately two times the ±2σ analytical precision across the interval ~34.0 to ~32.0 Ma, where the data density is greatest. Normalised benthonic foraminiferal $\delta^{18}O$ values increased from ~1.2 ‰ within Middle Eocene biozone CP14b, at ~39.5 Ma, to ~1.5 ‰ within Late Eocene biozone CP15, at ~36.9 Ma. Unequivocal identification of $\delta^{18}O$ trends within biozone CP15 is difficult since data are sparse between 36.6 and 34.2 Ma, hindering detailed interpretation over this stratigraphic interval. Nevertheless, despite the low density of data and evident scatter, available $\delta^{18}O$ values averaged ~1.5 ‰ throughout Late Eocene biozone CP15. From the base of latest Eocene to Earliest Oligocene biozone CP16a (34.2 Ma) normalised benthonic foraminiferal $\delta^{18}O$ values increased by ~0.4 ‰, from ~1.5 ‰ to ~1.9 ‰, over ~400 kyr, increasing by a further 0.7 ‰, from ~1.9 to 2.6 ‰, over <200 kyr during the earliest Oligocene (Figure 5.8). Maximum normalised benthonic foraminiferal $\delta^{18}O$ values were reached at ~33.6 Ma, immediately before the base of Early Oligocene biozone CP16b. Normalised benthonic foraminiferal $\delta^{18}O$ values then decreased abruptly by ~0.4 ‰ over ~200 kyr, before increasing to a second maximum of ~2.4 ‰ at 33.2 Ma. By the base of Early Oligocene biozone CP16c/CP17 (33.0 Ma), $\delta^{18}O$ values had once again decreased to ~2.0 ‰ and oscillated around ~2.0 ‰ until the base of Early Oligocene biozone CP18 (32.0 Ma; Figure 5.8). For the stratigraphic interval younger than 32.0 Ma, the data density is insufficient to identify any definite trends, although a change to more positive values is present within the running average.

5.6.6 Benthonic foraminiferal composite $\delta^{13}C$ record

Normalised benthonic foraminiferal $\delta^{13}C$ ratios vary between ~-0.9 and ~0.7 ‰. Over ~200 kyr intervals, scatter within the normalised benthonic foraminiferal composite $\delta^{13}C$ record is typically of the order of three times the ±2σ analytical error, although scatter is reduced between ~34.0 and ~32.0 Ma, where data density is greatest. Middle Eocene (biozone CP14b; ~39.5 to ~37.8 Ma) normalised benthonic foraminiferal $\delta^{13}C$ values averaged ~0.0 ‰ and varied between -0.4 and 0.2 ‰. Normalised benthonic foraminiferal

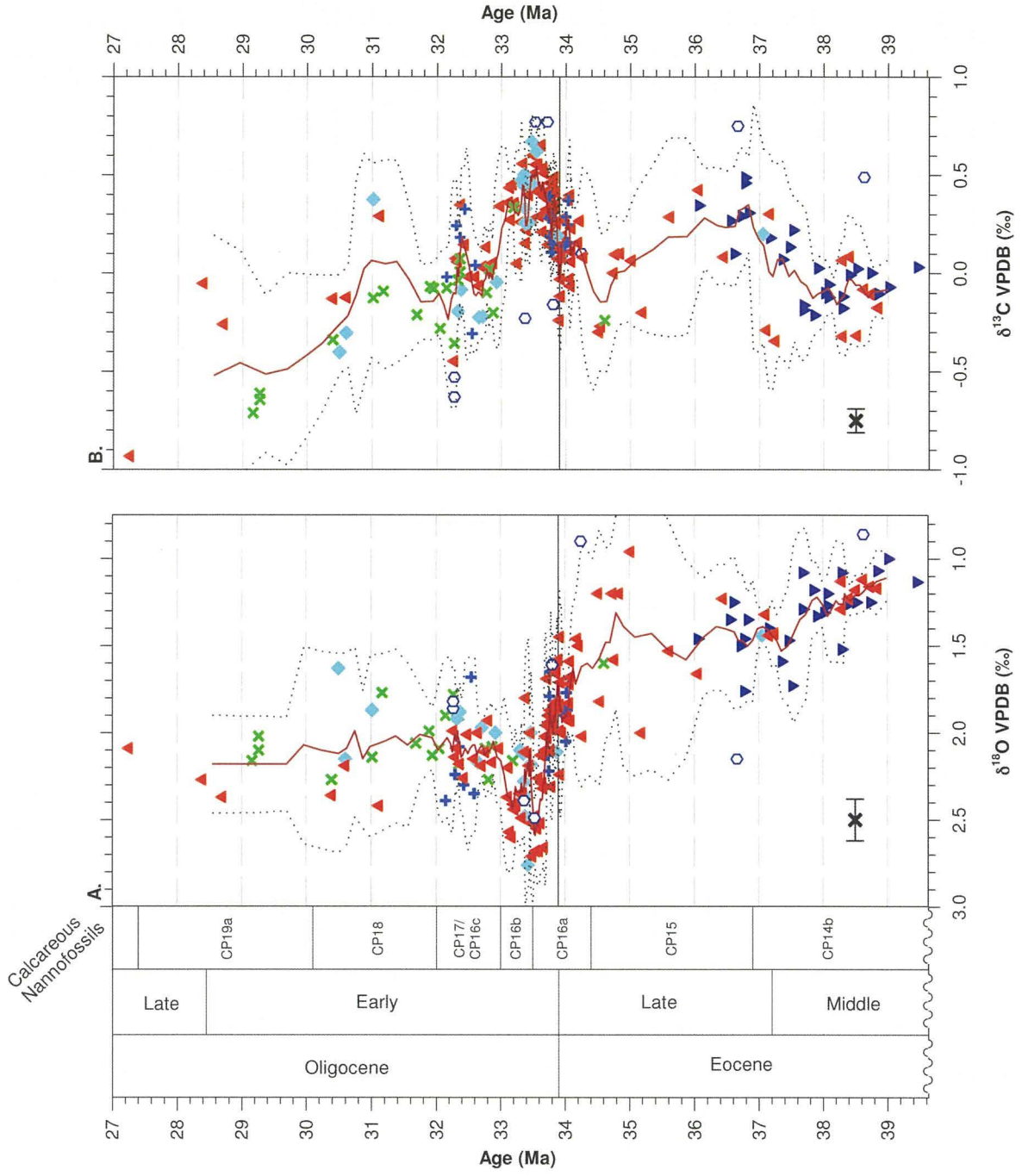

Figure 5.11: Benthonic foraminiferal composite stable-isotope records, with 5-point running averages and ± 2σ (95 %) confidence intervals included for descriptive purposes, plotted against numerical age. Symbols are as used in Figure 5.7 and the unfilled symbols are stable-isotope values rejected by filtering of the composite stable-isotope datasets, as described in the text (one value is not shown on the plot as it lay at 9.5 ‰ and 3.7 ‰ for $\delta^{18}O$ and $\delta^{13}C$ respectively).

$\delta^{13}C$ values then increased towards the end of Middle Eocene to ~0.4 ‰ at 36.8 Ma, i.e. immediately prior to the base of Late Eocene biozone CP15. Due to the scarcity of benthonic foraminifera few isotope data are available for the time interval between 36.6 and 34.2 Ma, but by 35.4 Ma normalised benthonic foraminiferal $\delta^{13}C$ values had decreased to ~0.0 ‰ and varied around this value until the Late Eocene base of biozone CP16a (~34.4 Ma). Normalised benthonic foraminiferal $\delta^{13}C$ values then increased through biozone CP16a, across the Eocene–Oligocene boundary, reaching the highest values of

~0.6 ‰ by the Early Oligocene base of biozone CP16b (33.4 Ma). $\delta^{13}C$ values remained relatively high, i.e. >~0.3 ‰ throughout biozone CP16b, before decreasing to ~0.0 ‰ at the Early Oligocene base of biozone CP16c/CP17 (33.0 Ma). Throughout biozone CP16c/CP17 normalised benthonic foraminiferal $\delta^{13}C$ values varied between -0.3 and 0.5 ‰. Between ~32.0 and ~27.0 Ma data density is low, although running average normalised benthonic foraminiferal $\delta^{13}C$ values decreased to -0.5 ‰ by the late Early Oligocene base of biozone CP19a.

5.7 Planktonic foraminiferal stable-isotope data

Stable-isotope records from Hole C were developed for four species of planktonic foraminifera: *Acarinina bullbrooki* and *Subbotina senni* (Middle Eocene) and *Catapsydrax unicavus* and *Turborotalia ampliapertura* (Early Oligocene), each of which are considered individually below. Stable-isotope data generated for these planktonic foraminifera were filtered using the same method that was applied to the benthonic foraminifera and <38 μm fine-fraction isotope records (see Sections 5.5 and 5.6) and are plotted against depth and numerical age in Figures 5.12 and 5.13, respectively. Filtering removed 3 of 88 samples (~3 %) for *C. unicavus* and 4 of 37 samples (~11 %) for *T. ampliapertura* (filled symbols in Figure 5.13); filtering had no effect on the *A. bullbrooki* and *S. senni* datasets due to the small number of samples and isotope ratio analyses completed.

5.7.1 Planktonic foraminiferal $\delta^{18}O$ data

$\delta^{18}O$ values for planktonic foraminifera range between ~-1.1 and ~2.1 ‰ (Figures 5.12A and 5.13A). The planktonic foraminiferal $\delta^{18}O$ records display relatively little scatter on an ~1.0 m scale, with the degree of scatter being a similar order of magnitude to the $\pm 2\sigma$ analytical precision. *S. senni* $\delta^{18}O$ values varied between ~-1.0 and ~-0.3 ‰ and there was a gradual increase in magnitude (from ~-1.0 to ~-0.3 ‰) through the Middle Eocene stratigraphic range of analyses (biozones CP13b and CP14b; ~99.2 to ~93.8 rmcd, Figure 5.12A; 39.7–37.5 Ma, Figure 5.13B). $\delta^{18}O$ values for *A. bullbrooki* are restricted to Middle Eocene biozone CP13b and averaged ~0.5 ‰, being higher than $\delta^{18}O$ values for *S. senni* from the same samples. The Middle Eocene *S. senni* and *A. bullbrooki* $\delta^{18}O$ values are lower than those recorded for the Oligocene planktonic foraminifera, when the lowest value was ~-0.1 ‰.

Between 37.5 and ~34.0 Ma no planktonic foraminifera stable-isotope data are available due to the insufficient numbers of single species of planktonic foraminifera within this interval, either due to fragmentation or samples being barren of planktonic foraminifera.

$\delta^{18}O$ records for both the Oligocene species begin at ~34.1 Ma, within latest Eocene to Early Oligocene biozone CP16a. *T. ampliapertura* $\delta^{18}O$ values varied between ~-0.1 and ~1.0 ‰, with values increasing by ~1.0 ‰ across the Eocene–Oligocene boundary, i.e. through biozone CP16a. *T. ampliapertura* $\delta^{18}O$ values stabilised at ~0.8 ‰ by the Early Oligocene base of biozone CP16b (33.5 Ma, ~84.0 rmcd), and remained at this value throughout biozone CP16b into Early Oligocene biozone CP17/CP16c (up to ~32.8 Ma; ~79.0 rmcd). *C. unicavus* exhibited higher $\delta^{18}O$ values than *T. ampliapertura* and ranged between ~0.4 and ~2.1 ‰. *C. unicavus* $\delta^{18}O$ values increased by >1.0 ‰ through Eocene–Oligocene boundary biozone CP16a, and had reached the highest values during Early Oligocene biozone CP16b (~33.4 Ma; ~83.0 rmcd). From the highest values at ~83.0 rmcd, *C. unicavus* $\delta^{18}O$ values decreased by ~0.7 ‰ over <100 kyr (~1.0 m), before increasing to ~2.0 ‰ over 200 kyr (~33.0 Ma, 80.0 rmcd) by Early Oligocene biozone CP16c/CP17. *C. unicavus* $\delta^{18}O$ values then decreased by ~0.4 ‰ by 32.8 Ma (79.0 rmcd), and then varied about ~1.6 ‰ through biozones CP16c/CP17. The most positive $\delta^{18}O$ values for *C. unicavus* occurred after the most positive $\delta^{18}O$ values recorded by both *T. ampliapertura* and the normalised benthonic foraminiferal composite $\delta^{18}O$ record (cf. Figure 5.8 and 5.11). Scatter in the *C. unicavus* and *T. ampliapertura* $\delta^{18}O$ is greater than the $\pm 2\sigma$ of the analytical precision throughout the dataset.

5.7.2 Planktonic foraminiferal $\delta^{13}C$ data

Planktonic foraminiferal $\delta^{13}C$ values range between ~0.6 and ~2.4 ‰. $\delta^{13}C$ values for *A. bullbrooki* range between ~2.1 and ~2.4 ‰ and generally increased by ~0.3 ‰ within Middle Eocene biozone CP13b, although there are only five data values. The *A. bullbrooki* $\delta^{13}C$ values overlap those of *S. senni*, which ranged between ~1.8 and ~2.4 ‰, with values for the latter species exhibiting a slight negative trend during Middle Eocene biozone CP14b, i.e. from ~39.6 to ~37.4 Ma (~98.0 to ~93.8 rmcd).

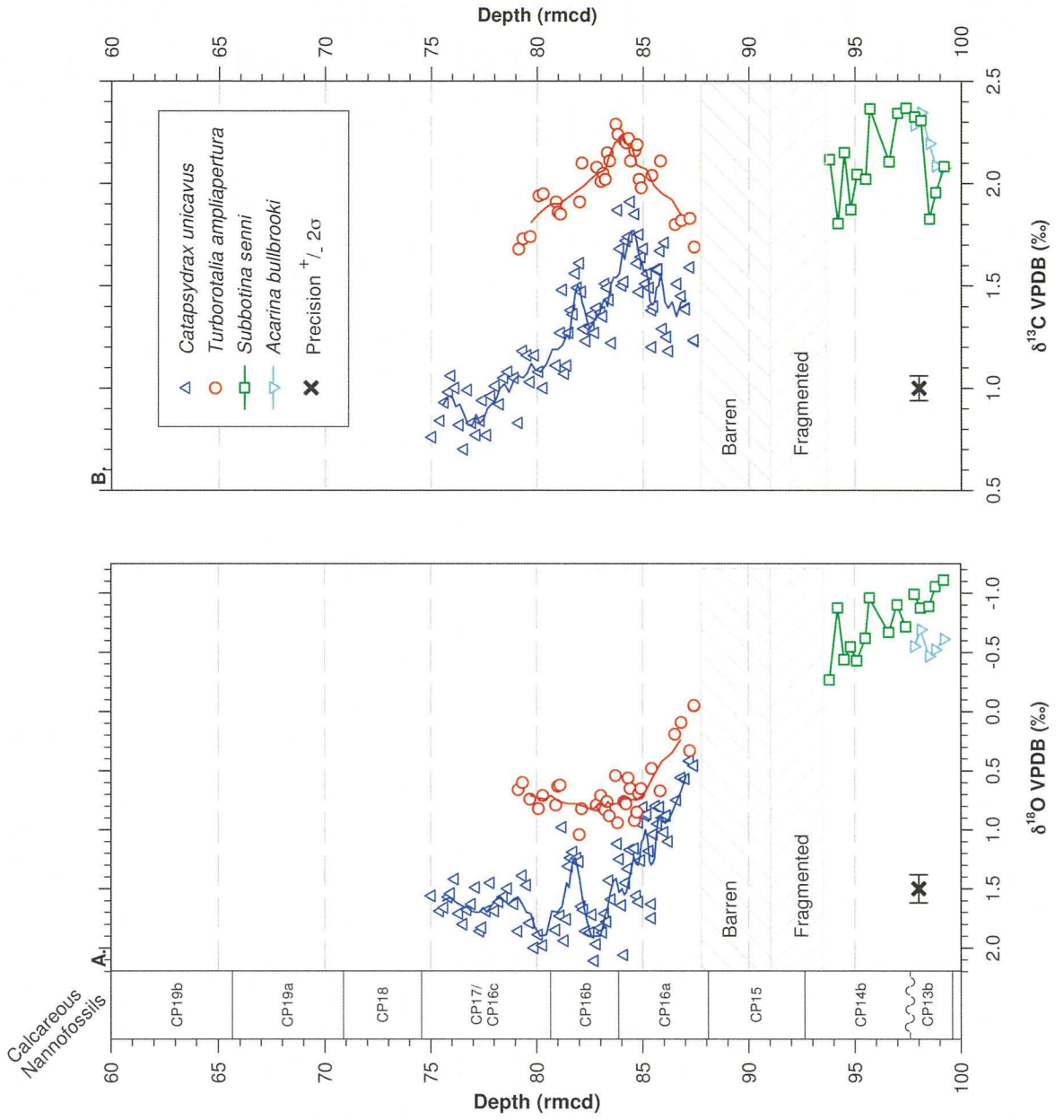

Figure 5.12: Planktonic foraminiferal stable-isotope data plotted against depth for Site 1211. A - $\delta^{18}O$. B - $\delta^{13}C$. 5-point running averages are also plotted through the *C. unicavus* and *T. ampliapertura* data. Analytical precision is shown at ±2σ (95 %) confidence intervals.

C. unicavus and *T. ampliapertura* $\delta^{13}C$ values range between ~0.6 and ~2.0 ‰ and from ~1.7 to ~2.3 ‰, respectively. As observed for the $\delta^{18}O$ values, scatter is greater than ±2σ of the analytical precision. $\delta^{13}C$ values for both of these species increased across the Eocene–Oligocene boundary, through biozone CP16a, attaining maximum values for both species close to the base of Early Oligocene biozone CP16b (~33.6 Ma). Following these maxima, $\delta^{13}C$ values for both species decreased throughout the remainder of the dataset, i.e. through Early Oligocene biozones CP16b and CP16c/CP17 (to 32.3 and 32.8 Ma, respectively). The better-defined *C. unicavus* $\delta^{13}C$ record decreased in magnitude by >1.0 ‰ over ~1.5 myr, although this decrease was not monotonic. *T. ampliapertura* $\delta^{13}C$ declined by ~0.6 ‰ from maximum values between 33.6 and 32.8 Ma. *C. unicavus* $\delta^{13}C$

values also are consistently lower than those for *T. ampliapertura* over the stratigraphic interval where data for both species were collected.

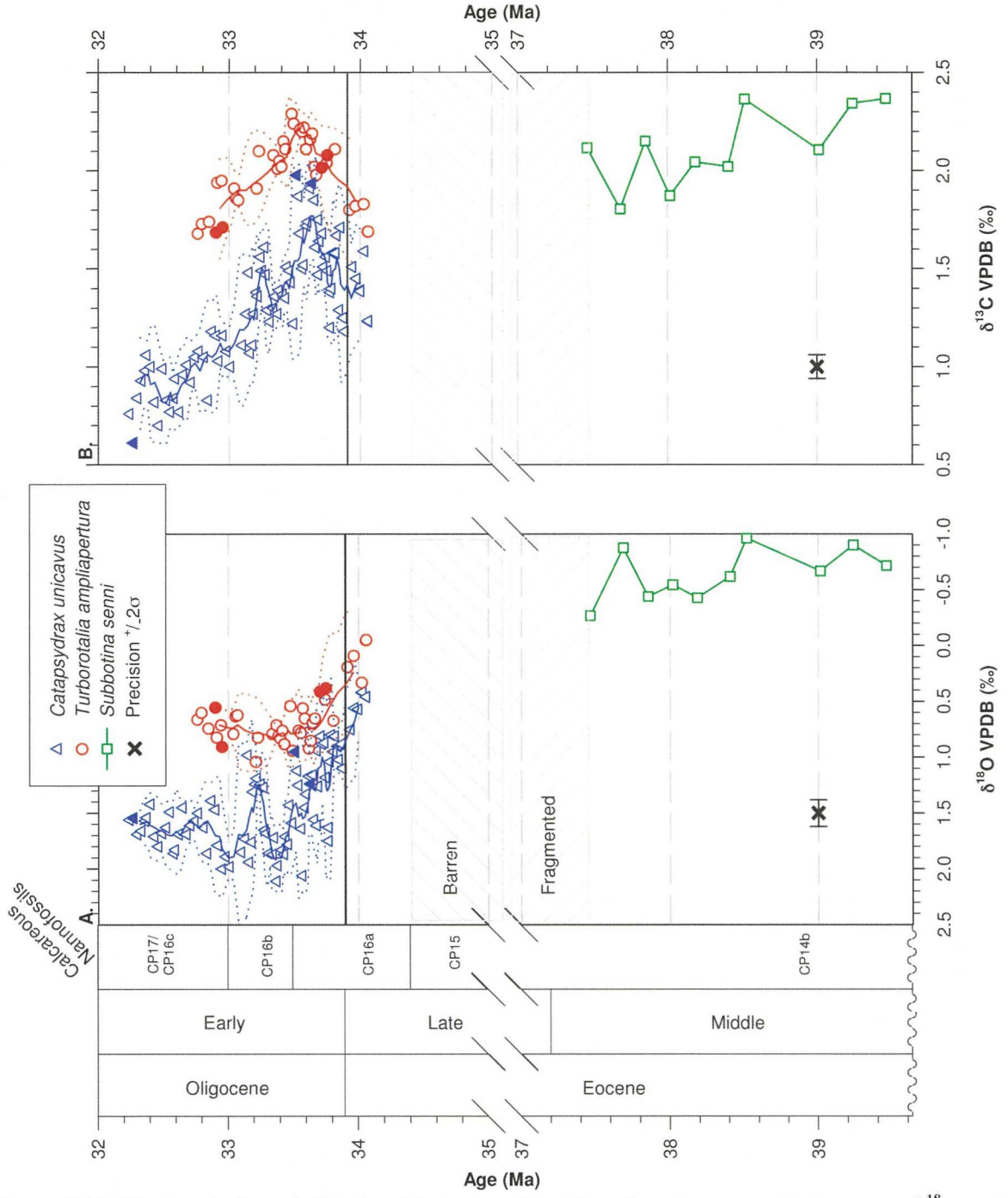

Figure 5.13: Planktonic foraminiferal stable-isotope data plotted against numerical age. A - $\delta^{18}O$. B - $\delta^{13}C$. Analytical precision is also shown at the ±2σ (95 %) confidence intervals. 5-point running averages with ± 2σ (95 %) confidence intervals are plotted through the *C. unicavus* and *T. ampliapertura* datasets. Filled symbols represent data points excluded from dataset as a result of falling outside the ±2σ filtering for either $\delta^{13}C$ or $\delta^{18}O$. Note that the age range is shorter than previous figures due to the restricted range of sampling of planktonic foraminifera in this study.

5.8 Foraminiferal preservation and SEM photomicrographs

The key foraminiferal species used in this study, i.e. *C. unicavus*, *N. truempyi*, *O. umbonatus* and *T. ampliapertura*, were photographed under a scanning electron microscope, to assess their preservation and the presence of any secondary calcite within chambers and/or overgrowth of the test walls. The photomicrographs taken (Plates 5.5 and 5.6) are described below and a related interpretation of preservation follows in Section 6.1.

Oridorsalis umbonatus

Selected specimens of *O. umbonatus* from Site 1211 are shown in Plate 5.5 (images A–F). All of the *O. umbonatus* specimens analysed in this study exhibited preservation similar to that shown in these SEM images; specimens with visible staining or test alteration, i.e. adhered carbonate, were not selected for geochemical proxy analyses. Plate 5.5 also includes images of opened *O. umbonatus* tests and a close-up of wall structure. Test surfaces had a granular appearance with little adhered calcite, either secondary carbonate growths or calcareous nannofossils (Plate 5.5; images A–C). Opened tests revealed some infilling carbonate, but this was limited to a few coccoliths present within chambers and the aperture (Plate 5.5; highlighted in images D and E). The *O. umbonatus* test wall structure is granular and relatively uniformly sized, similar to the texture of the outer wall of the test (Plate 5.5; images D-F).

Nuttaloides truempyi

Selected specimens of *N. truempyi*, exhibiting preservation typical of those sampled from Site 1211, are shown in Plate 5.5 (images G–K). The SEM photomicrographs reveal a granular wall texture, with limited evidence for adhered secondary carbonate or calcareous nannofossils (Plate 5.5; images G–I). Broken tests show that the granular texture is pervasive throughout the test wall cross section (Plate 5.5; image J), whilst infilling with secondary calcite or calcareous nannofossils was minor (Plate 5.5; images J and K).

Catapsydrax unicavus

Selected specimens of *C. unicavus* are shown in Plate 5.6 (images A–J). A cancellate wall structure is preserved, with semi-open unfilled pores. Observation of the outer test wall at higher magnification shows the presence of some coccolith plates within pores and also adhered to the test surface (Plate 5.6; images E and F). SEM photomicrographs of *C. unicavus* wall sections reveal generally open pores (Plate 5.6; images G–J) and two distinct

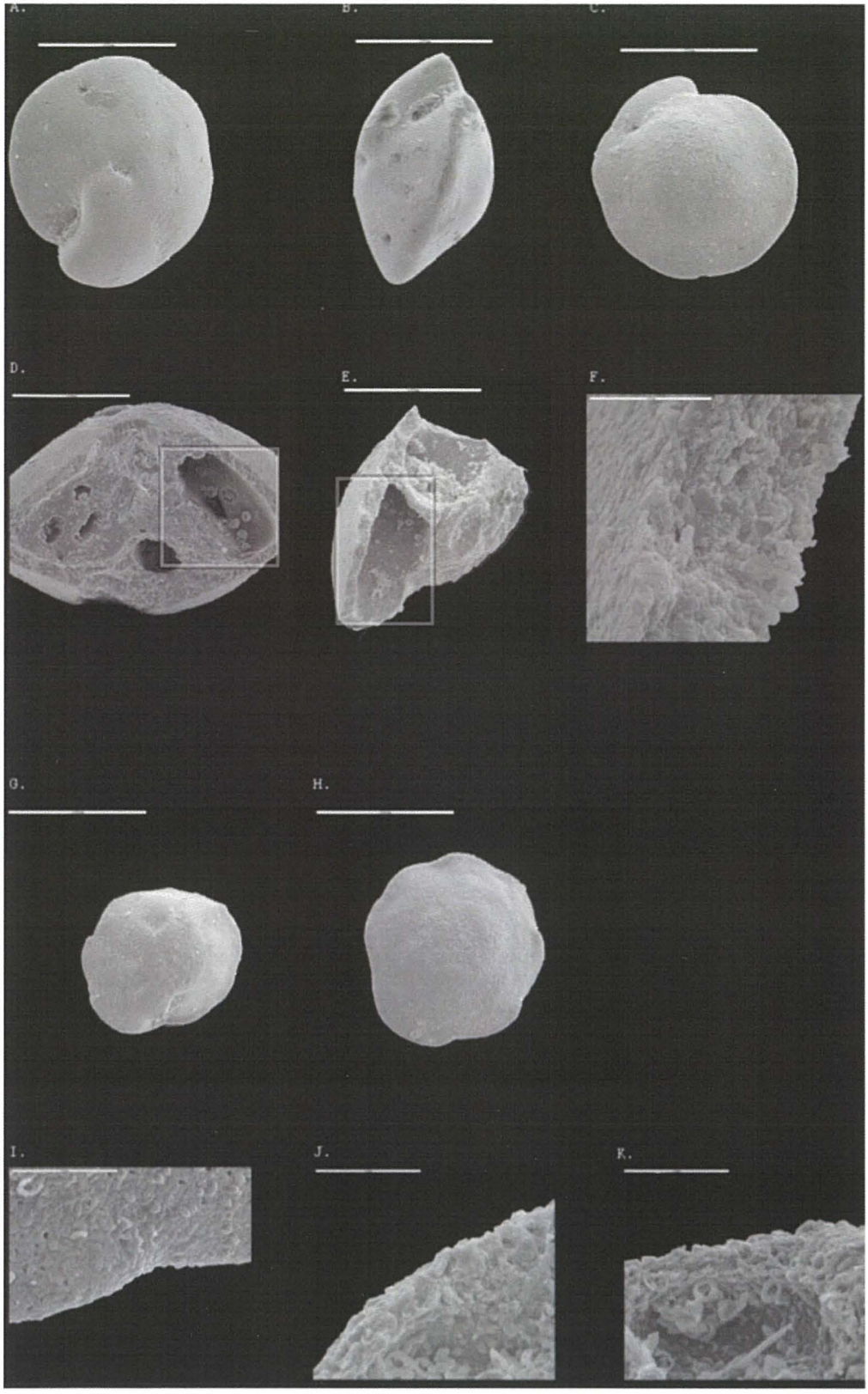

Plate 5.5: Photomicrographs of selected specimens of *Oridorsalis umbonatus*: A = dorsal view, B = lateral view, C = ventral view, D = opened specimen (all at 250x magnification, scale bars = 200 μm), E = opened chamber (500x magnification, scale bar = 100 μm) and F = close-up of wall structure (5000x magnification, scale bar = 10 μm). Highlight boxes in E and F show that infill of chambers was insignificant. Photomicrographs of selected specimens of *Nuttaloides truempyi*: G = dorsal view, H = ventral view (both at 250x magnification, scale bars = 200 μm), I = outer test wall, J = close-up of wall structure and K = inner wall surface of opened chamber (all at 2500x magnification, scale bar = 20 μm).

layers (Plate 5.6; images I–J). Image I clearly shows the presence of pores on the inner wall of the *C. unicavus* chambers, supporting the interpretation that the two layer wall structure is original, rather than a recrystallised overprint. Coccoliths are present within the chambers of opened tests (Plate 5.6; images G-J), suggesting the presence of some infilling, but secondary carbonate overgrowths are absent.

Turborotalia ampliapertura

Selected specimens of *T. ampliapertura* are shown in Plate 5.6 (images K–O). Images K–M clearly show the characteristic defoliation of the test wall that removes the outer pustulose layer either during deposition or sample processing (Plate 5.6; image M; left-hand side is not defoliated, right-hand side is defoliated; Pearson et al., 2006). The test wall pores appear to be open, with the occasional presence of isolated coccoliths either within pores or adhered to the test wall (Plate 5.6; images K–M). Sections through the test walls reveal a pervasive granular texture, whilst some coccolith infill also is present in chambers (Plate 5.6; images N and O).

In summary, SEM photomicrograph assessment of benthonic foraminifera does not reveal any obvious secondary carbonate and test chambers are open with only limited coccolith infill. Opened specimens of planktonic foraminifera again show little obvious secondary carbonate, but some coccolith infill was observed, particularly within *T. ampliapertura*. Chambers of opened planktonic foraminifera are, however, not completely infilled, suggesting that measured stable-isotope ratios will primarily reflect the foraminiferal test calcite. The implications of these observations of the foraminiferal test with respect to diagenesis and preservation of primary palaeoceanographic signals are discussed further in Section 6.1.

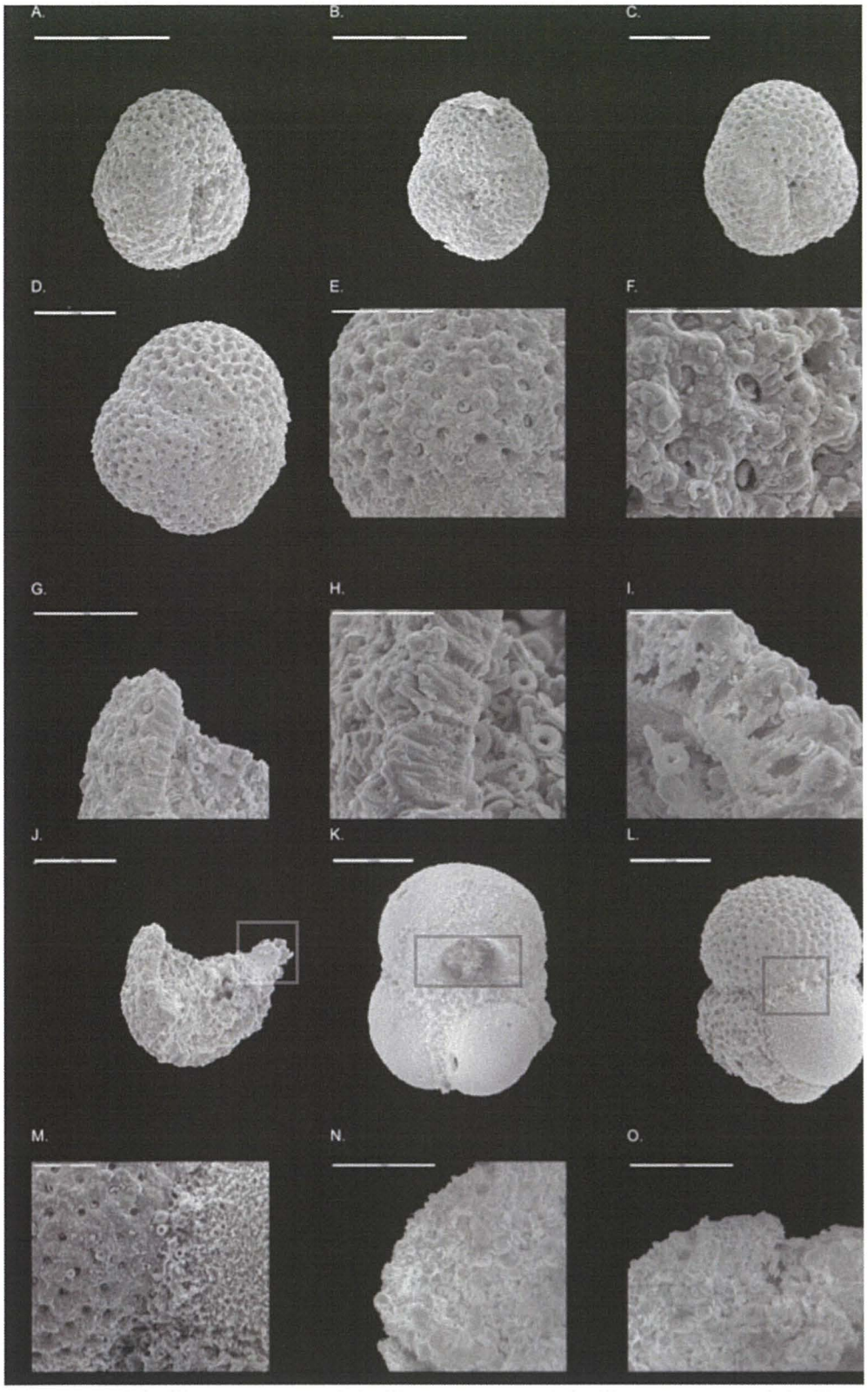

Plate 5.6: Photomicrographs of selected specimens of *Catapsydrax unicavus*: A and C = dorsal views, B and D = ventral views, E and F = close-ups of the external wall structure, G, H, I and J = close-ups of the internal wall structure. Highlight box in J features the presence of pores on the inner wall of the test. Photomicrographs of selected specimens of *Turborotalia ampliapertura*: K = dorsal view, L = ventral view, M = close-up of external wall texture, N and O = internal wall structure and chamber infill. Highlight in K shows infill of the aperture by fine-fraction material and in L shows the difference between defoliated and original test wall. Images A to D, and K and L were taken at 250x magnification with scale bars = 200 μm. Images E, G, N and O were taken at 1000x magnification with scale bars = 50 μm. Images F, H and I were taken at a magnification of 2500x with a scale bar of 20 μm. Images J and M were taken at 300x magnification with scale bars of 100 μm.

5.9 Surface-ocean to bottom-water isotope gradients ($\Delta\delta^{18}O$ and $\Delta\delta^{13}C$)

Surface-ocean to bottom-water isotope gradients (expressed as $\Delta\delta^{18}O$ and $\Delta\delta^{13}C$ values) have been calculated by subtracting *O. umbonatus* stable-isotope values from the stratigraphically equivalent planktonic foraminiferal and <38 μm fine-fraction stable-isotope data. The resulting records of $\Delta\delta^{18}O$ and $\Delta\delta^{13}C$ are plotted in Figures 5.14 and 5.15 with a propagated analytical precision at 95 % (±2σ) confidence limits; five-point running averages, with associated 95 % confidence intervals (±2σ) are also plotted to aid description and subsequent interpretation. No $\Delta\delta^{18}O$ and $\Delta\delta^{13}C$ values have been plotted for Eocene planktonic foraminifera, since only two *S. senni – O. umbonatus* paired isotope-ratio analyses fell within the stratigraphic range to which numerical age determinations have been assigned, which prevents any meaningful description or interpretation for that time interval.

5.8.1 Surface-ocean to bottom-water $\Delta\delta^{18}O$ gradients

The *T. ampliapertura–O. umbonatus* $\Delta\delta^{18}O$ gradient (hereafter $\Delta\delta^{18}O_{T.\ amp}$) is of greater magnitude than that of *C. unicavus–O. umbonatus* (hereafter $\Delta\delta^{18}O_{C.\ uni}$; Figure 5.14A). $\Delta\delta^{18}O_{T.\ amp}$ exhibits a degree of scatter, with values between ~-1.0 and ~-2.0 ‰ throughout Early Oligocene biozones CP16a and CP16b; this scatter is reflected in the relatively broad 95 % confidence intervals, typically ~±0.5 ‰. Running mean values show no overall trend in $\Delta\delta^{18}O_{T.\ amp}$ across this stratigraphic interval. The $\Delta\delta^{18}O_{C.\ uni}$ record is at higher stratigraphic resolution and spans a greater stratigraphic range than that of $\Delta\delta^{18}O_{T.\ amp}$, thus allowing more detailed description. $\Delta\delta^{18}O_{C.\ uni}$ varied between ~-0.2 and ~-1.7 ‰ during Early Oligocene biozones CP16a and CP16b, with the running average suggesting a ~400 to ~500 kyr cycle of ~1.0 ‰ with maxima in running average gradients of ~-1.3 ‰ at ~33.7 and ~33.2 Ma and minimum running average gradients of ~-0.4 ‰ at ~33.4 Ma. During Early Oligocene biozones CP16c/CP17, the $\Delta\delta^{18}O_{C.\ uni}$ gradient reduced in magnitude to between ~-0.2 and ~-0.8 ‰, with running average values remaining at ~-0.5 ‰ for the remainder of the dataset until ~32.2 Ma. Again, scatter within the dataset, as shown by the 95 % confidence interval with an envelope of ~1.0 ‰ for much of the dataset, was considerably greater than the analytical precision.

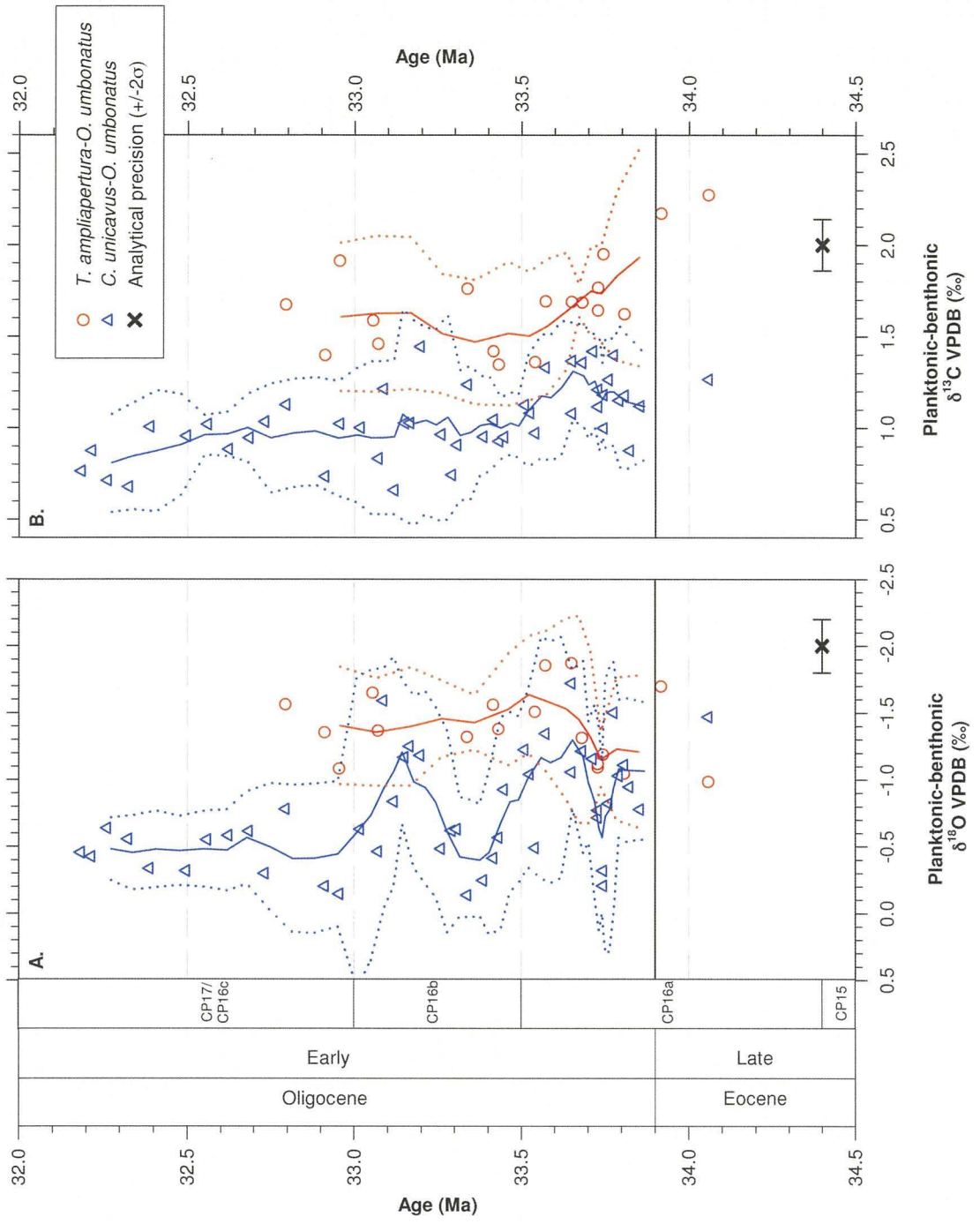

Figure 5.14: Plots of surface-ocean to bottom-water stable-isotope ratio gradients, i.e. planktonic to benthonic foraminiferal $\Delta\delta^{18}O$ (A.) and $\Delta\delta^{13}C$ (B.) values for *T. ampliapertura–O. umbonatus* (red circles), *C. unicavus–O. umbonatus* (blue triangles). The 95 % (±2σ) analytical error shown is that propagated for the benthonic and planktonic foraminifera stable-isotope records. The red and blue lines are 5-point running averages with 95 % (±2σ) confidence intervals (dotted) through the *T. ampliapertura–O. umbonatus* and *C. unicavus–O. umbonatus* gradient records, respectively. The magnitude of 95 % confidence intervals show that surface-ocean to bottom-water gradients are poorly constrained by the records from Site 1211.

Values for the <38 µm fine-fraction–*O. umbonatus* $\Delta\delta^{18}O$ gradient (hereafter $\Delta\delta^{18}O_{ff}$) varied between ~-1.0 and ~-2.3 ‰ between 39.0 and 28.4 Ma, with the majority of values between -1.0 and -2.3 ‰ (Figure 5.15A). The running average $\Delta\delta^{18}O_{ff}$ gradient remained constant within the 95 % analytical precision during the Middle and Late Eocene until ~35.4 Ma, increasing by ~0.5 ‰ between 35.4 and 34.8 Ma. For the stratigraphic interval

from 35.0–32.0 Ma the running average $\Delta\delta^{18}O_{ff}$ gradient ranged between -1.5 and -2.1 ‰, after which $\Delta\delta^{18}O_{ff}$ values are sparse. The scatter within the dataset and wide 95 % confidence intervals for both analytical precision and running averages (>0.5 ‰) prevent identification of short-term variation.

5.9.2 Surface-ocean to bottom-water $\Delta\delta^{13}C$ gradients

The *T. ampliapertura–O. umbonatus* $\Delta\delta^{13}C$ gradient (hereafter $\Delta\delta^{13}C_{T.\ amp}$) is more positive than the *C. unicavus–O. umbonatus* gradient (hereafter $\Delta\delta^{13}C_{C.\ uni}$; Figure 5.14B). $\Delta\delta^{13}C_{T.\ amp}$ running average values display little variation between ~34.1 and ~32.7 Ma. The $\Delta\delta^{13}C_{C.\ uni}$ gradient exhibits a range of values between ~0.6 to ~1.5 ‰ during Early Oligocene biozones CP16a, CP16b and CP16c/CP17. During biozone CP16a, running average $\Delta\delta^{13}C_{C.\ uni}$ values increased by ~0.2 ‰, reaching a maximum of ~1.3 ‰ at ~33.7 Ma. The magnitude of the $\Delta\delta^{13}C_{C.\ uni}$ gradient decreased following the maximum at ~33.7 Ma, to ~1.0 ‰ by biozone CP16b (~33.5 Ma), with running average values remaining at ~1.0 ‰ throughout the remainder of that biozone and into biozone CP16c/CP17. Scatter within the data was greater than the analytical precision, whilst the 95 % confidence interval varied depending on the density of data points.

Running average <38 μm fine-fraction (hereafter $\Delta\delta^{13}C_{ff}$) gradients were ~1.6 ‰ between ~39.0 and 35.0 Ma, before decreasing to ~1.3 ‰ at ~35.0 Ma (Figure 5.15B). $\Delta\delta^{13}C_{ff}$ data are, however, relatively sparse across this stratigraphic interval. The gradient then increased sharply during biozone CP16a by ~0.3 ‰, continuing to increase gradually throughout the remainder of the dataset to >2.0 ‰. 95 % confidence intervals around the 5-point running average were large (~2.0 ‰) outside of the interval 35.0 to 32.0 Ma (~0.5 ‰), reflecting the high degree of scatter. The magnitude of confidence intervals between 35.0 and 32.0 Ma were equivalent to those observed for the $\Delta\delta^{13}C_{T.\ amp}$ and $\Delta\delta^{13}C_{C.\ uni}$ gradients.

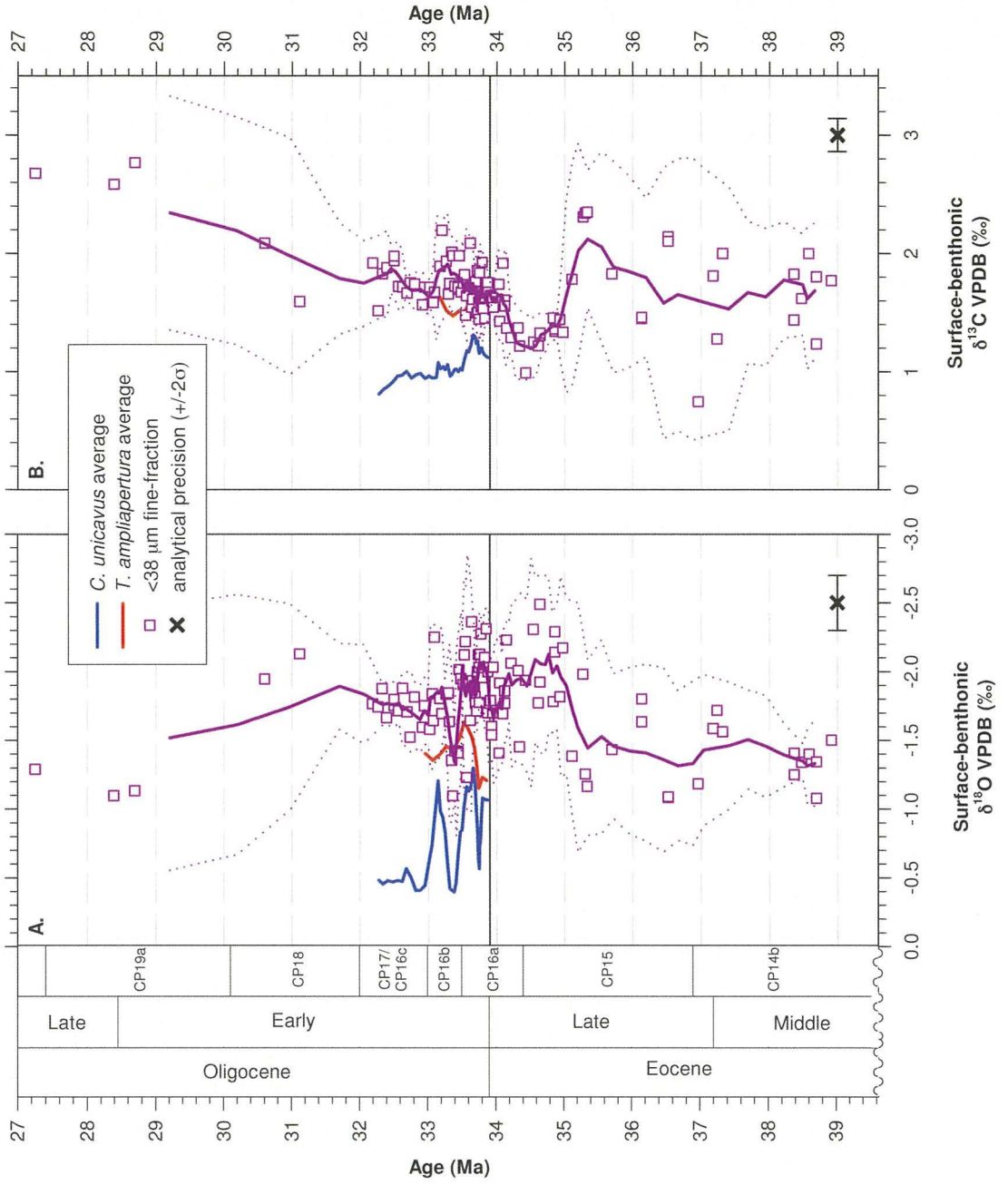

Figure 5.15: Plots of surface-ocean to bottom-water stable-isotope ratio gradients, i.e. the <38 µm fine-fraction to *O. umbonatus* $\Delta\delta^{18}O$ (A.) and $\Delta\delta^{13}C$ (B.) values, shown as purple squares with a 5-point running average (purple line) and 95 % (± 2σ) confidence interval (dotted purple line). 5-point running averages for *T. ampliapertura* to *O. umbonatus* (red line) and *C. unicavus* to *O. umbonatus* (blue line) $\Delta\delta^{18}O$ and $\Delta\delta^{13}C$ values from Figure 5.14 also are plotted. Analytical precision (± 2σ) for the analytical error propagated in calculating the records is also shown (cross and error bars at 39 Ma). It can be observed that scatter within the data are greater than the analytical precision, whilst the 95 % confidence interval indicates that the surface-ocean to bottom-water gradient was not well constrained, with a minimum envelope of ~0.5 ‰ at ~34 Ma.

5.10 Benthonic foraminiferal element/Ca ratios

Element/Ca ratios from the benthonic foraminifera analysed during the course of this study were filtered prior to plotting and description. The first consideration taken when filtering the element/Ca ratio dataset was identification of contaminated samples, which was

achieved through consideration of Mn/Ca and Ti/Ca ratios. A Mn/Ca ratio of >0.1 mmol/mol has been taken as evidence for the occurrence of significant Mn-oxide overgrowths on the foraminiferal test that likely indicate the presence of authigenic phases and potentially elevated and erroneous Mg/Ca ratios (Boyle, 1983; Yu et al., 2007). Ti/Ca ratios were considered in the context of non-carbonate silicate contamination, but generally were below analytical detection limits (>80 % of samples). Use of alternative, more rigorous, "cut-off" Mn/Ca (0.05 and 0.01 mmol/mol) and Ti/Ca (0.01 mmol/mol) threshold ratios were investigated; however, these more stringent data rejection criteria did not make systematic differences to the dataset, i.e. did not remove elevated Mg/Ca ratios that could have been associated with contamination, and thus were not deemed necessary. Of the 174 benthonic foraminiferal element/Ca ratio analyses completed only five had Mn/Ca values >0.1 mmol/mol (<3 % rejection rate) (Figure 5.16A). Samples that had Ti concentrations above analytical detection limits revealed a weak significant relationship between Mg/Ca and Ti/Ca ratios (Figure 5.16B; $r^2 = 0.12$, p-values = 0.05), while 28 of 34 (82 %) >LDL Ti/Ca ratios generally were <0.01 mmol/mol, with all samples <0.06 mmol/mol. Sr/Ca ratios plotted against Mg/Ca ratios are also shown in Figure 5.16C to assess whether there was any inter-relationship between these ratios; there is a weak but statistically significant relationship ($r^2 = 0.1873$, $p < 0.0001$). The significance of Mg/Ca to Sr/Ca ratios is considered in Section 6.1. Neither the Ti/Ca nor Sr/Ca relationship to Mg/Ca supports the use of a threshold value for contamination based on the results from Site 1211.

Following rejection of the small number of benthonic foraminiferal samples with Mn/Ca ratios >0.1 mmol/mol, the relationship between Ca concentrations measured in solution and determined Mg/Ca ratios then was assessed (Figure 5.17). This assessment was completed because sample solutions with low Ca concentrations would indicate a small quantity of foraminiferal material remained after the chemical cleaning procedures (see Section 3.6), which likely would have resulted in low Mg concentrations that could have yielded erroneous Mg/Ca ratios as the measured Mg concentration approaches analytical detection limits. Solution Ca concentrations of ~2 to ~70 μg/ml were measured, with the majority (~97 %) of the samples having Ca concentrations in solution <40 μg/ml. Across this range of Ca concentrations, benthonic foraminiferal Mg/Ca ratios ranged between ~0.8 and ~4.1 mmol/mol, with the majority (~88 %) of Mg/Ca ratios from ~1.0 to ~3.0 mmol. There is no statistically significant relationship between Ca concentrations in solution and Mg/Ca ratios ($r^2 = 0.0012$, $p = 0.66$) and, as such, there is no justifiable reason to apply any

filtering of the benthonic foraminiferal element/Ca ratio dataset based on Ca concentration measured in solution.

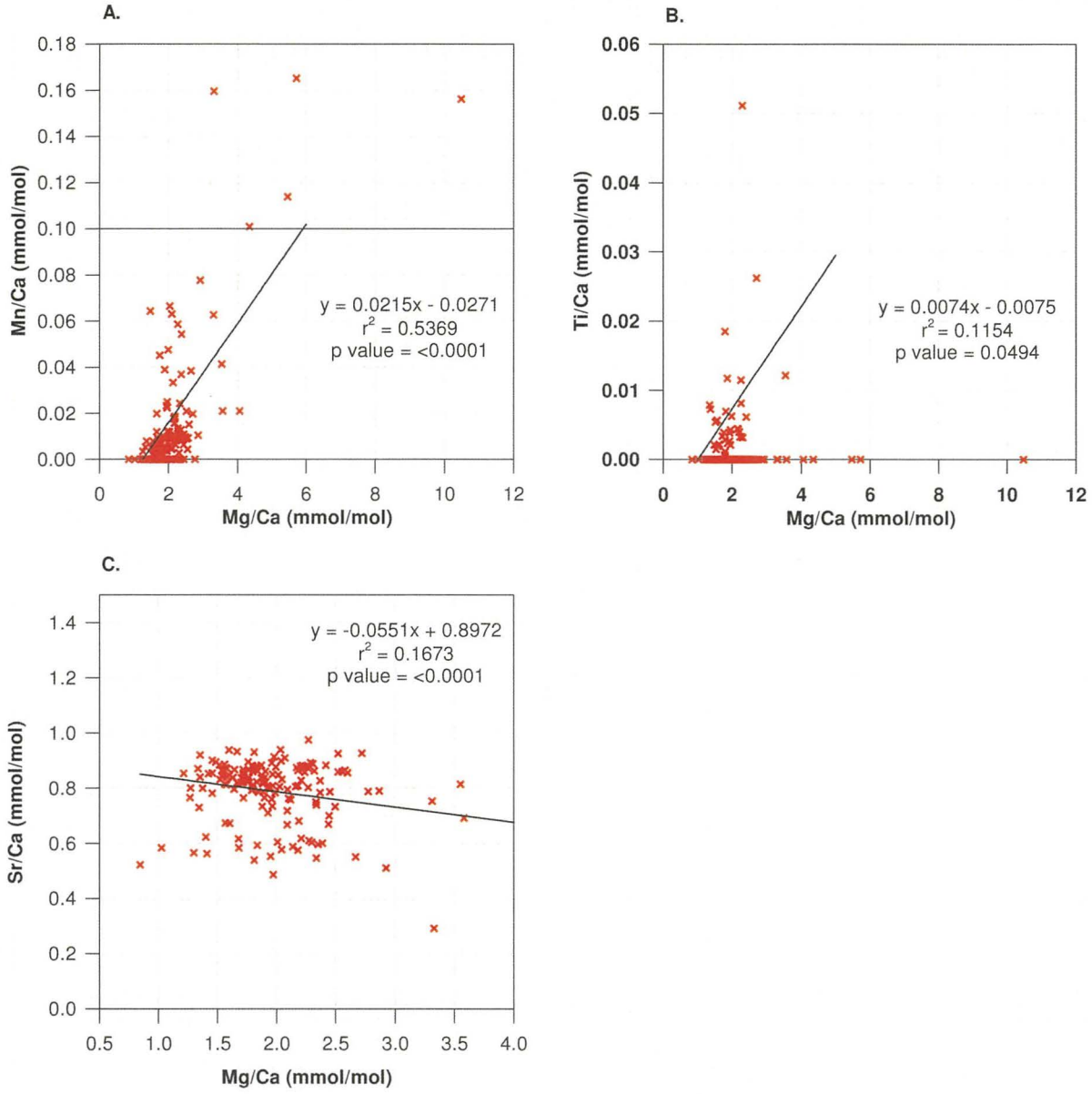

Figure 5.16: Plots of Mn/Ca (A), Ti/Ca (B) and Sr/Ca (C) ratios against Mg/Ca ratios, to assess contamination from authigenic phases (Mn) and silicates (Ti). Regression lines indicate the relationships between element/Ca and Mg/Ca ratios for all non-zero ratios; there is a statistically significant (p-value <0.001) moderate strength correlation (r^2 = 0.54) between Mn/Ca and Mg/Ca ratios, supporting the use of an upper limit for Mn/Ca ratios to remove samples likely to have a significant authigenic component; Ti/Ca and Sr/Ca ratios both show statistically significant (p-values <0.05), but very weak, relationships with Mg/Ca ratios, indicating no requirement to filter the dataset based on these element/Ca ratios. It can be observed that the majority of samples had very low Mn/Ca and Ti/Ca ratios, indicating that contamination was not a significant problem.

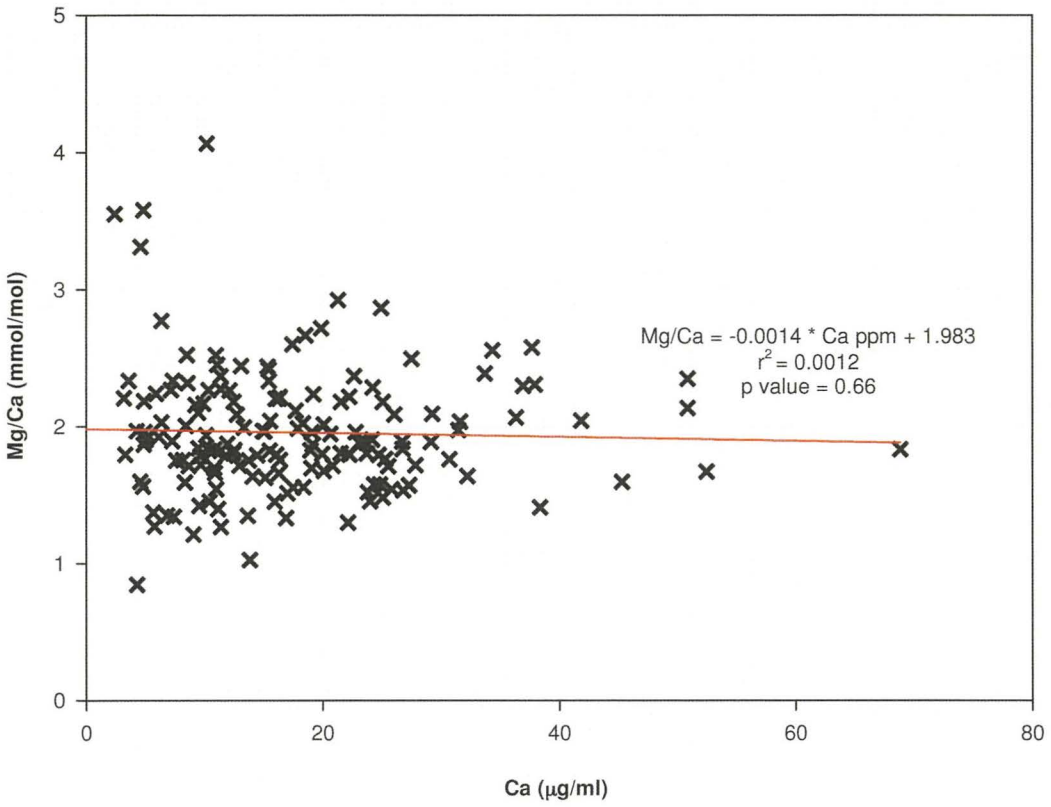

Figure 5.17: Mg/Ca ratios plotted against Ca concentrations measured in solution, excluding those samples with Mn/Ca ratios >0.1 mmol/mol. It is clear from the regression that there is no statistically significant systematic variation of Mg/Ca ratio with Ca concentration measured in solution and, as a consequence, no filtering based on solution Ca concentration has been applied to the element/Ca ratio dataset.

The final filtering step applied followed calculation of mean Mg/Ca and Sr/Ca ratios for one-million-year bins and rejection of data values that were outside of a 95 % confidence interval for each one million year bin, i.e. a mean $\pm 2\sigma$ rejection criterion, as applied also to the stable-isotope ratio datasets (cf. Section 5.5 and 5.6). The filtering step was applied to data from Hole C that was to be used for subsequent description and interpretation. This filtering approach removed a further 19 benthonic foraminiferal element/Ca ratio data points (~14 % rejection rate), in addition to the 3 % removed due to having Mn/Ca ratio >0.1 mmol/mol, leaving 121 robust benthonic foraminiferal element/Ca analyses (~85 % of the total number of samples measured). Benthonic foraminiferal element/Ca ratios are plotted in Figures 5.18 and 5.19, against depth and numerical age, respectively. Figure 5.18 also shows the element/Ca ratios by day of analysis, as well as those analyses rejected by the filtering approaches

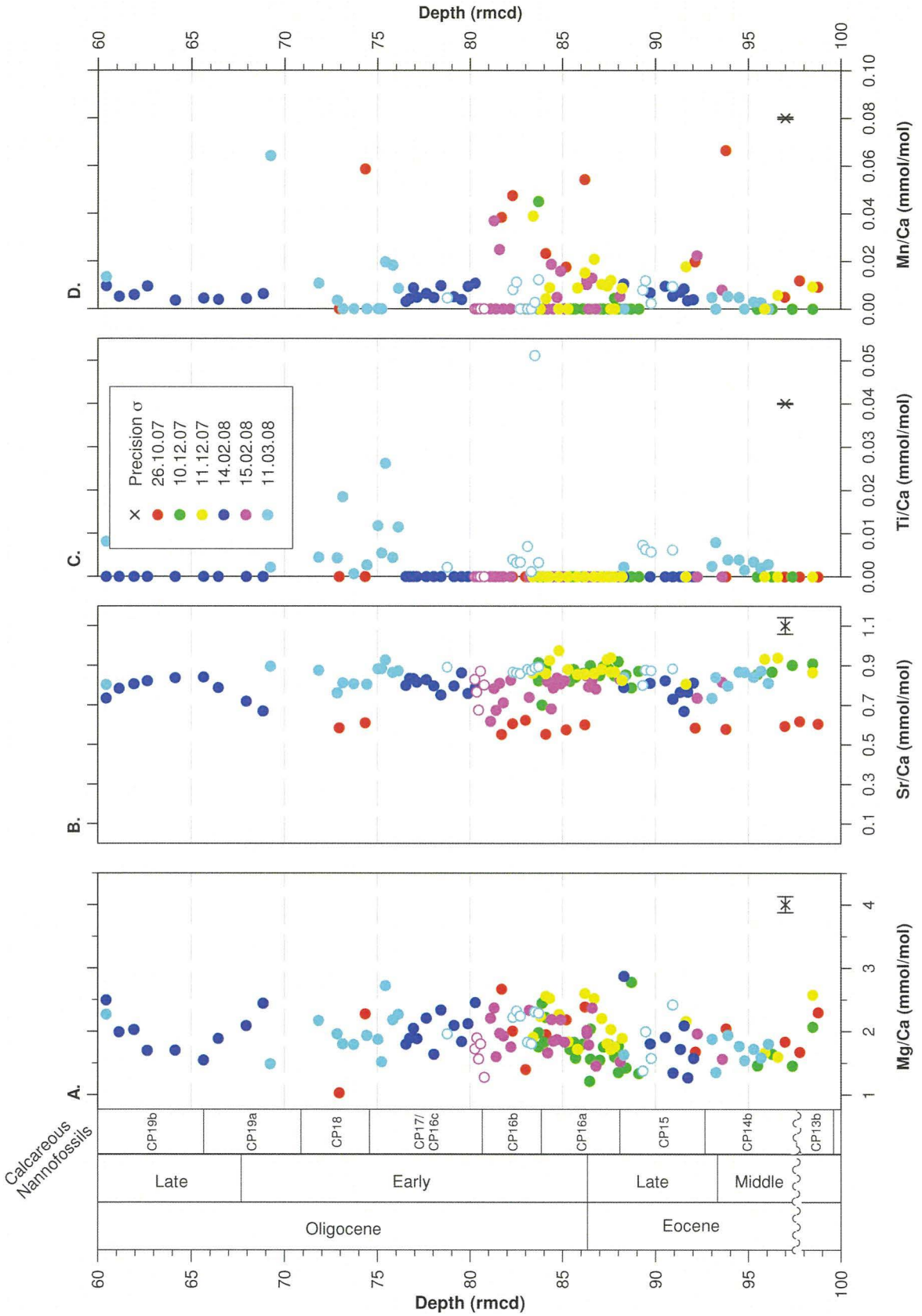

Figure 5.18: Plots of Site 1211 benthonic foraminiferal (*O. umbonatus*) element/Ca ratios (A = Mg/Ca, B = Sr/Ca, C = Ti/Ca and D = Mn/Ca; all in mmol/mol). Element/Ca ratios are plotted by day of analysis in different colours, showing that there is no systematic inter-day bias in measured element/Ca ratios, except for Sr/Ca from the 26th October, 2007. The analytical precision (±2σ) for each element/Ca ratio is shown in the bottom right of each panel. Element/Ca ratios from foraminifera picked from Hole A are shown as unfilled symbols in the colour of the day of analysis.

described above. Figure 5.19 includes the final accepted Mg/Ca and Sr/Ca ratios from Hole C with five-point running averages. Analytical precisions (±2σ) are also shown for each element/Ca ratio on Figures 5.18 and 5.19 and each element/Ca ratio dataset is described in turn below.

5.10.1 Benthonic foraminiferal Ti/Ca and Mn/Ca ratios

As described above, Ti/Ca and Mn/Ca ratios were measured primarily to allow an assessment of contamination and data filtering; however, identification of any stratigraphic trends within these data also has potential to further indicate the presence of any down-core trends in contamination, thus they are described before Mg/Ca and Sr/Ca ratios. Ti/Ca ratios ranged from 0.0011 to 0.0511 mmol/mol and Mn/Ca ratios ranged between 0.0024 and 0.0780 mmol/mol (Figure 5.16C and D). For both Mn/Ca and Ti/Ca ratios, a large proportion of the samples (51 of 121, 42 %, for Mn/Ca; 100 of 121, ~83 %, for Ti/Ca), recorded counts per second signals that were below the lower limit of detection (LLD), specified within this study as 3σ of the average value of procedural blank solutions, and thus have been assigned nominal Ti/Ca and Mn/Ca ratios of zero (although of course this is not actually the case). LLD values for Mn had a mean of 4033 ±3383 counts (N=6), LLD for Ti/Ca had a mean of 115 ± 133 counts (N=6). The stratigraphic records of benthonic foraminiferal Ti/Ca alnd Mn/Ca ratios are both insufficiently defined by measured values >LLD to allow the identification of any systematic trends across the stratigraphic range of this study.

5.10.2 Benthonic foraminiferal Mg/Ca ratios

Filtered benthonic foraminiferal Mg/Ca ratios range from ~1.0 to ~2.9 mmol/mol (Figures 5.18A and 5.19A) and do not show any systematic inter-day offset(s). Scatter throughout the dataset was much greater (4–5 times) than the analytical precision (at ±2σ level) and, within <1 m stratigraphic intervals (e.g. at ~86 rmcd) Mg/Ca ratios vary between ~1.1 and 2.5 mmol/mol compared to an analytical precision of ±0.12 mmol/mol. Mg/Ca ratios were relatively stable during Middle Eocene biozone CP14b and Late Eocene biozone CP15 (39.6 to ~34.2 Ma), averaging ~1.7 mmol/mol, although the running average through the data identifies a trend to slightly higher Mg/Ca ratios over this time interval. Data density is highest between the base of latest Eocene biozone CP16a through to the base of Early Oligocene biozone CP18, leading to an increase in variability of the running average in

Mg/Ca ratios. Mg/Ca ratios increased at the base of biozone CP16a to an average value of ~2.0 mmol/mol by 34.0 Ma. Between 34.0 and 32.0 Ma, during Eocene–Oligocene biozone CP16a and Early Oligocene biozones CP16b and CP16c/CP17, Mg/Ca ratios exhibited a large degree of scatter, between 1.2 and 2.7 mmol/mol, with the five-point running average varying between~1.8 and ~2.1 mmol/mol. In general, running average Early Oligocene Mg/Ca ratios were higher than those measured for the Middle–Late Eocene. Measured benthonic foraminiferal ratios from Early–Late Oligocene biozones CP18 and CP19a are at much lower stratigraphic resolution, than the earlier part of the stratigraphic record, hindering robust identification of trends, although running average Mg/Ca ratios remained higher than Middle–Late Eocene values.

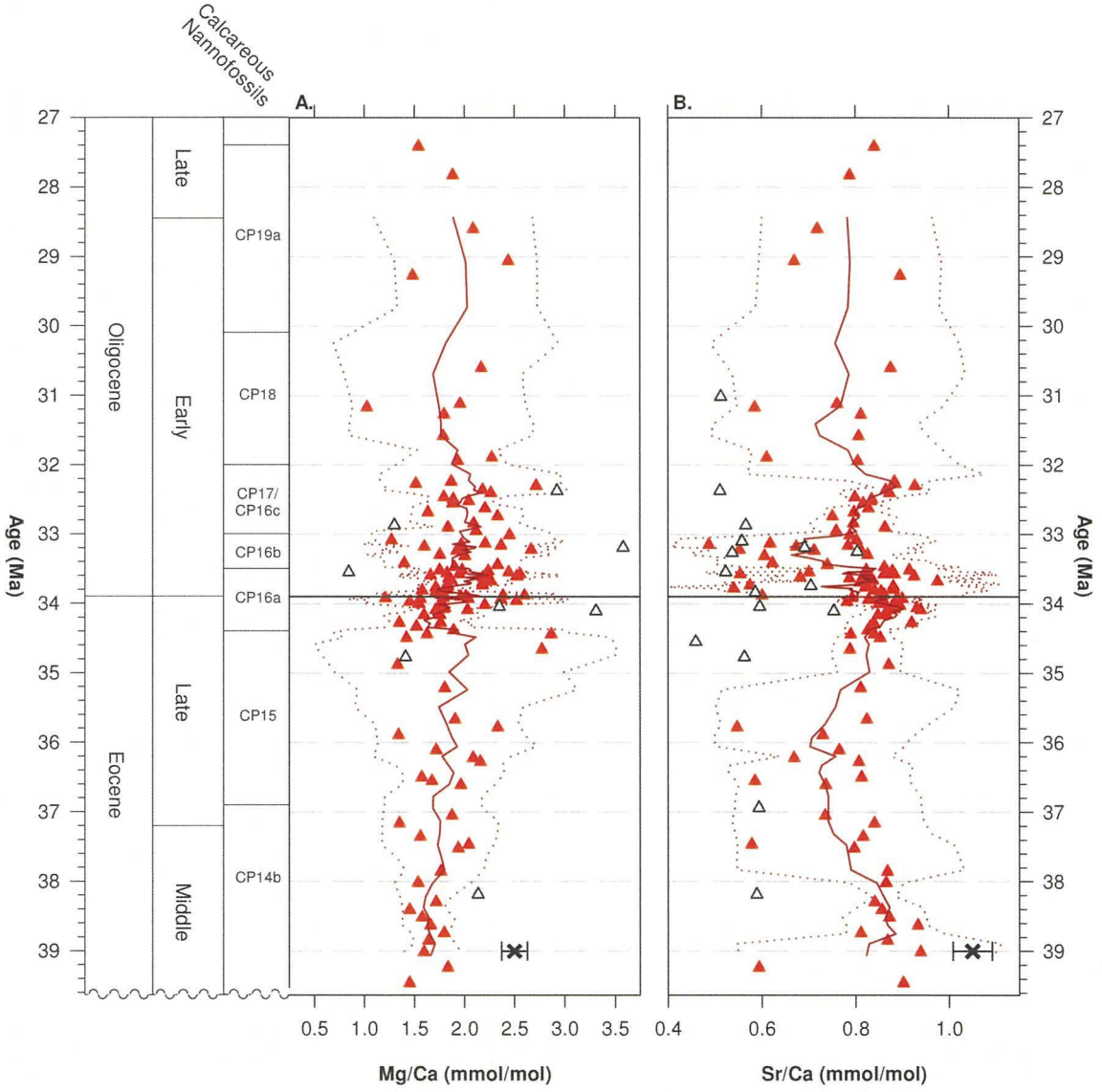

Figure 5.19: Plot of Site 1211 benthonic foraminiferal *O. umbonatus* element/Ca ratios against numerical age, including five-point running averages and 95 % (± 2σ) confidence intervals through each dataset. Although both Mg/Ca and Sr/Ca ratios display scatter greater than the analytical precision, 95 % (±2σ) confidence limits shown, Mg/Ca ratios display a much greater range of scatter than Sr/Ca ratios. Unfilled symbols represent samples removed by the mean ±2σ filtering approach (see text).

5.8.3 Benthonic foraminiferal Sr/Ca ratios

Filtered benthonic foraminiferal Sr/Ca ratios ranged from 0.55 to 0.98 mmol/mol, with an overall average value of 0.81 mmol/mol (Figures 5.18B and 5.19B). As with Mg/Ca ratios, scatter within the Sr/Ca ratio dataset was greater than the analytical precision, although less than that seen in the Mg/Ca ratio dataset (cf. the 5-point running averages and ±2σ envelopes in Figure 5.19). Sr/Ca ratios for the 26th October, 2007 plot away from the main group of Sr/Ca ratio determinations for unknown reasons; these values are not excluded by the filtering as they do not lie outside ±2σ of the 1 Myr averages. Running average Sr/Ca ratios decreased from ~0.90 to ~0.75 mmol/mol between Middle Eocene biozone CP14b and early Late Eocene biozone CP15 (~39.0 to ~36.5 Ma), at which point this trend reversed with an increase in running average Sr/Ca ratios to 0.85 mmol/mol over the next million years, i.e. to ~35.5 Ma. Running average Sr/Ca ratios stayed at ~0.85 mmol/mol until the latest Eocene base of biozone CP16a, at 34.4 Ma, before increasing to >0.90 mmol/mol by ~34.0 Ma. An irregular decrease in running average Sr/Ca ratios to ~0.70 mmol/mol then occurred across the Eocene–Oligocene boundary to ~33.2 Ma, i.e. prior to the base of Early Oligocene biozone CP16c/CP17. Running average Sr/Ca ratios subsequently increased throughout Early Oligocene biozones CP16c/CP17 to ~0.89 mmol/mol at 32.2 Ma, albeit with constant running average Sr/Ca ratios between 32.8 and 32.4 Ma. Running average Sr/Ca ratios then decreased by 0.2 mmol/mol into Early Oligocene biozone CP18, although the data density decreases in this stratigraphic interval. For samples younger than ~31.0 Ma Sr/Ca ratio data are too sparse to identify any trends.

5.11 Planktonic foraminiferal element/Ca ratios

Planktonic foraminiferal element/Ca records were assessed and filtered using the same criteria as applied to the *O. umbonatus* dataset (Section 5.8), i.e. Mn/Ca and Ti/Ca ratios were used to assess contamination, Ca concentrations in solution to assess the presence of any relationship to Mg/Ca ratios and possible analytical bias, as well as the final filtering step to reject samples with ratios ±>2σ of the mean Mg/Ca and Sr/Ca ratios determined for one-million-year bins.

Planktonic foraminiferal Mn/Ca and Ti/Ca ratios are plotted against Mg/Ca ratios in Figure 5.20. All Mn/Ca values were below the 0.1 mmol/mol threshold identified as indicating the

presence of authigenic phases (Boyle, 1983; Yu et al., 2007), with only one (for *C. unicavus*) approaching that concentration. Similarly, all Ti/Ca ratios were relatively low (<0.05 mmol/mol), which would indicate that there was no silicate contamination. Regressions for each planktonic species through the non-negative (i.e. >LLD) data values are also plotted (Figure 5.20); the regression statistics indicating that there is no statistically significant relationship between Mn/Ca or Ti/Ca ratios and Mg/Ca ratios (Table 5.5), suggesting that neither Mn/Ca nor Ti/Ca ratio identifies contaminated samples in this study. Planktonic foraminiferal Sr/Ca ratios against Mg/Ca ratios are also plotted in Figure 5.20 and also show no statistically significant relationship (considered in Section 6.1). None of the relationships shown in Figure 5.20 reveal clear species-specific differences in Mn/Ca, Ti/Ca or Sr/Ca ratios, with all species having element/Ca ratios over a similar range, as described in subsequent Sections 5.9.1, 5.9.2 and 5.9.3.

Planktonic foraminiferal Mg/Ca ratios are plotted against Ca concentration in solution in Figure 5.21, with regressions through each of the individual planktonic foraminiferal species datasets. As seen for *O. umbonatus,* there is no statistically significant relationship between Mg/Ca ratios and Ca concentration in solution for any planktonic foraminiferal species, indicating the absence of any consistent analytical bias to measured Mg/Ca ratios and no reason to apply a data filter based on Ca concentration measured in solution.

The final filtering step rejected data values that were >±2σ of the mean Mg/Ca and Sr/Ca ratios determined for one-million-year bins, with the resulting dataset described below and plotted against rmcd in Figure 5.22 and against numerical age in Figure 5.23. This filtering step removed 5 of the 52 (~10 %) *T. ampliapertura* element/Ca ratio analyses and 7 of the 72 (~10 %) *C. unicavus* element/Ca ratio analyses, but had no effect on the *A. bullbrooki* or *S. senni* element/Ca ratio datasets.

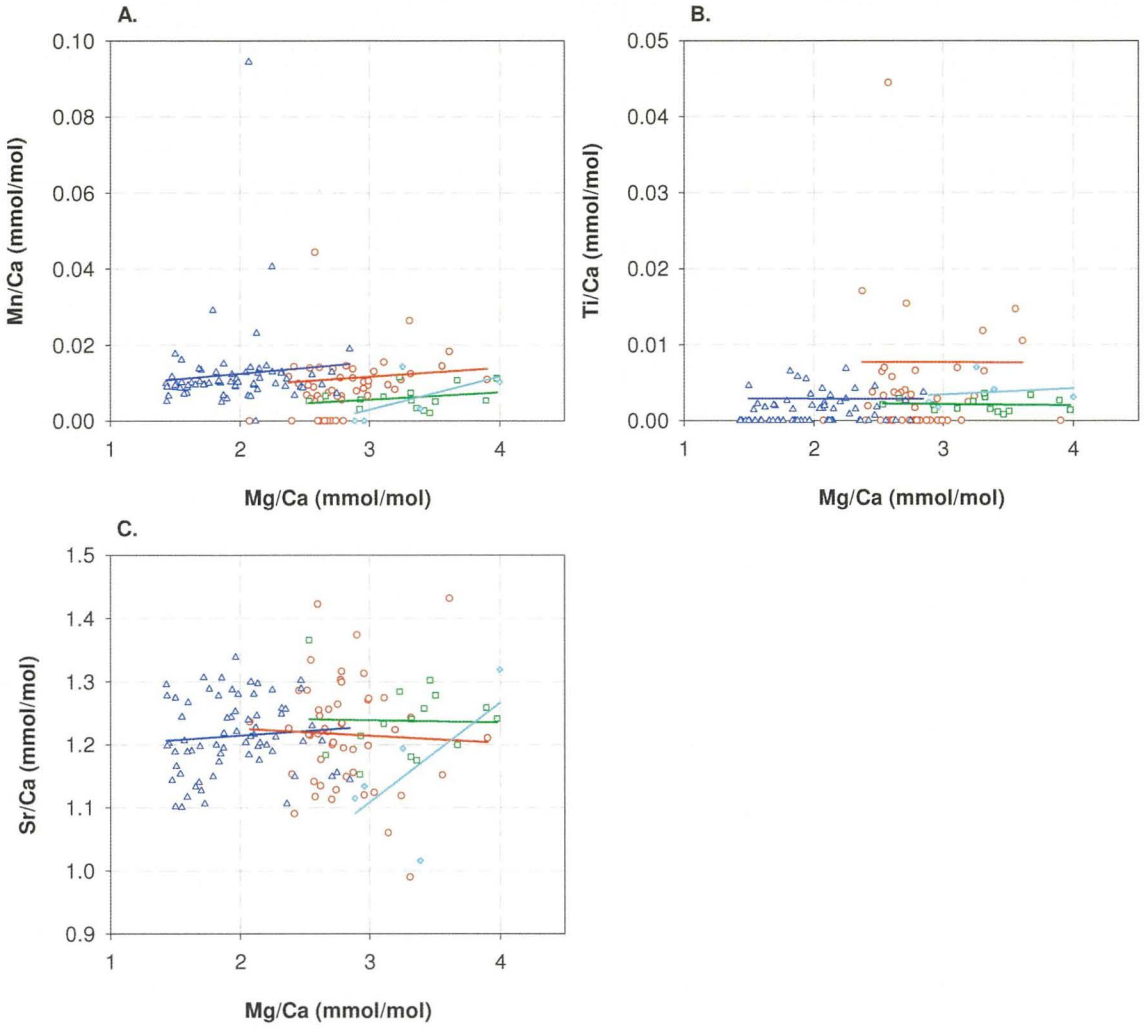

Figure 5.20: Plots of Mn/Ca (A), Ti/Ca (B) and Sr/Ca (C) ratios against Mg/Ca ratios, the two former ratios to assess contamination from authigenic phases and silicates, respectively. Regression lines indicate the relationships between element/Ca and Mg/Ca ratios for all non-zero ratios; the relationships for Mn/Ca, Ti/Ca and Sr/Ca ratios against Mg/Ca ratios are insignificant (low r^2 and statistically insignificant p-values; Table 5.5). On plot A, all Mn/Ca values were <0.1 mmol/mol, and thus do not indicate the presence of authigenic phases. In summary, it can be observed that the majority of samples had very low Mn/Ca and Ti/Ca ratios suggesting contamination was not a significant problem.

	Mn/Ca		Ti/Ca		Sr/Ca	
Species	r^2	p-value	r^2	p-value	r^2	p-value
A. bullbrooki	2.60E-04	0.28	3.17E-02	0.77	3.95E-03	0.26
C. unicavus	1.06E-02	0.44	7.58E-05	0.96	7.57E-03	0.48
S. senni	6.92E-02	0.34	4.25E-03	0.82	5.98E-05	0.93
T. ampliapertura	1.37E-02	0.47	4.88E-06	0.99	1.93E-03	0.76

Table 5.5: Statistics for the regressions shown in Figure 5.18. Correlations between Mn/Ca, Ti/Ca and Sr/Ca ratios and Mg/Ca ratios were weak and statistically insignificant.

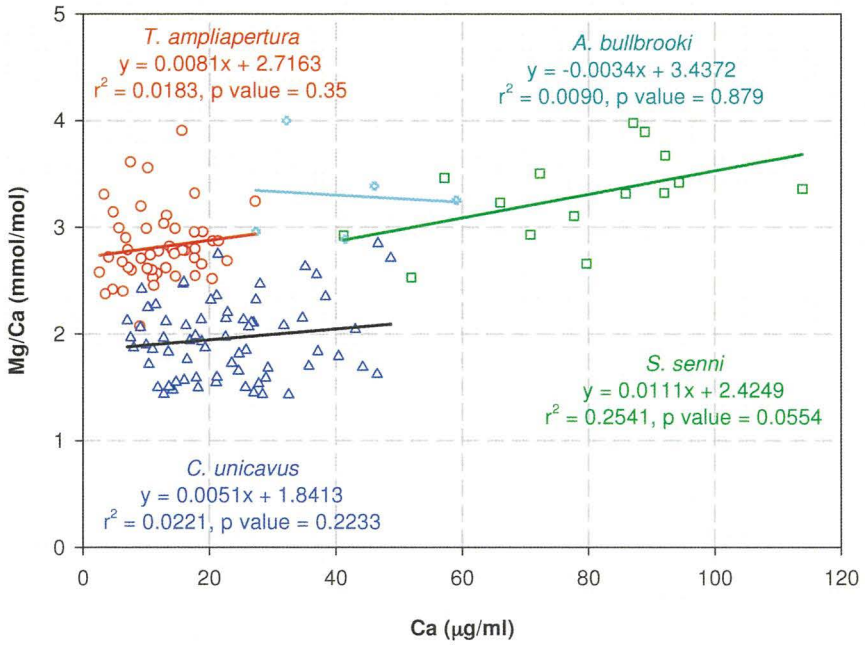

Figure 5.21: Mg/Ca ratios plotted against Ca concentrations in solution for each planktonic foraminiferal species: *A. bullbrooki* (light blue circles), *C. unicavus* (blue triangles), *S. senni* (green squares) and *T. ampliapertura* (red circles), with associated regression statistics. None of the regressions exhibit statistically significant ($p < 0.05$) relationships between Mg/Ca ratios and Ca concentrations in solution for any species and, as a consequence, no filtering based on Ca concentration measured in solution has been applied to the planktonic foraminiferal element/Ca ratio dataset.

The planktonic foraminiferal element/Ca ratios plotted against numerical age in Figure 5.23, cover a restricted age range (32.0 to ~39.6 Ma), compared to previous figures, and also omit the barren and/or fragmented foraminifera interval between 35.0 and 37.0 Ma to allow the stratigraphically limited planktonic element/Ca ratio data to be observed in more detail.

5.11.1 Planktonic foraminiferal Ti/Ca and Mn/Ca ratios

As with the element/Ca ratios measured for *O. umbonatus*, minor element/Ca ratios are described first as Ti and Mn have potential to reveal systematic down-core contamination within the sample set.

Measured planktonic foraminiferal Ti/Ca ratios were between 0.0007 and 0.0440 mmol/mol, although a large proportion (63 of 142 samples, ~44 %) of Ti/Ca ratio measurements were <LLD and were assigned nominal Ti/Ca ratios of zero. These <LLD Ti/Ca ratio measurements were for the Oligocene planktonic foraminifera and constituted

approximately half of each species dataset (Figure 5.22C). All but one planktonic foraminiferal Ti/Ca ratio fell within the two standard deviation of the analytical precision, thus it was not possible to describe stratigraphic trends in planktonic foraminiferal Ti/Ca ratios.

Mn/Ca ratios for the three species of planktonic foraminifera varied between 0.002 and 0.094 mmol/mol, with a minority of samples (14 of 142 planktonic analyses, ~10 %) having Mn concentrations <LLD and thus were assigned nominal Mn/Ca ratios of zero. *A. bullbrooki* Mn/Ca ratios were from 0.003 to 0.014 mmol/mol, with two of five measured samples analysed having values <LLD (40 %). *S. senni* Mn/Ca ratios were between 0.002 and 0.012 mmol/mol. For *C. unicavus,* Mn/Ca ratios varied between 0.005 and 0.094 mmol/mol, with seven of 66 (~11 %) analyses being <LLD. Mn/Ca ratios for *T. ampliapertura* ranged between 0.006 and 0.044 mmol/mol, with 23 of 51 (45 %) analyses <LLD. No stratigraphic trends can be observed in the >LLD Mn/Ca ratios measured (Figure 5.22 C and D).

5.11.2 Planktonic foraminiferal Mg/Ca ratios

The Eocene planktonic foraminifera *A. bullbrooki* and *S. senni* recorded Mg/Ca ratios between ~2.5 and ~4.0 mmol/mol (Figure 5.22A). Mg/Ca ratios for the Oligocene planktonic foraminiferal species plot as two relatively distinct populations: *C. unicavus* Mg/Ca ratios ranged between ~1.4 and ~2.9 mmol/mol, whilst *T. ampliapertura* Mg/Ca ratios ranged between ~2.1 and ~3.7 mmol/mol (Figure 5.22A). The majority (98 %) of the *T. ampliapertura* Mg/Ca ratios are, however, >~2.3 mmol/mol and, for a given sample depth, are higher than *C. unicavus* Mg/Ca ratios.

S. senni Mg/Ca ratios increased abruptly from 2.5 mmol/mol in the oldest age-assigned sample at ~39.5 Ma to 4.0 mmol/mol at ~39.2 Ma, before decreasing through Middle Eocene biozone CP14b to ~2.9 mmol/mol at 37.4 Ma (Figure 5.23). Data resolution is, however, relatively low at ~200 kyrs between samples for this time interval, thus not sampling any shorter-term variability. *C. unicavus* Mg/Ca ratios show a general decreasing trend through latest Eocene to Early Oligocene biozones CP16a, CP16b and CP16c/CP17, with running-average values decreasing by ~0.8 mmol/mol over the ~1.4 Myr period

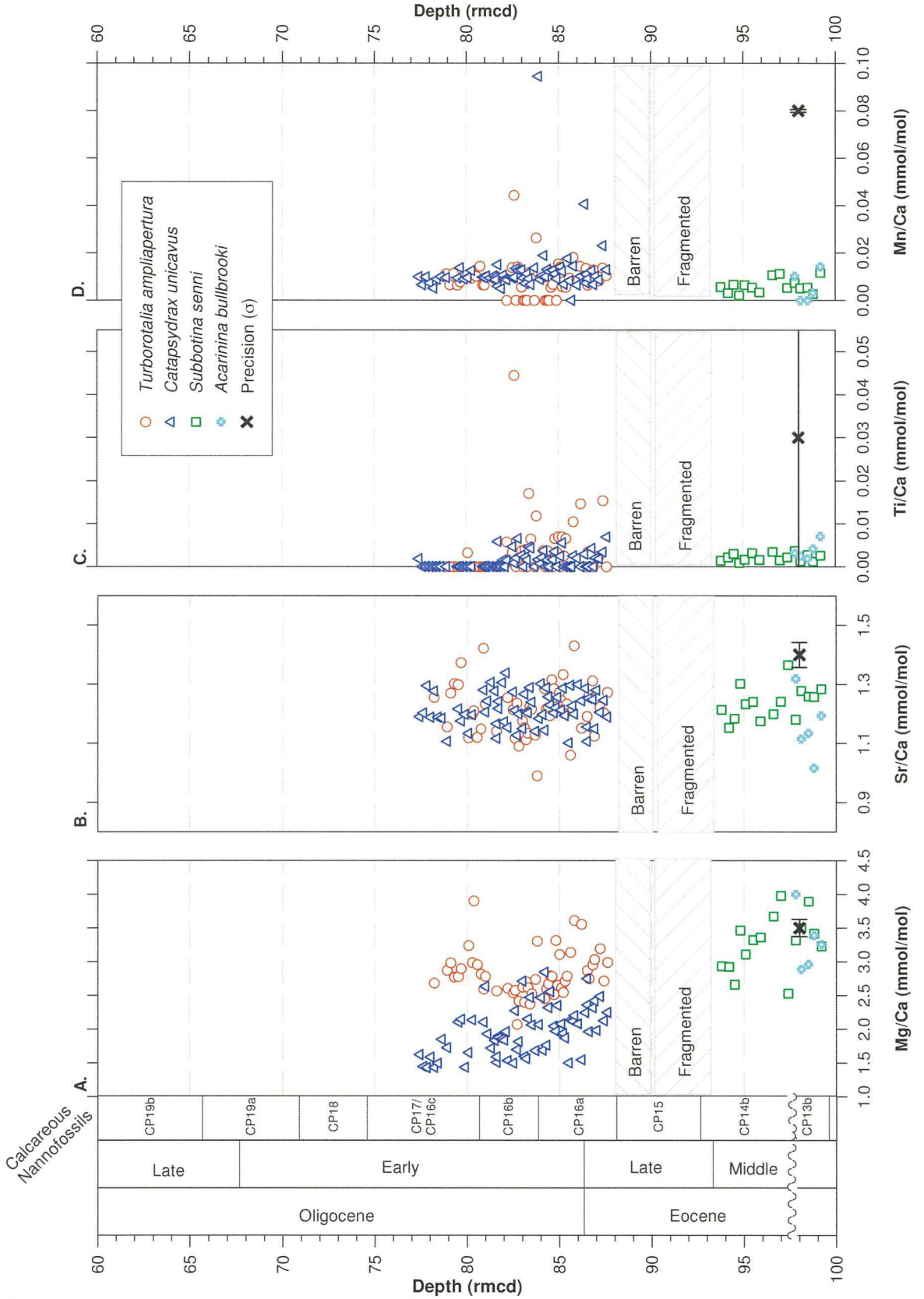

Figure 5.22: Element/Ca ratios for planktonic foraminifera plotted against depth. Analytical precision is shown as ±2σ, indicating that scatter within all datasets, except Ti/Ca, was greater than the analytical precision and so is actual variability within the dataset.

represented by that planktonic foraminiferal species. Scatter throughout the dataset was relatively uniform and greater than the ±2σ analytical precision. Running-average *T. ampliapertura* Mg/Ca ratios increased across the Eocene–Oligocene boundary, from 3.0 to

~3.3 mmol/mol, before decreasing to ~2.4 mmol/mol by ~33.4 Ma, i.e. within Early Oligocene biozone CP16b. Running-average *T. ampliapertura* Mg/Ca ratios then increased to 3.0 mmol/mol by the base of Early Oligocene biozone CP16c/CP17. Short-term scatter (within ~1 m or ~200 kyrs) was relatively uniform (maximum range of ~0.5 mmol/mol) throughout the *T. ampliapertura* Mg/Ca ratio dataset and greater than the analytical precision, but was typically less than that observed for *C. unicavus* (~1.0 mmol/mol).

5.11.3 Planktonic foraminiferal Sr/Ca ratios

Unlike for Mg/Ca ratios, all planktonic foraminiferal species have a restricted range of Sr/Ca ratios (~1.1 to ~1.4 mmol/mol), with a limited number (15 of 139, ~11 %) of data points falling outside of this range (Figures 5.22B and 5.23B). Of the two Eocene species, *A. bullbrooki* Sr/Ca ratios ranged between ~1.0 and ~1.3 mmol/mol, whilst *S. senni* Sr/Ca ratios ranged between ~1.2 and ~1.4 mmol/mol. Of the two Oligocene species, *C. unicavus* Sr/Ca ratios ranged between ~1.1 and ~1.3 mmol/mol, whilst *T. ampliapertura* Sr/Ca ratios ranged from ~1.0 to ~1.4 mmol/mol. There is no consistent offset in Sr/Ca ratios between these two Oligocene planktonic foraminiferal species. Plotting Sr/Ca ratios for each of the three planktonic foraminiferal species against numerical age assignments reveals no clear stratigraphic trends for the Early Oligocene species *C. unicavus* and *T. ampliapertura,* whereas Late Eocene *S. senni* Sr/Ca ratios decreased by ~0.1 mmol/mol over the stratigraphic range measured (Figure 5.23B). Scatter within the *C. unicavus* and *T. ampliapertura* Sr/Ca ratio dataset was about three times analytical precision (at the $\pm 2\sigma$ level), with both species exhibiting a similar range and magnitude of scatter in Sr/Ca ratios.

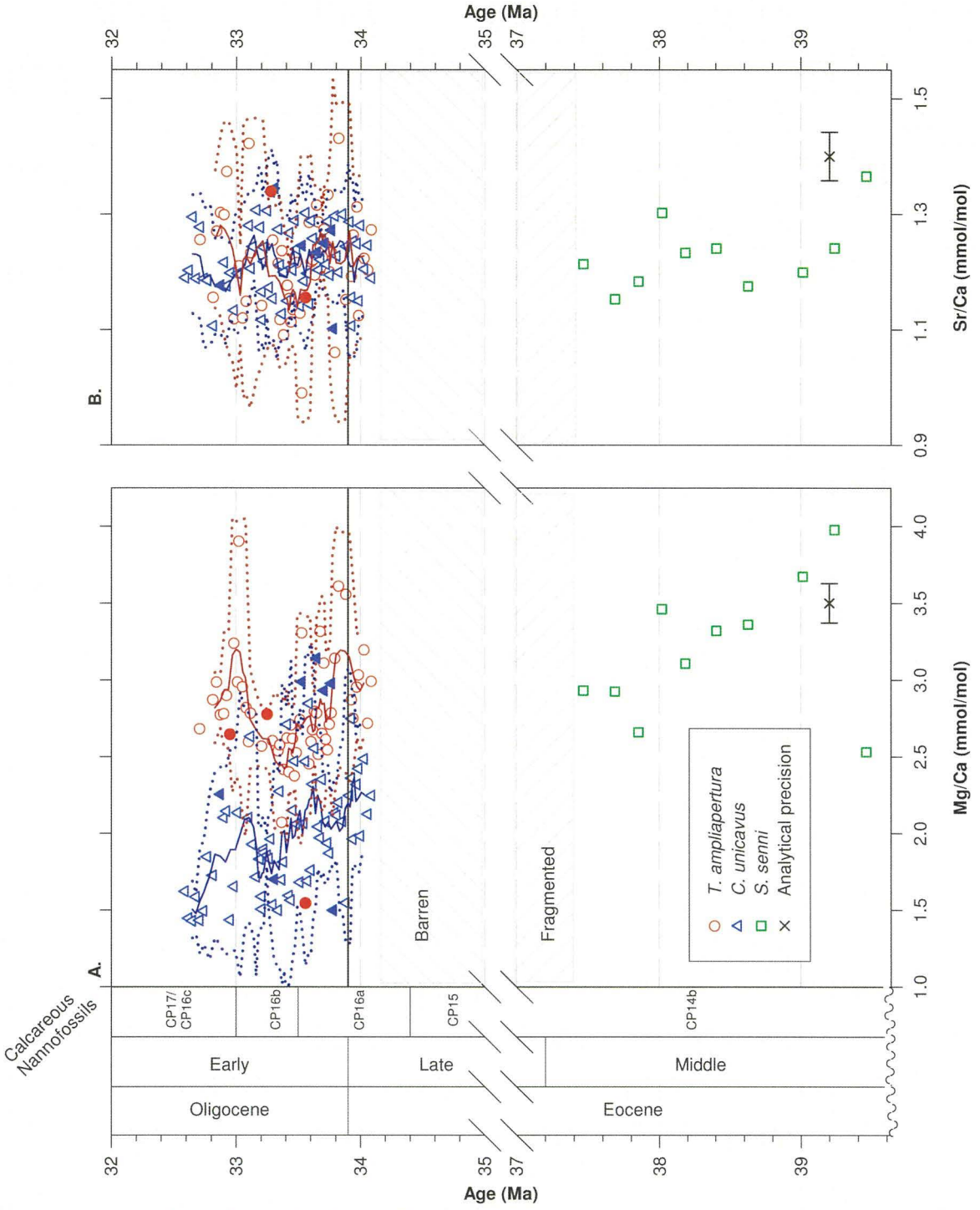

Figure 5.23: Site 1211 planktonic foraminiferal element/Ca ratios plotted against numerical age. Five-point running averages and 95% (±2σ) confidence interval are drawn through element/Ca ratios for *T. ampliapertura* and *C. unicavus*. Samples excluded by mean ±2σ filtering are plotted as solid symbols where values are within graph axes. Analytical precision at 95 % (±2σ) confidence limits are also shown. It can be observed that Mg/Ca ratios for *C. unicavus* and *T. ampliapertura* plot as relatively distinct groups, with the latter species having consistently higher ratios. The same offset is not present within the Sr/Ca ratios, where all the planktonic species plot within a restricted range of Sr/Ca ratios.

Chapter 6 - Discussion

6.1 Assessment of preservation and the influence of diagenesis on geochemical proxy records

6.1.1 Syn- and post-depositional diagenetic processes

Alteration of biogenic carbonates can commence upon the death of the calcifying organism, occurring both within the water column (syn-depositional) and within the sediment column (post-depositional). Syn-depositional alteration of biogenic carbonates takes the form of dissolution, i.e. loss of shell mass, and subsequent fragmentation as the carbonate material sinks through the water column or remains on the sediment surface. Syn-depostional alteration occurs as a result of carbonate saturation decreasing with increasing water depth. The level of dissolution depends on a multitude of variables, the degree of undersaturation, the "robustness" of foraminiferal shells and the supply of organic matter (Berger, 1971), with less robust planktonic foraminiferal particularly susceptible to dissolution (Murray, 1989). Studies of carbonate preservation have noted that foraminiferal dissolution and fragmentation occurs above the lysocline (Peterson and Prell, 1986; Lohmann, 1995) and thus is likely to have occurred at Site 1211 (see Section 6.3). Lohmann (1995) notes that over 50 % of *Globigerinoides sacculifer* can be dissolved prior to fragmentation beginning, thus even though only whole foraminifera were selected for geochemical analyses, the effect of dissolution on test geochemistry may be significant.

The effect of dissolution on planktonic foraminiferal stable-isotope geochemistry is to bias geochemical measurements towards those typical of deeper waters (Savin and Douglass, 1973; Lohmann, 1995, Rosenthal et al., 2000), i.e. $\delta^{18}O$ values become more positive, $\delta^{13}C$ values become less positive. Dissolution and fragmentation can also bias planktonic foraminiferal assemblages towards a deeper, cooler water signal as "warmer" water foraminifera and carbonates are typically more susceptible to dissolution (Berger, 1968; Parker and Berger, 1971; Savin and Douglass, 1973). As benthonic foraminifera do not calcify across a range of environments, it would seem logical that $\delta^{18}O$ and $\delta^{13}C$ remained relatively consistent throughout the test and thus dissolution would have little effect. McCorkle et al. (1995), however, observed weak dissolution related decrease in $\delta^{13}C$ from a species of *Cibicidoides*. Although the negative change with depth observed was close to the analytical precision and thus difficult to attribute and identify with great certainty.

Dissolution appears to be more of an issue for foraminiferal element/Ca ratios. Evidence suggests that dissolution preferentially removes high Ba/Ca, Cd/Ca, Mg/Ca and Sr/Ca foraminiferal carbonate (e.g. McCorkle et al., 1995; Brown and Elderfield, 1996; Elderfield et al., 2000; Rosenthal et al., 2000; Dekens et al., 2002; Regenberg et al., 2006; Mekik and Francois, 2006; Mekik et al., 2007; Huang et al., 2008), dissolution commencing in water depths above the lysocline (Regenberg et al., 2006; Huang et al., 2008). The preferential removal of high Mg/Ca carbonate appears to be due to foraminiferal test carbonate having two layers with contrasting Mg/Ca ratios (Nouet et al., 2007), the layer with increased Mg/Ca being poorly crystallized and leading to a much greater degree of susceptibility to dissolution.

The extent of dissolution at a single site, such as Site 1211, will depend on the changes in ocean carbonate chemistry across a studied interval. The carbonate compensation depth (CCD) history at Site 1211 is discussed in Section 6.3, however, there appears to be a deepening of CCD between ~34.5 and ~34.0 Ma, with a shallower CCD prior to ~34.5 Ma and uniformly deeper CCD after ~34.0 Ma. The absence of resolvable CCD variation and increased sedimentation rates at Site 1211 after ~34.0 Ma (Chapter 4) should mean that variance in the degree of dissolution is minor, although not absent, for the individual Oligocene planktonic foraminifera species dataset, which span ~34.0 to 32.5 Ma. Quantification of dissolution requires knowledge of original and post-dissolution sediment test weight and such is not possible for Site 1211. However, observations made during picking and foraminiferal preparation for geochemical analyses, of greater numbers of shell fragments and less effort being required to open shells during cleaning, suggested that *T. ampliapertura* tests were more delicate than *C. unicavus* test, which may mean that the former species experienced greater dissolution. Despite the likely absence of variable dissolution on the Oligocene planktonic foraminifera, the magnitude of the dissolution and its effect on Mg/Ca and $\delta^{18}O$ is uncertain and impossible to quantify with the available data. Differential dissolution may have affected benthonic foraminiferal Mg/Ca ratios especially proximal to the interval of CCD deepening. Greater dissolution prior the CCD deepening would lower Mg/Ca ratios relative to tests with reduced dissolution after the deepening, thus could potential introduce artefacts into the benthonic records. Study into the effect of dissolution on Mg/Ca and $\delta^{18}O$ values by Rosenthal et al. (2000), however, suggests that the relationship between the two proxies is maintained throughout dissolution

and so estimates of $\delta^{18}O_{sw}$ should remain viable. De Villiers (2003) also noted that dissolution did not increase the variability observed, which suggests dissolution does not obscure primary trends in foraminiferal Mg/Ca records.

Upon deposition and subsequent burial, i.e. post-depositional processes, a progressive down-core sequence of lithification in carbonate sediments was described in early Deep Sea Drilling Project (DSDP) studies (Schlanger and Douglass, 1973; Van der Lingen and Packham, 1975). Early stage diagenesis and lithification starts rapidly after settling, with gravitational compaction causing physical breakdown and dissolution/reprecipitation, i.e. diagenesis or recrystallisation, being limited to the more susceptible calcareous nannofossils, i.e. Discoasters. Recently, Borre and Fabricius (1998) have suggested that recrystallisation has an equal to or larger role than compaction in the diagenesis of carbonate ooze sediments, and thus may have a greater effect than the classic descriptions (Schlanger and Douglass, 1973; Van der Lingen and Packham, 1975). Further secondary precipitation follows with the overgrowth of the proximal and distal shields of calcareous nannofossils, recrystallisation of foraminifera and growth of discrete secondary euhedral crystals. Below 200–300 m sediment depth, carbonate ooze sediments lithify to chalks, a process controlled by sediment composition as well as burial depth. With greater depth, the chalks lithify further into limestones, through continued compaction and recrystallisation reactions.

The lithology of the sediments recovered from Site 1211 was carbonate ooze throughout (Shipboard Scientific Party, 2002b) as would be expected from the shallow burial depth (≤160 mbsf) and studies of down core lithification (Van der Lingen and Packham, 1975; Borre and Fabricius, 1998). Thus the suggestion of Borre and Fabricius (1998) that recrystallisation is the dominant process in the carbonate ooze interval has implications for the preservation of primary geochemical signals at Site 1211, requiring the effect of recrystallisation as well as physical changes on the carbonate geochemistry to be considered below.

Textural observations as to the nature of the fine-fraction carbonate that makes up >95 % of the studied intervals ooze sediments (Figure 5.1; also Shipboard Scientific Party, 2002b) have potential to reveal information about extent of post-depositional and burial processes.

The descriptions of down-core change on SEM images of carbonate sediment by Van der Lingen and Packham (1975) provide a benchmark for the expected effect of diagenesis on the sediment appearance. The Van der Lingen and Packham (1975) study observed that micritic, anhedral "micarb" particles are precipitated through the dissolution of foraminifera and easily dissolvable coccoliths. Further precipitation is then observed on these "micarb" particles and on fossil fragments and in particular Discoasters. Discoasters being particularly susceptible to reprecipitation and overgrowths, most likely as a result of them being single crystals and thus ideal nucleation sites (see Van der Lingen and Packham, 1975). Study of SEM images of Site 1211 fine-fraction should allow assessment of whether precipitated overgrowths and "micarb" particles are present, as well as any depth related increase in fragmentation. Foraminiferal carbonate is considered in Section 6.1.3.

SEM photomicrographs of the <38 μm fine-fraction carbonate were described in Section 5.5.4. Reprecipitation within coccolith shields appears to have been minimal, although some overgrowth of Discoasters is observed (Plate 5.3h and 5.4b). It is difficult to quantify reprecipitation/overgrowths reliably but observation suggests little, if any, systematic increase down-core. These observations would indicate that the fine-fraction sediment at Site 1211 was not undergoing progressive recrystallisation and that reprecipitation was not a significant factor. The presence of "micarb" particles is uncertain, many SEM images apparently have individual crystals (e.g. Plate 5.1b,f; 5.2b,f and 5.3f) but their origin is uncertain as they appear to be a component of many coccolith shields suggesting a biogenic rather than inorganic origin. An increase in fragmentation is identified in Section 5.5.4 (Table 5.2), associated with the interval immediately prior to the increase in $\delta^{18}O$ in fine-fraction and benthonic foraminifera associated with the initiation of the EOT (~88 rmcd; see Section 6.2). The interval of increased fragmentation was not associated with any progressive down-core trends in fragmentation, with relatively low levels of fragmentation stratigraphically above and below, so it seems unlikely that the fragmentation resulted from compaction. The coincidence of increased fragmentation and shallower lysocline/CCD (see Section 6.3) indicates the fragmentation resulted from syn-depositional and sediment surface dissolution. The absence of significantly increased reprecipitated carbonate in this interval would also argue for non-sediment column dissolution, i.e. dissolved carbonate is not being locally reprecipitated. SEM images thus do not suggest that Site 1211 biogenic carbonates have been subject to significant

diagenesis during burial. Despite the lack of textural evidence for diagenesis consideration of the geochemical effects of diagenesis is necessary.

6.1.2 Effect of diagenesis on primary $\delta^{18}O$ and $\delta^{13}C$ values

The effects of diagenesis in unlithified calcareous ooze are two-fold, consisting of dissolution and reprecipitation of a secondary, inorganic carbonate. Diagenetic dissolution has the same effect as syn-depositional dissolution in removing "warm" water, i.e. negative $\delta^{18}O$, primary carbonate. However, depending on the "openness" of the sediment pore-water system, dissolved primary carbonate may influence secondary carbonate. Within an open system, pore waters circulate throughout the sediment meaning dissolved primary carbonate has an insignificant effect on isotopic composition of pore-water fluids, whilst the reverse is true within a closed system. Inorganic secondary or diagenetic carbonate forms in isotopic equilibrium with sediment pore waters (Schrag et al., 1995). Thus the effect of precipitation of diagenetic carbonate depends both on the degree of reprecipitation relative to primary carbonate, the openness of the diagenetic environment, and on the difference between the stable-isotope values of the primary and diagenetic carbonates. The difference in stable-isotope values of primary and diagenetic carbonates reflecting the difference between the primary and secondary precipitation environments.

The effect of diagenesis on $\delta^{18}O$ and $\delta^{13}C$ values of biogenic carbonates is different. The $\delta^{13}C$ within pore-waters is typically that dissolved from biogenic carbonates, and thus resembles a closed system leading to recrystallisation homogenising $\delta^{13}C$ values (Crowley and Zachos, 2000; Pearson et al., 2001). At the opposite extreme, $\delta^{18}O$ from dissolved carbonate is only a minor component of pore-water $\delta^{18}O$ and thus $\delta^{18}O$ of diagenetic carbonate depends on the processes controlling pore-water $\delta^{18}O$. Pore-water $\delta^{18}O$ profiles have been observed to become more negative with respect to $\delta^{18}O$ with depth (Lawrence et al., 1975; Gieskes and Lawrence, 1976; McDuff, 1984; Rudnicki et al., 2001). This general depletion in $\delta^{18}O$ with depth results from low-temperature alteration of the basaltic basement and diffusion of the pore-water fluids (Lawrence et al., 1975; McDuff and Gieskes, 1976). The diagenetic carbonate forms in thermodynamic equilibrium with the pore-water leading to a further decrease in $\delta^{18}O$ with depth as a consequence of geothermal gradients (Schrag et al., 1995), thus a progressive trend of recrystallisation with depth would lead to increasingly depleted and homogenised shell $\delta^{18}O$. Models of the processes

leading to the more negative $\delta^{18}O$ values with depth and the effects of subsequent diagenesis are discussed in Section 6.1.4.

6.1.3 Effects of diagenesis on Mg/Ca and Sr/Ca ratios

As described earlier, dissolution of primary carbonate preferentially removes high Mg and Sr carbonate from single shells/tests and thus reduces the population average Mg/Ca and Sr/Ca ratio (Brown and Elderfield, 1996; Rosenthal et al., 2000; De Villiers, 2003). However, De Villiers (2003) highlight that if only samples with minimal dissolution are considered there is no reduction in Mg/Ca variability, suggesting that despite dissolution-induced change a temperature signal is captured.

The reprecipitation aspect of diagenesis has a greater potential to alter element/Ca ratios. Partition coefficients of Mg^{2+} into inorganic carbonate precipitated from seawater have been measured as being much greater than for biogenic precipitation (Oomori et al., 1987; Lea et al., 1999b), thus inorganic carbonate should contain more Mg^{2+}. The applicability of laboratory defined partition coefficients to marine systems has, however, been questioned (Morse and Bender, 1990; Sexton et al., 2006), with recrystallised tests having only minor enrichments. That said, substantially raised Mg/Ca values have been used to identify altered samples (Lear et al., 2004). Sr^{2+} partition coefficients appear to be controlled by a variety of factors including precipitation rate and Mg^{2+} concentration of carbonate (See Morse and Bender, 1990 for review). Diagenetic recrystallisation of biogenic carbonates has been observed to lower Sr/Ca (Baker et al., 1982; Elderfield et al., 1982; Ando et al., 2006), and down-core sediment profiles of bulk carbonate Sr/Ca have been considered to reveal diagenetic histories (Elderfield et al., 1982; Ando et al., 2006).

Minor element sediment pore water profiles have also been used to infer the presence of diagenetic carbonate. The depletion of the $\delta^{18}O$ of pore-waters described above correlates with a decrease in the concentration of Mg^{2+} ions and an increase in concentration of Ca^{2+} ions indicating that the pore-water profiles of these ions result from low-temperature alteration of the underlying basalt (Lawrence et al., 1975; McDuff and Gieskes, 1976). Alteration of the basalt leads to the exchange of Mg^{2+} for Ca^{2+} ions as the basalt is altered to clays and zeolites (Lawrence et al., 1975; McDuff and Gieskes, 1976), with diffusion

leading to the described pore-water profiles. Sr^{2+} pore water profiles increase rapidly with depth, reaching a maximum associated with the ooze-chalk transition, before decreasing gradually with depth (Elderfield and Gieskes, 1982; Gieskes et al., 1986). The decrease in Sr^{2+} shows no relationship to pore-water Ca^{2+} or Mg^{2+} suggesting an alternative controlling factor (Elderfield et al., 1982). The increase in Sr^{2+} concentration has been interpreted to result from the dissolution of primary high Sr^{2+} carbonates and subsequent recrystallisation of low-Sr^{2+} secondary carbonates. The maximum in Sr^{2+} concentrations has been interpreted as the interval of maximum recrystallisation (Baker et al., 1982; Gieskes et al., 1986).

Pore-water profiles for Site 1211 are described in Shipboard Scientific Party (2002b), and reveal that Sr^{2+} reached maximum values at ~60 mbsf (~66 rmcd) before declining gradually. Based on the diagenesis interpretation, i.e. Sr^{2+} concentrations are derived from recrystallising biogenic carbonate, Site 1211 pore-water profiles suggest maximum diagenesis at ~60 mbsf indicating the studied interval is likely to have undergone recrystallisation. More recently, however, Rudnicki et al. (2001) questioned whether pore-water fluids were indicative of diagenetic history at shallowly buried sites and that sediments could be considered chemically inert, recrystallisation limited to the early sedimentation history (~10 Ma). Rudnicki et al. (2001) noted that pore-water profiles and changes in lithology were unrelated in shallowly buried Cenozoic sediments from ODP Leg 171B. Whilst detailed pore-water profiles are not available for Site 1211, the Sr^{2+} concentration maximum at ~60 mbsf was not associated with the ooze-chalk transition, carbonate ooze being the lithology present throughout the recovered sections (~165 mbsf, Shipboard Scientific Party, 2002b). The absence of relationship between pore-water Sr^{2+} concentrations and lithology at Site 1211 indicates, as suggested by Rudnicki, that pore water chemistry is not controlled by on-going recrystallisation of the carbonate sediments and that the sediments are likely to be chemically inert.

Foraminiferal element/Ca ratios from Site 1211 were screened for any values outside the million year mean $\pm 2\sigma$ (see Section 5.10 and 5.11), which was applied to remove any values from dissolution or recrystallisation effected samples. Neither element/Ca ratio record, however, showed a systematic increase or decrease with age (down-core), suggesting that progressive diagenesis was not occurring (Figures 5.19 and 5.23). Sr/Ca ratios from Site 1211 were equivalent to ratios measured for Eocene *O. umbonatus* tests

recovered from sites in the South Atlantic (Site 523) and Southern Ocean (Site 689; Lear et al., 2003), the equivalence of ratios from three geographically distant sites and different burial depths would suggest that a palaeoceanographic ratio is recorded. The reasoning behind this suggestion being, that progressive diagenesis would be expected to lower the Sr/Ca ratios in samples from greater sediment depths, a trend that is not observed.

6.1.4 Models of diagenesis

As discussed in Section 6.1.2, carbonate stable-isotope values can be altered by diagenesis in the sediment column. Briefly, the diagenetic secondary carbonate depends on changes in the pore-water geochemical composition and geothermal gradient, so one approach to assess the importance and identify the tell-tale signs of diagenesis in marine carbonate records has been to model the effects of diagenesis (Killingley, 1983; Schrag et al., 1995). Modelling studies have focused on the effect of diagenesis on $\delta^{18}O$ records of bulk carbonate samples due to the difficulty in estimating recrystallisation rates of individual foraminifera. The effect of diagenesis on $\delta^{13}C$ has been subject to less attention as a result of pore-water $\delta^{13}C$ being primarily controlled by the bulk sedimentary carbonate $\delta^{13}C$ (Crowley and Zachos, 1999; Pearson et al., 2001) and thus homogenisation to an average biogenic carbonate values expected. The basis for modelling the effects of down-core diagenesis have worked on pore-water $\delta^{18}O$ chemistry being controlled by alteration reactions within the underlying basalt and subsequent diffusion of more negative $\delta^{18}O$ pore-waters upwards towards the sediment-ocean boundary (Lawrence et al., 1975; McDuff and Gieskes, 1976; Schrag et al., 1992). Schrag et al. (1992) modelled the effect of progressive recrystallisation on carbonates within these pore-waters, and with the effect of geothermal increases in temperature with depth. Modelled profiles suggest that, with a constant recrystallisation rate to explain progressive down-core degradation on foraminiferal preservation, carbonate $\delta^{18}O$ at first increases, before a general negative trend with depth (Schrag et al., 1992). Sedimentation rate, temperature gradient, $\delta^{18}O$ depth gradient and recrystallisation rate all acting to control the magnitude of the diagenetic alteration. Importantly Schrag et al. (1992) modelled that whilst the amplitude of variation in the $\delta^{18}O$ values was reduced, the events were not altered in duration or timing by diagenesis. By varying the initial carbonate $\delta^{18}O$ to simulate high-latitude planktonic and benthonic foraminifera and low-latitude planktonic foraminifera, Schrag et al. (1992) show the effect of diagenesis with depth on $\delta^{18}O$ from each respective area (Figure 6.1). This modelling indicated that benthonic and high-latitude planktonic

foraminifera were relatively unaffected by early recrystallisation, recrystallisation occurring in pore-waters of similar chemistry and temperature to those of primary calcification, followed by a trend to more negative $\delta^{18}O$ values with depth. Low-latitude planktonic $\delta^{18}O$ values, however, were shifted to initially to more positive values, as a consequence of calcification in a cooler environment than that of calcification, followed by a negative trend at depth. These modelled results have implications for the development of palaeoceanographic records as they suggest targeting shallowly buried sites for high-latitude and benthonic foraminiferal records to minimise the effect of diagenesis. However, such shallowly buried sites would lead to a greater effect of diagenesis on warm-surface water $\delta^{18}O$.

Schrag et al. (1992; 1995) suggested that diagenetic recrystallisation leads to the most significant deviation from primary $\delta^{18}O$ values for low-latitude planktonic foraminifera. This deviation from primary $\delta^{18}O$ values is due to the large difference between the pore water equilibrium $\delta^{18}O$ values and the $\delta^{18}O$ of the primary carbonate that formed in considerably warmer surface waters. The increase in tropical planktonic foraminifera $\delta^{18}O$ values suggested by Schrag et al. (1992) helps to explain the so-called "cool-tropics" paradox. In summary, a feature of many late 20th century reconstructions of Cretaceous and Palaeogene sea-surface temperatures (SSTs) were "cool-tropics" (e.g., Zachos et al., 1994; Huber et al., 1995), i.e. SST estimations that were less than equivalent locations in the modern ocean. These cool-tropics contrasted with warm high-latitude temperatures for the same time intervals (Zachos et al., 1994; Huber et al., 2002), resulting in reduced meridional temperature gradients, a situation that climate models have struggled to replicate (e.g. Huber and Sloan, 2001). As Site 1211 was selected for the shallow burial of Cenozoic sedimentation, the modelled results of Schrag et al., (1992; 1995) suggest that the surface-water records will record a "cool tropics" signal. Comparison of Site 1211 palaeotemperature predictions with "glassy" foraminifera (see Section 6.1.3) and alkenone proxy records may allow some quantification of the diagenetic effect (Section 6.2.4 and 6.4.4; Pearson et al., 2001). The difference between planktonic foraminifera derived $\delta^{18}O_{sw}$ estimates compared to benthonic foraminiferal values could also allow quantification (Section 6.5.3).

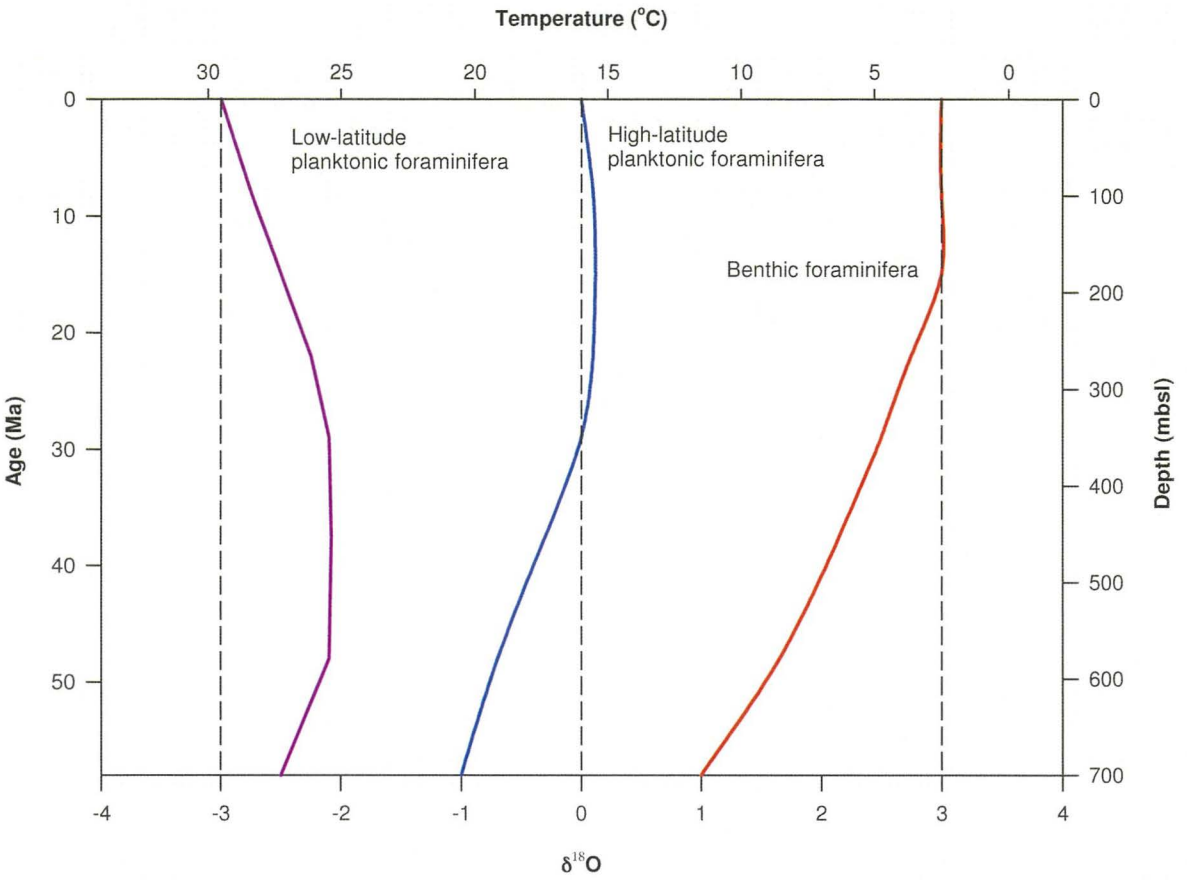

Figure 6.1: Model outputs for three different initial $\delta^{18}O$ values undergoing diagenesis in the sediment column, dashed lines indicating original values, modified from Schrag et al. (1992). It can be observed that the effect of diagenesis is more pronounced for more negative primary $\delta^{18}O$ values (i.e., low-latitude, warm-water planktonic foraminifera) than for more positive primary $\delta^{18}O$ values (i.e., high-latitude planktonic or benthonic foraminifera). In this study both the planktonic foraminifera and <38 µm fine-fraction coccolith material formed in low-latitude, warm-waters and thus could be more susceptible to diagenesis than the benthonic foraminifera. The modelled effect of diagenesis on Site 1211 sediments depends on whether diagenesis is a depth or time related process (note different vertical axes) and thus the magnitude could be either significant or minimal (see main text). Schrag et al. (1995) and Schrag (1999) have demonstrated that variation in Cenozoic $\delta^{18}O$ within low-latitude bulk sediments could be reproduced by their model, with little effect from recrystallisation rate, and as such could explain the so called "cool-tropics" paradox observed for the Cenozoic.

Whilst modelling the effects of diagenesis on Site 1211 fine-fraction, benthonic and planktonic foraminiferal carbonate is beyond the scope of this project, the modelled profiles of Schrag et al. (1992; 1995) can be used as a first-order assessment of diagenesis at Site 1211 (Figure 6.1). Although only two records extend across the full range of sampling, i.e. benthonic foraminifera *O. umbonatus* and the <38 µm fine-fraction, the modelled profiles of Schrag et al. (1992) suggest that these two datasets have potential to identify progressive down-core diagenesis. Comparison, however, is complicated by the sedimentation history at Site 1211 and the assumptions made about the recrystallisation and sedimentation rates in Schrag et al. (1992; 1995) have to be taken into account. Assumptions made concerning recrystallisation rates affect when and where recrystallisation occurs, a constant rate leading to a progressive change with time and thus burial, whilst a declining rate meaning diagenetic carbonate has an early burial bias.

Changes in sedimentation rates effect the depth within the sediment column at which recrystallisation is occurring, pore-water temperature increasing with depth due to the geothermal gradients, thus leading to less positive $\delta^{18}O$ thermodynamic equilibrium values. Thus, these variables have to be considered for Site 1211 carbonate records and the most suitable profiles of Schrag et al. (1992; 1995) used for comparison.

Considering recrystallisation rates, Schrag et al. (1992) use a constant rate to model foraminifera whilst a decreasing recrystallisation rate with time is used for bulk carbonates in Schrag et al. (1995) based on pore-water Sr concentrations in deep-sea sediments. Whilst the Schrag model has reproduced existing ODP site data, there has been suggestion that carbonates from shallowly buried sites are inert after their early (<10 Myr) diagenetic history (Rudnicki et al., 2001). If the latter scenario were the case then down-core profiles would not provide clear indication of diagenesis as recrystallisation will occur entirely within the upper few 10's of metres of sediment within similar pore-water conditions for all samples.

The second consideration is that of sedimentation rates, the Schrag $\delta^{18}O$ profiles were modelled for constant sedimentation rates, which were not observed at Site 1211. The biostratigraphy and depth–age model developed for Site 1211 indicate an unconformity between upper Lower Miocene and upper Oligocene sediments, and in the Middle Eocene (Shipboard Scientific Party, 2002b), as well as a three-fold increase in sedimentation rate between ~88.0 and ~75.0 rmcd (~34.0 – ~32.0 Ma, Figure 4.11), thus comparison of modelled profiles with $\delta^{18}O$ records is not straightforward. The unknown aspect of the comparison relates to the ~8.2 Myr hiatus at Site 1211 that occurred somewhere between ~27.0 and ~18.0 Ma (Shipboard Scientific Party, 2002a); was the hiatus erosional removing significant quantities of sediment so that Eocene/Oligocene sediments may have been buried much deeper and subject to diagenesis at greater depths or was the sedimentation and subsequent erosion minimal in terms of burial depth change. The history of sedimentation before and after the hiatus suggests the latter effect, sedimentation rates were low before and very low after, ~3.2 and ~0.4 m/Myrs respectively (Shipboard Scientific Party, 2002a). Thus even if the ~8.2 Myr hiatus in the sediment record was predominantly a period of sedimentation, the burial effects would have been small. Assuming 8 Myrs of sedimentation at ~3.2 m/Myrs, then sediment would have only been

buried to a greater depth of ~24 m, an increase in pore-water temperature of ~1 °C (assuming a 40 °C/km geothermal gradient, Schrag et al. 1995). This burial scenario would seem to be relatively implausible in terms of subsequent erosional rates and thus represents a maximum estimation.

With the above information, an expected pattern of diagenesis for Site 1211 can be hypothesised. The low sedimentation rates at Site 1211 suggest that sediments from the studied interval have never been deeply buried (<100 mbsf), which will emphasise the contrary effects of recrystallisation in near-surface pore-waters on fine-fraction and planktonic foraminifera compared to the benthonic foraminifera (Schrag et al., 1992). The <38 μm fine-fraction is predominantly comprised of calcareous nannofossils (see Section 5.5.4), which record shallow mixed-layer environments (Ennyu et al., 2002) and, as such, would have calcified in warm sub-tropical waters above Site 1211. Such biogenic carbonate thus would have been out of equilibrium with respect to the chemical composition of bottom-waters and shallowly buried sediment pore-waters, so any diagenetic recrystallisation would have been likely to cause $\delta^{18}O$ values to become more positive with depth/age (Figure 6.1; Schrag et al., 1992, 1995). Increased rates of early recrystallisation would enhance the positive shift in $\delta^{18}O$ in the fine-fraction relative to the planktonic foraminifera recrystallising at constant rate. *O. umbonatus,* however, is a shallow epifaunal benthonic species which would undergo recrystallisation in an environment close to that of primary calcification at relatively low rates of diagenesis, thus little $\delta^{18}O$ change would be expected. The progressive recrystallisation with time would lead to a greater proportion of diagenetic carbonate within the benthonic tests, whilst the relatively small increase in geothermal temperature would lead to a gradual negative trend in $\delta^{18}O$ with depth. The trends within single records would lead to $\delta^{18}O$ gradients between fine-fraction and benthonic foraminifera (surface to bottom water gradients) reducing down-core. Increased secondary carbonate in the fine-fraction relative to the planktonic foraminifera due to greater initial recrystallisation should also lead to more positive $\delta^{18}O$ values for the fine-fraction in comparison to the surface mixed layer dwelling *T. ampliapertura.*

Considering the actual observed $\delta^{18}O$ changes in fine-fraction, planktonic and benthonic foraminifera (Figures 5.7, 5.9, 5.11, 5.12, 5.13; Table 6.1) as well as surface to bottom

water gradients (Figure 5.14 and 5.15; Table 6.2), the presence of these hypothesised changes can be assessed. Considering both the stable-isotope data against depth (Figures 5.7A, 5.9 and 5.12) and against age (Figures 5.7B, 5.11 and 5.13) allows identification of trends accounting for diagenesis being a depth or time controlled effect. It is clear from each of the $\delta^{18}O$ profiles (Figures 5.7, 5.9, 5.11, 5.12 and 5.13) that short-term variability over a few metres remains (i.e. <38 μm fine-fraction between 85 to 90 rmcd) indicating that a true palaeoceanographic signal is present at Site 1211. The fine-fraction $\delta^{18}O$ records suggest a negative trend in $\delta^{18}O$ with depth/age (Figure 5.7, Table 6.1), opposite to that described above from progressive recyrstallisation in shallowly buried sediments. As a consequence of the restricted stratigraphic range of the planktonic foraminifera and the short-term variation, no clear down-core trend is visible in $\delta^{18}O$ that could be attributed to diagenesis (Figures 5.12 and 5.13). Benthonic foraminiferal $\delta^{18}O$ does exhibit a general negative shift with depth as would be expected from progressive recrystallisation, albeit with the Eocene–Oligocene boundary shift superimposed upon the trend (Figures 5.9 and 5.11; Table 6.1). The negative trend, however, is in line with the expected trend of bottom water warming seen in global compilations of benthonic foraminiferal data so is likely to represent an oceanographic signal (Zachos et al., 2001; 2008). Surface to bottom water gradients do not appear to change significantly over the studied stratigraphic interval (Figure 5.14 and 5.15; Table 6.2), which again would argue against progressive recrystallisation. Whilst the down-core profiles do not suggest a progressive recrystallisation with time/depth effect on any of the carbonate records from Site 1211, the state of foraminiferal preservation is discussed in the following two sections. A summary of the qualitative model predictions will be considered with the other sections evidence in Section 6.1.5.

6.1.5 "Frosty" versus "glassy" - foraminiferal preservation

In Section 6.1.1, the textural evolution of the fine-fraction was interpreted to indicate that significant fragmentation and diagenesis had not occurred at Site 1211. However, this interpretation was based solely on images of fine-fraction assemblages and not the whole foraminiferal tests that have been analysed to determine the majority of the geochemical records. Recently, much attention has focussed on the state of preservation of planktonic foraminifera used within palaeoceanographic studies, in particular the merits of "glassy" versus "frosty" textural preservation (Pearson et al., 2001; Norris et al., 2002; Wilson et

		$\delta^{13}C$		$\delta^{18}O$	
	RMCD	**Mean**	σ	**Mean**	σ
Cibicidoides spp.					
	60–70	0.52	0.22	2.04	0.18
	70–80	0.90	0.13	1.85	0.16
Gyrinoides spp.					
	70–80	0.50	0.25	2.03	0.19
	80–90	1.03	0.13	2.37	0.17
Nuttaloides truempyi					
	90–97.6	0.68	0.20	0.98	0.19
	97.6–100	0.19	0.05	0.27	0.04
Osungularia mexicana					
	70–80	0.76	0.14	2.25	0.12
	80–90	0.80	0.20	1.84	0.26
Oridorsalis umbonatus					
	60–70	-0.36	0.23	2.38	0.17
	70–80	0.02	0.19	2.15	0.14
	80–90	0.22	0.22	1.96	0.38
	90–97.6	-0.03	0.26	1.30	0.17
	97.6–100	-0.13	0.23	0.59	0.28
<38 µm fine-fraction					
	60–70	1.93	0.23	0.76	0.29
	70–80	1.88	0.13	0.29	0.11
	80–90	1.84	0.37	0.09	0.43
	90–97.6	1.82	0.23	-0.10	0.18
	97.6–100	1.79	0.07	-0.21	0.18
Catapsydrax unicavus					
	70–80	0.95	0.14	1.64	0.15
	80–90	1.43	0.22	1.36	0.44
Turborotalia ampliapertura					
	70–80	1.71	0.03	0.67	0.07
	80–90	2.03	0.15	0.67	0.25
Acarinina bullbrooki					
	97.6–100	2.20	0.12	-0.57	0.09
Subbotina senni					
	90–97.6	2.12	0.20	-0.64	0.23
	97.6–100	2.04	0.21	-0.98	0.12

Table 6.1: Mean and standard deviation $\delta^{13}C$ and $\delta^{18}O$ values for 10 m stratigraphic intervals for each planktonic and benthonic foraminiferal species and <38 µm fine-fraction carbonate. The trends observed in the foraminiferal and <38 µm fine-fraction records do not follow the hypothesised depth-$\delta^{18}O$ evolution suggested in Section 6.1.4.

	$\delta^{18}O$		
RMCD	**<38 µm f-f**	***O. umbonatus***	**Difference**
60–70	0.76	2.38	-1.61
70–80	0.29	2.15	-1.86
80–90	0.09	1.96	-1.87
90–97.6	-0.10	1.30	-1.40
97.6–100	-0.21	0.59	-0.80

	$\delta^{13}C$		
RMCD	**<38 µm f-f**	***O. umbonatus***	**Difference**
60–70	1.93	-0.36	2.29
70–80	1.88	0.02	1.86
80–90	1.84	0.22	1.62
90–97.6	1.82	-0.03	1.85
97.6–100	1.79	-0.13	1.92

Table 6.2: <38 µm fine-fraction – *O. umbonatus* $\delta^{18}O$ differences for 10 m stratigraphic intervals. As the lowermost interval (90–100 rmcd) contains a hiatus, with a gap in sedimentation of ~3 Myrs at 97.6 rmcd, the 90–97.6 rmcd interval is also tabulated. It can be observed that the exclusion of this interval makes little difference to <38 µm fine-fraction stable-isotopes and *O. umbonatus* $\delta^{13}C$ but causes an increase in *O. umbonatus* $\delta^{18}O$ evolution comparable to that observed in the published record of benthonic foraminiferal $\delta^{18}O$ (Zachos et al., 2001).

al., 2002; Sexton et al., 2006). So-called "glassy" foraminifera have an appearance akin to recently living specimens, and have been recovered from hemipelagic clay-rich sediments (Pearson et al., 2001; Norris et al., 2002; Wilson et al., 2002; Sexton et al., 2006), while "frosty" foraminifera are typically recovered from pelagic carbonate-rich sections. Oxygen-isotope analyses of Cretaceous and Eocene "glassy" foraminifera have produced palaeotemperature estimates warmer than those of modern-day, as expected for a warmer greenhouse world (Norris and Wilson, 1998; Pearson et al. 2001; Norris et al., 2002; Wilson et al., 2002), a contrast to previous "cool tropics" records (See Section 6.1.4).

Study of "frosty" planktonic foraminifera under the SEM indicates that the frosty appearance results from neomorphism, i.e. *in-situ* replacement of the primary carbonate, that has inconsistent effects on foraminiferal test geochemistry when compared to inorganic carbonate precipitation (Sexton et al., 2006). $\delta^{18}O$ values from "frosty" specimens are typically more positive, i.e. indicative of cooler SSTs, than for equivalent $\delta^{18}O$ values obtained from "glassy" planktonic foraminifera. More positive $\delta^{18}O$ values follow the modelled behaviour of warm-water planktonic foraminifera expected by Schrag et al. (1992, 1995), with early recrystallisation occurring in cooler conditions than those of the primary carbonate. $\delta^{13}C$ values and preservation of interspecies offsets in $\delta^{18}O$ values for both "glassy" and "frosty" planktonic foraminifera suggest, however, that the primary palaeoceanographic signal is not entirely overprinted. Mg/Ca ratios of "frosty" foraminifera do not, however, fit with the expected inorganic precipitation. As described in

Section 6.1.3, recrystallised inorganically precipitated carbonate was expected to have a greater Mg^{2+} content than the primary biogenic carbonate, due to inorganic partition coefficients being an order of magnitude greater. Despite the supposedly large degree of neomorphism identified from SEM micrographs and $\delta^{18}O$ values of Sexton et al. (2006), Mg/Ca ratios were elevated only by ~0.5 mmol/mol, much less than would be expected using laboratory defined inorganic partition coefficients. Importantly, despite the significant neomorphism present in "frosty" planktonic foraminifera, relative temperature trends remain, although far less confidence can be placed in absolute temperatures.

As would be expected from the location and mineralogy of the sediment cores, planktonic foraminifera from Site 1211 typically exhibited "frosty" preservation when viewed under a binocular microscope (Plate 5.6). Although great care was taken to select the well-preserved or 'best-looking' specimens, i.e. complete tests lacking obvious staining or infill, the work of Pearson et al. (2001) and Sexton et al. (2006) described above suggests that even these foraminifera were likely to have been subject to neomorphism and offsetting of primary palaeoceanographic signals. SEM photomicrographs of the planktonic foraminifera described in Section 5.8 (Plate 5.6) show test walls that clearly are not pristine when compared to "glassy" specimens (Figure 6.2).

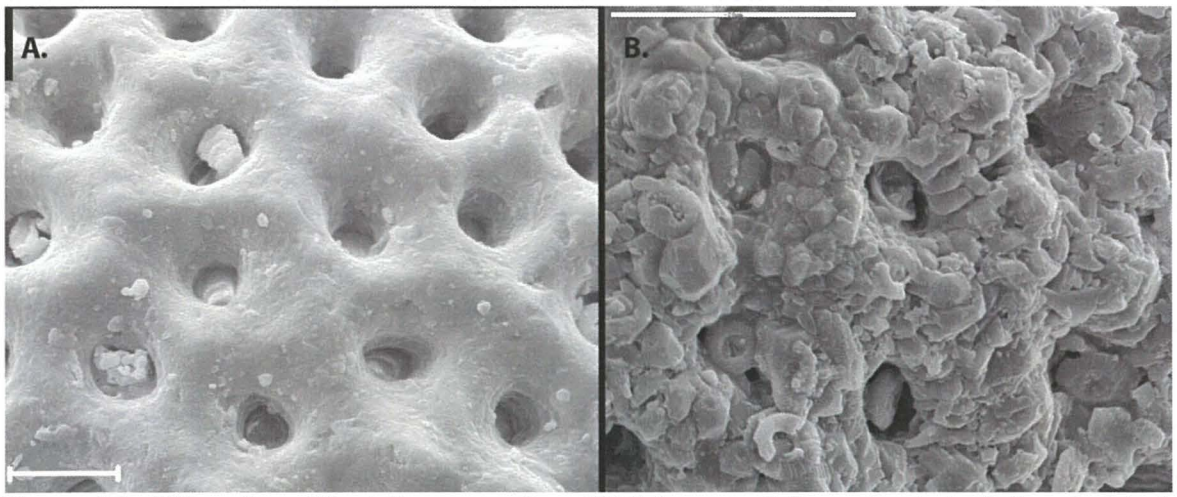

Figure 6.2: "Glassy" vs "frosty" preservation, SEM images of the outer test of the planktonic foraminiferal *C. unicavus* from Sexton et al. (2006, A, scale bar 10 µm) and from Site 1211 (B, scale bar 20 µm). The difference in preservation between the "glassy" (A) and "frosty" (B) specimens is clear, frosty foraminifera display a "weathered" appearance with adhered coccoliths and other secondary calcite covering the test wall.

The outer wall structure of both *Catapsydrax unicavus* and *Turborotalia ampliapertura* closely resembles the neomorphic "frosty" tests studied by Sexton et al. (2006; Figure 6.2), whilst wall cross sections display the same granular altered texture. Both wall surface and wall cross section textures show the weathered appearance identified by Sexton et al.

(2006) as resulting from neomorphic carbonate. These textures suggest that the Oligocene planktonic foraminifera have pervasively recrystallised shells as the neomorphic texture is not limited to the outer surface. Thus, based on the observations of Sexton et al. (2006), $\delta^{18}O$ values for Site 1211 foraminifera should have been shifted to more positive values and Mg/Ca to greater concentrations, i.e. indicating lower and higher palaeotemperatures respectively. Whilst the likely neomorphism suggests that absolute temperature estimation has been compromised, Section 6.1.6 considers whether inter-specific differences remain. The presence of inter-specific differences would suggest a palaeoceanographic signal remains and thus the relative trends retain palaeoceanographic information.

Studies of foraminiferal dissolution have identified that near-surface species tend to be more susceptible to dissolution than deeper-dwellers, so it may be hypothesised that such dissolution susceptibility leads to enhanced diagenesis, i.e. dissolution and reprecipitation. SEM images of the wall structures of *T. ampliapertura* and *C. unicavus* do suggest that the former species, a near surface dwelling foraminifera, has a wall structure consisting solely of micrometre scale crystals unlike the clear two-layer wall structure of the latter. *Turborotalia* species display a "peeling" effect occurring either during deposition or sample processing (Sexton et al., 2006; Pearson, *pers. comm.* 2008), which removes the outer wall structure, thereby exposing featureless internal wall structures. Peeling was noted during picking of *T. ampliapertura*, as well as under the SEM (Plate 5.6 K-M), so the micrometer granular texture and absence of clear structure may be the result of this peeling effect rather than a total neomorphism. No wall structure SEM images were obtained through "unpeeled" *T.* ampliapertura tests, so this hypothesis remains untested. The absence of calcareous nannofossils "welded" to the outer surface of the "inner" wall of *T. ampliapertura*, like those observed for the outer walls of *C. unicavus* and benthonic foraminiferal specimens, supports the idea that the outer wall and thus structure has been lost to "peeling". Whilst the SEM imagery does not clearly indicate whether *T. ampliapertura* has a greater susceptibility, subsequent interpretation of stable-isotope and element/Ca ratios must consider the possibility.

The issue of benthonic foraminiferal preservation and the effect of diagenesis on geochemistry has received little attention compared to the planktonic foraminiferal "glassy" vs "frosty" studies. The lack of attention has primarily resulted from models of diagenesis predicting recrystallisation occurs early within the burial history (Rudnicki et

al., 2001) in sediment pore-waters of similar temperature and chemical composition to those of primary calcification (Schrag et al., 1992; 1995). Early stage diagenesis in such conditions is believed to minimise the potential for diagenetic artefacts in benthonic stable-isotope records, particularly $\delta^{18}O$ records, an assumption recently questioned by Sexton and Wilson (2009). Sexton and Wilson studied the difference in both preservation and $\delta^{18}O$ geochemistry from Middle Cretaceous benthonic foraminifera deposited prior to a hiatus. They noted that foraminifera located immediately below the hiatus displayed wall structures indicative of very poor preservation and $\delta^{18}O$ values substantially more positive than foraminifera of identical age that were not exposed to an immediate hiatus and had similar outer wall structure preservation. Based on these observations, Sexton and Wilson (2009) suggest that the modelled diagenesis profiles for bulk sediments (e.g. Rudnicki et al., 2001) are not appropriate for benthonic foraminifera. Diagenesis of benthonic foraminifera would seem to be a longer-term process dependant on lithology and sedimentation rate controlling both the interaction of benthonic foraminifera with pore-water fluids and the pore-water fluid profiles. The effect of neomorphic carbonate on benthonic foraminiferal Mg/Ca has not been considered in detail, although inorganic reprecipitation following the behaviour of planktonic foraminifera would seem likely.

Benthonic foraminiferal preservation at Site 1211 was described in Section 5.8, the general observation being that across the stratigraphic range of study there was no clear variation in wall structure and no infill of chambers with diagenetic carbonate. Etching and dulling of the outer surface of benthonic foraminiferal tests have been identified as indicators of sub-lysocline dissolution (Corliss and Honjo, 1980), although this is not observed to be associated with any significant reprecipitation. Wall textures display a more granular appearance than the "weathered" texture of the planktonic foraminifera. Benthonic foraminiferal wall texture, however, is similar to that observed in diagenetically altered tests by Sexton and Wilson (2009) and so suggestive of a degree of neomorphism. These observations suggest that Site 1211 benthonic foraminifera had experienced diagenetic alteration, but there was no clear down core trend, i.e. visible diagenesis was approximately equivalent at all levels. Whilst lithology does not change greatly over the stratigraphic interval, being carbonate ooze throughout, the conclusions of Sexton and Wilson indicate the changing sedimentation rate may have an effect on the geochemistry of the diagenesis. As Chapter 4 details, sedimentation rates treble at ~34 Ma, thus sediments immediately older and younger could have differing diagenetic environments, as the

younger sediments were buried more quickly. However, given that, despite the increase, sedimentation rates were low (<7 m/Myr.), diagenetic environments would not have differed greatly, thus the change in burial is unlikely to have produced significant artefacts in to the benthonic foraminiferal geochemistry.

6.1.6 Inter-species differences in foraminiferal isotope values

For foraminiferal carbonate, inter-species differences in stable-isotope ratios have been used by many studies to suggest that neomorphism was limited within foraminiferal tests (Pearson et al., 1993; Norris and Wilson, 1998; Wade and Palike, 2004). Sexton et al. (2006), however, show that inter-species differences in planktonic foraminiferal isotope values could remain, despite considerable neomorphism; thus the presence of inter-species offsets in foraminiferal stable-isotopes does not indicate the absence of diagenetic carbonate. However, the presence of inter-specific offsets does indicate that diagenesis has not completely removed the primary stable-isotope signal, and thus allows relative trends to be interpreted in a palaeoceanographic sense (Sexton et al., 2006).

Figure 6.3 and Table 6.1 show interval mean $\delta^{13}C$ against $\delta^{18}O$ values for the foraminifera and fine-fraction analysed, the intervals being 60–70, 70–80, 80–90, 90–97.60 and 97.6–100 rmcd, the latter two intervals shown on the panel D. These clearly show no homogenisation with depth of the biogenic carbonate $\delta^{18}O$ and $\delta^{13}C$, as would be expected by complete recrystallisation, whilst as discussed above benthonic to fine-fraction $\delta^{18}O$ gradients do not show a clear trend (Table 6.2).

6.1.7 Implications for preservation of primary oceanographic records at Site 1211

Considering the evidence described above for the Site 1211 carbonate microfossils used to generate geochemical proxy records, the picture of diagenesis is somewhat blurred. The influence of dissolution on primary geochemical signals is unquantifiable, although it would appear to be more significant for planktonic foraminifera leading to a "cooler" record. Significant dissolution was only observed during a late Eocene interval (~36 to ~34.5 Ma), coincident with a slight decrease in carbonate sediment proxies suggesting a shoaling of the CCD (see Section 6.3). Fine-fraction stable-isotopes, however, do not change as would be expected from an increase in dissolution, i.e. there is a negative $\delta^{18}O$

shift unrelated to sediment proxies between 90 and 89 rmcd (35.2 and 35.0 Ma). Few foraminiferal records exist from the "dissolution" interval hindering identification of any relationship between dissolution and the stable-isotope record.

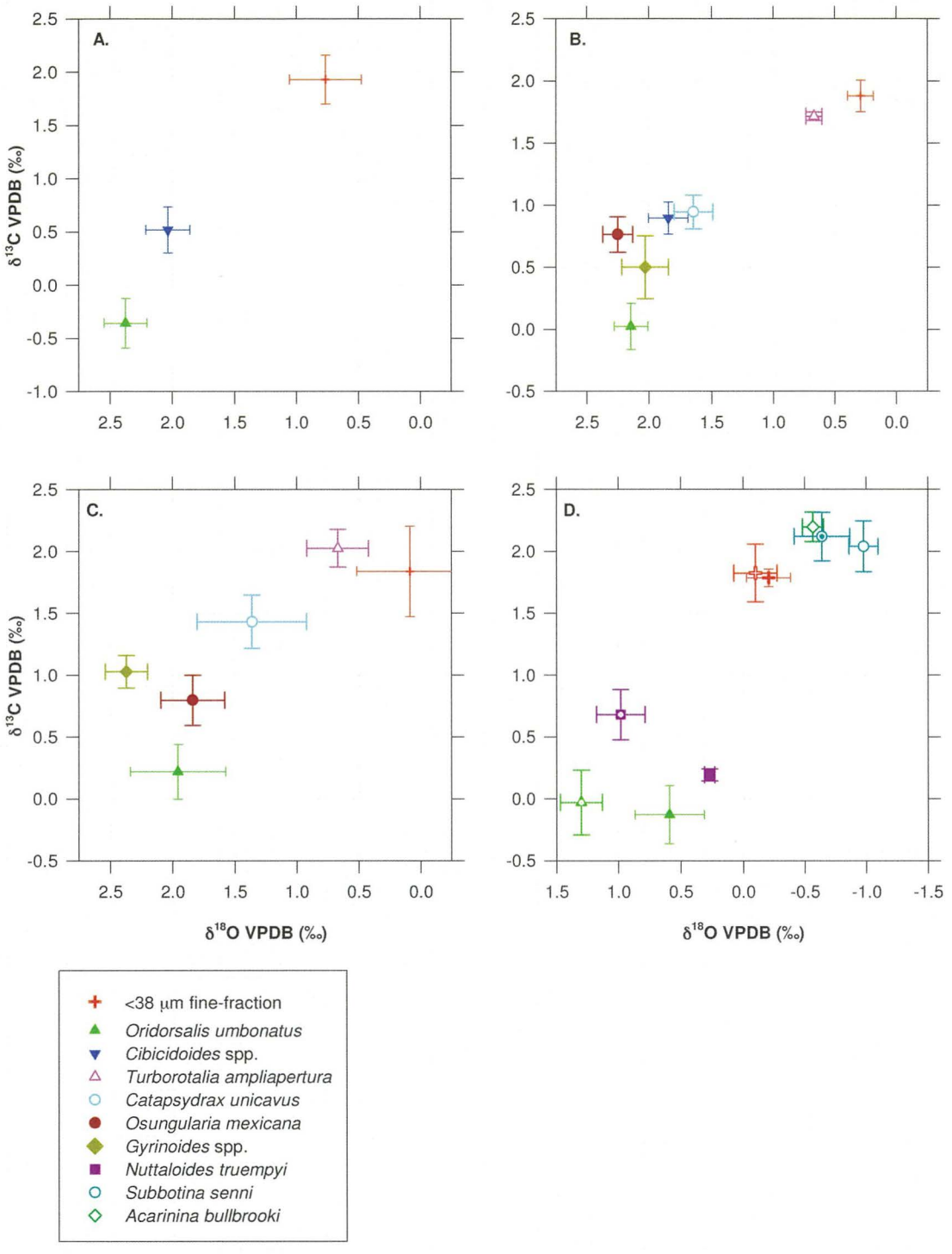

Figure 6.3: $\delta^{13}C$ versus $\delta^{18}O$ plots for four Site 1211 stratigraphic intervals: A. 60–70 rmcd, B. 70–80 rmcd, C. 80–90 rmcd, D. 90–97.6 and 97.6–100 rmcd. In panel D, symbols with a crosshair in D. are for the stratigraphic interval 90-97.6 rmcd, those without the 97.6–100 rmcd interval. These two stratigraphic intervals are separated due to a ~3 million years hiatus (see Chapter 4), which could introduce a more negative $\delta^{18}O$ signal into the data due to palaeoceanographic differences, i.e. the Middle Eocene was warmer than the Late Eocene (Zachos et al., 2001; 2008). The five stratigraphic intervals show no clear homogenisation of either $\delta^{18}O$ or $\delta^{13}C$ that would indicate significant progressive down core recrystallisation.

Neither SEM images of the fine-fraction nor down-core trends in foraminiferal stable-isotope and element/Ca values suggest progressive diagenesis with time. However, SEM images of the foraminifera, whilst not suggesting down core trends, do indicate the foraminiferal tests have been subject to considerable neomorphism. Thus there seems to be a basic contradiction between the possible indicators of diagenesis. The contradiction can be resolved if diagenesis occurred early within the burial history of the Site 1211 sediments and sediments are virtually chemically inert at its present depth, as suggested by Rudnicki et al. (2001) for a similarly shallow buried site. The presence of a Sr^{2+} pore-water maximum unrelated to changes in lithification may support sediments being inert at current locations, although further work looking at preservation across the maximum concentrations is required. Early diagenesis would influence surface-water stable-isotope records to a much greater extent than benthonic foraminiferal records, and thus it is likely that the planktonic foraminiferal and fine-fraction records have more positive $\delta^{18}O$ values than that of primary carbonate alone. Despite the likely diagenetic carbonate component, surface-water records should still record relative trends in $\delta^{18}O$ (and Mg/Ca). Later comparison of $\delta^{18}O_{sw}$ values calculated from each of the foraminiferal stable-isotope and element/Ca records may allow further assessment of the effects of diagenesis (See Section 6.5).

Overall the geochemistry of Site 1211 carbonates should reflect palaeoceanographic trends across the studied interval. Whilst progressive diagenesis was not apparent, there is a definite diagenetic component, as evidenced by the foraminiferal preservation. As such, the possibility of diagenetic influence must be considered where there is reason to expect that differential diagenesis may have taken place, i.e. at changes in sedimentation rate or sedimentary carbonate. These will be considered in the subsequent sections.

6.2 Site 1211 stable-isotopic evidence for the initiation of Antarctic glaciation

The <500 kyrs, two-stage >1.0 ‰ increase in benthonic foraminifera $\delta^{18}O$ values and associated ~1.0 ‰ positive $\delta^{13}C$ excursion are the most recognisable signals of EOB climate change. The event, described in Sections 2.2.3 and 2.3.3 (Figure 2.2), has been observed from the Atlantic Ocean (Miller and Fairbanks, 1983; Zachos et al., 1996; Riesselmann et al., 2007), the Indian Ocean (Pearson et al., 2008), Gulf of Mexico (Katz et al., 2008), the Pacific Ocean (Keigwin, 1980; Miller and Thomas, 1985; Coxall et al., 2005), and the Southern Ocean (Shackleton and Kennet, 1974; Zachos et al., 1992; 1996) as well as being a standout feature in global compilations of the datasets (Keigwin and Corliss, 1986; Zachos et al., 2001; 2008; Figure 1.1). The subsequent discussion identifies the stages of stable-isotope change within records from Site 1211, considering their magnitude and timing. Comparison between surface and bottom waters at Site 1211 and with published records then follows.

6.2.1 Site 1211 bottom-water isotope records

$\delta^{18}O$ values of the composite benthonic foraminifera record (see Section 5.6.4), i.e. bottom waters, are interpreted in Figure 6.4. The bottom-water $\delta^{18}O$ records were interpreted based on the assumption that significant ice-volumes were absent prior to the EOB (Zachos et al., 2001; see Section 2.1 and 2.2.3). Composite benthonic foraminiferal $\delta^{18}O$ records indicate that during the Middle to earliest Late Eocene (39.6 to 37.0 Ma), bottom-water temperatures decreased. The ~0.5 ‰ positive shift in $\delta^{18}O$ being approximately equivalent to a >2 °C decrease in bottom-water temperature, using the $\delta^{18}O$–calcification temperature calibration of Revello and Hillaire-Marcel (2007). Relatively few values were determined for much of the Late Eocene (~37 to 34.2 Ma), and those that were show a high degree of scatter preventing certainty as to the variation in bottom-waters during the interval. There appears, however, to be no systematic variation in bottom-water $\delta^{18}O$ prior to the initiation of the EOT, and thus no change in average bottom-water temperature or $\delta^{18}O_{sw}$.

Bottom-water $\delta^{13}C$ was typically ~-0.1 ‰ during the Middle and Late Eocene, but moved to more positive values (~0.25 ‰) between 37.5 and 35.5 Ma (Figure 5.11). The positive excursion does not correspond to any equivalent event in bottom-water $\delta^{18}O$. Such a positive step could correspond to either an increase in productivity at Site 1211 or a change

in bottom-water source region. Without further proxy records, however, it is not possible to determine which is the case.

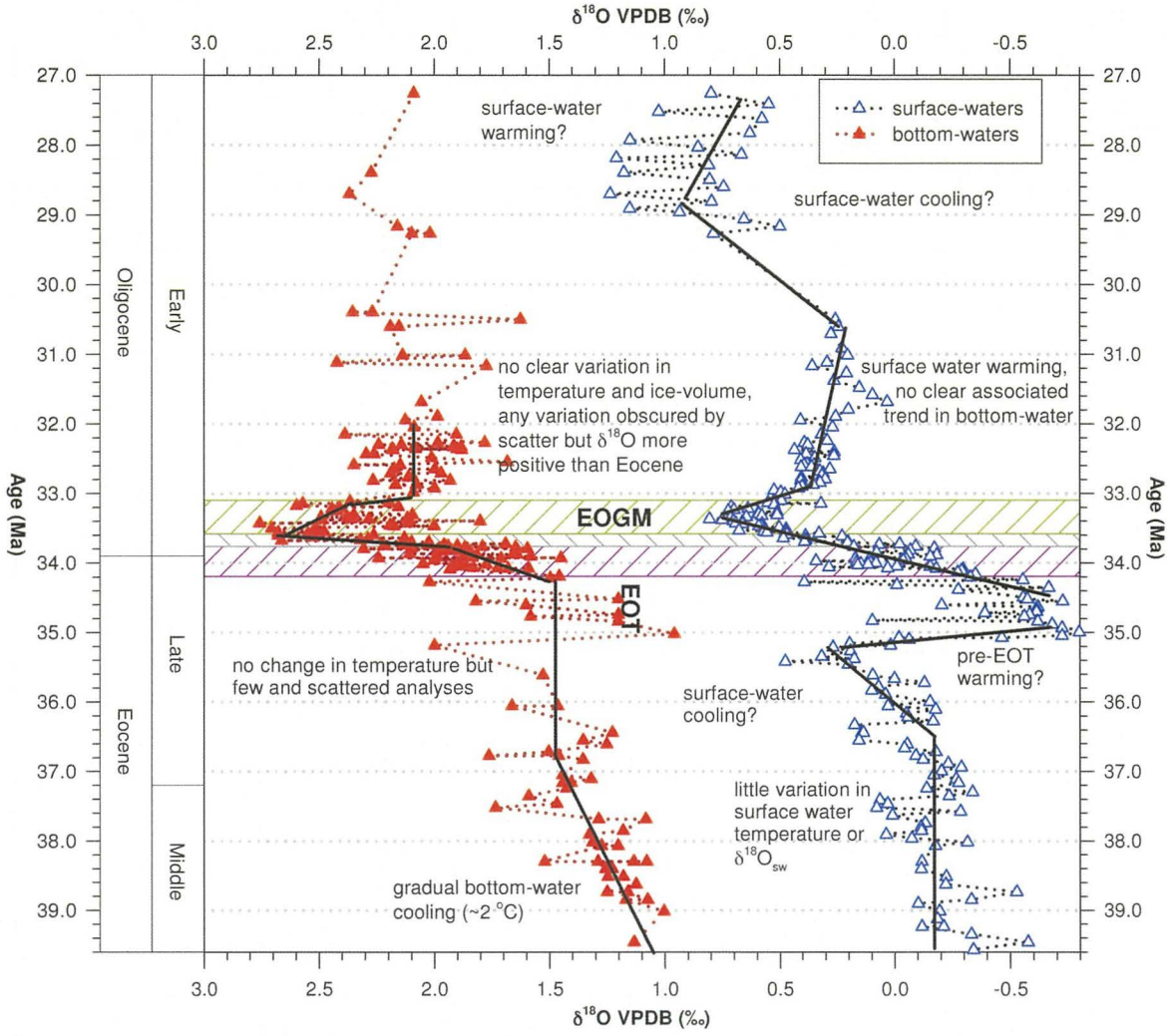

Figure 6.4: Interpreted bottom and <38 μm fine-fraction surface-water variation across the stratigraphic interval studied. Variation across the Eocene–Oligocene boundary is interpreted on Figure 6.5. Surface and bottom waters appear to evolve differently across the Middle Eocene to Early Oligocene, with greater variability in the surface-waters. Bottom-water records exhibited a high degree of scatter and were sampled at insufficient resolution between 37.0 to 34.2 Ma to provide an unambiguous late Eocene record. Surface-water records are discussed in Section 6.2.2.

The key interval within the bottom-water stable-isotope record is the EOB itself. The variation over the boundary has been identified as a series of stages, the two-step Eocene–Oligocene transition (EOT) and Eocene–Oligocene glacial maximum (EOGM; Coxall and Pearson, 2007). The scatter within the composite benthonic foraminiferal $\delta^{18}O$ hinders unambiguous identification of the initiation of the EOT. Scatter within ~34.2 to ~33.5 Ma interval is typically ≥0.5 ‰ over a 100 kyr period, obscuring short-term palaeoceanographic variation. Figure 6.5 shows an interpretation, based on trends occurring in benthonic foraminiferal $\delta^{18}O$, using a framework based on previously

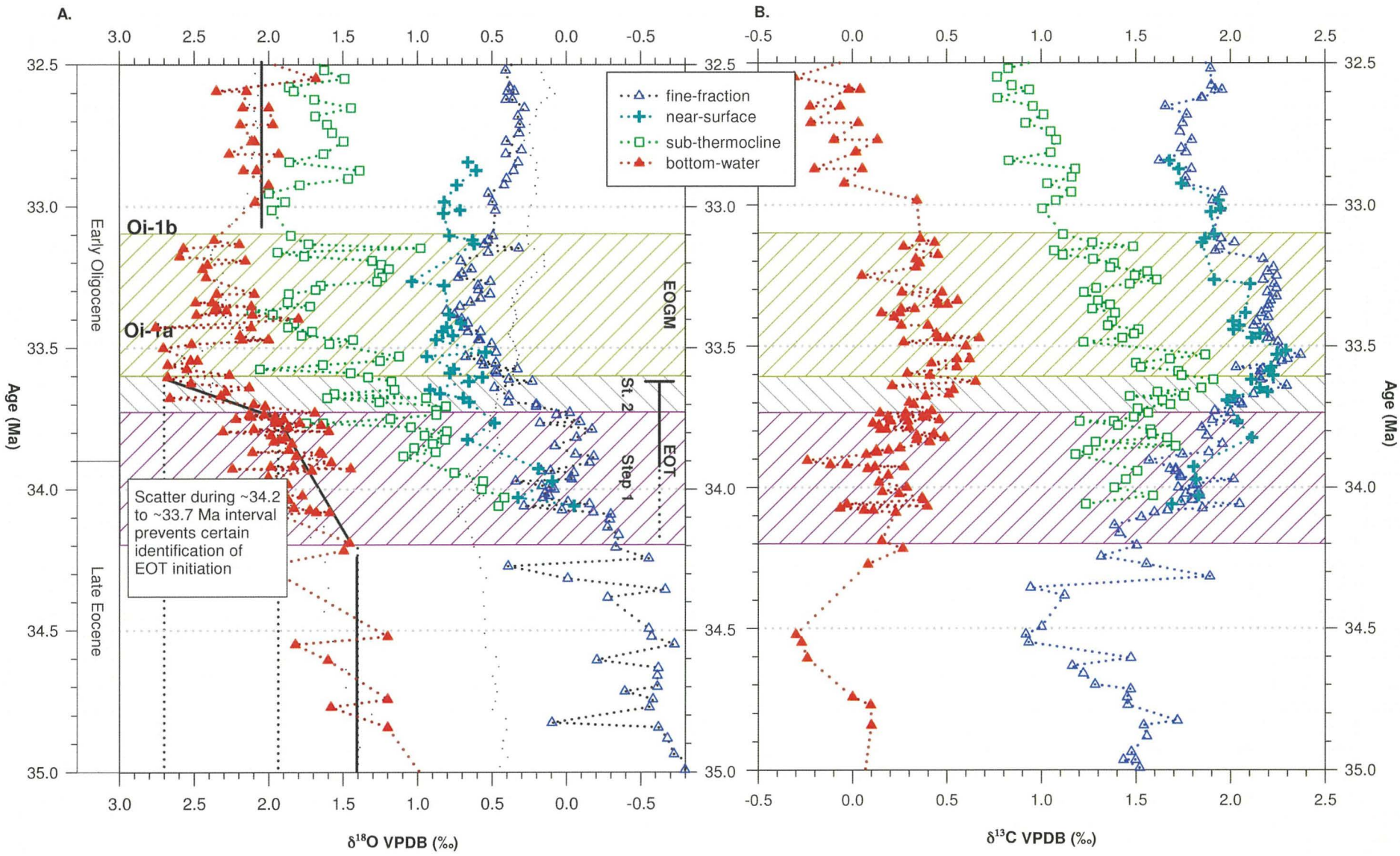
A.
B.
fine-fraction
near-surface
sub-thermocline
bottom-water
Oi-1b
Oi-1a
EOGM
St. 2
Step 1
EOT
Early Oligocene
Late Eocene
Scatter during ~34.2 to ~33.7 Ma interval prevents certain identification of EOT initiation
Age (Ma)
δ18O VPDB (‰)
δ13C VPDB (‰)

Figure 6.5: Late Eocene to Early Oligocene stable-isotope records for Site 1211, A. $\delta^{18}O$ and B. $\delta^{13}C$. Using the composite benthonic foraminiferal $\delta^{18}O$ record, the two steps of the EOT and the EOGM have been identified. Step 1 from ~34.2 to 33.75 Ma involves an increase in $\delta^{18}O$ of ~0.5 ‰, whilst step 2 from 33.75 to 33.6 Ma involves a ~0.8 ‰ increase. Benthonic foraminiferal composite $\delta^{13}C$ does not show a two-stepped increase related to that interpreted in $\delta^{18}O$. The extreme $\delta^{18}O$ of the EOGM lasts ~500 kyrs before a ~0.5 ‰ decrease to a new Oligocene level. The Oi-1a and Oi-1b events labelled by Miller et al. (1991) and Zachos et al. (1996) are also present. Neither of the planktonic foraminiferal stable-isotope records span the entire EOT, but both these and the fine-fraction indicate an increase in $\delta^{18}O$ of between ~1.0 and ~1.5 ‰ across the available EOT records. Surface-water $\delta^{18}O$ reaches maximum values after the maximum observed in the bottom-water records. As with bottom-water $\delta^{13}C$, the planktonic foraminiferal $\delta^{13}C$ does not show a relationship to $\delta^{18}O$ records. Fine-fraction $\delta^{18}O$ and $\delta^{13}C$, however, do increase in a similar manner.

published records (Figure 2.2; Site 744, Zachos et al., 1996). The interpretation in Figure 6.5 shows two steps, the first over ~350 kyr with a gradual increase in $\delta^{18}O$ of ~0.5 ‰ and the second over ~150 kyrs with an increase of ~0.8 ‰. The positioning of the initiation of the EOT is, however, ambiguous and could occur anywhere between ~33.9 and ~34.2 Ma.

The initiation of the EOGM can be identified in the composite benthonic foraminiferal $\delta^{18}O$ record at ~33.6 Ma. At this point $\delta^{18}O$ values, even including scatter, were more positive than at any other point within the dataset with average values of ~2.6 ‰. The maximum in benthonic foraminiferal $\delta^{18}O$ is coincident with maximum values of $\delta^{13}C$ observed for bottom and surface-water records. Within the EOGM, both Oi-1a and Oi-1b, as identified by Miller et al. (1991), can be observed within the benthonic foraminiferal composite $\delta^{18}O$ (Figure 6.5), separated by a mid-EOGM decrease. The termination of the EOGM is also evident within the composite benthonic foraminiferal $\delta^{18}O$, as a ~0.5 ‰ decrease to less positive average and discrete values at ~33.1 Ma. The benthonic foraminiferal stable-isotope values suggest that the EOGM had a duration of ~500 kyrs at Site 1211.

Post EOGM (between ~33.1 and ~32.0 Ma), bottom-water $\delta^{18}O$ values remain elevated by ~0.6 to ~0.8 ‰ above late Eocene values, indicating that bottom-waters remained cooler and/or a continental scale ice sheet remained. As a consequence of the scatter pervasive throughout the dataset, it is not possible to determine any periodicity within the small-scale variation, thus the presence of orbital cycles cannot be assessed. Whilst the stratigraphic sampling resolution was reduced for samples younger than ~32.0 Ma, there is no suggestion of a return to Eocene bottom-water conditions.

Bottom-water $\delta^{13}C$ does not show a clear relationship to the steps interpreted in the $\delta^{18}O$ record. $\delta^{13}C$ values remain constant at ~0.2 ‰ throughout much of the first stage of the EOT, gradually increasing from ~33.9 Ma to a maximum of ~0.7 ‰ at ~33.6 Ma. Published benthonic foraminiferal $\delta^{13}C$ records have been developed from epifaunal *Cibicidoides* species rather than the infaunal *O. umbonatus*. Shackleton et al. (1984) noted that *O. umbonatus* had an erratic $\delta^{13}C$ composition, possibly as a result of the species inhabiting a range of depths within the sediment (Rathburn et al., 1996), whilst Katz et al. (2003) discuss the species changing offsets with respect to other benthonic species over time. Recently, Rathmann and Kuhnert (2008) observed no relationship between shell $\delta^{13}C$ and seawater $\delta^{13}C$ for *O. umbonatus*, indicating a local pore-water $\delta^{13}C$ control, dependant on the oxidation of organic matter in the sediment. Such a control on $\delta^{13}C$, combined with a range of habitat depths, would explain the absence of a clear relationship with $\delta^{18}O$ increase at Site 1211; although the fact that a $\delta^{13}C$ excursion was observed indicates an overall control from global ocean $\delta^{13}C$ values. From maximum values at Oi-1a, $\delta^{13}C$ becomes less positive throughout the early Oligocene. As with the structure of $\delta^{13}C$ change across the EOT, there was little relationship between variation in bottom-water $\delta^{18}O$ and $\delta^{13}C$ during the EOGM or early Oligocene, thus identification of the temporal relationship between $\delta^{18}O$ and $\delta^{13}C$ is not possible.

As described in Chapter 2, the $\delta^{18}O$ isotope shift has been attributed to both a temperature decrease, an ice-volume increase or a combination of the two factors. Mg/Ca ratios are used to calculate palaeotemperatures in Section 6.4, which are subsequently used in Section 6.5 with $\delta^{18}O$ values to calculate changes in $\delta^{18}O_{sw}$ across the EOB. However, an estimate of the extent of ice-growth/cooling can be developed from the $\delta^{18}O$ palaeotemperature equation of Bemis et al. (1998; Equ. 6.1) using a few key assumptions. The assumptions being that the Late Eocene was free of continental scale ice and thus $\delta^{18}O_{sw}$ was ~-1.2 ‰ (Shackleton and Kennett, 1975) and that EOB bottom-water palaeotemperatures could not be less than those of a modern-day ocean (Miller et al., 1987; Zachos et al., 1996).

$$T = 16.5 - 4.8 * (\delta^{18}O_c - \delta^{18}O_{sw}) \quad \text{[Eqn 6.1]}$$

Modern-day temperatures in the western Pacific at depths equivalent to the palaeodepth of Site 1211 are ~2 °C (Talley, 2007), which corresponds to a $\delta^{18}O$ of ~1.8 ‰; therefore if average $\delta^{18}O$ exceeds ~1.8 ‰, then further $\delta^{18}O$ increase must result from the development of continental ice. Figure 6.6 shows the hypothesised evolution of bottom-water temperatures as determined using the assumptions described above. Palaeotemperatures remained, on average, >2 °C until ~33.8 Ma suggesting that the first stage of the EOT resulted from a bottom-water temperature decrease of ~2 °C. After ~33.8 Ma, average palaeotemperatures were <2 °C with $\delta^{18}O$ increasing by up to ~0.9 ‰ beyond the 1.8 ‰ (2 °C) threshold, indicating ice growth occurred during the second stage of the EOT.

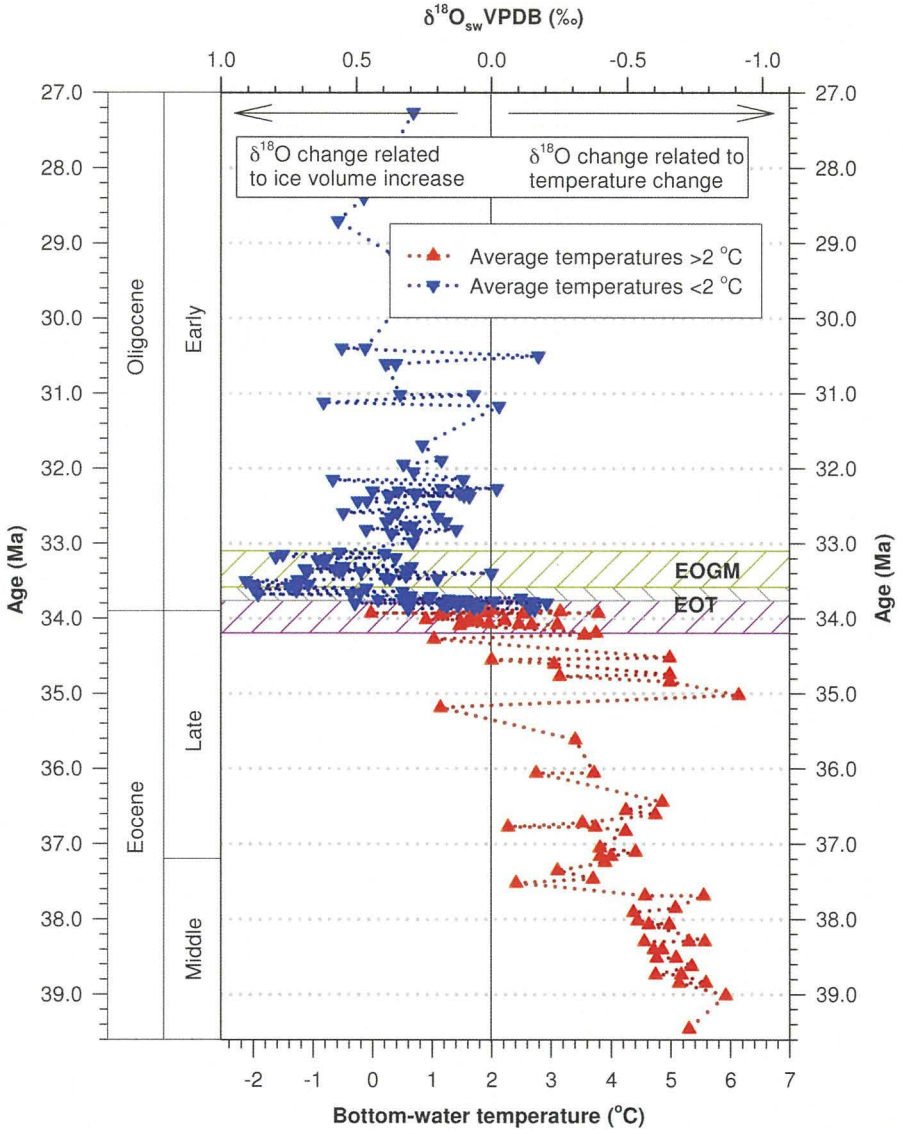

Figure 6.6: Benthonic foraminiferal $\delta^{18}O$ interpreted in terms of temperature change and $\delta^{18}O_{sw}$ increase, using a $\delta^{18}O$ value for a bottom-water of 2 °C as an indication that continental ice growth is occurring. Using this approach bottom-waters cool by ~3 °C prior to ~33.8 Ma, at which point the average temperatures become <2 °C and $\delta^{18}O_{sw}$ increases by up to 0.9 ‰. After the EOGM, $\delta^{18}O_{sw}$ declined to a level approximately ~0.4 ‰ above the ice-free Eocene ocean. These values will be compared to $\delta^{18}O_{sw}$ values calculated using benthonic foraminiferal Mg/Ca palaeotemperatures and $\delta^{18}O$ values in Section 6.5.

Following the EOGM, $\delta^{18}O$ excess decreases to ~0.4 ‰ above the 1.8 ‰ (2 °C) threshold indicating a much reduced post-EOGM ice sheet. Whilst the estimate of 0.9 ‰ is useful to demonstrate that a component of the bottom-water $\delta^{18}O$ positive shift must have resulted from an ice-volume component, uncertainty with regards the Eocene $\delta^{18}O_{sw}$ prevent this being considered an accurate assessment.

6.2.2 Surface-water variation at Site 1211

Surface-water stable-isotope variation is plotted on Figure 6.4 ($\delta^{18}O$ fine-fraction) and 6.5 (all records). Middle Eocene planktonic foraminifera stable-isotopes were plotted on Figure 5.13. The Site 1211 $\delta^{18}O$ and $\delta^{13}C$ inter-relationships are in agreement with previously published data concerning the palaeohabitats of the planktonic foraminiferal species analysed (Figure 6.3). *T. ampliapertura*, and the <38 μm fine-fraction, both have the lowest $\delta^{18}O$ values and highest $\delta^{13}C$ values, with *C. unicavus* $\delta^{18}O$ and $\delta^{13}C$ values being intermediate between *T. ampliapertura* and the benthonic foraminifera. Assuming increasing $\delta^{18}O$ values as temperature decreases with water depth and decreasing $\delta^{13}C$ values from photosynthetic take up of ^{12}C in the surface-waters and subsequent remineralisation of sinking organic material in deeper waters, then the planktonic foraminiferal stable-isotope records agree with previous identification of their habitats. *T. ampliapertura* had a near-surface mixed-layer habitat (Wade et al., 2007; Wade and Pearson, 2008), i.e. more negative $\delta^{18}O$ and more positive $\delta^{13}C$, whilst *C. unicavus* had a sub-thermocline habitat (Poore and Matthews, 1984; van Eijden and Ganssen, 1995), i.e. more positive $\delta^{18}O$ and more negative $\delta^{13}C$.

Fine-fraction carbonate $\delta^{18}O$ records have been demonstrated to track single-species foraminifera $\delta^{18}O$ records, albeit often at a positive offset of up to 1 ‰ across recent glacial/interglacial intervals (Goodney et al., 1980; Paull and Thierstein, 1990, Ennyu et al., 2002). The close relationship of the <38 μm fine-fraction to *T. ampliapertura* $\delta^{18}O$ (Figure 6.5) suggesting the relationship holds for Site 1211. Thus, despite some evidence for increased variation in fine-fraction $\delta^{18}O$ (Dudley and Nelson, 1989), fine-fraction $\delta^{18}O$ can be used as a surface-water $\delta^{18}O$ proxy. Fine-fraction $\delta^{13}C$, however, has not been observed to consistently reflect surface water $\delta^{13}C$ (Ennyu et al., 2002). Considering Figure 6.5, however, fine-fraction $\delta^{13}C$ does track *T. ampliapertura* $\delta^{13}C$ during the EOT

and EOGM suggesting that fine-fraction $\delta^{13}C$ can reveal information as to the nature of surface water variation.

Throughout the Middle Eocene, both fine-fraction and *S. senni* $\delta^{18}O$ show a slight positive trend, although the trend is more gradual in the fine-fraction records. Subbotinids were a deep-dwelling planktonic foraminiferal species (Zachos et al., 1994; Dutton et al., 2005), so the greater positive trend in the *S. senni* $\delta^{18}O$ record compared to the fine-fraction may reflect a greater temperature decrease in deeper surface waters than in the near surface waters. The decline in *S. senni* $\delta^{13}C$ relative to the stable fine-fraction records could reflect an increased separation of surface and deep-surface waters; increased stratification causing deeper-surface water $\delta^{13}C$ to decrease as a result of remineralisation of organic matter and temperatures to decrease as a result of reduced mixing. Although further surface dwelling planktonic foraminiferal determinations are required to produce reliable surface water $\delta^{13}C$ records and test this hypothesis further.

Late Eocene surface-water variation is defined solely by the fine-fraction, suggesting a cooling interval (of ~2 °C) over >1 Myrs between ~36.6 and ~35.2 Ma followed by a rapid warming (of ~4 °C) over <400 kyrs to ~34.8 Ma (Figure 6.5). As discussed above, bottom-water records were sparse across the Late Eocene but average values do not support such large variation, neither does the compilation bottom-water $\delta^{18}O$ record of Zachos et al. (2001, 2008), which suggests that the fine-fraction variation is representative of a surface-water only trend. The positive and negative excursions within the fine-fraction $\delta^{18}O$ are also observed in the $\delta^{13}C$ record, although the correlation between the records is not perfect. Decline in fine-fraction $\delta^{13}C$ continues to ~34.5 Ma after decline in $\delta^{18}O$ has ceased, however, the synchronicity of the initiation of the negative trend in $\delta^{18}O$ and $\delta^{13}C$ at ~35.2 Ma indicates the events are likely to be related. One hypothesis would be that the negative shift in $\delta^{18}O$, resulting from either increasing temperature or decreasing salinity, caused a reduction in surface water and export productivity causing a decrease in surface water $\delta^{13}C$. Continuation of $\delta^{13}C$ decline after the termination of the $\delta^{18}O$ decline suggest the surface water changes influencing $\delta^{18}O$ had a lasting impact.

Whilst the increase in benthonic foraminiferal $\delta^{18}O$ associated with the EOT was identified to commence between 34.2 and 33.9 Ma, fine-fraction stable-isotope records increase from ~34.5 Ma. Fine-fraction $\delta^{18}O$ and $\delta^{13}C$ increasing together by ~1.0 ‰ and ~1.5 ‰ respectively over a series of steps to the EOGM (Oi-1a, Figure 6.5), $\delta^{18}O$ increasing by a further ~0.4 ‰ from Oi-1a to 33.4 Ma. Stable-isotope records for the planktonic foraminifera both commence at ~34.1 Ma, with sub-thermocline *C. unicavus* $\delta^{18}O$ showing an increase of ~1.5 ‰ across the two-stages of the EOT. Near surface records from *T. ampliapertura* show an increase of ~1.0 ‰ across the EOT, although fewer determinations are available than for the other surface-water records. There is little coherence in the pattern of $\delta^{18}O$ increase between surface, sub-thermocline or bottom-waters, which is likely to result from the scatter within each of the datasets.

As discussed above, the positive $\delta^{18}O$ shift across the EOT reflects a temperature and ice-volume change. As the ice-volume component must be equivalent at all depth levels throughout the ocean, then a constraint on the extent of this ice-volume is the covariation of $\delta^{18}O$ between surface and bottom-water records (Miller et al., 1987, 1991). A minimum positive shift of ~1.0 ‰ in surface water $\delta^{18}O$ was observed in the *T. ampliapertura* record, suggesting that no more than 1.0 ‰ of the $\delta^{18}O$ increase in bottom and sub-thermocline records was related to ice-volume. Change in $\delta^{18}O$ beyond the ~1.0 ‰ limit would reflect cooling within the sub-thermocline and bottom-waters. A potential caveat for this approach is that variation in salinity of surface-waters across the EOT is unconstrained and thus a negative shift in salinity could attenuate ice-volume related $\delta^{18}O_{sw}$ change.

Near-surface and sub-thermocline $\delta^{13}C$ records all show no clear relationship to the stages of the EOT identified in Section 6.2.1, with neither planktonic foraminferal $\delta^{13}C$ record showing similarity to the corresponding $\delta^{18}O$ record. All $\delta^{13}C$ records including bottom-waters, however, show an equivalent absolute increase from ~34.1 to ~33.6 Ma, the range of $\delta^{13}C$ variation at Site 1211 being ~0.8 ‰. The similarity in absolute increase indicating that the carbon cycle change effected the entire water-column at Site 1211 equally and thus was likely to be due to a global change in the carbon cycle. A local change in productivity would be likely to produce a change in gradient across the EOT, which is not seen in surface to bottom-water gradient profiles (Figure 5.14).

The Oi-1a event, that signals the EOGM, was identified at ~33.6 Ma using benthonic foraminiferal $\delta^{18}O$ and was coincident with maximum $\delta^{13}C$ records in all records, suggesting the interpretation of the event was robust. However, surface-water $\delta^{18}O$ records do not show a coincident maximum and sub-thermocline records show only a single-datapoint maximum. Following the transient maximum in sub-thermocline records, each of the surface-water $\delta^{18}O$ continue to increase for ~200 kyr following Oi-1a, by up to ~1.0 ‰, coincident with an average decline from maximum bottom-water $\delta^{18}O$ values of ~0.5 ‰. The contrary variation in sub-thermocline records can also be observed at the termination of the EOGM, and is visible as a reduction in sub-thermocline to bottom-water $\delta^{18}O$ gradients in Figure 5.14. The coincidence of increased sub-thermocline to bottom-water $\delta^{18}O$ gradients with intervals of peak glaciation, i.e. Oi-1a and Oi-1b, suggests that the peak glaciations lead to invigorated mixing in the surface-waters, warming the sub-thermocline. As the peak conditions subsided, surface water stratification increased leading to cooler sub-thermocline waters and reduced sub-thermocline to bottom-water gradients. The lack of change in $\delta^{13}C$ gradients, however, would not support this hypothesis, although this can be attributed to the *O. umbonatus* $\delta^{13}C$ not recording bottom-water $\delta^{13}C$ reliably (Rathmann and Kuhnert, 2008). Foraminiferal Mg/Ca ratio derived palaeotemperature and subsequent $\delta^{18}O_{sw}$ estimates will provide further clarification of the 33.6 to 33.4 Ma interval, allowing the palaeoceanographic evolution of Site 1211 to be further determined.

Unlike bottom-water $\delta^{18}O$, surface and sub-thermocline $\delta^{18}O$ do not show an abrupt EOGM termination. Fine-fraction $\delta^{18}O$ declines, at first rapidly by 0.4 ‰ from 33.4 to 33.0 Ma, then gradually from ~33.1 to ~30.0 Ma by <0.5 ‰; bottom-water records showing little evidence of decrease over this latter interval. Sub-thermocline records do not show any clear change at the end of the EOGM but remain relatively consistent within the range of scatter in the data to ~32.5 Ma. The divergent behaviour of surface and sub-thermocline $\delta^{18}O$ suggests that post EOGM sub-thermocline waters had become isolated from surface waters, i.e. the increased stratification described above.

6.2.3 Intersite comparison of bottom-water records

The absolute magnitude of the Site 1211 positive EOB $\delta^{18}O$ excursion, from ~34.2 Ma to Oi-1a at ~33.6 Ma was ~1.3 ‰, with the maximum positive $\delta^{13}C$ excursion across the same interval being 0.9 ‰. The $\delta^{13}C$ estimation, however, represents a maximum range of the EOT at Site 1211, with values typically increasing by only 0.5 ‰ over the EOT. Thus the magnitude of the positive $\delta^{18}O$ shift was within the range of values observed in previous medium/high stratigraphic resolution EOB studies (cf. Table 2.1, Zachos et al., 1996; Coxall et al., 2005; Riesselman et al., 2007), whilst the $\delta^{13}C$ excursions at Site 1211 seems to be towards the minimum range observed in published records and, as discussed above, poorly recorded.

To allow comparison of timings and relative rates of change within the Site 1211 EOT isotope records with published datasets, it has been necessary to migrate the published datasets to the most recent geological timescale, i.e. Luterbacher et al. (2004, in Gradstein et al., 2004) and normalise Site 1211 stable-isotope records to *Cibicidoides* spp. This migration was achieved by interpolation between the magnetic chrons specified for the Berggren et al.'s (1995) Cenozoic geological time scale and those of Luterbacher et al. (2004), and applying the resulting chron-specific correction factor to individual datapoints. Interpolation to the most recent geological timescale of Luterbacher et al. (2004) consistently shifts the absolute timing of isotope events by ~200 kyrs older during the EOT. However, interpolation has little effect on the duration of either the EOT or EOGM such that the source publication interpretations of these intervals remain valid (Figure 6.7). Normalisation to *Cibicidoides* spp. was undertaken using the species offsets calculated in Section 5.6.3 for Site 1211.

Consideration of the published $\delta^{18}O$ records in Figure 6.7 indicates that initiation of the EOT occurred at ~34.1 Ma in all datasets except that for Site 1218, where there was a dissolution event at that stratigraphic level (see Section 6.3). As described in Section 6.2.1, initiation of the EOT commences between 34.2 and 33.9 Ma at Site 1211 (shaded area, Figure 6.7). Despite the uncertainty in timing of the initiation of the EOT at Site 1211, development of the Site 1211 bottom water $\delta^{18}O$ is similar to that observed in records from Sites 522 in the South Atlantic, Site 744 in the Southern Ocean (Zachos et al., 1996). The actual duration of each stage at Site 1211, however, differs from the Zachos et al. (1996)

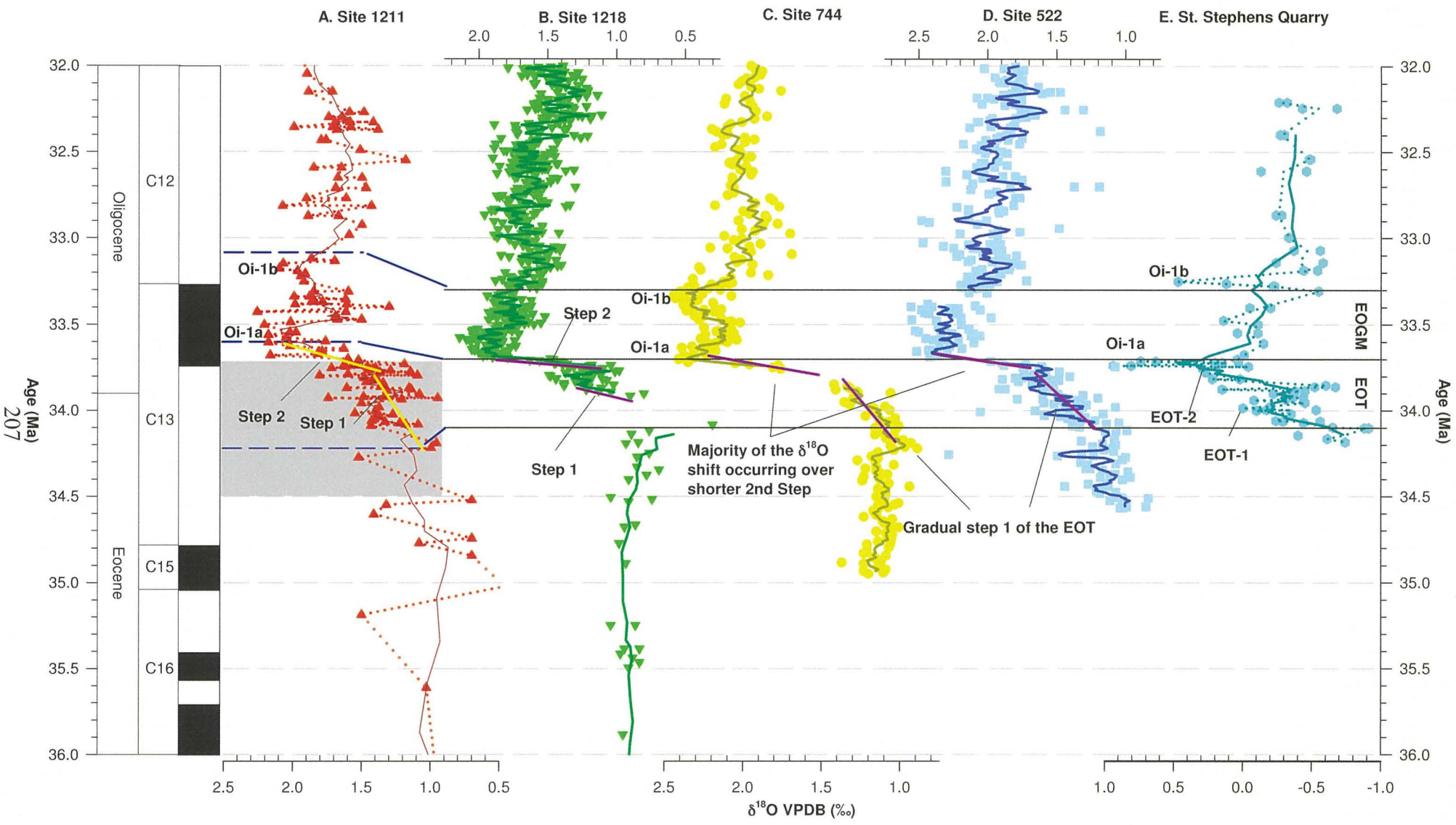
A. Site 1211
B. Site 1218
C. Site 744
D. Site 522
E. St. Stephens Quarry
Oligocene
Eocene
C12
C13
C15
C16
Oi-1b
Oi-1a
Step 2
Step 1
Majority of the δ18O shift occurring over shorter 2nd Step
Gradual step 1 of the EOT
EOGM
EOT
EOT-2
EOT-1
Age (Ma)
δ18O VPDB (‰)

Figure 6.7: $\delta^{18}O$ records across the Eocene–Oligocene boundary for Site 1211 (this study; A), Site 1218 (Lear et al., 2004; Coxall et al., 2005; B), Site 744 (Zachos et al., 1996; C), Site 522 (Zachos et al., 1996; D) and St Stephens Quarry (SSQ), Alabama (Katz et al., 2008; E). The Eocene–Oligocene transition (EOT) and Eocene–Oligocene glacial maximum (EOGM) are delimited by horizontal black lines at ~34.1, ~33.7 and ~33.25 Ma in panels B–E. The blue dashed lines on panel A indicate the interpreted Site 1211 EOT and EOGM (see text for discussion). The steps and features shown in panels B–E are from the respective studies. Data in plots B–E were converted to the timescale of Luterbacher et al. (2004, in Gradstein et al. 2004) by interpolating from the magnetochron ages of Cande and Kent (1995; data in panels C–E) and the astronomically derived magnetochron ages determined for Site 1218 (panel B). Solid lines through the datasets are 5-point running means. Panel E also includes the dotted line used to describe the variation at SSQ by Katz et al. (2008) for their interpretation. All isotope data are normalised to *Cibicidoides* spp. using the offsets calculated either within this study (see Section 5.6.3) or Shackleton et al. (1984; see Section 5.5.3 for details). Previous figures have shown the bottom-water normalised to *O. umbonatus*, the species used to develop the majority of the records, which calcifies $\delta^{18}O$ 0.5 ‰ more positive than *Cibicidoides* spp.

sites. At Site 522, the most complete record, the first step occurs over ~300 kyrs with the second taking <100 kyrs. The two-stages of the EOT at Site 1211 are longer than their equivalents at Site 522, which will be discussed later. It is interesting to note that the positive $\delta^{18}O$ shift recorded at Site 1211 does not clearly follow the two-step pattern observed by Coxall et al. (2005) for the equatorial Pacific, although determination of the significance of this absence is limited by the scatter within the Site 1211 data.

The EOGM lasted ~500 kyrs at Site 1211, however, the duration of the EOGM is constrained to magnetic chron C13n (<400 kyrs) at Sites 522, 744 and 1218 (Figure 6.7). The synchrony of records from the Atlantic, Southern and Pacific Oceans respectively and from different palaeodepths (Figure 6.7; Table 2.1) indicate a global event, thus the ~500 kyrs observed at Site 1211 must represent an overestimation of the length of the EOGM.

The stages of the EOT and the EOGM at Site 1211 were elongated compared to published records with magnetostratigraphy or orbitally tuned age models. The elongation of these global events indicates that the Site 1211 depth–age model underestimates sedimentation rates across the EOT and EOGM interval. As discussed in Chapter 4, the Site 1211 depth–age model was determined using a combination of biostratigraphy, Sr-isotope chemostratigraphy and tie-points to the Site 1218 isotope records. This approach made use of all the available Site 1211 age control data to produce the most robust depth–age model interpretation, based on correlation coefficients. In the absence of high-resolution chronostratigraphic records, such as orbitally tuned XRF or non-destructive core-logging data (cf. Westerhold et al., 2008 for the Palaeocene), refinement of the absolute depth-age model is limited. However, the depth-age model remains internally robust so common features remain present but shifted in absolute age and duration.

As described in Section 2.2.4, the $\delta^{18}O$ shift across the EOT was a result of changing bottom-water temperature and $\delta^{18}O_{sw}$. Assuming bottom-water salinity variation was minor, i.e. salinity changes of <0.5 ‰ (which would correspond to ~0.25 ‰ variation in $\delta^{18}O_{sw}$), then the majority of the $\delta^{18}O_{sw}$ change must result from ice-volume. As the temporal resolution of all palaeoceanographic studies is greater than the ocean mixing time, then the ice volume component is a global feature and therefore should be identical within each locations EOB record. Relative changes in the magnitude of the bottom-water $\delta^{18}O$ EOT shift between sites must, therefore, result from other palaeoceanographic differences, i.e. temperature, water depth.

Considering the EOGM $\delta^{18}O$ maxima between the sites then, Sites 1211 and 1218 have $\delta^{18}O$ values of ~2.1 ‰, whilst Site 522 and 744 have maximum values of ~2.5 ‰ (see Table 2.1 for locations). The offsets between $\delta^{18}O$ records at the sites were, on average, consistent across from the Late Eocene to the Early Oligocene, indicating the differences between the sites remained unaffected by the climate transition. The similarity of Sites 1211 and 1218 suggests these sites could have been bathed within similar water masses, the more positive $\delta^{18}O$ values at Sites 522 and 744 suggesting these sites were either cooler and/or more saline than Site 1211. However, each of the sites are geographically distant and the palaeodepths of the sites span ~2 km (Table 2.1), so further proxy control on the temperature and salinity differences are required. Following the termination of the EOGM, Figure 6.7 shows the evolution of $\delta^{18}O$ at the deep-water sites up to ~32.0 Ma. Post-EOGM $\delta^{18}O$ variation is different at each site reflecting local influences on $\delta^{18}O$ as well as the global $\delta^{18}O_{sw}$ component as a result of EOGM termination. These changes are likely to result from temperature, $\delta^{18}O$ suggesting that bottom-water temperature at Sites 744 and 1211 remained relatively constant, whilst Sites 522 and 1218 declined by up 0.3 ‰ (~1 °C). These trends may be elucidated further with the development of Mg/Ca palaeotemperature records in Section 6.4.5.

$\delta^{18}O$ values at Site 1211 were ~1.5 – ~2.0 ‰ more positive than those at St Stephens Quarry (SSQ), Alabama (Katz et al., 2008), a difference most likely resulting from the warm temperatures at the shallow tropical shelf sea location of SSQ (~15 to 20 °C). $\delta^{18}O$ records from St Stephens Quarry, Alablama (SSQ, Katz et al., 2008) show a similar EOT increase to the deep-water sites, although the EOT-2 step identified by Katz et al. is not

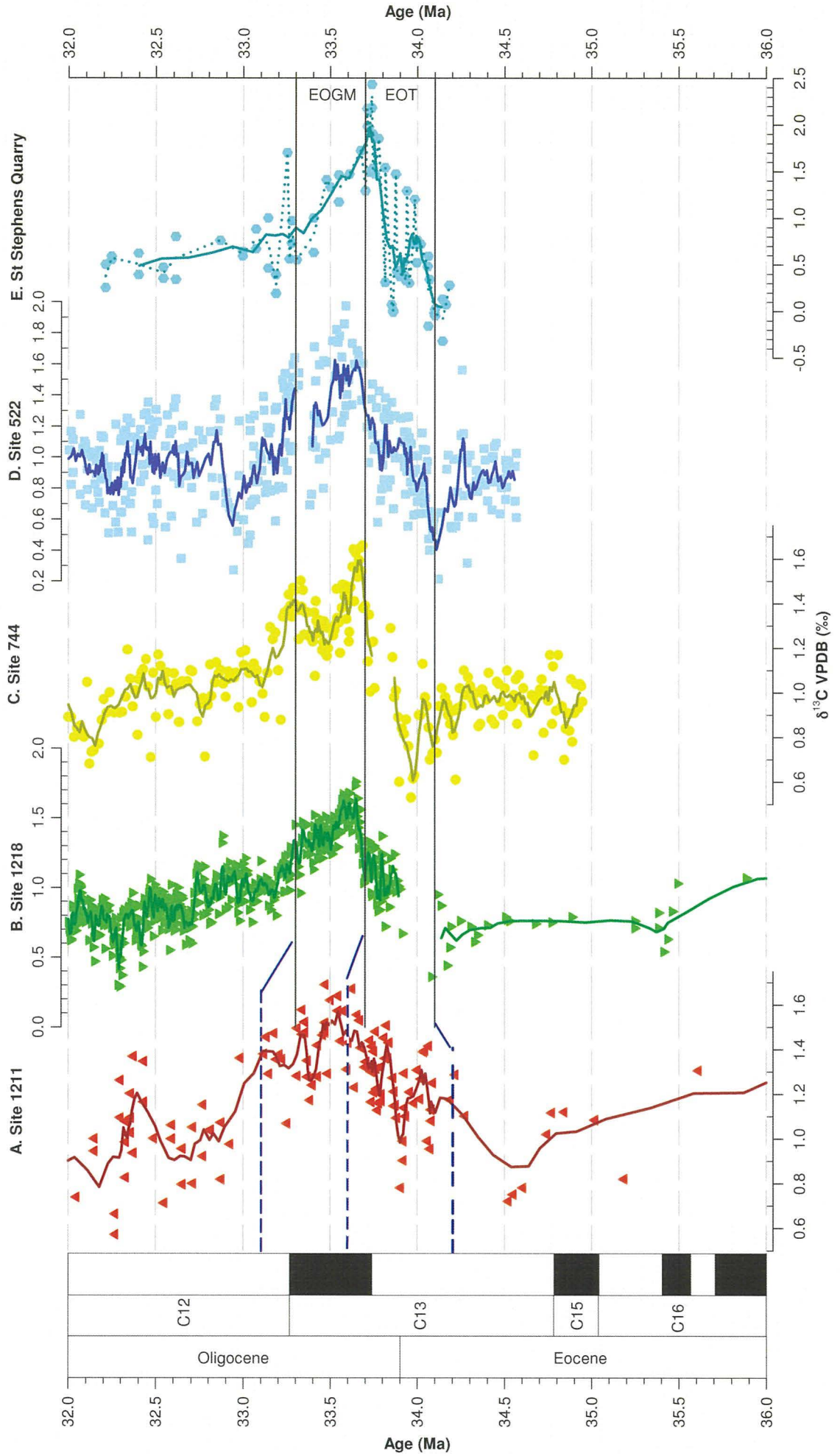
Age (Ma)
EOGM
EOT
E. St Stephens Quarry
D. Site 522
C. Site 744
B. Site 1218
A. Site 1211
δ13C VPDB (‰)
C12
C13
C15
C16
Oligocene
Eocene
Age (Ma)

Figure 6.8: $\delta^{13}C$ records across the Eocene–Oligocene boundary for Site 1211 (this study; A), Site 1218 (Lear et al., 2004; Coxall et al., 2005; B), Site 744 (Zachos et al., 1996; C), Site 522 (Zachos et al., 1996; D) and St Stephens Quarry (SSQ), Alabama (Katz et al., 2008; E). The Eocene–Oligocene transition (EOT) and Eocene–Oligocene glacial maximum (EOGM) are delimited by horizontal black lines at ~34.1, ~33.7 and ~33.25 Ma in panels B–E. The blue dashed lines on panel A indicate the interpreted Site 1211 EOT and EOGM (see text for discussion). Published deep-water and hemipelagic sites (B to E) all show a near identical, two-step transient increase in $\delta^{13}C$, that correlates with the steps in $\delta^{18}O$ shift at the sites, followed by a gradual decline to Eocene $\delta^{13}C$ values. The global similarity of the increase indicating the event is a global perturbation of the marine carbon-cycle. A two-step increase in $\delta^{13}C$ is not evident at Site 1211, although there is a clear transient perturbation in $\delta^{13}C$. The absence of the two-step evolution and relationship to $\delta^{18}O$ (Figure 6.4), supports the idea that *O. umbonatus* was not a reliable recorder of bottom-water $\delta^{13}C$ during the late Cenozoic.

apparent in Site 1211 or any published deep-water record. The EOGM at SSQ, however, does not follow the observed deep-sea behaviour, with a much more brief Oi-1 period of <100 kyrs. $\delta^{18}O$ then decreases rapidly throughout the EOGM, showing a further transient peak at ~33.3 Ma. These differences, when compared to the deep-water records, suggest that SSQ is influenced by a previously unidentified change in local hydrography across the EOGM that acts to produce an attenuated $\delta^{18}O$ signal, and thus SSQ seems not to be representative of deep-water $\delta^{18}O$ change.

$\delta^{13}C$ records for Site 1211 and published sites are shown in Figure 6.8. The $\delta^{13}C$ records from Sites 522, 744, 1218 and SSQ plotted in Figure 6.8 were based on *Cibicidoides* spp., whereas the $\delta^{13}C$ record from Site 1211 was normalised to *Cibicidoides* spp. It is clear that all five records exhibit a positive excursion corresponding to the EOT irrespective of the age mismatch and the attenuated excursion evident within the Site 1211 records. Evolution of published $\delta^{13}C$ records indicates a globally observed two-step positive excursion correlating with the positive shift in $\delta^{18}O$ is present within all records, indicating the $\delta^{13}C$ shift resulted from a perturbation in the marine carbon cycle (Zachos et al., 1996; Salamy and Zachos, 1999). The absence of the two-step increase and correlation with $\delta^{18}O$ at Site 1211 supports the idea that *O. umbonatus* is not a reliable recorder of bottom-water $\delta^{13}C$ (Section 6.2.1), limiting the significance of comparison between Site 1211 and published records.

6.2.4 Intersite Eocene–Oligocene surface water variation

Surface-water records across the EO boundary are plotted in Figure 6.9 and 6.10, having been interpolated onto the Gradstein et al. (2004) timescale as described for the bottom-water records (Section 6.2.3). Two records are bulk or fine-fraction carbonate from ODP

Site 1218 in the equatorial Pacific (Palike et al., 2006, bulk carbonate) and Site 748 in the Southern Ocean (Indian sector, Bohaty and Zachos, 2003, fine-fraction), whilst one is from the planktonic foraminifera *T. ampliapertura* recovered from the Tanzanian Drilling Project (TDP) Sites 12 and 17 (Pearson et al., 2008).

In Figure 6.9, the only feature present unambiguously within each records is the EOB shift in $\delta^{18}O$ at ~34 Ma. Surface waters thus evolved locally rather than showing a global control. Assuming that temperature is the dominant control on the surface-water $\delta^{18}O$, then Site 1211 $\delta^{18}O$ values indicate Site 748 was cooler and Site 1218 was warmer. The separation of the fine-fraction $\delta^{18}O$ records at ~1 ‰ (~4 °C) during the Eocene and ~1.5 ‰ (~6 °C) during the Oligocene, however, is much less than would be expected from the latitudinal differences indicating other factors are at work. One such factor could be salinity, Broecker (1989) observing ~1.5 ‰ gradient between low and high latitudes with more positive values at low-latitudes due to evaporation. The Broecker gradient would increase the latitudinal differences to ~2.5 to ~3.0 ‰ or ~10 to ~12 °C. Different species of calcareous nannofossils with contrasting vital effects, i.e. biological offsets from $\delta^{18}O$ equilibrium, could also affect the fine-fraction and bulk records altering the absolute $\delta^{18}O$ recorded at each site.

Considering the evolution of surface water $\delta^{18}O$, the sub-tropical record from Site 1211 shows less variability during much of the Middle Eocene than the high latitude record from Site 748. Site 748 shows a long term (>1 Myrs) positive and then negative shift in $\delta^{18}O$ of >0.5 ‰, whilst Site 1211 remains relatively constant. $\delta^{13}C$ records, however, are very similar between the two sites throughout the Middle Eocene. $\delta^{18}O$ variation during the Late Eocene shows that low and high latitudes surface waters varied greatly, with a collapse in $\delta^{18}O$ difference between ~36.2 and ~35.2 Ma. The collapse in $\delta^{18}O$ difference occurs with an increase in $\delta^{13}C$ at both sites, which could indicate an association with increased productivity; an increase in Southern Ocean productivity being observed near this time (Diester-Haass, 1996; Salamy and Zachos, 1999; Diester-Haass and Zahn, 2001). The collapse in $\delta^{18}O$ gradient suggests that surface water conditions, i.e. temperature or salinity, were similar at the two sites during the ~36.2 to ~35.2 Ma interval.

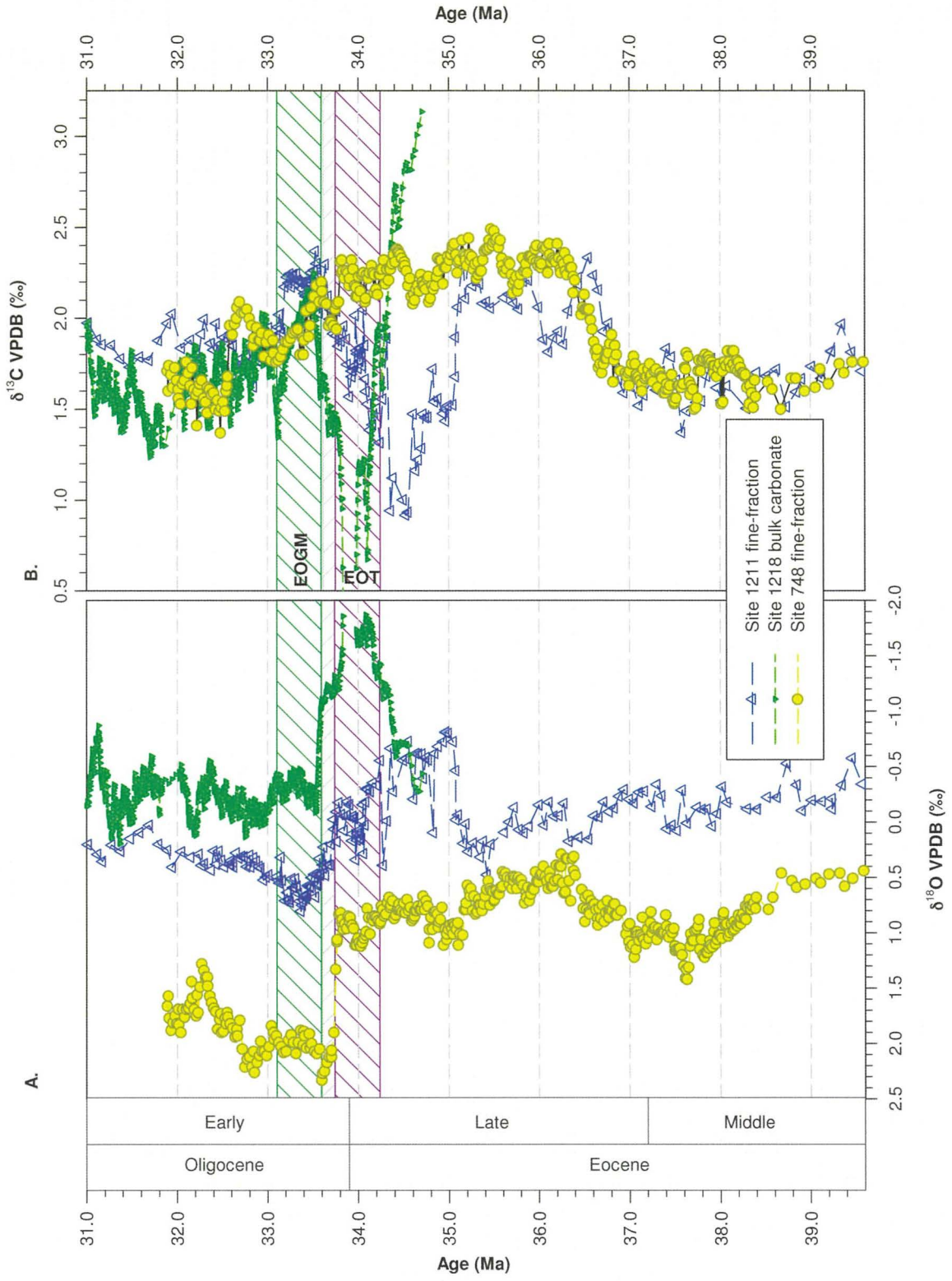

Figure 6.9: Surface-water stable-isotope records for Site 1211, Site 748 in the Southern Ocean and Site 1218 in the equatorial Pacific (Bohaty and Zachos, 2003; Palike et al., 2006). $\delta^{18}O$ is presented in panel A. and $\delta^{13}C$ is plotted in panel B. Shaded boxes refer to the two steps of the EOT and the EOGM for Site 1211 as identified in Section 6.2.1.

Site 748 and 1211 $\delta^{18}O$ and $\delta^{13}C$ diverge at 35.2 Ma, with a negative excursion in both $\delta^{18}O$ and $\delta^{13}C$ of ~1.0 ‰ at Site 1211 lasting until ~34.5 Ma, whilst Site 748 records remain relatively uniform. Similar changes to those observed at Site 1211 occurred at Site 1218, although those at Site 1218 were later and had greater magnitude. The different

relationship between decrease in $\delta^{13}C$ and $\delta^{18}O$ at the sites indicates each event is regional in extent. The contrasting changes in the latest Eocene between high and low-latitude suggest there was significant low-latitude surface-water change prior to the EOT. As described above (Section 6.2.2) the negative excursion in $\delta^{18}O$ and $\delta^{13}C$ suggests a large but transient increase in temperatures and/or salinity decrease, associated with a possible reduction in surface-water productivity. These changes clearly do not appear to have occurred in the high latitudes. Low-latitude planktonic foraminiferal records over this interval would be informative as whether the fine-fraction shifts are representative of a real oceanographic change or result from species composition variation.

Whilst all surface-water records exhibit a clear EOB $\delta^{18}O$ step of >1.0 ‰, the timings and development differ at each site due to local surface ocean changes (Figure 6.9). Interestingly, no EOB $\delta^{13}C$ excursion is recorded at Site 748, but following the EOGM decrease in the fine-fraction $\delta^{13}C$ records agree in trend and absolute magnitude, suggesting that the fine-fraction $\delta^{13}C$ records elements of both local and global carbon-cycle change.

Planktonic foraminiferal records at sufficient resolution to identify EOT and EOGM change are limited to a solitary record for *T. ampliapertura* from the TDP (Pearson et al., 2008; Lear et al., 2008). Foraminifera recovered by the TDP have exceptional "glassy" preservation (See Section 6.1.5) but are representative of a hemipelagic, not open-ocean, surface water environment. Stable-isotope records for *T. ampliapertura* are plotted in Figure 6.10 with those from Site 1211. Despite the relatively few Site 1211 *T. ampliapertura* determinations, $\delta^{18}O$ in the two records appear to increase by ~1.0 ‰ across the EOT. The observation of a clear EOT $\delta^{18}O$ increase from geographically surface-water settings confirming the global nature of the $\delta^{18}O_{sw}$ shift associated with ice-volume increase.

$\delta^{13}C$ for *T. ampliapertura* also shows a typical positive EOT excursion of approximately equivalent magnitude at both sites, ~0.6 ‰ from the initiation of the EOT to the Oi-1a. Site 1211 $\delta^{13}C$ is offset by up to ~1 ‰ from the TDP record, which may result from greater

export of ^{12}C rich organic material to deep-waters at Site 1211 (as indicated by less positive $\delta^{13}C$ for the sub-thermocline dwelling *C. unicavus*).

Site 1211 $\delta^{18}O$ values were typically ~2.5 to ~3.0 ‰ more positive than those from Tanzania. The difference between the sites possibly represents either cooler surface waters, more saline waters at Site 1211 or the presence of diagenetically altered carbonate. Pearson et al. (2001) notes that the location of the TDP sites was likely to be within a warm boundary current, so elevated palaeotemperatures, i.e. more negative $\delta^{18}O$, compared to the open-ocean sub-tropical Site 1211 may be expected. A ~2.5 ‰ difference in $\delta^{18}O$, however, suggests Site 1211 was ~12.0 °C cooler than TDP. Mg/Ca palaeotemperatures are estimated in Section 6.4.4 for Site 1211 *T. ampliapertura*, which are compared to TDP 12/17 in Section 6.4.5 so the relative temperature differences estimated by $\delta^{18}O$ and Mg/Ca will be produced. Salinity at Site 1211 would have to be ~6.0 ‰ more saline than at the TDP sites to account for the $\delta^{18}O$ difference (using the relationship identified by Broecker, 1989). Such a salinity difference would indicate that the hemipelagic TDP locations were influenced by a freshwater input, as modern-day open ocean locations such as Site 1211 are not recorded to have salinities deviating from average ocean salinity by more than ~2 ‰ (Zachos et al., 1994). A freshwater influence at the TDP sites has, however, not been identified (Pearson et al., 2001). Whilst neither palaeoceanographic difference is a feasible explanation alone for the difference in $\delta^{18}O$ between Site 1211 and TDP sites, neomorphism of the Site 1211 foraminifera has potential to explain the difference (Section 6.1.5). Site 1211 planktonic foraminifera were "frosty", rather than the "glassy" preservation of TDP sites, and exhibited a high degree of neomorphism upon study under SEM (Figure 6.2), which would suggest that the tests had been recrystallised. As discussed in Section 6.1.4/5, recrystallisation of warm-water planktonic foraminifera in cool deep-waters leads to more positive $\delta^{18}O$ values, which would explain the indication of the much cooler surface-water temperatures at Site 1211. Further discussion of the mismatch in temperature occurs in Section 6.4.4, where Mg/Ca palaeotemperatures are estimated.

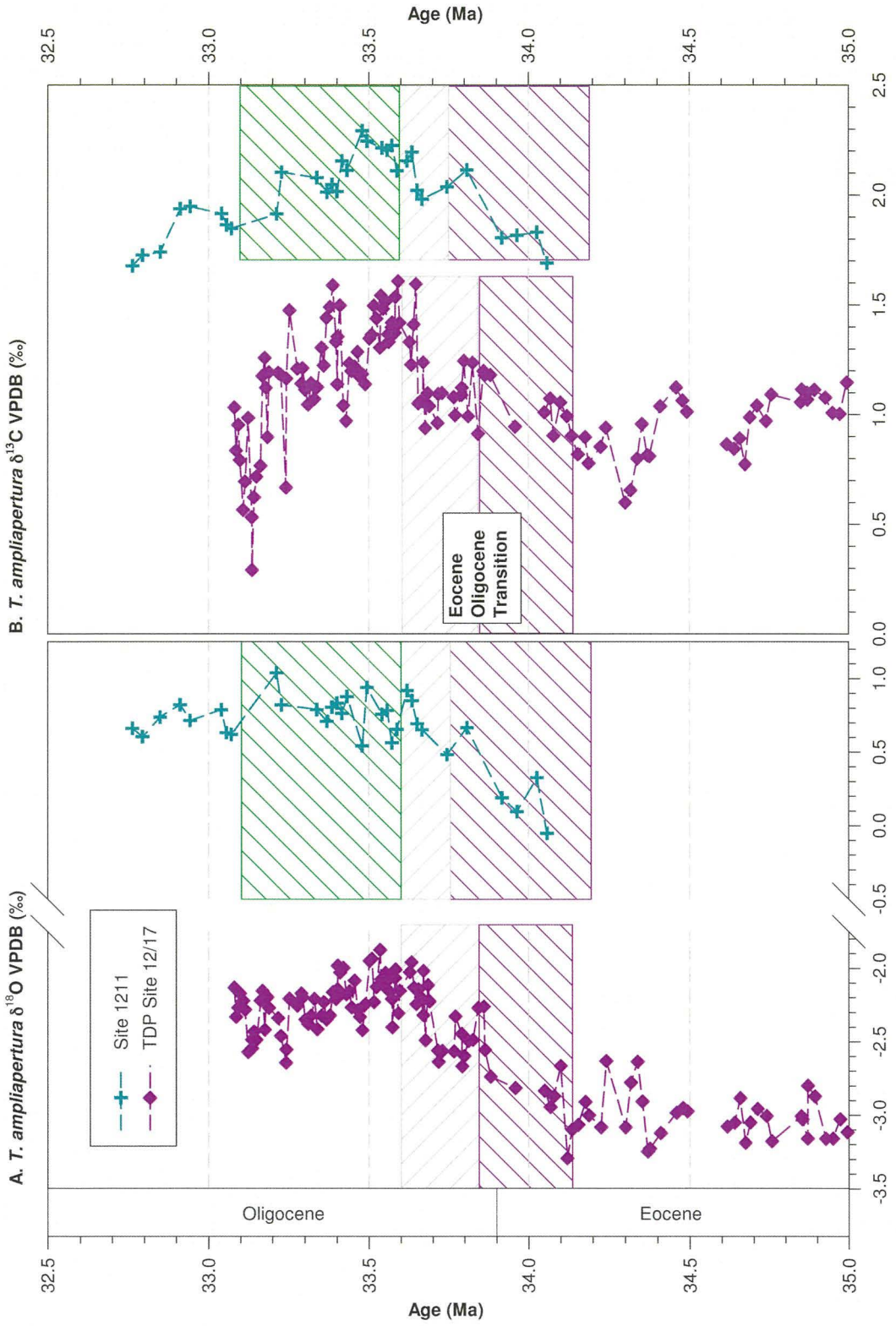

Figure 6.10: Stable-isotope records for *T. ampliapertura* for Site 1211 and TDP Site 12/17 (Pearson et al., 2008). Shaded boxes correspond to stages of the EOT (first stage purple, second stage grey) and the EOGM (dark green) as identified by this study for Site 1211 and Lear et al. (2008) for the TDP sites.

6.3 Eocene–Oligocene carbonate compensation depth (CCD) variation

Reconstructions of the Cenozoic Carbonate Compensation Depth (CCD) have revealed that the CCD varied temporally and spatially between Atlantic Ocean, Indian Ocean and Pacific Ocean basins (Figure 6.11; Van Andel, 1975; Peterson and Backman, 1990; Rea et al., 1995; Coxall et al., 2005; Rea and Lyle, 2005; Tripati et al., 2005; Kroon et al., 2007). While both regional and ocean-basin scale CCD variations are present within CCD reconstructions, a global deepening of the CCD occurred from the Late Eocene to the Early Oligocene. The absolute magnitude of this change in CCD position was variable, with a >1 km deepening determined for the equatorial Pacific Ocean over <300 kyrs (Van Andel, 1975; Rea and Lyle, 2005), with a more gradual late Eocene to Oligocene deepening of ~600–1000 m in the Atlantic Ocean (van Andel, 1975; Tripati et al., 2005; Kroon et al., 2007). Eocene–Oligocene Indian Ocean CCD variation is less well understood, but a several hundred metre deepening across the EOB seems likely (van Andel, 1975; Peterson et al., 1992). Equatorial Pacific CCD deepening across the Eocene–Oligocene boundary occurred synchronously with the $\delta^{18}O$ increase, and has been taken to indicate that glaciation at the EOB had a near immediate and direct impact on the global carbon cycle (Coxall et al., 2005). However, the absence of such rapid changes in CCD from other ocean basins across the EOB suggests the equatorial Pacific CCD deepening may not be indicative of global changes.

The deepening of CCD across the EOT led to an increase in deep-water carbonate ion saturation ($\Delta[CO_3^{2-}]$), which has been hypothesised to cause an increase in Mg uptake into benthonic foraminiferal tests. The enhanced uptake of Mg due to increasing $\Delta[CO_3^{2-}]$ resulting in the observed increase in benthonic foraminiferal Mg/Ca ratios (Lear et al., 2004; Coxall et al., 2005). Since the main aim of this study was to produce records of benthonic foraminiferal Mg/Ca ratios from a locality that experienced a reduced change in carbonate ion saturation, assessment and comparison of the pattern of CCD variation at Pacific Ocean Site 1211 (this study) to that at Site 1218 (Lear et al., 2004; Coxall et al., 2005) is necessary.

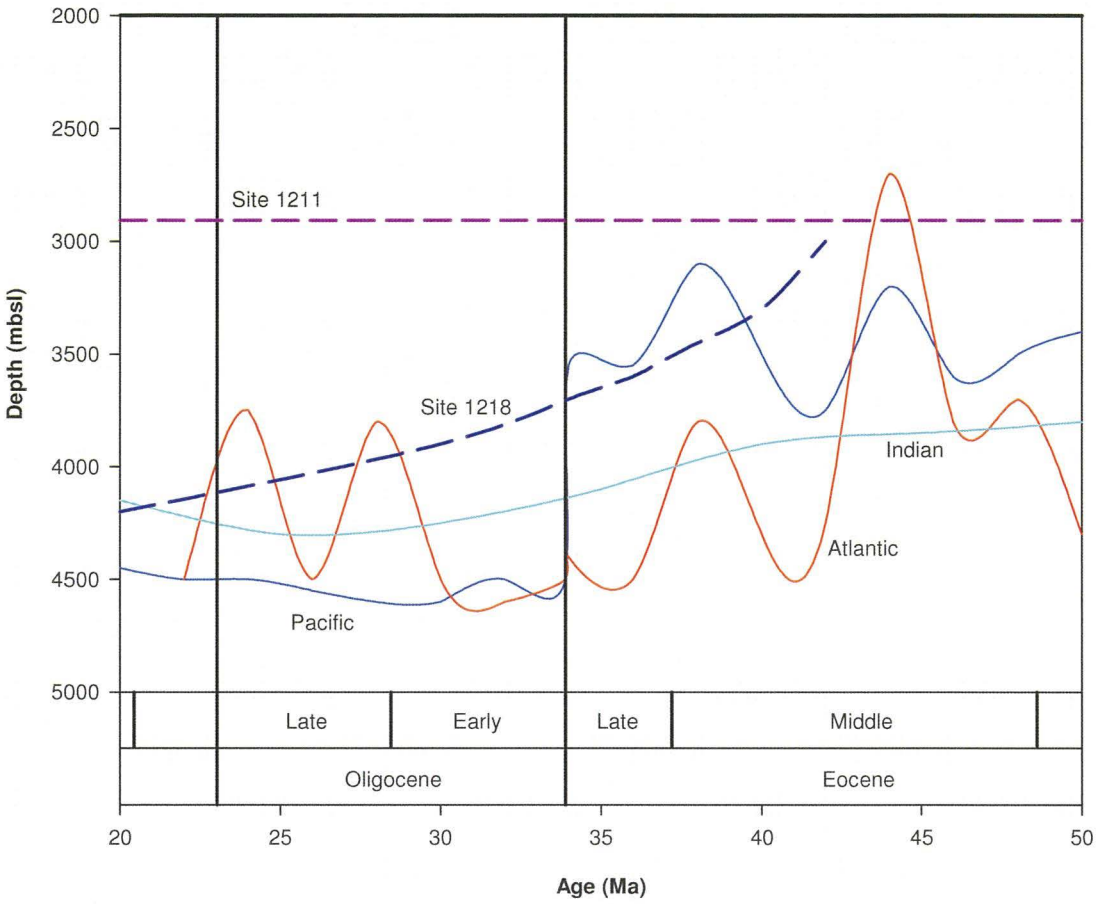

Figure 6.11: CCD variation during the Eocene and Oligocene for the Indian Ocean (Van Andel, 1975), tropical Atlantic Ocean and equatorial Pacific Ocean (Coxall et al., 2005; Tripati et al., 2005). The palaeodepth histories of Pacific Ocean ODP Sites 1211 (Ito and Clift, 1998; Shipboard Scientific Party, 2002b) and 1218 (Rea and Lyle, 2005) also are shown; Site 1211 being located at previous ODP Site 305 allowing the palaeodepth history of Site 305 to be used (Ito and Clift, 1998). In contrast to Site 1218, Site 1211 was located above the CCD during both the Eocene and Oligocene.

6.3.1 Comparison of geochemical proxies for CCD variability

The sediment proxies for CCD variability measured in this study, i.e. $\%CaCO_3$, % sand fraction and scanning X-ray fluorescence (XRF) Ca and Fe records, have been supplemented with colour reflectance and magnetic susceptibility data measured following Site 1211 core recovery (Shipboard Scientific Party, 2002b). The latter two records display close relationships with $\%CaCO_3$ (Figure 5.5A; Shipboard Scientific Party, 2002b), since increasing $\%CaCO_3$ leads to higher colour reflectance values and dilution of detrital Fe concentrations, thereby lowering magnetic susceptibility values. These proxy records of CCD variation are plotted along with the benthonic foraminiferal stable-isotope ratios in Figure 6.12.

The controls on $\%CaCO_3$ and % sand fraction were outlined in Sections 3.3.2 and 3.3.3, both proxies being dependent on a combination of preservation of $CaCO_3$, i.e. dependent

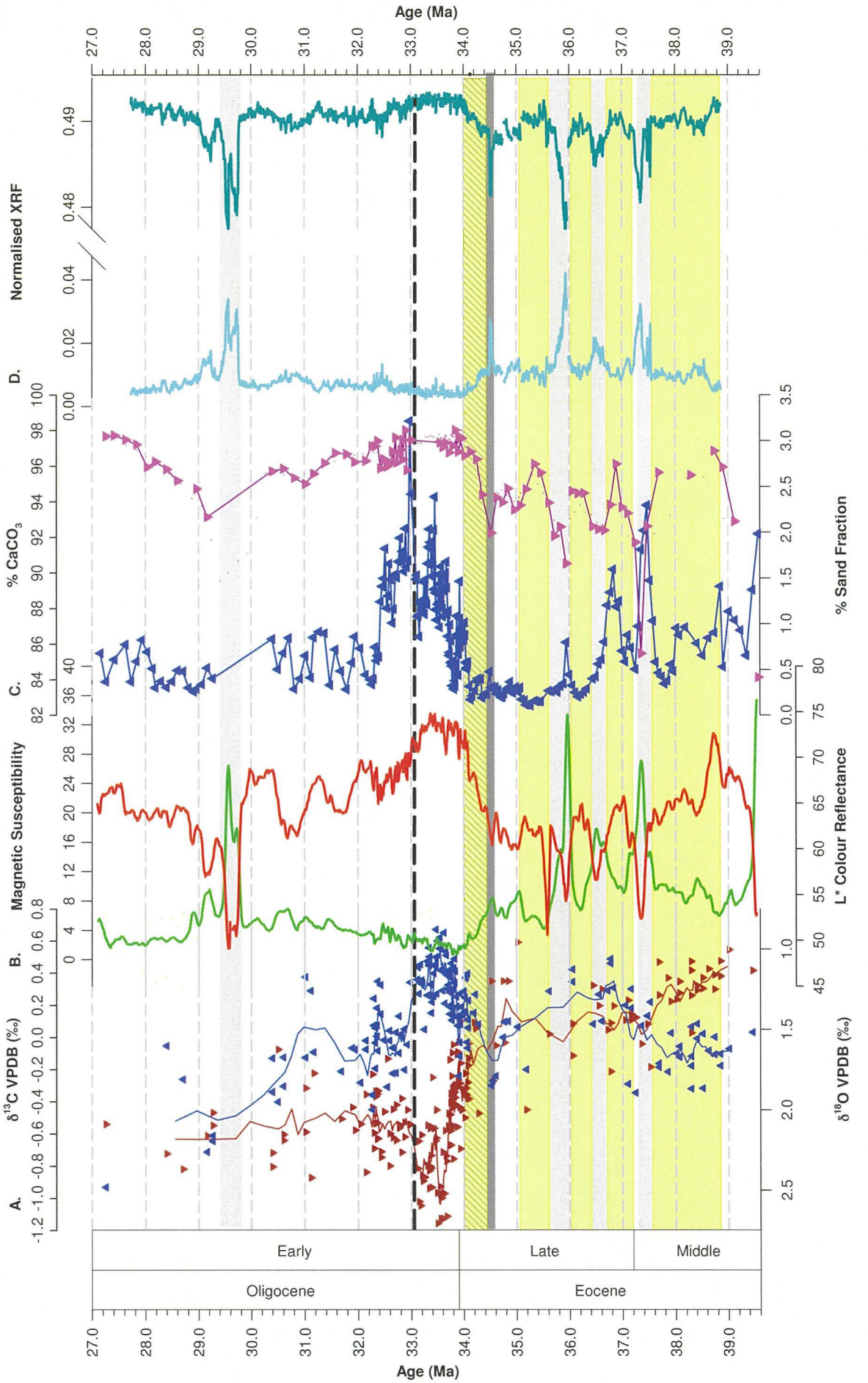
Age (Ma)
27.0
28.0
29.0
30.0
31.0
32.0
33.0
34.0
35.0
36.0
37.0
38.0
39.0
D.
Normalised XRF
0.49
0.48
0.04
0.02
0.00
C.
% CaCO3
100
98
96
94
92
90
88
86
84
82
40
36
32
B.
Magnetic Susceptibility
28
24
20
16
12
8
4
0
A.
δ13C VPDB (‰)
0.8
0.6
0.4
0.2
0.0
-0.2
-0.4
-0.6
-0.8
-1.0
-1.2
% Sand Fraction
3.5
3.0
2.5
2.0
1.5
1.0
0.5
0.0
80
75
70
65
60
55
50
45
L* Colour Reflectance
1.0
1.5
2.0
2.5
δ18O VPDB (‰)
Early
Late
Middle
Oligocene
Eocene
Age (Ma)

Figure 6.12: Panel A. 5-point running mean of benthonic foraminiferal $\delta^{18}O$ values (dark red) and $\delta^{13}C$ values (blue), Panel B. 5-point running mean of colour reflectance values (red) and magnetic susceptibility data (green; both Shipboard Scientific Party, 2002b), Panel C. % sand fraction (Blue, line is 5-point running mean) and $\%CaCO_3$ (pink, line is 5-point running mean), Panel D. Normalised X-ray fluorescence Fe (pale blue) and Ca (dark cyan) records. Pale-grey bars indicate intervals where co-variation of proxy records suggests enhanced dissolution and thus geologically short-term (<1 Myr) CCD shoaling events. Yellow bars correspond to relative deep Eocene CCD, with the EOT deepening of CCD hatched. Horizontal dark-grey bar corresponds to the pre-EOB CCD shoaling identified in published records (Coxall et al., 2005). Black dotted line marks the interpreted initiation of the Eocene–Oligocene transition. The heavy black dashed line marks the termination of the EOGM. CCD decrease across the EOT occurred prior to the bulk of the stable-isotope shift at Site 1211.

on carbonate ion saturation and hence CCD position, surface-ocean productivity, terrigenous inputs and winnowing, although CCD variation would seem to be the dominant influence on $\%CaCO_3$ and % sand fraction variability (Wu et al., 1990; Bassinot et al., 1994; Zhang et al., 2007; Anderson et al., 2008). Whilst CCD variation seems to be the dominant influence on $\%CaCO_3$ and % sand fraction, the sensitivity of these proxies to determine change in CCD can be compromised in certain conditions. When carbonate sedimentation is predominant, then even large changes in dissolution has little effect (Lyle, 2002; Lyle et al., 2005; Emerson and Hedges, 2008). The insensitivity of $\%CaCO_3$ to dissolution is best demonstrated by Lyle et al. (2005), taking a sediment that is 90 % carbonate and 10 % clay, dissolving half the original carbonate would only lead to a reduction of sediment $\%CaCO_3$ to 80 %. By comparison when % sand fraction is <10 %, % sand fraction can be dominated by changes in the fine-fraction proportion compromising its applicability as a CCD proxy (Hancock and Dickens, 2005). The effect of dissolution on % sand fraction records begins above the lysocline (Peterson and Prell, 1984; Lohmann, 1995), the lysocline being the depth at which ocean water becomes unsaturated with respect to the carbonate ion and carbonate dissolution begins. Such above lysocline fragmentation and reduction in % sand fraction, however, does not remove significant quantities of carbonate from the sediment rain but simply reduces the particle size (Peterson and Prell, 1984). In contrast, normalised scanning XRF records of Ca and Fe have been observed to vary with planktonic foraminifera fragmentation indices (Westerhold et al., 2008), with Fe increasing and Ca decreasing as fragmentation increases and *vice versa*, and thus should identify intervals of carbonate dissolution. While none of these CCD proxy records are solely dependant on the amount of $CaCO_3$ present within the sediment (See Section 3.3.2 and 3.3.3), CCD variation is the common variable between them that likely accounted for a significant proportion of variability in each proxy record; thus identification of common trends should allow the interpretation of relative CCD change across the EOB at Site 1211.

An approach that may allow quantification of the changes in CCD is the comparison of mass accumulation rates (MARs) from several closely located sites that did not experience significant variations in surface-ocean productivity (Peterson and Backman, 1990; Lyle et al., 2005). Surface-ocean productivity is important as calcium carbonate rain rate is a control on CCD, greater rain rates depressing the CCD and *vice versa*, thus similar surface ocean productivity reduces variation in $CaCO_3$ rain rate. This technique should be applicable to those ODP Leg 198 sites that were cored as part of the Shatsky Rise Cenozoic depth transect (Shipboard Scientific Party, 2002a) and will be used to identify mass accumulation rate gradients.

6.3.2 Variation in the CCD at Site 1211

As described in Section 6.3.1 above, covariation of the sediment proxies measured at Site 1211 will provide the strongest indication of CCD variation. Considering Figure 6.12, it is clear that XRF Ca, L* colour reflectance both vary with $\%CaCO_3$, whilst XRF Fe and Magnetic susceptibility are inversely correlated to $\%CaCO_3$. % Sand fraction shows little correlation to any other sedimentary carbonate proxy, a lack of correlation is likely to result from dissolution and fragmentation of foraminifera related to remineralisation of organic matter prior to the dissolution of carbonate, i.e. above the lysocline (Peterson and Prell, 1984).

Whilst the main theme of this section is relative variation in the depth of the CCD at Site 1211, the observations of $\%CaCO_3$ (Section 5.12) indicate that throughout the studied interval (~60 to 100 rmcd; ~27 to ~39.6 Ma) carbonate content was typically >90%. Such high carbonate contents would indicate that Site 1211 was above the CCD throughout, although the non-linearity of preservation of $CaCO_3$ and dissolution in $CaCO_3$ dominated realms (Rea and Lyle, 2005) means that the low variability could obscure larger variations in bottom-water saturation.

Given the uncertainties in the overall control on sedimentary carbonate proxies, care must be taken not to over interpret records. The general trends in sedimentary carbonate proxies shown in Figure 6.12 should therefore be identified first to provide a background to CCD change at Site 1211, prior to the interpretation of more transient variation. Eocene XRF Ca, L* colour reflectance and % $CaCO_3$ are typically less than Oligocene values, whilst

magnetic susceptibility and XRF Fe are typically greater. Such variation in sedimentary carbonate proxies indicates that CCD was shallower during the Eocene than the Oligocene. The deepening of CCD occurred gradually between ~34.5 and ~34.0 Ma, observed as an increase in XRF Ca, L* colour reflectance and $\%CaCO_3$ and a decrease in magnetic susceptibility and XRF Fe. A deepening during this interval agrees with the observation of $CaCO_3$ sediments at Site 1208, situated at a palaeodepth of 3346 mbsl on the Central High of Shatsky Rise (Shipboard Scientific Party, 2002e) at the EOB. The absence of $CaCO_3$ sediment at ~3300 mbsl indicates Site 1211 was within ~400 m of the CCD during the Eocene, a depth likely to place the site within the corrosive waters of the lysocline. Interestingly deepening of CCD at Site 1211 occurred prior to the initiation of the EOT at Site 1211, unlike the records of Coxall et al. (2005) where the two events are synchronous. The mismatch of the CCD and $\delta^{18}O$ isotope increase at Site 1211 suggests that CCD responded to a local forcing at Site 1211, possibly increased surface water productivity as suggested by the fine-fraction $\delta^{13}C$ increase, rather than a global carbon cycle change.

With the macro-scale development of CCD identified, fine-scale transient variation, i.e. <500 kyr, can be identified and interpreted. During the Middle to Late Eocene transient events are superimposed upon the sedimentary carbonate proxies suggesting a dynamic late Eocene CCD. Transient peaks in XRF Fe and magnetic susceptibility, with correlated troughs in XRF Ca, L* colour reflectance and $\%CaCO_3$ suggest CCD shoaling, whilst the reverse observation suggests CCD deepening (Figure 6.12, shoaling highlighted in grey, yellow highlights represent relatively deep CCD). Transient CCD shoaling occurs at ~37.4, ~36.5 and ~35.8 Ma. Studies (Lyle et al., 2005; Tripati et al., 2005) have linked variation in Middle to Late Eocene CCD to ephemeral glaciations, citing evidence of positive stable-isotope excursions related to deepening of CCD and *vice versa*. Such relationships between CCD variation and benthonic foraminiferal $\delta^{18}O$ (or $\delta^{13}C$) are not clear at Site 1211 (Figure 6.12); although as noted in Section 6.2 there is a high degree of scatter within stable-isotope records that may obscure relationships. The occurrence of these transient CCD events is compared to similar transient events observed in $\%CaCO_3$ records from the equatorial Pacific Ocean in Section 6.3.4.

Prior to the increase in sedimentary carbonate proxies at 34.5 Ma, covariation of the proxies (dark grey highlight in Figure 6.12) suggests only a minor increase in dissolution

or reduction in carbonate sedimentation compared to the earlier CCD variations (cf. event at ~35.8 or ~37.4 Ma with the event at ~34.5 Ma) and thus a very restricted shoaling of the CCD immediately prior to the EOB. A shoaling of CCD is recognised in other latest Eocene, pre-EOT sections (Sites 744, 1218 and 1263), although the event is much less clear in the records from Site 1211. The difference between Sites 1211 and 1218 will be covered in Section 6.3.4.

Following the EOGM (~33 Ma) XRF Ca and $\%CaCO_3$ decline slowly to ~30 Ma remaining above Eocene levels throughout, the inverse correlation observed in XRF Fe and magnetic susceptibility. Such a decline suggests a slight post-EOGM decline in calcium carbonate content of the sedimentary record, which would indicate a gradual and subtle shoaling of the CCD, along with much less temporal variability in CCD position than was evident during the Eocene. L* colour reflectance also declines across the 33–30 Ma interval but with a more pronounced decrease and greater variability than observed in XRF Ca and $\%CaCO_3$ records. Between 30 and 29 Ma the CCD proxy records indicate a decrease in sedimentary calcium carbonate, a change that would suggest a ~1 Myr shoaling of CCD. A Middle Oligocene CCD shoaling has not been identified in CCD records from Site 1218 for the equatorial Pacific Figure 6.11), although there are no detailed Oligocene CCD records from the sub-tropical Pacific Ocean. The CCD shoaling between 30 and 29 Ma occurred with an excursion to more negative <38 μm fine fraction $\delta^{13}C$ values, whilst <38 μm fine fraction $\delta^{18}O$ values became more positive, suggesting a surface-water influence on the CCD shoaling. Benthonic foraminiferal stable-isotope ratios did not, however, record any change in $\delta^{18}O$, although these analyses are sparsely distributed. The likely shoaling of the CCD between 30 and 29 Ma does not, however, impact the main aims of the study and thus is not considered further.

As noted above % sand fraction does not vary with the other sedimentary carbonate proxies. Using the assumption % sand fraction is primarily controlled by dissolution (Peterson and Prell, 1984), % sand fraction indicates a shallower Late Eocene CCD than during the Middle Eocene, an interpretation not supported by the other sedimentary carbonate proxies. The lack of covariation of % sand fraction and intervals of relatively deep CCD during the Late Eocene, e.g. at ~35.4 Ma, suggests that % sand fraction was not more sensitive to carbonate dissolution than $\%CaCO_3$ (enhanced sensitivity being

suggested by Wu et al., 1990; Bassinot et al., 1994). Low sensitivity of % sand fraction to carbonate dissolution is supported by comparison of the Middle Eocene and post-EOGM Oligocene % sand fractions, which indicate greater dissolution during the Oligocene than the Middle Eocene, i.e. a shallower post-EOGM Oligocene CCD than the Middle Eocene, contrary to the deepened Oligocene CCD indicated by the sedimentary carbonate proxies. % Sand fraction also increased 400 kyr after the other sedimentary carbonate proxies at ~34.1 Ma close to the initiation of the EOT, such variation lagging supposedly less sensitive indicators of increasing sedimentary carbonate would again argue that % sand fraction was not a more sensitive dissolution indicator at Site 1211 and that the % sand fraction was controlled by another factor. Peterson and Prell (1984) suggest that foraminiferal fragmentation is dependant on a balance between the remineralisation of organic matter and the degree of $\Delta[CO_3^{2-}]$. The near zero values observed during the Late Eocene could thus be explained by an increase in surface water productivity leading to enhanced remineralisation within the water column. As $\Delta[CO_3^{2-}]$ were relatively low during the Late Eocene, deeper waters would have been corrosive to foraminiferal tests, the two dissolution effects acting to remove much of the sand fraction leading to the low % sand fractions observed. Late Eocene increased productivity, however, would not seem to be supported by decline in fine-fraction $\delta^{13}C$ after ~35.2 Ma; a decline in fine-fraction $\delta^{13}C$ suggesting a reduction in the export of organic material from surface waters. Thus, % sand fraction records at Site 1211 do not appear to have a single dominant influence, rather representing a combination of several and so cannot be used to identify CCD change.

In summary, Site 1211 was above the CCD throughout the studied interval. CCD variation lead to variable dissolution during the Middle and Late Eocene, however, the degree of dissolution cannot be quantified with the available proxy data. The suggestion of a non-linear relationship between dissolution and $\%CaCO_3$ in sedimentary regimes dominated by $CaCO_3$ (Rea and Lyle, 2005) could mean that potentially large changes in dissolution are occurring for minimal proxy response. Carbonate MARs have potential to isolate changes in $CaCO_3$ sedimentation and are discussed below. The CCD deepened prior to the initiation of the EOT as indicated by the benthonic foraminiferal $\delta^{18}O$ increase and remained deep throughout the intensively studied interval, i.e. to 32.0 Ma. Whilst the carbonate proxies measured do allow qualitative assessment of Site 1211 CCD, further preservation proxies, such as foraminiferal fragmentation ratio, benthonic to planktonic foraminiferal ratios, could allow improved constraint.

6.3.3 Mass accumulation rates over Shatsky Rise – preservation or productivity

Whilst the sedimentary carbonate proxies allow CCD depth trends to be identified, they are unable to provide quantification of depth changes. Mass accumulation rates (MARs) from a depth transect of geographically closely located sites, which had similar levels and changes in productivity, however, may allow such quantification (Peterson and Backman, 1990; Lyle et al., 2005; Tripati et al., 2005). This technique should be applicable to those ODP Leg 198 sites that were cored as part of the Shatsky Rise Cenozoic depth transect (Shipboard Scientific Party, 2002a). $CaCO_3$ or % sand fraction MARs have been calculated using Equation 6.2, as described in Shipboard Scientific Party (2004).

$$\text{MAR (g/cm}^2\text{/k.y.)} = \%\text{ sand fraction or } CaCO_3 \text{ x LSR (m/m.y.) x dry bulk density (g/cm}^3\text{)/10} \quad \textbf{(Eq. 6.2)}$$

where LSR is the linear sedimentation rate (see Section 4.4, Table 4.3) and dry bulk density are those measured by the Shipboard Scientific Party (2002b). Dry bulk density determinations are, however, only available for Site 1211 at very low sampling resolution (~1.5 m), limiting the generation of high temporal resolution MAR records. As such, Site 1211 MARs were calculated over 1 million year intervals using the mean dry-bulk density values, where available, in combination with $\%CaCO_3$ and % sand fraction data. To provide a water column palaeodepth transect, MARs have also been calculated for Shatsky Rise ODP Leg 198 Sites 1209 and 1210. This approach involved the determination of depth–age models for each site (Figure 6.13) and use of the sedimentation rates to calculate mean $CaCO_3$ MARs for the intervals identified within the depth–age models. The $\%CaCO_3$ values determined by Averyt et al. (2005) have been used to calculate $CaCO_3$ MARs for Sites 1209 and 1210. The resulting MARs are plotted for all three sites in Figure 6.14.

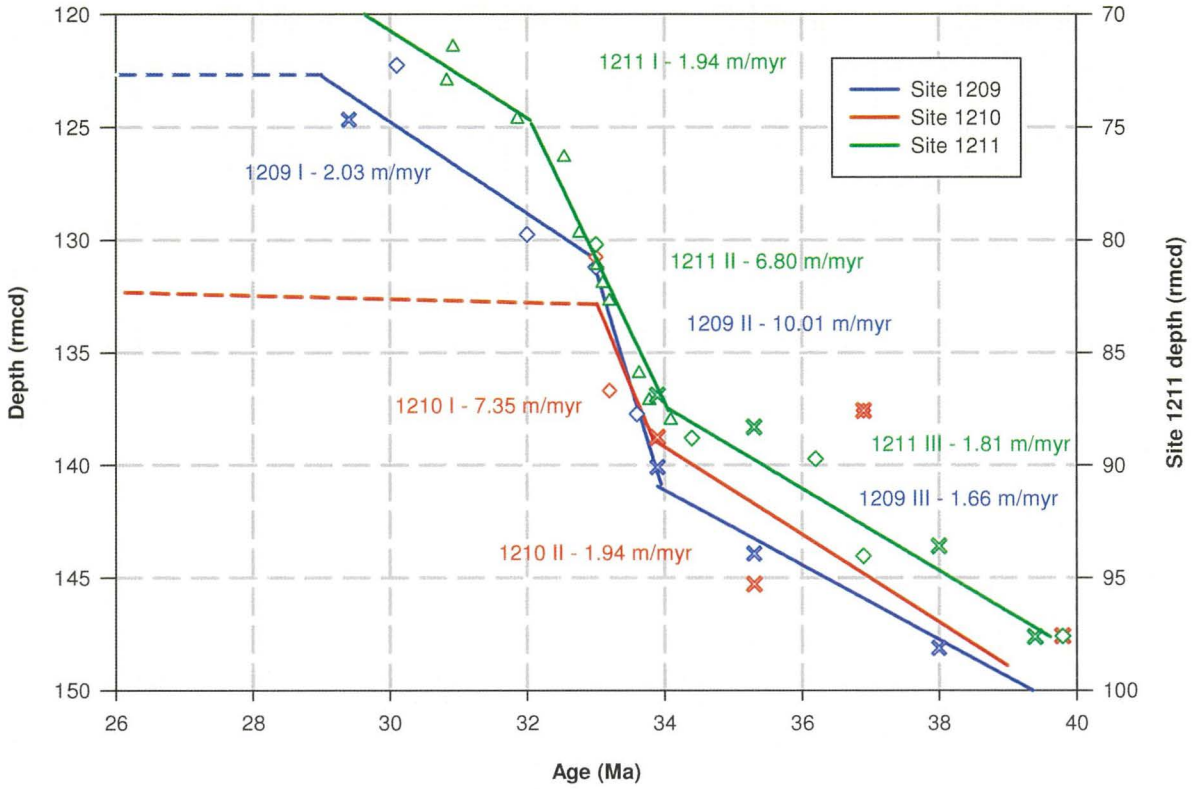

Figure 6.13: Depth–age relationships for ODP Sites 1209, 1210 and 1211. Depth–age relationships were determined by regression using the foraminiferal (crosses) and nannofossil (diamonds) biostratigraphic datums of Shipboard Scientific Party (2002c,d), Bralower (2005) and Petrizzo et al. (2005) and Sr-isotope ratios (triangles). It is of interest to note that sedimentation rates prior to and increase across the EOB were very similar across Sites 1209, 1210 and 1211, suggesting similar productivity and preservation changes during EOT and EOGM.

Palaeodepths were poorly constrained for Sites 1209, 1210 and 1211, benthonic foraminiferal assemblage derived estimates being between 2000–3000 metres during the Late Eocene to Early Oligocene (Shipboard Scientific Party, 2002a). However, crustal subsidence models indicate minimal subsidence of Shatsky Rise since the Early Eocene (Ito and Clift, 1998), so it is unlikely that there has been significant deviation from their present-day water depths (Site 1209, 2387 metres below sea level (mbsl); Site 1210, 2547 mbsl; Site 1211, 2907 mbsl). If, as would be expected, carbonate ion saturation decreases with depth then MARs should reflect this. It has to be recognised, however, that the $CaCO_3$ MARs were calculated using assumptions of linear sedimentation rates and averages of dry-bulk densities for sediment depth ranges that are equivalent to several million years of geological time. Consequently, this methodology will have masked any shorter-term variation(s) in MARs and related CCD changes.

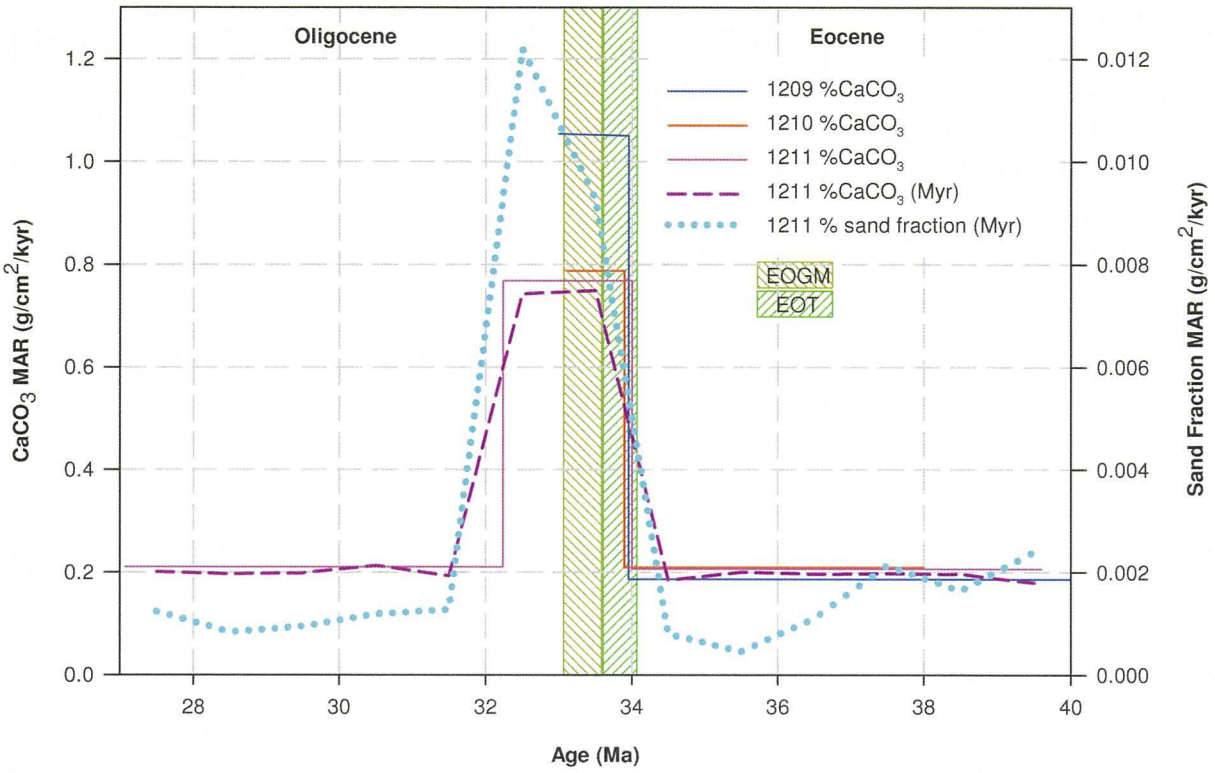

Figure 6.14: Mean $CaCO_3$ and sand fraction mass accumulation rates determined for sections of the depth–age model shown in Figure 6.13. $CaCO_3$ MAR calculated using the mean dry-bulk density, sediment accumulation rate and $\%CaCO_3$ of the intervals for Sites 1209 (blue), 1210 (red) and 1211 (pink). Also shown for Site 1211 are mean MARs for 1 Myr increments for $CaCO_3$ and sand fraction. $\%CaCO_3$ data for Sites 1209 and 1210 are taken from Averyt et al. (2006). Dry bulk densities are those determined by the Shipboard Scientific Party (2002b,c,d).

Before the EOB $CaCO_3$ MARs were essentially identical at ~0.2 g/cm^2/kyr for the three sites, indicating that calcium carbonate sedimentation and thus deep water carbonate ion saturation state was invariant with depth and locality. The absence of differences in the $CaCO_3$ MARs across the palaeodepth transect during the Eocene would suggest an above lysocline water depth for all three sites (Peterson and Prell, 1984). The CCD proxies shown in Figure 6.12, however, indicate that the Late Eocene was a time of relatively increased dissolution at Site 1211, compared to the Early Oligocene. Whilst Hancock and Dickens (2005) also observed that dissolution indices, $\%CaCO_3$, benthonic foraminiferal abundance and fragmentation, indicate an intensification of dissolution at Sites 1209 and 1211 between 37.0 and 33.9 Ma relative to the Middle Eocene. Across the EOB there was a greater than three-fold increase in $CaCO_3$ MARs at Sites 1210 and 1211, to ~0.75 g/cm^2/kyr, and a contemporaneous five-fold increase in $CaCO_3$ MAR at Site 1209, to ~1.0 g/cm^2/kyr, sustained throughout the EOT and EOGM. These increases result primarily from increased sedimentation rates, as increases in $\%CaCO_3$ were minimal (~3 %). The three- to five-fold increase in $CaCO_3$ MARs corresponds to similar increase in carbonate MAR across the EOB seen at Site 744 and 1218 (Salamy and Zachos, 1999; Coxall et al., 2005). Higher $CaCO_3$ MAR at Site 1209, compared to Site 1211, suggests increased

$CaCO_3$ preservation at the former shallower site. But, the similarity of the magnitude of the $CaCO_3$ MARs at Sites 1210 and 1211 despite the palaeodepth difference suggests that $CaCO_3$ preservation and thus $\Delta[CO_3^{2-}]$ was similar across the range of water depth between these two sites. Whilst $CaCO_3$ MARs are only available for Site 1211 after ~33.0 Ma, due to a lack of sediment data for Site 1209 and a hiatus at Site 1210, sedimentation accumulation rates at Site 1209 and 1211 decline to ~2.0 m/Myr (Figure 6.13). The marginal increase in Oligocene sediment accumulation compared to Eocene sediment accumulation (Site 1209, from ~1.7 to 2.0 m/Myr; 1211, from ~1.8 to ~1.9 m/Myr), argues against CCD remaining deep during the Oligocene (all other factors being equal). However, proxies for sedimentary carbonate do not indicate that Oligocene CCD shoals after the EOGM.

Sand fraction MAR follow the general trends described by the Site 1211 $CaCO_3$ MARs, i.e. a many fold early Oligocene increase from low Eocene and Oligocene background levels. Use of sand fraction MARs, rather than % sand fraction, removes the influence of changing fine-fraction sedimentation. Sand fraction MARs were similar during the Late Eocene and post-32.0 Ma Oligocene, despite the clear differences in planktonic foraminifera numbers and preservation, which would suggest a MAR productivity control across the EOB. The low resolution of the sand fraction MARs (1 Myr averages) prevents certain identification of the development of changes in productivity but suggest elevated productivity for ~2 Myrs following the EOT, although as with the $CaCO_3$ MARs this duration is dependant on the depth–age model developed in Chapter 4.

The $CaCO_3$ MARs calculated across Shatsky Rise thus do not display declining sedimentary carbonate preservation with depth, which would suggest $\Delta[CO_3^{2-}]$ was essentially constant in the bottom-waters that bathed Shatsky Rise. As MARs do not appear to represent preservation, productivity appears to control the similarities and differences between the sites; the increase in $CaCO_3$ and sand fraction MARs suggesting a several fold increase at the EOT. A similar increase in productivity across the EOT has been identified from the equatorial region of the Pacific Ocean (Moore et al., 2004) and Southern Ocean (Diester-Haass, 1996; Diester-Haass & Zahn, 1996; 2001). Records relating to productivity at Site 1211 (and Shatsky Rise) are poorly developed. The amount of barite in pelagic sections has been used as a proxy for export productivity (Averyt et al., 2005). %Barite levels have been observed to have a maximum lasting <300 kyr close to

the EOB at Site 1209 and 1210, before decreasing to similar background levels of ~0.02 % at both sites (Averyt et al., 2005; no data are available for Site 1211), which suggests a restricted pulse of enhanced surface-ocean productivity. Maximum %Barite levels were greater at Site 1209 than Site 1210, ~0.25 % compared to ~0.1 % respectively, which would further suggest increased productivity at Site 1209, although the data is insufficient to allow calculation of barite MARs. These observations are in agreement with the $CaCO_3$ MARs changes observed above, with greater productivity at Site 1209 relative to Site 1211 (and 1210) explaining the elevated $CaCO_3$ MAR at the former site over the EOT and EOGM. Planktonic to benthonic foraminiferal $\delta^{13}C$ gradients (see Figure 5.14 and Section 5.9.2) show maximum values during the Earliest Oligocene (during the EOT), declining throughout the EOGM suggesting a maximum in export-productivity at Site 1211, coeval with the increase %barite observed at Sites 1209 and 1210.

MARs were calculated in an attempt to calculate the depth of the CCD using gradients in the MARs with from a series of geographically restricted sites with different depths, using the approach described in Rea and Lyle (2005). However, as MAR gradients were not observed, depth calculation was not possible, thus comparison of Mg/Ca to CCD variation must be achieved through the sediment carbonate proxies alone. Productivity appears to be a significant factor in the apparent increase in preservation at Site 1211. CCD deepening at Site 1211 was identified as occurring prior to the initiation of the EOT, i.e. the $\delta^{18}O$ increase, an observation counter to the synchronous relationship observed between CCD deepening and $\delta^{18}O$ increase at Site 1218 (Coxall et al., 2005). If the Site 1211 CCD was controlled primarily by local productivity then a pre-EOT increase could explain the contradiction between Site 1211 and 1218 records. An increase in the stratigraphic resolution of dry bulk density measurements across the Late Eocene and Early Oligocene is required, however, to test the hypothesis that surface water productivity increased prior to the EOT as suggested in Section 6.3.2.

6.3.4 Comparison of CCD variability between Pacific Ocean Sites 1211 and 1218

Eocene to Oligocene CCD variation at Site 1218 has been determined and described by Coxall et al. (2005), Lyle et al. (2005) and Tripati et al. (2005). There are two key aspects for comparison between Sites 1211 and 1218, firstly assessment of the relative difference in carbonate ion saturation change across the Eocene–Oligocene boundary and secondly, to

compare CCD histories, i.e. were there significant differences between bottom-water carbonate ion saturations above each site that would suggest local rather than global controls.

The primary aim of this study was to produce benthonic foraminiferal Mg/Ca ratios across the EOB from a site that had undergone relatively little change in bottom-water carbonate saturation. These Mg/Ca ratios were to test the hypothesis that the absence of cooling and 2 °C warming across the EOB observed from benthonic foraminiferal Mg/Ca values at Site 1218, resulted as an effect of an increase in bottom-water carbonate ion saturation (Lear et al., 2004; Coxall et al., 2005). From the sedimentary carbonate records described above, Site 1211 clearly remained above the CCD throughout the Late Eocene and Early Oligocene unlike Site 1218 (Figure 6.11, 6.12 and 6.15). Quantification of the variation in bottom-water carbonate ion saturation or the magnitude of CCD deepening has not been possible from the CCD proxy records available for Site 1211, but an idea of the difference in changes between the sites can be gained from the variation in $\%CaCO_3$ observed. From Figure 6.15, $\%CaCO_3$ from Site 1211 can be observed, when plotted on the same axis, to show an insignificant level of variation compared to Site 1218, indicating that the change in bottom-water $\Delta[CO_3^{2-}]$ was likely to be much reduced at Site 1211. Assuming observations of Martin et al. (2002) and Elderfield et al. (2006) for a depression of the $\Delta[CO_3^{2-}]$ effect on benthonic foraminifera at increased $[CO_3^{2-}]$, then Site 1211 foraminifera should have been less effected by changes in $\Delta[CO_3^{2-}]$. Thus increase uptake in Mg^{2+} by Site 1211 benthonic foraminifera should be reduced in comparison to the Site 1218 records, if a $\Delta[CO_3^{2-}]$ effect is occurring. Comparison of Site 1211 and 1218 Mg/Ca palaeotemperature records in Section 6.4.5 should reveal whether a reduced effect is observed.

A series of carbonate accumulation events (CAEs) have been identified throughout the Middle to Late Eocene and indicate a dynamic equatorial Pacific CCD (Figure 6.15; Lyle et al., 2005; Tripati et al., 2005), whilst CCD variations have also been identified for the Atlantic and Indian Oceans (Peterson and Backman, 1990; Tripati et al., 2005). Tripati et al. (2005) link these transient CCD deepening to positive excursions in benthonic foraminiferal $\delta^{18}O$ of up to 1.5 ‰ at ~42.0, ~39.0 and ~36.2 Ma (using the Gradstein et al., 2004 timescale adopted in this study) suggesting significant transient ice-volume development related to changes atmospheric carbon dioxide concentrations. If the

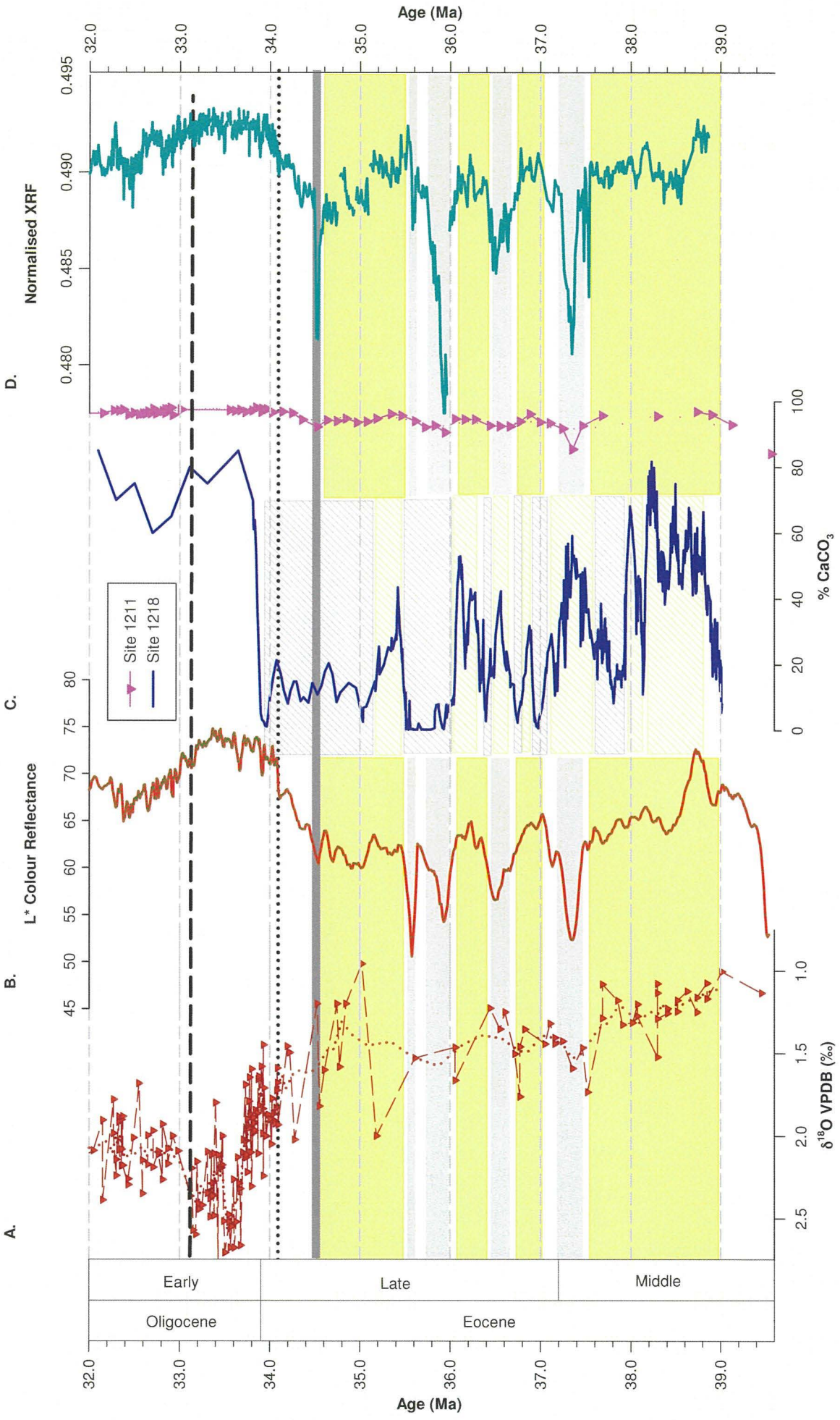
Age (Ma)
32.0
33.0
34.0
35.0
36.0
37.0
38.0
39.0
A.
B.
C.
D.
Normalised XRF
0.480
0.485
0.490
0.495
L* Colour Reflectance
45
50
55
60
65
70
75
80
Site 1211
Site 1218
% CaCO3
0
20
40
60
80
100
δ18O VPDB (‰)
2.5
2.0
1.5
1.0
Early
Late
Middle
Oligocene
Eocene

Figure 6.15: Site 1211 benthonic foraminiferal $\delta^{18}O$ (A) with L* colour reflectance (B), % $CaCO_3$ for Sites 1211 (pink) and 1218 (blue; C) and XRF Ca (D). %$CaCO_3$ was much greater at Site 1211 and experienced insignificant variation compared to Site 1218, which would indicate bottom-water carbonate ion saturation variation was much less at Site 1211 than at Site 1218. Yellow shadings indicate relative deep CCD intervals whilst grey shadings indicate CCD shoaling for Site 1211 as evidenced by covariation of the CCD proxies (Figure 6.12); hatched areas in panel C represent deep and shallow intervals at Site 1218. Correlation between CCD variation at Sites 1211 and 1218 is variable, although the major transient CCD deepening associated with $\delta^{18}O$ events identified by Tripati et al. (2005) at ~39 and ~36.2 Ma are present at Site 1211. Differences between the two sites are likely to represent the influence of local changes in productivity and thus carbonate rain rate. The dark grey bar indicates the minor shoaling identified prior to the permanent CCD deepening, again compared to the equivalent shoaling at Site 1218, the event is of minor significance at Site 1211.

hypothesis of transient glaciations during the Eocene is correct then similar transient CCD deepenings and $\delta^{18}O$ increases should be present in the records of Site 1211. Covariation of sedimentary carbonate proxies at Site 1211 is highlighted in Figure 6.15, along with relative CCD variation at Site 1218 and so the presence (or not) of the transient Tripati events can be assessed.

Covariation of sedimentary carbonate proxies at Site 1211 indicates irregular duration deep CCD intervals (yellow shaded bars in Figure 6.5). The major CAEs identified by Tripati et al. (2005) at ~39.0 and ~36.2 Ma are present at Site 1211, observation of these events at both sites suggesting an ocean-wide deepening. However, away from these major events, CCD deepening at the two sites does not correlate well. Independent variation of CCD would suggest that local factors, e.g. productivity, were the dominant influence on CCD at the two sites rather than global or ocean-wide controls. $CaCO_3$ MARs for Site 1211 are at too low a temporal resolution (~1 Myrs) compared to the duration of the events (≤200 kyr) to estimate the significance of the CCD depth changes and comparison to equivalent $CaCO_3$ MARs from Site 1218. The scattered and low-resolution nature of the composite benthonic foraminifera stable-isotope record during the Middle to Late Eocene (Section 5.6 and 6.2.1) also precludes identification of whether CCD and $\delta^{18}O$ covariation occurred.

A further aspect of CCD deepening at Site 1218 was the observation that the deepening occurred "lock-step", i.e. synchronously with the two-stepped $\delta^{18}O$ shift (Figure 1.2; Coxall et al., 2005), leading to the conclusion that glaciation caused CCD change through either a shift in carbonate sedimentation to the deep-ocean due to sea-level fall or as a result of increase siliceous productivity at the expense of carbonate productivity. As described in Section 6.3.2 CCD proxies lead (increasing from 34.5 Ma) the EOT initiation (at ~34.2 Ma) identified from benthonic foraminiferal $\delta^{18}O$ (Section 6.2.1), thus "lock-

step" behaviour of $\delta^{18}O$ and CCD deepening was not observed at Site 1211 across the EOT. Indeed the majority (~1.0 ‰) of the increase in $\delta^{18}O$ occurs with minimal increase in sedimentary carbonate proxies between 34.0 and Oi-1a at 33.5 Ma. The evidence from Site 1211 indicates the lead is a "real" event, not resulting from either the scatter in the stable-isotope data or errors in the age model (Section 6.3.2) but most likely from an increase in surface-water productivity.

The absence of "lock-step" change at Site 1211, or indeed at Sites 744 or 1263 (Zachos et al., 1996; Salamy and Zachos, 1999; Riesselman et al., 2007) indicates that Site 1218 CCD variation was atypical across the EOT. Changes in carbonate sedimentation and CCD deepening would have been more pronounced at Site 1218 as a result of its greater water depth (~3500 mbsl) compared to other sites (2000–3000 mbsl) and because of Site 1218s location in the equatorial upwelling zone. The greater water depth put Site 1218 close to the Eocene CCD, unlike Sites 744, 1211 and 1263 that were above the CCD as evidenced by $\%CaCO_3$ of >90 %, meaning small scale CCD variation would have much clearer effects on the carbonate in the sedimentary record at Site 1218, as shown by the different CCD histories between Sites 1211 and 1218. Site 1218s location within the Pacific equatorial upwelling zone would also have impacted carbonate sedimentation and thus CCD. The increase in latitudinal temperature gradients may be expected to increase the vigour of oceanic circulation (Zachos et al., 1994), and thus the vigour of upwelling. Increased upwelling would increase the supply of nutrients to the surface waters enhancing productivity (Diester-Haass, 1995; Salamy and Zachos, 1999; Diester-Haass and Zahn, 2001), which in turn could lead to enhanced export productivity and thus carbonate rain rate at Site 1218. Enhanced carbonate rain rate would locally depress the CCD, whilst the control of circulation vigour by increasing latitudinal gradients would link the productivity based deepening to the $\delta^{18}O$ record. Site 1211 located away from upwelling regions in the eastern tropical Pacific would experience a much-reduced increase in productivity and so experience a less pronounced deepening of CCD (cf. Eastern and Western Pacific productivity in Moore et al., 2004).

6.4 Mg/Ca palaeotemperature estimation

As discussed in Section 2.2.6, foraminiferal Mg/Ca ratios are related to the water temperature at which a foraminifera calcifies (Nurnberg et al., 1996; Rosenthal et al., 1997; Lea et al., 1999b; Elderfield and Ganssen, 2000; Lear et al., 2002; Anand et al., 2003 among others) allowing calculation of palaeotemperature records. These palaeotemperature records can subsequently be used within the $\delta^{18}O$ palaeotemperature equation (Section 2.2.4/6; 6.2.1 and 6.5.1) to estimate $\delta^{18}O_{sw}$. Mg/Ca ratios across the EOB were developed for two planktonic foraminiferal species, *T. ampliapertura* and *C. unicavus*, and one benthonic foraminiferal species, *O. umbonatus* (see Sections 3.6; 5.10 and 5.11), to allow the estimation of palaeotemperatures and $\delta^{18}O_{sw}$ from Site 1211. Estimation of Cenozoic palaeotemperatures from Mg/Ca ratios requires four issues to be addressed (Lear et al., 2000), three of which are relevant to this study. The fourth issue is that of species-specific effects but only a monospecific Mg/Ca record was developed for Site 1211. These issues are the preservation of the primary geochemical signal, i.e. biogenic carbonate (discussed in Section 6.1), the palaeo-seawater Mg/Ca ratio and the actual Mg/Ca ratio – water temperature calibration used to estimate palaeotemperatures. The latter two issues are discussed below.

6.4.1 Palaeo sea-water Mg/Ca ratios

Seawater Mg/Ca ratios are controlled by the balance of fluxes of Mg and Ca into and out of the ocean. Mg is supplied to the ocean by rivers, whilst it is removed by alteration of mid ocean ridge basalts (substituting Mg for Ca within the basalt, see Section 6.1.2/3) and by dolomitisation of carbonates; Ca is supplied by the rivers and at mid ocean ridges and is removed by carbonate accumulation (Wilkinson and Algeo, 1989, Elderfield and Schulz, 1996). The major sink for Mg in the modern ocean is mid-ocean ridge alteration (Wilkinson and Algeo, 1989), however, sediment mass balance constraints indicate that the dominant sink varied throughout the Phanerozoic and has typically been dolomite formation throughout this interval. Several approaches have been used to identify the evolution of Cenozoic Mg/Ca ratios including mass balance modelling of the sources and sinks as constrained by the geological record (Wilkinson and Algeo, 1989, Berner, 2004); modelling based on the relationship between crustal spreading rates and seawater alteration (Hardie, 1996; Stanley and Hardie, 1998), or through the measurement of fluid inclusions

within halite evaporite deposits (Zimmerman, 2000; Lowenstein et al., 2001; Horita et al., 2002). The estimates and modelled results of these studies are shown in Figure 6.16.

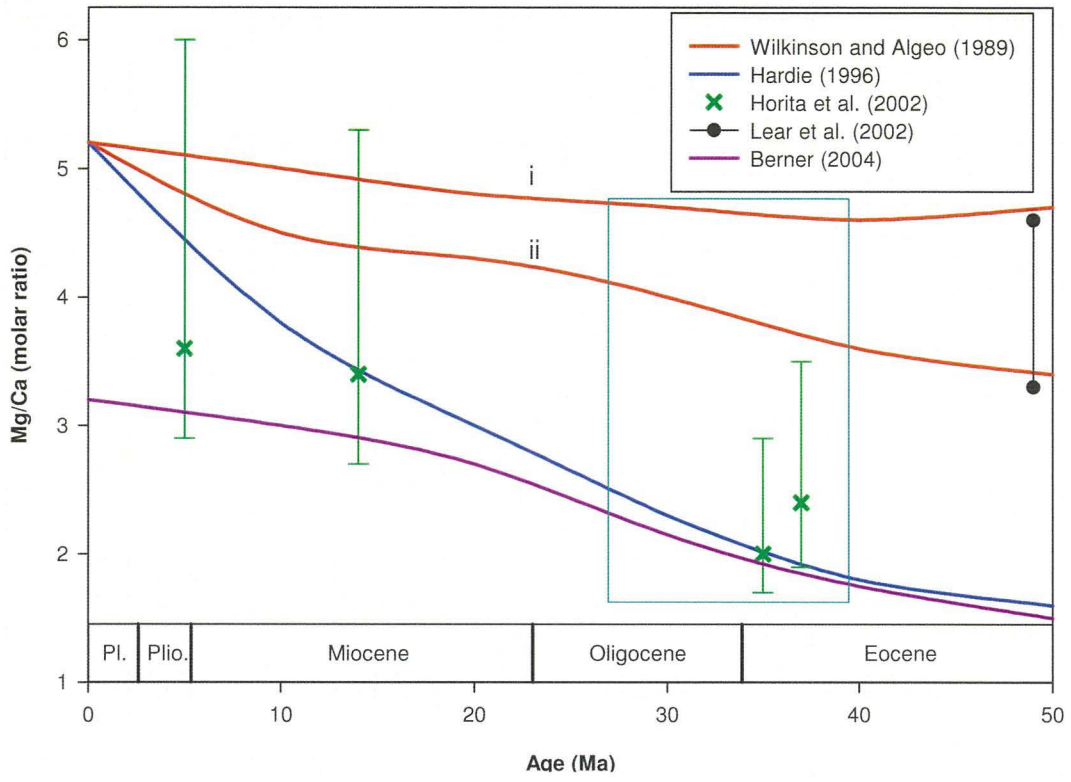

Figure 6.16: Seawater Mg/Ca ratio evolution over the past 50 Ma. Wilkinson and Algeo (1989) and Berner (2004) predictions are based on mass balance models of fluxes into and out of the system, whilst Hardie (1996) uses assumption with regards to crustal production and associated hydrothermal fluxes. The two curves i and ii from Wilkinson and Algeo (1989) relate to different assumptions with regards to the residence time of Mg within the ocean, i) reflects a 14 Myr residence time with regards to mid-ocean ridge circulation and ii) reflects a 0.6 Myr residence time with regards to dolomite formation. Horita et al. (2002) use fluid inclusions from halite evaporite deposits to determine seawater chemistry. Lear et al. (2002) used the Mg/Ca ratio-bottom water temperature calibration determined for the benthonic foraminifera *O. umbonatus* with Mg/Ca ratios and $\delta^{18}O$ palaeotemperature estimates for an ice-free time (~49 Ma) to constrain seawater Mg/Ca, the range of values reflects uncertainties within the pre- and exponential constants. The highlighted area (pale blue box) indicates the time interval covered by this study and the range of Mg/Ca ratios expected, the effect of this range of seawater Mg/Ca on palaeotemperature estimates is shown in Figure 6.17.

Each of the estimates of palaeo-seawater Mg/Ca ratio requires assumptions regarding the controls on and magnitudes of the fluxes of Mg and Ca into and out of the ocean (Figure 6.16). The lack of consensus in Figure 6.16 results from the differing assumptions made by studies, for example: Hardie (1996) links seawater alteration linearly to the rate of crustal production, increasing crustal production leading to increasing alteration reactions and thus decline in seawater Mg/Ca. Hardie's (1996) assumptions reproduce changes in the carbonate chemistry of hyper-calcifying organisms, i.e. whether low-Mg or high-Mg carbonate (Stanley and Hardie, 1998), however, both the effect of circulation on seawater Mg/Ca ratios and the degree of variation in crustal production over the Cenozoic have questioned (Holland et al., 1996; Rowley, 2002). Holland et al. (1996) suggested the effect

on Mg/Ca ratios of circulation through mid-ocean ridge was much less than assumed by Hardie (1996) and Stanley and Hardie (1998), whilst Rowley (2002) suggested that crustal production has been relatively invariant over the Cenozoic and thus cannot account for the Mg/Ca variation seen. Alternatively, Wilkinson and Algeo (1989) consider dolomitisation of marine carbonates to be the dominant sink of Mg, based on mass balance equations concerning the temporal distribution and volume of sedimentary carbonate sequences. Use of a mass balance technique assumes a perfect knowledge of sedimentary carbonate reservoirs so may be flawed by an imperfect knowledge of sedimentary carbonate reservoirs (Horita et al., 2002).

Measurement of fluid inclusions in evaporite deposits could provide an independent check on the modelled evolution of Mg/Ca ratios, however, fluid inclusions are susceptible to alteration and assumptions regarding the palaeo-chemistry of the seawater out of which they evaporated (see Horita et al., 2002 for discussion). Fluid inclusions Mg/Ca ratios appear to track the modified Hardie (1996) seawater Mg/Ca ratios (Stanley and Hardie, 1998), although the uncertainty related to assumptions about seawater Ca^{2+} concentrations means the constraint provided by fluid inclusions is relatively imprecise. An independent constraint on Cenozoic seawater Mg/Ca ratios was that of Lear et al. (2002), who use the Mg/Ca ratios from the extant (and long ranging) benthonic foraminifera *O. umbonatus* to estimate middle Eocene Mg/Ca by re-arranging the species calibration (see Section 6.4.2; Equ. 6.3) with the $\delta^{18}O$ palaeotemperature estimate from an assumed ice-free sample. The range of values shown in Figure 6.16 reflects the uncertainty within the Mg/Ca-bottom water temperature calibration. Lear et al.'s (2002) predicted Mg/Ca seawater values were much greater than those predicted by the Hardie (1996) model and estimated from fluid inclusions, and similar to the seawater Mg/Ca ratios predicted by Wilkinson and Algeo (1989).

The stratigraphic interval researched by this study is highlighted in Figure 6.16, and shows a wide variation in modelled or estimated seawater Mg/Ca ratios across the period, i.e. seawater Mg/Ca range from <2 to >5 mol/mol, so the effect of changing seawater Mg/Ca ratios on palaeotemperature estimates must be considered (Figure 6.17). Palaeotemperature estimates are derived from the generic benthonic foraminiferal Mg/Ca palaeotemperature calibration of Martin et al. (2002; see Section 6.4.2), using the range of seawater Mg/Ca values estimated for the studied interval. Figure 6.17 shows that choice of seawater Mg/Ca

ratio is critical to absolute temperature estimation, e.g. cf. temperature estimations for a foraminiferal Mg/Ca of 2 mmol/mol with a seawater Mg/Ca ratio of 3 and 4 mol/mol; temperatures calculated with a seawater Mg/Ca of 3 mol/mol are >2 °C warmer. Absolute temperature variation with time is also complicated by changing Mg/Ca with time, e.g. seawater Mg/Ca has increased by ~1 mol/mol between ~39.6 and ~27.0 Ma (the stratigraphic range of this study, highlighted box in Figure 6.16; Wilkinson and Algeo, 1989; Hardie, 1996), thus use of a single seawater Mg/Ca ratio may introduce artefacts into the palaeotemperature record. However, both Ca and Mg are conservative elements in seawater, with residence times of 0.6 and 14 Myrs (Wilkinson and Algeo, 1989), so estimation of relative change over restricted periods, i.e. <1 Myrs, should be robust (Lear et al., 2002).

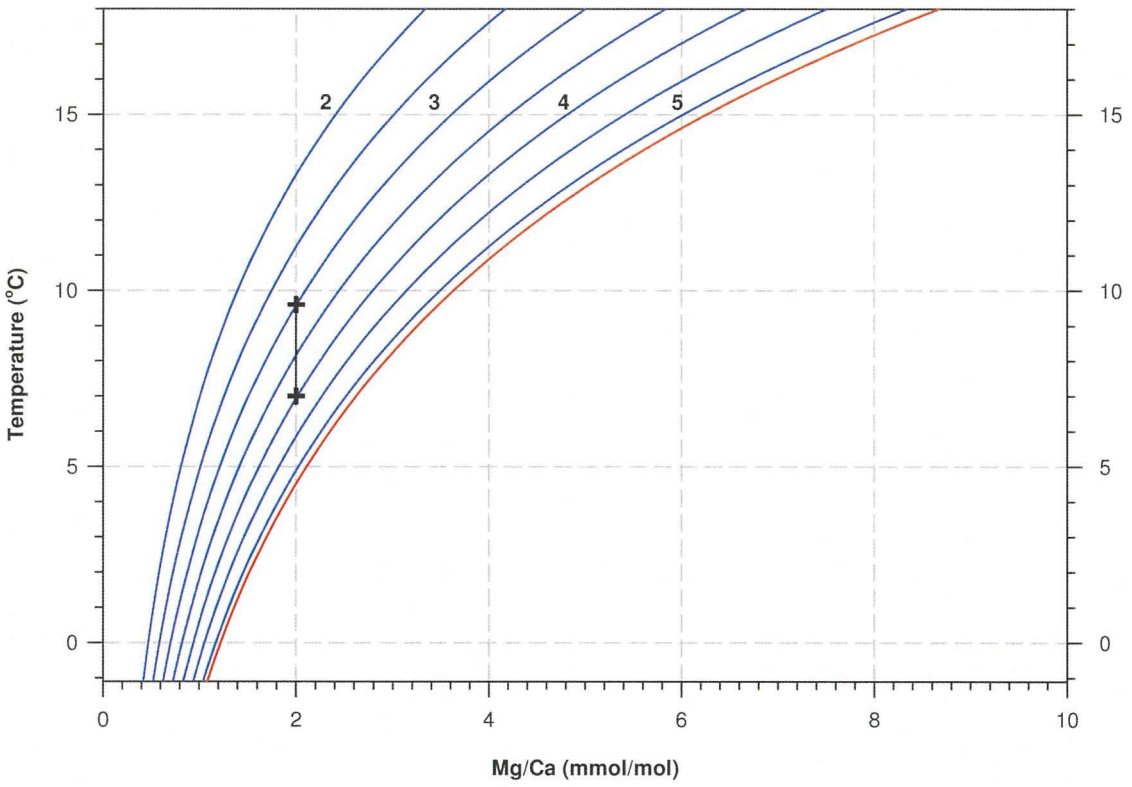

Figure 6.17: Mg/Ca temperatures (blue lines) calculated using the Martin et al. (2002) calibration for the range of seawater Mg/Ca estimations (2 to 5 molar ratio) expected for the interval covered by this study (highlighted pale blue box in Figure 6.16). The red line is the predicted temperature using modern day seawater Mg/Ca ratios of 5.2 mol/mol. At typical benthonic foraminiferal Mg/Ca (~2 mmol/mol) an increase of 1 molar ratio in seawater Mg/Ca (equivalent to the estimated increase of seawater Mg/Ca over 39 to 27 Ma from Wilkinson and Algeo (1989) and Hardie (1996) causes a temperature increase of >2 °C (black crosshairs).

Lear et al. (2004) use the modern day seawater Mg/Ca ratio to calculate palaeotemperatures for the Cenozoic, justifying their choice by suggesting that the lack of variation of Sr/Ca over the Cenozoic reflects relatively invariant Ca concentrations. Reasoning behind this decision being that any global changes in Ca concentration would

be reflected in both Mg/Ca and Sr/Ca records, so the absence of any trend indicates seawater Ca ratios did not vary greatly across their study interval, Ca having a shorter residence time in the ocean of ~0.6 Myrs than the 14 Myr residence time of Mg (Elderfield and Schulz, 1996), thus controlling variation. Figure 5.19 shows the Sr/Ca ratios determined for the studied interval (39.0 to 27.0 Ma) in this study, and it can be observed that there is no systematic trend within Sr/Ca, with values essentially varying closely around the mean (~0.8 mmol/mol). The similarity of Sr/Ca ratios throughout the interval suggests that, as at Site 1218 (Lear et al., 2004), there has not been a large change in Ca concentrations, suggesting that Mg/Ca has also been constant. The likely absence of significant change within Mg/Ca ratios means that a single seawater Mg/Ca ratio can be used to determine palaeotemperature estimates across the range of the study.

Although absolute temperature cannot be stated with great confidence due to the uncertainty in seawater Mg/Ca, the relative changes throughout the studied interval are likely to be robust. For the purposes of palaeotemperature reconstructions from foraminiferal Mg/Ca ratios developed within this study, seawater Mg/Ca molar ratios of 5.2 (modern-day), 4.3 (approximate EOB value of Wilkinson and Algeo, 1989) and 2.2 (Hardie, 1996) have been used to determine palaeotemperatures and the results discussed, as too which is most appropriate in Section 6.4.4.

6.4.2 Mg/Ca palaeotemperature calibrations

Calculation of palaeotemperatures from foraminiferal Mg/Ca ratios requires a foraminiferal Mg/Ca–water temperature calibration. Palaeotemperature calibrations for benthonic foraminiferal Mg/Ca are based on a limited number of core-top based studies concerning predominantly *Cibicidoides* spp. (Rosenthal et al., 1997; Lear et al., 2002; Martin et al., 2002; see Section 2.2.6). These have all followed the exponential relationship observed between planktonic foraminiferal Mg/Ca and temperature (Nurnberg et al., 1996; Lea et al., 1999b; Elderfield and Ganssen, 2000; Anand et al., 2003) and have equations of the form:

$$Mg/Ca_{foram} = B \exp (A * T) \qquad \text{(Eq. 6.3)}$$

where Mg/Ca_{foram} is the Mg/Ca of the foraminifera, B is a pre-exponential constant, A an exponential constant and T is the water temperature, both A and B are species-specific. A summary of the species pre- and exponential constants calculated and related errors are shown in Table 2.2

Deep-water Site 1211 Mg/Ca ratios were developed for this study from a single species *O. umbonatus* (Section 3.5), thus inter-specific effects are eliminated. Three Mg/Ca ratio – bottom water temperature calibrations for *O. umbonatus* have been developed by Lear et al. (2002), Rathmann et al. (2004) and Rathmann and Kuhnert (2008), plotted in Figure 6.18 with the *Cibicidoides* spp. calibration of Martin et al. (2002) and the linear *C. pachyderma* calibration of Marchitto et al. (2007) for comparison. The three *O. umbonatus* Mg/Ca – BWT relationships were developed through different methods at different locations (Table 2.2); Lear et al. (2002) used a compilation of core-top samples from a range of depths at six globally spread locations, Mg/Ca ratios were determined from solutions prepared from 6-20 foraminifera that had been cleaned rigorously using the "reductive" and "oxidative" cleaning methods (See Section 3.6.1). Rathmann et al. (2004) and Rathmann and Kuhnert (2008) Mg/Ca – BWT calibrations were determined from samples collected from a depth-transect off the coast of Namibia using average Mg/Ca ratios of several (5-7) foraminifera, Mg/Ca ratios for each foraminifera being determined using laser ablation, sampling the uncleaned individual tests five times and averaging the resulting ratios.

Choice of Mg/Ca ratios – BWT calibration equation has implications with regards to the absolute temperature estimated for a sample (Figure 6.18), with a difference of ~4 °C at a Mg/Ca ratio of 2 mmol/mol between Rathmann and Kuhnert (2008) and Lear et al. (2002) calibrations. The similarity (Table 2.2) of the exponential constant, however, shows that relative temperature change estimations will be similar. Whilst Rathmann and Kuhnerts (2008) calibration has a higher correlation coefficient ($r^2 = 0.75$ compared to $r^2 = 0.4$) than Lear et al. (2002), the Lear calibration was based on core-top samples from a global spread of locations and was undertaken on "cleaned" foraminifera, thus the Lear et al. (2002) calibration was used for the calculation of palaeotemperatures in this study.

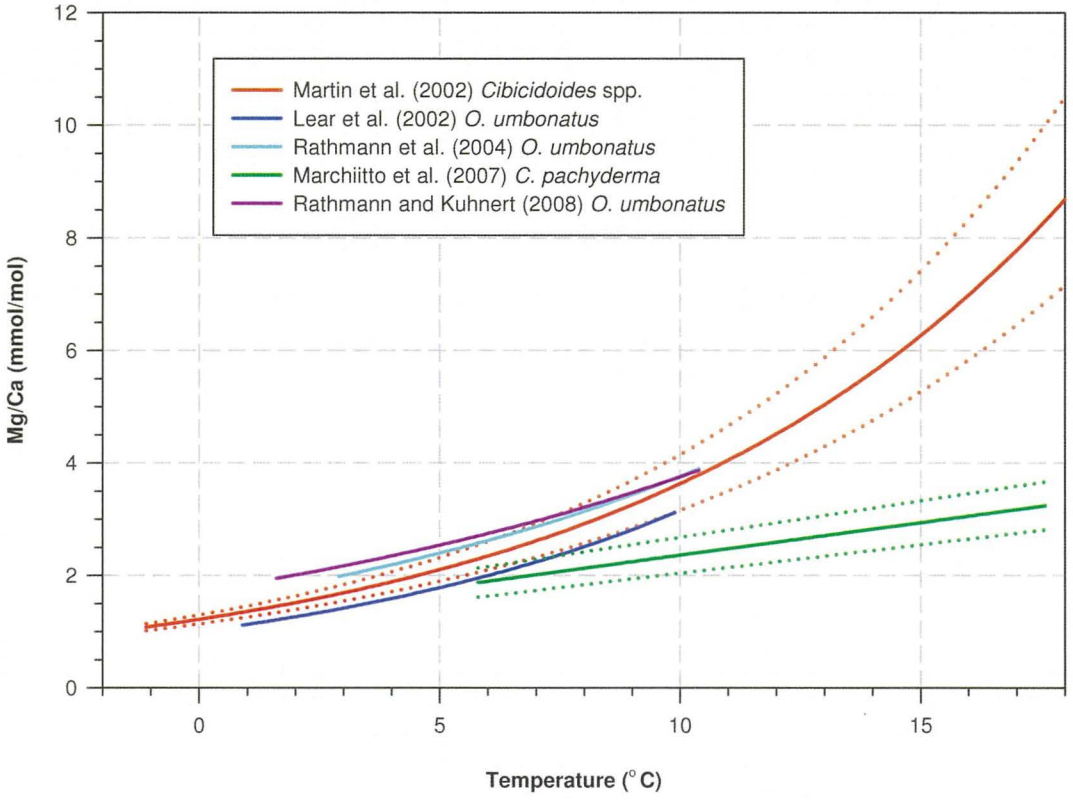

Figure 6.18: Selected foraminiferal Mg/Ca ratio – bottom water calibrations from Table 2.2, whilst absolute temperatures depend on the chosen calibration, similar relative temperature changes can be observed for the different exponential equations. Dotted lines are the 95% (±2σ) confidence intervals of the calibrations, where identified by the original study.

Selection of Mg/Ca ratio – calcification temperature relationships for the two Oligocene planktonic foraminifera, *C. unicavus* and *T. ampliapertura*, and the single Eocene species that fell within the depth–age relationship, *S. senni,* is more difficult as all species are extinct and thus no species-specific relationships exist. Calibrations for extant planktonic foraminifera species (Table 2.2) have been developed from culturing (Nurnberg et al., 1996; Lea et al., 1999b), from core-tops (Elderfield and Ganssen, 2000; Lea et al., 2000; Cleroux et al., 2008; Regenberg et al., 2009) and sediment trap studies (Anand et al., 2003). These studies all identified similar temperature sensitivities (Table 2.2) with a ~10 % change in Mg/Ca per °C, the differences in sensitivities identified not being significant considering the differences in methods used, analytical precision and statistical constraints on data caused by low numbers of samples and replicates (Rosenthal and Lothmann, 2002). Assuming the similarity in temperature sensitivity was also present in Eocene and Eocene/Oligocene planktonic foraminifera, then whichever Mg/Ca–temperature equation is used, relative changes within palaeotemperatures calculated for *C. unicavus*, *S. senni* and *T. ampliapertura* should be robust. Selection of a calibration equation to derive absolute temperatures is more uncertain, however, as the pre-exponential constants differ between

studies and species calibrations leading to very different palaeotemperature estimates (Table 2.2 and Figure 6.19).

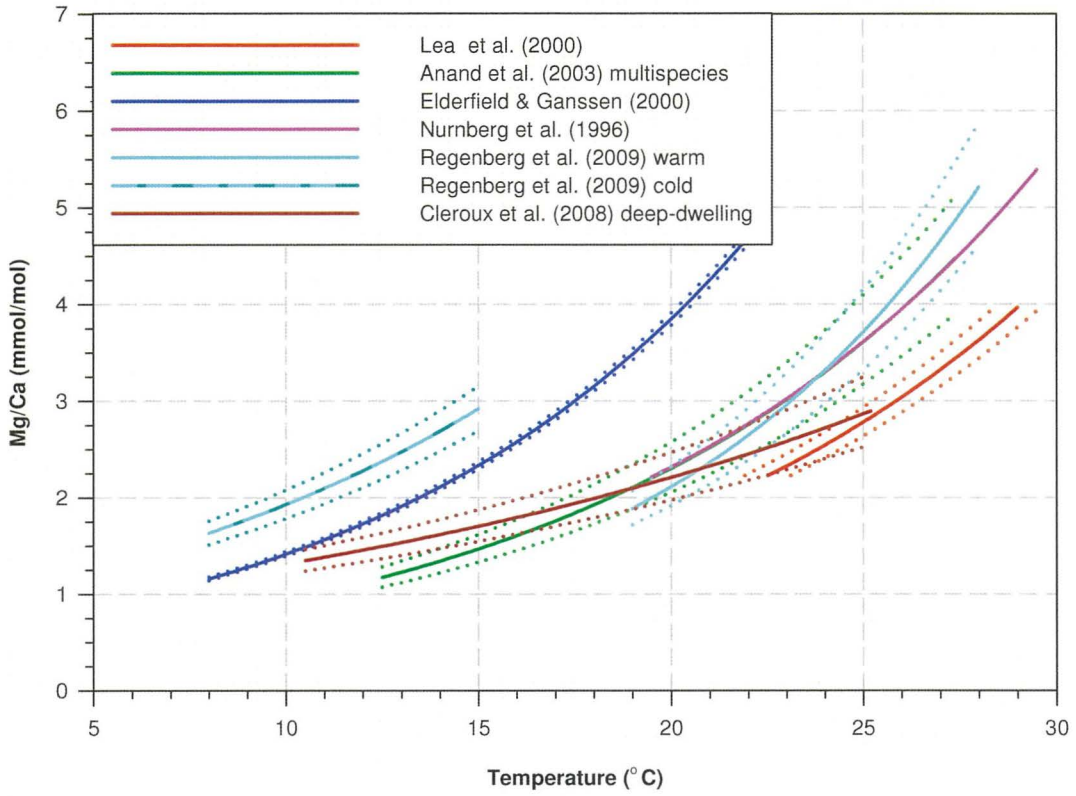

Figure 6.19: Selected planktonic foraminiferal Mg/Ca–calcification temperature calibrations over the applicable range of temperatures (see Table 2.2 for constants) with 95 % (±2σ) confidence intervals as published by the original studies. Choice of Mg/Ca–palaeotemperature equation can be observed to have significant effects on the absolute temperature determined, although relative changes in temperature would be similar

Palaeohabitats have been identified from $\delta^{18}O$ hierarchies of Eocene/Oligocene planktonic foraminifera, with *C. unicavus* identified as a sub-thermocline dwelling species and *T. ampliapertura* as a surface mixed layer species (Van Eijden and Ganssen, 1995; Pearson et al., 2006), thus a calibration suitable for application to both these habitats would be advantageous. Multispecies calibrations, derived from extant planktonic foraminifera species that inhabit a range of water depths, are likely to offer the best approach to estimating palaeotemperatures. Two such calibrations exist for surface mixed-layer to sub-thermocline deep-water dwelling planktonic foraminifera, both from the sub-tropical/tropical Atlantic Ocean (Anand et al., 2003; Regenberg et al., 2009, Figure 6.19). The two calibrations are in good agreement for temperatures >18 °C, but Regenberg et al. (2009) identify an offset of up to 8 °C for deep-dwelling, i.e. sub-thermocline dwelling, planktonic foraminifera (calcification temperatures <15 °C). Use of either equation makes the assumption that the extinct planktonic foraminifera had the same relationship between Mg/Ca and calcification temperature as extant species, an assumption difficult to test. Lear et al. (2008) develop Mg/Ca palaeotemperature estimates for *T. ampliapertura* using the

generic Mg/Ca-temperature equation (Equation 6.4, Table 2.2, Figure 6.19) of Anand et al. (2003); choosing this equation as *T. ampliapertura* is within the phylogenetic bracket of the modern groups used to develop the equation. However, no palaeotemperature estimates have been developed for *C. unicavus* or *S. senni*, as far as the author is aware. Use of a single equation for both species would remove any calibration based differences due to different (pre-) exponential constants, so the single calibration equation of Anand et al. (2003) has been used to estimate palaeotemperatures. Even if the absolute palaeotemperatures are erroneous as a result of this approach, relative variation within and between the records should be reliable as a result of the likely similarity in Mg/Ca–temperature relationship.

6.4.3 Site 1211 palaeotemperature estimates

Mg/Ca palaeotemperature estimates were calculated for *O. umbonatus* and *T. ampliapertura* to allow selection of the seawater Mg/Ca ratio that estimates the most reasonable temperatures compared to other data sources and published records (Figure 6.20 and 6.21). Palaeotemperatures were calculated assuming constant seawater Mg/Ca molar ratios of 2.2 (Hardie, 1996; Berner, 2004), 4.3 (Wilkinson and Algeo, 1989) and 5.2 (modern-day), using the calibration of Lear et al. (2002) for *O. umbonatus* and the Anand et al. (2003) calibration for *T. ampliapertura*, which are both of the form:

$$Mg/Ca_{foram} = \frac{Mg/Ca_t}{Mg/Ca_0} * B \exp(A * T) \qquad \{Equ\ 6.4\}$$

Where Mg/Ca_t was the seawater Mg/Ca ratio across the studied interval and Mg/Ca_0 is that of modern-day seawater (5.2) and A and B were constants, as listed in Table 2.2.

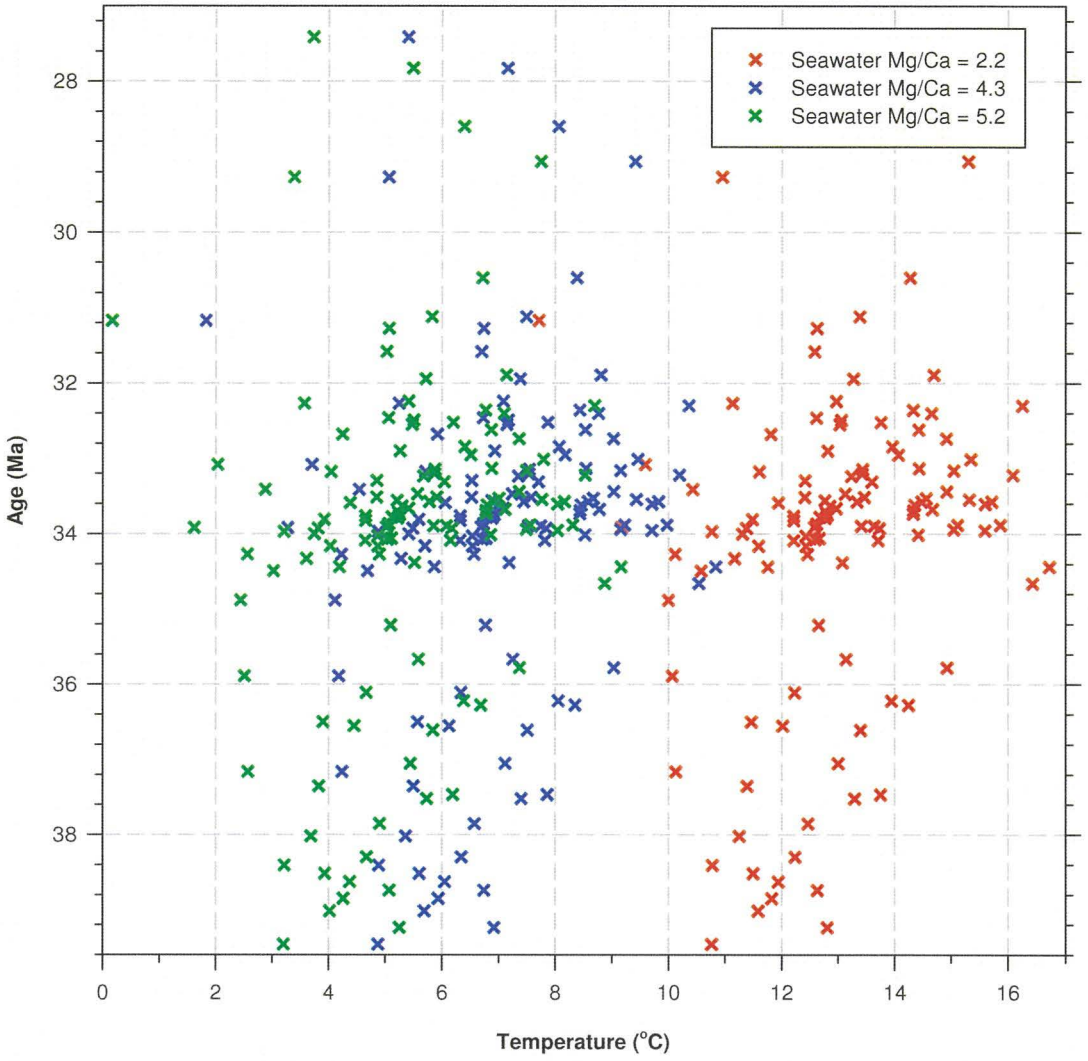

Figure 6.20: Absolute palaeotemperature estimates calculated using the *O. umbonatus* Mg/Ca – bottom water temperature calibration of Lear et al. (2002) and approximate Early Oligocene seawater Mg/Ca ratios (mol/mol) of 2.2 (Hardie, 1996), 4.3 (Wilkinson and Algeo, 1989) and 5.2 (Modern day seawater). Whilst absolute temperatures are offset due the different seawater Mg/Ca, relative changes and the range of temperature estimates are identical.

Bottom-water Mg/Ca palaeotemperature estimates vary between ~8 and ~17 °C around a mean of ~13 °C (seawater Mg/Ca of 2.2), ~2 and ~11 °C around a mean of 7 °C (seawater Mg/Ca of 4.3) and ~0 and ~9 °C around a mean of 5 °C (seawater Mg/Ca of 5.2). Modern day bottom waters at a depth of ~3000 m have a palaeotemperature of 1 to 2 °C (Talley, L.D., 2007), suggesting that bottom waters have cooled by between 3 and 12 °C since the study period, depending on the seawater Mg/Ca used. A ~12 °C bottom water temperature decrease over the last ~30 million years is equivalent to the entire change in deep-water temperature across the past 65 Ma (Lear et al., 2000; Zachos et al., 2001) and therefore is unlikely. Bottom-water temperature decreases of 3–6 °C, however, are similar to those observed by Lear et al. (2000) from the EOB to present day, so seawater Mg/Ca ratios of 4.3 or 5.2 mol/mol are possible.

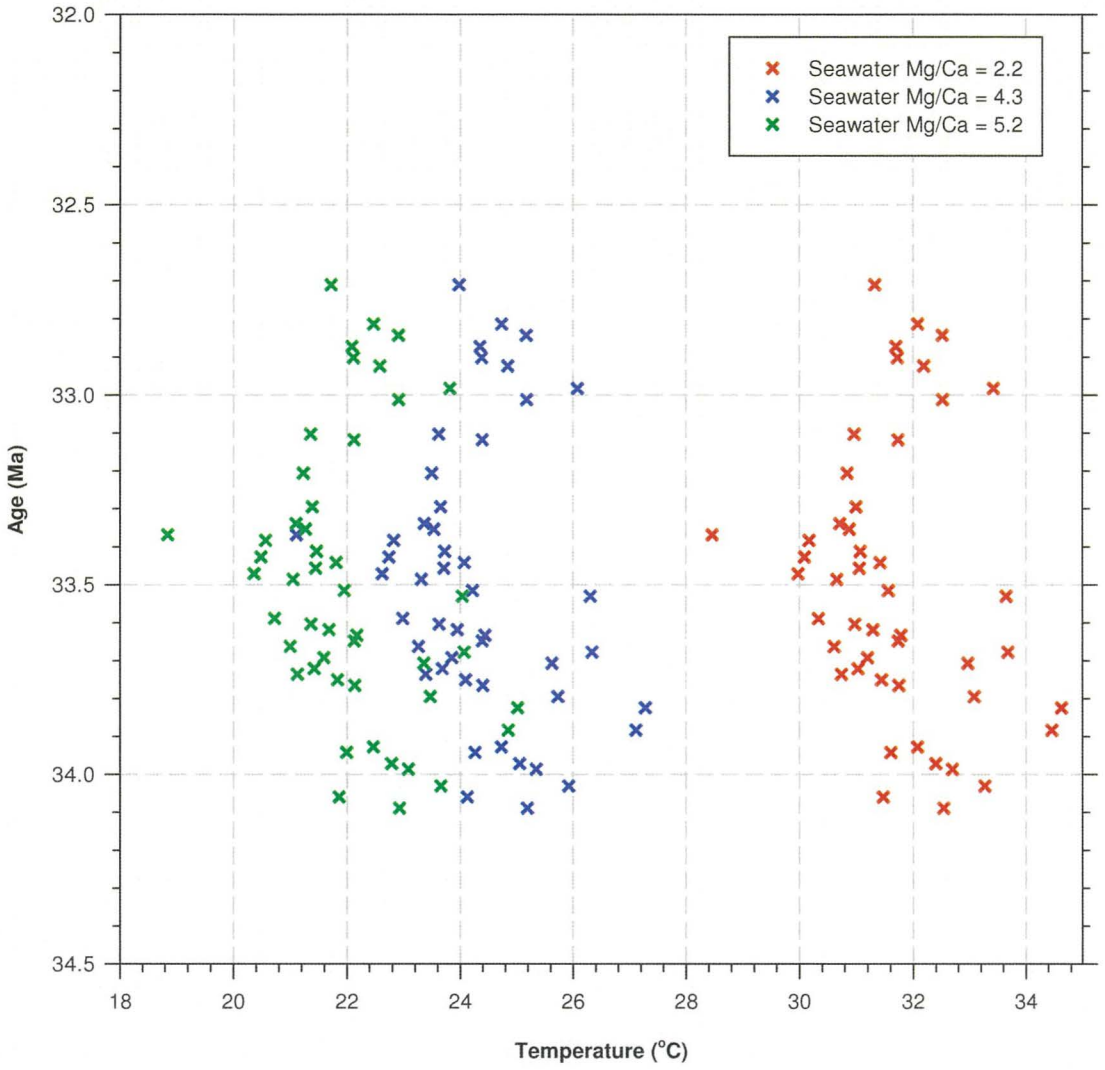

Figure 6.21: Absolute palaeotemperature estimates for *T. ampliapertura* calculated using the planktonic foraminifera Mg/Ca – calcification temperature calibration of Anand et al. (2004) and approximate Early Oligocene seawater Mg/Ca ratios (mol/mol) of 2.2 (Hardie, 1996), 4.3 (Wilkinson and Algeo, 1989) and 5.2 (Modern day seawater). As with the *O. umbonatus* Mg/Ca – bottom water temperature estimates, relative calcification temperature changes and the range of estimates are identical for all seawater Mg/Ca ratio.

T. ampliapertura palaeotemperatures with a seawater Mg/Ca ratio of 2.2 are high, with the near surface mixed-layer dwelling *T. ampliapertura* estimating between 30 and 35 °C. Lear et al. (2008) calculate palaeotemperatures from *T. ampliapertura* estimating temperatures of ~27 to 29 °C, whilst Liu et al. (2009) used alkenone unsaturation index ($U^{K'}_{37}$) and tetrather index (TEX_{86}) to calculate tropical surface temperatures to be between 29 and 31 °C. Thus, palaeotemperature estimates using seawater Mg/Ca of 2.2 appear to overestimate the sea surface temperatures. As seawater Mg/Ca of 2.2 mol/mol also produced unrealistic bottom-water temperatures, seawater Mg/Ca must have a value of >2.2 mol/mol during the late Eocene and early Oligocene.

T. ampliapertura surface palaeotemperature estimates are lower than those of Lear et al. (2008) and Liu et al. (2009) by ~3 to ~4 °C (once corrected to sea-surface values by +2 °C , Lear et al., 2008) for seawater Mg/Ca of 4.3 mol/mol and ~5 to ~6°C for a seawater Mg/Ca ratio of 5.2 mol/mol. Identical temperatures to these published records are unlikely as both Lear et al. (2008) and Liu et al. (2009) were for tropical rather than sub-tropical environments, and in the case of the alkenone based estimates of Liu et al. (2009) may not represent calcification during the same season. Seawater Mg/Ca ratios of 4.3 and 5.2 mol/mol produce range of bottom-water temperatures that are plausible for Site 1211 during the Eocene, neither requiring cooling greater than that expected from the $\delta^{18}O$ and Mg/Ca composite Cenozoic records of Lear et al. (2000) and Zachos et al. (2001). The seawater Mg/Ca ratio of 4.3 mol/mol, however, would seem to produce more reasonable palaeotemperature estimations for both benthonic and planktonic foraminifera, and so is used for subsequent calculations and figures. However, as relative changes are more significant than absolute temperatures, choice of Mg/Ca ratio is not critical provided consistency is maintained between records.

Considering Figures 6.20 and 6.21, a standout feature of these palaeotemperature estimates is the degree of scatter over short time intervals, e.g. *O. umbonatus* palaeotemperature estimates between 34.0 and 33.8 Ma have a ~5 °C range, bottom-water temperature variations of such a magnitude over relatively restricted time-intervals being palaeoceanographically unlikely. Mg/Ca ratios have been observed to be variable both within individual tests (Hathorne et al., 2003; Eggins et al., 2003; Rathmann et al., 2004; Anand and Elderfield, 2005; Rathmann and Kuhnert, 2008; Sadekov et al., 2008) and between replicate samples measured during calibration studies (Lear et al., 2002; Yu and Elderfield, 2008), suggesting that Mg/Ca ratios are highly variable within and between tests of a single sample. Despite the observed intra- and inter-test variability, Sadekov et al. (2008) demonstrated that mean foraminiferal Mg/Ca ratios for *Globogineroides ruber* displayed the exponential relationship with surface seawater temperature observed in previous studies (e.g. Lea et al., 2000; Anand et al., 2003 among others); however, the uncertainty and degree of scatter around the mean temperature calibration was related to the number of tests analysed and decreased with increasing sample size. Rathmann and Kuhnert (2008) observe variation of up to ~33 % at Mg/Ca ratios of ~2 mmol/mol (~4 °C) unrelated to either temperature or $(\Delta)[CO_3^{2-}]$ in *O. umbonatus*, even though a clear population Mg/Ca-temperature relationship over the core-transect was observed.

Variability of ~±33 % around an *O. umbonatus* Mg/Ca of ~2 mmol/mol could account for virtually all the variation in Site 1211 records, ±33 % equating to a range of ~1.34 to ~2.66 mmol/mol (cf. with the range of Mg/Ca values for Site 1211 in Figure 5.19). Like this study, Rathmann and Kuhnert (2008) analysed small numbers of foraminifera (5-10), thus the sample size dependent uncertainty about the mean ratio (and hence temperature) observed by Sadekov et al. (2008) for planktonic foraminifera may apply to benthonic foraminifera also.

Alternatively the inter and intra-specific variation described has also been attributed to a variety of others causes, including high-Mg carbonate, bioturbation, actual variability due to temperature and vital effects (Lear et al., 2002; Rathmann et al., 2004; Rathmann and Kuhnert, 2008; Yu and Elderfield, 2008), which require further consideration. Inter/intra sample variability is too great (>1 mmol/mol) to be explained by seasonality or bioturbation of benthonic foraminiferal Mg/Ca ratios, but the presence of high-Mg through contamination and/or through vital effects due to changes within the shell microenvironment seem to be possible controls (Rathmann et al., 2004).

Assessment of intra-test variability was not attempted in this study so the presence of significant changes in vital effects between samples cannot be assessed, however, the presence of contaminant phases has been considered. All foraminiferal specimens analysed at Site 1211 had "frosty" preservation (Section 6.1.5) indicating significant degree of neomorphism of the test walls and thus alteration of the primary carbonate (Pearson et al., 2001; Sexton et al., 2006; Sexton and Wilson, 2009). As described in Sections 6.1.3 and 6.1.5, neomorphism of foraminiferal carbonate leads to increase in the test Mg/Ca ratio (Sexton et al., 2006). Although to account for the scatter seen, neomorphism would have to be variable over restricted stratigraphic intervals, i.e. within <50 cm. A more plausible explanation may be that contamination of the foraminiferal test was insufficiently identified. Trace element/Ca ratios, i.e. Si, Ti and Mn, were measured to identify potential contamination, however, drift correction of the Si/Ca ratios was not possible and Ti was frequently below limits of machine sensitivity (Section 5.10 and 5.11). These two element/Ca ratios typically correspond to alumino-silicate contamination so the absence of continuous screening for this contamination could have allowed silicate contamination to remain unidentified. Reduction of the Mn/Ca threshold levels from 100 µmol/mol to 50 and 10 µmol/mol to assess the degree to which Mn overgrowth contamination contributed

to the scatter, however, did not cause any noticeable changes. Measurement of alternative element/Ca ratios, i.e. Fe/Ca and Al/Ca, would improve the confidence in screened Mg/Ca ratios in future studies.

A potential source of methodological error may lie in the calibration of Mg/Ca ratios with the synthetic standards or in the data processing filtering procedure undertaken. Calibration was achieved through use of a single Ca concentration (see Section 3.6.4) rather than accounting for the differing Ca contents in each sample; however, the effect of a slope calibration on scatter was shown to be insignificant (Figure 3.4). Similar magnitude of the scatter also remains if Mg/Ca ratios calculated from samples with restricted Ca concentrations, i.e. between 5 and 10 or 10 and 15 μm/ml, indicating the scatter is not a result of matrix effects due to changing sample Ca concentration. Planktonic foraminifera were cleaned by the "oxidative" method (see Section 3.6.1) rather than the more rigorous "reductive and oxidative" technique used to clean the benthonic specimens. However, as similar scatter was observed in both *C. unicavus* and *O. umbonatus*, despite different cleaning methods, preparatory methods are unable to explain the observed scatter.

As the degree of scatter requires high variability in contamination or neomorphism over restricted stratigraphic intervals, the limited number (typically less than 10 whole tests) of both planktonic and benthonic foraminifera for Mg/Ca ratio analysis (as per Sadekov et al., 2008) would therefore seem to be the most plausible explanation for the scatter observed in Site 1211 datasets. However, to investigate the degree to which within shell variability effects shell Mg/Ca at Site 1211 would require further investigation using laser ablation techniques on multiple single foraminifer tests from a range of stratigraphic locations (see Rathmann et al., 2004; Rathmann and Kuhnert, 2008). Despite the scatter observed in *O. umbonatus* by Rathmann et al. (2004) and Rathmann and Kuhnert (2008) and for *G. rubber* by Sadekov et al. (2008), temperature was the dominant control on mean Mg/Ca ratios and so this is assumed to be the case for Site 1211. The scatter, however, clearly prevents interpretation of short-term changes, i.e. <200 kyrs, so a time-averaging method has been applied to reveal the underlying temperature changes to be approximated. This method involved the calculation of, depending on sampling density, 250, 500 or 1,000 kyr averages and 95 % confidence limits throughout the dataset. The time-averaged approach could be modified by averaging the time intervals corresponding to the EOT and EOGM as identified from benthonic foraminiferal $\delta^{18}O$ records (Section 6.2.1). The former approach,

however, has the advantage of not making any assumptions as to the relationship of temperature change to the $\delta^{18}O$ record. Figure 6.22 shows the two methods have very similar results and suggest similar evolutions of palaeotemperature within Site 1211 bottom-waters. Site 1211 palaeotemperatures were subsequently interpreted from these averages.

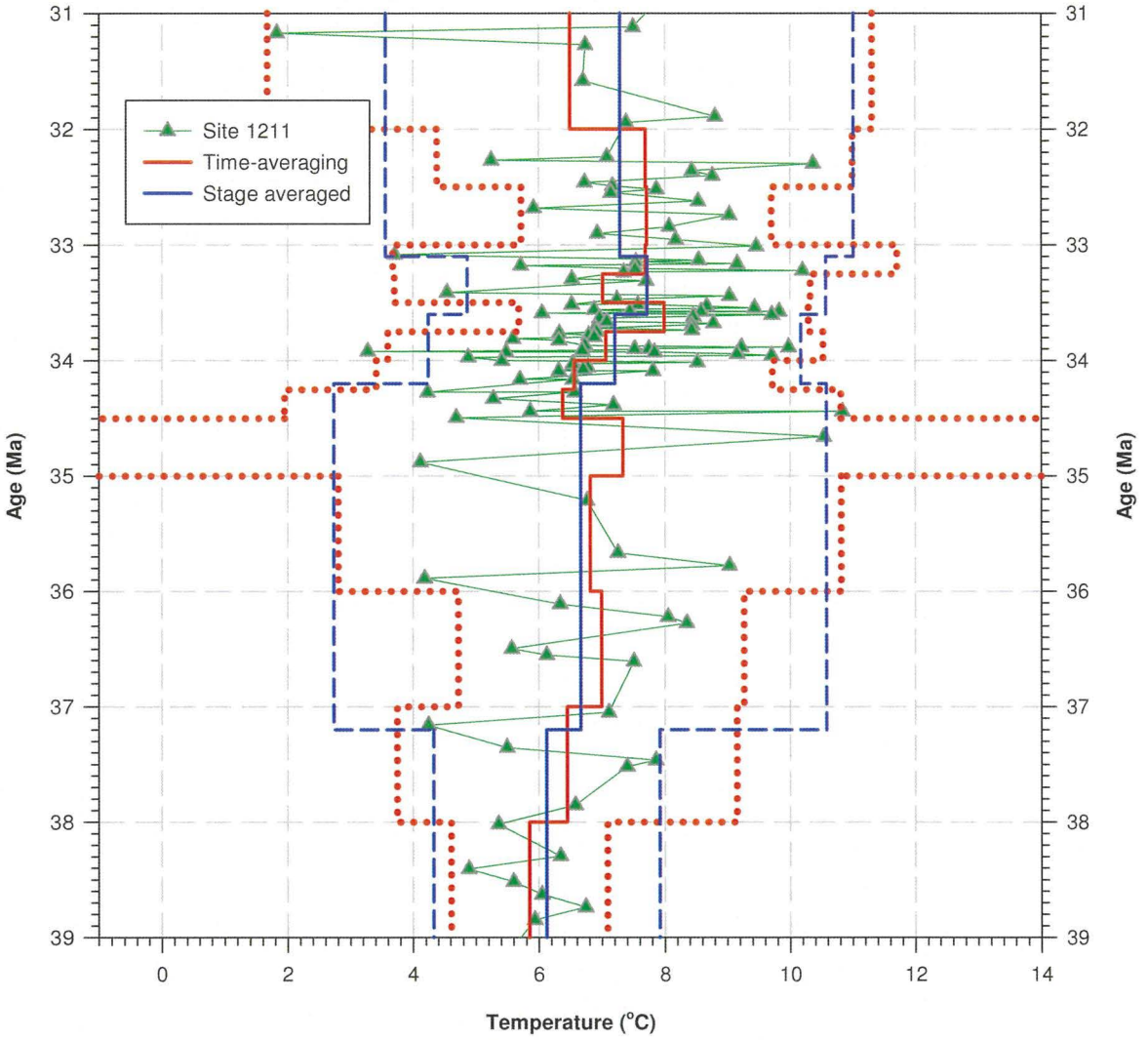

Figure 6.22: Bottom-water palaeotemperature estimates for Site 1211, calculated using a seawater Mg/Ca ratio of 4.3 mol/mol and the Mg/Ca–temperature calibration of Lear et al. (2002). The average lines with 95 % (±2σ) confidence levels correspond to either a time-averaged series, i.e. average Mg/Ca over 250 and 500 kyr intervals, or stage averaged, i.e. Middle Eocene, Late Eocene, EOT, EOGM and post-EOGM Oligocene. The two averaging techniques lead to very similar interpretations of the palaeotemperature change at Site 1211; although time-averaging may over interpret variation during the Eocene whilst stage averaging implicitly assumes a link between palaeotemperature change and the $\delta^{18}O$ increase across the EOB. Palaeotemperatures typically averaged between 6.0 and 6.5 °C during the Middle to Late Eocene, with confidence limits typically of >±2 °C. Average palaeotemperature increases from the latest Eocene, i.e. with the initiation of the EOT, reaching maximum values of ~8 °C coincident with Oi-1a, although the magnitude of the 95 % confidence intervals remains similar to the Eocene. Following the EOGM palaeotemperature values decrease by ~0.5 °C, indicating that Oligocene bottom-waters were ~1 °C warmer than Eocene.

6.4.4 Temperature variation at Site 1211

Figure 6.22 shows the bottom-water palaeotemperature estimates and time/stage-averaged values across the studied interval at Site 1211. The time-averaged approach indicates that Late Eocene bottom-water palaeotemperatures were ~6.5 °C until 34.0 Ma with varying degrees of confidence but typically >±2 °C (2σ). The absence of any clear trend in Mg/Ca palaeotemperature across this interval argues that there were no significant changes in seawater Mg/Ca across the Middle and Late Eocene. Increase from typical Eocene temperatures occurs through the intervals 34.25 to 34.0 and 34.0 to 33.75 Ma, with average temperatures rising by >0.5 °C over the two intervals. Between 34.0 and 33.75 Ma, average temperatures exceed the range of temperatures observed for the Eocene, with further increase of ~1 °C occurring during 33.75 to 33.5 Ma. Average temperatures then decline by <0.5 °C but typically vary ~1 C warmer than during the Eocene at ~7.5 °C until 31.5 Ma. The 31.5 to 31.0 Ma average suggests a decrease in temperature during the interval, but has >±5 °C confidence limits and is likely to be influenced greatly by one of the three values being very low (<2 °C) compared to ~7 °C of the other estimates. The increase in bottom-water palaeotemperatures mirrors that in the composite benthonic foraminiferal $\delta^{18}O$ (Figure 6.5), with the greatest increase occurring across the second stage of the EOT.

Plots of surface-water Mg/Ca palaeotemperature estimation are shown in Figure 6.23, together with those for bottom-waters at Site 1211, and have been plotted with the time-averaged values and 95 % confidence intervals (except for *S. senni* which has insufficient determinations to make a time-averaging approach valid). The 95 % confidence intervals for *C. unicavus* were ~±2 °C, i.e. similar in magnitude to those of *O. umbonatus*, whilst *T. ampliapertura* limits were typically ±1 °C. *C. unicavus* and *T. ampliapertura* palaeotemperature estimates, plot as distinct populations and *T. ampliapertura* 95 % confidence limits do not overlap the *C. unicavus* data indicating significantly different palaeotemperatures.

T. ampliapertura palaeotemperature estimates indicate that near surface water temperatures were cooler during the 33.75 to 33.5 Ma and 33.5 to 33.25 Ma intervals than before or after, i.e. during the EOGM compared to the early EOT and Oligocene. As pre-Eocene palaeotemperatures were not measured, determination of whether there was an

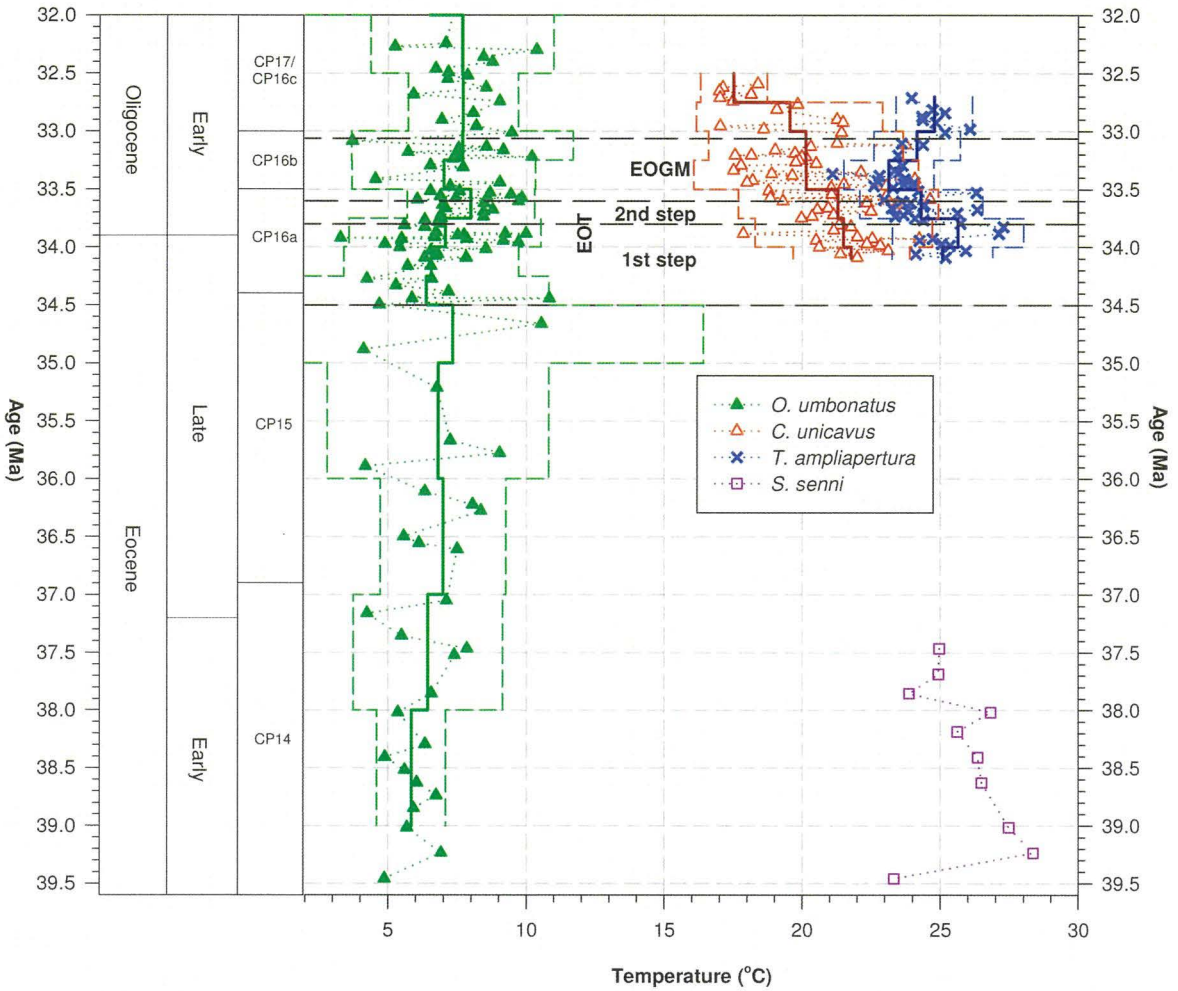

Figure 6.23: Mg/Ca palaeotemperatures and time-averaged values for *O. umbonatus* and the planktonic foraminifera, *C. unicavus* and *T. ampliapertura* determined for Site 1211, Mg/Ca palaeotemperatures only for *S. senni*. Scatter is large within all records with >3 °C in a 100 kyr period being typical, leading to the requirement for time-averaging (Section 6.4.3). Time-averaged bottom-water palaeotemperatures increase by ~1.5 °C across the EOT, whilst surface-water temperatures decrease by ~2 °C across the EOT before sub-thermocline and surface water records diverge at the end of the EOGM. Continued temperature decrease of sub-thermo cline records by ~2 °C suggests these waters became more isolated from the surface during the Oligocene compared to the EOT, possibly indicating increased stratification at Site 1211.

Eocene to Oligocene surface water-cooling is not possible. Average *C. unicavus* palaeotemperatures were cooler than *T. ampliapertura* and decrease from the EOT (34.1 to 33.75 Ma averages) by ~2 °C during the EOGM, followed by a further ~2 °C by 33.0 to 32.5 Ma. The temperature evolution of the two Oligocene planktonic foraminifera agree with the hypothesis of increased stratification isolating surface and sub-thermocline waters during the Oligocene (Section 6.2.2). *C. unicavus* records, however, display too great a level of scatter to identify temperature changes related to the contrary relationship of bottom and sub-thermocline water $\delta^{18}O$ values observed in Section 6.2.2. Surface-water temperature changes thus appear to be the opposite of those observed for bottom-waters at Site 1211 across the EOT, with both near-surface and sub-thermocline waters cooling by ~2 °C indicating surface and deep-waters evolved separately across the EOT. *S. senni* shows a general decrease in palaeotemperatures from the Middle Eocene into the Late

Eocene, mixed layer temperatures appear to have been as warm or warmer than surface waters across the EOT and EOGM as defined by *T. ampliapertura.*

6.4.5 Intersite Mg/Ca temperature differences.

Mg/Ca palaeotemperatures for Sites 522, 1218 and SSQ (Lear et al., 2000, 2004) are plotted with those of Site 1211 in Figure 6.24 to allow assessment of inter-site variability. Palaeotemperatures derived from *O. umbonatus*, i.e. Sites 522 and 1218, were calculated using the Lear et al. (2002) calibration and seawater Mg/Ca of 4.3 mol/mol, whilst palaeotemperatures from SSQ are those determined by Katz et al. (2008).

Considering the deep-sea sites first, i.e. Sites 522, 1211 and 1218, the general relationship was Site 1211 had average temperatures warmer than Site 1218 by at least ~2 °C. No clear relationship is observed between Sites 1211 and 522 palaeotemperature estimates, however, Site 522 sample estimates fall within the spread of Site 1211 data and 95 % confidence intervals. The difference between Sites 1211 and 522 was within the analytical precision at Site 1211 (±0.8 °C, 95 % (±2σ) confidence limits), all of which suggest the data was not statistically different. Whilst Site 1218 data also falls within the Site 1211 95 % confidence limits, the data clearly plots separately from the Site 1211 data and the Site 1218 95 % confidence limits do not overlap Site 1211 data, indicating that palaeotemperatures are different at the two sites. Comparing Site 1211 to SSQ is less informative as a result of SSQs location on the continental shelf, however, Site 1211 is ~10 °C cooler than SSQ where Mg/Ca palaeotemperatures are available.

Considering the absolute temperature differences, Sites 522 and 1211 were both at palaeodepths of ~3000 mbsl across the EOB, shallower than Site 1218 at a palaeodepth of ~3500 mbsl (Lear et al., 2000; Shipboard Scientific Party, 2002b; Coxall et al., 2005). Average Oligocene palaeotemperatures for Site 573 from the equatorial Pacific and also at a palaeodepth of ~3000 m, were observed to be ~1.4 °C warmer than Site 1218 (Lear et al., 2004), further supporting the idea of shallower bottom waters being measurably warmer than deeper bottom-waters. The temperature difference identified above should lead to $\delta^{18}O$ at Site 1211 offset to more negative values by ~0.5 ‰ than Site 1218, whilst Sites 1211 and 522 should be similar. Such a difference in $\delta^{18}O$ was not observed (Figure 6.7) as

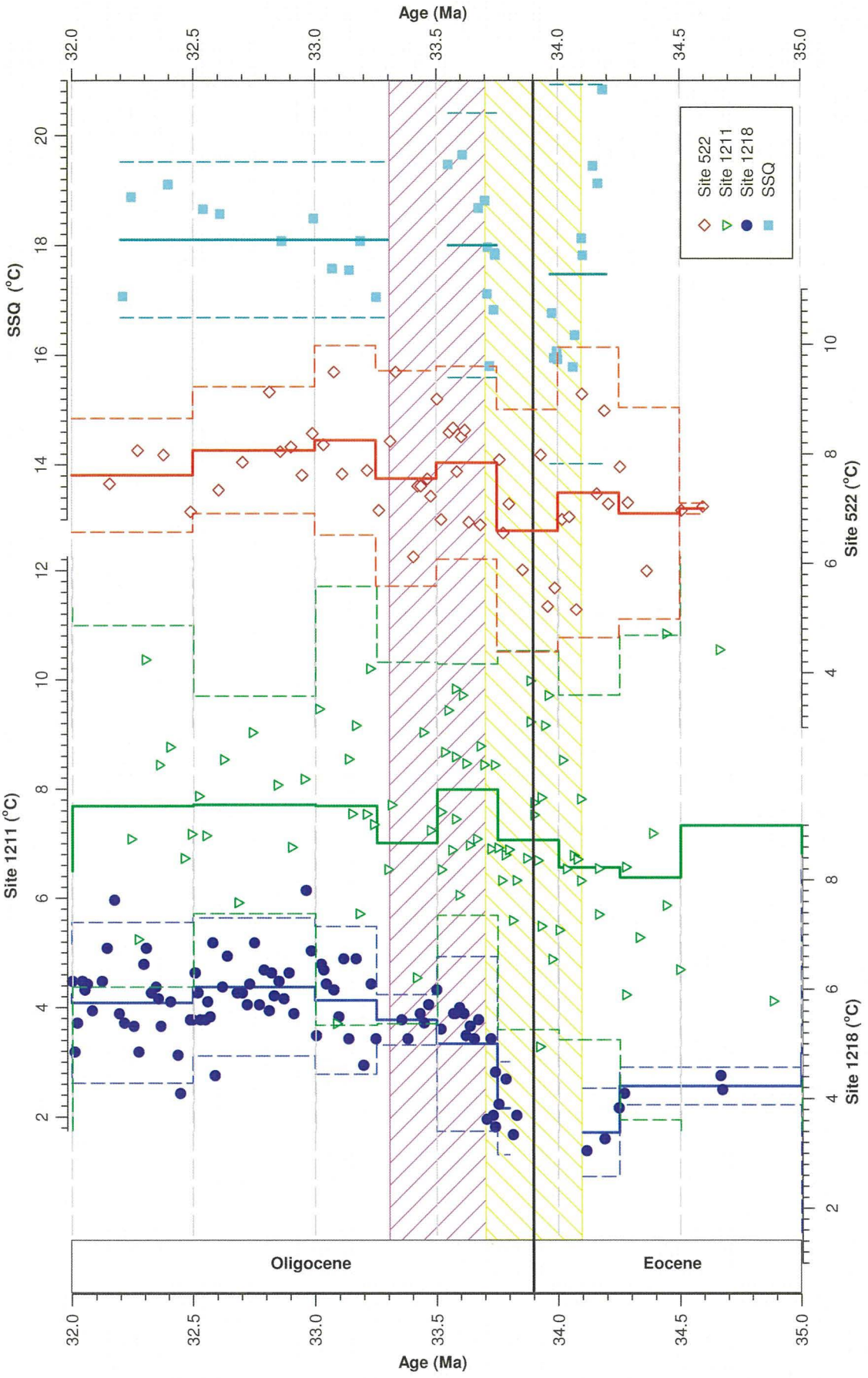
Age (Ma)
32.0
32.5
33.0
33.5
34.0
34.5
35.0
SSQ (°C)
Site 1211 (°C)
Site 522 (°C)
Site 1218 (°C)
Site 522
Site 1211
Site 1218
SSQ
Oligocene
Eocene

Figure 6.24: Palaeotemperature estimates from published Mg/Ca ratios for Site 522 and 1218 (Lear et al., 2000; 2004) and Site 1211 (this study) with time-averages and 95 % (±2σ) confidence intervals drawn through each dataset. SSQ are depth corrected Mg/Ca palaeotemperatures (Katz et al., 2008), the gaps between the averaged sections reflecting the absence of benthonic foraminifera for palaeotemperature determinations. Palaeotemperatures were calculated using the Mg/Ca-temperature calibration of Lear et al. (2002) and seawater Mg/Ca of 4.3 (mol/mol).

Sites 1211 and 1218 had similar $\delta^{18}O$, whilst Site 522 was more positive by up to ~0.5 ‰ than both Sites 1211 and 1218, these relationships indicate a further influence on benthonic foraminiferal $\delta^{18}O$.

Differences in preservation, methodological and laboratory offsets or bottom-water chemistry could all affect either Mg/Ca or $\delta^{18}O$ at Sites 522, 1211 and 1218. Preservation seems to have been typical at each site of pelagic carbonate sediment hosted benthonic foraminifera (Zachos et al., 1996; Lear et al., 2000; 2004; see Section 6.1.5). Preservation in such pelagic carbonate environments, however, does suggest that the foraminiferal tests will have been exposed to neomorphism (Sexton et al., 2006; Sexton and Wilson, 2009) that could influence test geochemistry. Site 1218 was buried to greater depths than Sites 522 and 1211, ~200 rmcd compared to ~100 rmcd, however, the modelled effect of diagenesis at these burial depths is expected to be insufficient to cause the negative shift in $\delta^{18}O$ at Site 1218 or positive shifts at Sites 522 and 1211 necessary to cause the $\delta^{18}O$ relationships seen (Figure 6.1; Schrag et al., 1992, 1995). Two further arguments also indicate that the $\delta^{18}O$ and Mg/Ca ratios observed did not result from diagenesis, firstly Rudnicki et al. (2001) indicate that in shallowly buried sites, diagenesis occurs early in the burial history, i.e. <10 Myrs, reducing the potential for diagenesis occurring in an environment significantly different to that of formation (Section 6.1.2); and secondly, Table 2.1 shows that the EOT $\delta^{18}O$ shift is greater at Site 1218 than Sites 1211 and 522, counter to the attenuation of $\delta^{18}O$ events modelled by Schrag et al. (1992;1995) for progressive recrystallisation. Neither do consistent down-core Sr/Ca ratios support the idea of substantial diagenesis (Section 6.1.3), thus preservation is unlikely to be the cause of the absence of the expected $\delta^{18}O$ relationships.

Methodological differences are likely to account for some of the difference between the three Mg/Ca derived temperature records. The more rigorous "reductive and oxidative" cleaning method of Boyle and Keigwin (1986) consistently produces Mg/Ca ratios that are ~10–15 % lower relative to the "oxidative" method (Barker et al., 2003). A ~10–15 %

difference is equivalent to a temperature decrease of 1 °C. Site 522, unlike Sites 1211 and 1218, was cleaned using the oxidative technique so Mg/Ca ratios may be expected to be ~1 °C greater than if cleaned by the "reductive and oxidative" approach. Were such a overestimation present then Site 522 would typically be ~1 °C warmer than Site 1218 and ~1 °C cooler than Site 1211, a 1 °C cooling of Site 522 relative to Site 1211 would equate to a more positive $\delta^{18}O$ by ~0.25 ‰, i.e. approximately half the $\delta^{18}O$ difference observed.

As a consequence of the inability of preservation and methodological differences to account for the differences observed in Mg/Ca palaeotemperatures and $\delta^{18}O$, then an oceanographic factor is the most likely explanation. Benthonic foraminiferal $\delta^{18}O$ at the three sites can be reconciled if bottom-waters had different salinities. Broecker (1989) observes a 1 ‰ change in salinity affects $\delta^{18}O_{sw}$ by 0.5 ‰ in the modern ocean, so assuming that the 2 °C increase in bottom water temperature at Site 1211 should have decreased the $\delta^{18}O_{bf}$ by ~0.5 ‰, then bottom-waters at Site 1211 would have to be 1 ‰ more saline than those at Site 1218 to explain the equivalent $\delta^{18}O_{bf}$. The relationship of Site 1211 to Site 522 is more complex, as a consequence of the likely overestimation of temperature. Correcting for the cleaning bias at Site 522, then Site 522 was ~1 °C cooler than Site 1211, but had $\delta^{18}O$ 0.5 ‰ more positive. Half of the more positive $\delta^{18}O$ can be explained by the cooler temperatures at Site 522, then a salinity 0.5 ‰ greater at Site 522 could reconcile the difference with Site 1211.

Despite the relative temperature differences between the deep-water sites, evolution of bottom-water palaeotemperatures was similar across the EOB with Oligocene palaeotemperatures being greater than those of the Eocene. Average palaeotemperatures increase by >1 °C between the same intervals at each site, i.e. ~34.0 to 33.75 Ma and 33.75 to 33.5 Ma, or the latter stages of the EOT and the EOGM. The increase between the ~34.0 to 33.75 Ma and 33.75 to 33.5 Ma intervals corresponds to the ~2 °C increase, noted by Lear et al. (2004) during the second phase of the EOT, and can be observed in the sample to sample palaeotemperature data for Sites 522 and 1218. Site 1211 reaches maximum average palaeotemperature during the EOGM, rather than the post-EOGM interval maxima observed at Sites 522 and 1218; Site 1218 palaeotemperatures increasing by a further ~1 °C from the 33.75 to 33.5 Ma interval explaining the negative $\delta^{18}O$ trend after the EOGM at the site (see Section 6.2.3; Figure 6.7). Prior to the increase associated with the EOGM,

Site 1211 differs from Sites 522 and 1218 in not showing a temperature decrease of ~0.8 °C associated with the initiation of the EOT. The most likely explanation for the absence of the temperature decrease is the scatter and low number of determinations during the Late Eocene.

Considering the SSQ palaeotemperature estimates and time-averaged values, time-averaged values clearly do not reflect the transient ~2 °C decreases in palaeotemperatures associated with the $\delta^{18}O$ increase across the first step of the EOT and the Oi-1 glacial (Katz et al., 2008). Given the fragmentary nature of the dataset from SSQ, missing the late Eocene and stages of the EOT and EOGM, the time-averaged approach is unlikely to provide a true comparison representative of palaeotemperature change across the boundary. However, the SSQ record has been proposed as representative of global events, despite the site's hemipelagic location, and the time-averaging approach would indicate that temperatures remained relatively constant across the EOB. It is interesting to note that there also appears to be a warming phase associated with the early EOGM, which could represent that observed in the deep-sea records.

Whilst no published Mg/Ca palaeotemperature records exist for the sub-thermocline dwelling *C. unicavus*, Lear et al. (2008) produce a Mg/Ca palaeotemperature record for *T. ampliapertura* (Figure 6.25) for the EOT. The Lear et al. (2008) record was produced from "glassy" specimens obtained from hemipelagic Tanzanian drilling project (TDP) Sites 12 and 17. Overlap between the Site 1211 record and that of Lear et al. (2008) is limited to the latter half of the first phase of the EOT and phase two of the EOT. The overlap suggests that palaeotemperatures were ~1 to 2 °C cooler at Site 1211, compared to the TDP sites. Overlap of the records, however, is insufficient to allow comparison of the evolution of the records.

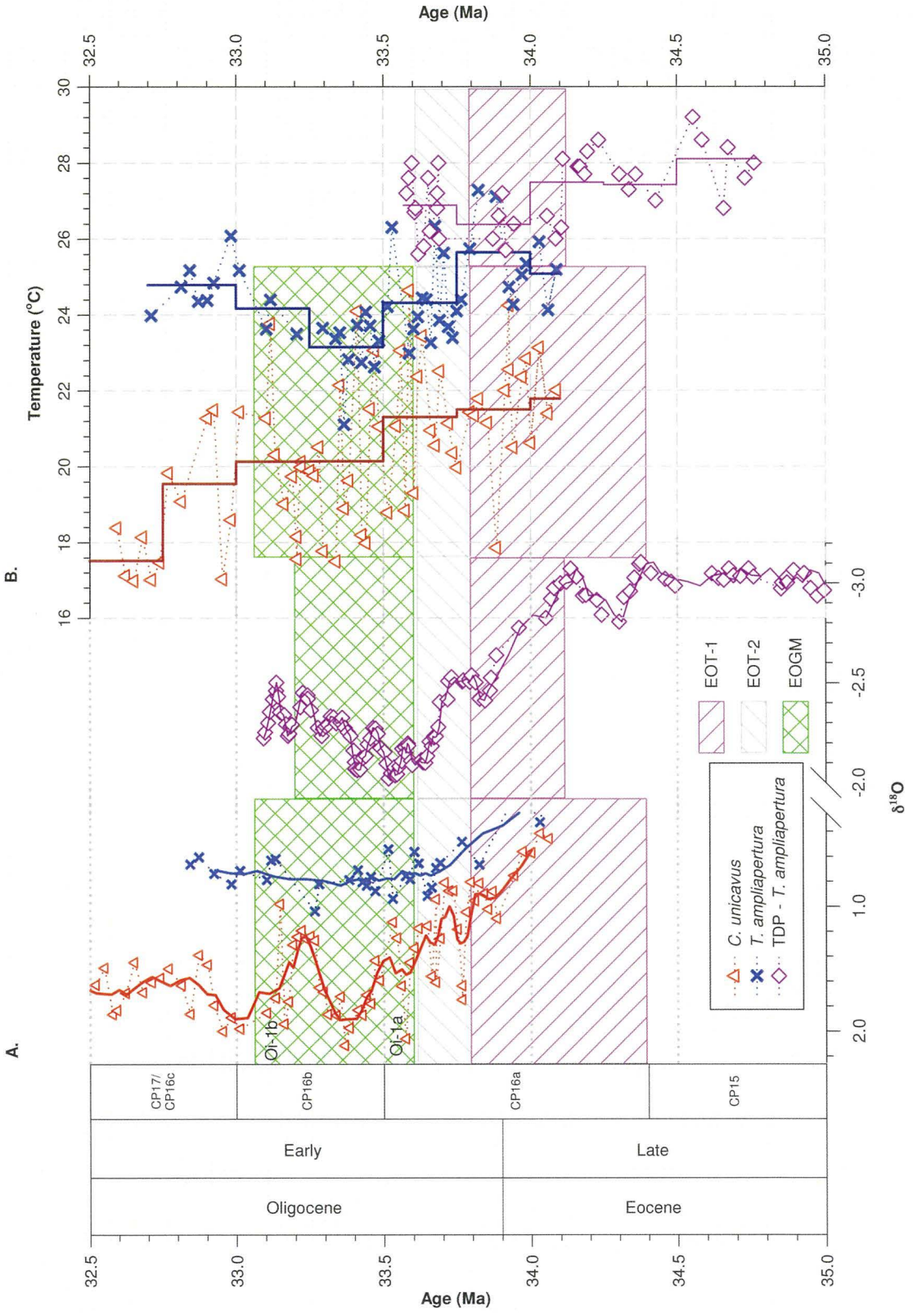

Figure 6.25: Comparison plot of Site 1211 planktonic foraminiferal data with published *T. ampliapertura* $\delta^{18}O$ (A.) and Mg/Ca palaeotemperature estimates (B.) of Lear et al. (2008) and Pearson et al. (2008), calculated using the Anand et al. (2004) calibration and seawater Mg/Ca of 4.3 mol/mol. Mg/Ca palaeotemperature estimates for equivalent ages were limited, but suggest that Site 1211 was at least 1 °C cooler than TDP 12/17 during EOT-1 and ~2 °C cooler during EOT-2.The positive offset of Site 1211 planktonic foraminiferal $\delta^{18}O$ compared to those from TDP and the homogenisation of Site 1211 *T. ampliapertura* records suggests that the planktonic foraminifera have a significant contribution from secondary carbonate (See Section 6.1).

Comparison of $\delta^{18}O$ values from Site 1211 and TDP 12/17 in Section 6.2.4 (Figure 6.10 and 6.25) revealed Site 1211 *T. ampliapertura* $\delta^{18}O$ were positively offset by ~3 ‰. A 3 ‰ difference of $\delta^{18}O$ equating to Site 1211 surface-temperatures being ~12 °C cooler than TDP 12/17, however, Mg/Ca palaeotemperatures indicate a temperature difference of between 1 and 2 °C. The disagreement in the relative differences in surface-water temperatures between Site 1211 and TDP 12/18 predicted by Mg/Ca palaeotemperatures and $\delta^{18}O$ values indicates that a further influence is present within the Site 1211 records. The most likely influence would seem to be preservation (as discussed in Section 6.2.4), neomorphism of planktonic foraminiferal carbonate has been observed to offset $\delta^{18}O$ to more positive values and increase Mg/Ca palaeotemperatures by a few degrees relative to the values suggested by "glassy" specimens (Sexton et al., 2006). Section 6.1.5 described that the planktonic foraminifera from Site 1211 had experienced significant neomorphism, and so the cooler palaeotemperature predicted by the $\delta^{18}O$ compared to Mg/Ca palaeotemperatures is in agreement with the observation of Sexton et al. (2006). The prediction of relatively low sea-surface temperatures at Site 1211 from diagenetically altered planktonic foraminifera, compared to unmodified specimens of Lear et al. (2008) and palaeotemperatures estimates derived from alkenone-based thermometry (Liu et al., 2009), adds further weight to the argument that the so-called "cool-tropics" paradox for the warmer Cenozoic worlds results can be explained by diagenesis (Section 6.1.3; Pearson et al., 2001).

6.4.6 Carbonate ion control on Site 1211 Mg/Ca?

An aim of this study was to produce paired benthonic foraminiferal $\delta^{18}O$ and Mg/Ca records from a site that had experienced a much reduced CCD change and thus reduced increase in $\Delta[CO_3^{2-}]$ across the Eocene-Oligocene transition (Section 1.1). This aim was based on previous interpretation by Lear et al. (2004) of the Site 522 and 1218 palaeotemperature records; they observed a ~2 °C cooling at Site 522 associated with the first stage of the EOT and a ~2 °C warming associated with the second stage at both Sites 522 and 1218. Whilst the temperature decrease across the first stage of the EOT may reflect an intermediate water mass cooling at Site 522, Lear et al. (2004) hypothesised that the absence of cooling in the Site 1218 temperature record may result from the dramatic increase in deep water $\Delta[CO_3^{2-}]$. Benthonic foraminiferal Mg/Ca ratios were observed to show a greater rate of decrease in cold deep waters with low $\Delta[CO_3^{2-}]$ than expected from the temperature dependence alone (Martin et al., 2002; Elderfield et al., 2006). Using the

departure from the exponential relationship in deep waters of Martin et al. (2002), Lear et al. (2004) suggest that the ~1 km deepening of CCD would lead to an increase in $\Delta[CO_3^{2-}]$ that would increase foraminiferal Mg/Ca by ~20 %, i.e. an amount equivalent to 2 °C, obscuring the cooling observed at Site 522 in the Site 1218 records. However, the CCD deepening at Site 1218 occurred "lock-step" with two-stage increase in benthonic foraminiferal $\delta^{18}O$ (Coxall et al., 2005; Section 6.2.3 and 6.4.4), which would indicate that any increase in $\Delta[CO_3^{2-}]$ occurred over both stages rather than just over the first step of the EOT. Neither would it fully explain the warming over the second step of the EOT observed at Sites 522 and 1218, thus the carbonate ion saturation hypothesis does not fully explain observations of Mg/Ca palaeotemperatures and their relationship to the CCD.

Benthonic foraminiferal Li/Ca and Zn/Ca have both been observed to demonstrate relationships with $[CO_3^{2-}]$ (Marchitto et al., 2000; 2002; Lear and Rosenthal, 2006) and attempts were made to measure these ratios to provide a carbonate ion constraint. Determination of these records was unsuccessful (see Section 3.6) so comparison of Site 1211 Mg/Ca palaeotemperatures with CCD variation is the only method available to consider the carbonate ion saturation hypothesis. The low number of determinations prior to the EOB and the scatter precludes correlation of Mg/Ca palaeotemperatures with the transient CCD shoaling identified in Section 6.3.2, i.e. at 35.8 or 37.2 Ma (see Figure 6.12), average values remaining virtually constant throughout (Section 6.4.4; Figure 6.23). Figure 6.26 shows Mg/Ca palaeotemperature estimates with the proxies for the CCD, (see Section 6.3.1/2) to allow identification of any relationships between the two records. During the CCD deepening average Mg/Ca palaeotemperatures do not show any clear deviation from the variation observed throughout the Eocene, although, as previously discussed, estimates display a high degree of scatter. Average palaeotemperatures increase by ~1 °C above Eocene levels during the earliest Oligocene, after the significant increase in CCD proxies has terminated. The relationship of an increase in Mg/Ca palaeotemperatures after the CCD deepening had terminated, indicates that the warming is unlikely to have occurred as a result of increasing $\Delta[CO_3^{2-}]$, as bottom waters are likely to have been supersaturated after 34.0 Ma. Thus, the observation of an increase in Mg/Ca ratios appears to be a real increase in bottom-water temperature. Across the CCD deepening, the relationship between Mg/Ca palaeotemperature and increasing $\Delta[CO_3^{2-}]$ is ambiguous, the scatter and low number of determinations preventing clear identification of the temperature change from the late Eocene (~35.0 Ma) across the CCD deepening (34.5

to 34.0 Ma). Palaeotemperature variation typical of the Eocene as a whole suggests no significant change in bottom-water temperatures.

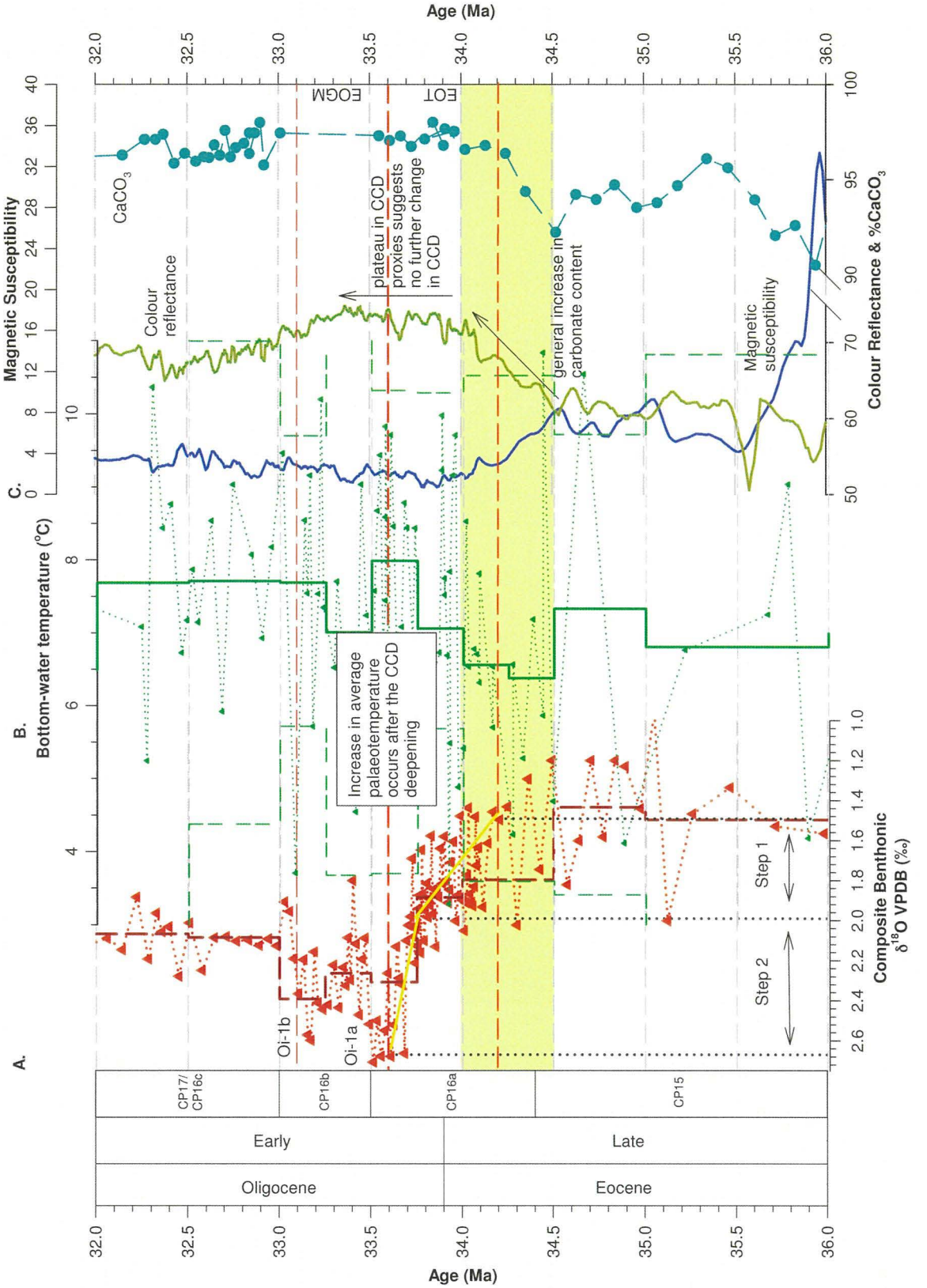

Figure 6.26: Comparison plots of benthonic foraminiferal $\delta^{18}O$ (A.), bottom-water temperature with time-averaged values and ±95 % (±2σ) confidence intervals (B.) and CCD proxies (C.). Yellow shaded area shows the interval of CCD deepening identified in Section 6.3.2, whilst red dashed lines correspond to the EOT and EOGM identified in Section 6.2.1. The increase in average Mg/Ca palaeotemperatures occurs following the deepening of the CCD, indication that the temperature increase was unlikely to be related in increase in bottom-water carbonate ion saturation.

Interpretation of Site 1211 records across the EOB is therefore similar to that of Lear et al. (2004) for Site 1218 (described above), and could be taken to support the presence of a $\Delta[CO_3^{2-}]$ effect. Section 6.3.4, however, indicated that CCD and therefore $\Delta[CO_3^{2-}]$ variation at Site 1211 was much reduced compared to Site 1218 and hypothesised that any $\Delta[CO_3^{2-}]$ effect would be less. Interpretation of the Site 522 and 1218 records in Section 6.4.3 also indicated that both sites experienced a similar average bottom-water temperature increase across the EOT to Site 1211 (Figure 6.24), despite apparent differences in $\Delta[CO_3^{2-}]$ as indicated by the different carbonate sedimentation at the sites (e.g. Figure 6.15; Shipboard Scientific Party, 1984; Zachos et al., 1996). The interpretation in Figure 6.24 also shows Site 1218 to have the temperature decrease observed by Lear et al. (2000) for Site 522, although the decrease is partially obscured by the hiatus, which perhaps questions a central feature of the argument for a $\Delta[CO_3^{2-}]$ control. The presence of a cooling at Site 1218 would suggest that the increase in $\Delta[CO_3^{2-}]$ did not obscure the bottom-water temperature decrease observed at Site 522, and therefore that the $\Delta[CO_3^{2-}]$ increase is not a significant control on Mg/Ca at Site 1218. The Mg/Ca record prior to and across the CCD deepening being insufficiently constrained for Site 1211 to identify a temperature decrease, rather than absence of cooling indicating a definite $\Delta[CO_3^{2-}]$ effect. The degree of covariation between the sites does argue for the effect of changing $\Delta[CO_3^{2-}]$ being limited in the deep-water Mg/Ca ratios, and thus that the palaeotemperature increase is "real".

Other evidence argues that the *O. umbonatus* Mg/Ca palaeotemperature records do not reflect a changing $\Delta[CO_3^{2-}]$. Elderfield et al. (2006) observe a reduced influence on Mg/Ca of infaunal as opposed to epifaunal benthonic foraminiferal species, whilst Rathmann and Kuhnert (2008) note no effect from either $[CO_3^{2-}]$ or $\Delta[CO_3^{2-}]$ on *O. umbonatus* Mg/Ca. The reduction in effect of $\Delta[CO_3^{2-}]$ hypothesised to result from pore-waters equilibrating quickly to reduced $\Delta[CO_3^{2-}]$ to saturation (Elderfield et al., 2006), thus changing bottom-water $\Delta[CO_3^{2-}]$ has little effect on the pore-water chemistry in which epifaunal foraminifera calcify in. As described previously, however, benthonic foraminifera appear to show a high degree of natural scatter in Mg/Ca (Rathmann et al., 2004; Rathmann and Kuhnert, 2008; Yu and Elderfield, 2008), which does not seem to be related to either temperature or $(\Delta)[CO_3^{2-}]$. Until greater understanding of the influences on the natural scatter is achieved, Cenozoic benthonic foraminiferal Mg/Ca ratios must be viewed with some caution. However, the above described covariation indicates that temperature was the predominant effect on benthonic foraminiferal Mg/Ca and so the relative records can be

viewed as accurate. The similarity between published sites and Site 1211 suggests that the assumption that temperature was the dominant control, beneath the scatter (see Section 6.4.3), was reasonable. Thus, Site 1211 Mg/Ca palaeotemperatures can be used to determine $\delta^{18}O_{sw}$ values to assess the magnitude of ice sheet development at the EOB.

6.5 $\delta^{18}O_{sw}$ Estimations

As discussed in Section 2.2.1, foraminiferal $\delta^{18}O$ is primarily dependent on the temperature of calcification and the $\delta^{18}O_{sw}$, the latter variable being controlled by the extent of global ice-volume and salinity, although salinity is likely to have minor effects in the deep-ocean. Paired foraminiferal $\delta^{18}O$ and Mg/Ca palaeotemperature estimates provide the most promising method of constraining changes in $\delta^{18}O_{sw}$ across the EOB (See Section 2.2.4). The $\delta^{18}O_{sw}$ component of foraminiferal $\delta^{18}O$ can be derived using a rearranged $\delta^{18}O$-palaeotemperature equation (Equ 6.5) using the Mg/Ca palaeotemperatures estimated in Section 6.4.

$$\delta^{18}O_{sw} = (T - 16.5 + 4.8 * \delta^{18}O_{planktic}) / (4.8 + 0.27) \quad \textbf{Equ. 6.5}$$

The $\delta^{18}O$-palaeotemperature equation of Bemis et al. (1998) has been used to calculate $\delta^{18}O_{sw}$ for Site 1211 benthonic and planktonic foraminifera. The Bemis equation was developed through laboratory based culture studies on the planktonic foraminifera *O. universa*, and has been demonstrated to provide close approximations of calcification temperatures for plankton-tow and core-top assemblages. The equation also predicts *Cibicidoides* spp. calcification temperatures; Duplessy et al. (2002) observed a relationship similar to that determined for *Uvigerina* spp. by Shackleton (1974) once the *Cibicidoides* data had been corrected to equilibrium. Correction to equilibrium is unnecessary at Site 1211 as *O. umbonatus*, the predominant species used in the composite benthonic foraminiferal stable-isotope records calcifies in equilibrium to sea-water $\delta^{18}O$ (Shackleton et al., 1984). Use of the Bemis et al. (1998) $\delta^{18}O$-temperature calibration leads to $\delta^{18}O_{sw}$ estimations offset by an average of 0.5 ‰ ±0.14 (±2σ) relative to the alternative benthonic foraminiferal equation of Shackleton (1974), but a similar pattern to $\delta^{18}O_{sw}$ evolution. Absolute magnitude of the $\delta^{18}O_{sw}$ estimates depends on the Mg/Ca temperature; however, relative changes over short time intervals (<1 Myrs) should be robust and reflect palaeoceanographic change allowing quantification of the extent of ice-volume.

6.5.1 Site 1211 $\delta^{18}O_{sw}$

$\delta^{18}O_{sw}$ for both benthonic and planktonic foraminifera has been calculated from paired analyses, i.e. sample depths with both $\delta^{18}O$ and Mg/Ca palaeotemperatures, from $\delta^{18}O$ and Mg/Ca palaeotemperatures interpolated at a 50 kyr spacing and for time-averaged means

(see Section 6.4.4). Interpolation of Mg/Ca and $\delta^{18}O$ values at a 50 kyr spacing used the "Interp" program of Howell et al. (2006), estimating the values of a datapoint using a linear relationship between the two nearest datapoints; this method was used by Lear et al. (2004) and Katz et al. (2008) to produce $\delta^{18}O_{sw}$ estimations. Whilst the paired analysis approach allows direct quantification of $\delta^{18}O_{sw}$, in practice the high degree of scatter present within the Mg/Ca palaeotemperatures (see Section 6.4.3) leads to highly variable $\delta^{18}O_{sw}$ estimations. Examples of the effect of the Mg/Ca palaeotemperature scatter can be seen in Figure 6.27A at 33.0 and 31.2 Ma, where $\delta^{18}O_{sw}$ values appear to decrease sharply relative to surrounding interpolated or mean values. These two decreases in $\delta^{18}O_{sw}$ are related to low palaeotemperature estimates from the foraminiferal Mg/Ca ratio record, and thus are likely to be artefacts of the scatter. Paired analyses were also limited especially between 36.5 and 34.2 Ma, limiting quantification of $\delta^{18}O_{sw}$ change across the interval and the EOB. However, both interpolated and time-averaged estimates allow the calculation of $\delta^{18}O_{sw}$ across the interval covered in this study. Considering Figure 6.27, time-averaged $\delta^{18}O_{sw}$ offer the clearest record of bottom-water $\delta^{18}O_{sw}$ change across the studied interval, and are thus used to interpret changes in $\delta^{18}O_{sw}$. Interpolated $\delta^{18}O_{sw}$ values suggesting cyclic variation of $\delta^{18}O_{sw}$ throughout the Middle and Late Eocene would require repeated waxing and waning of continental scale ice sheets, such variation has not been identified in previous studies (e.g. Lear et al., 2004, Coxall et al., 2005) but can be explained by the limited number and scatter in the foraminiferal Mg/Ca ratios measured.

Three features stand out from the time-averaged $\delta^{18}O_{sw}$ record; first of all there is an increase in $\delta^{18}O_{sw}$ during the Middle Eocene of ~0.5 ‰, secondly, Late Eocene $\delta^{18}O_{sw}$ is essentially constant and thirdly, there is a major increase in $\delta^{18}O_{sw}$ across the EOT. Increase in bottom-water $\delta^{18}O_{sw}$ during the Middle Eocene questions that the interpretation made in Section 6.2.1 of benthonic foraminiferal $\delta^{18}O$ increase during the Middle Eocene. In Section 6.2.1, benthonic foraminiferal $\delta^{18}O$ increase during the Middle Eocene was identified as a bottom-water temperature decrease (Figure 6.4), however, the $\delta^{18}O_{sw}$

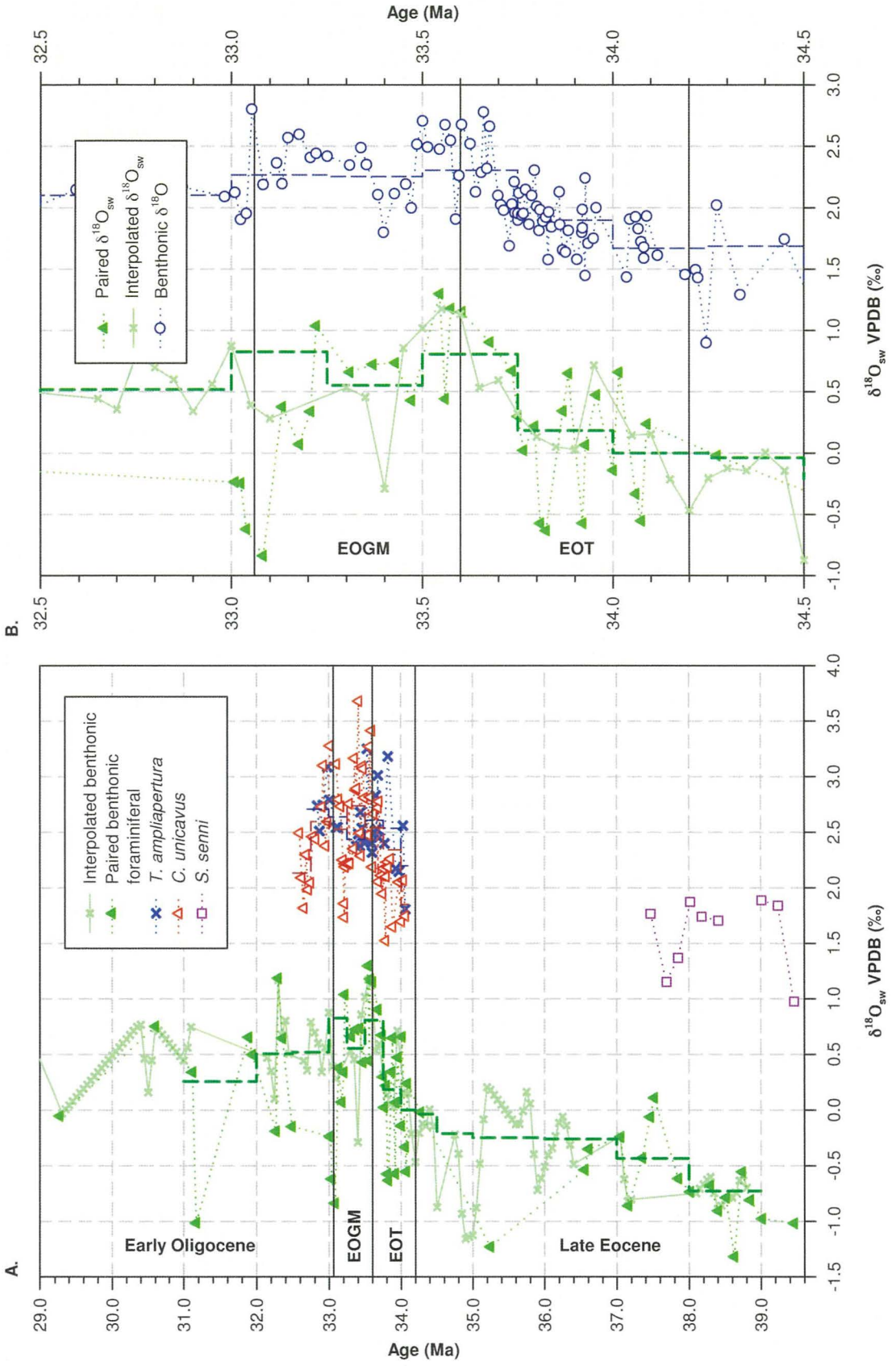
B.
Age (Ma)
32.5
33.0
33.5
34.0
34.5
Paired $\delta^{18}O_{sw}$
Interpolated $\delta^{18}O_{sw}$
Benthonic $\delta^{18}O$
EOGM
EOT
$\delta^{18}O_{sw}$ VPDB (‰)
3.0
2.5
2.0
1.5
1.0
0.5
0.0
-0.5
-1.0
A.
Interpolated benthonic
Paired benthonic foraminiferal
T. ampliapertura
C. unicavus
S. senni
Early Oligocene
EOGM
EOT
Late Eocene
29.0
30.0
31.0
32.0
33.0
34.0
35.0
36.0
37.0
38.0
39.0
Age (Ma)
$\delta^{18}O_{sw}$ VPDB (‰)
4.0
3.5
3.0
2.5
2.0
1.5
1.0
0.5
0.0
-0.5
-1.0
-1.5

Figure 6.27: $\delta^{18}O_{sw}$ estimations across the studied stratigraphic interval (39.6 to 29 Ma) from benthonic and planktonic foraminifera (A.) and an expanded Eocene/Oligocene transition section including benthonic foraminiferal $\delta^{18}O$. Dashed lines indicate $\delta^{18}O_{sw}$ calculated from time-average Mg/Ca and $\delta^{18}O$ values. Time-averaged benthonic foraminiferal $\delta^{18}O_{sw}$ indicates there was a ~1.2 ‰ increase, average with Oligocene values being >0.7 ‰ greater than average Eocene values. Both paired and interpolated $\delta^{18}O_{sw}$ values are compromised by the high degree of scatter in the Mg/Ca palaeotemperature estimations. Both records display in variation in $\delta^{18}O_{sw}$ suggesting a highly dynamic continental ice sheet that has not been identified from either previous paired proxy studies or sea level estimations across the Late Eocene and Early Oligocene (Pekar et al., 2002; Lear et al., 2004; Coxall et al., 2005). Due to the unavailability of latest Eocene samples, surface water $\delta^{18}O_{sw}$ variation across the EOB has not been determined. The timing and duration of the EOT and EOGM are those identified in Section 6.2.1.

records indicate that the increase was not the result of cooling. Similar Middle Eocene increase in $\delta^{18}O_{sw}$ is also observed by Billups and Schrag (2003) from two sites, Site 689 and 757 in the Weddell Sea and sub-tropical Indian Ocean respectively, which would suggest a global increase in $\delta^{18}O_{sw}$ from ~40 Ma. A global increase in $\delta^{18}O_{sw}$ would indicate the change was a result of the growth of continental ice prior to the EOB. Evidence from clay mineral assemblages of a shift in Antarctic weathering to a cooler physical regime at ~40 Ma could be interpreted as support for the initiation of Antarctic glaciation (Zachos et al., 1999). A caveat to the interpretation of the $\delta^{18}O_{sw}$ increase during the Middle Eocene is the seawater Mg/Ca ratio, a single seawater Mg/Ca ratio being assumed in both this study and Billups and Schrag (2003) despite the study intervals duration being longer than the oceanic residence time of Ca (~1 Myr). Seawater Mg/Ca ratios are discussed in Section 6.4.1 (Figure 6.16) where the wide range of estimates for Cenozoic seawater Mg/Ca are described. An increase in seawater Mg/Ca during the Middle Eocene could account for the absence of a temperature change and thus introduce a $\delta^{18}O_{sw}$ artefact. A detailed record of surface water $\delta^{18}O_{sw}$ over the Middle Eocene could allow further constraint of any seawater Mg/Ca or global $\delta^{18}O_{sw}$ variation, however, the low-resolution planktonic foraminiferal $\delta^{18}O_{sw}$ record from Site 1211 is ambiguous. Further planktonic foraminiferal determinations are required to clarify the surface water record. $\delta^{18}O_{sw}$ – ice-volume equivalence is discussed in Section 6.5.3, but the addition of a further 0.5 ‰ increase in the ice-volume inventory prior to the EOB has significant implications for global ice-sheet extent.

Average $\delta^{18}O_{sw}$ and hence ice volumes remain constant throughout the Late Eocene, following the typical interpretation of the benthonic foraminiferal $\delta^{18}O$ record (Zachos et al., 2001). The need to time-average Site 1211 data, however, obscures any transient glaciations such as those suggested by Tripati et al. (2005) at ~39 and ~36 Ma. EOT

increase in $\delta^{18}O_{sw}$ at Site 1211 indicates all of the benthonic foraminiferal $\delta^{18}O$ increase results from ice volume, with time averaged $\delta^{18}O_{sw}$ values increasing by ~1.25 ‰ (interpolated values by >1.5 ‰). The increase in $\delta^{18}O_{sw}$ of ~1.25 ‰ is greater than the two estimates of ~0.9 and ~1.0 ‰ made in Section 6.2, using either benthonic foraminiferal $\delta^{18}O$ and assumptions relating to bottom-water temperatures (Section 6.2.1) or the maximum covariation of $\delta^{18}O$ between planktonic and benthonic foraminiferal (Section 6.2.2). The difference primarily accountable for by the warming of ~1 °C identified in Mg/Ca palaeotemperature records masking a ~0.25 ‰ increase in benthonic foraminiferal $\delta^{18}O$ and the absence of the initiation of the EOT in planktonic foraminiferal records. Post Oi-1a, $\delta^{18}O_{sw}$ values decrease gradually by ~0.3 ‰, with Early Oligocene values varying ~0.9 ‰ above typical Eocene values. The ~0.9 ‰ more positive $\delta^{18}O$ of the Oligocene compared to the Eocene indicates that Antarctica remained glaciated following the EOGM. Time-averaged increase in the planktonic foraminiferal records were much less at ~0.5 ‰, although absolute changes were ~1.0 ‰. The reduction in magnitude partially results from the absence of pre-EOT Late Eocene determinations but also may reflect changes in surface water salinity, as both planktonic foraminiferal records show post Oi-1a maxima in $\delta^{18}O_{sw}$ and little relationship to bottom-water $\delta^{18}O$ (as was observed for foraminiferal $\delta^{18}O$ in Section 6.2.2).

Surface water $\delta^{18}O_{sw}$, have been calculated for the Middle Eocene and Early Oligocene, however, change in surface-water $\delta^{18}O_{sw}$ across the EOB has not been identified due to an absence of Late Eocene determinations, thus comparison with the evolution of deep-water $\delta^{18}O_{sw}$ has not been possible. Both Middle Eocene and Early Oligocene surface-water $\delta^{18}O_{sw}$ were ~2 ‰ more positive than values for bottom-waters. The significance of the offset is uncertain, possibly reflecting a salinity difference between surface and deep-waters. As previously discussed, latitudinal salinity gradients of ~2-3 ‰ have been observed in the modern ocean (Broecker, 1989; Zachos et al., 1994) leading to elevated $\delta^{18}O_{sw}$ at low-latitudes and vice-versa. Assuming a modern-day type circulation, i.e. deep-waters form at high-latitudes and sink to fill the deep ocean, then such a salinity gradient could explain the observed difference in $\delta^{18}O_{sw}$. A salinity effect could be combined with the effects of diagenesis, the presence of neomorphic carbonate in the planktonic foraminiferal test leading to more positive $\delta^{18}O$ (Schrag et al., 1992, 1995; Sexton et al., 2006). Site 1211 planktonic foraminifera displayed pervasive neomorphism (Section 6.1.3), so $\delta^{18}O$ values were likely to be shifted to more positive values. An offset of ~3.0

‰ was observed between Site 1211 and TDP *T. ampliapertura* $\delta^{18}O$ records (Section 6.2.4 and 6.4.5), the offset suggesting either unrealistically cool surface waters at Site 1211 or low salinities at TDP. A positive 2 ‰ neomorphic shift would reconcile the $\delta^{18}O$ ratios, suggesting a more reasonable ~4 °C or 2 ‰ salinity difference between the subtropical Site 1211 and tropical TDP. Neomorphism would also attenuate the $\delta^{18}O$ shift in planktonic foraminifera (Schrag et al., 1992; 1995), possibly explaining the differences in planktonic and benthonic foraminiferal EOT $\delta^{18}O_{sw}$ magnitude.

6.5.2 Comparison of estimates of changing $\delta^{18}O_{sw}$ across the EOB

$\delta^{18}O_{sw}$ estimations for published Mg/Ca palaeotemperature and benthonic foraminiferal $\delta^{18}O$ values were calculated for Sites 522, 1218 and SSQ using the data discussed in Section 6.2.3 and 6.4.5 respectively. Records for Site 522 and 1218 were determined using Mg/Ca palaeotemperatures and $\delta^{18}O_{bf}$ values interpolated from the original dataset at 50 kyr resolution using the "Interp" program (Howell et al., 2006, see above), whilst SSQ $\delta^{18}O_{sw}$ were calculated from paired values. Time-averaged $\delta^{18}O_{sw}$ were then calculated using the method described in Section 6.4.4 and are plotted with equivalent values for Site 1211 in Figure 6.28 to allow comparison.

The key aspects of Figure 6.28 are the $\delta^{18}O_{sw}$ increases across the EOB, i.e. from the minimum values in the latest Eocene to the maximum EOGM values, and the similar pattern of $\delta^{18}O_{sw}$ evolution at Sites 1211 and 522. Time-averaged $\delta^{18}O_{sw}$ increases at Site 1211 was the lowest of the deep-water sites at ~1.25 ‰, compared to Site 522 at ~1.4 ‰ and Site 1218 at ~1.5 ‰, but much greater than the time-averaged increases observed from the hemipelagic SSQ and TDP that increase by ~0.8 and ~0.6 ‰ respectively. The average $\delta^{18}O_{sw}$ from the hemipelagic sites being remarkably similar to the ~0.7 ‰ maximum modelled by DeConto et al. (2008), although SSQ values show much greater absolute variability (up to ~1.2 ‰). The large discrepancy in $\delta^{18}O_{sw}$ increase partially reflects the time-averaging method, i.e. the averaging interval is much longer than the duration of the maximum ~1.2 ±0.3 ‰ increase at SSQ. The similarity in deep-water Mg/Ca palaeotemperature estimates was taken to indicate that carbonate ion saturation was not a significant control on deep-water benthonic foraminiferal Mg/Ca (Section 6.4.6), so the reduced magnitude of hemipelagic records suggests that local changes in hydrography are

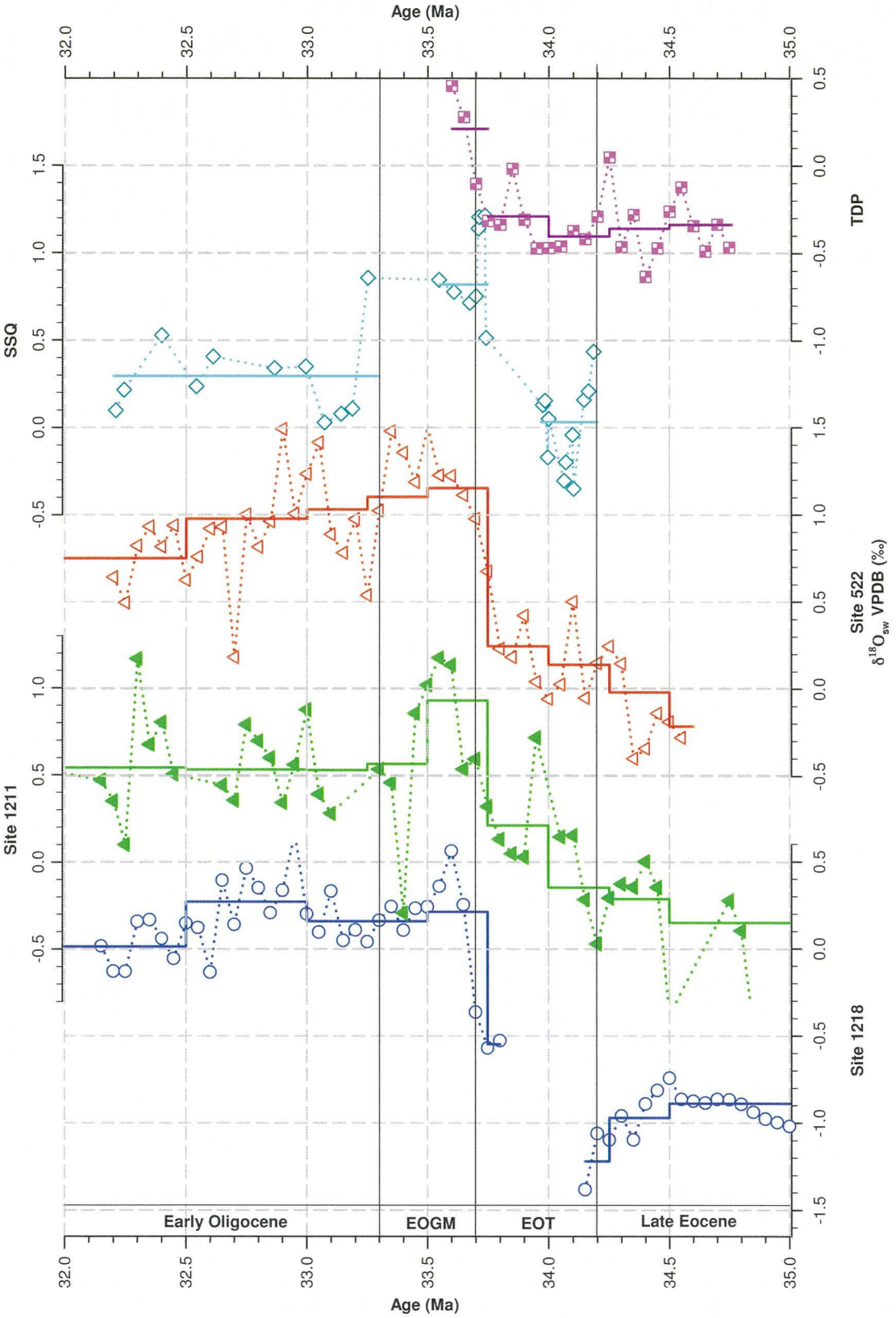

Figure 6.28: $\delta^{18}O_{sw}$ estimates for ODP Site 522 (Southern Atlantic), 1211 (tropical Pacific) and 1218 (Equatorial Pacific), St Stephens Quarry (SSQ), Alabama (Gulf of Mexico) and TDP 12/17 (tropical Indian Ocean). The three deep-water sites, Sites 522, 1211 and 1218, all show similar $\delta^{18}O_{sw}$ evolutions and magnitudes across the EOB, and approximately twice increase observed in the hemipelagic SSQ and TDP records. Estimates for Site 522 and 1218 were calculated using the palaeotemperature equation of Bemis et al. (1998) using the method described in Section 6.5.2 using the data of Zachos et al. (1996), Lear et al. (2000), Lear et al. (2004) and Coxall et al. (2005). $\delta^{18}O_{sw}$ for SSQ and TDP are those calculated by Katz et al. (2008) and Lear et al. (2008) respectively. EOT and EOGM intervals are those identified from the published datasets (see Section 6.2.3)

influencing the records. The atypical development of the $\delta^{18}O$ shift across the EOT and EOGM at SSQ may suggest that bottom water evolution at the site was not representative of the global ocean (Section 6.2.4).

Considering the two complete deep-ocean records, i.e. Sites 1211 and 522, then the increase in $\delta^{18}O_{sw}$ appears to have occurred relatively equally over the two phases of the EOT, with a more gradual first stage of increase over 300 to 400 kyr and a more abrupt second stage over <150 kyr. Following maximum $\delta^{18}O_{sw}$ values, there is then a decline through the termination of the EOGM and into the early Oligocene at Sites 1211 and 522, indication the ~1.0 ‰ increase in Oligocene $\delta^{18}O$ relative to Eocene $\delta^{18}O$ results from a sustained, if less extreme, continental glaciation.

6.5.3 Estimation of sea level change and ice volume from Site 1211.

In Section 6.4.6, Site 1211 was determined to have a geochemical record with minimal influence from carbonate ion saturation changes and $\delta^{18}O_{sw}$ increase is similar to the average estimated by Katz et al. (2008) for carbonate ion saturation corrected deep-water sites. Thus, the Site 1211 $\delta^{18}O_{sw}$ record is used to determine the increase in ice-volume and consider sea level changes across the EOT. $\delta^{18}O_{sw}$ to sea level calibrations have been determined for the Pleistocene with a $\delta^{18}O$ increase of 0.11 ‰ per 10 m sea-level fall (Fairbanks and Matthews, 1978) and for the Oligocene by comparison of backstripping of Oligocene sediments and benthonic $\delta^{18}O$ change to between 0.10 to 0.13 ‰ per 10 m sea level fall (Pekar et al., 2002). As the Pleistocene calibration falls within the range of the Oligocene calibration, the latter calibration range has been used to provide an estimate of the sea-level fall indicated by a ~1.25 ‰ increase in $\delta^{18}O_{sw}$ at Site 1211. The time-averaged increase of 1.25 ‰ at Site 1211 corresponds to a sea-level fall of between ~100 and 125 metres. Site 1211 post-EOGM Oligocene $\delta^{18}O_{sw}$ values were ~0.9 ‰ greater than the Eocene, indicating that Oligocene sea levels were between 70 and 90 metres lower than the Eocene.

Estimates of sea level variation have been developed from backstripping of Oligocene sedimentary sequences from the New Jersey continental margin (Figure 6.29; Kominz and

Pekar, 2001; Pekar et al., 2002). Correcting for the isostatic loading of the crust by multiplying eustatic estimates by 1.48 (Kominz and Pekar, 2001), an apparent sea level decrease of ~100 m from the Eocene to the EOGM was identified, i.e. at the lowest end of estimates of sea level change suggested by the Site 1211 $\delta^{18}O_{sw}$ increase. The relationship of Site 1211 $\delta^{18}O_{sw}$ change to the apparent sea level changes identified from the New Jersey margin therefore indicates a 0.13 ‰ per 10 m water depth change, i.e. inline with the maximum estimates of Pekar et al. (2002) and similar to the 0.12 ‰ per 10 m of Katz et al. (2008).

Figure 6.29 shows the Site 1211 bottom-water $\delta^{18}O_{sw}$ record with the apparent sea level estimates determined from backstripping and benthonic foraminiferal depth facies from the New Jersey Margin (Kominz and Pekar, 2001; Pekar et al., 2002). Despite the scatter in the Site 1211 record, there is a broad correlation between Site 1211 $\delta^{18}O_{sw}$ and the New Jersey margin throughout the Oligocene, assuming a $\delta^{18}O_{sw}$–sea level calibration of 0.13 ‰ per 10 m. The only exception to the correlation is at ~32.7 Ma, where the New Jersey record suggests a significant high-stand, yet Site 1211 records suggest relatively constant $\delta^{18}O_{sw}$. Lear et al. (2004) also observed a mismatch between $\delta^{18}O_{sw}$ and apparent sea level at ~32.7 Ma, indicating the mismatch is a Pacific wide feature. The reason for the mismatch is uncertain with the <1 Myr duration suggesting that the New Jersey sea level change did not result from tectonoeustacy but $\delta^{18}O_{sw}$ ruling out glacioeustacy (Lear et al., 2004; Miller et al., 2005).

Estimations of the EOGM and Oligocene ice-volume growth and ice sheet $\delta^{18}O$ can be made using a simple mass balance equation and assumptions regarding the $\delta^{18}O$ isotopic composition and volume of the pre-glacial ocean (Coxall et al., 2005; Katz et al., 2008; Lear et al., 2008). The equation and approach described below replicates the results of Coxall et al. (2005) and Lear et al. (2008), if the $\delta^{18}O_{sw}$ variation from these studies is used to calculate the Oligocene $\delta^{18}O_{sw}$. The mass balance equation is of the form

$$(OV_{Eocene} * \delta^{18}O_{sw}^{Eocene}) + (IV_{Eocene} * \delta^{18}O_{ice}) = (OV_{Oligo} * \delta^{18}O_{sw}^{Oligo}) + (IV_{Oligo} * \delta^{18}O_{ice})$$

Equ. 6.6

Where OV is the ocean volume and IV is the ice volume for the Eocene and Oligocene. The values used within the equation are those of Shackleton and Kennett (1975), where OV_{Eocene} was $1380*10^6$ km^3, $\delta^{18}O_{sw}{}^{Eocene}$ is -1.2 ‰, OV_{Oligo} was $1360*10^6$ km^3. $\delta^{18}O_{sw}{}^{Oligo}$ was the Eocene value with the EOGM or Oligocene shift in $\delta^{18}O_{sw}$ from this study added, i.e. 1.25 and 0.9 ‰ for the EOGM and Oligocene respectively. The assumption is made that Eocene ice volume was insignificant, whilst both IV_{Oligo} and $\delta^{18}O_{ice}$ are unknown. A series of IV_{Oligo} were calculated by assuming $\delta^{18}O_{ice}$ values range from that of modern day Antarctica (~-50 ‰, Shackleton and Kennett, 1975) through values of Greenland (~40 ‰, Blunier and Brook, 2001) to the values of -35 to -30 ‰ as modelled by DeConto and Pollard (2008; Table 6.3) and comparing the calculated volumes to the present day volume of Antarctic ice ($25.4 * 10^6$ km^3; Lythe et al., 2001). The $\delta^{18}O$ of Oligocene ice is uncertain, DeConto et al. (2008) used a water isotope tracer model to calculate earliest Oligocene Antarctic ice sheets had an average composition of -35 to -30 ‰, which would lead to bipolar glaciation with a $\delta^{18}O_{sw}$ increase of ~1.2 ‰. More positive Oligocene $\delta^{18}O_{ice}$ results from the assumption of lower latitudinal temperature gradients and thus reduced fractionation (Coxall et al., 2005). However, modelling simulations of the Eocene have not indicated latitudinal thermal gradients were substantially different to the modern day (Huber and Sloan, 2001), which would suggest modern $\delta^{18}O_{ice}$ values were attainable.

Table 6.3 shows the modelled ice-volume determined for Site 1211 and comparison to modern day and LGM Antarctic ice volume. Ice volumes calculated for the EOGM increase in $\delta^{18}O_{sw}$ were in excess of modern day with all $\delta^{18}O$ ice values, Oligocene $\delta^{18}O_{ice}$ of -70 ‰ required to restrict ice to modern day Antarctic levels. Predicted ice volumes were approximately equivalent to the maximum Antarctic ice volume during the Last Glacial Maximum (LGM) with ice $\delta^{18}O$ of -50 and -45 ‰. If $\delta^{18}O$ values of ice >-45 ‰ were used, then the ice volumes require contemporaneous Northern Hemisphere glaciation. Whilst there is limited evidence for a Northern Hemispheric glaciation, i.e. Eldrett et al. (2007), Tripati et al. (2008), there is no evidence for extensive glaciation away from Antarctica. As Site 1211 records indicate minimal influence from $\Delta[CO_3^{2-}]$, then the assumption of Antarctic ice sheet $\delta^{18}O$ more positive than ~-45 ‰ is not supported; thus Site 1211 records indicate that Oligocene $\delta^{18}O_{ice}$ was similar to modern day and ice volume was similar to the LGM during the EOGM. With ice sheet $\delta^{18}O$ of between -45 to -50 ‰, the Site 1211 records suggest a sustained ice-volume equivalent of up to 90 % of the modern Antarctic ice sheet. These ice volumes estimated for Site 1211 are in excess of

those modelled by DeConto and Pollard (2003) for the EOT, i.e. 20 x 10^6 km^3 or ~80 % of the modern day extent. However, DeConto and Pollard's study did not include any West Antarctic ice or the effect of West Antarctic ice buttressing the East Antarctic ice sheet, both of which would be likely to increase modelled ice volumes.

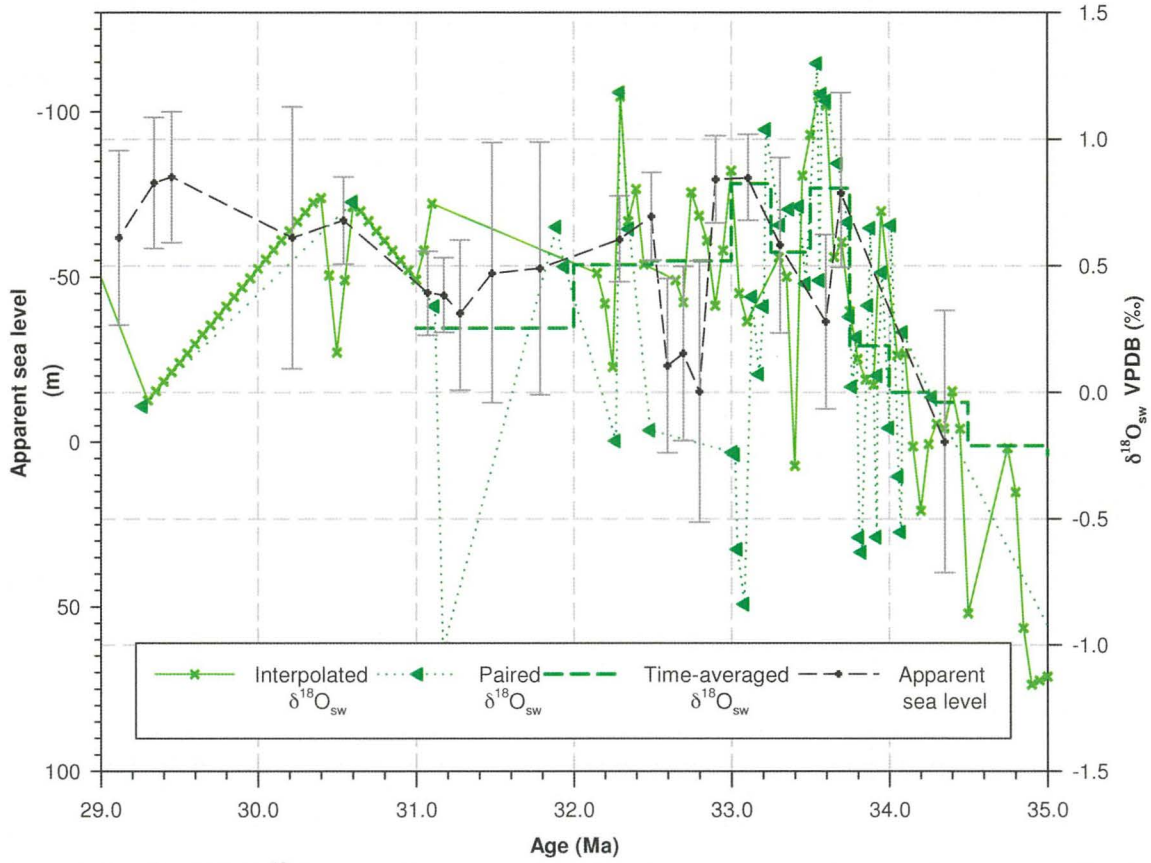

Figure 6.29: Site 1211 $\delta^{18}O_{sw}$ records compared to the apparent sea level curve of Kominz and Pekar (2001), i.e. eustatic changes multiplied by 1.48 to account for isostatic responses. Depth and $\delta^{18}O_{sw}$ scales are calibrated to a 0.13 ‰ per 10 m depth change as calculated for Site 1211. Site 1211 $\delta^{18}O_{sw}$ increase, when calibrated to 0.13 ‰ per 10 m sea level change, shows a broad correlation with the trends of the apparent sea level estimates. The Kominz and Pekar (2001) record has been interpolated on to the Gradstein et al. (2004) chronology to allow comparison with Site 1211, using the method described in Section 6.2.3.

Interval	Assumed composition of glacial ice $\delta^{18}O$ (‰)	Calculated ice volume (km^3)	% Modern Antarctic Ice sheet	% LGM Antarctic Ice Sheet
EOGM	-50	34.6 x 106	136	92
EOGM	-45	38.5 x 106	151	102
EOGM	-40	43.3 x 106	170	115
EOGM	-35	49.4 x 106	195	131
EOGM	-30	57.7 x 106	227	153
EOGM	-25	69.2 x 106	273	184
Oligocene	-50	20.9×10^6	82	67
Oligocene	-45	22.8×10^6	90	74
Oligocene	-40	25.1×10^6	99	83
Oligocene	-35	27.9×10^6	110	95
Oligocene	-30	31.4×10^6	123	111
Oligocene	-25	35.8×10^6	141	133

Table 6.3: EOGM and Oligocene ice volumes assuming a 1.25 and 0.9 ‰ increase in $\delta^{18}O_{sw}$ respectively from pre glacial $\delta^{18}O_{sw}$ of -1.2 ‰ (Shackleton and Kennett, 1975), using the mass balance equation (Equ. 6.6) and parameter values described above. Current and LGM ice volumes were taken as 25.4 x 10^6 and 37.7 x 10^6 km^3 (Lythe et al., 2001; Huybrechts, 2002).

Whilst the above changes describe the EOT increase in ice volume and $\delta^{18}O_{sw}$, a Middle Eocene increase in bottom-water $\delta^{18}O_{sw}$ was observed in Figure 6.27 and by Billups and Schrag (2003). If this increase in $\delta^{18}O_{sw}$ is attributable to ice volume growth then the ice volumes calculated in Table 6.3 are increased by more than a third, which would require Northern Hemisphere glaciation with even the most negative continental ice sheet $\delta^{18}O$. With the clear lack of evidence for such an extent of ice, there must be a further influence on the bottom-water Mg/Ca record. Until questions about Northern Hemisphere glaciation can be answered positively, records of $\delta^{18}O_{sw}$ can only be viewed as a broad approximation.

6.6 Site 1211 Synthesis

6.6.1 Cenozoic Shatsky Rise

Combining this studies benthonic foraminiferal stable-isotope ratio records with records from Site 1209 (Dutton et al., 2005) allows the compilation of a record of bottom-water evolution at Shatsky Rise throughout much of the Palaeogene (65 to 27 Ma). Dutton et al. (2005) determined stable-isotope values from a range of benthonic foraminiferal species throughout the Palaeocene, Early and Middle Eocene, which have been normalised to equilibrium values, i.e. to *O. umbonatus* for $\delta^{18}O$ and *Cibicidoides* spp. for $\delta^{13}C$, using the calibrations of Katz et al. (2003). Site 1211 benthonic foraminiferal compilation data was normalised using the offsets calculated earlier (see Section 5.6.3). Site 1209 rmcd depths were converted to numerical age using a depth–age model based on planktonic foraminifera and calcareous nannofossils biostratigraphy and the most recent geologic timescale (Figure 6.30; Gradstein et al., 2004; Bralower et al., 2005; Petrizzo et al., 2005), with depth-age relationships identified through selection of the best regression coefficients. The resulting dataset was compiled with that of Site 1211 and the 5-point running average through the dataset calculated (Figure 6.31).

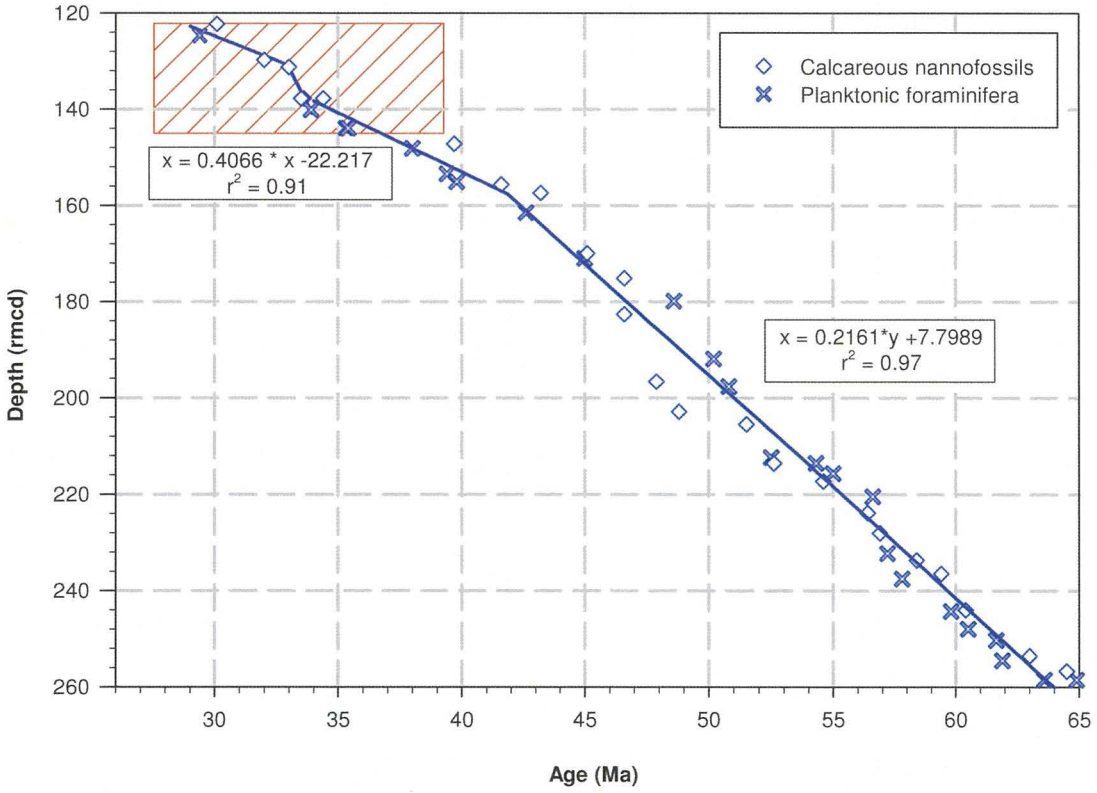

Figure 6.30: Depth–age relationship for Site 1209, Shatsky Rise based on correlation coefficients between calcareous nannofossil and planktonic foraminiferal biostratigraphies (Shipboard Scientific Party, 2002c; Bralower, 2005; Petrizzo et al., 2005). Red-hatched box indicates Site 1209 depth age model in Figure 6.13.

Shatsky Rise bottom-water stable-isotope chemistry follows the trends observed in the 5-point running average of the global compilation of Zachos et al. (2001; 2008), with Shatsky Rise data points typically falling within the global data cloud of the Zachos compilation. Short-term events, such as the Palaeocene/Eocene thermal maximum (PETM) at ~55.7 Ma or the isotope variation at ~41.0 Ma, are not recorded at Shatsky Rise due to the relatively low Palaeocene and Eocene sampling resolution (Dutton et al., 2005). Whilst the general trends are followed, Shatsky Rise $\delta^{18}O$ evolution departs from the global dataset with a positive excursion at ~51.0 Ma and a negative excursion between ~48.0 and ~43.0 Ma. Dutton et al. (2005) suggest the former excursion results from a rapid shift to more saline deep-waters in the Pacific Ocean, noting the excursion corresponds to a collapse in surface-bottom water $\delta^{13}C$ gradients at equatorial Pacific Site 865. Between ~48.0 and ~43.0 Ma, Shatsky Rise $\delta^{18}O$ were ~0.5 ‰ less positive than the average compilation and fall away from the population as a whole, which would indicate that Shatsky Rise bottom-waters were either warmer or less saline during this interval. Shatsky Rise $\delta^{18}O$ move into the spread of the global dataset between ~43 and ~37 Ma.

6.6.2 Cenozoic Mg/Ca palaeotemperature veracity?

Dutton et al. (2005) also produced a low-resolution benthonic foraminiferal Mg/Ca record for Site 1209. A Shatsky Rise Cenozoic record was compiled by normalising the foraminiferal Mg/Ca to *O. umbonatus*, using the offsets calculated by Lear et al. (2000) and then calculating palaeotemperatures as described in Section 6.4.3. As seawater Mg/Ca has almost certainly changed over the Cenozoic (see Section 6.4.1), a simple linear version of the Wilkinson and Algeo (1989) seawater Mg/Ca evolution through the Cenozoic was used to enable calculation of palaeotemperatures (ii in Figure 6.16). Variable seawater Mg/Ca ratios were calculated using a linear equation derived from a simple end member relationship of seawater Mg/Ca at 33.9 Ma being 4.3 mol/mol and at 60 Ma being 3.5 mol/mol, using sample age to calculate the appropriate seawater Mg/Ca ratio. Assumption of the alternative Wilkinson and Algeo (1989) model (I in Figure 6.16) leads to a reduced gradient and lower temperatures, whilst the Hardie (1996) model results in unrealistically high bottom-water temperatures (see Section 6.4.3).

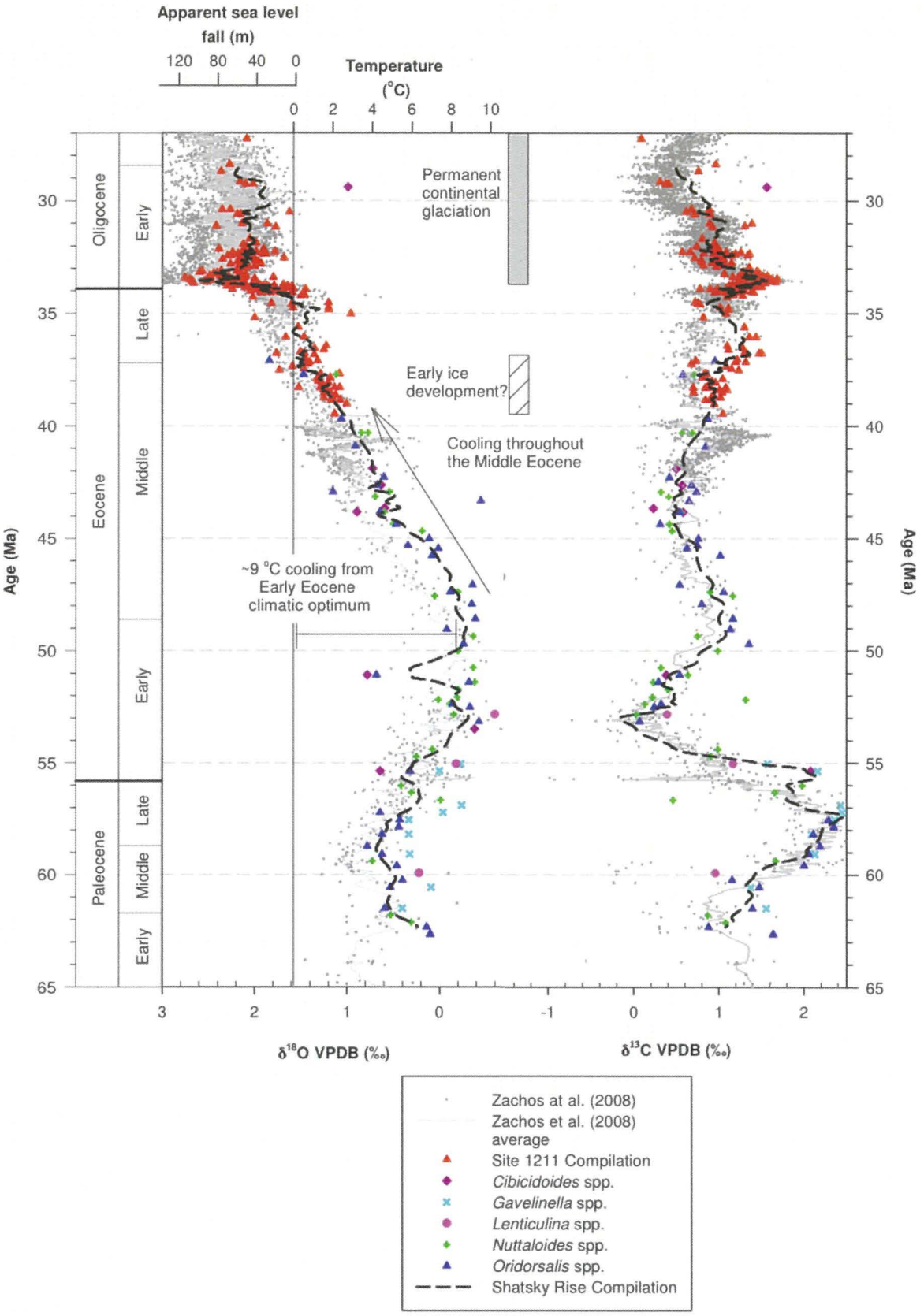
Apparent sea level fall (m)
120 80 40 0
Temperature (°C)
0 2 4 6 8 10
Oligocene
Eocene
Paleocene
Early
Late
Middle
Early
Late
Middle
Early
Permanent continental glaciation
Early ice development?
Cooling throughout the Middle Eocene
~9 °C cooling from Early Eocene climatic optimum
Age (Ma)
30 35 40 45 50 55 60 65
3 2 1 0 -1
δ18O VPDB (‰)
0 1 2
δ13C VPDB (‰)
Zachos at al. (2008)
Zachos et al. (2008) average
Site 1211 Compilation
Cibicidoides spp.
Gavelinella spp.
Lenticulina spp.
Nuttaloides spp.
Oridorsalis spp.
Shatsky Rise Compilation

Figure 6.31: Shatsky Rise Palaeogene compilation plot overlain on top of the global stable-isotope compilation of Zachos et al. (2001; 2008), both datasets normalised to equilibrium values, i.e. *O. umbonatus* and *Cibicidoides* spp. for $\delta^{18}O$ and $\delta^{13}C$ respectively (Shackleton et al., 1984). Normalisation was achieved using the species offsets of Katz et al. (2003) for Dutton et al. (2005) data or the offsets developed in Section 5.6.3 for Site 1211. The lines through each dataset correspond to five-point running averages. There is good long-term agreement between both Shatsky Rise $\delta^{18}O$ and $\delta^{13}C$ and the global dataset equivalent throughout the Palaeogene; although the low stratigraphic resolution of Shatsky Rise means that short-term events, i.e. the Palaeocene/Eocene thermal maximum, are absent. Relative temperature changes prior to ice sheet development are shown with the $\delta^{18}O$ values, using the initiation of the EOT as an indicator of continental ice growth and sea level fall (as calculated in Section 6.5.3). Shatsky Rise data suggest an ~9 °C temperature decrease during the Middle Eocene, although the questionable Middle Eocene ice growth interval is highlighted. Data from Zachos et al. (2008) was migrated onto the geologic timescale of Gradstein et al. (2004) through interpolating between magnetochrons as per previous data migrations (see Section 6.2.3).

Shatsky Rise Mg/Ca palaeotemperature variation over the Cenozoic does not follow the trends expected from the benthonic foraminiferal $\delta^{18}O$ record, i.e. warming during the latest Palaeocene or the ~9 °C cooling observed from the Middle Eocene to the Late Eocene (Figure 6.32). Several explanations for the lack of covariation can be hypothesised, such as changing seawater Mg/Ca ratios, changing $\delta^{18}O_{sw}$, diagenesis, or the veracity of benthonic foraminiferal Mg/Ca on deep-time scales. As described in Section 6.4.1, seawater Mg/Ca ratios have been modelled to have varied throughout the Cenozoic (Figure 6.16), and a simplified version of one modelled scenario was used to calculate Shatsky Rise palaeotemperatures. Variation in seawater Mg/Ca could explain the divergence of benthonic foraminiferal Mg/Ca palaeotemperatures and $\delta^{18}O$, however, for this to be the case, seawater Mg/Ca would have to be highly variable throughout the Cenozoic. To account for intervals where relative $\delta^{18}O$ temperatures and Mg/Ca palaeotemperatures converge or diverge, such as between ~56.0 and ~53.0 Ma or ~47.5 and ~42.5 Ma, seawater Mg/Ca would have to decrease or increase over these intervals (respectively) but remain relatively constant before and between them. Seawater Mg/Ca ratios are controlled by hydrothermal alteration, i.e. mid-ocean ridge spreading, and dolomitisation (Wilkinson and Algeo, 1989; Hardie, 1996), then the alteration and dolomitisation would have to show equivalent variance. Evidence for significant short-term (<2 Myr) variation in mid-ocean ridge spreading or dolomitisation has not been observed during the Cenozoic (Wilkinson and Algeo, 1989; Rowley, 2002), suggesting seawater Mg/Ca did not change in the manner required. This is not to say that seawater was not variable and changed in the similar linear fashion used within this study, but simply that variation was more likely on a gradual >5 Myr scale than over more short-term timescales.

Equally, $\delta^{18}O_{sw}$ change due to ice volume seems to be highly unlikely. The changing relationship between $\delta^{18}O$ and Mg/Ca would require continental ice sheets within the

Palaeocene, a requirement not supported by evidence of widespread glaciation or the observation of warm high-latitude temperatures (Zachos et al., 1994). Diagenesis could account for the decrease in $\delta^{18}O$ with age during the Middle Eocene (see Figure 6.1; Section 6.1.2/5), however, the reversal of this trend during the Palaeocene would argue against a diagenetic cause. Similarly, the relatively invariant Mg/Ca between ~63.0 and ~50.0 Ma would suggest that diagenesis had either ceased or had reached a diagenetic calcite end member, whilst $\delta^{18}O$ continues to show variations that suggest primary carbonate remained. Thus, the relationship between Mg/Ca and $\delta^{18}O$ cannot be explained by diagenesis.

The most likely scenario, thus, seems to be the veracity of the benthonic foraminiferal Mg/Ca ratios. The assumption has been made that the relationship between foraminiferal Mg/Ca and temperature has not changed, and that the offsets in Mg/Ca ratios have remained uniform throughout the entire Cenozoic. However, as noted in Section 6.4.3, even in modern benthonic foraminiferal Mg/Ca, not all variation can be accounted for by temperature alone (e.g. Lear et al., 2002; Martin et al., 2002; Elderfield et al., 2006; Yu and Elderfield, 2008, Rathmann and Kuhnert, 2008). Hypotheses relating to a balance between temperature and carbonate ion saturation have been suggested (Martin et al., 2002; Elderfield et al., 2006), whilst carbonate ion saturation has been cited to explain the EOB Mg/Ca record (Lear et al., 2004; Coxall et al., 2005). Records from Site 1211, whilst interpreted to be carbonate free (Section 6.4.6), displayed a significant degree of scatter that could be explained by the natural variation observed by Yu and Elderfield (2008) and Rathmann and Kuhnert (2008). Dutton et al. (2005) also identified unexplained differences between Mg/Ca palaeotemperature records from the same location (Site 689) as measured by Lear et al. (2000) and Billups and Schrag (2003). This evidence all suggests that Cenozoic benthonic foraminiferal Mg/Ca records cannot be solely interpreted as temperature records and that the globally observed benthonic foraminiferal $\delta^{18}O$ record is currently the best indicator of deep-sea temperature available. Common features within the Mg/Ca record from a global array of locations, however, suggest a single global control. If this is the case then the increase in Mg/Ca palaeotemperature at the EOB is likely to represent palaeoceanographic temperature change.

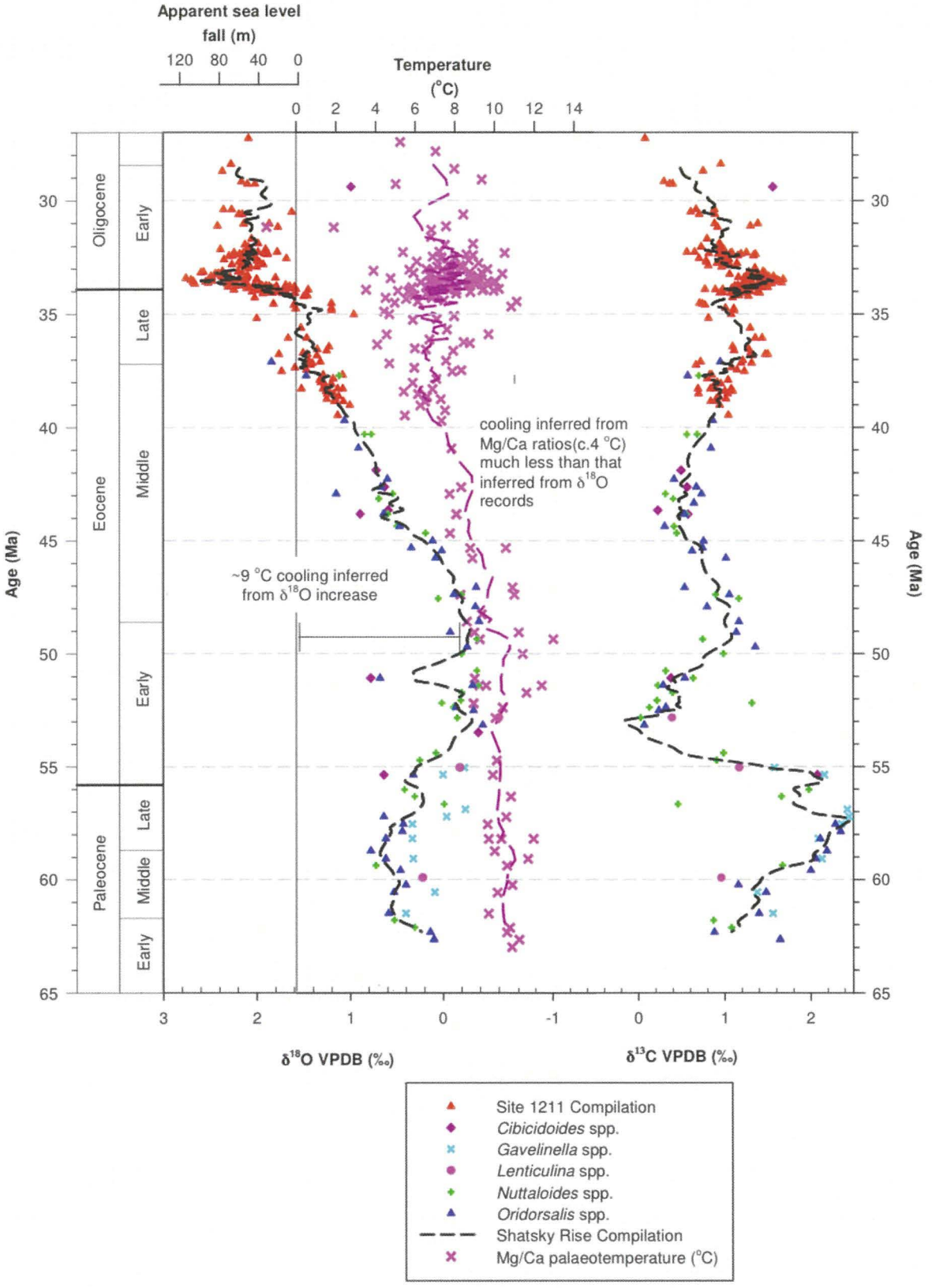
Apparent sea level fall (m)
120 80 40 0
Temperature (°C)
0 2 4 6 8 10 12 14
Oligocene
Eocene
Paleocene
Early
Late
Middle
Early
Late
Middle
Early
Age (Ma)
30 35 40 45 50 55 60 65
cooling inferred from Mg/Ca ratios(c.4 °C) much less than that inferred from δ18O records
~9 °C cooling inferred from δ18O increase
3 2 1 0 -1
δ18O VPDB (‰)
0 1 2
δ13C VPDB (‰)
Site 1211 Compilation
Cibicidoides spp.
Gavelinella spp.
Lenticulina spp.
Nuttaloides spp.
Oridorsalis spp.
Shatsky Rise Compilation
Mg/Ca palaeotemperature (°C)

Figure 6.32: Shatsky Rise stable-isotope compilation (as Figure 6.31) with Mg/Ca palaeotemperatures. Mg/Ca palaeotemperatures were calculated using a simple linear version of Wilkinson and Algeos (1989) seawater Mg/Ca ratio (ii in Figure 6.16). Bottom-water Mg/Ca palaeotemperatures show little covariation with the relative benthonic foraminiferal $\delta^{18}O$ temperature record throughout the Cenozoic. Expected warming during the Early Eocene is not observed, whilst less half of the interpreted ~9 °C Middle Eocene cooling in $\delta^{18}O$ values is present. In order to match Mg/Ca palaeotemperatures to relative $\delta^{18}O$ palaeotemperatures then seawater Mg/Ca variation would have to be dynamic. For example to match the Middle Palaeocene to Early Eocene record (~63 to ~50 Ma), seawater Mg/Ca would have remained constant throughout the Middle to Late Palaeocene, decrease during earliest Early Eocene (~57 to ~53 Ma) before becoming constant again until ~50 Ma. Similar relative changes would be required during the Middle and Late Palaeocene. Changes to seawater Mg/Ca such as those described would require Mg^{2+} and Ca^{2+} cycling to vary dramatically, i.e. significant, short-term changes in the hydrothermal alteration and dolomitisation reactions that control sea water Mg/Ca (Wilkinson and Algeo, 1989; Hardie, 1996). Evidence for such variation during the Cenozoic is not forthcoming, with relatively invariant sea-floor spreading rates and low variation in dolomitisation (Wilkinson and Algeo, 1989; Rowley, 2002). An alternative hypothesis would be that benthonic foraminiferal $\delta^{18}O$ values represented changes in $\delta^{18}O_{sw}$ rather than temperature; however, this would infer continental ice sheets had been present during the Palaeocene. Continental ice sheet development during the Palaeocene is not supported by either sedimentogical evidence (see Section 2.1) or the observation of low-latitudinal temperature surface-water gradients (Zachos et al., 1994).

6.6.3 Atypical carbon cycle changes at Site 1211?

Published records indicate that the $\delta^{13}C$ excursion lags the positive shift in $\delta^{18}O$, whilst the CCD deepening occurs synchronously (Zachos et al., 1996; Coxall et al., 2005; Riesselman et al., 2007). The relationships between $\delta^{13}C$ and CCD deepening have been taken to indicate that the development of continental ice, i.e. the $\delta^{18}O$ shift, caused perturbations in the carbon-cycle. Of the possible reasons for an excursion in $\delta^{13}C$, both evidence and modelling suggest an increase in export and siliceous microfossil productivity as a result of continental glaciation was the most likely cause (Diester-Haass, 1995; 1996; Diester-Haass and Zahn, 1996; 2001; Salamy and Zachos, 1999; Robert et al., 2002; Diester-Haass and Zachos, 2003; Anderson and Delaney, 2005; Zachos and Kump, 2005). An increase in oceanic circulation and seasonality linked to an increase in latitudinal temperature gradients as a result of high-latitude cooling suggested as the most likely cause for the increase in productivity (Zachos et al., 1996; Salamy and Zachos, 1999; Zachos and Kump, 2005).

Various hypotheses have been suggested for CCD deepening and its relationship to $\delta^{18}O$ increase across the Eocene–Oligocene boundary. These hypotheses have focused on three possible causes: i) changes in seasonality and an increase in the proportion of siliceous primary producers relative to carbonate responsible for surface-ocean productivity leading to elevated organic-carbon burial; ii) changes in the inputs of Ca^{2+} and CO_3^{2-} into the

oceans as result of increased glacial weathering and iii) shifts in the location of carbonate burial as a result of sea-level fall (Zachos et al., 1996; Salamy and Zachos, 1999; Ravizza and Peucker-Ehrenbrink, 2003; Coxall et al., 2005; Zachos and Kump, 2005). Merico et al. (2008) used a geochemical model to assess each of the three suggested hypotheses and only the shift in location of carbonate production as a result of sea level fall could replicate observations. The $\delta^{13}C$ excursion resulting from the erosion of early Cenozoic carbonates as they became exposed by the sea level fall, thus both carbon-cycle changes occur as a result of EOB glaciation. Rea and Lyle (2005) have, however, questioned whether the sea level fall and shelf exposure is sufficient to have caused the observed increase in deep-sea carbonate sedimentation.

Considering Figure 6.12, the relationship of the $\delta^{13}C$ excursion and CCD deepening to the $\delta^{18}O$ step at Site 1211 is contrary to the relationships described above from other high-resolution studies and thus indicates the opposite conclusion. At Site 1211, CCD and carbon-cycle change lead glaciation, with the relationship between the sedimentary carbonate proxies and $\delta^{13}C$ suggesting that an increase in burial of organic carbon relative to inorganic carbonate had acted to depress CCD and cause the $\delta^{13}C$ excursion prior to the EOT (Salamy and Zachos, 1999; Zachos and Kump, 2005). Although the veracity of the $\delta^{13}C$ record is uncertain, as it lacks the clear two-step increase observed in published records (Figure 6.8), there is a clear excursion with the $\delta^{18}O$ record, thus the Site 1211 records seem to contradict the published sites.

Assuming that the synchronicity of CCD deepening and EOT initiation, and corresponding lag of $\delta^{13}C$ (Zachos et al., 1996; Coxall et al., 2005; Riesselman et al., 2007), is typical of the global signal of the climatic changes over the EOB, then the CCD deepening in advance of $\delta^{18}O$ increase at Site 1211 needs to be explained. Two explanations could reconcile the absence of shoaling prior to and lead of CCD deepening over EOT initiation; either the lead of CCD at Site 1211 is controlled by variation in local palaeoceanography as opposed to a global climate, or that the depth–age model overestimates the age of sediments between 34.5 and 34.2 Ma. Several lines of reasoning support the former hypothesis over the latter. The $\delta^{18}O$ shift from ~34.2 Ma is of equivalent magnitude to that observed in published records (Section 6.2.3), whilst there is no clear increase in the running average $\delta^{18}O$ values from 34.5 to 34.2 Ma (see Figure 6.2 EOB), a definite

increase in $\delta^{18}O$ being expected if CCD deepening and EOT initiation had occurred simultaneously at Site 1211. These two lines of evidence would suggest the Site 1211 depth-age model is broadly correct. Figure 6.5 shows that fine-fraction $\delta^{18}O$ and $\delta^{13}C$ start to become more positive at 34.5 Ma, i.e. with CCD deepening, which could indicate that surface-waters cooled and became more productive at this time. The control on $CaCO_3$ MARs across the Shatsky Rise by productivity, shown by the absence of carbonate ion saturation gradients with depth (Section 6.3.3) suggests that increased surface water productivity and subsequent export productivity would lead to an increase in carbonate rain rate, depressing the CCD, and thus alter the relationship between $\delta^{18}O$ and CCD at Site 1211. Local productivity controls were suggested by Tripati et al. (2005) as an explanation of the difference in CCD deepening at Site 1218 in the equatorial Pacific and that observed for other ocean basins (Figure 6.11). With $\%CaCO_3$ at Site 1211 being >97 % by ~34.0 Ma, the impact of a further global deepening of CCD related to the EOT would be minor on $\%CaCO_3$ levels and thus the apparent link between glaciation and CCD deepening would be obscured. Why Shatsky Rise experienced an increase in surface-water productivity prior to the EOT is uncertain, and would require more detailed records of both productivity related and surface water proxies across the latest Eocene and into the Oligocene.

6.6.4 Eocene–Oligocene palaeoceanography of Site 1211

The primary aim of this study was to produce a multi-proxy record of palaeoceanographic change at Site 1211 over the Eocene–Oligocene climate transition (Section 1.1). The individual proxy records have been discussed in the previous sections but not considered as a whole to produce an oceanographic evolution of Site 1211; this section produces such a description.

Throughout the Middle Eocene bottom-waters at Site 1211 show increasing $\delta^{18}O$ and $\delta^{13}C$ but no average Mg/Ca palaeotemperature change leading to an increase in $\delta^{18}O_{sw}$ of ~0.5 ‰. Declining $\delta^{18}O$ during the Middle Eocene has been observed from a global range of locations and was assumed to result from bottom-water temperature decrease prior to the EOB (Figure 6.31; Zachos et al., 2001). Assuming an ice-free Middle Eocene (see Section 6.2.1 for calculation details), then the $\delta^{18}O$ decrease equates to a temperature decrease of ~1.5 °C. The increase in $\delta^{18}O_{sw}$ between ~39.6 and ~37.5 Ma, however, indicates the

increase in benthonic foraminiferal $\delta^{18}O$ does not result from temperature change. Billups and Schrag (2003) observe similar increase in $\delta^{18}O_{sw}$ from ~40 Ma from shallower palaeodepth (~1.5 km) sites from the Indian and Southern Ocean; observation of an increase of ~0.5 ‰ from several widespread locations suggesting that continental ice sheet growth began at ~40 Ma. Growth of Antarctic continental ice at ~40 Ma agrees with evidence from changing clay mineralogies from Antarctica, suggesting an increase in physical weathering and cooling (Zachos et al., 1999). However, the veracity of bottom-water Mg/Ca palaeotemperatures is questionable over a ~3.0 Myr period as a result of changing seawater Mg/Ca and the lack of similarity in deep-water Mg/Ca palaeotemperatures with the $\delta^{18}O$ record (see Section 6.6.2). The increase in bottom-water $\delta^{18}O_{sw}$ is not observed in deep-dwelling planktonic foraminiferal $\delta^{18}O_{sw}$ (Figure 6.27), neither do fine-fraction $\delta^{18}O$ show covariation with benthonic foraminiferal $\delta^{18}O$ increase during the Middle Eocene (Figure 6.4), both of which arguing against the early development of continental ice. As discussed in Section 6.5.3, $\delta^{18}O_{sw}$ increase can be empirically linked to ice-volume growth, the development of Middle Eocene ice would lead to bipolar glaciation at the EOB, which is not supported by sedimentary evidence (Section 6.5.3). An alternative explanation for $\delta^{18}O_{sw}$ increase would be an increase in salinity of ~1 ‰ at Site 1211 (0.5 ‰ corresponding to a 1.0 ‰ increase in $\delta^{18}O_{sw}$; Broecker, 1989), although the global observation of a deep-water $\delta^{18}O$ increase would suggest bottom-water salinity increase was a global occurrence (see Figure 6.31). Any such change in global deep-ocean salinity would impact the surface-water salinity to a much greater degree due to the requirement for salt conservation (Miller et al., 1991), which is not evident in the surface water records of Site 1211; thus the cause for the late Middle Eocene $\delta^{18}O$ increase remains enigmatic.

During the Late Eocene, average $\delta^{18}O$ and Mg/Ca palaeotemperatures remained constant at Site 1211. The apparent lack of variability in bottom waters has to be considered in light both the scatter and relatively low number of determinations across the ~36.0 to ~34.2 Ma interval, both of which hinder identification of any short-term events within the record. A lack of significant variation in $\delta^{18}O$ during the Late Eocene would follow the global deep-water pattern as observed at other sites (see Section 6.6.1). The local maximum between 37.0 and ~36.0 to ~35.0 Ma (unclear as a result of a lack of determinations) in bottom-water $\delta^{13}C$, unrelated to any variability in either surface of bottom-water $\delta^{18}O$, suggests a moderate $\delta^{13}C$ excursion during this interval. An excursion could result from either local

changes, such as an increase in productivity at Site 1211 or a change in bottom-water mass bathing the site, or global changes in the burial of $\delta^{13}C$. Records of CCD fluctuations over the 37.0 to 35.0 Ma interval of the Late Eocene do not correlate with stable-isotope variation (Figure 6.12) suggesting that the $\delta^{13}C$ excursion was not a result of a new geochemically distinct water mass. % Sand fraction, however, was low throughout the interval indicating fragmentation of foraminifera was high, fragmentation being associated with increased oxidation of organic matter in the sediment column and hence increased export productivity (Peterson and Prell, 1984; Diester-Haass, 1995). Whilst less pronounced than at Site 1211, the Zachos et al. (2001; 2008) compilation (Figure 6.31) shows a minor $\delta^{13}C$ excursion at this time and there is evidence of increased productivity and siliceous microfossil burial at ~37.0 Ma from the Atlantic and Southern Oceans (Diester-Haass, 1995; Diester-Haass and Zahn, 1996; Anderson and Delaney, 2005; Ravizza and Paquay, 2008). Enhanced export productivity and siliceous microfossil burial would both act to remove $\delta^{12}C$ from the ocean causing the $\delta^{13}C$ excursion (Zachos et al., 1996; Salamy and Zachos, 1999). Proxies relating to productivity, i.e. benthonic accumulation rates, sedimentary Ba, and improved records of CCD variation are required to test whether productivity increased at Site 1211 between ~37.0 and ~35.0 Ma or whether the $\delta^{13}C$ excursion resulted from a global event.

Average bottom-water $\delta^{18}O_{sw}$ values for the late Eocene (37.0 to 34.5 Ma) show little variation (Figure 6.27), suggesting that global ice volumes did not change significantly during the interval. The variance seen in interpolated records assumed to result from the scatter in the Mg/Ca palaeotemperature records (Section 6.4.3), occurring as a result of either contamination, neomorphism of the foraminiferal tests or through unexplained variation in the uptake of Mg by *O. umbonatus* (Rathmann and Kuhnert, 2008). During the late Eocene interval fine-fraction $\delta^{18}O$ shows marked variation, in particular a gradual positive shift between ~36.6 and ~35.2 Ma, followed by a ~1.0 ‰ increase between ~35.2 and ~35.0 Ma. These changes would suggest that surface waters either first cooled by ~2 °C before warming by ~4 °C, increased in salinity by ~1.0 ‰ before a ~2.0 ‰ decrease, or a combination of the two. An increase in surface-water temperatures between ~35.2 to ~34.9 Ma seems more likely than a decrease in salinity, as a salinity decrease of the magnitude of ~2 ‰ would be equivalent to the modern day high to low-latitude salinity gradient (Zachos et al., 1994) and require a major change in evaporation and precipitation at Site 1211. Fine-fraction $\delta^{13}C$ also becomes less positive between ~35.2 and ~35.0 Ma,

although the trend continues to ~34.5 Ma. Despite Ennyu et al. (2002) indicating that fine-fraction $\delta^{13}C$ does not reflect seawater $\delta^{13}C$, fine-fraction $\delta^{13}C$ does track *T. ampliapertura* $\delta^{13}C$ closely across the EOT and EOGM. The similarity of planktonic foraminiferal and fine-fraction $\delta^{13}C$ suggests that the fine-fraction $\delta^{13}C$ can be taken to have recorded surface-water $\delta^{13}C$ across the Late Eocene and Early Oligocene. The negative change in fine-fraction $\delta^{13}C$ values could indicate that surface-waters became less productive at ~35.2 Ma, a change related to the decrease in $\delta^{18}O$. The development of planktonic foraminiferal records across this interval would allow the development of these ideas but was not possible due to the lack of whole specimens observed.

Across the EOB, $\delta^{18}O$ variation at Site 1211 appears to follow a "classic" two-step pattern, i.e. an initial gradual increase followed by a more abrupt second step; although increase in *O. umbonatus* $\delta^{13}C$ does not faithfully track seawater $\delta^{13}C$ variation as has been observed in published records (Section 6.2.1). The pattern of glaciation follows published records with an extreme EOGM period, that abruptly decreases by about one third at ~33.1 Ma. A ~1.0 °C increase in bottom-water temperatures indicated from Mg/Ca ratios suggests that the EOGM $\delta^{18}O_{sw}$ increase was ~1.25 ‰ resulting from an ice volume equivalent to the LGM assuming modern ice sheet $\delta^{18}O$ values (Section 6.5.1/3). Post-EOGM Oligocene $\delta^{18}O_{sw}$ increase was ~0.9 ‰ equivalent to glaciation on the scale of modern day Antarctic glaciation. Due to the scatter within the benthonic foraminiferal $\delta^{18}O$ records, it is not possible to identify any orbital variation within the post EOGM Oligocene as observed for the equatorial Pacific by Wade and Palike (2004). Unlike published records (c.f. Coxall et al., 2005; Riesselman et al., 2007), CCD deepening leads the development of continental ice. However, as discussed above (see Section 6.6.3), CCD deepening increase is coincident with fine-fraction stable-isotope increase suggesting that there may have been an increase in surface water productivity that locally depressed the CCD.

Planktonic foraminiferal and fine-fraction stable-isotope records indicate surface-waters evolved differently across the EOT and EOGM. Each of the surface-water records has peak $\delta^{18}O$ values after the Oi-1a peak in bottom-water records (Figure 6.5), which together with planktonic foraminiferal Mg/Ca palaeotemperature estimates indicates that surface waters cooled across the EOT and into the EOGM. Following the EOT, there is a reduction in the sub-thermocline–bottom water $\delta^{18}O$ and $\delta^{13}C$ gradients but little change in the

surface–bottom-water gradient indicating that stratification between the surface and deeper waters became stronger (Figures 5.13 and 5.14). The contrary behaviour of sub-thermocline $\delta^{18}O$ to bottom-water $\delta^{18}O$ observed at the Oi-1a and Oi-1b event could represent enhanced mixing of surface waters relating to increases in the vigour atmospheric/oceanic circulation caused by the extreme climate state. Whilst bottom-water records are sparse younger than ~32.0 Ma, fine-fraction records get gradually more negative between ~33.0 and ~30.0 Ma suggesting a ~1.0 °C warming, before a positive shift of up to ~1.0 ‰ at ~29.8 Ma. These surface-water changes have no corollary in the limited bottom-water records available, so determination of whether these are whole ocean events is not possible.

As described in Section 2.4, declining atmospheric pCO_2 is the leading hypothesis as to the cause of glaciation at the Eocene–Oligocene boundary (DeConto and Pollard, 2003; 2008; Coxall and Pearson, 2007). Comparing Site 1211 bottom-water $\delta^{18}O$ and Mg/Ca palaeotemperatures with Eocene–Oligocene pCO_2 variation shows a similar relationship to that identified by Pearson et al. (2009) for TDP records (Figure 6.33). The gradual initiation of the $\delta^{18}O$ shift corresponds to the decline in pCO_2 towards Antarctic threshold values, whilst palaeotemperatures remaining in the range of values observed for the Late Eocene (Figure 6.22). The majority of the increase in $\delta^{18}O$ occurs with the increase of pCO_2 to Eocene levels, the pCO_2 increase coincident with the majority of the increase in bottom-water palaeotemperatures. Lear et al. (2004) hypothesised that the development of continental ice would lead to a decline in weathering. Declining weathering rates would lead to an increase in atmospheric pCO_2 that would act as a negative feedback on the glaciation and cause the warming observed by Lear et al. (2000; 2004), as well as in the new records developed by this study for Site 1211. Figure 6.33 shows that the Lear et al. (2004) hypothesis is supported by the pCO_2 records of Pearson et al. (2009).

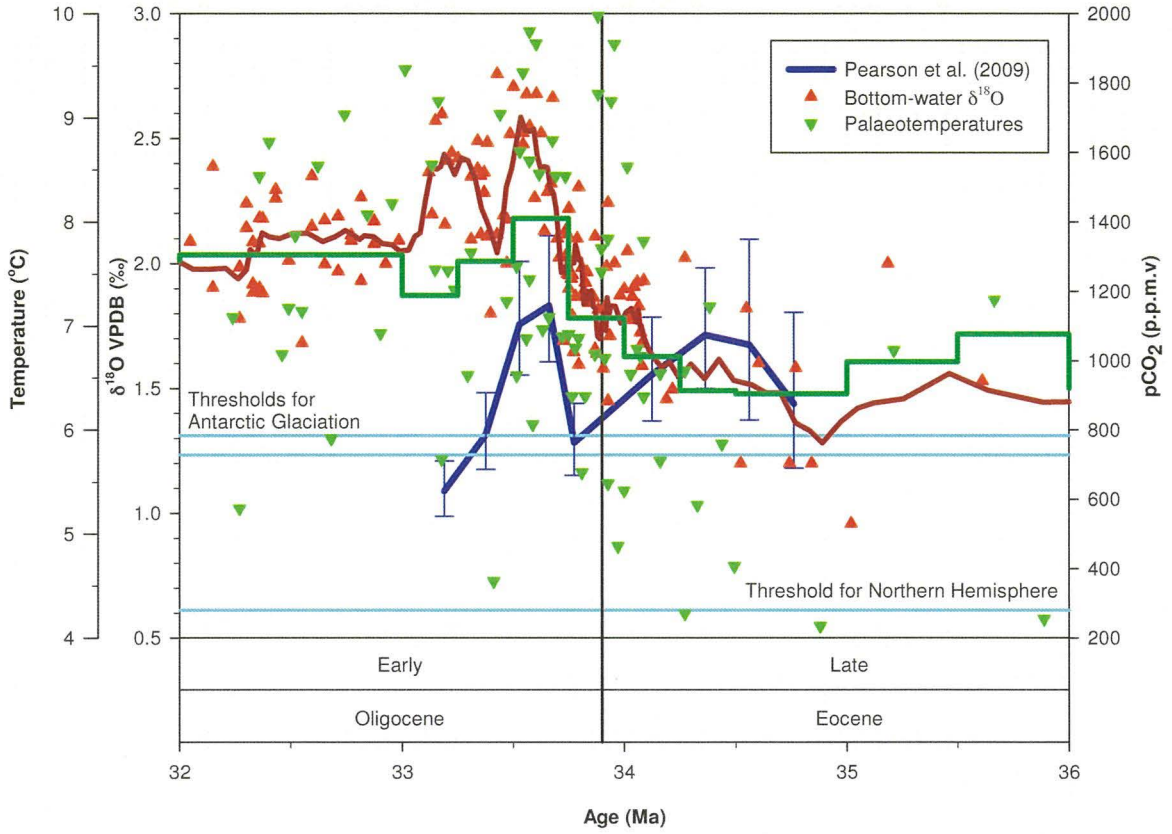

Figure 6.33: Bottom-water $\delta^{18}O$ and Mg/Ca palaeotemperature records plotted against the foraminiferal ^{11}B-derived estimates of pCO_2 of Pearson et al. (2009; see Section 2.3.6), with the pCO_2 thresholds calculated for the development of Antarctic and Northern Hemispheric ice sheets (DeConto and Pollard, 2003; DeConto et al., 2008). Initiation of the $\delta^{18}O$ increase occurs with the decrease in pCO_2 towards the threshold for Antarctic glaciation, whilst the majority of the $\delta^{18}O$ shift occurs with an increase in pCO_2. Palaeotemperatures increase throughout the pCO_2 decrease, although the greater proportion of the warming occurs with the pCO_2 increase, possibly suggesting the reduction in weathering due to ice growth lead to an increase in atmospheric pCO_2 (Lear et al., 2004).

Chapter 7: Conclusion

This study was initiated with the two clear aims relating to climate change across the Eocene–Oligocene boundary. Firstly, the study aimed to produce a new multiproxy record of Late Eocene to Early Oligocene oceanography from the Pacific Ocean. The rationale being the Pacific Ocean is, and was during the late Cenozoic, the largest ocean on Earth so would have the most globally representative record of EOB oceanographic and climatic change; further to this the Pacific Ocean is a major influence on modern day climates so has potential to influence global climate change across the EOB (Lyle et al., 2008). However, despite the size and importance of the Pacific Ocean, only a single high-resolution study exists from the Pacific Ocean from the equatorial Site 1218 (Coxall et al., 2005), thus the development of a new Pacific EOB record was viewed as a priority. Secondly, whilst features of the EOB deep-ocean record are relatively well constrained, with a globally recognised >1.0 ‰ increase in $\delta^{18}O$ and a transient positive excursion in $\delta^{13}C$ (cf. Miller et al., 1991; Zachos et al., 1996; Coxall et al., 2005; Riesselman et al., 2007), the causes of the increase are much less well constrained. The cause of the benthonic foraminiferal $\delta^{18}O$ increase is the key question across the EOB, as globally similar changes in $\delta^{18}O$ can only result from either temperature decrease and/or ice volume development. Constraint of the proportion of the $\delta^{18}O$ shift attributable to deep-water temperature change and the proportion attributable to ice-volume increase an important requirement, if the development and causes of the EOB are to be understood. Attempts to deconvolute these records have been inconclusive, the most promising approach being that of paired benthonic foraminiferal $\delta^{18}O$ and Mg/Ca ratios, the latter proxy allowing temperature estimation from equivalent samples to the $\delta^{18}O$ value (e.g. Lear et al., 2002). Application of the technique to deep-ocean sediments, however, has lead to further questions regarding both the EOB and the Mg/Ca proxy. Mg/Ca ratio palaeotemperature estimates indicate the deep-ocean either remained the same temperature or warmed across the EOB (Lear et al., 2000; 2004; Billups and Schrag, 2003), counter to the expectation that high latitude cooling lead to ice development. The lack of cooling in the deep-ocean had two implications, either EOB ice development could account for all the $\delta^{18}O$ shift observed or the benthonic foraminiferal Mg/Ca ratios had another control across the EOB. Changing deep water carbonate ion saturation has been hypothesised to influence Mg uptake (Lear et al., 2004; Coxall et al., 2005), the Mg/Ca ratio record indicating EOB warming being obtained from Site 1218 where there was a rapid (<300 kyr) deepening of CCD by >1.0 km (Coxall et al., 2005). However, the effect of changing carbonate ion saturation on benthonic foraminiferal Mg/Ca has been observed to be variable between

species and different habitats (Yu and Elderfield, 2006; Rathmann and Kuhnert, 2008). Thus, the second aim of this study was to produce paired foraminiferal records from a location with a reduced, if not absent, change in carbonate ion saturation so as to isolate a true bottom-water temperature record.

7.1 Site 1211 key results

Site 1211 recovered during ODP Leg 198 to Shatsky Rise was identified as a suitable location, Shipboard Scientific Party (2002a, b) indicating that the site had a complete calcium carbonate sediment record across the EOB and remained above the CCD throughout the Late Eocene to Early Oligocene. A multiproxy record designed to reveal information regarding the evolution of both the physical oceanographic evolution of waters above Site 1211 and the carbonate ion saturation of deep-waters was produced.

Bottom-water Late Eocene to Early Oligocene $\delta^{18}O$ and $\delta^{13}C$ records from Site 1211 show an evolution of stable-isotope records comparable to published records. A two-step increase in $\delta^{18}O$ of ~1.2 ‰ was identified at Site 1211, following the evolution of published records from Site 522, 744 and 1263 (Zachos et al., 1996; Riesselman et al., 2007), i.e. a gradual first step of less than half the total shift followed by a more rapid second step increase. A ~500 kyr interval of high $\delta^{18}O$ values followed representing the Eocene Oligocene glacial maximum, before $\delta^{18}O$ decreased to an Oligocene value ~0.7 ‰ more positive than average Eocene $\delta^{18}O$. A clear $\delta^{13}C$ excursion was also observed, although the excursion appeared to be attenuated relative to that observed in published records. The attenuation is likely to have resulted from *O. umbonatus* calcifying in relation to sediment pore water $\delta^{13}C$ rather than seawater $\delta^{13}C$ (Rathmann and Kuhnert, 2008). Site 1211 was confirmed to be above the CCD throughout the Late Eocene and Early Oligocene with sediment %CaCO values typically >95 % suggesting bottom-waters were not undersaturated to a significant degree. During the Late Eocene, Site 1211 CCD underwent periodic, transient shoaling events, however, foraminiferal stable-isotope records are insufficiently detailed to allow identification of any climatic shift associated with the shifts. CCD deepening at Site 1211 occurred prior to the first stage of the EOT, and sedimentary carbonate proxies reached maximum values (~98 %) during the first stage of the EOT (~34.0 Ma), after which CCD remained deep and invariant throughout the Early Oligocene. Attempts to constrain the actual depth of the CCD using $CaCO_3$ mass

accumulation rate gradients were unsuccessful; $CaCO_3$ mass accumulation rates indicating no carbonate ion saturation gradient across bottom-waters above Shatsky Rise. Mass accumulation rates at Site 1211 appear to have been controlled solely by surface water productivity, leading to the hypothesis the deepening of the CCD prior to the EOT resulted from an increase in surface water productivity as evidenced by a positive shift in fine-fraction $\delta^{13}C$ with the CCD deepening.

Site 1211 Mg/Ca ratio displayed a high degree of scatter, most likely attributable natural inter- and intra-test variability and insufficient numbers of tests analysed. The scatter meant palaeotemperature records had to be determined from time-averaged values, which indicated up to ~1.5 °C warming of bottom-waters across the second stage of the EOT and into the EOGM. Bottom-water palaeotemperatures remained elevated into the Oligocene, indicating a permanent warming of bottom-waters. The majority of the increase in Mg/Ca palaeotemperatures observed occurred after the deepening of CCD, between ~34.0 and ~33.5 Ma compared to between ~34.5 and 34.0 respectively. Thus palaeotemperature increase occurred during the interval when sedimentary carbonate proxies indicate little change in bottom-water carbonate ion saturation, a relationship that suggests that the palaeotemperature increase resulted from warming rather than changing bottom-water carbonate ion saturation.

The relationship of Mg/Ca palaeotemperatures across the CCD deepening was ambiguous, given the scatter and low number of determinations completed. Assessment was made using the two published deep-water records, interpreted using the time-averaged approach required for Site 1211. The similarity of the palaeotemperature evolution from the EOT of Sites 522 and 1218, despite significantly different carbonate sedimentation histories, was interpreted as indicating that carbonate ion saturation was not the dominant influence on benthonic foraminiferal Mg/Ca across the EOB. The absence of pre-EOT cooling at Site 1211, results from scatter rather than increasing carbonate ion saturation.

In the interpreted absence of a carbonate ion saturation effect, averaged foraminiferal $\delta^{18}O$ and Mg/Ca palaeotemperatures indicated an increase in $\delta^{18}O_{sw}$ of ~1.25 ‰. An increase in $\delta^{18}O_{sw}$ of ~1.25 ‰ suggesting an ice sheet equivalent to that present on Antarctica during

the Last Glacial Maximum, if Oligocene $\delta^{18}O_{ice}$ was equivalent to modern day values (~-45 ‰). Oligocene $\delta^{18}O_{ice}$ more positive than ~-40 ‰ leads to unrealistically large ice volumes, as has been observed in previous EOB studies, i.e. Coxall et al. (2005) and Katz et al. (2008).

Further records were developed from planktonic foraminifera and <38 μm fine-fraction carbonates, the latter shown to be predominantly calcareous nannofossils, that describe the evolution of surface waters at Shatsky Rise across the Late Eocene to Early Oligocene. Surface-water $\delta^{18}O$ and $\delta^{13}C$ also exhibit the classic $\delta^{18}O$ shift and $\delta^{13}C$ excursion, although the full event is only recorded in the <38 μm fine-fraction. Surface-waters evolved independently from bottom-waters with $\delta^{18}O$ increase continuing beyond that observed in the bottom-waters. Planktonic foraminiferal Mg/Ca ratios show a temperature decrease across the Eocene–Oligocene transition, although the decrease was only maintained in the sub-thermocline dwelling species. $\delta^{18}O_{sw}$ from both planktonic foraminifera indicates an increase of up to ~1.0 ‰, although neither record is complete across the EOT or is representative of Late Eocene conditions. Periods of extreme glaciation, i.e. maxima in bottom-water $\delta^{18}O$, suggest that surface-waters became less stratified suggesting that atmospheric and oceanic circulation was most vigorous at these intervals.

7.2 Site 1211 caveats

Despite the apparent agreement, outlined above, of many of the Site 1211 records with previously published records, there remains a significant level of doubt concerning the interpretation of records from Site 1211. The key records developed to achieve the aims of the study, the benthonic foraminiferal stable-isotope and Mg/Ca ratios displayed a significant degree of scatter throughout much of their range, which is very apparent when comparing to records from Site 1218 (Figures 6.7 and 6.24). Scatter within the benthonic foraminiferal $\delta^{18}O$ and $\delta^{13}C$ is less obstructive to interpretation than that in Mg/Ca, likely a result of the magnitude of the changes in these records. However, when considered in detail, $\delta^{13}C$ records clearly do not follow the typical evolution observed in published records (Figure 6.8) or show a relationship to Site 1211 $\delta^{18}O$. Explanation for this would appear to be that the infaunal *O. umbonatus* calcifies in relation to the pore-water as opposed to seawater $\delta^{13}C$ as well as having a variable depth habitat within the sediment

(Rathburn et al., 1994; Rathmann and Kuhnert, 2008). The observation that *O. umbonatus* $\delta^{13}C$ has variable relationships with time to other benthonic foraminiferal species has been made previously (i.e. Shackleton et al., 1984; Katz et al., 2003), although the offsets developed in this study do not suggest that the variability is any greater than that of $\delta^{18}O$. Thus, the $\delta^{13}C$ results from Site 1211 suggest that *O. umbonatus* is not a suitable species to develop bottom-water stable-isotope results from.

The scatter is most evident and problematic, however, in the Mg/Ca ratio records from *O. umbonatus* (Figure 6.20), most likely as a result of the restricted number of foraminifera available for analysis. The *O. umbonatus* Mg/Ca ratios could only be interpreted through the use of a time-averaged approach such was the degree of scatter, which raises doubts as to the veracity of both the temperature increase identified and subsequent $\delta^{18}O_{sw}$ calculated. The scatter combined with the low number of determinations between ~35.0 and ~34.0 Ma also also obscures clear identification of the evolution of Mg/Ca temperature change and CCD deepening. Much of the strength of the interpretation of Site 1211 Mg/Ca palaeotemperatures and seawater $\delta^{18}O$ comes from the similarity of time-averaged published Mg/Ca ratio palaeotemperature evolution (Figure 6.24), Site 1211 data alone being insufficiently well constrained to confidently interpret the changes. The scatter in Mg/Ca ratios for Site 1211 seems likely to result from a combination of variable preservation/contamination and natural scatter observed upon calcification (cf. Lear et al., 2002; Rathmann and Kuhnert, 2008). A hypothesis could be suggested that the Mg/Ca ratios at Site 1211 do not represent a dominant temperature signal but primarily reflect natural variation; the increase in temperatures at ~34.0 Ma reflecting an increase in the number of samples completed as a result of the increase in carbonate preservation. Support for this hypothesis may be gained from relative and absolute range of Mg/Ca palaeotemperatures observed being similar throughout the dataset and the broadly similar 95 % ($\pm 2\sigma$) confidence range around the 5-point running averages during both Eocene and Oligocene. The observation that dissolution preferentially removes high Mg-carbonate (McCorkle et al., 1995; Elderfield et al., 2000; Rosenthal et al., 2000 among others) could explain the lower average temperatures calculated during the Eocene. However, even though natural scatter of up to a third has been identified in *O. umbonatus* (Rathmann and Kuhnert, 2008), a Mg/Ca–temperature dependence has been noted for the species by several studies (Lear et al., 2002; Rathmann et al., 2004; Rathmann and Kuhnert, 2008). The identification of a Mg/Ca–temperature relationship arguing that Site 1211 records

must have a temperature component and that a time-averaged approach would likely to reveal any temperature changes Mg/Ca from Site 1211. Thus, the increase in palaeotemperatures does appear to be "real" at Site 1211, although much less certainty can be placed on the relationship to CCD deepening.

A further question relating to Site 1211 records is the constraint on the CCD deepening. The proxies for CCD variation are unambiguous in indicating that CCD deepened close to/prior to the EOB and that Site 1211 was above the CCD throughout the Late Eocene and Early Oligocene. However, Site 1211 sedimentation is dominated by calcium carbonate throughout, e.g. $\%CaCO_3$ is >95 %, which would suggest that proxies based on sedimentary carbonate are not particularly informative as to the level of dissolution and hence bottom-water carbonate ion saturation. Reasoning behind this idea being that if sediment rain is ~5% non-carbonate and 95% carbonate, a minimum assumption for the carbonate proportion of the sediment rain at Site 1211 (as even after dissolution prior to the CCD deepening Site 1211 $\%CaCO_3$ are typically >95 %), then dissolution of significant quantities of the $CaCO_3$ rain does not significantly effect that the $\%CaCO_3$ in the sediment (see Lyle et al., 2005). The non-linearity could explain the absence of a pre-EOB dissolution event as has been observed within EOB records from Site 744 and 1218 (Zachos et al., 1996; Coxall et al., 2005). The effect of a predominantly carbonate sediment rain obscuring changes in dissolution can be minimised through the use of mass accumulation rates, which was attempted in Section 6.3.3. However, greater numbers of determination of both dry bulk density and preservation related variables, such as $\%CaCO_3$, % sand fraction and benthonic foraminiferal counts, need to be made from Shatsky Rise sites across the Cenozoic depth transect, i.e. Sites 1208 to 1211, to allow constraint of MAR gradients and thus carbonate ion saturation. In addition to this, a greater variety of dissolution/CCD proxies need to be developed, records such as benthonic foraminiferal abundance, planktonic to benthonic foraminiferal ratios and foraminiferal fragmentation indices, to allow a greater control on CCD variation to recognised from Site 1211.

7.3 Summary and further work

Baring in mind the problems with the dataset from Site 1211 discussed above, this study has only partially achieved its initial aims, in that a new Pacific Ocean dataset has been

produced. However, the key question as to whether a carbonate ion saturation effect exists on benthonic foraminiferal Mg/Ca remains unanswered. The bottom-water temperature increase at Site 1211 was clearly post EOB CCD deepening which, along with the temperature increase in all deep-water sites, suggests that bottom-waters did warm with the development of maximum glaciation. Mg/Ca palaeotemperatures from the interval during the CCD deepening, however, are ambiguous. Arguments for or against a carbonate saturation effect can be made; although, on the balance of evidence, a carbonate ion saturation effect would seem to be a relatively minor control on deep-water Mg/Ca. The scatter in Mg/Ca palaeotemperatures indicates that foraminiferal Mg/Ca was not solely controlled by temperature, with a large degree of natural variability in uptake apparent. Further research into the controls on Mg uptake by benthonic foraminifera is clearly required to identify the causes of the variability seen and whether the effects are species specific. The scatter in all the geochemical proxy records from Site 1211, however, might suggest that Site 1211 sediments are not typical of a purely primary carbonate record. Consideration of the heterogeneity of single foraminiferal shells from a range of sample depths throughout the studied interval could lead to clearer identification of whether the neomorphism observed is variable between shells and/or whether the heterogeneity observed in modern specimens is present.

Assuming the geochemical records from Site 1211 are that of primary carbonate, then Site 1211 poses a number of questions about palaeoceanography of Shatsky Rise. An improved record of both benthonic foraminiferal stable-isotope and element/Ca ratios including, as was planned in this study, trace element/Ca ratios, i.e. Li/Ca, Zn/Ca and Cd/Ca would help constrain both questions regarding the carbonate ion saturation change as well as the scatter in the Mg/Ca record. The development of stable isotope records from *Cibicidoides* spp. could answer the question as to the non-correlation of $\delta^{18}O$ and the $\delta^{13}C$ records observed from *O. umbonatus*. Increased resolution of records particularly between ~35.0 and ~34.0 Ma, i.e. across the build up and initiation of the EOB, could clarify the relationship between stable-isotope and apparent CCD deepening. The records of trace element/Ca ratios could constrain the increase in bottom-water carbonate ion (saturation) with the positive shift in the foraminiferal $\delta^{18}O$ record. These records must be undertaken with a spread of contaminant sensitive element/Ca ratios, as well as careful consideration of shell preservation, to minimise the potential for contaminant scatter within the record.

A refinement of the multiproxy approach attempted within this study in identification of CCD changes is required also, as described above would allow deconvolution of more of the possible influences on the CCD. Again, a more focussed consideration of the key ~35.0 to ~34.0 Ma interval, along with the EOT and EOGM, would allow the development of the EOB climate change to be identified from the site. On a more regional scale, the $CaCO_3$ MARs from Sites 1209 to 1211 indicate no clear gradient in bottom-water carbonate ion saturation, despite being within ~400 m of the CCD. A multiproxy, depth transect across the Shatsky Rise would reveal whether this scenario was the case.

8.0 References:

Anand, P., and H. Elderfield (2005), Variability of Mg/Ca and Sr/Ca between and within the planktonic foraminifers Globigerina bulloides and Globorotalia truncatulinoides, Geochemistry Geophysics Geosystems, 6. Q11D15, doi:10.1029/2004GC000811.

Anand, P., H. Elderfield, and M. H. Conte (2003), Calibration of Mg/Ca thermometry in planktonic foraminifera from a sediment trap time series, Paleoceanography, 18(2), PA1050, doi:10.1029/2002PA000846.

Anderson, L. D., and M. L. Delaney (2005), Use of multiproxy records on the Agulhas Ridge, Southern Ocean (Ocean Drilling Project Leg 177, Site 1090) to investigate sub-Antarctic hydrography from the Oligocene to the early Miocene, Paleoceanography, 20(3). PA1013, doi:10.1029/2004PA001043.

Anderson, R. F., M. Q. Fleisher, Y. Lao, and G. Winckler (2008), Modern CaCO3 preservation in equatorial Pacific sediments in the context of late-Pleistocene glacial cycles, Marine Chemistry, 111(1-2), 30-46.

Ando, A., H. Kawahata, and T. Kakegawa (2006), Sr/Ca ratios as indicators of varying modes of pelagic carbonate diagenesis in the ooze, chalk and limestone realms, Sedimentary Geology, 191(1-2), 37-53.

Averyt, K.B., M. Calhoun, L. Schmalz, and A. Paytan, (2005), Data report: carbonate and barite trends across the Eocene/Oligocene boundary at Shatsky Rise, ODP Leg 198. In Bralower, T.J., Premoli Silva, I., and Malone, M.J. (Eds.), Proc. ODP, Sci. Results, 198: College Station, TX (Ocean Drilling Program), 1–16. doi:10.2973/odp.proc.sr.198.106.2005.

Baker, P. A., J. M. Gieskes, and H. Elderfield (1982),Diagenesis of carbonates in deep-sea sediments – evidence from Sr/Ca ratios and interstitial dissolved Sr2+ date, , Journal of Sedimentary Petrology, 52(1), 71-82.

Barker, P. F., B. Diekmann, and C. Escutia (2007a), Onset of Cenozoic Antarctic glaciation, Deep-Sea Research Part Ii-Topical Studies in Oceanography, 54(21-22), 2293-2307.

Barker, P. F., G. M. Filippelli, F. Florindo, E. E. Martin, and H. D. Scher (2007b), Onset and role of the Antarctic Circumpolar Current, Deep-Sea Research Part Ii-Topical Studies in Oceanography, 54(21-22), 2388-2398.

Barker, S., M. Greaves, and H. Elderfield (2003), A study of cleaning procedures used for foraminiferal Mg/Ca paleothermometry, Geochemistry Geophysics Geosystems, 4. 8407, doi:10.1029/2003GC000559.

Barnola, J. M., D. Raynaud, Y. S. Korotkevich, and C. Lorius (1987), Vostok ice core provides 160,000 year record of atmospheric CO2, Nature, 329(6138), 408-414.

Bassinot, F. C., L. Beaufort, E. Vincent, L. D. Labeyrie, F. Rostek, P. J. Muller, X. Quidelleur, and Y. Lancelot (1994), Coarse fraction fluctiations in pelagic carbonate sediments from the tropical Indian Ocean – A 1500-kyr record of carbonate dissolution, Paleoceanography, 9(4), 579-600.

Be, A. W. H. (1980), Gametogenic calcification in a spinose planktonic foraminfera, Globiderinoides sacculifer (Brady), Marine Micropaleontology, 5(3), 283-310.

Bemis, B. E., H. J. Spero, J. Bijma, and D. W. Lea (1998), Reevaluation of the oxygen isotopic composition of planktonic foraminifera: Experimental results and revised paleotemperature equations, Paleoceanography, 13(2), 150-160.

Bemis, B. E., H. J. Spero, D. W. Lea, and J. Bijma (2000), Temperature influence on the carbon isotopic composition of Globigerina bulloides and Orbulina universa (planktonic foraminifera), Marine Micropaleontology, 38(3-4), 213-228.

Berger, W. H. (1968), Planktonic foraminifera – selective solution and paleoclimatic interpretation, Deep-Sea Research, 15(1), 31-43

Berger, W. H. (1971), Sedimentation of planktonic foraminifera, Marine Geology, 11(5), 325-358.

Berggren, W. A., and P. N. Pearson (2005), A revised tropical to subtropical paleogene planktonic foraminiferal zonation, Journal of Foraminiferal Research, 35(4), 279-298.

Berggren, W. A., D. V. Kent, C. C. I. Swisheri, and M.-P. Aubry (1995), A revised Cenozoic geochronology and chronostratigraphy, SEPM (Society for Sedimentary Geology) Special Publication; Geochronology, time scales and global stratigraphic correlation, 129-212.

Berner, R. A. (1993), Weathering and its effect on atmospheric CO2 over Phanerozoic time, Chemical Geology, 107(3-4), 373-374.

Berner, R. A. (2003), The long-term carbon cycle, fossil fuels and atmospheric composition, Nature, 426(6964), 323-326.

Berner, R. A. (2004), A model for calcium, magnesium and sulfate in seawater over Phanerozoic time, American Journal of Science, 304(5), 438-453.

Bice, K. L., D. Birgel, P. A. Meyers, K. A. Dahl, K. U. Hinrichs, and R. D. Norris (2006), A multiple proxy and model study of Cretaceous upper ocean temperatures and atmospheric CO2 concentrations, Paleoceanography, 21(2), PA2002, doi:10.1029/2005PA001203.

Bijma J., H.J. Spero and D. W. Lea (1999), Reassessing Foraminiferal Stable Isotope Geochemistry: Impact of the Oceanic Carbonate System (Experimental Results). In Fischer, G., G. Wefer (Eds.) from Use of Proxies in Paleoceanography: Examples from the South Atlantic, 489-512

Billups, K., and D. P. Schrag (2002), Paleotemperatures and ice volume of the past 27 myr revisited with paired Mg/Ca and 18O/16O measurements on benthic foraminifera, Paleoceanography, 17(1), 3.1-3.11.

Billups, K., and D. P. Schrag (2003), Application of benthic foraminiferal Mg/Ca ratios to questions of Cenozoic climate change, Earth and Planetary Science Letters, 209(1-2), 181-195.

Blum, J. D., and Y. Erel (1995), A silicate weathering mechanism linking increases in marine Sr-87/Sr-86 with global glaciation, Nature, 373, 415-418.

Blunier, T., and E. J. Brook (2001), Timing of millennial-scale climate change in Antarctica and Greenland during the last glacial period, Science, 291(5501), 109-112.

Bohaty, S. M., and J. C. Zachos (2003), Significant Southern Ocean warming event in the late middle Eocene, Geology, 31(11), 1017-1020.

Bolli, H. M., J.-P. Beckmann, and J. B. Saunders (1994), Benthic foraminiferal biostratigraphy of the south Caribbean region, Benthic foraminiferal biostratigraphy of the south Caribbean region., i-xi, 1-408.

Borre, M., and I. L. Fabricius (1998), Chemical and mechanical processes during burial diagenesis of chalk: an interpretation based on specific surface data of deep-sea sediments, Sedimentology, 45(4), 755-769.

Boyle, E., and Y. Rosenthal (1996a), Chemical hydrography of the South Atlantic during the last glacial maximum: Cd vs. delta C-13, South Atlantic, 423-443.

Boyle, E., and Y. Rosenthal (1996b), Chemical hydrography of the South Atlantic during the last glacial maximum: Cd vs. delta C-13, 423-443 pp.

Boyle, E. A. (1983), Manganese carbonate overgrowths on foraminifera tests, Geochimica Et Cosmochimica Acta, 47(10), 1815-1819.

Boyle, E. A., and L. D. Keigwin (1985), Comparison of Atlantic and Pacific paleochemical records for the last 215,000 years – changes in deep ocean circulation and chemical inventories, Earth and Planetary Science Letters, 76(1-2), 135-150.

Bralower, T.J. (2005), Data report: Paleocene–early Oligocene calcareous nannofossil biostratigraphy, ODP Leg 198 Sites 1209, 1210, and 1211 (Shatsky Rise, Pacific Ocean). In Bralower, T.J., Premoli Silva, I., and Malone, M.J. (Eds.), Proc. ODP, Sci. Results, 198: College Station, TX (Ocean Drilling Program), 1–15. doi:10.2973/odp.proc.sr.198.115.2005.

Broecker. W.S. (1989), The salinity contrast between the Atlantic and Pacific oceans during glacial time. Paleoceanography, 4, 207-212

Broecker, W.S., and T.S. Hung (1982), Tracers in the sea, Palisades, N.Y. Lamont-Doherty Geological Observatory, Columbia University, 1982

Brown, S. J., and H. Elderfield (1996), Variations in Mg/Ca and Sr/Ca ratios of planktonic foraminifera caused by postdepositional dissolution: Evidence of shallow Mg-dependent dissolution, Paleoceanography, 11(5), 543-551.

Bukry, D. (1973), Low-latitude coccolith biostratigraphic zonation. In Edgar, N.T., Saunders, J.B., et al., Init. Repts. DSDP, 15: Washington (U.S. Govt. Printing Office), 685–703.

Bukry, D. (1975), Biostratigraphy of Cenozoic marine sediment by calcareous nannofossils. Micropaleontology, 24:44–60.

Cande, S. C., and D. V. Kent (1995), Revised calibration of the geomagnetic polarity timescale for the Late Cretaceous and Cenozoic, Journal of Geophysical Research-Solid Earth, 100(B4), 6093-6095.

Cleroux, C., E. Cortijo, P. Anand, L. Labeyrie, F. Bassinot, N. Caillon, and J. C. Duplessy (2008), Mg/Ca and Sr/Ca ratios in planktonic foraminifera: Proxies for upper water column temperature reconstruction, Paleoceanography, 23(3), PA3214, doi:10.1029/2007PA001505.

Corliss, B. H., and S. Honjo (1981), Dissolution of deep-sea foraminifera, Micropaleontology, 27(4), 356-378.

Coxall, H. K., P. A. Wilson, H. Palike, C. H. Lear, and J. Backman (2005), Rapid stepwise onset of Antarctic glaciation and deeper calcite compensation in the Pacific Ocean, Nature, 433(7021), 53-57.

Coxall, H. K. and P. N. Pearson, (2007), The Eocene–Oligocene transitions, in M. Williams, A. M. Haywood, F. J. Gregory, and D. N. Schmidt (eds), Deep-time perspectives on climate change: marrying the signal from computer models and biological proxies. The Micropalaeontological Society Special Publications, The Geological Society, London, 351-387.

Crowley, T.J., and J.C. Zachos (2000), Comparisons of zonal temperature profiles for past warm time periods, in Huber, B.T., K.S. Macleod and S.C. Wing (eds) from Warm Climates in Earth History, Cambridge University Press, Cambridge, 50-76.

Dalai, T. K., and G. Ravizza (2006), Evaluation of osmium isotopes and iridium as paleoflux tracers in pelagic carbonates, Geochimica Et Cosmochimica Acta, 70, 3928-3942.

Dalai, T. K., G. E. Ravizza, and B. Peucker-Ehrenbrink (2006), The Late Eocene Os-187/Os-188 excursion: Chemostratigraphy, cosmic dust flux and the Early Oligocene glaciation, Earth and Planetary Science Letters, 241(3-4), 477-492.

de Villiers, S. (2003), Dissolution effects on foraminiferal Mg/Ca records of sea surface temperature in the western equatorial Pacific, Paleoceanography, 18(3). 1070, doi:10.1029/2002PA000802.

DeConto, R., D. Pollard, and D. Harwood (2007), Sea ice feedback and Cenozoic evolution of Antarctic climate and ice sheets, Paleoceanography, 22(3), PA3214, doi:10.1029/2006PA001350.

DeConto, R. M., and D. Pollard (2003), Rapid Cenozoic glaciation of Antarctica induced by declining atmospheric CO2, Nature, 421(6920), 245-249.

DeConto, R. M., D. Pollard, P. A. Wilson, H. Palike, C. H. Lear, and M. Pagani (2008), Thresholds for Cenozoic bipolar glaciation, Nature, 455(7213), 652--652.

Dekens, P. S., D. W. Lea, D. K. Pak, and H. J. Spero (2002), Core top calibration of Mg/Ca in tropical foraminifera: Refining paleotemperature estimation, Geochemistry Geophysics Geosystems, 3. 4, doi:10.1029/2001GC000200.

Diester-Haass, L. (1991), Eocene Oligocene paleoceanography in the Antarctic Ocean, Atlantic sector (Maud Rise, ODP Leg 113, Site 689B and Site 690B), Marine Geology, 100(1-4), 249-276.

Diester-Haass, L. (1995), Middle Eocene to Early Oligocene paleoceanography of the Antarctic Ocean (Maud Rise, ODP Leg 113, Site 689) – change from a low to a high productivity ocean, Palaeogeography Palaeoclimatology Palaeoecology, 113(2-4), 311-334.

Diester-Haass, L. (1996), Late Eocene-Oligocene paleoceanography in the southern Indian Ocean (ODP Site 744), Marine Geology, 130(1-2), 99-119.

Diester-Haass, L., and R. Zahn (1996), Eocene-Oligocene transition in the Southern Ocean: History of water mass circulation and biological productivity, Geology, 24(2), 163-166.

Diester-Haass, L., and R. Zahn (2001), Paleoproductivity increase at the Eocene-Oligocene climatic transition: ODP/DSDP sites 763 and 592, Palaeogeography Palaeoclimatology Palaeoecology, 172(1-2), 153-170.

Diester-Haass, L., and J.C. Zachos (2003), The Eocene – Oligocene transition in the Equatorial Atlantic (ODP Site 925): Paleoproductivity increase and positive δ13C excursion, in: Prothero, D., L. Ivany and E.A. Nesbitt (eds) from Greenhouse to Icehous, New York, Columbia University Press, 397-418

Diester-Haass, L., C. Robert, and H. Chamley (1993), Paleoceanographic and paleoclimatic evolution in the Weddell Sea (Antarctica) during the Middle Eocene-Late Oligocene , from a coarse sediment fraction and clay mineral data (ODP Site 689), Marine Geology, 114(3-4), 233-250.

Diester-Haass, L., C. Robert, and H. Chamley (1996), The Eocene-oligocene preglacial-glacial transition in the Atlantic sector of the Southern Ocean (ODP site 690), Marine Geology, 131(3-4), 123-149.

Dudley, W. C., and C. S. Nelson (1989), Quaternary surface-water stable isotope signal from calcareous nannofossils at DSDP Site 593, Southern Tasman Sea, Marine Micropaleontology, 13(4), 353-373.

Duplessy, J. C., L. Labeyrie, and C. Waelbroeck (2002), Constraints on the ocean oxygen isotopic enrichment between the Last Glacial Maximum and the Holocene: Paleoceanographic implications, Quaternary Science Reviews, 21(1-3), 315-330.

Dutton, A., K. C. Lohmann, and R. M. Leckie (2005), Insights from the Paleogene tropical Pacific: Foraminiferal stable isotope and elemental results from Site 1209, Shatsky Rise, Paleoceanography, 20(3). PA3004, doi:10.1029/2004PA001098.

Edgar, K. M., P. A. Wilson, P. F. Sexton, and Y. Suganuma (2007), No extreme bipolar glaciation during the main Eocene calcite compensation shift, Nature, 448(7156), 908-911.

Edmond, J. M. (1992), Himalayan tectonics, weathering processes, and the strontium isotope record in marine limestones, Science, 258(5088), 1594-1597.

Eggins, S., P. De Deckker, and J. Marshall (2003), Mg/Ca variation in planktonic foraminifera tests: implications for reconstructing palaeo-seawater temperature and habitat migration, Earth and Planetary Science Letters, 212(3-4), 291-306.

Ehrmann, W. U., and A. Mackensen (1992), Sedimentological evidence for the formation of an East Antarctic ice-sheet in Eocene Oligocene time, Palaeogeography Palaeoclimatology Palaeoecology, 93(1-2), 85-112.

Ehrmann, W. U., M. Melles, G. Kuhn, and H. Grobe (1992), Significance of clay mineral assemblages in the Antarctic Ocean, Marine Geology, 107(4), 249-273.

Elderfield, H., and J. M. Gieskes (1982), Sr-isotopes in interstitial waters of marine sediments from Deep-Sea Drilling Project cores, Nature, 300(5892), 493-497.

Elderfield, H., and A. Schultz (1996), Mid-ocean ridge hydrothermal fluxes and the chemical composition of the ocean, Annual Review of Earth and Planetary Sciences, 24, 191-224.

Elderfield, H., and G. Ganssen (2000), Past temperature and delta O-18 of surface ocean waters inferred from foraminiferal Mg/Ca ratios, Nature, 405(6785), 442-445.

Elderfield, H., C. J. Bertram, and J. Erez (1996), Biomineralization model for the incorporation of trace elements into foraminiferal calcium carbonate, Earth and Planetary Science Letters, 142(3-4), 409-423.

Elderfield, H., M. Cooper, and G. Ganssen (2000), Sr/Ca in multiple species of planktonic foraminifera: Implications for reconstructions of seawater Sr/Ca, Geochem. Geophys. Geosyst., 1, 1017, doi:10.1029/1999GC000031.

Elderfield, H., J. Yu, P. Anand, T. Kiefer, and B. Nyland (2006), Calibrations for benthic foraminiferal Mg/Ca paleothermometry and the carbonate ion hypothesis, Earth and Planetary Science Letters, 250(3-4), 633-649.

Elderfield, H., J. M. Gieskes, P. A. Baker, R. K. Oldfield, C. J. Hawkesworth, and R. Miller (1982), 87Sr/86Sr and 18O/16O ratios, interstitial water chemistry and diagenesis in deep-sea carbonate sediments of the Ontong Java Plateau, Geochimica Et Cosmochimica Acta, 46(11), 2259-2268.

Eldrett, J. S., I. C. Harding, P. A. Wilson, E. Butler, and A. P. Roberts (2007), Continental ice in Greenland during the Eocene and Oligocene, Nature, 446(7132), 176-179.

Emerson, S.R., and J.I. Hedges (2008), Chemical oceanography and the marine carbon cycle, Cambridge University Press, Cambridge.

Ennyu, A., M. A. Arthur, and M. Pagani (2002), Fine-fraction carbonate stable isotopes as indicators of seasonal shallow mixed-layer paleohydrography, Marine Micropaleontology, 46(3-4), 317-342.

Epstein, S., R. Buchsbaum, H. A. Lowenstam, and H. C. Urey (1953), Revised carbonate-water isotopic temperature scale, Geological Society of America Bulletin, 64(11), 1315-1325.

Erez, J., and B. Luz (1983), Experimental paleotemperature equation for planktonic foraminifera, Geochimica Et Cosmochimica Acta, 47(6), 1025-1031.

Fairbanks, R. G., and R. K. Matthews (1978), Marine oxygen isotope record in Pleistocene coral, Barbados, West Indies, Quaternary Research, 10(2), 181-196.

Farmer, E. C., P. B. deMenocal, and T. M. Marchitto (2005), Holocene and deglacial ocean temperature variability in the Benguela upwelling region: Implications for low-latitude atmospheric circulation, Paleoceanography, 20(2), PA2018, doi:10.1029/2004PA001049.

Gieskes, J. M., H. Elderfield, and M. R. Palmer (1986), Strontium and its isotopic composition in interstitial waters of marine carbonate sediments, Earth and Planetary Science Letters, 77(2), 229-235.

Gieskes, J. M., H. Elderfield, J. R. Lawrence, J. Johnson, B. Meyers, and A. Campbell (1982), Geochemistry of interstitial waters and sediments, Leg 64, Gulf of California, Initial Reports of the Deep Sea Drilling Project, 64(OCT), 675-694.

Goodney, D. E., S. V. Margolis, W. C. Dudley, P. Kroopnick, and D. F. Williams (1980), Oxygen and carbon isotopes of recent calcareous nannofossils as paleoceanographic indicators, Marine Micropaleontology, 5(1), 31-42.

Greaves, M., S. Barker, C. Daunt, and H. Elderfield (2005), Accuracy, standardization, and interlaboratory calibration standards for foraminiferal Mg/Ca thermometry, Geochemistry Geophysics Geosystems, 6, Q02D13, doi:10.1029/2004GC000790.

Greaves, M., et al. (2008), Interlaboratory comparison study of calibration standards for foraminiferal Mg/Ca thermometry, Geochemistry Geophysics Geosystems, 9, Q08010, doi:10.1029/2008GC001974.

Grossman, E. L. (1984a), Carbon isotopic fractionation in live benthic foraminifera – comparison with inorganic precipitate studies, Geochimica Et Cosmochimica Acta, 48(7), 1505-1512.

Grossman, E. L. (1984b), Stable isotope fractionation in live benthic foraminifera from the Southern California borderland, Palaeogeography Palaeoclimatology Palaeoecology, 47(3-4), 301-327.

Hamilton, C. P., H. J. Spero, J. Bijma, and D. W. Lea (2008), Geochemical investigation of gametogenic calcite addition in the planktonic foraminifera Orbulina universa, Marine Micropaleontology, 68(3-4), 256-267.

Hancock, H.J.L., and G.R. Dickens, (2005), Carbonate dissolution episodes in Paleocene and Eocene sediment, Shatsky Rise, west-central Pacific. In Bralower, T.J., Premoli Silva, I., and Malone, M.J. (Eds.), Proc. ODP, Sci. Results, 198: College Station, TX (Ocean Drilling Program), 1–24. doi:10.2973/odp.proc.sr.198.116.2005.

Hardie, L. A. (1996), Secular variation in seawater chemistry: An explanation for the coupled secular variation in the mineralogies of marine limestones and potash evaporites over the past 600 my, Geology, 24(3), 279-283.

Hathorne, E. C., O. Alard, R. H. James, and N. W. Rogers (2003), Determination of intratest variability of trace elements in foraminifera by laser ablation inductively coupled plasma-mass spectrometry, Geochemistry Geophysics Geosystems, 4, 8408, doi:10.1029/2003GC000539.

Hay, W. W., S. Flogel, and E. Soding (2005), Is the initiation of glaciation on Antarctica related to a change in the structure of the ocean?, Global and Planetary Change, 45(1-3), 23-33.

Healey, S. L., R. C. Thunell, and B. H. Corliss (2008), The Mg/Ca-temperature relationship of benthic foraminiferal calcite: New core-top calibrations in the < 4 degrees C temperature range, Earth and Planetary Science Letters, 272(3-4), 523-530.

Holland, H. D., J. Horita, and W. E. Seyfried (1996), On the secular variations in the composition of Phanerozoic marine potash evaporites, Geology, 24(11), 993-996.

Horita, J., H. Zimmermann, and H. D. Holland (2002), Chemical evolution of seawater during the Phanerozoic: Implications from the record of marine evaporites, Geochimica Et Cosmochimica Acta, 66(21), 3733-3756.

Howarth, R. J., and J. M. McArthur (1997), Statistics for strontium isotope stratigraphy: A robust LOWESS fit to the marine Sr-isotope curve for 0 to 206 Ma, with look-up table for derivation of numeric age, Journal of Geology, 105(4), 441-456.

Howell, P., N. Pisias, J. Ballance, J. Baughman, and L. Ochs (2006), ARAND Time-Series Analysis Software, Brown University, Providence RI.

Hsu, K. J., J. A. McKenzie, H. Oberhansli, and H. Weissert (1984a), South Atlantic Cenozoic paleoceanography, Initial Reports of the Deep Sea Drilling Project, 73(JAN), 771-785.

Hsu, K. J., et al. (1984b), Site-522, Initial Reports of the Deep Sea Drilling Project, 73(JAN), 187-270.

Huang, K. F., C. F. You, H. L. Lin, and Y. T. Shieh (2008), In situ calibration of Mg/Ca ratio in planktonic foraminiferal shell using time series sediment trap: A case study of intense dissolution artifact in the South China Sea, Geochemistry Geophysics Geosystems, 9, Q04016, doi:10.1029/2007GC001660.

Huber, B. T., D. A. Hodell, and C. P. Hamilton (1995), Middle-Late Cretaceous climate of the southern high-latitudes – stable isotopic evidence for minimal equator to pole thermal gradients, Geological Society of America Bulletin, 107(10), 1164-1191.

Huber, B. T., R. D. Norris, and K. G. MacLeod (2002), Deep-sea paleotemperature record of extreme warmth during the Cretaceous, Geology, 30(2), 123-126.

Huber, M., and L. C. Sloan (2001), Heat transport, deep waters, and thermal gradients: Coupled simulation of an Eocene Greenhouse Climate, Geophysical Research Letters, 28(18), 3481-3484.

Huber, M., and D. Nof (2006), The ocean circulation in the southern hemisphere and its climatic impacts in the Eocene, Palaeogeography Palaeoclimatology Palaeoecology, 231(1-2), 9-28.

Huber, M., H. Brinkhuis, C. E. Stickley, K. Doos, A. Sluijs, J. Warnaar, S. A. Schellenberg, and G. L. Williams (2004), Eocene circulation of the Southern Ocean: Was Antarctica kept warm by subtropical waters?, Paleoceanography, 19(4), PA4026, doi:10.1029/2004PA001014.

Huybrechts, P. (2002), Sea-level changes at the LGM from ice-dynamic reconstructions of the Greenland and Antarctic ice sheets during the glacial cycles, Quaternary Science Reviews, 21(1-3), 203-231.

Ito, G., and P. D. Clift (1998), Subsidence and growth of Pacific Cretaceous plateaus, Earth and Planetary Science Letters, 161(1-4), 85-100.

Ivany, L. C., S. Van Simaeys, E. W. Domack, and S. D. Samson (2006), Evidence for an earliest Oligocene ice sheet on the Antarctic Peninsula, Geology, 34(5), 377-380.

Jansen, J. H. F., S. J. Van der Gaast, B. Koster, and A. J. Vaars (1998), CORTEX, a shipboard XRF-scanner for element analyses in split sediment cores, Marine Geology, 151(1-4), 143-153.

Kastner, M., and J. M. Gieskes (1976), Interstitial water profiles and sites of diagenetic reactions, Leg 35, DSDP, Bellingshausen abyssal plain, 11-20 pp., Elsevier, Amsterdam.

Katz, M. E., and K. G. Miller (1991), Early Paleogene benthic foraminiferal assemblages and stable isotopes in the Southern Ocean, Proceedings of the Ocean Drilling Program Scientific Results, 114, 481-512.

Katz, M. E., D. R. Katz, J. D. Wright, K. G. Miller, D. K. Pak, N. J. Shackleton, and E. Thomas (2003), Early Cenozoic benthic foraminiferal isotopes: Species reliability and interspecies correction factors, Paleoceanography, 18(2), 1024, doi:10.1029/2002PA000798.

Katz, M. E., K. G. Miller, J. D. Wright, B. S. Wade, J. V. Browning, B. S. Cramer, and Y. Rosenthal (2008), Stepwise transition from the Eocene greenhouse to the Oligocene icehouse, Nature Geoscience, 1(5), 329-334.

Keigwin, L., and G. Keller (1984), Middle Oligocene cooling from equatorial Pacific DSDP Site 77B, Geology, 12(1), 16-19.

Keigwin, L. D. (1980), Paleoceanographic change in the Pacific at the Eocene-Oligocene boundary, Nature, 287(5784), 722-725.

Keigwin, L. D., and B. H. Corliss (1986), Stable isotopes in late Middle Eocene to Oligocene foraminifera, Geological Society of America Bulletin, 97(3), 335-345.

Kennett, J. P. (1977), Cenozoic evolution of Antarctic glaciation, circum-Antarctic ocean, and their impact on global paleoceanography, Journal of Geophysical Research-Oceans and Atmospheres, 82(27), 3843-3860.

Kennett, J. P., and N. J. Shackleton (1976), Oxygen isotopic evidence for development of psychrosphere 38 Myr ago, Nature, 260(5551), 513-515.

Kennett, J. P., and L. D. Stott (1990), 49. Proteus and Proto-oceanus: ancestral Paleogene oceans as revealed from Antarctic stable isotopic results; ODP Leg 113, Proceedings of the Ocean Drilling Program Scientific Results, 113, 865-880.

Kennett, J. P., N. J. Shackleton, and P. Vella (1974), Cenozoic paleo-oceanography and glacial history recorded in deep-sea drilled sites from the south Pacific, 41 pp., Int. Counc. Sci. Unions--UNESCO Paris.

Killingley, J. S. (1983), Effects of diagenetic recrystallisation of 18O/16O values of deep-sea sediments, Nature, 301(5901), 594-597.

Kominz, M. A., and S. F. Pekar (2001), Oligocene eustasy from two-dimensional sequence stratigraphic backstripping, Geological Society of America Bulletin, 113(3), 291-304.

Kroon, D., Zachos, J.C., and Leg 208 Scientific Party (2007), Leg 208 synthesis: Cenozoic climate cycles and excursions. In Kroon, D., Zachos, J.C., and Richter, C. (Eds.), Proc. ODP, Sci. Results, 208: College Station, TX (Ocean Drilling Program), 1–55. doi:10.2973/odp.proc.sr.208.201.2007.

Latimer, J. C., and G. M. Filippelli (2002a), Eocene to Miocene terrigenous inputs and export production: geochemical evidence from ODP Leg 177, Site 1090, Palaeogeography Palaeoclimatology Palaeoecology, 182(3-4), 151-164.

Latimer, J. C., and G. M. Filippelli (2002b), Eocene to Miocene terrigenous inputs and export production: geochemical evidence from ODP Leg 177, Site 1090, Palaeogeography Palaeoclimatology Palaeoecology, 182(3-4), 151-164.

Lawrence, J. R., J. M. Gieskes, and W. S. Broecker (1975), Oxygen isotope and cation composition of DSPD pore waters and alteration of layer-II basalts, Earth and Planetary Science Letters, 27(1), 1-10.

Lawver, L. A., and L. M. Gahagan (2003), Evolution of Cenozoic seaways in the circum-Antarctic region, Palaeogeography Palaeoclimatology Palaeoecology, 198(1-2), 11-37.

Lea D.W., J. Bijma, H.J. Spero and D. Archer (1999a), Implications of a Carbonate Ion Effect on Shell Carbon and Oxygen Isotopes for Glacial Ocean Conditions. In Fischer, G., G. Wefer (Eds.) from Use of Proxies in Paleoceanography: Examples from the South Atlantic, 513-522

Lea, D. W., T. A. Mashiotta, and H. J. Spero (1999b), Controls on magnesium and strontium uptake in planktonic foraminifera determined by live culturing, Geochimica Et Cosmochimica Acta, 63(16), 2369-2379.

Lea, D. W., D. K. Pak, and H. J. Spero (2000), Climate impact of late quaternary equatorial Pacific sea surface temperature variations, Science, 289(5485), 1719-1724.

Lea, D. W., P. A. Martin, D. K. Pak, and H. J. Spero (2002), Reconstructing a 350 ky history of sea level using planktonic Mg/Ca and oxygen isotope records from a Cocos Ridge core, Quaternary Science Reviews, 21(1-3), 283-293.

Lear, C. H., and Y. Rosenthal (2006), Benthic foraminiferal Li/Ca: Insights into Cenozoic seawater carbonate saturation state, Geology, 34(11), 985-988.

Lear, C. H., H. Elderfield, and P. A. Wilson (2000), Cenozoic deep-sea temperatures and global ice volumes from Mg/Ca in benthic foraminiferal calcite, Science, 287(5451), 269-272.

Lear, C. H., Y. Rosenthal, and N. Slowey (2002), Benthic foraminiferal Mg/Ca-paleothermometry: A revised core-top calibration, Geochimica Et Cosmochimica Acta, 66(19), 3375-3387.

Lear, C. H., H. Elderfield, and P. A. Wilson (2003), A Cenozoic seawater Sr/Ca record from benthic foraminiferal calcite and its application in determining global weathering fluxes, Earth and Planetary Science Letters, 208(1-2), 69-84.

Lear, C. H., Y. Rosenthal, H. K. Coxall, and P. A. Wilson (2004), Late Eocene to early Miocene ice sheet dynamics and the global carbon cycle, Paleoceanography, 19(4), PA4015, doi:10.1029/2004PA001039.

Lear, C. H., T. R. Bailey, P. N. Pearson, H. K. Coxall, and Y. Rosenthal (2008), Cooling and ice growth across the Eocene-Oligocene transition, Geology, 36(3), 251-254.

Liu, Z. H., M. Pagani, D. Zinniker, R. DeConto, M. Huber, H. Brinkhuis, S. R. Shah, R. M. Leckie, and A. Pearson (2009), Global Cooling During the Eocene-Oligocene Climate Transition, Science, 323(5918), 1187-1190.

Livermore, R., A. Nankivell, G. Eagles, and P. Morris (2005), Paleogene opening of Drake Passage, Earth and Planetary Science Letters, 236(1-2), 459-470.

Lohmann, G. P. (1995), A model for variation in the chemistry of planktonic foraminfera due to secondary calcification and selective dissolution, Paleoceanography, 10(3), 445-457.

Lowenstein, T. K., M. N. Timofeeff, S. T. Brennan, L. A. Hardie, and R. V. Demicco (2001), Oscillations in Phanerozoic seawater chemistry: Evidence from fluid inclusions, Science, 294(5544), 1086-1088.

Luterbacher, H.P., J. R. Ali, H. Brinkhuis, F. M. Gradstein, J. J. Hooker, S. Monechi, J. G. Ogg, J. Powell, U. Röhl, A. Sanfilippo, and B. Schmitz (2004), The Paleogene period, in Gradstein, F.M., J. G. Ogg and A. G. Smith (eds) from A Geologic Time Scale 2004, Cambridge University Press

Lyle, M. (2003), Neogene carbonate burial in the Pacific Ocean, Paleoceanography, 18(3), 1059, doi:10.1029/2002PA000777

Lyle, M., Olivarez Lyle, A., Backman, J., and Tripati, A. (2005), Biogenic sedimentation in the Eocene equatorial Pacific—the stuttering greenhouse and Eocene carbonate compensation depth. In Wilson, P.A., Lyle, M., and Firth, J.V. (Eds.), Proc. ODP, Sci. Results, 199: College Station, TX (Ocean Drilling Program), 1–35. doi:10.2973/odp.proc.sr.199.219.20.

Lyle, M., J. Barron, T. J. Bralower, M. Huber, A. O. Lyle, A. C. Ravelo, D. K. Rea, and P. A. Wilson (2008), Pacific ocean and Cenozoic evolution of climate, Reviews of Geophysics, 46(2), RG2002, doi:10.1029/2005RG000190.

Lythe, M. B., D. G. Vaughan, and B. Consortium (2001), BEDMAP: A new ice thickness and subglacial topographic model of Antarctica, Journal of Geophysical Research-Solid Earth, 106(B6), 11335-11351.

Mackensen, A., and W. U. Ehrmann (1992), Middle Eocene through Early Oligocene climate history and paleoceanography in the Southern Ocean – stable oxygen and carbon isotopes from ODP sites on Maud Rise and Kerguelen Plateau, Marine Geology, 108(1), 1-27.

Marchitto, T. M., W. B. Curry, and D. W. Oppo (2000), Zinc concentrations in benthic foraminifera reflect seawater chemistry, Paleoceanography, 15(3), 299-306.

Marchitto, T. M., D. W. Oppo, and W. B. Curry (2002), Paired benthic foraminiferal Cd/Ca and Zn/Ca evidence for a greatly increased presence of Southern Ocean Water in the glacial North Atlantic, Paleoceanography, 17(3), 3, doi:10.1029/2000PA000598.

Marchitto, T. M., S. P. Bryan, W. B. Curry, and D. C. McCorkle (2007), Mg/Ca temperature calibration for the benthic foraminifer Cibicidoides pachyderma, Paleoceanography, 22(1), PA1203, doi:10.1029/2006PA001287.

Martin, P. A., and D. W. Lea (2002), A simple evaluation of cleaning procedures on fossil benthic foraminiferal Mg/Ca, Geochemistry Geophysics Geosystems, 3, 8401, doi:10.1029/2001GC000280.

Martin, P. A., D. W. Lea, Y. Rosenthal, N. J. Shackleton, M. Sarnthein, and T. Papenfuss (2002), Quaternary deep sea temperature histories derived from benthic foraminiferal Mg/Ca, Earth and Planetary Science Letters, 198(1-2), 193-209.

Matthews, R. K., and R. Z. Poore (1980), Tertiary delta-18O record and glacio-eustatic sea-level fluctuations, Geology, 8(10), 501-504.

McArthur, J. M., R. J. Howarth, and T. R. Bailey (2001), Strontium isotope stratigraphy: LOWESS version 3: Best fit to the marine Sr-isotope curve for 0-509 Ma and accompanying look-up table for deriving numerical age, Journal of Geology, 109(2), 155-170.

McCorkle, D. C., P. A. Martin, D. W. Lea, and G. P. Klinkhammer (1995), Evidence of a dissolution effect on benthic foraminiferal shell chemistry – delta 13C, Cd/Ca, Ba/Ca, and Sr/Ca results from the Ontong Java Plateau, Paleoceanography, 10(4), 699-714.

McDuff, R. E. (1984), The chemistry of interstitial waters from the upper ocean crust, Site 395, Deep-sea Drilling Project Leg 78B, Initial Reports of the Deep Sea Drilling Project, 78(AUG), 795-799.

McDuff, R. E., and J. M. Gieskes (1976), Calcium and Magnesium profiles in DSDP interstitial waters – diffusion or reaction, Earth and Planetary Science Letters, 33(1), 1-10.

Mekik, F., and R. Francois (2006), Tracing deep-sea calcite dissolution: Agreement between the Globorotalia menardii fragmentation index and elemental ratios (Mg/Ca and Mg/Sr) in planktonic foraminifers, Paleoceanography, 21(4), PA4219, doi:10.1029/2006PA001296.

Mekik, F., R. Francois, and M. Soon (2007), A novel approach to dissolution correction of Mg/Ca-based paleothermometry in the tropical Pacific, Paleoceanography, 22(3), PA3217, doi:10.1029/2007PA001504.

Merico, A., T. Tyrrell, and P. A. Wilson (2008), Eocene/oligocene ocean de-acidification linked to Antarctic glaciation by sea-level fall, Nature, 452(7190), 979-U976.

Miller, K. G., and R. G. Fairbanks (1983), Evidence for Oligocene Middle Miocene abyssal circulation changes in the Western North-Atlantic, Nature, 306(5940), 250-253.

Miller, K. G., and E. Thomas (1985), Late Eocene to Oligocene benthic foraminiferal isotopic record, Site 574, Equatorial Pacific, Initial Reports of the Deep Sea Drilling Project, 85(OCT), 771-777.

Miller, K. G., J. D. Wright, and R. G. Fairbanks (1991), Unlocking the ice house – Oligocene-Miocene oxygen isotopes, eustasy and margin erosion, Journal of Geophysical Research-Solid Earth and Planets, 96(B4), 6829-6848.

Miller, K. G., J. D. Wright, and J. V. Browning (2005a), Visions of ice sheets in a greenhouse world, Marine Geology, 217(3-4), 215-231.

Miller, K. G., J. V. Browning, M. P. Aubry, B. S. Wade, M. E. Katz, A. A. Kulpecz, and J. D. Wright (2008), Eocene-Oligocene global climate and sea-level changes: St. Stephens Quarry, Alabama, Geological Society of America Bulletin, 120(1-2), 34-53.

Miller, K. G., M. A. Kominz, J. V. Browning, J. D. Wright, G. S. Mountain, M. E. Katz, P. J. Sugarman, B. S. Cramer, N. Christie-Blick, and S. F. Pekar (2005b), The phanerozoic record of global sea-level change, Science, 310(5752), 1293-1298.

Moore, T. C., P. D. Rabinowitz, P. E. Borella, N. J. Shackleton, and A. Boersma (1984), History of the Walvis Ridge, Initial Reports of the Deep Sea Drilling Project, 74(MAR), 873-894.

Moore, T. C., J. Backman, I. Raffi, C. Nigrini, A. Sanfilippo, H. Palike, and M. Lyle (2004), Paleogene tropical Pacific: Clues to circulation, productivity, and plate motion, Paleoceanography, 19(3), PA3013, doi:10.1029/2003PA000998.

Moran, K., et al. (2006), The Cenozoic palaeoenvironment of the Arctic Ocean, Nature, 441(7093), 601-605.

Morse, J. W., and M. L. Bender (1990), Partition-coefficients in calcite – examination of factors influencing the validity of experimental results and their application to natural systems, Chemical Geology, 82(3-4), 265-277.

Mortyn, P. G., H. Elderfield, P. Anand, and M. Greaves (2005), An evaluation of controls on planktonic foraminiferal Sr/Ca: Comparison of water column and core-top data from a North Atlantic transect, Geochemistry Geophysics Geosystems, 6, Q12007, doi:10.1029/2005GC001047.

Mulitza S., H. Arz, S. Kemle-von Micke, C. Moos, H.-S. Niebler, J. P‰tzold and M. Segl (1999), The South Atlantic Carbon Isotope Record of Planktic Foraminifera 427-445 In Fischer, G., G. Wefer (Eds.) from Use of Proxies in Paleoceanography: Examples from the South Atlantic, 513-522

Murray, J. W. (1989), Syndeposition dissolution of calcareous foraminifera in modern shallow-water sediments, Marine Micropaleontology, 15(1-2), 117-121.

Nilsen, E. B., L. D. Anderson, and M. L. Delaney (2003), Paleoproductivity, nutrient burial, climate change and the carbon cycle in the western equatorial Atlantic across the Eocene/Oligocene boundary, Paleoceanography, 18(3), 1057, doi:10.1029/2002PA000804.

Norris, R. D., and P. A. Wilson (1998), Low-latitude sea-surface temperatures for the mid-Cretaceous and the evolution of planktic foraminifera, Geology, 26(9), 823-826.

Norris, R. D., K. L. Bice, E. A. Magno, and P. A. Wilson (2002), Jiggling the tropical thermostat in the Cretaceous hothouse, Geology, 30(4), 299-302.

Nouet, J., and F. Bassinot (2007), Dissolution effects on the crystallography and Mg/Ca content of planktonic foraminifera Globorotalia tumida (Rotaliina) revealed by X-ray diffractometry, Geochemistry Geophysics Geosystems, 8, Q10007, doi:10.1029/2007GC001647.

Nurnberg, D., J. Bijma, and C. Hemleben (1996), Assessing the reliability of magnesium in foraminiferal calcite as a proxy for water mass temperatures, Geochimica Et Cosmochimica Acta, 60(5), 803-814.

Nurnberg, D., A. Muller, and R. R. Schneider (2000), Paleo-sea surface temperature calculations in the equatorial east Atlantic from Mg/Ca ratios in planktic foraminifera: A comparison to sea surface temperature

estimates from U-37(K '), oxygen isotopes, and foraminiferal transfer function, Paleoceanography, 15(1), 124-134.

Ogg, J.S., and A.G. Smith (2004), The geomagnetic polarity time scale, in Gradstein, F.M., J. G. Ogg and A. G. Smith (eds) from A Geologic Time Scale 2004, Cambridge University Press

Okada, H., and D. Bukry (1980), Supplementary modification and introduction of code numbers to the low-latitude coccolith biostratigraphic zonation (Bukry, 1973, 1975), Marine Micropaleontology, 5(3), 321-325.

O'neil, J. R., R. N. Clayton, and T. K. Mayeda (1969), Oxygen isotope fractionation in divalent metal carbonates, Journal of Chemical Physics, 51(12), 5547

Oomori, T., H. Kaneshima, Y. Maezato, and Y. Kitano (1987), Distribution coefficient of Mg2+ ions between calcite and solution at 10-50 °C, Marine Chemistry, 20(4), 327-336.

Oppo, D. W., and R. G. Fairbanks (1989), Carbon isotope composition of tropical surface water during the past 22,000 years, Paleoceanography, 4(4), 333-351.

Ortiz, J. D., A. C. Mix, W. Rugh, J. M. Watkins, and R. W. Collier (1996), Deep-dwelling planktonic foraminifera of the northeastern Pacific Ocean reveal environmental control of oxygen and carbon isotopic disequilibria, Geochimica Et Cosmochimica Acta, 60(22), 4509-4523.

Oslick, J. S., K. G. Miller, M. D. Feigenson, and J. D. Wright (1994), Oligocene-Miocene strontium isotopes – stratigraphic revisions and correlations to an inferred glacioeustatic record, Paleoceanography, 9(3), 427-443.

Pagani, M., J. C. Zachos, K. H. Freeman, B. Tipple, and S. Bohaty (2005), Marked decline in atmospheric carbon dioxide concentrations during the Paleogene, Science, 309(5734), 600-603.

Pak, D. K., and K. G. Miller (1995), Isotopic and faunal record of Paleogene deep-water transitions in the North Pacific, Proceedings of the Ocean Drilling Program Scientific Results, 145, 265-281.

Palike, H., R. D. Norris, J. O. Herrle, P. A. Wilson, H. K. Coxall, C. H. Lear, N. J. Shackleton, A. K. Tripati, and B. S. Wade (2006), The heartbeat of the oligocene climate system, Science, 314(5807), 1894-1898.

Palmer, M. R., and J. M. Edmond (1992), Controls over the Strontium isotope composition of river water, Geochimica Et Cosmochimica Acta, 56(5), 2099-2111.

Paull, C. K., and H. R. Thierstein (1990), Comparison of fine-fraction with monospecific foraminiferal stable isotopic stratigraphies from pelagic carbonates across the last glacial termination, Marine Micropaleontology, 16(3-4), 207-217.

Pearson, P. N., and M. R. Palmer (2000), Atmospheric carbon dioxide concentrations over the past 60 million years, Nature, 406(6797), 695-699.

Pearson, P. N., N. J. Shackleton, and M. A. Hall (1993), Stable isotope paleoecology of Middle Eocene planktonic foraminifera and multispecies isotope stratigraphy, DSDP Site 523, South Atlantic, Journal of Foraminiferal Research, 23(2), 123-140.

Pearson, P. N., G. L. Foster, and B. S. Wade (2009), Atmospheric carbon dioxide through the Eocene-Oligocene climate transition, Nature, 461(7267), 1110-U1204.

Pearson, P. N., R. K. Olsson, B. T. Huber, C. Hemleben, and W. A. Berggren (2006), Atlas of Eocene planktonic foraminifera, Cushman Foundation for Foraminiferal Research Special Publication, 41, 1-507.

Pearson, P. N., I. K. McMillan, B. S. Wade, T. Dunkley Jones, H. K. Coxall, P. R. Bown, and C. H. Lear (2008), Extinction and environmental change across the Eocene-Oligocene boundary in Tanzania, Geology, 36(2), 179-182.

Pearson, P. N., P. W. Ditchfield, J. Singano, K. G. Harcourt-Brown, C. J. Nicholas, R. K. Olsson, N. J. Shackleton, and M. A. Hall (2001), Warm tropical sea surface temperatures in the Late Cretaceous and Eocene epochs, Nature, 413(6855), 481-487.

Pegram, W. J., and K. K. Turekian (1999), The osmium isotopic composition change of Cenozoic sea water as inferred from a deep-sea core corrected for meteoritic contributions, Geochimica Et Cosmochimica Acta, 63(23-24), 4053-4058.

Pekar, S. F., N. Christie-Blick, M. A. Kominz, and K. G. Miller (2002), Calibration between eustatic estimates from backstripping and oxygen isotopic records for the Oligocene, Geology, 30(10), 903-906.

Peterson, L. C., and W. L. Prell (1985), Carbonate dissolution in recent sediments of the eastern equatorial Indian Ocean – preservation patterns and carbonate loss above the lysocline, Marine Geology, 64(3-4), 259-290.

Petrizzo, M.R., I. Premoli Silva, and P. Ferrari (2005), Data report: Paleogene planktonic foraminifer biostratigraphy, ODP Leg 198 Holes 1209A, 1210A, and 1211A (Shatsky Rise, northwest Pacific Ocean). In Bralower, T.J., Premoli Silva, I., and Malone, M.J. (Eds.), Proc. ODP, Sci. Results, 198: College Station, TX (Ocean Drilling Program), 1–56. doi:10.2973/odp.proc.sr.198.110.2005.

Peucker-Ehrenbrink, B., and G. Ravizza (2000), The marine osmium isotope record, Terra Nova, 12(5), 205-219.

Poore, R. Z., and R. K. Matthews (1984), Oxygen isotope ranking of Late Eocene and Oligocene foraminifers – implications for Oligocene sea-surface temperatures and global ice-volume, Marine Micropaleontology, 9(2), 111-134.

Rathburn, A. E., B. H. Corliss, K. D. Tappa, and K. C. Lohmann (1996), Comparisons of the ecology and stable isotopic compositions of living (stained) benthic foraminifera from the Sulu and South China seas, Deep-Sea Research Part I-Oceanographic Research Papers, 43(10), 1617-1646.

Rathmann, S., and H. Kuhnert (2008), Carbonate ion effect on Mg/Ca, Sr/Ca and stable isotopes on the benthic foraminifera Oridorsalis umbonatus off Namibia, Marine Micropaleontology, 66(2), 120-133.

Rathmann, S., S. Hess, H. Kuhnert, and S. Mulitza (2004), Mg/Ca ratios of the benthic foraminifera Oridorsalis umbonatus obtained by laser ablation from core top sediments: Relationship to bottom water temperature, Geochemistry Geophysics Geosystems, 5, Q12013, doi:10.1029/2004GC000808.

Ravello, A.C., and C. Hillaire-Marcel (2007), The use of oxygen and carbon isotopes of foraminifera in paleoceanography, in Hillaire-Marcel, C., and A. De Vernal (eds) from Proxies in Late Cenozoic paleoceanography, Elsevier, 735-764.

Ravizza, G., and B. Peucker-Ehrenbrink (2003), The marine Os-187/Os-188 record of the Eocene-Oligocene transition: the interplay of weathering and glaciation, Earth and Planetary Science Letters, 210(1-2), 151-165.

Ravizza, G., and F. Paquay (2008), Os isotope chemostratigraphy applied to organic-rich marine sediments from the Eocene-Oligocene transition on the West African margin (ODP Site 959), Paleoceanography, 23(2), PA2204, doi:10.1029/2007PA001460.

Raymo, M. E., and W. F. Ruddiman (1992), Tectonic forcing of late Cenozoic climate, Nature, 359(6391), 117-122.

Raymo, M. E., W. F. Ruddiman, and P. N. Froelich (1988), Influence of late Cenozoic mountain building on ocean geochemical cycles, Geology, 16(7), 649-653.

Rea, D. K., and M. W. Lyle (2005), Paleogene calcite compensation depth in the eastern subtropical Pacific: Answers and questions, Paleoceanography, 20(1), PA1012, doi:10.1029/2004PA001064.

Rea, D. K., et al. (1995), Scientific results of drilling the North Pacific Transect, 577-596 pp., Texas A & M University Ocean Drilling Program, College Station, TX.

Regenberg, M., S. Steph, D. Nurnberg, R. Tiedemann, and D. Garbe-Schonberg (2009), Calibrating Mg/Ca ratios of multiple planktonic foraminiferal species with delta O-18-calcification temperatures: Paleothermometry for the upper water column, Earth and Planetary Science Letters, 278(3-4), 324-336.

Regenberg, M., D. Nurnberg, S. Steph, J. Groeneveld, D. Garbe-Schonberg, R. Tiedemann, and W. C. Dullo (2006), Assessing the effect of dissolution on planktonic foraminiferal Mg/Ca ratios: Evidence from Caribbean core tops, Geochemistry Geophysics Geosystems, 7, Q07P15, doi:10.1029/2005GC001019.

Reilly, T. J., K. G. Miller, and M. D. Feigenson (2002), Latest Eocene-earliest Miocene Sr isotopic reference section, Site 522, eastern South Atlantic, Paleoceanography, 17(3), 1046, doi:10.1029/2001PA000745.

Riesselman, C.R., R.B. Dunbar, D.A. Mucciarone and S.S. Kitasei (2007), High resolution stable isotope and carbonate variability during the early Oligocene climate transition: Walvis Ridge (ODP Site 1263), in Antarctica: A Keystone in a Changing World – Online Proceedings of the 10th ISAES, edited by A.K. Cooper and C.R. Raymond et al., USGS Open File Report 2007–1047, Short Research Paper 095, 7 p.; doi:10.3133/of2007-1047.srp095.

Robert, C., and J. P. Kennett (1997), Antarctic continental weathering changes during Eocene-Oligocene cryosphere expansion: Clay mineral and oxygen isotope evidence, Geology, 25(7), 587-590.

Robert, C., L. Diester-Haass, and H. Chamley (2002), Late Eocene-Oligocene oceanographic development at southern high latitudes, from terrigenous and biogenic particles: a comparison of Kerguelen Plateau and Maud Rise, ODP Sites 744 and 689, Marine Geology, 191(1-2), 37-54.

Röhl, U., et al. (2000), High-resolution, downhole, and nondestructive core measurements from sites 999 and 1001 in the Caribbean Sea, edited, pp. 191-203, Texas A & M University Ocean Drilling Program, College Station, TX.

Röhl, U., T. J. Bralower, R. D. Norris, and G. Wefer (2000), New chronology for the late Paleocene thermal maximum and its environmental implications, Geology, 28(10), 927-930.

Rohling, E. J., and S. Cooke (1999), Stable oxygen and carbon isotopes in foraminiferal carbonate shells, 239-258 pp.

Romanek, C. S., E. L. Grossman, and J. W. Morse (1992), Carbon isotopic fractionation in synthetic aragonite and calcite – effects of temperature and precipitation rate, Geochimica Et Cosmochimica Acta, 56(1), 419-430.

Rosenthal, Y., and G. P. Lohmann (2002), Accurate estimation of sea surface temperatures using dissolution-corrected calibrations for Mg/Ca paleothermometry, Paleoceanography, 17(3), 1044, doi:10.1029/2001PA000749.

Rosenthal, Y., E. A. Boyle, and N. Slowey (1997), Temperature control on the incorporation of magnesium, strontium, fluorine, and cadmium into benthic foraminiferal shells from Little Bahama Bank: Prospects for thermocline paleoceanography, Geochimica Et Cosmochimica Acta, 61(17), 3633-3643.

Rosenthal, Y., M. P. Field, and R. M. Sherrell (1999), Precise determination of element/calcium ratios in calcareous samples using sector field inductively coupled plasma mass spectrometry, Analytical Chemistry, 71(15), 3248-3253.

Rosenthal, Y., G. P. Lohmann, K. C. Lohmann, and R. M. Sherrell (2000), Incorporation and preservation of Mg in Globigerinoides sacculifer: Implications for reconstructing the temperature and O-18/O-16 of seawater, Paleoceanography, 15(1), 135-145.

Rowley, D. B. (2002), Rate of plate creation and destruction: 180 Ma to present, Geological Society of America Bulletin, 114(8), 927-933.

Royer, D. L., R. A. Berner, and D. J. Beerling (2001), Phanerozoic atmospheric CO2 change: evaluating geochemical and paleobiological approaches, Earth-Science Reviews, 54(4), 349-392.

Rudnicki, M. D., P. A. Wilson, and W. T. Anderson (2001), Numerical models of diagenesis, sediment properties, and pore fluid chemistry on a paleoceanographic transect: Blake Nose, Ocean Drilling Program Leg 171B, Paleoceanography, 16(6), 563-575.

Sadekov, A., S. M. Eggins, P. De Deckker, and D. Kroon (2008), Uncertainties in seawater thermometry deriving from intratest and intertest Mg/Ca variability in Globigerinoides ruber, Paleoceanography, 23(1), PA1215, doi:10.1029/2007PA001452.

Salamy, K. A., and J. C. Zachos (1999), Latest Eocene Early Oligocene climate change and Southern Ocean fertility: inferences from sediment accumulation and stable isotope data, Palaeogeography Palaeoclimatology Palaeoecology, 145(1-3), 61-77.

Savin, S. M., and R. G. Douglas (1973), Stable isotope and magnesium geochemistry of recent planktonic foraminifera from South Pacific, Geological Society of America Bulletin, 84(7), 2327-2342.

Scher, H. D., and E. E. Martin (2004), Circulation in the Southern Ocean during the Paleogene inferred from neodymium isotopes, Earth and Planetary Science Letters, 228(3-4), 391-405.

Scher, H. D., and E. E. Martin (2006), Timing and climatic consequences of the opening of Drake Passage, Science, 312(5772), 428-430.

Schlanger, S. O., R. G. Douglas, Y. Lancelot, T. C. Moore, Jr., and P. H. Roth (1973), Fossil preservation and diagenesis of pelagic carbonates from the Magellan Rise, central North Pacific Ocean, 407-427 pp., Texas A & M University Ocean Drilling Program, College Station, TX.

Schrag, D. P. (1999), Effects of diagenesis on the isotopic record of late paleogene tropical sea surface temperatures, Chemical Geology, 161(1-3), 215-224.

Schrag, D. P., D. J. Depaolo, and F. M. Richter (1992), Oxygen isotope exchange in a 2-layer model of oceanic crust, Earth and Planetary Science Letters, 111(2-4), 305-317.

Schrag, D. P., D. J. Depaolo, and F. M. Richter (1995), Reconstructing past sea-surface temperatures – correcting for diagenesis of bulk marine carbonate, Geochimica Et Cosmochimica Acta, 59(11), 2265-2278.

Sexton, P. F., and P. A. Wilson (2009), Preservation of benthic foraminifera and reliability of deep-sea temperature records: Importance of sedimentation rates, lithology, and the need to examine test wall structure, Paleoceanography, 24, PA2208, doi:10.1029/2008PA001650.

Sexton, P. F., P. A. Wilson, and P. N. Pearson (2006), Microstructural and geochemical perspectives on planktic foraminiferal preservation: "Glassy" versus "Frosty", Geochemistry Geophysics Geosystems, 7, Q12P19, doi:10.1029/2006GC001291.

Shackleton, N. J., 1974. Attainment of isotopic equilibrium between ocean water and the benthonic Foraminifera genus Uvigerina: Isotopic changes in the ocean during the last glacial. C.N.R.S. Colloquium, 219:203-209.

Shackleton, N. J., and J. P. Kennett (1974), Palaeotemperature history of the Cenozoic from oxygen isotope studies in D.S.D.P. Leg 29, 66 pp., Int. Counc. Sci. Unions--UNESCO Paris.

Shackleton, N. J., and J. P. Kennett (1975a), Late Cenozoic oxygen and carbon isotopic changes at DSDP Site 284, 801-807 pp., Texas A & M University Ocean Drilling Program, College Station, TX.

Shackleton, N. J., and J. P. Kennett (1975b), Paleotemperature history of the Cenozoic and the initiation of Antarctic glaciation, 743-755 pp., Texas A & M University Ocean Drilling Program, College Station, TX.

Shackleton, N. J., M. A. Hall, and A. Boersma (1984), Oxygen and carbon isotope data from Leg 74 foraminifers, Initial Reports of the Deep Sea Drilling Project, 74(MAR), 599-612.

Shackleton, N.J, J. D. H. Wiseman, and H. A. Buckley (1973), Nonequilibrium isotopic fractionation between seawater and planktonic foraminiferal tests, Nature, 242(5394), 177-179.

Shackleton, N. J., M. A. Hall, D. Pate, L. Meynadier, and P. Valet (1993), High resolution stable-isotope stratigraphy from bulk sediment, Paleoceanography, 8(2), 141-148.

Shevenell, A. E., and J. P. Kennett (2007), Cenozoic Antarctic cryosphere evolution: Tales from deep-sea sedimentary records, Deep-Sea Research Part Ii-Topical Studies in Oceanography, 54(21-22), 2308-2324.

Shipboard Scientific Party (2002a), Leg 198 summary. In Bralower, T.J., I. Premoli Silva, M.J. Malone, et al., Proc. ODP, Init. Repts., 198: College Station, TX (Ocean Drilling Program), 1–148. doi:10.2973/odp.proc.ir.198.101.2002.

Shipboard Scientific Party (2002b), Site 1211. In Bralower, T.J., I. Premoli Silva, M.J. Malone, et al., Proc. ODP, Init. Repts., 198: College Station, TX (Ocean Drilling Program), 1–148. doi:10.2973/odp.proc.ir.198.101.2002.

Shipboard Scientific Party (2002c), Site 1209. In Bralower, T.J., I. Premoli Silva, M.J. Malone, et al., Proc. ODP, Init. Repts., 198: College Station, TX (Ocean Drilling Program), 1–148. doi:10.2973/odp.proc.ir.198.101.2002.

Shipboard Scientific Party (2002d), Site 1210. In Bralower, T.J., I. Premoli Silva, M.J. Malone, et al., Proc. ODP, Init. Repts., 198: College Station, TX (Ocean Drilling Program), 1–148. doi:10.2973/odp.proc.ir.198.101.2002.

Shipboard Scientific Party (2002e), Leg 199 summary. In Bralower, T.J., I. Premoli Silva, M.J. Malone, et al., Proc. ODP, Init. Repts., 198: College Station, TX (Ocean Drilling Program), 1–148. doi:10.2973/odp.proc.ir.198.101.2002.

Shipboard Scientific Party (2004), Explanatory notes. In Zachos, J.C., D. Kroon, P. Blum, et al., Proc. ODP, Init. Repts., 208: College Station, TX (Ocean Drilling Program), 1–63. doi:10.2973/odp.proc.ir.208.102.2004.

Spero, H. J. (1992), Do planktonic foraminifera accurately record shifts in the carbon isotopic composition of seawater sigma CO2, Marine Micropaleontology, 19(4), 275-285.

Spero, H. J., and D. F. Williams (1988), Extracting environmental information from planktonic foraminiferal δ13C, Nature, 335(6192), 717-719.

Spero, H. J., and D. W. Lea (1993), Intraspecific stable-isotope variability in the planktic foraminifera Globigerinoides sacculifer – results from laboratory experiments, Marine Micropaleontology, 22(3), 221-234.

Spero, H. J., and D. W. Lea (1996), Experimental determination of stable isotope variability in Globigerina bulloides: Implications for paleoceanographic reconstructions, Marine Micropaleontology, 28(3-4), 231-246.

Spero, H. J., J. Bijma, D. W. Lea, and B. E. Bemis (1997), Effect of seawater carbonate concentration on foraminiferal carbon and oxygen isotopes, Nature, 390(6659), 497-500.

St John, K. (2008), Cenozoic ice-rafting history of the central Arctic Ocean: Terrigenous sands on the Lomonosov Ridge, Paleoceanography, 23(1), PA1S05, doi:10.1029/2007PA001483.

Stanley, S. M., and L. A. Hardie (1998), Secular oscillations in the carbonate mineralogy of reef-building and sediment-producing organisms driven by tectonically forced shifts in seawater chemistry, Palaeogeography Palaeoclimatology Palaeoecology, 144(1-2), 3-19.

Stott, L. D., J. P. Kennett, N. J. Shackleton, and R. M. Corfield (1990), 48. The evolution of Antarctic surface waters during the Paleogene: inferences from the stable isotopic composition of planktonic foraminifers, ODP Leg 113, Proceedings of the Ocean Drilling Program Scientific Results, 113, 849-863.

Talley, L.D. (2007), Hydrographic Atlas of the World Ocean Circulation Experiment (WOCE). Volume 2: Pacific Ocean (eds. M. Sparrow, P. Chapman and J. Gould), International WOCE Project Office, Southampton, U.K., ISBN 0-904175-54-5.

Thomas, E., and A. J. Gooday (1996), Cenozoic deep-sea benthic foraminifers: Tracers for changes in oceanic productivity?, Geology, 24(4), 355-358.

Toggweiler, J. R., and H. Bjornsson (2000), Drake Passage and palaeoclimate, Journal of Quaternary Science, 15(4), 319-328.

Tripati, A., J. Backman, H. Elderfield, and P. Ferretti (2005), Eocene bipolar glaciation associated with global carbon cycle changes, Nature, 436(7049), 341-346.

Tripati, A. K., M. L. Delaney, J. C. Zachos, L. D. Anderson, D. C. Kelly, and H. Elderfield (2003), Tropical sea-surface temperature reconstruction for the early Paleogene using Mg/Ca ratios of planktonic foraminifera, Paleoceanography, 18(4), 1-13.

Tripati, A. K., et al. (2008), Evidence for glaciation in the Northern Hemisphere back to 44 Ma from ice-rafted debris in the Greenland Sea, Earth and Planetary Science Letters, 265(1-2), 112-122.

Urey, H. C. (1947), The thermodynamic properties of isotopic substances, Journal of the Chemical Society(MAY), 562-581.

Van der Lingen, G. J., and G. Packham (1975), Relationships between diagenesis and physical properties of biogenic sediments of the Ontong-Java Plateau (sites 288 and 289, Deep Sea Drilling Project), 443-481 pp., Texas A & M University Ocean Drilling Program, College Station, TX.

Van Andel, T. H. (1975), Mesozoic-Cenozoic calcite compensation depth and global distribution of calcareous sediments, Earth and Planetary Science Letters, 26(2), 187-194.

Van Eijden, A. J. M., and G. M. Ganssen (1995), An Oligocene multispecies foraminiferal oxygen and carbon-isotope record from ODP hole 758A (Indian Ocean) – paleoceanographic and paleo-ecological implications, Marine Micropaleontology, 25(1), 47-65.

Vinot-Bertouille, A. C., and J. C. Duplessy (1973), Individual isotopic fractionation of carbona and oxygen in benthic foraminifera, Earth and Planetary Science Letters, 18(2), 247-252.

Vonhof, H. B., J. Smit, H. Brinkhuis, A. Montanari, and A. J. Nederbragt (2000), Global cooling accelerated by early late Eocene impacts?, Geology, 28(8), 687-690.

Wade, B. S., and H. Palike (2004), Oligocene climate dynamics, Paleoceanography, 19(4), PA4019, doi:10.1029/2004PA001042.

Wade, B. S., and P. N. Pearson (2008), Planktonic foraminiferal turnover, diversity fluctuations and geochemical signals across the Eocene/Oligocene boundary in Tanzania, Marine Micropaleontology, 68(3-4), 244-255.

Wade, B. S., W. A. Berggren, and R. K. Olsson (2007), The biostratigraphy and paleobiology of Oligocene planktonic foraminifera from the equatorial Pacific Ocean (ODP Site 1218), Marine Micropaleontology, 62(3), 167-179.

Wefer, G., and W. H. Berger (1991), Isotope paleontology – growth and composition of extance calcareous species, Marine Geology, 100(1-4), 207-248.

Westerhold, T., and U. Röhl, (2006) Data report: revised composite depth records for Shatsky Rise Sites 1209, 1210, and 1211. In Bralower, T.J., Premoli Silva, I., and Malone, M.J. (Eds.), Proc. ODP, Sci. Results, 198: College Station, TX (Ocean Drilling Program), 1–26. doi:10.2973/odp.proc.sr.198.122.2006

Westerhold, T., U. Rohl, J. Laskar, I. Raffi, J. Bowles, L. J. Lourens, and J. C. Zachos (2007), On the duration of magnetochrons C24r and C25n and the timing of early Eocene global warming events: Implications from the Ocean Drilling Program Leg 208 Walvis Ridge depth transect, Paleoceanography, 22(1), PA2201, doi:10.1029/2006PA001322.

Westerhold, T., U. Rohl, I. Raffi, E. Fornaciari, S. Monechi, V. Reale, J. Bowles, and H. F. Evans (2008), Astronomical calibration of the Paleocene time, Palaeogeography Palaeoclimatology Palaeoecology, 257(4), 377-403.

Wilkinson, B. H., and T. J. Algeo (1989), Sedimentary carbonate record of calcium magnesium cycling, American Journal of Science, 289(10), 1158-1194.

Wilson, P. A., R. D. Norris, and M. J. Cooper (2002), Testing the Cretaceous greenhouse hypothesis using glassy foraminiferal calcite from the core of the Turonian tropics on Demerara Rise, Geology, 30(7), 607-610.

Woodruff, F., S. M. Savin, and R. G. Douglas (1980), Biological fractionation of oxygen and carbon isotopes by recent benthic foraminifera, Marine Micropaleontology, 5(1), 3-11.

Wu, G., J.C. Herguera, and W.H. Berger (1990), Differential dissolution: Modification of late Pleistocene oxygen isotope records in the western equatorial Pacific, Paleoceanography, 5, 581-594

Yu, J. M., and H. Elderfield (2007), Benthic foraminiferal B/Ca ratios reflect deep water carbonate saturation state, Earth and Planetary Science Letters, 258(1-2), 73-86.

Yu, J. M., and H. Elderfield (2008), Mg/Ca in the benthic foraminifera Cibicidoides wuellerstorfi and Cibicidoides mundulus: Temperature versus carbonate ion saturation, Earth and Planetary Science Letters, 276(1-2), 129-139.

Yu, J. M., H. Elderfield, and B. Honisch (2007a), B/Ca in planktonic foraminifera as a proxy for surface seawater pH, Paleoceanography, 22(2), PA2202, doi:10.1029/2006PA001347.

Yu, J. M., H. Elderfield, M. Greaves, and J. Day (2007b), Preferential dissolution of benthic foraminiferal calcite during laboratory reductive cleaning, Geochemistry Geophysics Geosystems, 8, Q06016, doi:10.1029/2006GC001571.

Zachos, J., M. Pagani, L. Sloan, E. Thomas, and K. Billups (2001), Trends, rhythms, and aberrations in global climate 65 Ma to present, Science, 292(5517), 686-693.

Zachos, J. C., and L. R. Kump (2005), Carbon cycle feedbacks and the initiation of Antarctic glaciation in the earliest Oligocene, Global and Planetary Change, 47(1), 51-66.

Zachos, J. C., J. R. Breza, and S. W. Wise (1992), Early Oligocene ice-sheet expansion on Antarctica – stable isotope and sedimentological evidence from the Kerguelen Plateau, Southern Indian Ocean, Geology, 20(6), 569-573.

Zachos, J. C., L. D. Stott, and K. C. Lohmann (1994), Evolution of early Cenozoic marine temperatures, Paleoceanography, 9(2), 353-387.

Zachos, J. C., T. M. Quinn, and K. A. Salamy (1996), High-resolution (10(4) years) deep-sea foraminiferal stable isotope records of the Eocene-Oligocene climate transition, Paleoceanography, 11(3), 251-266.

Zachos, J. C., G. R. Dickens, and R. E. Zeebe (2008), An early Cenozoic perspective on greenhouse warming and carbon-cycle dynamics, Nature, 451(7176), 279-283.

Zachos, J. C., B. N. Opdyke, T. M. Quinn, C. E. Jones, and A. N. Halliday (1999), Early cenozoic glaciation, antarctic weathering, and seawater Sr-87/Sr-86: is there a link?, Chemical Geology, 161(1-3), 165-180.

Zachos, J. C., M. W. Wara, S. Bohaty, M. L. Delaney, M. R. Petrizzo, A. Brill, T. J. Bralower, and I. Premoli-Silva (2003), A transient rise in tropical sea surface temperature during the Paleocene-Eocene Thermal Maximum, Science, 302(5650), 1551-1554.

Zeebe, R. E. (1999), An explanation of the effect of seawater carbonate concentration on foraminiferal oxygen isotopes, Geochimica Et Cosmochimica Acta, 63(13-14), 2001-2007.

Zeebe, R. E., and P. Westbroek (2003), A simple model for the CaCO3 saturation state of the ocean: The "Strangelove", the "Neritan", and the "Cretan" Ocean, Geochemistry Geophysics Geosystems, 4, 1104, doi:10.1029/2003GC000538.

Zhang, J. Y., P. X. Wang, Q. Y. Li, X. R. Cheng, H. Y. Jin, and S. Y. Zhang (2007), Western equatorial Pacific productivity and carbonate dissolution over the last 550 kyr: Foraminiferal and nannofossil evidence from ODP Hole 807A, Marine Micropaleontology, 64, 121-140.

Zimmermann, H. (2000), Tertiary seawater chemistry - Implications from primary fluid inclusions in marine halite, American Journal of Science, 300(10), 723-767.